Universidade do Minho
Escola de Engenharia

Joaquim Miguel Antunes de Oliveira

New nanotechnology approaches using dendrimers modified with natural polymers for controlling stem cells behaviour in tissue engineering strategies

Março de 2009

New nanotechnology approaches using dendrimers modified with natural polymers for controlling stem cells behaviour in tissue engineering strategies

Joaquim Miguel Antunes de Oliveira

UMinho | 2009

Universidade do Minho
Escola de Engenharia

Joaquim Miguel Antunes de Oliveira

New nanotechnology approaches using dendrimers modified with natural polymers for controlling stem cells behaviour in tissue engineering strategies

Tese de Doutoramento em
Ciência e Tecnologia de Materiais:
Engenharia de Tecidos - Materiais Híbridos

Trabalho efectuado sob a orientação do
Professor Rui Luís Gonçalves dos Reis
Professor João Filipe Colardelle da Luz Mano
Doutor Hajime Ohgushi

Março de 2009

To my parents, my sister and Natacha

‘*Every day you may make progress. Every step may be fruitful. Yet there will stretch out before you an ever-lengthening, ever-ascending, ever-improving path. You know you will never get to the end of the journey. But this, so far from discouraging, only adds to the joy and glory of the climb*’. Sir Winston Churchill (1874-1965).

The Olive Trees

Vincent van Gogh, 1889

Oil on canvas

It makes figurative meaning to Donald Tomalia inspiration from nature and a poetic analogy of the dendrimers to nature's architecture and geometric forms.

ACKNOWLEDGEMENTS.

This thesis was only possible to accomplish due to the unique contribution of several people and institutions. To them, I would like to deeply express my gratitude and dedicate this dissertation.

I would like to gratefully acknowledge my thesis supervisor, the Professor Rui L. Reis, for in first place believe in me. I am indebted to Professor Rui L. Reis whose assistance and provided opportunity is invaluable. I wish to highlight his continuous efforts and enthusiastic supervision during my PhD. He was always there to listen and to give me valuable advices. He was an example to follow, with his character, leadership and inteligence, he was an inspiration and mentor. Without his warm encouragement and constant guidance, I could not have finished this thesis, he brought out the good ideas in me and my work. I herein express my admiration. I also thank the possiblity gaven to be involved in parallel projects, which were most important to me and to my career. The principle, to see the good in everything and be a constructive part of the whole, made me feel more responsible.

A special thanks goes to my trully inspiring co-supervisor, Professor João F. Mano, who is most responsible for helping me all the way through the entire review process of several papers and complete the writing of this thesis, as well as the challenging research that lies behind it. He taught me how to ask questions and express my ideas. Professor João F. Mano has been a good friend and mentor. He was always there to meet and talk about my ideas, to proofread papers and improve its contents.

I must express my admiration to the National Institute of Advanced Industrial Science and Technology (AIST); Tissue Engineering Research Group, Research Institute of Cell Engineering (RICE), Osaka, Japan, whose facilities are outstanding. I want to express my deeply-felt thanks to Doctor Hajime Ohgushi who formally accepted to be my co-supervisor and guided my research during the stay at AIST.

This thesis was partially developed at the Department of Polymer Engineering (DEP), University of Minho, thus I would also like to take this opportunity to thank the staff of our department for their warmth and responsiveness as their administrative work, certainly facilitate my research work.

Both thanks of gratitude and appreciation are addressed to all my 3B's colleagues, whom directly and indirectly contribute for this thesis.

For both friendship and for the clear professionalism with which they present me, I would like to express my gratitude to Patricia Malafaya, Tiago Silva, Vitor Correlo and Rui Amandi.

II would also like to thank my friends namely, Silgia Costa and Simone S. Silva for their constant help and support through the thesis.

I acknowledge Adriano Pedro for being a good friend, help me secure the data and provide a valuable assistance for solving problems with my laptop.

I wish to give my sincere thanks to António Salgado for collaborating with me and help to explore new possibilities and ideas.

Additionally, I would like to seize this opportunity to thank the following people for their help and support throughout the PhD thesis:

I have benefited enormously from the support of Márcia Rodrigues, Alexandra Marques and Rogério Pirraco with the cell culture studies.

I am also sincerely grateful to asssistance of Liliana Gomes and Claúdia Costa.

Others who deserve particular gratitude are the members of the 3B's management team especially, Tánia Alves, Ariana Santos and Virginia**.**

I also appreciated the support and help of Elsa Ribeiro during the SEM/EDS analyses.

To Mr. António Sousa Azevedo for his technical assistance in the X-ray diffraction analyses.

To Noriko Kotobuki, I want to express how grateful I am for her patience and help on cell culture and molecular biology assays, and with whom I explored new ideas.

Thanks also to Mika Tadokoro for assistance during the histological studies.

To Motohiro Hirose and staff of AIST, whom directly and indirectly contribute for the success of *in vivo* experimentation.

Many thanks to all my Japanese friends and to Murphy's football team from Osaka, whom inspired me how to work hard and play hard. A special thanks to Krzysztof and Minami who teach me Japanese culture and how to enjoy the 'Sento' (public bathhouses) to reduce stress!

This thesis would be incomplete without a special thanks to the entities and projects that provided the financial support to conduct research. To the executives, managers and employees of the Portuguese Foundation for Science and Technology (FCT) for the PhD grant (Ref. SFRH/BD/21786/2005) supported through the POCTI and FEDER programs.

To Rotary Club de Caldas das Taipas, and Foundation Calouste Gulbenkian (FCG) for the short-term scholarships (Ref. SV – AR 91221 and Ref. SV – AR 437063) that allow me to attend several international meetings.

The support of Canon Foundation in Europe is also gratefully acknowledged.

This thesis would also not be possible to accomplish without the finacial support under the scope of the European NoE EXPERTISSUES (NMP3-CT-2004-500283) and European Union HIPPOCRATES STREP Project (NMP3-CT-2003-505758).

To Materialise (Belgium) for the μ-CT software provided and LBI (Vienna, Austria) for the μ-CT scans carried out under the scope of HIPPOCRATES project.

My truly and deeply-felt thanks to all my family, my father José, especialy my late mother, Emilia, this thesis is a tribute to you both. Your prayers and taughts formed part of my vision and myself, these have been invaluable throughout my research.

To my grandparents, Avelino and Maria, especially to my deceased and beloved grandmother, who was a second mom to me. You gave me so much. I will never forget you.

Special mention to my sister Ana and my brother-in-law António which have been always supportive in the good and bad moments, a special thank. To their sons, Carolina and Eduardo, whom with their joy gave me strength to go on.

To Natacha parents, Ana and Horácio for their warm support.

At last but not least, to Natacha, my girlfriend and other half. For her patience, kindness, love and friendship whether I was present or absent, thanks for the uninterrupted support during the PhD period.

New nanotechnology approaches using dendrimers modified with natural polymers for controlling stem cells behaviour in tissue engineering strategies

ABSTRACT.

In the recent years, great progress has been done in the emerging field of tissue engineering. Despite the important advances the performance of cells-scaffold constructs, one of the several tissue engineering approaches, remains limited in part due to the need for optimize cell culture techniques and culture media. Nanocarrier systems have generated a significant amount of interest in the *ex vivo* cell maintenance, and control of the cellular fate *in vivo* mainly due to their internalization efficiency, drug loading capacity, and to favorably modulate the solubility and pharmacokinetics of drugs. Dendrimers are synthetic, monodispersive, spherical and highly branched macromolecules that present unique advantages and fulfills most requirements as carriers for drug delivery; however, it has been found that high generation dendrimers are often cytotoxic. Thus, in this thesis we focused our attention in this fundamental problem and explore the development of novel nanobiomaterials based on the grafting of carboxymethylchitosan (CMCht) onto low generation poly(amidoamine) (PAMAM) dendrimers, the so-called CMCht/PAMAM dendrimer nanoparticles. These macromolecular vehicles were developed to explore a new concept consisting on the intracellular and controlled delivery of bioactive molecules aimed at control stem cells functions in a more effective manner *ex vivo*, and maintain the cellular phenotype *in vivo* upon re-implantation. Thus, by combining nanotechnology-based systems and traditional tissue engineering strategies, we expect to develop a novel therapeutic solution for the efficient treatment of damage/diseased cells and tissues. To validate this new concept, there is the need to evaluate the performance of the developed nanocarriers, *in vitro* and *in vivo*. Firstly, the uptake efficiency and internalization mechanism of fluorescent-labeled CMCht/PAMAM dendrimer nanoparticles was investigated using different cell types. Fluorescence microscopy studies revealed that the developed nanocarriers could be efficiently internalized, either by cell lines and primary cultures, after a few hours. Flow cytometry studies revealed that rat bone marrow stromal cells (RBMSCs) cultured in the presence of colchicine, an alkaloid that inhibits endocytosis, decreased the internalization of the nanoparticles. These data showed that uptake by cells was primarily via an active endocytotic mechanism, but not exclusively. Preliminary studies were also carried out to evaluate the possible applicability of the CMCht/PAMAM dendrimer nanoparticles in the central nervous system. Internalization rate, cell viability and metabolic activity studies were performed using rat post-natal hippocampal neurons and cortical glial cells that revealed their ability for being taken up by these cells and its non cytotoxicity. Complementarily, dexamethasone (Dex), a glucocorticoid known to have

important role on the proliferation and expression of osteoblastic differentiation markers, was used as a model drug and incorporated into the bulk of the nanoparticles. Physicochemical characterization and *in vitro* biological studies have demonstrated that the Dex-loaded CMCht/PAMAM dendrimer nanoparticles were successfully synthesized, were not cytotoxic in the range of concentration below 1 $mg.mL^{-1}$ and promote osteogenesis (2-D system). To assess the true value of the Dex-loaded CMCht/PAMAM dendrimer nanoparticles systems for application in tissue engineering strategies, we use different biomaterials to develop a set of novel scaffolds both ceramic and polymeric or formulations. These scaffolds were found to be suitable for applications in bone, cartilage and osteochondral tissue engineering. *In vitro* studies have shown that combination of scaffolds, bone marrow stromal cells and Dex-loaded CMCht/PAMAM dendrimer nanoparticles (3-D system) enhanced osteogenesis. Finally, *in vivo* studies have shown that the novel Dex-loaded CMCht/PAMAM dendrimer nanoparticles may be beneficial as intracellular nanocarrier, supplying Dex in a regimented manner, while avoiding the need of culturing stem cells for long periods of time *in vitro*, towards promoting the osteogenic differentiation. Remarkably, the proposed strategy allow modulate and direct stem cells differentiation towards osteogenic phenotype, enhance *in vivo* proteoglycan extracellular matrix synthesis and promote superior *de novo* bone formation. This thesis mark the transition from the '*proof-of-concept'* to useful intracellular nanocarrier tool, as the Dex-loaded CMCht/PAMAM dendrimer nanoparticles show promise for application in direct stem cell to a particular cell fate, *in vitro* and *in vivo*.

Novas abordagens da nanotecnologia recorrendo a dendrímeros modificados com polímeros naturais para o controlo das funções celulares de células estaminais e utilização em estratégias de engenharia de tecidos

RESUMO.

Grandes progressos têm sido feitos nos últimos tempos no emergente campo científico da engenharia de tecidos. No entanto, a eficiência dos sistemas células-matriz tridimensional porosa, uma das estratégias usadas nas abordagens em engenharia de tecidos, tem sido limitada, em parte, pela necessidade de se optimizarem as técnicas e os meios de cultura usados. Sistemas de nanopartículas para o transporte de moléculas bioactivas têm suscitado grande interesse na área da biomedicina, nomeadamente no que respeita à possível aplicação como suplementos em meios de cultura *ex vivo*, e no controlo das funções celulares *in vivo*. Isto deve-se, principalmente, à sua eficiência de internalização, elevada capacidade de incorporação de fármacos, e ao facto de favorecerem a solubilidade de moléculas hidrofóbicas e de possibilitarem a modulação da sua farmacocinética. Os dendrímeros são sistemas macromoleculares sintéticos altamente ramificados que apresentam características únicas, tais como monodispersividade e uma estrutura esférica, e que preenchem a maioria dos requisitos para serem usados como veículos para a libertação controlada de fármacos. Não obstante, tem-se verificado que dendrímeros de elevada geração apresentam tipicamente uma citotoxicidade indesejada. Assim, nesta tese a atenção focou-se na resolução deste problema fundamental. Para tal foi explorado o desenvolvimento de novos nanobiomateriais tendo como estratégia a ligação química do polímero carboximetilquitosano (CMCht) a dendrímeros de poliamidoamina (PAMAM) de baixa geração, que se denominaram por nanopartículas de carboximetilquitosano/poliamidoamina (CMCht/PAMAM). Estas macromoléculas foram desenvolvidas e um novo conceito aplicativo foi testado relacionado com a sua aplicação em medicina regenerativa como veículos de libertação controlada e intracelular de moléculas bioactivas, de forma a ser possível controlar efectivamente as actividades celulares, tais como a proliferação e a diferenciação de células estaminais *ex vivo*, e a manutenção do fenótipo dessas mesmas células após o seu implante. Assim, recorrendo à nanotecnologia e a estratégias usadas na engenharia de tecidos, espera-se que seja possível desenvolver uma nova solução terapêutica que possa possibilitar, de uma forma eficiente, o tratamento de células e tecidos danificados ou que apresentem algum tipo de patologia. De forma a validar este novo conceito, é necessário avaliar o potencial dos nanosistemas desenvolvidos, *in vitro* e *in vivo*. Primeiramente, a eficiência e o mecanismo de internalização de nanopartículas de CMCht/PAMAM ligadas a um marcador fluorescente foram investigados, recorrendo a estudos

celulares, *in vitro*. Estudos de microscopia de fluorescência revelaram que as nanopartículas desenvolvidas são internalizadas por diferentes tipos de células após algumas horas em cultura, incluindo linhas celulares e culturas primárias. Estudos envolvendo a citometria de fluxo mostraram que quando células multipotentes do estroma da medula óssea de rato (RBMSCs), foram cultivadas na presença de colchicina, um alcalóide inibidor da endocitose, exibiam menor capacidade de internalização das nanopartículas. Assim, a internalização das nanopartículas pelas células ocorre principalmente por um mecanismo de endocitose, mas que este não é o único. Foram também realizados estudos para determinar a taxa de internalização, viabilidade celular e actividade metabólica, recorrendo a neurónios isolados do hipocampo de rato pós-natais e células da glia. Estes estudos mostraram que as nanopartículas são internalizadas por estas células, e não afectam negativamente a viabilidade da cultura das células. A dexametasona (Dex), uma molécula pertencente à família dos glucocorticóides e conhecida pelo seu papel na modulação da proliferação e expressão dos marcadores de diferenciação osteoblástica, foi usada como fármaco modelo e incorporada nas nanopartículas de CMCht/PAMAM. A caracterização físico-química e estudos biológicos *in vitro* demonstraram que as nanopartículas de CMCht/PAMAM carregadas com Dex foram sintetizadas com sucesso, não apresentaram citotoxicidade em concentrações até 1 $mg.mL^{-1}$ e promoveram a osteogénese (sistema de cultura 2-D). Por forma a avaliar o verdadeiro potencial aplicativo das nanopartículas de CMCht/PAMAM carregadas com Dex em estratégias de engenharia de tecidos, diferentes biomateriais foram usados no desenvolvimento de estruturas tridimensionais porosas, incluindo cerâmicos, polímeros e formulações contendo ambos. Estas estruturas tridimensionais porosas mostraram-se adequadas para serem usadas em engenharia de tecidos de osso, cartilagem e defeitos osteocondrais. Estudos *in vitro* revelaram que a abordagem constituída por estruturas tridimensionais porosas, RBMSCs e nanopartículas de CMCht/PAMAM carregadas com Dex (sistema de cultura 3-D) promoveu um aumento significativo da osteogénese. Por último, estudos *in vivo* mostraram que as nanopartículas de CMCht/PAMAM carregadas com Dex são um sistema de libertação intracelular altamente eficiente, uma vez que possibilitaram a libertação de Dex com um perfil cinético adequado, permitindo assim evitar os longos períodos de cultura *in vitro*, necessários à diferenciação osteogénica de células estaminais. A estratégia proposta permite modular e direccionar a diferenciação das células estaminais para o fenótipo osteogénico, aumentar a síntese de proteoglicanos da matriz extracelular e promover a formação de osso num estado de maturação mais avançado. Esta tese marca a transição de "prova de conceito" para uma ferramenta aplicativa das nanopartículas desenvolvidas na libertação intracelular de fármacos, uma vez que as nanopartículas de CMCht/PAMAM carregadas com Dex se mostraram promissoras no direccionamento das células estaminais para um determinado fenótipo, *in vitro* e *in vivo*.

TABLE OF CONTENTS.

LIST OF ABBREVIATIONS.

12-AS	12-(9-anthroyloxy) stearic acid
2-D	two-dimensional;
3-D	three-dimensional;
3-TC	lamivudine;
5-ASA	5-aminosalicylic acid;

A

A/B	antibiotic-antimycotic;
Ac	acetylated;
AChE	acetylcholinesterase;
AF	alexaFluor;
AFM	atomic force microscopy;
ALP	alkaline phosphatase;
Alpha-MEM	minimal essential medium Eagle alpha modification;
AMP	2-amino-2-methyl-1,3-propanediol;
ATP	adenosine triphosphate;
ATRP	atom transfer radical polymerization;

B

b-FGF	basic fibroblast growth factor;
BAPTA-AM	1,2-bis-(o-aminophenoxy) ethane-N,N,N',N',-tetraacetic acid-acetoxymethyl ester;
BBB	blood brain barrier;
BCA	bicinchoninic acid;
BMVEC	brain micro-vessel endothelial cells;
BNTC	boron neutron capture therapy;
BSA	bovine serum albumin;
BV/TSV	bone volume density;

C

CLB	chlorambucil;
CD	cyclodextrins;
CED	convection enhanced delivery;
CHT	chitosan;
CMCht	carboxymethylchitosan;
CMCht/HAp	carboxymethylchitosan/hydroxylapatite composite scaffolds;
CMCht/PAMAM	carboxymethylchitosan/poly-(amidoamine);
CNS	central nervous system;
CT	computed tomography;

D

DAPI blue	4,6-diamidino-2-phenylindole, dilactate;
DCC	dicyclohexylcarbodiimide;
DD	degree of deacetylation;
DDS	drug delivery system;
Dex	dexamethasone;
di-BOC	di-tert-butyl dicarbonate;
DLS	dynamic light scattering;
DMB	dimethylmethylene blue;
DMEM	Dulbecco's modified Eagle medium;
DMSO	dimethyl sulfoxide;
DNA	deoxyribonucleic acid;
DOPE	1,2-dioleyl-3-phosphatidyletha-nolamine;
DOTAP	N-(1-(2,3-dio-leoyloxy)propyl) N,N,N-trimethyl ammonium methylsulfate;
Dox	doxorubicin;
DS	degree of substitution;
ε	dielectric constant;

E

E	modulus;
EBV	Epstein Barr virus;
ECACC	European collection of cell cultures;
ECM	extracellular matrix;
EDA	ethylenediamine;
EDC	1-ethyl-3(3-dimethylamino-propyl);
EDTA	ethylenediaminetetraacetic acid;
EG	ethylene glycol;
EGF	epidermal growth factor;
EGFP	green fluorescent protein;
ELISA	enzyme-linked immunosorbent assay;
ENFET	enzyme field effect transistor;
ES	embryonic stem cells;
EtdD-1	ethidium homodimer-1;

F

FA	folic acid;
FACS	fluorescence-activated cell sorting;
FBS	fetal bovine serum;
FITC	fluorescein isothiocyanate;
FTIR	Fourier-transform infra-red spectroscopy;
FUdR	5-fluoro-2'-deoxiuridina;
F344/N	Fischer 344 rat;

G

G	generation number;
GAGs	glycosaminoglycans;
GBMSCs	goat bone marrow stromal cells;
GFs	growth factors;
GLUT 1	glucose transporter;
GOX	glucose oxidase;

H

HA	hyaluronan or hyaluronic acid;
HAp	hydroxylapatite;
HAp/CHT	hydroxylapatite/chitosan bilayered scaffolds;
HAS	human serum albumin;

HBP	hyperbranched polymer;
HER-2	human growth receptor;
H&E	haematoxylin & eosin;
HIV	human immunodeficiency virus;
HIV-1	human immunodeficiency virus type 1;
HMGB1	high mobility group box 1 plasmid;
HPLC	high performance liquid chromatography;
HSGP	heparin or heparan sulfate proteoglycan;
f(Ka)	Henry´s function;

I

ICP-OES	inductively-coupled plasma optical emission;
iPs	induced pluripotent stem cells;

L

LCST	lower critical solution temperature;
LDV	laser Doppler velocimetry;
LH	light-harvesting;

M

2-MAP	mouse anti-rat microtubule associated protein 2;
M	molar;
MA	methacrylate;
MAPs	multiple antigen peptides;
Man	mannose;
MEM	Eagle's minimum essential medium;
Mimics®	Materialise interactive medical image control system;
M_n	number-average molecular weight;
Mo/Mac	monocyte/macrophages;
MPPI	poly(propyleneimine);
MRI	magnetic resonance imaging;
mRNA	messenger ribonucleic acid;
MS	multiple sclerosis;
MTS	3-(4,5-dimethylthiazol-2-yl)-5-(3-carboxymethoxyphenyl)-2-(sulfophenyl)-2H-tetrazolium;
MTX	methotrexate;
M_w	weight-average molecular weight;
M_w/M_n	polydispersity index;
μg	micrograms;
μL	microliters;
μm	micrometers;
μ-CT	micro-computed tomography;

N

NaHA	sodium hyaluronate;
NMR	nuclear magnetic resonance spectroscopy;
NSAIDs	non-steroidal anti-inflammatory drugs;

O

OEI	oligoethylenimine;
OG	Oregon green;
ONs	antisense oligonucleotides;

P

PABA	*p*-aminobenzoic acid;
PAMAM	poly(amidoamine);
PAMAM-CT	poly(amidoamine)-carboxylic terminated dendrimers;
PAH	*p*-aminohippuric acid;
PBS	phosphate buffer saline;
PCI	photochemical-internalization;
PDMA	poly(*N*,*N*-dimethylaminoethyl methacrylate);
PEG	poly(ethylene glycol);
PEG-DA	poly(ethylene glycol)-dialdehyde;
PEI	poly(ethyleneimine);
PEPE	polyether-copolyester;
PETIM	poly(propyl ether imine);
PLGA	poly(lactide-*co*-glycolide);
PLGSA	poly(glycerol-succinic acid);
PLL	poly-(L-lysine);
PNIPAAM	poly(N-isopropylacrylamide);
pNP	p-nytrophenol;
PNS	peripheric nervous system;
PP	primaquine phosphate;
PPI	poly(propyleneimine);
PrPSc	protease-resistant isoform of the prion protein;
PSMA	prostrate specific membrane antigen;
PTX	paclitaxel;

R

RAFT	reversible addition-fragmentation transfer;
RBMSCs	rat bone marrow stromal cells;
RGD	tripeptide Arg-Gly-Asp;
RNA	ribonucleic acid;
ROS	reactive oxygen species;

S

SaOs-2	human osteoblast-like cells;
SBF	simulated body fluid;
SCI	spinal cord injury;
SEM	scanning electron microscopy;
siRNA	small interfering RNA;
shRNA	small hairpin RNA;
SPCL	starch-polycaprolactone;

T

t-BOC	N-tert-butoxycarbonyl;
TCPS	tissue culture polystyrene;
TEM	transmission electron microscopy;
TE	tissue engineering;
TGA	thermogravimetric analysis;
TGF-β	transforming growth factor beta;
ThT	thioflavin T;
TMA-DPH	1-(trimethylammoniumphenyl)-6-phenyl-1,3,5 hexatriene *p*-toluenesulfonate;
Tris	Tris(hydroxymethyl)aminomethane;

U

UE	electrophoretic mobility;
UV	ultraviolet;
UV-VIS	ultraviolet-visible spectrophotometry;

V

VEGF	vascular endothelial growth factor;
VOI	volume of interest;
η	viscosity;

W

WLs	weight loss;
WUs	water-uptake;

X

XRD	X-ray diffraction;

Z

Z	zeta potential;

LIST OF FIGURES.

LIST OF TABLES.

SHORT *CURRICULUM VITAE*.

In 1977, Joaquim Miguel A. Oliveira was born in Caldas das Taipas - Guimarães, Portugal. Nowadays, he lives in Caldas das Taipas and works, as a researcher in the 3B's Research Group, Department of Polymer Engineering at University of Minho, Headquarters of the European Institute of Excellence on Tissue Engineering and Regenerative Medicine at Avepark, Caldas das Taipas - Guimarães, Portugal. This research group is directed by its founder, Professor Rui L. Reis. This group has been considered as excellent by the Portuguese Foundation for Science and Technology, and is one of the associated units of the Institute for Biotechnology and Bioengineering.

His background includes a graduation in Biochemistry at Faculty of Sciences of University of Porto. During the final year, he developed is final research project on the theme Electrochemistry Applied to the Development of Biosensors in the Department of Chemistry, Faculty of Sciences, Porto University of Porto, Porto, Portugal. This work was supervised by Professor Carlos Pereira and as a consequence, his first paper was published in the Journal of Analytical Chemistry.

In 2002, he was enrolled in a Doctoral Program in Biomedical Engineering (2002/2003) at Faculty of Engineering, Porto University, Porto, Portugal. During this period he developed research on the development of hybrid materials for biomedical applications, at the Institute of Biomedical Engineering (INEB), Lab. of Biomaterials, Porto University, Porto, Portugal under the supervision of Professor José D. Santos. He also carried out research (research fellow) at Nara Institute of Science and Technology (NAIST), Nara, Japan for a short period of time. This work was performed under the supervision Professor Chikara Ohtsuki.

In 2004, he was invited to move the 3B's Research Group as researcher under the scope of the Hippocrates project. He formally started his PhD at the 3B's Research Group, in 2005, after being awarded with a grant from the FCT under the supervision of Professor Rui L. Reis, in collaboration with the National Institute of Advanced Industrial Science and Technology (AIST); Tissue Engineering Research Group, Research Institute of Cell Engineering (RICE), Osaka, Japan under the local supervision of Doctor Hajime Ohgushi. During the year of 2005, his work was distinguished with the Best Student Award (Oral Presentation), for the paper entitled "Innovative Technique for the Preparation of Porous Bilayer Hydroxyapatite/Chitosan Scaffolds for Osteochondral Applications", as part of the 18th International Symposium on Ceramics in Medicine - Bioceramics 18, held in Kyoto, Japan. In 2008, he

was distinguished with the Tissue Engineering and Regenerative Medicine International Society **-** EU Chapter (TERMIS-EU) '50 Best Ranked Abstract' AWARD, Porto Meeting, Portugal.

As a researcher in the 3B's, he was enrolled in the elaboration of several approved projects (National and European), as part of the organization of several scientific meetings (e.g. InVents-Series of events and the 2008 Annual Meeting of Tissue Engineering and Regenerative Medicine-European Chapter), and in the development of the business plan of STEMMATTERS, which is the biotechnological spin-off of the 3B's Research Group. He has been also involved in the supervision of several under-graduated students (e.g. Seminars of Mechanics: 3rd year Biomedical Engineering and final year of Polymer Chemistry both at University of Minho). He was one of the mentors of the new facilities of the 3B's Research Group and the Headquarters of the European Institute of Excellence on Tissue Engineering and Regenerative Medicine at Avepark, Caldas das Taipas-Guimarães, Portugal. In addition, he is referee in several scientific and international journals, such as the Journal of Cellular and Molecular Medicine: Reviewer Invitation, Tissue Engineering*,* Marine Biology and Journal of Tissue Engineering and Regenerative Medicine. Moreover, he is currently the elected treasurer of Tissue Engineering and Regenerative Medicine International Society-Student and Young Investigator Section in Europe.

As a result of his research efforts within the field of tissue engineering and regenerative medicine, presently he is author or co-author of more than 16 publications in international journals, 10 proceedings in international meetings and participated as oral presenter/poster presenter in approximately 40 international meetings.

LIST OF PUBLICATIONS.

The research work carried out during the PhD period resulted in the following publications:

INTERNATIONAL JOURNALS WITH REFEREE, AS FIRST AUTHOR

Oliveira JM, Malafaya PB, Silva SS, Kotobuki N, Hirose M, Sousa RA, Mano JF, Reis RL and Ohgushi H, Dexamethasone-loaded carboxymethylchitosan/poly(amidoamine) dendrimer nanoparticles induces osteogenic differentiation of rat bone marrow stromal cells and ectopic bone formation (2009), submitted.

Oliveira JM, Salgado AJ, Sousa N, Mano JF, and Reis RL, Dendrimers and derivatives as a potential therapeutic tool in regenerative medicine strategies: a review (2009), submitted.

Oliveira JM, Kotobuki N, Tadokoro M, Hirose M, Mano JF, Reis RL and Ohgushi H, *Ex vivo* culturing of rat bone marrow stromal cells with dexamethasone-loaded carboxymethylchitosan/poly(amidoamine) dendrimer nanoparticles enhances ectopic bone formation on tissue engineered constructs (2009), submitted.

Oliveira JM, Kotokuki N, Marques AP, Pirraco RP, Benesch J, Hirose M, Costa SA, Mano JF, Ohgushi H and Reis RL, 2008, Surface engineered carboxymethyl-chitosan/poly(amidoamine) dendrimer nanoparticles for intracellular targeting, Advanced Functional Materials, **18**: 1840-1853.

Oliveira JM, Sousa RA, Kotobuki N, Tadokoro M, Hirose M, Mano JF, Reis RL and Ohgushi H, 2009, The osteogenic differentiation of rat bone marrow stromal cells cultured with dexamethasone-loaded carboxymethylchitosan/poly(amidoamine) dendrimer nanoparticles, Biomaterials, **30**: 804-813.

Oliveira JM, Rodrigues MT, Silva SS, Malafaya PB, Gomes ME, Viegas C A A, Azevedo JT, Dias IR, Mano JF and Reis RL, 2006, Novel hydroxyapatite/chitosan bilayered scaffold for osteochondral tissue-engineering applications: scaffold design and its performance when seeded with goat bone marrow stromal cells, Biomaterials, **27**: 6123-6137 (Hot paper).

Oliveira JM, Salgado AJ, Pirraco RP, Pereira VH, Fraga JS, Marques AP, Neves NM, Mano JF, Reis RL and Sousa N, Carboxymethylchitosan/poly(amidoamine) dendrimer nanoparticles in central nervous system regenerative medicine: Effects on neurons/glial cell viability/proliferation and internalization efficiency (2009), submitted.

Oliveira JM, Silva SS, Malafaya PB, Rodrigues MT, Kotokuki N, Hirose M, Gomes ME, Mano JF, Ohgushi H and Reis RL, 2008, Macroporous hydroxyapatite scaffolds for bone tissue engineering applications: physicochemical characterization and assessment of rat bone marrow stromal cells viability, Journal of Biomedical Materials Research: Part A – In Press, Corrected Proof, (doi:10.1002/jbm.a.32213).

Oliveira JM, Costa SA, Leonor IB, Malafaya PB, Mano JF and Reis RL, 2009, Novel hydroxyapatite/carboxymethylchitosan composite scaffolds prepared combining an innovative '*autocatalytic*' electroless co-precipitation route, Journal Biomedical Materials Research: Part A, **88A(2)**: 470-480.

Oliveira JM, Grech JM, Leonor IB, Mano JF and Reis RL, 2007, Calcium-phosphate derived from mineralized algae for bone tissue engineering applications, Materials Letters, **61**: 3495-3499.

BOOK CHAPTERS AND CONFERENCE PROCEEDINGS WITH REFEREE, AS FIRST AUTHOR

Oliveira JM, Sousa RA, Kotobuki N, Malafaya PB, Hirose M, Mano JF, Reis RL and Ohgushi H, 2008, Dexamethasone-loaded carboxymethylchitosan/poly(amidoamine) dendrimer nanoparticles enhances bone formation *in vivo*, Tissue Engineering: Part A, **14**: 721.

Oliveira JM, Salgado AJ, Pirraco RP , Pereira VH, Fraga JS, Marques AP, Neves NM, Mano JF, Sousa N and Reis RL, 2008, *In vitro* characterization on the interactions between carboxymethyl-chitosan/poly(amidoamine) dendrimer nanoparticles and neurons/glial cells, Tissue Engineering: Part A, **14**: 744.

Oliveira JM, Kotobuki N, Hirose M, Mano JF, Reis RL and Ohgushi H, 2007, Intracellular carboxymethylchitosan/poly(amidoamine) nanocarriers loaded with dexamethasone enhances osteogenic differentiation of RBMSCs *in vitro*, Tissue Engineering, **13(7)**: 1719.

Oliveira JM, Silva SS, Mano JF and Reis RL, 2006, Innovative technique for the preparation of porous bilayered hydroxyapatite/chitosan scaffolds for osteochondral applications, In Key Engineering Materials, Trans Tech Publications Ltd., **309-311**: 927-930.

Oliveira JM, Leonor IB and Reis RL, 2005, Preparation of bioactive coatings on the surface of bioinert polymers through an innovative auto-catalytic electroless route, In Key Engineering Materials, Trans Tech Publications Ltd., **284-286**: 107-110.

INVITED LECTURES

Oliveira JM, Mano JF and Reis RL, Nanotechnology based stem cell therapies for regenerative medicine, 6th Marie Curie Cutting Edge Conference 'Stem Cells: from the Petri dish to the clinical application, Algarve, Portugal, October 2008.

Oliveira JM, Mano JF and Reis RL, Bone Tissue Engineering, Young Scientist Meeting 2008, Porto, Portugal, September 2008.

Oliveira JM, Silva SS, Mano JF and Reis RL, Hybrid Materials, VI Materials Engineering Forum, Guimarães, Portugal, May 2005.

ORAL PRESENTATIONS IN INTERNATIONAL MEETINGS, AS FIRST AUTHOR

Oliveira JM , Salgado AJ, Pirraco RP , Pereira VH, Fraga JS, Marques AP, Neves NM, Mano JF, Sousa N and Reis RL, *In vitro* characterization on the interactions between carboxymethyl-chitosan/poly(amidoamine) dendrimer nanoparticles and neurons/glial Cells, Annual Tissue Engineering and Regenerative Medicine International Society - TERMIS-EU Meeting, Porto, Portugal, June 2008.

Oliveira JM, Sousa RA, Kotobuki N, Malafaya PB, Hirose M, Mano JF, Reis RL and Ohgushi H, Dexamethasone-loaded carboxymethylchitosan/poly(amidoamine) dendrimer nanoparticles enhances bone formation *in vivo*, Annual Tissue Engineering and Regenerative Medicine International Society - TERMIS-EU Meeting, Porto, Portugal, June 2008.

Oliveira JM, Sousa RA, Kotokuki N, Tadokoro M, Hirose M, Mano JF, Reis RL and Ohgushi H, Carboxymethylchitosan/poly(amidoamine) dendrimer nanoparticles loaded with dexamethasone promotes ectopic bone formation, 8th World Biomaterials Congress, Amsterdam, Netherlands, May 2008.

Oliveira JM, Kotokuki N, Hirose M, Mano JF, Reis RL and Ohgushi H, Dexamethasone-loaded carboxymethylchitosan/poly(amidoamine) dendrimer nanoparticles enhances ectopic bone formation in tissue engineered constructs: proof-of-concept, 3rd International Meeting of the Portuguese Society for Stem Cells and Cell Therapies (SPCE-TC), Faro, Portugal, April 2008.

Oliveira JM, Kotobuki N, Tadokoro M, Hirose M, Mano JF, Reis RL and Ohgushi H, *Ex vivo* culturing of rat bone marrow stromal cells with dexamethasone-loaded carboxymethylchitosan/poly(amidoamine) dendrimer nanoparticles enhances ectopic bone formation on tissue engineered constructs, 5th Marie

Curie Cutting-Edge Conference on "Synthesis and applications of self-assembling materials at nano-scale", Funchal, Portugal, April 2008.

Oliveira JM, Sousa RA, Kotobuki N, Tadokoro M, Hirose M, Mano JF, Reis RL and Ohgushi H, Carboxymethylchitosan/poly(amidoamine) dendrimer nanoparticles loaded with dexamethasone induces osteogenic differentiation of RBMSCs seeded onto HA and SPCL scaffolds: *In vitro* study, 1st Annual Meeting of Tissue Engineering and Regenerative Medicine, TERMIS-AP Chapter, Tokyo, Japan, December 2007.

Oliveira JM, Kotokuki N, Tadokoro M, Hirose M, Mano JF, Reis RL and Ohgushi H, Carboxymethyl-chitosan/poly(amidoamine) nanospheres loaded with dexamethasone induces the osteogenic differentiation of rat bone marrow stromal cells: *In vitro* study, INVENTS: 4th Marie Curie Cutting Edge Conference on "4th Marie Curie Cutting Edge Conference Biocompatibility evaluation and biological behaviour of polymeric biomaterials, Alvor, Algarve, Portugal, October 2007.

Oliveira JM, Kotokuki N, Hirose M, Mano JF, Reis RL and Ohgushi H, Intracellular carboxymethyl-chitosan/poly(amidoamine) nanocarriers loaded with dexamethasone enhances osteogenic differentiation of RBMSCs *in vitro*, 1st Annual Meeting of Tissue Engineering and Regenerative Medicine, TERMIS-EU Chapter, London, United Kingdom, September 2007.

Oliveira JM, Kotokuki N, Mano JF, Reis RL and Ohgushi H, Carboxymethylchitosan/poly(amidoamine) dendrimer nanocarriers: loading of dexamethasone and assessment of its internalization by fluorescence microscopy and FACS analysis, 8th International Symposium on Frontiers in Biomedical Polymers-FBPS 07, Ghent, Belgium, June 2007.

Oliveira JM, Kotokuki N, Mano JF, Ohgushi H and Reis RL, Carboxymethylchitosan/poly(amidoamine) dendrimer nanocarriers for tissue engineering applications: biocompatibility and assessment of its internalization by fluorescence microscopy and FACS analysis, 2nd Annual International Meeting of the Portuguese Society for Stem Cells and Cellular Therapy (SPCE-TC), Coimbra, Portugal, April 2007.

Oliveira JM, Marques AP, Benesch J, Mano JF and Reis RL, Preparation and characterization of novel carboxymethyl-chitosan/PAMAM dendrimers to be used as drug delivery carriers for tissue engineering applications, Regenerate: World Congress on Tissue Engineering and Regenerative Medicine (TERMIS), Pittsburgh, United States of America, April 2006.

Oliveira JM, Silva SS, Mano JF and Reis RL, Innovative technique for the preparation of porous bilayered hydroxyapatite/chitosan scaffolds for osteochondral applications, Bioceramics 18, Kyoto, Japan, December 2005.

Oliveira JM, Costa SA, Leonor IB and Reis RL, Carboxymethylchitosan/calcium phosphate hybrid materials prepared by an innovative auto-catalytic co-precipitation method, Bioceramics 17, New Orleans, United States of America, December 2004.

Oliveira JM, Leonor IB and Reis RL, Preparation of bioactive coatings on the surface of bioinert polymers through an innovative auto-catalytic electroless route, Bioceramics 17, New Orleans, United States of America, December 2004.

POSTER PRESENTATIONS IN INTERNATIONAL MEETINGS, AS FIRST AUTHOR

Oliveira JM, Kotokuki N, Mano JF, Reis RL and Ohgushi H, Carboxymethyl-chitosan/poly(amidoamine) nanoparticles for being used as an intracellular DDS for bone tissue engineering applications: investigation of the mechanism of internalization and intracellular fate, INVENTS: 3rd Marie Curie Cutting Edge Conference on "Biomineralisation of polymeric materials, bioactive biomaterials and biomimetic methodologies, and 1st TERMIS-EU Summer School: The European Chapter of the Tissue Engineering and Regenerative Medicine International Society, Funchal, Portugal, June 2007.

Oliveira JM, Kotokuki N, Mano JF, Reis RL and Ohgushi H, Novel FITC-labelled carboxymethyl-chitosan (CMC)/PAMAM nanoparticles to be used as intracellular drug delivery carriers: assessment of its internalization by fluorescence microscopy, Japanese Biomaterials Society Meeting, Tokyo, Japan, November 2006.

Oliveira JM, Pirraco RP, Marques AP, Costa SA, Mano JF and Reis RL, Novel carboxymethyl-chitosan/poly(amidoamine) nanospheres to be used as a targeted-drug delivery carrier: assessment of its internalization using fluorescent probes, 2nd Marie Curie Cutting Edge Conference - Recent advances on polymeric based systems for controlled delivery of bioactive agents: Applications in Tissue Engineering, Alvor, Portugal, October 2006.

Oliveira JM, Costa SA, Leonor IB, Mano JF and Reis RL, Carboxymethylchitosan/calcium phosphate hybrid materials prepared by an innovative auto-catalytic co-precipitation method, 19th European Conference on Biomaterials (ESB2005), Sorrento, Italy, September 2005.

INTERNATIONAL JOURNALS WITH REFEREE, AS CO-AUTHOR

Antunes JC, **Oliveira JM**, Reis RL, Soria JM, Gómez-Ribelles and Mano JF, Novel poly(L-lactic acid)/hyaluronic acid macroporous hybrid scaffolds: characterization and assessment of cytotoxicity, Journal of Biomedical Materials Research: Part A – Submitted.

Santos TC, Marques AP, Silva SS, **Oliveira JM**, Mano JF, Castro AG and Reis RL, 2007, *In vitro* evaluation of the behaviour of human polymorphonuclear neutrophils in direct contact with chitosan-based membranes, Journal of Biotechnology, **132(2)**: 218-226.

Mano JF, Silva GA, Azevedo HS, Malafaya PB, Sousa RA, Silva SS, Boesel LF, **Oliveira JM**, Santos TC, Marques AP, Neves NM and Reis RL, 2007, Natural origin biodegradable systems in tissue engineering and regenerative medicine: present status and some moving trends, Journal of the Royal Society Interface , **4(17)**: 999-1030.

Silva SS, **Oliveira JM**, Mano JF and Reis RL, 2006, Physicochemical characterization of novel chitosan-soy protein/TEOS porous hybrids for tissue engineereing applications, Advanced Materials Forum III, **514-516**: 1000-1004.

BOOK CHAPTERS AND CONFERENCE PROCEEDINGS WITH REFEREE, AS CO-AUTHOR

Santos TC, Marques AP, Silva SS, **Oliveira JM**, Mano JF, Castro AG, van Griensven M, Redl H and Reis RL, 2008, Chitosan/soy-based membranes enhance wound re-epithelialization in partial thickness skin wounds, Tissue Engineering Part A, **14(5)**: 711.

Gomes ME, Azevedo HS, Malafaya PB, Silva SS, **Oliveira JM**, Silva GA, Sousa RA, Mano JF and Reis RL, 2007, Natural polymers in tissue engineering applications, In Textbook on tissue engineering, eds. C Van Blitterswijk, A Lindahl, P Thomsen, D Williams, J Hubbell, R Cancedda, Elsevier, Academic Press, Amsterdam, **Chapter 6**, 145-192.

Correlo VM, Gomes ME, Tuzlakoglu K, **Oliveira JM**, Malafaya PB, Mano JF, Neves NM and Reis RL, 2007, Tissue engineering using natural polymers, In Biomedical Polymers , eds. Mike Jenkins, Woodhead publishing Ltd , Cambridge, 197-217.

Silva SS, **Oliveira JM**, Mano JF and Reis RL, 2006, Physicochemical characterization of novel chitosan-soy protein/TEOS porous hybrids for tissue engineering applications, In Advanced Materials Forum III, Pts 1 and 2, 1000-1004.

Costa SA, **Oliveira JM**, Leonor IB, Mano JF and Reis RL, 2005, Carboxymethylchitosan/calcium phosphate hybrid materials prepared by an innovative auto-catalytic co-precipitation method, In Key Engineering Materials, Trans Tech Publications Ltd., **284-286**: 701-704.

ORAL PRESENTATIONS IN INTERNATIONAL MEETINGS, AS CO-AUTHOR

Marques AP, Santos TC, da Silva RMP , Silva SS, **Oliveira JM**, van Griensven M, Mano JF, Redl H and Reis RL, Chitosan improves the *in vivo* biological response to soy-based biomaterials, Translational Biomaterial Research Symposium, Atlanta, United States of America, September 2008.

Santos TC, Marques AP, Silva SS, **Oliveira JM**, Mano JF, Castro AG, van Griensven M, Redl H and Reis RL, Chitosan/soy-based membranes enhance wound re-epithelialization in partial thickness skin wounds, TERMIS-EU 2008 Meeting, Porto, PT, Tissue Engineering (2008), Porto, Portugal, June 2008.

Santos TC, Marques AP, Silva SS, **Oliveira JM**, Mano JF, Castro AG and Reis RL, *In vitro* evaluation of the behaviour of polymorphonuclear neutrophils in direct contact with chitosan-based membranes, 6th European Symposium on Biochemical Engineering Science, Salzburg, Austria, August 2006.

Rodrigues MT, **Oliveira JM**, Gomes ME, Viegas CAA, Azevedo JT, Dias IR, Mano JF and Reis RL, Preliminary studies on single- and bilayered- hydroxyapatite/chitosan scaffolds seeded with osteoblasts or chondrocytes differentiated from goat marrow cells for the regeneration of bone and cartilage defects, 1st Marie Curie Cutting Edge Conference, Funchal, Portugal, June 2006.

Rodrigues MT, **Oliveira JM**, Gomes ME, Viegas CAA, Dias IR, Mano JF and Reis RL, Novel hydroxyapatite/chitosan bilayer scaffolds for the regeneration of osteochondral defects using a tissue engineering approach based on culturing and differentiation of goat marrow cells into osteoblasts or chondrocytes, World Congress on Tissue Engineering and Regenerative Medicine, Pittsburg, United States of America, April 2006.

Baran ET, Pashkuleva I, Costa SA, **Oliveira JM** and Reis RL, Peptide synthesis on chitin and chitosan for bioactive biomaterial preparation, Society for Biomaterials 30th Annual Meeting and Exposition: New Applications and Technologies, Memphis, United States of America, April 2005.

POSTER PRESENTATIONS IN INTERNATIONAL MEETINGS, AS CO-AUTHOR

Marques AP, Santos TC, da Silva RMP, Silva SS, **Oliveira JM**, van Griensven M, Mano JF, Redl H and Reis RL, Chitosan improves the *in vivo* biological response to soy-based biomaterials, Society for

biomaterials-Advancing discoveries from the laboratory to the clinic, Atlanta, United States of America, September 2008.

Salgado AJ, **Oliveira JM**, Pereira VH, Pirraco RP, Marques AP, Neves NM, Mano JF, Reis RL and Sousa N, Carboxymethyl-chitosan/poly(amidoamine) dendrimer nanoparticles as intracellular drug delivery systems in central nervous system regenerative medicine: effects on neurons/glial Cell viability/proliferation and internalization efficiency, 8th World Biomaterials Congress, Amsterdam, Netherlands, May 2008.

Gomes S, Rodrigues MT, **Oliveira JM**, Gomes ME, Leonor IB, Mano JF and Reis RL, Hydrothermal conversion of Corallina officinalis algae into calcium phosphate scaffolds for bone tissue engineering strategies, 3rd Marie Curie Cutting-Edge Conference "Biomineralisation of polymeric materials, bioactive biomaterials and biomimetic methodologies", Funchal, Portugal, June 2007.

Silva SS, **Oliveira JM**, S.M. Luna, Gomes ME, Mano JF and Reis RL, Development of Chitosan hybrid bioactive membranes prepared through an in situ cross-linking process, 19th European Conference on Biomaterials (ESB2005), Sorrento, Italy, September 2005.

Silva SS, **Oliveira JM**, S.M. Luna, Gomes ME, Mano JF and Reis RL, Biocompatibility assessment of novel chitosan hybrid bioactive membranes prepared by means of an in situ cross-linking process, 6th International Symposium on Frontiers in Biomedical Polymers, Granada, Spain, June 2005.

Silva SS, **Oliveira JM**, Mano JF and Reis RL, Preparation and characterization of novel chitosan-soy protein porous hybrids for tissue engineering applications, XII Portuguese Materials Society Meeting, Aveiro, Portugal, March 2005.

Silva SS, **Oliveira JM**, Mano JF and Reis RL, Preparation of novel chitosan/soy protein porous structures for tissue engineering applications, Biomaterials In Regenerative Medicine: The Advent of Combination Products, Philadelphia, United States of America, October 2004.

INTRODUCTION TO THE THESIS FORMAT.

This thesis contains two main parts namely, the preliminary part which is related with authorship and thesis information, and body of the thesis. The late is organized in four sections that include a total of eleven chapters. The body of thesis chapters is based on the series of related papers published in international journals or submitted for publication, which are specified with each chapter. Thus, each thesis chapter is presented in manuscript form in a style consistent with the papers, i.e. an abstract, introduction, materials and methods, results, discussion and conclusions sections. A list of references is also provided as a subsection within each chapter. The order of thesis chapters is as given below.

SECTION 1:

The first chapter is this thesis introduction and is concerned on reviewing the exploratory research merging nanotechnology and regenerative medicine. It also summarizes the fundamentals on the synthesis and macromolecular structure, ability to design and improve the biological performance of dendrimers and its derivatives. Special focus is devoted on the novel applications and recent work involving dendrimers in the fields of tissue engineering and central nervous system, but extends into gene delivery and theranostics, which are succinctly reviewed. Some remarks on the need to conduct comprehensive research *in vivo* are provided, and new research directions are also proposed.

SECTION 2:

Chapter II fully describes the experimental work and protocols related to the obtained results. Along with Chapter I, it provides a guideline of the rationale for the research, namely on the aspects related with the selection of the materials, on the developed processing routes, and characterization strategies and protocols used.

SECTION 3:

The thesis chapters included within this section are based on the series of related papers that resulted from research work already published or submitted for publication.

Chapter III describes a novel "*autocatalytic*" electroless deposition route for production of composite scaffolds composed of hydroxylapatite (HAp) and carboxymethylchitosan (CMCht) for bone tissue

engineering scaffolding applications. The physicochemical characterization in terms of architecture, degradability and bioactivity is presented herein.

Chapter IV reports a new methodology for developing HAp scaffolds by using an organic sacrifice template, and its potential to find applications in bone tissue engineering scaffolding investigated. The novelty of this work consists on the possibility of obtaining porous and highly interconnected scaffolds mimicking the sacrificial component. It were evaluated the physicochemical properties of the HAp scaffolds. Cytotoxicity of the HAp scaffolds was investigated by both carrying direct observation of mouse fibroblasts cells (L929 cell-line) death and performing a luminescent cell viability assay rat bone marrow stromal cells (RBMSCs).

Chapter V describes the development of novel hydroxylapatite/chitosan (HAp/CHT) bilayered scaffold by combining a freeze-drying technique for the cartilage region and a layer for bone regeneration based on the HAp supports developed in the previous chapter. The developed HAp/CHT bilayered scaffolds are aimed at find applications in osteochondral TE strategies, and were characterized herein by different techniques. The intrinsic cytotoxicity of the HAp scaffolds and HAp/CHT bilayered scaffolds extract fluids was investigated by carrying out a cellular viability assay (MTS test) using mouse fibroblastic-like cells. Moreover, *in vitro* cell culture studies were carried out to evaluate the capacity of HAp and CHT layers to separately, support the growth and differentiation of goat bone marrow stromal cells (GBMSCs) into osteoblasts and chondrocytes, respectively.

Chapter VI describes the synthesis of surface engineered carboxymethylchitosan/poly(amidoamine) dendrimer (CMCht/PAMAM) nanoparticles for applications as a intracellular nanocarrier. Such structures are proposed to be used as carriers to deliver bioactive molecules aimed at controlling the behaviour of stem cells, namely their proliferation and differentiation. Cytotoxicity and internalization efficiency was investigated using both human osteoblast-like cells and RBMSCs, under fluorescence-activated cell sorting and fluorescence microscopy analyses. As a model drug, dexamethasone (Dex) was incorporated into CMCht/PAMAM dendrimer nanoparticles and release rates were determined by high performance liquid chromatography. Moreover, the Dex-loaded CMCht/PAMAM dendrimer nanoparticles osteogenic potential was also investigated using RBMSCs and compared to that of typical osteogenic media, *in vitro*.

Chapter VII preliminary evaluates the possible applicability of the CMCht/PAMAM dendrimer nanoparticles in central nervous system (CNS). Internalization rate, cell viability and metabolic activity studies were performed using post-natal hippocampal neurons and cortical glial cells.

Chapter VIII was designed to investigate the effect of combining novel Dex-loaded CMCht/PAMAM dendrimer nanoparticles and, both HAp (developed in Chapter IV) and SPCL scaffolds (3-D system) on the proliferation and osteogenic differentiation of RBMSCs, *in vitro.* A detailed biological characterization is presented.

Chapter IX is the first of two *in vivo* studies and exploits the potential of the combinatorial strategy in tissue engineering principles employing CMCht/PAMAM dendrimer nanoparticles towards the intracellular release and regimented supply of Dex aimed at control stem cells osteogenic differentiation in the absence of typical osteogenic inducers, *in vivo*. The effect of initial cell number seeded in the HAp scaffolds on the bone forming ability of the constructs was also investigated. Qualitative and quantitative new bone formation was evaluated using the non-destructive micro-computed tomography analysis of the explants, and Haematoxylin & Eosin staining of the explant sections, followed by histomorphometrical analysis.

Chapter X reports deeper studies on the chemistry of the Dex-loaded CMCht/PAMAM dendrimer nanoparticles namely the data on proton nuclear magnetic resonance, dynamic light scattering and zeta potential analyses. Dex-loaded CMCht/PAMAM dendrimer nanoparticles internalization efficiency, osteogenic potential and bone forming ability were also evaluated, *in vitro* and *in vivo*. For this study, SPCL scaffolds were used as the 3-D matrix, as these scaffolds exhibit lower attenuation coefficient than bone, thus we can envision investigate qualitatively and quantitatively the calcified tissue within the explants using a non-destructive and time-saving technique such as micro-computed tomography.

SECTION 4:

This thesis ends with Chapter XI, which is the summary and conclusions of the research work under the scope of this thesis.

SECTION 1.

CHAPTER I.

Dendrimers and derivatives as a potential therapeutic tool in regenerative medicine strategies: a review

CHAPTER I.

Dendrimers and derivatives as a potential therapeutic tool in regenerative medicine strategies: a review

Abstract

Since the pioneering work dealing with the synthesis and physicochemical aspects of dendrimers, a predictable and tunable set of compositions for therapeutic, scaffolding and imaging systems has been reported. Although many of the work involving dendrimer synthesis and traditional applications has been well documented many hot issues should be examined and thus need to be reviewed, namely those related with most recent and notable advances of dendritic polymers that show promise in the field of regenerative medicine. Herein, a review is given on dendritic nanopolymers, especially on dendrimer and dendrons technology and their surface engineering to deliver and target drugs or bring imaging agents to the targets where they are required. This review begins with a brief overview on the exploratory research merging nanotechnology and regenerative medicine. Fundamentals on the synthesis and macromolecular structure of dendritic polymers are provided. The unique advantages of dendrimers comparing to traditional macromolecular architectures (e.g. linear, cross-linked, branched) are a consequence of their inherent properties, i.e. large surface area, shape, functionalization, and high efficiency for the cellular uptake which possibly dendrimers fulfill the requirements as carriers for gene, nucleic acids, bioactive molecules and peptide/protein delivery. The huge portfolio of degradable and non-degradable controlled-release vehicles are being investigated for their processing into nanocarriers, several new emerging nanomaterials are being studied for their biodegradability, controlled-release and stimuli-responsive properties. Therefore, the release of different or multiple bioactive agents, each with its own kinetic profile, which can be released under the action of specific stimuli, is becoming possible. However, to make use of this potential, toxicological, drug loading capacity and host-guest chemistries in dendrimers must be addressed. These issues are included within the scope of this review. Moreover, we will discuss possible strategies that can be taken to overcome some of the dendrimers limitations. Further attention is given on the progress in the targeting strategies and it is discussed its importance in the therapeutic efficiency and in avoiding the undesired secondary effects of several drugs. Therefore, their ability to target delivery to specific sites in the human body possibly the improvement of the bioavailability of therapeutic molecules, decrease the dosage and frequent re-dosage needs. In addition, integration of the nanocontrolled-release systems with other

desirable functions to create new and cross-discipline applications can also be realized by means of using dendrimer technology. In the following sections of this review, special focus is provided on the novel applications and recent work involving dendrimers in both fields of tissue engineering and central nervous system. In regenerative medicine field, dendrimer-based polymers have been attracting great attention as drug delivery system (DDS) to deliver bioactive molecules aimed at modulate the behavior of stem cells, i.e. their proliferation and differentiation, *in vitro* and *in vivo*. Moreover, due to their innovative character other applications beyond DDS became possible, namely as scaffolding and chemoattractants for tissue regeneration, and implantable biodegradable nanomaterial-based medical devices integrated with drug delivery functions (theranostics). Finally, within the scope of this review we highlight promising areas for further research and succinctly comment on how and why dendrimers and dendrons technology should be viewed as the next generation of biomaterials for the 21st century.

This chapter is based on the following publication: **Oliveira JM**, Salgado AJ, Sousa N, Mano JF, and Reis RL, Dendrimers and derivatives as a potential therapeutic tool in regenerative medicine strategies: a review, (2009), submitted.

---

1. INTRODUCTION

During the 20th century, we have assisted to great innovations on polymer synthesis and advances in the design of biodegradable chemistries. These achievements allowed obtaining macromolecules of multiple compositions and novel architectures possessing unique physicochemical and biological properties. Synthetic polymers can be divided into four key architectural classes: linear, cross-linked, branched, and dendritic structures. The first three types have been studied extensively in the past. The fourth comprises the nature-inspired dendrimers and its derivatives and are reviewed herein. These are highly branched and nanospherical macromolecules, and are the most prominent example of nano-polymer revolution. The first report is attributed to Tomalia et al. [1] and dates to the early 1980s. These novel structures differ from typical linear polymers, since their architecture is extremely precise and controlled conferring them with tunable and predictable molecular weights, biodegradability and biocompatibility. This chemistry revolution igniting many possibilities and it is not surprisingly that we now assist to their burst exploitation in a variety of medical applications.

In this review, we report on the noteworthy scientific advances and most recent literature, dealing with the dendritic polymers nanotechnology and brief discuss on the convergence of nanotechnology and regenerative medicine. Fundamentals on dendrimers will be succinctly provided. Numerous synthetic strategies have been reported for the preparation of dendrimer-based materials. The present review will also focus on the most recent advances in the dendrimers surface engineering, which allowed obtaining novel and promising complexities (architectures and chemical functionalities) such as the dendronized polymers. Interesting features reported for dendronized polymers are also discussed, as well as some suggestions for potential applications such as tissue engineering (TE), central nervous system (CNS), gene delivery and theranostics will be also highlighted wherein.

1.1. CONVERGENCE OF NANOTECHNOLOGY AND REGENERATIVE MEDICINE

In 1959, Richard Feynman [2] coined nanotechnology as a futuristic approach to the development of materials atom by atom. The ultimate goal of nanotechnology can be described as the ability to apply the nanoscale principles and work at the atomic, molecular and supramolecular levels (on the range of 1-100 nm) to understand, and create material systems by assembling molecules into objects or vice-versa. Nanotechnology provides solutions for the transformation of biosystems and provides a broad collection of technologies, techniques and processes for real life purposes. Current and potential applications of nanotechnology in medicine range from research involving diagnostic devices, drug

delivery vehicles, nanoscale surgery, biosensors and body part repair/regeneration and cancer therapy. By its turn, regenerative medicine uncovers fundamental biological processes, self-repairing, self-replicating, and tissue regeneration mechanisms and offers inspiration models to nanotechnology [3-5]. Several examples of applications of nanotechnology in regenerative medicine will be provided further, but the currently undergoing explosive developments are summarized in Table 1.

Table 1. Nanotechnology applications in regenerative medicine.

Application (s)	Examples of material structures, devices and systems at nanoscale	Ref. (s)
Targeted and controlled drug delivery	Nanoshells (layered colloids with a nonconducting nanoparticle core covered by a thin metal shell) and nanorods (e.g. copolymers, gold) are used in combination with specific wavelengths of lights and heat technology for cancer therapy.	[6-9]
	Dendrimer-antibody or peptide-major histocompatibility complex ligand constructs for sensitive detection and drug delivery (e.g. doxorubicin) to T cells. Using this type of strategy guided therapy is possible.	[10,11]
	Quantum dots (central core of elements of groups II- or III-VI of the periodic table, i.e. CdSe, CdTe, PbSe, ZnSe, GaAs, InP, GaN capped with ZnS) cross-linked to antibody conjugates (e.g. monoclonal antibodies, biotin, avidin), oligonucleotides molecule ligands to render them specific to biological targets.	[12-14]
	Liposomes (lipid-based vesicles with size ranging from 50-100 nm) and surface modified-liposomes (e.g. PEGylated lipids trademarked as QuSomes™) for drug delivery and treatment of several diseases (e.g. cancer therapy, and inflammatory arthritis). Surface modified sialyl Lewis X-liposomes demonstrate their efficiency as a targeted drug delivery system for preventing stenosis after angioplasty.	[15-19]
	Fullerenes (i.e. clusters of 60 carbon atoms) for intracellular drug delivery, as their structure mimic that of clathrin known to mediate endocytosis.	[20-22]
Medical devices	Contrast agents as the superparamagnetic nanoparticles (e.g. FePt, iron oxide, PLGA coated iron oxide with size ranging from 10 to 20 nm) and quantum-dot-based nanoparticles (e.g. biotinylated gadolinium-annexin A5-streptavidin) for use in magnetic resonance imaging (MRI). Radiopaque iodinated polymeric nanoparticles for X-ray imaging applications have also been developed.	[23-27]
	T1 agents to target folate receptors using dendrimer-based agent that can be decorated with both ligands and gadolinium.	[28]
	Proteins such as antibodies, antigens, and enzymes can be immobilized on protein chips for application in early diagnosis of disease, tailored drug therapy, and detection of various pathogens.	[29-33]
	Silicon nanopore membranes for find applications in hemodialysis and hemofiltration.	[34]
Cell/Tissue engineering	Carbon single-wall nanotube (size <100 nm) sheets to develop artificial muscle.	[35,36]
	Systems to determine or reduce immune rejection of organs.	[37,38]
	Nanostructured materials for nerve, bone, and cartilage regeneration.	[39-41]
	Collagen-dendrimer hydrogels for ocular tissue engineering.	[42]
Gene delivery	Polycationic polymers (e.g. SuperFect dendrimers, poly-(L-lysine)) as synthetic non-viral vectors with decrease cytotoxicity.	[43-45]
	Cationic liposomes and formulations (e.g. lipid-coated magnetic nanoparticles, liposomal bubbles) for the delivery of oligonucleotides to different cells. Liposomal formulations for triggered release of siRNA have also been developed.	[46-51]
Molecular tags (*in vitro* and *in vivo imaging)*	Semi-conductor nanocrystals quantum dots (e.g. CdSe, ZnS), nanocrystals that fluoresce in different colours depending on their sizes and may find application for targeting multiple types of cells in living organisms. The quantum dots may be also linked with ligand molecules for receptor labeling and visualization.	[52-55]
	Metal-chelate-dendrimer coupled to monoclonal antibody for radiotherapy and imaging.	[11]
	Fluorescent labeled-nanoparticles (e.g. fluorescein isothiocyanate (FITC)-labeled PAMAM dendrimer-drug conjugate) for assessing cellular uptake.	[56]
	Gold and silver nanoparticles (size <50 nm) for molecular detection and separation.	[57-59]
	Gold nanorods for cancer cell imaging.	[9]
Biosensors, bioanalysis and microfluidics	Carbon-nanotubes arrays as immunosensors for detection of antigen-antibody binding.	[60]
	Electrochemical immunosensor based on dendrimer-assisted self-assembled monolayers functionalized with enzyme-tagged antibody.	[61,62]
	Dendrimer-modified electrodes for application as biosensors. PAMAM–CdS nanocomposites for biological assays.	[63-66]
	Nanowire field-effect transistors for detection of biomolecules.	[67,68]
	High-throughput (e.g. extracellular matrix microarray, high-throughput screening of gene functions) analysis as a tool for evaluating cell fate and drug discovery.	[69-71]
Theranostics (i.e. combined therapeutics and diagnostic)	Polymer-based nanosystems for therapeutic and diagnostic of several diseases.	[72,73]
	Liposomes (e.g. polyethylene glycol (PEG)-coated liposomes-doxorubicin, ^{111}Indium-vinorelbine-liposomes) for imaging, therapy and diagnosis of variety of cancers.	[74,75]
	Fullerenes (e.g. PEG-coated fullerenes containing gadolinium ions) for MRI and efficient photodynamic therapy of tumors.	[76]

Exploratory research in nanotechnology is considered to be emerging, disruptive and multidisciplinary [77]. Since it offers ever more exciting promises of new diagnoses and cures, it can greatly impact every aspect of society. Consequently, there have been tremendous investments in this area [5].

2. DENDRITIC POLYMERS-DENDRIMERS AND DENDRONS: FUNDAMENTALS AND BIOTECHNOLOGICAL APPLICATIONS

Dendrimers are a unique class of synthetic polymers which play an important role in emerging nanotechnology [78,79]. The term ‘‘dendrimer’’ (from greek: *dendra*, tree and *meros*, part of) describes the architecture of this emerging class of polymeric macromolecules which possess 3-D features that resemble a tree (Figure 1).

Figure 1. The typical dendron structure resembles the architecture of a tree (Photo obtained from Casa Milà also known as La Pedrera-Barcelona, and makes figurative meaning to Tomalia inspiration from nature and a poetic analogy of the dendrimers to nature’s architecture and geometric forms).

Presently, the dendritic architectural class can be divided into four subclasses: random hyperbranched polymers, dendrigraft polymers, dendrons, and dendrimers [79]. More than 100 different dendrimers and 1,000 surface chemistries are currently known.

In this section we will deal with the dendrimers fundamental aspects. A typical dendrimer structure consists of three basic components (Figure 2): multifunctional central core (○) where other molecules can be trapped [80], branched units (Y) that emanates from the central core and external capping-groups (E). The highly regular branching units are organized in layers called ‘‘generations’’, and represent the repeating monomer unit of these synthetic macromolecules [79]. Therefore, dendrimers can be synthesized from simple branched monomer units, in a precise and controlled fashion from trunk to

branch and to leaf ‘‘surface groups’’. Dendrimers can be designed to provide a quite versatile choice of external functional groups [73] in order to reduce cytotoxicity, enhance transepithelial transport [80,81], for interaction with coupling molecules such as natural-based polymers [82] and fluorescent probes [83]. The surface groups may also act as passive or reactive gates controlling entry or departure of molecules from the dendrimer interior. Surface properties can also allow control clearance and biodistribution in the body.

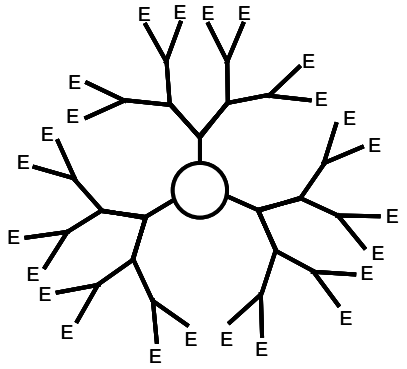

Figure 2. Schematic representation of the dendrimer typical structure.

Their size, shape, and topology, as well as flexibility and surface functionality, are controlled at the molecular level (all three architectural components), which makes them useful building blocks and carrier molecules at the nanometer level, but also possibly to precisely manipulate both molecular weight and chemical composition. This new class of synthetic [84-86], highly branched, nanospherical macromolecules presents unique features in comparison to the traditional linear, cross-linked and branched polymers [79,87], thus many researchers have explored their potential in many biological applications. An advantage is related with the fact that the narrow molecular weight distributions (M_w/M_n = 1.0000-1.05) can provide reproducible pharmacokinetic behavior [79].

There are different types of dendrimers which are classified as: (i) glycodendrimers and (ii) peptide dendrimers. Glycodendrimers have been showing a great potential as drug carrier. The term ‘glycodendrimer’ has been used to describe dendrimers that include carbohydrates into their architecture. The vast majority of glycodendrimers have saccharide residues on their outer surface, but glycodendrimers containing a sugar unit as the central core from which all branches emanate have also been described. Generally, glycodendrimers can be classified as: (i) carbohydrate-centred, (ii) carbohydrate-based and (iii) carbohydrate-coated dendrimers. The late will be further exploited in section 3, the so-called dendronized polymers.

By its turn, Sadler et al. [88] broadly defined peptide dendrimers as ''radial or wedge-like branched macromolecules consisting of a peptidyl branching core and/or covalently attached surface functional units''. Thus, this definition includes any dendrimer with an amino acid core, branching units, surface functional groups or any combination of the three as a peptide dendrimer. In dendrimer synthesis, aminoacids are also appealing building blocks because peptide-coupling techniques can be used. Despite, most research on dendritic polymers has been conducted with glycodendrimers.

Both the synthesis and applications of glycodendrimers and peptide dendrimers have been reviewed by many [88-91]. Succintly, two different synthetic strategies are currently explored for synthesizing structurally well defined dendritic polymers, namely the divergent [87,92] and convergent growth [93-95] approaches. Most of the commercially available dendrimers, such as the Tomalia's dendrimers poly(amidoamine) (PAMAM) dendrimers from Dendritech Inc. (Midland, MI, USA) and poly(propyleneimine) (PPI) dendrimers from DSM (Geleen, The Netherlands) are produced by divergent method. This methodology involves *in situ* branch-cell construction in stepwise and iterative stages around a desired core to produce core-shell structures. In the convergent method (Fréchet approach) dendrons are synthesized according to the divergent approach and then are anchored to a multifunctional core. Both strategies possess advantages and disadvantages and the appropriate route depends mainly on the type of monomer used and the desired structure. Although there are different routes to synthesise dendrimers, their maximum size is typically in the order of ~10-20 nm [96,78]. Recently, a novel synthetic route has been proposed for new low-cost Priostar dendrimers [97,98].

Unlike traditional polymers, the unique characteristics of dendritic polymers make possible their use in a wide range of applications. Among the myriad of possibilities, dendritic polymers can find applications as a delivery carrier of drugs [80,99,100], and on the development of synthetic vaccines [101] and antitumour systems [102,103] and immunology [104,105]. Other applications in the bioscience field includes blood anticoagulant [106] and microbicidal [107-109] activities. For example, Jiang [110] reported on a poly-(L-lysine) (PLL) dendrimer with a polyanionic outer surface consisting of 32 naphthalene disulfonate units, also know as Vivagel (Starpharma Ltd., Melbourne, Australia) to be used as topical vaginal microbicide for HIV prevention. These were found to be safe and prevent HIV-1 infection by binding to receptors on the viral coat. The promising results potentate VivaGel entering phase II clinical trials in humans [111]. Other dendrimer-based DDS have also proved to effectively enhance anti-viral activity by reducing the viral load, *in vitro* [112,113]. Dendrimers have also been useful in prion research [114-116] since cationic dendrimers are shown to perturb peptide fibrillation in a process dependent on the nature of the charged groups on the dendrimer surface.

Regarding the antitumour systems, dendrimers mimicking the surface structure of proteins involved in angiogenesis inhibition have been developed [117,118]. Angiogenesis is an important process for tumour growth and is initiated by angiogenic factors, such as vascular endothelial growth factor (VEGF) and basic fibroblast growth factor (b-FGF). These growth factors bind to their receptors on endothelial cells with the dependence of heparin or heparan sulfate proteoglycan (HSPG) in extracellular matrix (ECM). The participation of binding to heparin or HSPG leads to potential targets for antiangiogenic activity. Endostatin, a weel-known endogenous angiogenic protein binds to heparin or HSPG and inhibits some functions of endothelial cells, resulting in potent suppression of angiogenesis. To find a new potent angiogenic inhibitors, Shimamura and coworkers [118] have focused their attention on characteristic positive-charge-rich surface of endostatin and the interaction between its arginine residues and either heparin or HSPG. This group design novel arginine-rich dendrimers, TX-1943 (8 Arg residues) and TX-1944 (16 Arg residues), which mimic the surface structure of endostatin and evaluated their antiangiogenic ability, *in vitro* and *in viv*o. *In vitro* studies demonstrated that both dendrimers bound to heparin [118]. During this study, it was also observed that angiogenesis inhibition of b-FGF stimulated proliferation and tube formation of endothelial cells, *in vitro*; however TX-1944 antiangiogenic activity was stronger than that of TX-1943. Moroever, both type of dendrimers exhibited potent antiangiogenic activity in the chicken embryo chorioallantoic membrane assay, *in vivo*. These data suggest that arginine dendrimer can be used in prevention of the growth and metastasis of solid tumours.

The innovative synthetic procedures increased the accessibility to the functionalization of dendrimers with transition metals in the core, finding interesting applications in catalysis [119-122]. Actually, dendrimers can combine the advantages of homogenous and heterogeneous catalysts. Homogenous catalysts are known for having a good accessibility of active sites. Despite, one of the disadvantages lie on the fact that it is difficult to separate from the reaction stream. On the contrary, heterogeneous catalysts are easy to separate from the reaction mixture but the disadvantage is that kinetics of the reaction is limited by mass transport. Dendrimers have a multifunctional surface and all catalytic sites are always exposed towards the reaction mixture. Metallodendrimer research has been steadily gaining ground during the last few years. Several authors have been proposing the use of dendrimers to develop complexes with metals such as Pt [123], Ag [124,125], Fe [126], Cu and Ni [127].

Benito et al. [128,129] demonstrated the synthesis of carbosilane dendrimers with N,N'-pyridylimine molybdenum and platinum at their periphery. In addition, similar complexes have also been described by Al-Hamra [130]. This work reports on the synthesis of second and third generation dendrimers based on PLL with a pentaamine cobalt (III) metal complex at the core, following a divergent synthetic

approach. The use of the cobalt complex served as the C-terminal protecting group, which facilitate purification and enhanced the dendrimers' solubility in aqueous and organic solvents. Similarly, Bellis [131] synthesised a series of surface-functionalized proline-modified PPI dendrimers as metal-free catalysts for asymmetric aldol reactions which showed improved solubility in organic solvents. Another group [132] reported on the synthesis of lipophilic dendrimers, containing crown ether moieties with different sizes as the core, surrounded by poly(aromatic ether) wedges of different generations. The synthesis route consisted on the use of bis(bromomethyl)-substituted crown ethers and Fréchet-type poly(benzyl ether) dendrons as building blocks.

Most metallodendrimers are built from organic skeletons, in particular from dendrimers of types PAMAM or PPI. However, a lot of examples are also known for fluorinated [133] and phosphorus-containing dendrimers [134,135].

It has been demonstrated that dendrimers containing phenylene ethylene units exhibit a correlation between the molecular geometry and the electronic properties [136]. In addition, it was also shown that the light-gathering properties increase with the generation although the excitation transfer efficiency to the core decreases for generations higher than the sixth [136,137]. Dendrimers are mainly attracting the interest of many scientists because of their unique physicochemical characteristics and geometry [138]. Light harvesting dendrimers own their efficiency to a highly directed process that delivers captured light energy to the core [139]. For example, Akai et al. [140,141] have studied the energy transfer and shielding effect in different types of dendrimers. The most recent work, reports on the wire-type dendrimers possessing a poly-(*p*-phenylenevinylene) backbone and having oligophenylene light-harvesting (LH) antenna. This study has demonstrated the ability of wire-type dendrimer with a LH-antenna as highly efficient light-emitting material. Andrews et al. [142], reported a new approach for modeling the multi-step flow and that possibly to reveal the character and patterns of internal energy flow in dendrimeric materials. Similar applications have been proposed for fullerodendrimers, i.e. the fullerene-based PAMAM-type dendrons. Thus, dendrimers have been useful for encapsulation of core moieties. Although the conformation that a dendrimer assumes around a core moiety cannot be directly determined, the effect of increasing dendrimer size on the photophysical and electrochemical properties of the core has been exploited. Araki et al. [143] have been developing fullerodendrimers for application as artificial photosynthesis systems. Their work has shown that the rate constants and quantum yields of photo-induced electron transfer with the added aromatic amine donors in benzonitrile tend to decrease with the dendron generation. These data thus indicated that the bulky dendron groups acted as barriers for the donor molecules to approach the C_{60} moiety in the core of the dendrimers. Other

works [144,145] have shown much promise of iridium-based phosphorescent and phenylazomethine dendrimer complexes as light emitting materials for efficient organic light emitting diodes.

As proposed by Ceroni [146], metal-containing dendrimers can be classified from structural viewpoint as: (i) dendrimers built around a metal complex as a core; (ii) dendrimers containing metal complexes as branching centers; (iii) dendrimers containing metal complexes as peripheral units; (iv) dendrimers that can coordinate metal ions by ligand units that are present in the branches; and (v) dendrimers with a core which is able to coordinate a metal ion.

It is likely that improving design of dendrimers will lead to coordination compounds capable of performing even more sophisticated functions, such as energy up-conversion and electrochemiluminescence.

Applications of dendrimers in more traditional technologies such as coatings and inks have also been exploited, as their spherical shape shows unique rheological characteristics [147]. Dendrimers versatility further explains their importance in optic, electronics and magnetic applications [148-150]. Interestingly, a recent work [151] propose the use PAMAM dendrimers adsorved onto native oxide surfaces of silicon wafers as a strategy to direct the integration of metal electrodeposition with silicon microfabrication processes and selective deposition by dendrimer patterning.

Alonso et al. [152] have describe the development of an amperometric enzyme electrode for glucose monitoring. This high sensitive electrode consisted on the electrostatic immobilization of the enzyme glucose oxidase onto C and Pt electrodes modified with mixed ferrocene-cobaltocenium dendrimers. This work showed that higher generation dendrimers to be more efficient electron transfer mediators, and can find applications as sensors. In another study [153], PPI dendrimer cores functionalised with octamethylferrocenyl units were deposited onto a Pt electrode. Amperometric biosensors for glucose were prepared by immobilization of glucose oxidase (GOX) onto the electrodes and their applications as hydrogen peroxide and glucose sensor was investigated. It was also shown that electrodes modified with polymethylferrocenyl dendrimer promote the redox reactions of hydrogen peroxide and its efficiency was affected by structural characteristics of the dendrimers when low working potentials are used. Despite, the biosensors developed possess a good linear response region, and superior sensitivity and reproducibility as compared with other ferrocene-mediated glucose sensors.

Yao et al. [154] have reported on enzyme field effect transistor (ENFET) for determining glucose. This biosensor was produced with dendrimer encapsulated Pt nanoparticles and GOX via a layer-by-layer self-assembly method. This work demonstrated that the developed biosensor possess good stability, enhanced sensitivity and extended lifetime as compared to conventional ones. By its turn Buschbeck

[155] has been proposing the surface modification of low generation dendrimers with triethylene glycol methyl ether units to develop ionophores for chemical sensors.

Another work [156] using erythrocyte ghosts demonstrated that the addition of fourth generation PAMAM dendrimer and PAMAM-OH has a dual effect on the activity of human erythrocyte membrane acetylcholinesterase (AChE). Low dendrimer (25 μM) concentrations caused a statistically significant increase of the enzyme activity. For dendrimer concentrations higher than 100 μM, it was observed an inhibition of AChE. The efficiency of the inhibition was similar for both amine- and hydroxyl-terminated PAMAM dendrimers; however, the maximum of activation occurred at a different range of dendrimer concentration; 25 μM for PAMAM-OH (G4) and 100 μM for PAMAM (G4). The advanced explanation for the changes of AChE activity upon addition of dendrimers was related with the alteration in protein structure, but may be associated with the structural changes in the whole membrane. A study reported by Shcharbin [157] aimed at clarify whether AChE inhibition was a result of direct action of dendrimers on the enzyme or a result of indirect changes in lipid bilayer of membrane. By performing fluorescence analysis it was demonstrated that anionic and cationic dendrimers changed AChE conformation and the strongest effect was induced by carboxylic-tterminated PAMAM dendrimers (G3.5). It was also demonstrated that changing on AChE conformation and catalytic activity depended on type and concentration of the dendrimer.

Another interesting work reported by Kubát et al. [158], investigated the interaction of porphyrins with PAMAM dendrimers of different generation and external groups, in aqueous solution. In that work, the binding of porphyrins to PAMAM dendrimers is controlled mainly by electrostatic interactions between porphyrins and terminal groups of PAMAM dendrimers (amine or carboxylic groups), and depended on both porphyrin peripheral functionalization and pH of the solution. Moreover, low and high generation dendrimers formed complexes with porphyrins.

Shcharbin et al. [159,160] have been studying the interaction of serum albumins with cationic dendrimers. In their first study [159], they investigated the interaction of a fourth generation PAMAM dendrimer and serum albumins from human (HAS) and bovine (BSA) origin. This study demonstrated that serum albumins and PAMAM G4 dendrimer form complexes with stoichiometry of 4-6:1 for PAMAM:HSA and 4-5:1 for PAMAM:BSA molar ratio. Results obtained from circular dichroism, fluorescence polarization and zeta-potential experiments have shown that dendrimers did not significantly change the secondary structure of proteins, and interactions between protein and dendrimer were weak. Based on the 3-D crystal structures of HSA and BSA, they identified five non-specific anionic regions for binding of cationic dendrimers. Another study [160] investigated the effect of the generation of PAMAM dendrimers

(G2 and G6) on the binding to bovine serum albumin (fatty acids free and loaded with different fatty acids). This comprehensive work has shown that although proteins loaded with fatty acids have more stable structures and were less sensitive to the action of dendrimers, BSA-fatty acid complexes bound to PAMAM dendrimers. Results suggested that the efficiency of the interaction depended on the fatty acids loaded on the protein, i.e. PAMAM dendrimers were able to compete with BSA for fatty acids if two or three fatty acids were loaded per protein.

An important characteristic of dendritic molecules is their improved solubility in a large number of organic solvents [161,162]. An understanding of the interfacial interactions is important to the biomedical applications of these polymers. In this respect, it has been shown that dendrimers are able to change their conformation on the different alkanethiol surfaces due to their flexibility. Abdelhady et al. [163] have conducted an atomic force microscopy (AFM) study to understand the factors affecting the interactions of fourth generation PAMAM dendrimers with substrates of defined surface chemistry. Their results also suggest that the surface conformation of such dendrimer molecules can depend upon the nature of the different functionalized substrates.

Recently, Allabashi [164] has reported on an easy method for manufacturing composite filters cross-linked with silylated dendritic polymers and cyclodextrins (CD). Triethoxysilylated derivatives of PPI dendrimer, PPI and polyglycerol hyperbranched polymers and *β*-cyclodextrin (*β*-CD) were impregnated into Al_2O_3, SiC and TiO_2 membranes and were tested for the removal of a variety of organic pollutants from water. The obtained data proved their efficiency on removing up to 99% polycyclic aromatic hydrocarbons, 93% of the monocyclic aromatic hydrocarbons, and up to 43% of pesticides, among others.

Cromer and coworkers [165] have proposed the use of functionalized dendrimers as endotoxin sponges. Using *in vitro* and *in vivo* models of septic shock, they demonstrated that PAMAM dendrimers partially modified by hydrophobic groups effectively bind and sequester bacterial lipopolysaccharides. Therefore, these systems potentially can be useful for the therapy of Gram-negative sepsis. Interestingly, Labieniec et al. [166] studies provide the first evidence of the therapeutic effect of fourth generation PAMAM dendrimers. These were found to lower plasma glucose and suppress long-term markers of diabetic hyperglycaemia, *in vivo*.

Despite the many advantages and superior performance of the dendrimers highlighted herein, few can be obtained with high generations, with exception of PAMAM, PPI, polyphosphane, and triallyl phenol. Synthesis of high generation dendrimers, useful for exploring the nature of the dendritic architecture, depends critically on the nature of the constituent monomers, their reactivities, and the method of their

preparation. Krishna et al. [167] have previously shown that poly(propyl ether imine) (PETIM) dendrimers (G3) possessing alcohol, amine, nitrile, ester or carboxylic acid groups at the peripheries can be obtained. Moreover, during their studies it was demonstrated that PETIM dendrimers with carboxylic acid groups were non-toxic over two different cell lines: human breast cancer T47D and African green monkey kidney (CV-1) cells. Jayamurugan et al. [168] have also reported on the synthesis of high generation PETIM dendrimers. This group obtained PETIM dendrimers up to G6 by carrying out simple iterative steps consisting of two alternate Michael additions and two reduction reactions. The disadvantage is that the procedure is long, but the overall yields are quite good for lower generations. They have shown to be possible tailoring the peripheries of these dendrimers by introducing different groups such as alcohols, amines, carboxylic acids, esters, or nitriles, and up to 128 external groups, thereby opening up new properties and possibilities for several applications.

The well-defined hyperbranched structure of dendrimers has motivated chemists to explore the possibility for mimicking protein functions with dendritic macromolecules [169], such as O_2-carrying hemoproteins [170] and Coenzyme B_{12} [171]. In the next section, this issue will be explored further.

3. DENDRITIC POLYMERS IN REGENERATIVE MEDICINE

3.1. DRUG DELIVERY APPLICATIONS OF DENDRIMERS AND DENDRONIZED POLYMERS

The development of nanotechnology-based efficient drug delivery systems for small molecules, proteins and DNA has been attracting great deal of attention over the last few years. Unlike traditional polymers, dendrimers can be obtained in precise molecular weights even at high generations, which as previously highlighted can provide a reproducible pharmacokinetic behaviour. This feature makes them ideal candidates for drug delivery applications. Despite, a efficient drug delivery systems should meet other criteria, such as: (i) structural control over size and shape of drug or imaging-agent cargo-space; (ii) biocompatibility, non-toxic polymer/pendant functionality; (iii) precise, nanoscale-container and/or scaffolding properties with high drug loading capacity; (iv) well-defined scaffolding and/or surface modifiable functionality for cell-specific targeting moieties; (v) lack of immunogenicity; (vi) appropriate cellular adhesion and internalization, (vii) adequate bio-elimination or biodegradation; (viii) controlled or stimuli-responsive drug release features; (ix) molecular level isolation and protection of the drug against inactivation during transit to target cells; (x) minimal non-specific cellular and blood-protein binding properties; (xi) ease of consistent, reproducible, clinical grade synthesis.

In regenerative medicine, the control of cells behavior at the nanoscale is addressed via cell-adhesion receptors. The surface of eukaryotic cells is covered with an array of glycoconjugates, (e.g. glycoproteins and glycolipids). Extracellularly, carbohydrates in some of the glycoconjugates play a key role in the process of cell-cell and cell-pathogen adhesion. Furthermore, they also participate in such fundamental processes as glycan cross-linking in the ECM. Intracellularly, carbohydrate receptors are involved in such key biological processes as protein folding and sorting of proteins (e.g. the degradative lysosomal enzymes). It is the weak binding of most carbohydrate ligands for their protein receptors, that requires these carbohydrates to be clustered in order to attain biologically meaningful affinities toward their receptors (e.g. lectin type) [172]. In order to refine the biological activities and drug delivery by dendritic polymers, efficient carbohydrate ligands of the glycodendrimer-type are emerging as potent ligands for carbohydrate-binding proteins. Such type of molecules can be obtained through surface engineering using a carbohydrate coating on the dendrimeric system, the so-called dendronized polymers (Figure 3).

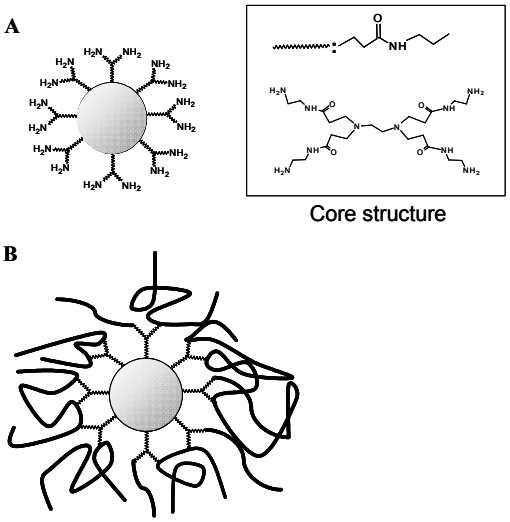

Figure 3. Comparison of the structure of (A) PAMAM dendrimer (G2), (B) PAMAM dendrimer bearing carbohydrate end groups (dendronized polymer).

Dendrimers modified with the terminal carbohydrate polymers constitute a new class of biopolymers with many interesting applications. Dendronized polymers can be conveniently synthesized with a good yield using both divergent and convergent approaches or using as well chemoenzymatic approaches [173]. Another advantage of these systems is related with the chemical nature of the synthetic linker and the possibility of tailoring the type of glycosidic linkages in these compounds, which gives us additional flexibility to meet demands from the point of view of hydrophobicity, and biodegradability [172]. Moreover,

these compounds can grow to considerable size by successive cycles of branching, which give them a unique possibility to vary the degree of carbohydrate clustering required by the carbohydrate receptors. Potentially, such type of molecules can be used for treatment and control of metabolic disorders involving carbohydrates, and protection against certain types of infections.

Dendronized polymers with a variety of shapes, core molecules, carbohydrate residues and valences are made available for the biological evaluation. This new class of materials is expected to exhibit entirely new properties since the structures might have sizes larger than 10 nm and different surface properties [85]. In fact, the linking of terminal sugar residues such as heparin on dendrimers can create a multivalent display that mimic cell-surface glycans [174]. This strategy showed that heparin dendrimers promote FGF-2-mediated mitogen-activated kinase activation in L6 myoblasts. Thus, these glycodendrimers can modulate heparin-protein interactions.

It has been found [175] that high generation dendrimers (G7) with amine capping-groups causes haemolysis and changes the morphology of red cells, since they bind to membranes of cells (negatively charged) in a non-specific manner and can cause toxicity *in vitro* and *in vivo*. Similar findings were reported by Domanski et al. [176] that investigated the effect of PAMAM dendrimers concentration and generation (G2, G3 and G4) on human red blood cells. This paper demonstrated that erythrocyte shape changed and was accompanied by dendrimer-induced haemolysis when these cells were exposed to nanoparticules concentrations ranging between 1 nM and 1 µM. Moreover, it was conclusive that when higher dendrimer generation was used, a lower concentration of PAMAM dendrimer was needed to cause haemolysis. These observations were supported by the work of Jevprasesphant et al. [177]. The cytotoxicity of unmodified PAMAM dendrimers towards Caco-2 cells was appreciably higher for cationic (whole generation) compared with anionic (half generation) dendrimers and for both types increased with increasing size (generation) and concentration. King Heiden et al. [178] have also demonstrated that PAMAM dendrimers amine-terminated (G4) are toxic and attenuated growth and development of zebrafish embryos at sublethal concentrations. However, PAMAM dendrimers carboxylic terminated (G3.5) were not toxic to zebrafish embryos. Dutta et al. [179] study corroborated previous findings that demonstrated the cytotoxic behaviour of PPI dendrimer amine-terminated (G5), *in vitro*. Recently, Libieniec et al. [166] have also shown the cytotoxic effects of PAMAM dendrimers (G4), *in vivo*. It was found that PAMAM dendrimers increased mortality of streptozotocin-diabetic rats. In a study reported by Neerman [180], melamine dendrimer were developed and their potential as a vehicle for drug delivery applications was investigated. The preliminary i*n vitro* study has shown a decrease in Clone 9 cells viability at 0.1 $mg.mL^{-1}$ as compared to that of cells cultured in the presence of dextran. For the *in vivo*

study, mice were administered with increasing concentrations of dendrimer via i.p. injection. At a higher concentration (160 $mg.kg^{-1}$), 100% mortality was observed and histopathological data revealed hepatoxicity. At low concentrations (2.5-40 $mg.kg^{-1}$) of the dendrimers, no mortality was seen, and no hepatic damage was found. These data suggest that the toxicity of the melamine-based dendrimer is comparable to the cationic PAMAM dendrimers, and further studies needs to be carried out to evaluate their potential as DDS.

Surface engineered dendrimers with carbohydrates should make it also possible to avoid the cytotoxic effects of cationic and high generation dendrimers and reduce the haemolytic toxicity by reduction/shielding of the positive charge on the dendrimer surface, while enhancing the peripheral congestion to improve container properties. The development of strategies for the synthesis of dendrimers based on novel cores and branches continues to be one of the important aspects of dendrimer chemistry due to the need for tailoring rigidity and density to refine drug release kinetics. Sashiwa and coworkers [82,181-183] have established the synthesis of a variety of chitosan-dendrimer dendronized polymers mainly by two procedures: i) dendrimers bearing aldehyde and a spacer are synthesized, and then these are reacted with chitosan by reductive N-alkylation, and ii) linking of chitosan to the dendrimer surface. The first approach has the advantage of no crosslinking during the reaction. The second allows use of commercially available amino-dendrimers such as PAMAM and poly(ethyleneimine) (PEI) dendrimers. At least two binding points are available; however, this can be a drawback as it can cause an undesired crosslinking. Following these studies, Oliveira and coworkers [184] have proposed surface engineer PAMAM dendrimers with the water-soluble carboxymethylchitosan (CMCht) to develop novel sphere-like nanoparticles aimed at find application as carriers to deliver intracellularly bioactive molecules. These are aimed at control from inside the behavior of stem cells, namely their proliferation and differentiation. Dubber et al. [185] previously reported on the synthesis of a carbohydrate-centered PAMAM dendrimers. First, D-glucose was converted into its per-aminoethyl-functionalized derivative, which was then submitted to the multi-step reaction for obtaining the PAMAM branches. Domanski et al. [186] also shown that thiophosphate dendrimers (G5) were neither haemotoxic nor cytotoxic within the concentration range from 100 pM to 10 μM, thus being good candidates for drug delivery. A marked decrease in the cytotoxicity of amine-terminated PAMAM dendrimers was noted when the surface was modified with the addition of six lauroyl or four PEG chains [177]. Dutta et al. [179] have demonstrated that the surface modification of PPI (G5) dendrimers with mannose and N-tert-butoxycarbonyl (t-Boc) decrease haemolitic toxicity and cytotoxicity over HepG2 and COS-7 cell lines, *in vitro*. Moreover, an *in vivo* study [187] using Wistar rats showed that administration of PPI dendrimers

(G5) caused haemolysis and tissue degeneration, after 24 hours. On the contrary, no signs of toxicity were observed in animals to which surface-modified PPI dendrimers were administered, suggesting that functionalization of dendrimers leads to drastic reduction of toxicity and increases biocompatibility. Makimura and coworkers [188] have investigated glycodendrimers with a lysine core and with different carbohydrates on the exterior. Compared to the mono-functional structure, L-lysine dendrimers with 8 or 16 sialic acid residues show enhance binding properties and efficiently suppress the hemagglutination of erythrocytes.

A surface engineering strategy was also on the basis of Jevprasesphant et al. [189] work to improve the properties of dendrimers. It was found that conjugation of cationic PAMAM dendrimers with lauroyl chloride decreased their cytotoxicity and increased their permeation through Caco-2 cell monolayers. Another study [178] has demonstrated that when the tripeptide Arg-Gly-Asp (RGD) was conjugated to PAMAM dendrimers (G4), these were less potent in causing embryo toxicity as compared to nonconjugated dendrimers.

Dendronized polymers can display a higher loading capacity and allow the bulk incorporation of bioactive molecules of higher molecular weights and of different chemistry, while maintaining high internalization and transfection efficiency as compared to conventional dendrimer (Figure 4). For example, Kono et al. [190] designed PEG-modified dendrimers having a shell of hydrophobic amino acid residues in the peripheral moiety of the dendrimer to increase their encapsulation ability. L-phenylalanine or γ-benzyl-l-glutamate residues were introduced to all chain ends of fourth generation PAMAM dendrimers, and then PEG (M_w 2000) chains were attached to the amino acid residues. Results have shown that the surface engineering of the PAMAM dendrimers improved the binding of Rose Bengal guest molecules than the dendrimer without the external layer.

Dendritic polymers offer an interesting possibility as complexing agents for enhanced transdermal delivery of hydrophobic drugs [100]. Several dendrimers have shown solubility enhancement of drugs such as dexamethasone (Dex), nifedipine, camphotecin, quinolones and indomethacin that are hydrophobic or not very soluble in water [92,100,191,192]. Other studies [193,194] have also demonstrated the ability of PAMAM dendrimers to enhance the solubility of non-steroidal anti-inflammatory drugs (NSAIDs), such as naproxen, ketoprofen, ibuprofen and diflunisal.

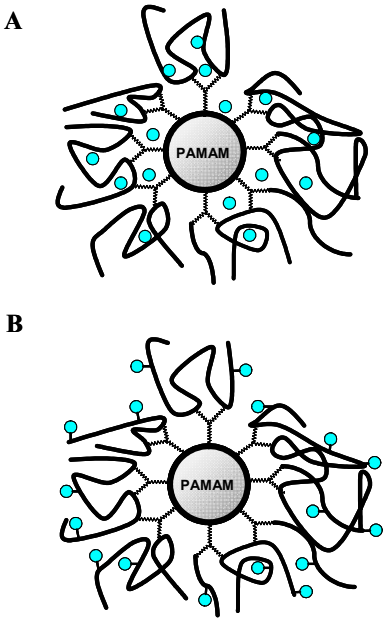

Figure 4. Dendronized polymer loaded with a drug: incorporation in the bulk (A) and covalent bonding to functional groups (B).

The existence of inner cavities with different architectures in the dendrimers can be used to design controlled delivery systems [195], where the drug pharmacokinetics can be modulated as desired [100,196-198]. The interior of the dendrimers needs to be hydrophobic so that a drug can be loaded. The exterior of the dendrimer, however, usually needs to be hydrophilic to improve the bioavailability in the body [198]. Factors such as the ionization state of the drug have also been reported to affect the release of drug from PAMAM dendrimers [199].

On the other hand, high drug loading influences the water solubility of the product and the biodistribution of the conjugates [200]. Agashe et al. [201] have studied the biodistribution pattern of the PPI dendrimer-based carbohydrate (mannose and lactose)-coated glycodendrimers (G5) in mice, in order to explore the potential of these systems as drug carriers. These complexes were found to be stable both *in vitro* and *in vivo*. All systems were cleared rapidly from circulation. Moreover, clearance of mannose-coated PPI dendrimer and lactose-coated PPI dendrimer was faster than PPI alone. All complexes accumulated in liver, but only those with terminal carbohydrate moieties were retained for a longer period of time, which was related to lectin-carbohydrate interactions. This information is significant since it serve as a useful platform in designing carbohydrate-coated dendrimers for the delivery of bioactive agents to liver.

The attraction of dendronized polymers as DDS arises from the possibility to control and refine drug delivery. Actually, they can allow a temporally controlled delivery of single or multiple compounds, since

step-wise degradation can be achieved due to the variety of chemical linkages within their structure (Figure 5).

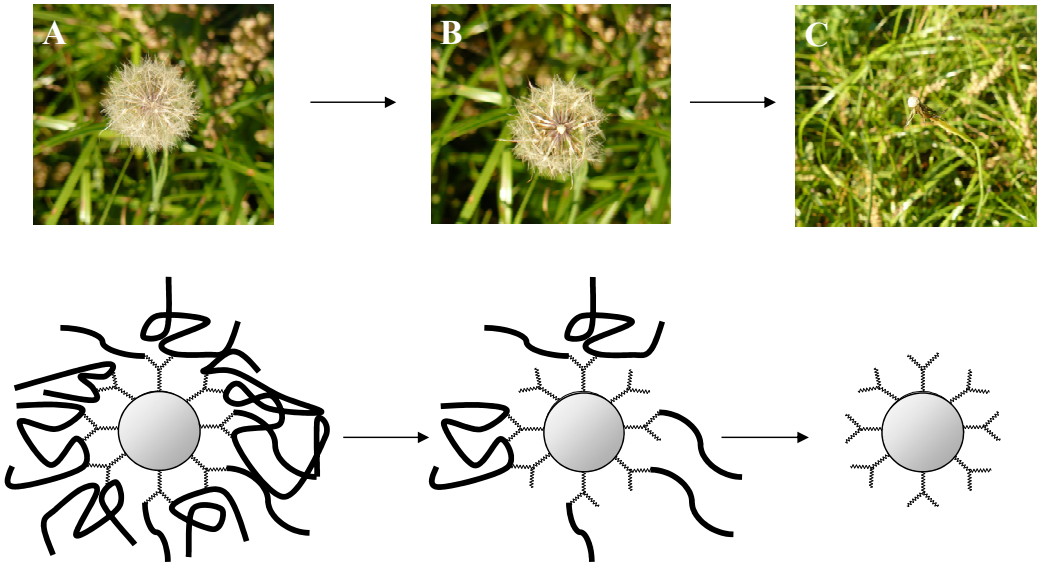

Figure 5. Photos of dendrons and figurative representation of nature's architecture and controlled-release strategy (top). Schematic representation of the step-wise (A→C) degradation of dendronized polymers, from periphery to core (bottom).

Response to certain stimulus is a fundamental process of living systems. Learning from nature inspired scientists to develop materials that respond to external stimuli such as temperature, pH, light, electric field, chemicals and ionic strength [202]. Thus, smart or stimuli-responsive polymers respond to specific changes in their environment and as a consequence dramatic changes in their physical properties occurs (e.g. shape, surface characteristics, solubility, formation of an intricate molecular self-assembly or a sol-to-gel transition). The versatility of smart polymeric materials makes them one of the most appealing interfaces of chemistry and biology. Interestingly, it has been reported [203-206] dendrimers whose degradation can be initiated by different induced-reactions either at the periphery and core, which lead to their complete depolymerization, the so-called self-immolative dendrimers. Hiu et al. [207] have reported on dendritic PAMAM core (G3) and poly(*N*,*N*-dimethylaminoethyl methacrylate) (PDMA) synthesized via a atom transfer radical polymerization (ATRP), the so-called G3-PAMAM-*g*-PDMA. Chlorambucil (CLB), an anticancer drug was used as a model drug. The controlled drug release from polymers with different average graft length of PDMA was investigated by UV spectroscopy. Results have shown that the rate of the drug release could be controlled by pH. Actually, release of CLB from the dendrimer derivative was faster at pH 1.4 than at pH 10.0. Moreover, the release of CLB from G3-PAMAM-*g*-PDMA was apparently slower as compared to that from CLB

incorporated into the PAMAM dendrimer. In addition, these studies have also shown that G3-PAMAM-*g*-PDMA presented a typical thermo-responsive character.

Pistolis et al. [208] have reported on amine-terminated diaminobutane PPI dendrimers (DAB-32 or DAB-64) as pH-sensitive controlled-release systems. As a model system, pyrene was incorporated into the PPIs dendrimers. Release studies revealed that pyrene incorporation is favored in basic environments and mainly close to the core of PPI dendrimers, while its release is induced in acidic media.

Zheng et al. [209] have synthesized dendrimer-star poly(N-isopropylacrylamide) (PNIPAAM) polymers with narrow M_w using dithiobenzoate-terminated PPI dendrimer (G2 and G3) via a reversible addition-fragmentation transfer (RAFT). The aqueous solution of the dendrimer-star PNIPAAM was found to be thermo-sensitive with a LCST around 32˚C. Thus, the use of methacrylic acid along with NIPAAM, not only induce changes in the lower critical solution temperature (LCST) but also allows obtaininge materials responsive to both temperature and pH.

pH and T-activated polymers demonstrated to be successful drug delivery systems. By its turn, photochemical-internalization (PCI) allows site-specific delivery, i.e. escape of the macromolecules from endocytic vesicles into the cytosol. Lai et al. [210] have conjugated doxorubicin (Dox) to PAMAM dendrimers via pH-sensitive and insensitive linkers, acid-labile hydrazone linkages (PAMAM-hyd-Dox) and amide (PAMAM-amide-Dox), respectively. In their study they combined doxorubicin-dendrimers with different PCI strategies to evaluate the cytotoxic effects. Results showed that both PCI strategies promoted the PAMAM-amide-Dox cytosolic distribution, but significantly enhanced the cytotoxicity of free Dox on human gingival cancer (Ca9-22) cells at higher concentrations. The authors failed to develop a multi-modality cancer treatment, but their data provided insights on possible research directions, namely the need to exploit other spacers besides amide-linkage, in drug-polymer complexes.

Papagiannaros et al. [211] have screened the cytotoxic of Dox-PAMAM dendrimer complex attached to liposomes using different human cancer cell lines (e.g. lung, colon, breast, central nervous system and prostate). In this innovative work Dox was incorporated into PAMAM dendrimers (3:1 molar ratio) (1) with an efficiency of 97%, and the anticancer activity investigated. Dox-PAMAM complex was also attached to hexadecylphosphocholine:eggphosphatidylcholine:stearylamine 10:10:0.1 (molar ratio) (2) and eggphosphatidylcholine:stearylamine 10:0.1 (molar ratio) (3) liposomes and the incorporation efficiency was 91 and 95%, respectively. The *in vitro* cytotoxicity tests revealed that Dox-PAMAM dendrimers retained high growth inhibiting activity which was decreased when the complex attached to liposome 3. The activity of Dox was enhanced when hexadecylphosphocholine was incorporated to

liposomal formulation (2). Formulation 2 was superior from all the three formulations against all cell lines tested. It is of interest that the dendrimeric liposomal formulation enhanced the activity of Dox against one type of breast cells. The most sensitive cell lines were those originated from lung cancer, suggesting a selective action of Dox as compared to the rest of the cell lines. This was an incouranging and promosing data, showing that dendrimeric liposomal formulations may be a valuable strategy for the superior performance of DDS aimed at treat several types of cancer.

Wiwattanapatapee [212] investigated the use of dendrimers for colon-specific drug delivery applications. In their studies, 5-aminosalicylic acid (5-ASA) was bound to the water-soluble dendrimer using different spacers containing azo-bond (e.g. *p*-aminobenzoic acid, PABA and *p*-aminohippuric acid, PAH). PAH provide the polymer conjugates a higher loading capacity (3 times) for 5-ASA as compared to that of dendrimer conjugates with PABA as the spacer. *In vitro* studies with cecal content of rats were carried out for investigating drug release from dendrimer conjugates. The release of 5-ASA from both conjugates was significantly slower as compared to that of sulfasalazine (SA), a commercial prodrug. Moreover, the conjugate with PAH linker showed significant higher amount of initial drug release than the conjugate with the PABA linker. As a consequence, the amount of drug released from PAMAM-PAH-SA was significantly higher than that of PAMAM-PABA-SA conjugate. This study nicely illustrated the potential use of PAMAM dendrimer for colon-specific drug delivery, and the important role of the spacers for the optimization of drug release.

Ghorai and coworkers [213] have described the first molecules of anthracene capped chiral dendrimers derived from a 1,3,5-trisubstituted aromatic core and carbohydrate units in the interior and periphery. These are claimed to be suitable for anchoring other useful functionalities aimed at find applications as DDS and light harvesting materials.

It is known that carbohydrate substructures of cell surface glycoconjugates constitute important binding sites for pathogen infection. Dendrimeric systems for use in a lectin-binding assays have been developed [214]. Mannose receptors are present in the surface of monocyte/macrophages (Mo/Mac), alveolar macrophages, astrocytes in brain, and hepatocytes in liver. For example, targeting of anti retroviral drugs to macrophages, which by its turn are the target cells for HIV, could be an attractive approach in improving the therapeutic efficacy and reducing the toxicity of antiretroviral drugs. In this context, Dutta [113] explored the targeting potential and anti-HIV activity of lamivudine (3TC, antiretroviral drug) loaded mannosylated fifth generation poly(propyleneimine) dendrimers (MPPI). The entrapment efficiency of 3TC loaded MPPI and PPI dendrimers (G5) were found to be ~43 and ~36%, respectively. The i*n vitro* release profile showed that mannose-modified PPI slows down drug release as compared to

that of unmodified PPI dendrimers. The results of *in vitro* internalization studies showed significant increase in lymphoblast human T (MT2) cells uptake of 3TC when MPPI was used as compared to that for PPI and free drug. This result evidence that MPPI interacts with the lectin receptors present on the surface of MT2 cells leading to its enhanced cellular uptake. Antiretroviral activity was determined using MT2 cell lines by estimating p24 antigen by ELISA, which is a widely accepted method of quantifying the viral load in HIV infection. 3TC loaded PPI and MPPI formulations were found to possess higher anti-HIV activity, mainly due to the enhanced cellular uptake of 3TC. These data suggest that the proposed MPPI drug delivery carrier has great potential to increase the efficacy and reduce the toxicity of antiretroviral therapy.

Tuftsin, a natural macrophage activator tetrapeptide constituted of Thr-Lys-Pro-Arg, presents a broad spectrum of activities and binds to several cells of immune system. For example, Dutta et al. [112] have synthesized a tuftsin conjugated PPI dendrimers (G5) for targeting to circulating Mo/Mac. These systems proved to hold potential for the controlled and targeted delivery of antiretroviral drugs. Tuftsin-conjugated-PPI stimulated the phagocytic activity of the Mo/Mac especially in HIV infected cells, contributing to the anti-HIV activity of the drug due to its inherent antiretroviral activity. These materials were also found to be non-cytotoxic, *in vivo* [187].

Research on dendrimeric-based artificial virus receptors has been attracting great deal of attention. Yamada et al. [215] successfully synthesized a novel class of carbosilane dendrimer periphery-functionalized lacto-*N*-neotetraose, which is aimed at mimic dengue virus receptor. In another work [214], they synthesized carbosilane dendrimers periphery-functionalized with lactotriaose (GlcNAcβ1-3Galβ1-4Glc) with valencies of three, four, six, and twelve for use in a lectin-binding assay. The hexavalent glycodendrimer showed a 2500-fold larger binding effect than that of free lactotriaose, though the dodecavalent one exhibited only a 1200-fold larger binding effect. Interestingly, the same group also reported [216] on the potential of carbosilane dendrimers periphery-functionalized with galabiose (three, four, and six galabiose residues) for use as artificial inhibitors against Shiga toxins. Bhadra et al. [217] have synthesized PPI dendrimers-coated with galactose and investigated the efficienct on delivering primaquine phosphate (PP, a liver schizonticide) directly to liver cells. Results showed that the coating of PPI systems with galactose increases the drug entrapment efficiency, prolonged circulation and drug release as compared to uncoated PPI delivery systems. Another interesting work reported by Agrawal [218] demonstrated a method for synthesize galactose-coated PLL dendrimers having polyethyleneglycol (PEG-1000) as core. This method consisted on alternating protection and deprotection steps of L-lysine by di-tert-butyl dicarbonate (di-BOC) until the formation of peptide dendrimer (G4) took place. Moreover,

they successfully loaded these macromolecules with chloroquine phosphate, which is extensively employed for the suppression and treatment of malaria. The internalization studies of uncoated and coated drug dendrimer formulations in macrophages revealed almost 5 times reduced phagocytosis due to galactose coating. Galactose coated peptide dendrimers drastically reduced haemolytic activity compared to uncoated PLL formulation. Haematological data suggested that galactose-coating strategy decrease immunogenicity as compared to uncoated formulations.

Carbosilanes bearing saccharide residues on their surface were first introduced by Matsuoka et al. [219]. An innovative work [220], described the synthesis of glycodendrimer via carbosiloxane formation. In this work, a hydrosilylation route for attaching carbohydrate derivatives to carbosilane backbones without using any hetero atoms was described.

Prieto et al. [221] have investigated the cytotoxicity of sulfadiazine complexed with fourth generation PAMAM dendrimers. Cell culture studies using fibroblasts (Vero cells) and macrophages (J-774 cells) have revealed that the dendrimeric sulfadiazine complexes did not affect membrane integrity at low concentrations (0.03 μM). Moreover, cytotoxicity tests using human intestinal adenocarcinoma cells line (Caco-2 cells) results showed that dendrimeric sulfadiazine did not reduce viability of Caco-2 cells over the tested concentrations as compared to that for PAMAM (G4). Remarkably, the *in vivo* study has shown that brain and muscle of Wistar rats are the main targets of intravenous administration of dendrimeric sulfadiazine, which can be advantegeous for drug delivery applications directed to central nervous system.

For efficient encapsulation and delivery of 5-fluorouracil (anti-cancer drug), Bhadra [222] also exploit the surface modification route of PAMAM dendrimers with PEG. PEGylation of the systems was found to increase the drug-loading capacity of the nanocarrier, reduce the drug release rate and haemolytic toxicity. In another work [223], PEGylated PPI (G5) dendrimers were developed for sustained delivery of famotidine, a H_2 receptor antagonist. *In vivo* investigations demonstrated that there was a marked difference in the percentage of drug distribution from the bound drug through PEGylated dendrimer when compared with the free drug. Similar studies were carried out by Haba et al. [224]. They have prepared biocompatible nanocapsules consisting of polyamidoamine (G4) dendrimer having both a PEG chain and a methacryloyl group at every chain end of the dendrimer through an L-lysine residue. Therefore, these works support previous findings showing that PEGylation can increase circulation time, the sustained release of therapeutic molecules and improve haemocompatibility. Recently, Kono et al. [225] provided deeper insights on the designing of dendrimer-based carriers for accurate drug delivery. They have developed PAMAM dendrimers (G4) that have a glutamic acid (Glu) residue at every chain

end of the dendrimer. Then, to obtain PEG-modified dendrimers with sites for conjugation, PEG chains were attached to amino groups of Glu residues. Dox was linked to side chains of the Glu residues by an amide bond, [PEG-Glu(Dox)-G4], or hydrazone bond, [PEG-Glu(NHN-Dox)-G4]. The developed systems were stable under physiological conditions, and Dox molecules were released from PEG-modified dendrimers in acidic environments such as those of endosomes/lysosomes. The Dox-bearing dendrimers showed much lower toxicity to HeLa cells as compared to free drug. However, it was evident that the conjugates with hydrazone bonds exhibited higher cytotoxic effects than those with amide bonds. These results suggest the importance of pH-sensitive hydrazone linkage for high cytotoxicity. Furthermore, the PEG-modified dendrimers exhibited a similar level of toxicity to that of Dox-resistant (SBC-3/ADR100) cells and their parent Dox-sensitive SBC-3 cells.

Early studies have been performed with peptide dendrimers and other peptide-binding dendrimers, to evaluate peptide-protein and protein-protein interactions. These showed that dendrimer-based research can be a valuable tool for elucidating these processes. For example, Tam et al. [105] proposed peptide dendrimers to act as immunogens, also known as multiple antigen peptides (MAPs).

CD derivatives bearing peptides may be useful as carriers for transporting drugs to biological targets containing specific peptide receptors. Thus, the peptide bio-recognizability together with the CD host-guest complexation properties makes such systems suitable templates for the application in site-specific drug delivery. Much effort has been made to complex low generation dendrimers with other polymers. For example, Dodziuk et al. [226] have reported on their attempts to complex a first generation dendrimer having four branches with α-, β- or γ-cyclodextrins, however, NMR studies showed that were not successful. Muhanna et al. [227] have reported a different strategy. Their study has shown the synthesis of tetradecavalent amino acid and peptide dendrimers based on a β-CD core. These were found to have great potential for application in MAP concept as a means to increase the peptide-receptor binding and hence improve the site specificity of the drug delivery system. Imae [228] investigated the binding of PAMAM dendrimer to sodium hyaluronate (NaHA). They successfully synthesized the PAMAM/NaHA complexes. Moreover, the static light scattering data showed that when the dendrimers bind to the NaHA chain, the wormlike character of NaHA is scarcely changed at low mixing $[NH_2]/[COO^-]$ ratios. However, the structure of NaHA changed to a rodlike one at high $[NH_2]/[COO^-]$ values, where the terminal numbers of dendrimers exceed at least five times the repeating unit numbers of a NaHA chain. They postulated that electrostatic interaction is essential but not sufficient to connect such large numbers of dendrimers to NaHA, because the number of amino terminal groups is 42 times larger than the number of carboxylates. Therefore, they concluded that hydrogen-bonding interaction, besides the

electrostatic interaction, should play an important role in the formation of these complexes. For rational design of intracellular nanocarriers, it is important to better understand the transport mechanisms across biological barriers. In general transport of nanosystems is dependent on one hand, on their nature namely their location, function and permeability and on the other, on the nature of the nanocarrier molecules (e.g. molecular weight, charge, hydrophobicity, flexibility) and geometry [229]. Figure 6 shows a simplified representation of the endocytotic route of nanoparticle aimed at act as intracellular reservoir of drugs. Ultimately, these are expected to be release inside the cells and both modulate and control the cell machinery.

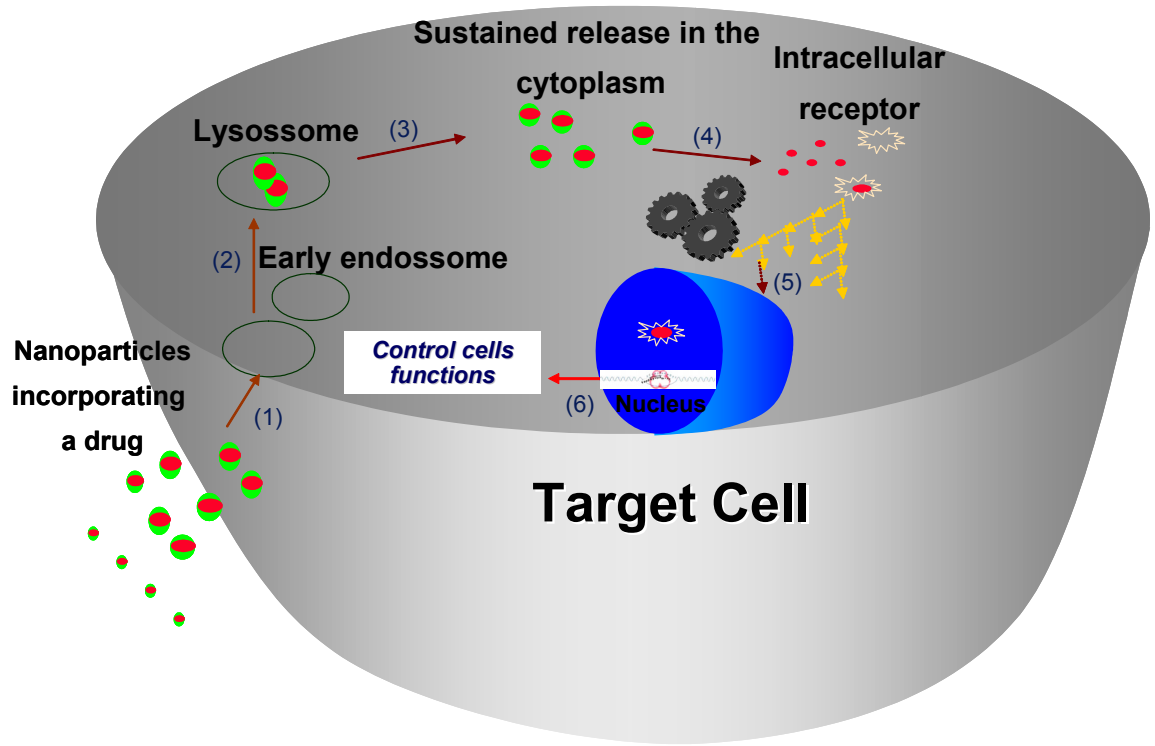

Figure 6. Simplified representation of the nanoparticle intracellular reservoir for the sustained release of drugs, which are aimed at modulate the cell machinery. (1) internalization contact and crossing of the cell membrane; (2) uptake of the vector complex into intracellular endosome; (3) nanoparticles release from the endosome into cytoplasm; (4) sustained drug release and interaction with the intracellular receptor release from the endosome into the cytoplasm; (5) activation of cells machinery or translocation of the complex receptor/drug into the nucleus; (6) gene expression: mRNA transcription and protein translation from mRNA.

Recently, Perumal et al. [230] have investigated the effect of surface functionality on cellular trafficking of dendrimers. In this report, different dendrimers (G4 OH-terminated, G4 amine-terminated and G3.5)

were firstly, labeled with FITC. Results revealed that dendrimers are internalized by human lung carcinoma epithelial cells (A549 cell line). Using inhibitory drugs (e.g. sucrose, chlorpromazine, filipin, nocodazole and cytochalasins) for endocytosis, they found that nanoparticles uptake is mainly by fluid-phase endocytosis, independently of the external functionality. Although, significant differences in uptake mechanisms were seen. For example, anio-nic dendrimers appear to be mainly internalized by caveolae mediated endocytosis in A549 lung epithelial cells, while there were evidences of cationic and neutral dendrimers internalization by a non-clathrin, non-caveolae mediated mechanism that may be by electrostatic interactions or other non-specific fluid-phase endocytosis. Confocal microscopic studies revealed that cationic dendrimers were mostly localized in the endosomes in the cell periphery. By its turn, both anionic and neutral dendrimers were found to localize in the lysosomes. These data have shown that the surface charge of the dendrimers strongly influences their uptake by cells and intracellular localization, thus opening up new possibilities of targeting therapeutic agents to subcellular organels. Pisal [231] investigated the permeability of arginine- and ornithine-conjugated PAMAM dendrimers (G4) across Caco-2 cell monolayers. Firstly, conjugates were obtained by linking the polyamines to the amine groups of the PAMAM dendrimers (G4) using an Fmoc synthetic route, and then conjugates were labeled with fluoroscein isothiocyanate (FITC). The *in vitro* cell culture studies revealed that surface-modification of dendrimers increase permeability. The mechanisms by which the polyamines improve the permeation of the dendrimers remain unclear. Despite, the authors speculated on the disruption of intercellular tigh junctions as one possible mechanism. Similarly, Seib et al. [232] have reported on the endocytic properties and intracellular trafficking of both linear and branched PEIs, and cationic PAMAM dendrimers (G2-4) in B16F10 murine melanoma cells. All polymers were first conjugated to Oregon Green (OG) and carefully characterised in respect of pH- and concentration-dependence of fluorescence. Flow cytometry studies revealed that uptake rate for PAMAM (G4) was the highest, followed by branched PEI, linear PEI, PAMAM (G3) and at last PAMAM (G2). Cells were cultured in the presence of the dendrimers and chlorpromazine or wortmannin to assess the mechanisms of uptake. The precise mechanisms of PAMAM internalisation were once not totally clarified, but the authors suggest that PAMAM (G4) internalisation can be cholesterol-dependent.

When comparing to traditional macromolecular architectures (i.e. linear, crosslinked, branched), the unique features of the dendrimers and dendrimeric systems can improve the cellular uptake, bioavailability of therapeutic molecules inside the cells for long time periods, and consequently decrease the dosage and frequent re-dosage needs. For developing safer and even more efficient dendrimeric

nanocarriers, there is the need to intensify the comprehensive research on the mechanisms of cellular uptake.

3.2. TISSUE ENGINEERING (TE) APPLICATIONS OF DENDRIMERS AND DENDRONIZED POLYMERS

In the recent years, great advances have been done in the emerging field of TE and regenerative medicine. Many important data have been published, and thus there is a need to overview the most recent achievements and scientific considerations in this particular area of research. The objective of this section is to highlight the most recent and relevant reports in the field of TE and regenerative medicine, and stress its utility and feasibility by giving some examples of successful clinical treatments. Due to the multidisciplinary nature of this field we were encouraged to cover many other related issues, even if succinctly. The regenerative potential of different cells (and its sources), and the control of its functions by means of using different bioactive agents will be discussed. The TE strategies used for the regeneration of specific body parts are also addressed as well as the requirements (e.g. cell/material interactions and surface chemistry) that should be met for optimal performance of the TE cells-scaffold constructs. The role of bioreactors in TE is also briefly discussed. Finally, new promising strategies are proposed, namely the use nanocarriers such as dendrimers and dendronized polymers for the controlled and targeted delivery of bioactive agents that are aimed at modulate the cells functions such as proliferation and differentiation.

3.2.1. TE strategies: an overview

In our body there are different cell types, which can be categorized as follows: (i) germ cells, (ii) somatic cells, and (iii) stem cells. Germ cells are cells that give rise to gametes, male and female. Somatic cells are the specialized ones and make-up the adult body. In their differentiated state they may possess one or more copies of the genome, with the exception of erythrocytes which do not possess any. Finally, stem cells can be defined as cells that possess the capacity of divide indefinitely (proliferate) in culture and potentially may also differentiate into functionally distinct lineages [233]. Stem cells can be grouped according to the source or tissue of origin. Alternatively, they can also be classified for their capacity of differentiation or “cell plasticity” as: (i) totipotent, i.e. can differentiate in all types of specialized cells of the body, including entire fetus and placenta; (ii) pluripotent, i.e. can differentiate in several cells types of all three germ layers (ectoderm, mesoderm and endoderm), but not the whole organism; (iii) multipotent, i.e. can only differentiate in limited type of specialized cells; and (iv) unipotent, i.e. can only give rise to one differential cell lineage.

Due to the limited regenerative capacity of the body, there is the need for developing more effective treatments to cure the several spontaneous and injuries-related diseases. It is well known that in mammalian tissue repair mechanisms results from the activation of pre-existing stem cells or progenitors cells. Moreover, the identification of several stem cells sources and their isolation promise to revolutionize the concept of regenerative medicine, since allows us to develop numerous cell-based therapies.

In the early 1990s, Langer and Vacanti [234] coined TE as ''an interdisciplinary field of research that applies the principles of engineering and the life sciences towards the development of biological substitutes that restore, maintain, or improve tissue function''. This concept is based on understanding of how tissue formation and regeneration occurs, and instead of traditional implantation of new spare parts it envisions to induce new functional tissues. To accomplish this goal, three main therapeutic strategies have been proposed [235]: (i) implantation at injury site of freshly isolated cells (e.g. own patient cells) or cultured cells (differentiated cells alone or in combination with stem cells, for example); (ii) *in situ* tissue regeneration, i.e. implantation of a scaffold at the diseased/damaged tissue aimed at promote healing/repair by the patients own cells; and (iii) implantation of tissues obtained from combining cells and scaffolds that are cultured *in vitro* with or without the presence of bioactive molecules. Thus, the basic TE triad consists of cells, scaffolds and bioactive agents which can be used separately or in combination. By its turn, regenerative medicine uses the cell and tissue engineering principles for the regeneration of damaged/disead body tissues.

For cell therapy, either differentiated (e.g. autologous chondrocytes) [236] or undifferentiated (e.g. stem cells) cells [233,237] can be used. Despite, the use of stem cells in clinical practice is still limited since raises many problems and concerns, specially a sub-type of stem cells, the embryonic stem (ES) cells. This problematic is not only due to ethical/religious issues [238,239], safety [240,241] or technical limitations, but also to the legislative/regulatory constraints [233,242]. Adult stem cells are seen as an alternative to ES cells, as their clinical use seems to be safe, without complications and major ethical issues concerns [243,244]. Stem cells can proliferate and differentiate beyond the tissues in which they normally reside or may be artificially placed [245]. In fact, it has been shown that bone marrow-derived stem cells cannot only reconstitute bone marrow but are capable of forming several types of mesenchymal tissues, including bone [246], muscle cells [247], lung and gut [248]. For example, cell sheet transplantation has been proving to be a breakthrough therapeutic strategy for treatment myocardial infarction [249], among others.

The intensive research efforts and technological advances allowed to identify and isolate different types of stem cells from germ cells, embryo, fetus (e.g. fetal blood, placenta and umbilical cord blood), and

adult tissues and organs [250-255]. In addition, it was reported the isolation of stem cells derived from amniotic fluid that express embryonic and adult stem cell markers [256]. The amniotic fluid-derived stem cells were found to be pluripotent, meaning that has the potential to differentiate into cell types representing each embryonic germ layer, including cells of adipogenic, osteogenic, myogenic, endothelial, neuronal and hepatic lineages.

Interestingly, differentiated cells can be reprogrammed to a pluripotent state by transfer of nuclear contents into oocytes, by fusion with ES cells, and for male germ cells by cell culture alone. Recently, Takahashi and Yamanaka [257,258] demonstrated that pluripotent stem cells can be directly generated from fibroblast cultures, the so-called induced pluripotent stem (iPs) cells by retrovirus-mediated transfection with four transcription factors, namely Oct3/4, Sox2, c-Myc, and Klf4, under ES cell culture conditions. The four factors, however, can not fully explain iPs cell induction [259]. Though, this step further has major implications in regenerative medicine as for the first time, it is possible to create pluripotent cells directly from somatic cells of humans [260].

For *in situ* tissue regeneration and tissue implantation there is the need to use temporary matrices for tissue growth, the so-called scaffolds [261,262]. Though, as stressed by different authors [263,264] the strategy to implant cells with scaffolds (constructs) is oftenly considered wiser, as it allow a rapid and correct vascularization of the tissue to be repaired. Scaffolds with special design [265], tunable degradability and mechanical properties [266,267], biocompatible and capable of sustaining dense populations of cells [268,269] are being developed. The role of the scaffold is temporary, but crucial to the success of the therapeutic strategy. Thus, the criterious selection of a biomaterial is of major importance. Synthetic biomaterials have been processed in a variety of matrices [270-272], other used for their bioactive ability [273], and new cell-scaffold constructs strategies [274,275] are being designed to allow the development of biological and mechanically functional artificial tissues/organs.

Scaffolds architecture, namely porosity, pore size and interconnectivity of the biomaterial scaffolds are also known to play a critical role in tissue formation [276]. However, the balanced porosity/mechanical performance of the scaffolds is an issue that cannot be forgotten, and thus should also be exploited further.

Surface properties of the scaffolds also dictate the response of cells and possibly tunning cell behaviour, and promote cell adhesion, cell orientation and cell motility [277-279], etc. Various techniques have been used to fabricate micropatterned surfaces of different materials, including microlithography [280], microcontact printing [281,282], and many others.

Growth factors (GFs) and other bioactive molecules may be provided to control the cellular functions either from culture media [283,284] or simply by incorporation into the scaffold [285,286] which can be more advantageous. The cells on their scaffold need to be typically cultured in custom-designed bioreactors [236,287] as mechanical forces may be required [288,289], either through fluid stresses or structural stresses, in order to provide further stimuli to cell function. Quite oftenly, this process may take days or weeks until it forms a tissue similar to that aimed at repair/regenerate. With simple tissues only one cell type may be involved (e.g. chondrocytes in cartilage repair), but in other situations, more than one cell type may be needed, as tissue to be regenerated consists of multiple structures (e.g. osteochondral tissues) [290,291]. Thus, this will require considerable sophistication with respect to the bioreactor system itself. To achieve superior tissue formation *in vitro*, great efforts have been made to develop and improve a wide variety of bioreactors, including spinner flasks [292,293], recirculation bioreactors [294,295], rotating wall vessels (e.g. uni- and bi-axial bioreactor rotation) [296-298], among others.

3.2.2. Dendrimers and dendronized polymers in TE

The use of dendrimers architectures in cells and TE applications is still in its infancy. Few examples have been reported, and these are mainly related with applications in cell adhesion studies as nanopatterning [299]. Interestingly, ligand-modified dendrimers have been proposed for use as substratum for cell culture and high performance bioartificial organs [300].

On the other hand, it has been reported [87] that when a dendrimer reaches a certain generation (a variable factor according to the dendritic structure but in general equal to or greater than G4), significant conformational change occurs, and the structure assumes a densely packed globular shape. Several authors [79,87,301] have been discussing the potential of tunning dendrimers to develop macromolecules that can mimic globular proteins. In fact, partial core shell-filled tecto(dendrimers) can be obtained by covalently assembling PAMAM dendrimers (nucleophilic or electrophilic) around other electrophilic or nucleophilic core dendrimers [302]. This feature allows many new technological applications. One possibility is to take advantage of dendrimer architecture towards resembling the role of different proteins in the cells culture media. For example, dendrimers may be a valuable tool on the development of synthetic serum-free culture media and adequate substratum for superior cell culturing. Fluorescence spectroscopy, differential scanning calorimetry and fluorescent probes studies [303,304] showed that dendrimers interact with proteins giving rise to stable complexes by establishing both electrostatic and non-electrostatic interactions.

Kim et al. [305] have also investigated the response of human epithelial cells to dendrimer-immobilized substrates with or without D-glucose displayed as a terminal ligand. When the topographic surface possessed a roughness of 4 nm epithelial cells cultured on naked dendrimer surface without D-glucose were somewhat stretched in their morphology compared with those on a nonmodified plain surface. However, for the roughness values higher than 4 nm cell stretching was inhibited, thus resulting in the predominant existence of round-shaped cells. The change in cell morphology was quite evident on the surfaces with D-glucose-displayed dendrimers. Fluorescence microscopic observation showed that when the roughness value increased up to 4.5 nm on these surfaces, an enhancement of cell stretching occurs. These results suggested that surface roughness and D-glucose display induce changes in cellular morphology caused by the cytoskeleton formation accompanied by marked cell elongation. Therefore, this study demonstrated that dendrimer surfaces can offer a promising design for optimizing cells culture conditions.

In the work reported by Benhabbour and colleagues [306], it was demonstrated that cells showed a greater affinity for the dendronized surfaces as compared to the Au surfaces (control). Moreover, *in vitro* cell culture studies with mouse 3T3 fibroblasts showed that cell attachment was diminished for the PEG-grafted Au surfaces as compared to the control Au and G1-G4 dendronized surfaces. These results showed that dendronized surfaces presenting a large number of hydroxyl groups can be a reliable alternative to the use of peptides to promote cell adhesion and proliferation.

3.2.2.1. Bone TE

Bone is a very dense and specialized form of connective tissue, highly specialized in the several regions that constitutes it and acts as a support for the body. Bone lesions above a critical-sized segmental defect still remain a huge challenge to reconstructive surgery and regenerative medicine. This is mainly due to the fact that bone has a limited ability to heal [307,308]. In many clinical situations there is the need for a surgical intervention and use of autografts [309,310], allografts or xenografts [310,311] transplantation. Still, the preferred clinical strategy is the autologous transplantation, since it avoids the problem of immune rejection [312] and consequent administration of drugs for immunosupression of the host [313]. Therefore, we can state that the currently available treatment possibilities are far from being a truly ideal solution. Recently, it has been applied the TE principles [314], i.e. by seeding bone marrow stem cells onto scaffolds (constructs) [315] or prostheses [316] to recreate an regenerative environment at the defect area and achieve a superior bone healing. Despite the important advances, the performance of constructs remains limited, in part due to the need of optimize cell culture techniques [317]. To circumvent

these limitations great efforts are focused on developing novel nanocarriers aimed at modulate cells behaviour. Previously, our group [184] has investigated investigated if the Dex-loaded CMCht/PAMAM dendrimer nanoparticles can play a crucial role in the regulation of osteogenesis, *in vitro*. In this work, the uptake efficiency and mechanism of FITC-labeled CMCht/PAMAM dendrimer nanoparticles using rat bone marrow stromal cells (RBMSCs) was investigated. Fluorescence microscopy studies revealed that the developed nanocariers could be efficiently internalized by RBMSCs, after a few hours (Figure 7). Flow cytometry studies revealed that RBMSCs cultured in the presence of colchicine, an endocytotic inhibitor, reduce the internalization of the nanoparticles. These data showed that uptake by cells was primarily via an active endocytosis mechanism, but not exclusively. Moreover, the biochemical data demonstrated that the Dex-loaded CMCht/PAMAM dendrimer nanoparticles were not cytotoxic and promote osteogenesis (2-D system).

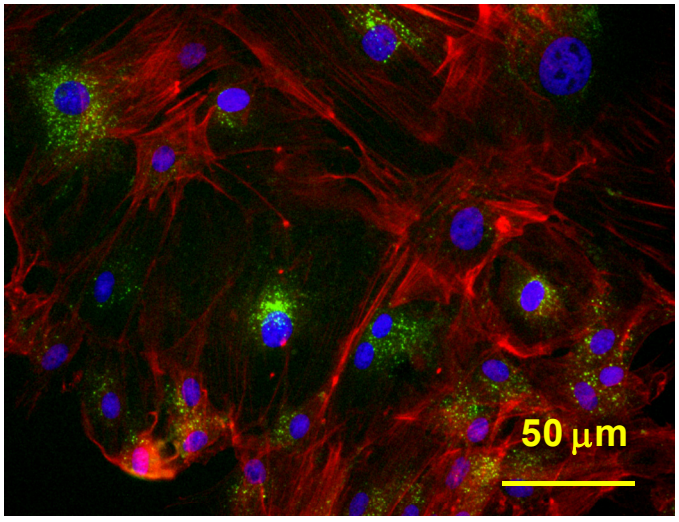

Figure 7. Fluorescence microscopy image of the RBMSCs cultured in the presence of FITC-labeled CMCht/PAMAM dendrimer nanoparticles (green) for 7 days. Nuclear DNA and cytoskeleton were labeled with Hoechst 33258 (blue) and Texas-Red phalloidin (red), respectively.

Recent studies [318,319] have shown that combination of hydroxyapatite (HAp) scaffolds, bone marrow stromal cells and Dex-loaded CMCht/PAMAM dendrimer enhanced osteogenesis *in vitro* (3-D systems), and *de novo* bone formation as compared to controls, *in vivo* (Figure 8). Remarkably, animal studies have shown that the novel Dex-loaded CMCht/PAMAM dendrimer nanoparticles may be beneficial as intracellular nanocarrier, supplying Dex in a regimented manner, while avoiding the need of culturing the cells *in vitro* for long periods of time. Moreover, this strategy allows modulate and direct stem cells differentiation towards the osteogenic phenotype, and enhance *in vivo* proteoglycan ECM synthesis and

de novo bone formation. It has also been exploited dendritic monomers as components in dentistry applications to allow polymerization to extend further, as incomplete polymerized matrixes can cause irritation, allergy or toxicological effects [320]. In fact, photopolymerized dendritic copolymers and particulate filler composites have been combined to be used as dental restorative materials [321]. In that study, dendritic monomers were found to enhance the copolymerization of methyl methacrylate and to lower the viscosity, which can be advantegous to improve biocompatibility of the fillers.

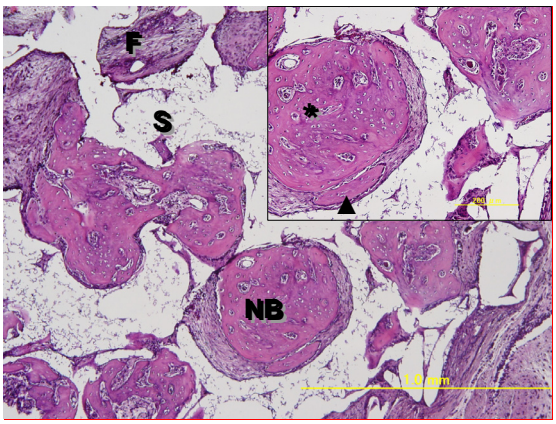

Figure 8. Light microscopy photographs of the HAp-RBMSCs implant section (decalcified), stained with Haematoxylin & Eosin after 4 weeks of subcutaneous implantation: HAp scaffold seeded with $1x10^6$ RBMSCs that were expanded *in vitro* (7 days), in MEM medium supplemented with 0.01 $mg.mL^{-1}$ Dex-loaded CMCht/PAMAM dendrimer nanoparticles, prior implantation. It is possible to observe representative areas of the HAp scaffold (S), *de novo* bone formation (NB), fibrous tissue (F). Black arrows reveal the cells lining which is suggestive of active osteoblasts. Osteocytes can also be visualized (*).

3.2.2.2. Cartilage TE

In the human body, it can be found two main types of cartilage, namelly the “unstressed” and “stressed” cartilage, in ear and joints, respectively. General features of cartilage tissue includes: (i) a small number of chondrocytes (less than 10% of the weight of articular cartilage) with low proliferation rate and having both catabolic and anabolic functions; (ii) a high content of water (75% of the wet weight of articular cartilage); (iii) an abundant ECM composed by proteoglycan and different types of collagens (mainly type II), corresponding to 15-30 and 50-73% of the solid ECM weight, respectively; and (iv) possess no nerve and vascular systems [322,323]. Although a classical wound healing response is initiated, articular cartilage lesions are repaired without complete restoration of the components and architecture of the

native tissue. This is explained by the fact of being an avascular tissue, regenerative cells cannot migrate to the defect void unless the lesion goes beyond the subchondral bone plate [324,325]. Therefore, a regenerative response will be only possible when it is provided an artificial access by the marrow [326]. This consideration is subjacent on several clinical strategies that are currently employed on the treatment of small cartilage lesions namely, the subchondral abrasion, Pridie's perforations, micro-fracture, and transplantation of osteochondral plugs [325,327-329]. Although, in most cases after clinical intervention the repaired tissue tends to degenerate and occur the formation of the undesired fibrocartilage [324,330,331]. Many attempts have been made to develop biomaterials for cartilage repair/regeneration. Few have exploited the advantages of dendrimers for this type of applications. Sontjens and colleagues [332] have synthesized a photocrosslinkable hydrogel scaffold for cartilage repair based on triblock copolymer consisting of PEG core and methacrylated-poly(glycerol-succinic acid) (PLGSA) terminal blocks. *In vitro* chondrocyte encapsulation studies demonstrated that the developed hydrogels supported synthesis of proteoglycans and type II collagen, which denote cartilaginous extracellular matrix formation. Morever, encapsulated chondrocytes showed no signs of dedifferentiation. Despite the promising results *in vitro*, the authors discussed the need to improve mechanical properties and tailor the degradation rate of the developed hydrogels for the superior performance of the hydrogels, *in vivo*.

3.2.2.3. Ocular wounds

Another example of dendrimer applications in TE is related with the attempts to improve the biological response of different biomaterials. In another study [42], laminin-based peptide YIGSR was introduced into the dendrimer-collagen hydrogel by linking the peptide to the residual dendrimer amine groups. The incorporated YIGSR peptide promoted the adhesion and proliferation of the corneal epithelial cells cultures onto the collagen hydrogel, *in vitro*. Moreover, neurite extension and nerve cell density was enhanced on these materials relative to unmodified gels or controls. This work is an unprecedented example of the ability to tune the biological function through the dendrimer crosslinker and a new strategy towards obtaining polymer-based tissue-engineering scaffolds with improved biological performance.

Inspired by the functional significance of collagen in nature and its remarkable physiological roles, Khew et al. [333] have developed enzymatically crosslinked collagen-mimetic dendrimers. These were obtained in two-step procedure: (i) collagen-mimetic peptides supplemented with a cell-binding sequence (GFOGER) and enzyme-specific crosslinking domains (EDGFFKI and APQQEA) were conjugated onto

a PAMAM dendrimers (G2), resulting in a crosslinkable collagen-mimetic dendrimer, and (ii) enzyme-mediated crosslinking the different collagen-mimetic dendrimers by tissue transglutaminase. Collagen-mimetic dendrimers were first assessed for their cytotoxicity and then adhesion studies were carried out using L929 mouse fibroblasts and a hepatoma cell line (Hep3B cells), respectively. Results were indicative of the non-cytotoxic nature of the polymers. The adhesion studies have proven that enzymatic protein crosslinking, which is a common physiological event in the extracellular environment, can significantly improve cell adhesion on the novel collagen-like biomaterial. Moreover, it was observed that combining of collagen-like structural domain and biologically relevant epitopes (e.g. cell-binding sequence and enzyme-substrates) into the molecular design of a biomimetic collagen could be a promising approach for mimicking more closely its biological function.

Repair of wounds after traumatic or surgical injury is of significant clinical and research importance. For example, corneal wounds arise from surgical procedures (e.g. transplants, incisions for cataract removal and intraocular lens implantation, laser-assisted in situ keratomileusis), infections (ulcers), and traumatic injury (lacerations, perforations). Nowadays, these wounds are repaired using nylon sutures but this technique is not ideal because the suture material does not actively participate in healing and the procedure is inherently invasive. Therefore, alternative strategies using adhesive polymers have been tested. For example, Duan et al. [334] crosslinked collagen with multifunctional dendrimers. PPI octaamine dendrimers (G2) were used to generate highly crosslinked collagen hydrogels with mechanical properties that would make it appropriate for use as a corneal TE scaffold.

For the superior performance of ocular wounds, hydrogel adhesives should meet some criteria, namely: (i) adhere to the moist corneal surface and seal the wound to withstand high intraocular pressures; (ii) possess adequate rheological properties to permit a controlled and rapid placement; (iii) ability to seal the corneal wound in a controlled manner and restore the intraocular pressure; (iv) maintain the structural integrity of the eye and possess a refractive properties resembling as much as possible to native cornea; (v) be biocompatible and provide a microbial barrier; and (vi) be biodegraded or bioabsorbed on a time scale consistent with tissue regeneration.

Grinstaff and coworkers [335] have developed a set of dendrimeric adhesives composed of dendrimers of different generation (G1, G2 G3) combined with PEG, glycerol, and succinic acid for finding application in the repair of corneal wounds. The polymer was modified to contain terminal methacrylate (MA) groups, [G1]-PGLSA-MA)$_2$-PEG. Two strategies to develop the ocular adhesives were explored: (i) the use of a photocrosslinking reaction to form the dendrimer-PGLSA-MA)$_2$-PEG, and (ii) the use a peptide ligation reaction to couple the individual dendrimers together to form the lysine-based dendron with

terminal cysteines adhesive hydrogel G2-$(Lys)_3$-Cys_4) and PEG-dialdehyde (PEG-DA). Both strategies strategies afford hydrogels that are adhesive, transparent, elastic, hydrophilic, and soft. The *in vivo* studies in chicken eyes have shown that the photocrosslinkable ([G1]-PGLSA-MA)$_2$-PEG adhesive completely sealed the linear lacerations on post-operative day. By its turn, the histological studies demonstrated that wounds sealed with these adhesive gels appeared to be more complete as compared to sutured wounds, after 28 days. By its turn, the dendron ([G2]**-**$(Lys)_3$-Cys_4) and PEG-DA show to be effective on the repair of corneal lacerations and required less surgical time than conventional suturing, *ex vivo*. The advantage of the photocrosslinked gels lies on the ability of the polymer to crosslink and adhere to the tissue where the clinician directs the light. However, the limitation is the potential risks with ocular damage when using light. Thus, the crosslinking strategy based on peptide bonding show to be more attractive since it can avoid the need for light and the reaction is performed at neutral pH; thus the polymer can be crosslinked upon placement on the tissue.

3.2.2.4. Diagnosis and inflammation

In autograft transplantation, biopsies are performed harvesting the smallest amount of tissue possible from patients to prepare starter cells. Oftenly, tissue is lised and cells are expanded. During culturing changes in intracellular states can cause variation in individuality in a cell population and cells behavior. Moreover, due to terminal differentiation cellular senescence can occur. Therefore, there is the need to investigate the cellular status, prior implantation into the patient. In this context, Hata el al. [336] have proposed a novel image analysis methodology based on the observation of the partial anchoring of the cells to a glucose-dendrimer immobilized culture surface as a mean to evaluate the formation of the cellular cytoskeleton in a non-invasive manner. In this study, formation of the cellular cytoskeleton was correlated with the growth cellular potential. This innovative method allowed observation of the cells morphology, and conclude on the regenerative potential of the cells to be used in TE strategies.

In the last few years, there has been a great interest [337,338] in the mediators responsible for the selective recruitment and activation of immune cells at inflammatory site. Among these mediators, chemokines have received particular attention in *in vivo* studies involving the investigation of cytokine-associated responses to biomaterials [234]. Chemokines are a large family of small (7,000-15,000 Da, from 67 to 127 amino acids in length), structurally related heparin-binding proteins, which are classified into 4 subfamilies according to the configuration of cysteine residues near the N-terminus, depending on whether the first 2 cysteines are separated (CXC, CX3C) or not (CC, C) by an intervening amino acid [339].

Chemokine messages are decoded by specific receptors [340-342] that initiate signal transduction events, leading to a multitude of cellular responses, including chemotaxis and activation of inflammatory and bone cells. Thus, the development of synthetic chemoattractants by linking small peptide sequences that are known to interact with chemokine receptors to dendrimers and, when appropriate, chemokine inhibitors [343] can be envisioned. In regenerative medicine, the development of dendrimer-based chemoattractants can find interesting applications towards recruiting stem cells [344]. This unexploited area can open up new therapeutic avenues, not only for treating autoimmune diseases but also, to be used in innovative TE strategies, since it can lead to the superior repair/regeneration of damaged/diseased tissues by endogenous cells.

3.3. CENTRAL NERVOUS SYSTEM (CNS) APPLICATIONS OF DENDRIMERS AND DENDRONIZED POLYMERS

In spite of deeply studied, the brain and the central nervous system (CNS) still encase many mysteries, and therefore its pathologies still represent a major challenge for biomedical science. Neurodegenerative disorders such as Parkinson's or Alzheimer's disease, stroke, brain tumours or multiple sclerosis (MS) are among leading debilitating diseases within our society to which a feasible and long lasting therapeutic approach is yet to be found. In the next lines we will give a short overview on the CNS properties, as well as how drug delivery systems, and in particular dendrimers, may be used to develop strategies that hinder some of the symptoms of the above referred therapies.

3.3.1. The central nervous system: basic concepts

The nervous system is structurally divided in two sections [345,346]: (i) central nervous system, and (ii) peripheric nervous system (PNS). The first is constituted by the brain and spinal cord, and is considered to be the "command post" of the nervous system. It is responsible for the interpretation and processing of the information that is hand over by the PNS, which is constituted by an array of nerves, that are spread out through the body and connected to the spinal cord, and have as main function to gather information from the outer/inner environment. In this sense the spinal cord can be looked as an information "highway" transmitting information from and into the brain, playing therefore a leading role on the normal functioning of the CNS.

From the cell biology point of view the CNS is composed of two cell types, neurons and glial cells.

Neurons are considered to be the structural and functional unit of the CNS. Its main characteristic is based on the ability to respond and conduct electrochemical impulses, being their actions mainly mediated through the release of chemical regulators known as neurotransmitters [346,347]. Although

neurons can considerably change in shape and size, they are normally divided in three areas: the cell body or soma, dendrites and the axons [346]. The cell body, as its name implies is the area where all nucleus and the remaining organelles are located, and therefore is considered as the "nutritional centre" of the neuron, as it is the place where macromolecules found to be essential to neuronal survival are produced [348]. The dendrites can be looked as extensions of the cell body that provide an extended surface area for the reception of the nervous impulses, transmitted by neighbouring neurons, to the cell bodies [347]. Finally, the axon can also be looked as an extension protruding from the cell body, although much more differentiated than the dendrites. It is through this structure that the nervous impulses are conducted from the cell body to the axon terminals, where neurotransmitters will be released to adjacent neurons to an area denominated as synaptic cleft [346,347]. The axon is normally surrounded by a lipoproteic sheath of myelin. The latter acts mainly as an electric insulator, allowing in this sense a faster transmission of the nervous impulse. The areas of the brain that are rich in myelinated fibers are known as white matter while the areas containing the cell bodies are known as grey matter [346,347].

The glial cells are the second cell type of the central nervous system. They are more abundant than the neurons. Glial cells are mainly involved in supporting functions, such as the maintenance of the ionic balance of neurons, the modulation of the synaptic transmission and the re-establishment of the neurological function upon neuronal damage, although, this is not always possible, as in the case of spinal cord injury (SCI). Three cell populations can be found among glial cells [346]: (i) astrocytes, (ii) oligodendrocytes, and (iii) microglial cells.

Astrocytes are the most abundant glial cell type. They are commonly located in the vicinities of blood vessels and neurons, and are, among others, responsible for mediating the synaptic transmission by removing, from the synaptic cleft, neurotransmitters that will be later on "recycled" and made available again to neurons.

Oligodendrocytes are the cells involved on the production of the myelin sheath, that encases the neurons, and thus are of the utmost importance within the CNS [345].

Microglial cells play an important role within the CNS, as they are considered to be the immune mediators of the latter, possessing a macrophage-like behaviour, eliminating death tissue and cells by phagocytosis, as well foreign agents. They possess two states, which mainly reflect their state of activation. Ramified microglial cells are considered to be in the resting state. They are characterized by possessing long cytoplasmastic processes, a small cell body and few lysosomes. On the other hand activated microglia is characterized by ameboid morphology, with a large cell body and a large number of lysosomes, which indicates a high phagocytotic capacity [349].

3.3.2. Blood brain barrier (BBB)

The brain is protected from the rest of the body by structures known as barriers that most oftenly represent a major hurdle for the delivery of diagnostic and therapeutic agents [350]. In fact most of the systemically administered drugs do not enter the brain in adequate amounts, which most of the times leads to an increase of dosage that can lead to undesirable side effects. The most well known barrier is the BBB, which consists of “walls” of capillaries that separate brain from the circulating blood [350]. Its low permeability is mostly attributed to brain micro-vessel endothelial (BMVEC) cells which form tight junctions and have a low pinocytic potential [350-353]. Moreover, the BBB is also formed by astrocytic processes, leptomeningeal cells and a parenchymal membrane that overall isolate the brain from unwanted molecules [350]. However, not all molecules are “unwanted” by the BBB. For instance, the latter provides for selective transport of small molecules, lipophilic and low molecular weight compounds, polypeptides ad even cells to the CNS. In particular, nutrients and endogenous compounds such as amino acids, glucose, essential fatty acids, vitamins, minerals, electrolytes' are effectively carried by the BBB. Most of these processes are based on receptor-mediated endocytosis [351]. Receptors such as insulin, transferrin, endothelial growth factors, amino acids, glucose (GLUT 1) transporter are known to be expressed by the BBB, for example [351]. In this sense the BBB can be seen as regulatory membrane, which selectively allows the passage of essential molecules to the homeostasis of the CNS, while inhibiting what is believed to be “harmful” ones. Thus, when designing a strategy to deliver a therapeutic agent into the CNS one must understand the properties of the BBB in order to allow an efficient delivery nanocarrier to the target site (s).

3.3.3. Dendrimers and dendronized polymers in CNS

As referred before drug delivery to the CNS is tremendously challenging. Initially films, tablets, microspheres and intracranial polymeric materials were tested for these applications. However, as recently reviewed by Kabanov and Gendelman [350], such strategies had limited success namely due to their invasiveness, inflammatory responses to implants and limited distribution of therapeutic molecules around the implantation site. It was in this context that nanomedicine based approaches started to be put forward as a possible solution. Within these one can found liposome’s [354,355], polymeric nanoparticles [356,357], and nanogels [358]. Particularly interesting for the above referred applications are also dendrimers [359]. Surprisingly, their application to the CNS is also still quite scarce. Nevertheless, some nice examples can be drawn from the literature of the possible applications of these systems for drug delivery in the CNS. For instance Suppatone and co-workers [360,361] suggested the use of

dendrimers for the removal of prion effection. In a couple of studies it was reported that branched polyamines, including PAMAM, PPI and PEI dendrimers, were able to purge PrPSc, the protease-resistant isoform of the prion protein, from scrapie-infected neuroblastoma (ScN2a) cells in culture. The removal of PrPSc by these compounds depended mainly on both the concentration of branched polymer and the duration of exposure. Structure-activity analysis revealed that a high surface density of primary amino groups was required for polyamines to eliminate PrPSc effectively from cells. In a subsequent study it was also demonstrated that exposure of ScN2a cells to 3 $mg.mL^{-1}$ of PPI (G4) for 4 weeks not only reduced PrPSc to a level undetectable by Western blot but also eradicated prion infectivity as determined by bioassays in mice. Moreover exposure of purified RML prions to branched polyamines *in vitro* disaggregated the prion rods, reduced the β-sheet content of PrP 27-30, and rendered PrP 27-30 susceptible to proteolysis.

Cationic phoshorous dendrimers have also been proposed for the same applications, also through inhibition of fibril assembly [362]. Spectrofluorometric assays with thioflavin T (ThT) and Fourier transformed infra-red (FTIR) spectroscopy show that these class of phosphorous dendrimers were able to clearly interfere with PrP 185-208 aggregation process by both slowing down the formation of aggregates (by causing a decrease of the nucleation rate) and by lowering the final amount of amyloid fibrils, a common hallmark of conformational diseases. In fact, time-course experiments demonstrated that phosphorus dendrimers were able to remove quickly existing PrPSc molecules and the clearance occurred within 4 hours of treatment [115]. The mechanism behind these actions is mostly unknown. However, similarly to what happens with PAMAM dendrimers, the breakage of oligomers or whole fibrils caused by dendrimers has probably a strong role on the observed phenomena. A similar report was also put forward by Klajnert et al. [114]. In this particular study, PAMAM dendrimers (G3) were used to control the nucleation rate of amyloid plaques. The outcome of these studies revealed that dendrimers can modulate the aggregation process by affecting the nucleation rate at low concentrations. However, at higher concentrations it seemed that dendrimers promoted the elongation of this nucleation chains. Therefore, the interest in the reported effect of dendrimers has to be considered within the ongoing search for compounds that can affect amyloid formation and in relation to the structural intermediates in this process which are responsible for the cytotoxic effects. In this sense low dendrimer concentrations could contribute to a decrease of the lifetime of low molecular weight intermediates and contribute to decrease the potential cytotoxic effects of the peptides. For instance Patel et al. [363] described the use of modified PAMAM dendrimers for Alzheimers' disease. In this particular case sialic-acid-conjugated

PAMAM dendrimers using a physiologically relevant attachment of the sialic acid to the dendrimeric termini were prepared.

Another route to use dendrimers for CNS related applications, namely for transfection purposes, is by coating the latter with specific peptides. An example of such an approach was the one presented by Kim and colleagues [364,365], in which arginine-grafted PAMAM dendrimers were used. In this case these PAMAM-Arg dendrimers were complexed with expression of both a reporter gene (luciferase expression plasmid pCN-Luci) and a high mobility group box 1 (HMGB1) shRNA transgene-expressing plasmid for gene knock down. Results revealed that these PAMAM-Arg/DNA complexes showed particularly high transfection efficiencies and low cytotoxicity in primary cortical cells, as compared to other gene carriers such as native PAMAM.

Other classes of dendrimers have also been purposed for CNS regenerative medicine, such as those based on polyesters. In a report put forward by Dhanikula and colleagues [195,359] it was suggested the use of polyether-copolyester (PEPE) dendrimers conjugated with D-glucosamine and loaded with methotrexate (MTX), in order to allow a better delivery across the BBB. Results revealed that the efficacy of MTX-loaded dendrimers was established against U87 MG and U 343 MGa cells (two glioma cell lines). *In vitro* studies revealed that glucosylated dendrimers were found to be endocytosed in significantly higher amounts than nonglucosylated dendrimers by both the cell lines. Moreover, the amount of MTX-transported across an *in vitro* model of the BBB was three to five times more after loading in the dendrimers, which indicates that glucosylation further increased the cumulative permeation of dendrimers across BBB and hence increased the amount of MTX available across it. This work showed a different set of dendrimers as well as different strategy to potentate their delivery across the BBB. However, it should be looked with caution as only *in vitro* models were used and therefore the *in vivo* proof of concept is yet to be demonstrated. A similar strategy (e.g. cell targeted particles) was followed by Wu et al. [366], which have developed a vehicle for boron neutron capture therapy (BNTC), instead of MTX. Similarly to what happened before a heavily boronated PAMAM dendrimer was chemically linked to C225 by means of the heterobifunctional reagents N-succinimidyl 3-(2-pyridyldithio)-propionate and N-(k-maleimido undecanoic acid)-hydrazide. Initial *in vitro* studies revealed that the already mentioned F98EGFR glioma cells specifically internalize the particles when compared to receptor negative F98 wild-type cells. Further *in vivo* studies were conducted by stereotactically implanting F98EGFR cells into the brains of Fischer rats. The targeted boronated dendrimers were administered 14 days after either convection enhanced delivery (CED) or direct intratumoral (i.t.) injection. Results revealed that not only the targeted dendrimers were receptor specific *in vivo*, but that

also animals that were exposed to the tested therapy disclose higher survival rated when compared to controls. In this sense it appears that this strategy for using dendrimers as targeted particles for therapeutic usage is more favorable than the former. Another *in vitro* study [367] described yet another set of polyester based dendrimers denominated as PLGSA. The results reported are quite scarce regarding CNS applications, but still it was demonstrated that these dendrimers could encapsulate camptothecins and could be internalize by glioblastoma cells (SF-268 cell line). Finally, another study [368] suggested a possible source of delivery vehicles based on dendrimers denominated as CMCht/PAMAM dendrimer nanoparticles. Experiments with post-natal hippocampal neurons and cortical glial cells revealed that both cell populations were able to taken up the CMCht/PAMAM dendrimer nanoparticles. The internalization rates changed according to the cell populations, reaching a maximum peak after 48 hours of incubation. Overall astrocytes and microglial cells disclosed higher internalization rates (around 100% of the total cell sub-population) followed by neurons and oligodendrocytes (up to 80-90% of the observed cells). Further experiments for periods of up to 7 days revealed that the periodical addition of CMCht/PAMAM dendrimer nanoparticles was needed to maintain the levels of internalization. Finally it was also observed that cell viability and proliferation were not significantly affected by the presence of the above referred nanoparticles. These results were quite promising, but similarly to what it was described for other studies herein described, further *in vivo* proof of concept needs to be done.

3.4. GENE DELIVERY APPLICATIONS OF DENDRIMERS AND DENDRONIZED POLYMERS

The ability to transfer genetic material efficiently, into the nucleus and cytoplasm of eukaryotic cells may allow treatment of a variety of genetic disorders. There are two types of vectors to gene delivery: (i) viral and (ii) non-viral. Viral-mediated DNA vehicles (infection) have played a major role in gene therapeutics. Unfortunately, initial enthusiasm associated to the high infection yields, has been tempered by growing concerns regarding the safety issues such as toxicity, immunogenicity and oncogenicity [369,370]. On the other hand, synthetic DNA delivery systems “transfection” provides potential alternatives for gene therapy and DNA vaccination. Major drawback of current transfection technology is the low efficiency compared to infection techniques, although new materials are being exploited.

Genetic material is usually imported into the cell by endocytosis where, via the endosomes, it may be transported to lysosomes, to other intracellular membrane compartments or to the cytosol. Thus, they first reach mildly acidic endosomes (pH 5.0-6.5) and then end up in lysosomes where they face much lower pH conditions and possible enzymatic degradation. Therefore, the

importance of transferring genetic material into the cytosol is an extremely important process in the development of effective gene therapies. Moreover, transport of the gene into the nucleus must occur without imparting damage/inactivation from the vehicle itself. This renewed the interest in pH-responsive dendrimeric nanocarriers as a mean to enable these macromolecules to reach their subcellular targets.

Dendrimers play a significant role in the development of non-viral vectors for gene delivery due to the high charge density and tunable surface functional groups, thus allowing optimize condensation and formation of nanostructures with DNA, the so-called “dendriplexes”. Amine-terminated PAMAM dendrimers (polycationic) can interact with negatively charged phosphate groups of nucleic acids. This ensures consistent formation of transfection complexes. In fact, the transfection reagent called SuperFect™ consisting of activated dendrimers is commercially available. Activated dendrimers can carry higher amounts of genetic material as compared to that of viruses. SuperFect-DNA complexes are characterised by high stability and provide more efficient transport of DNA into the nucleus than liposomes. It has been advanced that the high transfection efficiency of dendrimers may not only be due to their well-defined shape but may also be caused by the low pK of the amines (3.9 and 6.9). The low pK permit the dendrimer to buffer the pH change in the endosomal-lysosomal compartment. This can be beneficial since it can direct towards polymeric swelling, thus allowing disruting the membrane of the organelle and promoting the complex release or DNA itself. Therefore, they have an intrinsic endosomolytic escape capacity, or can mediate their escape by degradable spacers. Another advantage is that these vectors can also prevent fast degradation of DNA by endo- and exo-nucleases. PAMAM and other cationic dendrimers such as PPI, thus fulfill these requirements. Initial work by Szoka and colleagues [371] have shown that the three dimensional spherical structure of the PAMAM dendrimers (G5) could be broken by heating and, surprisingly the fractured dendrimers led to significant enhanced transfection efficiency over naked plasmid DNA. Recently, Kim et al. [372] have proposed the use of poly(amino ester) obtained by bulk condensation of two monomers-containing multiple reacting groups towards obtaining a non-viral and cationic polymer-based gene delivery system. The particular feature of this system consisted on the low cytotoxicity and slow degradation which possibly long-term therapeutic applications.

There are many factors affecting the efficiency of non-viral gene delivery systems. For successful gene therapy first of all, we need that genetic material can be permanently integrated and expressed by cells. In this context, Galetti et al. [373] have demonstrated that antisense oligonucleotides (ONs, gene-specific sequences of nucleic acids with 15 to 25 bases) directed to LMP1 mRNA, effectively suppressed LMP1 gene expression which plays a key role for growth transformation and immortalization of B lymphocytes.

The efficiency of three cationic carriers on the delivery of anti-LMP1-ON to their site of action in Epstein Barr virus (EBV)-infected B lymphocytes was investigated. Results have shown that liposomes, dendrimers or transferrin-PLL-conjugated ON were internalized by the cells at an extent several fold higher than that of the naked oligomers. Using Superfect®, a dendrimeric polycation with terminal amine groups, a higher intracellular concentration of ON was obtained as observed by both cytofluorimetric and confocal microscopy analysis. However, there were some evidences of toxicity induced by the positively charged dendrimers on the lymphocytes' membranes and the lack of intracellular mRNA-ON duplex formation and of LMP1 mRNA degradation, indicated a failure of this carrier.

To improve transfection efficiency, different strategies have been proposed. In this respect, Arima and coworkers [374] prepared a novel conjugate consisting of a dendrimer (G3) with α-cyclodextrin bearing mannose (Man-α-CDE conjugates) with various degrees of substitution of the mannose moiety. This system Man-α-CDE conjugate (G3, DSM10) provided the highest gene transfer activity in different cells type and provided new insights on the cellular association of polyplex with Man-α-CDE conjugate (G3, DSM10). Results also suggested that the conjugate has less cytotoxicity and were able to escape from endosome and to be translocated into the nucleus.

Luo et al. study [375] revelead the low cytotoxicity of PEG-modified PAMAM and their efficiency on the DNA delivery. These systems were obtained using low generation dendrimers with PEG chains, which mimics the fractured high-generation dendrimers. In fact, the proposed molecules showed a 20-fold increase in transfection efficiency as compared to that of partially degraded dendrimer controls.

Zhang and coworkers [376] have investigated the effect of the core structure and generation of PAMAM dendrimers on the formation and transfection efficiency of the dendriplexes. This work evaluated *in vitro,* the transfection efficiency of a series of dendrimers with a trimesyl core (DT, three-arm) using COS-7 cells, HeLa cells and primary hepatocytes. Dendrimers derived from pentaerythritol (DP, four-arm) and inositol (DI, six-arm) were used for comparison. Results revealed that the minimal generation of DT for complex with DNA was 6, while for DP and DI was 5. Thus, the difference in core structure resulted in different dendrimer flexibilities, and consequently influenced the interaction between the dendrimers and the DNA. As expected, the optimal generation numbers at which dendrimers showed higher transgene expression was 5 for DPs and DIs and 6 for DTs. Importantly, DT dendriplexes show higher transfection efficiency, which can be related to its buffer capacity inside the endosome.

Boussif work [377] use PEI to test its potential for gene delivery. PEI is a protonable amino nitrogen atom, which makes the polymeric network an effective ‘‘proton sponge’’ at virtually any pH and can protect

DNA from nuclease activity. The PEI/luciferase reporter gene complex was transfered into a variety of cell lines and primary cells gave results comparable to that of lipopolyamines (gold standard).

Interestingly, Dung et al. [378] have prepared deriplexes of cholesteryl dendrimers with antisense oligonucleotides (5:1). These were biologically active and mediated delivery of antisense oligonucleotide into HeLa cells in a moderate level. The enhanced delivery of the antisense oligomer into nucleus of the cells resulted in the expression of the reporter gene product, a luciferase. Thus, that work demonstrated that the increase of hydrophobicity by the conjugation of cholesterol to dendrimer enhanced the delivery efficiency of antisense oligonucleotide into cells.

Recently, Russ et al. [379] have synthesize grafted-PPI dendrimers of PPI dendrimers (G2 and G3) by surface modification with either oligoethylenimine (OEI) via ester-degradable or PPI dendrimer (G2). In that study, it was investigated their potential as vectors for gene delivery both *in vitro* and *in vivo*. *In vitro* transfection studies with the polyplexes (surface-modified PPI dendrimers and plasmid DNA pCMVLuc-firefly luciferase reporter gene) was carried out using both Neuro2A neuroblastoma cells (ATCC®, CCl-131) and B16F10 murine melanoma cells. Results have shown that all compounds were not cytotoxic and grafting of either G2 or G3 core units with OEI led to enhanced transfection efficiency, irrespective of the investigated core generation used. Increase of dendrimers' generation did not enhance transfection efficiency *in vitro*. Prior *in vivo* studies, it was screened possible haemolytic activity of the compounds. Contrarily to the previously reported PEI-induced erythrocyte aggregation, this work showed that all developed vectors did not induce erythrocyte aggregation. *In vivo*, it was observe a clear influence of the dendrimers in the the tumor gene expression levels, i.e. higher dendrimer core generation increased gene expression, demonstrating that surface modification and incorporation of ethylenimine core are key factors contributing to improve biocompatibility and transfection efficiency.

Tziveleka et al. [380,381] have been proposing different synthetic vectors for the prospective application as gene transfection agents. Interestingly, fourth generation PPI dendrimers partially or fully surface-modified with guanidinium groups were able to complex with plasmid DNA (pEGFP-C2 and pGL3 luciferase reporter vectors). *In vitro* studies using human embryonic kidney (HEK 293) and the monkey kidney fibroblast (COS-7) cells, showed that complete replacement of primary amino groups with the hydroxylated moieties resulted in complete loss of transfection efficiency. Contrarily, functionalization of the dendrimers with guanidinium groups enhanced transfection efficiency. This enhancement was dependent on the number of guanidinium groups at dendrimer periphery and cell type. In fact, the fully guanidinylated-modified dendrimer showed the best transfection efficiency. The advanced explanation is related with the accumulation of the guanidinium group at the dendrimeric surface, which can improve

their penetrating ability. However, cytotoxicity studies demonstrated that increase in the degree of guanidinylation increase dendrimer's cytotoxicity. Thus, at light of these data, we can once state that functionalization strategies can be valuable strategy for superior transfection efficiency, but special attention should be addressed in respect to cytotoxicity, which as in the present work can limit gene transfer potency.

Choi [382] adopted a different strategy to improve transfection efficiency of PAMAM dendrimers. In his work, it was demonstrated the positive effect on the transfection efficiency of polyplexes by bonding Dex to PAMAM dendrimers. *In vitro* studies using human embryonic kidney (293) and mouse neuroblastoma (Neuro2A) cells, showed that PAMAM-Dex/plasmid DNA (pCMV-Luc) complex had a higher transfection efficiency as compared to PEI and PAMAM, in the presence of serum proteins. Using 1,2-bis-(o-aminophenoxy) ethane-N,N,N',N',-tetraacetic acid-acetoxymethyl ester (BAPTA-AM), a glucocorticoid receptor inhibitor, they have proved that Dex-induced translocation of the glucocorticoid receptor facilitate transport of complexes into nucleus, thus enhancing by this mean transfection efficiency.

Great efforts have also been made as an attempt to clarify the mechanism (s) of transfection. Manunta et al. [383] have reported on the route by which dendriplexes are internalised, and mediate gene transfer. This work demonstrated that internalization is dependent on the cell type, and it is a successful example of dendrimer application as a non-viral vector for gene delivery. This report showed that transfection of the dendriplexes may occur via different pathways, but in cells expressing caveolae, results suggest that gene delivery might be occurring by a caveolin-dependent pathway. Ruponen et al. [384] carried out a comparative study to investigate the performance of both cationic lipids (e.g. N-(1-(2,3-dio-leoyloxy) propyl)-N,N,N-trimethyl ammonium methylsulfate (DOTAP) and 1,2-dioleyl-3-phosphatidylethanolamine (DOPE)) and polymers (e.g. PEI, PAMAM dendrimers and PLL) for gene delivery. Moreover, the effect of interactions of extracellular polyanionic glycosaminoglycans (GAGs) such as hyaluronic acid (HA), chondroitin sulfate, and heparan sulfate with positively charged plasmid DNA complexes on the transfection efficiency was investigated. Results have shown that polycations condensed DNA more effectively as compared to that of monovalent lipids. Furthermore, polyplexes (PEI, PLL) were internalized by the cells more efficiently than lipoplexes. It was also found that sulfated GAGs (heparan sulfate, chondroitin sulfates B and C) completely blocked transfection, except in the case of liposomes with DOPE. Moreover, it was evidenced that sulfated GAGs induced DNA release from PEI complexes, but DNA release from the complexes was not required for the inhibition of transfection. By its turn, HA also inhibited transfection by PEI, PAMAM dendrimers. This comphreensive study suggested that cell surface GAGs, namely heparan sulfate can inhibit transfection mediated by both cationic lipids and

polymers indicating that mechanistic information can help to develop more efficient vectors for gene delivery.

On the other hand, the protection of DNA from *in vivo* degradation by the vectors is another key feature for success in gene delivery. Recently, new step forward report by Diaz-Mochon [385] showed that a hybrid combination of PAMAM and peptide dendrimers, the so-called peptoid dendrimers were able to transfect cells with higher efficiency than the PAMAM counterpart and were also non-toxic. In part, this work supported previous findings which demonstrated that combination of primary and secondary amines generates a ‘‘proton sponge’’ effect which can facilitate the DNA transfection process, by facilitating the release of the plasmid from the cytoplasmic lysosome. Thus, efficiency of dendrimer/DNA complexes may be favoured by prolonging the release of plasmid.

An early stage work reported by Herrmann [386] described the synthesis of polyphenylene dendrimers functionalized with lysine residues or substituted with short peptide sequences composed of five lysine or glutamic acid repeats and a C- or N-terminal cysteine residue. This group postulated that these amino acid and peptide functionalized dendrimers may be of interest as model compounds to study DNA complexation.

There are few papers which employ dendritic PLL as a gene delivery carrier, either alone or in combination with linear polymers or PEG. However, Männistö et al. [387] have been shown that the shape and charge of these non-viral vectors greatly influences their complexation with DNA and ultimately their transfection efficiency. Their study showed the ability of PLL dendrimers for complexing with DNA. Linear polymers were more efficient than dendritic ones. At low M_w of PLL, DNA binding and condensation were less efficient, particularly with dendrimers. PEGylation did not decrease DNA condensation of PLLs at less than 60% (fraction of M_w) of PEG. Moreover, introduction of PEG stabilized the complexes sterically. Internalization of PLL/DNA complexes was high and PEGylation increased the transfection efficacy. However, overall transfection level of PLL was low possibly due to inadequate escape of the complexes from endosomes or poor release of DNA from the complexes. Higashi et al. [388] have been studying the interaction of water soluble PLL-shelled dendrimers possessing various PLL segment (*n* = 5-40) with DNA by circular dichroism spectroscopy, dynamic light scattering, and melting behavior of double-stranded DNA. Double helical DNAs were found to complex with dendritic PLLs (G3) [5, 10, and 20] primarily via electrostatic interactions. Moreover, a longer PLL-containing (G3) was found to interact with DNA more effectively than a shorter one. Okuda et al. [389] have also investigated the effect of substituting terminal cationic groups in PLL on the gene delivery into cells, in particular, the effect of guanidinium groups on the transfection. Monodispersed PLL (G6)

dendrimers in which external amino acids were replaced by arginines and histidines were synthesized. A particular attention was given to clarify whether histidine shows the activity as an endosomal disruption agent. DNA-binding and transfection studies revealed that arginine-terminated PLL dendrimers could bind to the DNA more efficiently, and presented higher transfection efficiency as compared to those for histidine-terminated PLL. In fact, histidine-terminated PLL did not mediate transfection. Despite, the terminal histidines of PLL dendriemrs, especially the imidazole groups, had a key role in the pH-dependent complex formation and transfection (neutral and acidic pH´s). The unique character of histidine-PLL dendrimers is most promising.

As aforementioned, cationic PAMAM dendrimers have been proving to efficiently mediate transfection of DNA into a variety of mammalian cells, *in vitro*. However, as highlighted the major drawback of high generation cationic dendrimers is their associated cytotoxicity. Anionic dendrimers, on the other hand, have shown no cytotoxic effect on cells over a broad range of concentrations. Hussain et al. [390] have reported the successful use of ONs conjugated with pentaerythritol-based anionic dendrimers in inhibiting cancer cell growth. *In vitro* studies using cancer cells showed that ONs-dendrimer conjugates enhance the cellular uptake, up to 4 times as compared to that for naked ONs. These data clearly demonstrated that anionic ONs-dendrimer conjugates may represent attractive alternatives to cationic non-viral vectors for the delivery of gene silencing ONs. However whether the system may facilitate the delivery of duplex siRNA for gene silencing by RNA interference need to be answer. Therefore, further studies are necessary to evaluate the full potential of the delivery system.

Electrophoretic studies carried out by Kuo et al. [391] have demonstrated that fifth generation PAMAM and PPI dendrimers altered or blocked the mobility of RNA isolated from human macrophage-like cells (U937 cell line) and mouse fibroblast NIH/3T3cells previously exposed to DNA/dendrimer complexes. At higher dendrimer:DNA ratio, dendrimers interacted with RNA after isolation, but gene expression of these complexes was not affected. Electrostatic forces were found to be responsible for the dendrimer-induced alteration in RNA mobility. Because RNA isolation is routinely used for biological applications, such dendrimer-induced alteration in RNA mobility should be accounted for when further processing RNA for related applications, and the use of high ionic strength solvents (2 M NaCl solution) to disrupt the electrostatic forces binding dendrimers to RNA is advised.

A final key aspect in the gene delivery is related to the need for controlling gene transfection. This can be accomplished by developing controllable and nontoxic gene delivery systems that are stimuli-responsive. For example, Nishiyama et al. [392] proposed an innovative strategy based on PCI gene delivery. In their work, they have developed a ternary complexes (size between 100 and composed of a

core of and cationic peptides ($C(YGRKKRRQRRRG)_2$) that were enveloped in the second generation aryl ether dendrimers (32 carboxyl groups at the periphery) with a phtalocyanine core (photosensitizer). *In vitro* transfection studies using human cervical epithelioid carcinoma (HeLa) cells demonstrated that this ternary system enhance (>100-fold) transgene expression as compared to conventional reagents such as PEI and Lipofectamine, *in vitro*. Moreover, it was shown that PCI-mediated gene delivery reduced phototoxicity of the ternary complexes. For the *in vivo* studies a reported gene was used. Fluorescence microscopy studies of rat conjunctival tissue revealed that the ternary complex positively induced gene delivery by PCI. That work demonstrated that polyplex-polycations significantly affects both transfection efficiency and toxicity. Therefore further optimization of this type of systems should involve research on the use of other polycations. Thus, PCI provides us with an opportunity to develop efficient light-inducible gene delivery systems. Shieh et al. [393] also investigated phototriggered gene transfection by core-modified PAMAM dendrimers (G4). In their work, a 5,10,15-tri(4-acetamidophenyl)-20-mono(4-carboxylphenyl) porphyrin (hydrophobic core) was introduced into the PAMAM dendrimers by activation with DCC and N-hydroxysuccinimide. *In vitro* characterization studies revealed that porphyrin core-PAMAM dendrimer conjugates were able to complex with green fluorescent protein (EGFP) plasmid DNA and that the internalization by HeLa cells was concentration-dependent. Moreover, results from phototoxicity showed that without irradiation more than 94% of the cells survived when incubated with conjugates at a concentration of 20 μM. However, the complexes induced toxicity at 50 μM. For photodynamic therapy, results show that conjugation of porphyrin core to dendrimers did not increase the cytotoxicity of the PAMAM dendrimer below 20 μM, but significantly induced cell death after suitable irradiation. Despite, the expression of EGFP was enhanced in HeLa cells using the PCI treatment. Thus, that study demonstrated that PAMAM dendrimers conjugated with porphyrin core can be an efficient and safe vector for PCI-mediated gene delivery.

Dendrimers are one of the most useful nonviral gene delivery systems. Their ability to transfect cells without inducing toxicity and be tuned for stimuli-induced gene delivery confers a great advantage over other gene delivery vectors for use *in vivo*.

3.5. THERANOSTICS APPLICATIONS OF DENDRIMERS AND DENDRONIZED POLYMERS

Although opportunities to develop nanotechnology-based drug delivery systems extend into all therapeutic classes of pharmaceuticals, the development of effective diagnose and therapeutic, i.e. one-package systems that can target different tissues while releasing one or multiple therapeutic agents under a external stimuli have been attracting a great deal of attention. For example, in cancer therapy,

anticancer agents can damage both malignant and normal cells alike. Additional problems include instability of the drugs/GFs in the biological milieu and short half-time, systemic migration, and premature drug loss through either rapid clearance by Mo/Mac, and/or metabolism. The design of most sophisticated systems should also consider the need for temporal release of the drug (s). Thus, dendrimers can be tuned for: (i) be stimuli-responsive nanocarriers, (ii) include molecular tags, (iii) possess high payload efficiency, (iv) decrease dosage requirements as well as re-dosage frequency and (v) target delivery and minimize drug migration, thus suppressing secondary effects during drug (s) treatment. For example, Kuo and colleagues [394] have investigated *in vivo*, the interactions of second and third generation PPI dendrimers with human macrophages U-937, since these molecules are primarily removed from circulation by the mononuclear phagocyte system. The effect of the type of dendrimer and concentration on the content of ntracellular responses-reactive oxygen species (ROS), mitochondria membrane potential, cell size and complexity, and cell cycle profiles were investigated. Although the concentrations of PPI dendrimers used (40-300 $\mu g.mL^{-1}$) were not cytotoxic, various intracellular responses in dendrimer-treated macrophages occurred in a time-dependent manner. Moreover, the intracellular responses were found to be dependent on the dendrimer generation. This work nicely illustrates that a better understanding of the molecular action of these nanosystems in the cellular system may be an advantage for best design of safer and more effective delivery systems.

As previously stated herein, dendrimers fulfill these requirements as they can be stimuli-responsive and controlled-release systems for nucleic acids, bioactive molecules and peptide/protein delivery. Due to the possibility of tailoring the end groups, dendrimers are able to interact with the target, such as cell walls and/or proteins [159]. The external functional groups may allow the simultaneous, covalent bonding to therapeutic drugs, targeting devices and fluorescent probes (Figure 9).

Recently, a combination of polymer chemistry and imaging science approaches has led to the generation of polymer-based bioimaging probes for the diagnosis and treatment of different diseases. The ultimate goal of *in vivo* imaging is to achieve highly sensitive and reliable imaging techniques viable for diagnosis in personalized medicine for delivering drugs, following their distribution, and monitoring therapy. This concept (theranostics) is based on the “find, fight and follow” approach. New probes with enhanced capabilities and performance should be developed specific to nano-imaging techniques. Key research priorities for targeted delivery and *in vivo* imaging should address: (i) design of nanostructures with stealth properties that prevent them from being opsonised or cleared before reaching the target cells, (ii) ability to penetrate into cells and crossover biological barriers like the BBB, uptake and recycling of nanostructures, (iii) nanocarriers or strategies that selectively targets diseased cells, tissues

and organs, (iv) trans-endocytosis of nanostructures, (v) safety evaluation (*in vitro*/*in vivo* cytotoxicity, haemo-compatibility and immunogenicity), *in vivo* carrier biodistribution, and (vi) compatibility with external activation by magnetic field, ultrasound, X-ray, or optics to trigger the therapeutic activity. For example, the Kobayashi and coworkers [395] have shown that a dendrimer-based magnetic resonance contrast agent may be useful for *in vivo* detection of renal tubular damage. By its turn, Rietveld et al. [396] developed dendrimers with tetrabenzoporphyrin cores for *in vivo* oxygen imaging. While it is promising to both incorporate therapeutic agents and molecular-tags on the dendrimers and improve their potency [73], the possibility of combining diagnosis and therapy in multi-functional dendrimer-based nanosystems can allow the early detection, targeting and treatment of several diseases.

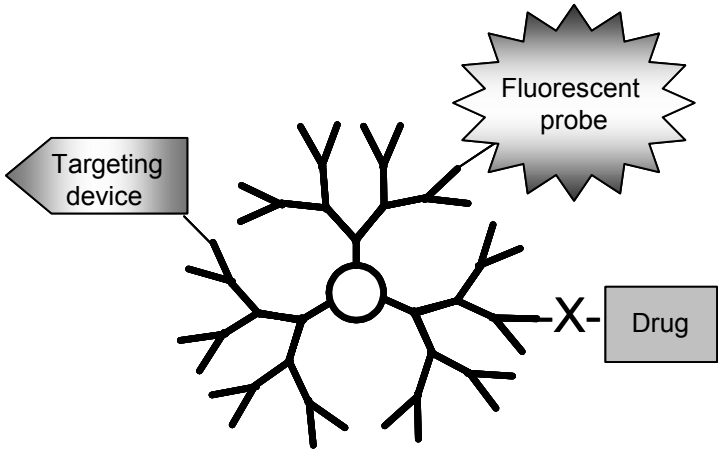

Figure 9. Schematic representation of dendrimers with the external binding of the drug and fluorescent probes for applications in theranostics (one package system). It is possible follow the biodistribution, internalization and intracellular trafficking within cells. The use of targeting devices such as antibodies to augment specificity is also possible. The drug can linked to dendrimers using different spacers or bonds (X), which can be cleaved under a certain external stimuli, thus stimuli- or bio-responsive release is an additional possibility.

Thomas et al. [397] have linked PAMAM dendrimers (G5) with FITC for tracking, and two different antibodies 60bca and J591 antibodies that bind to CD14 and prostrate specific membrane antigen (PSMA), respectively. This work showed the receptor specificity as the conjugates bound to specific antigen expressing cells. By its turn, Shukla and coworkers [398] have synthesized PAMAM dendrimers (G5) conjugated to anti-HER2 monoclonal antibody by tagging the formulation with alexaFluor (AF). Flow cytometric studies revealed the uptake of conjugate by HER2 expressing cells while no such affinity was found for MCA-207 control cells that did not express HER2, *in vitro*.

According to the literature, the success of entrapping small molecules inside the dendrimer depends on the mutual properties between the host and the guest molecules. For example, Domanski et al. [83] reported on the attempts to entrap of small fluorescent probes commonly used to evaluate membrane fluidity inside the dendrimer. This work has shown that the 12-(9-anthroyloxy) stearic acid (12-AS), a non-polar fatty acid derivative, was successfully incorporated into the PAMAM dendrimers cavities, while on the contrary 1-(trimethylammoniumphenyl)-6-phenyl-1,3,5 hexatriene *p*-toluenesulfonate (TMA-DPH), a amphiphilic salt possessing positive charge, was not.

Kolhe et al. [399] have demonstrated that ibuprofen predominantly forms a complex with PAMAM (G3 and G4) dendrimers because of the ionic interaction between the $-NH_2$ end groups and the carboxyl group of ibuprofen. In this work, they demonstrated that the *in vitro* release of ibuprofen from drug-dendrimer complex is appreciably slower compared to pure ibuprofen. Moreover, the FITC-labeled dendrimer-complexed drug enters human lung epithelial carcinoma A549 cells much faster than pure drug suggesting that dendrimers may be able to carry the complexed drug inside cells efficiently. That group [56] synthesized a fourth generation PAMAM (PAMAM-OH) dendrimer covalently linked to ibuprofen using dicyclohexylcarbodiimide (DCC) as a coupling agent. A high payload nanocarrier was obtained; 58 molecules of ibuprofen were covalently conjugated to one molecule of PAMAM-OH (G4) dendrimer. FITC-labeled dendrimer-drug conjugate nanoparticles internalization was evaluated *in vitro* once using A549 cells. The pharmacological activity of the dendrimer-ibuprofen conjugate was compared to pure ibuprofen at various time points by measuring the suppression of prostaglandin E2. Results demonstrated the high internalization efficency of the FITC-labeled dendrimer-drug conjugate and superior therapeutic activity due to faster prostaglandin E2 suppression. Thus, the results suggest that dendrimer-ibuprofen conjugate improve the drug efficacy by enhanced cellular delivery, and may produce a rapid pharmacological response. For example, several ligands are known to be associated with tumour. Ligand based dendritic polymers have been attracting great deal of attention for find applications in cancer-cell-specific targeting [102] and tumour therapy [400].

Transferrin is a β-globulin (β_1-glycoprotein) and facilitates the transport of ferric ion (Fe^{3+}) through transferrin receptors on the plasma membrane. In fact use of transferrin as a ligand has been explored as a suitable delivery system for site-specific delivery to tumours [401]. PLL covalently linked with transferrin for delivery of ONs when exposed to human leukemic (HL-60) cells have been stated to promote apoptosis to a greater extent as compared to free ONs. Another paper [402] demonstrated that PEGylated poly(cyanoacrylate) nanoparticles conjugated to transferrin were effective on the delivery of paclitaxel (PTX), an antitumour drug. PEGylation prevented aggregation of nanoparticles and transferrin

effectively determined tumour site. An excellent study by Choi and coworkers [102] is appropriate to highlight herein. Their innovative wotk consisted on the development of dendrimers conjugated to different biofunctional moieties [FITC for imaging, and folic acid (FA) for targeting], and then were link together using complementary DNA oligonucleotides to produce clustered molecules for targeting tumour cells through folate receptors. This step forward allowed both obtain efficient DNA-linked dendrimer clusters for intracellular imaging and therapeutics, and circumvent the tedious synthesis of multiply-functionalized dendrimers.

Instead of linking oligonucleotides to the dendrimers, Majoros [403] synthesized a multifunctional PAMAM dendrimer (G5) conjugated with FITC, FA, and PTX. *In vitro* studies have shown that drug-free dendrimer conjugates were not cytotoxic even at high concentrations. On contrary, drug-loaded dendrimer conjugates were toxic to both folate receptor-positive and folate receptor-negative cells as a result of non-specific binding at concentrations around 200 nM.

Another good example of PAMAM dendrimer based multifunctional devices (target the desire cells, releasing the desired drug and monitoring their internalization-fluorescent probe) has been reported by Islam et al. [404]. This group partially acetylated PAMAM dendrimers (G5) that were then conjugated with FITC, FA and MTX. These intended for targeting tumour cells through the folate receptor, while releasing intracellularly an antitumour drug. Interestingly, they have shown that HPLC analysis is a valuable technique to determine the purity and stability of dendrimer-based complexes. Yang et al. [405] have synthesized FITC- and biotin-linked PAMAM dendrimer (G5) conjugates and investigated their ability for targeting cancer cells. The bifunctional conjugate (FITC-biotin-dendrimer) exhibited much higher internalization by HeLa cells than the conjugate without biotin. The uptake was found to be energy and dose-dependent, and could be effectively blocked by dendrimer-conjugated biotin. Results indicate that the biocompatible biotin-dendrimer conjugate can be a promising nano-platform for therapy and diagnosis of tumours.

Epidermal growth factor (EGF) is an important factor that controls the disposition of neoplastic cells and potentiates transcription and proliferation of cells. Human growth receptor (HER-2) is a member of EGF family and their number is augmented in several tumours [406], and hence, it provides a potential target for immunotherapeutic agent.

Nanoparticles having size range of 1-10 nm have capacity to diffuse easily inside the tumour cells. This helps to overcome limitations relating to chemotherapy using free drug such as poor *in vivo*/*in vitro* correlation and overcome other possible resistances offered by tumours. In fact, Tomalia [407] has also been proposing the use of ~5 nm sodium salt-PAMAM dendrimers (G4.5) nanoparticles possessing a

1,4-diaminobutanecore, as multi-purpose nanodevices for oncology drug delivery and diagnostic MRI contrast agents.

Relevant scientific data was recently reported by Saad et al. [408]. In this interesting work they investigated on the role of different nanocarriers (linear polymer, PAMAM dendrimer and liposomes) containing the same bioactive agents, in tumour-specific treatment and imaging. Which nanocarrier is most efficient was investigated. In their comphreensive work it was demonstrated for the first time, that the targeting of nanocarriers to tumor-specific receptors minimize the influence of the architecture, composition, size and M_w of nanocarriers on the efficacy of imaging and cancer treatment. This step forward, once illustrate that the nanocarriers potential can only be fully exploited with a much better understanding of how such structures interact with the body and its components, *in vitro* and *in vivo*.

4. CONCLUDING REMARKS AND FUTURE OUTLOOK

Nanotechnology and medicine research are merging with other fields leading to completely new science and superior technological platforms such as those recently reported for regenerative medicine and neurosciences. The main aim of this review article was to summarize the unique properties, ability to design and improve the biological performance of dendrimers. This novel class of polymers and their derivatives has been exhibiting unique physicochemical and biological properties which have great potential to be used in a variety of applications, including tissue engineering and regenerative medicine, which have been discussed herein.

It was also emphasized their compatibility with nanoscale building blocks such as genetic material, bioactive molecules and fluorescent-probes, which make them even more versatile than other nanomaterials, indeed probably unique feature to be used in theranostics. Dendrimers arises in a time when common medical practice is based on symptom control, and research is focused on the best drugs to relieve the impact and progression of a given disease. Dendrimers may be used as tools to diagnose pathologies in an early stage thus helping manage disease in a sustainable manner. There is however, the need to conduct comprehensive research *in vivo*, to better understand and assess their true value as multifunctional packages. In particular, we still do not know whether these synthetic polymers, once they entered the body can cause damage to other tissues. Thus, much effort needs to be done in future, to evaluate the risk of bioaccumulation and redistribution. Research on their adsorption and interaction with biological surfaces, the associated uptake mechanisms, long-term effects, and bioelimination needs also to be determined. Hence new and unexplored characteristics of nanoscale are opened, and unsettled issues of biocompatibility, which will remain a key challenge

without a definitive near term answer, progress in the field of dendritic polymers will certainly depend on other not less important aspects. In order to be effective, dendrimer-based products should be based on scientific evidence for their uselfulness and must be easier to translate from laboratory to the clinic, in other words be quality-controlable, cost-effective and sustainable. At last but not least, their application should be validated from the regulator's viewpoint, worldwide.

As a final remark, the process of converting basic discoveries into marketable products can be long and hard but certainty arise, since the discovery of dendrimers we can envision things never possible before and expect many innovations in the puzzled field of regenerative medicine.

REFERENCES

1. Tomalia, D.A., et al., *A new class of polymers: Starburst-dendritic macromolecules.* Polymer Journal, 1985. **17**: p. 117.
2. Feynman, R., *There's plenty of room at the bottom*, in *American Physical Society*. 1959: California Institute of Technology, Pasadena, CA.
3. Pridgen, E.C., R. Langer, and O.C. Parokhzad, *Biodegradable, polymeric nanoparticle delivery systems for cancer therapy.* Nanomedicine, 2007. **2**(5): p. 669.
4. Muller, D.J., et al., *Observing structure, function and assembly of single proteins by AFM.* Progress in Biophysics and Molecular Biology, 2002. **79**: p. 1.
5. Roco, M.C., *Nanotechnology: convergence with modern biology and medicine.* Current Opinion in Biotechnology, 2003. **14**(3): p. 337.
6. Bikram, M., et al., *Temperature-sensitive hydrogels with SiO2-Au nanoshells for controlled drug delivery.* Journal of Controlled Release, 2007. **123**(3): p. 219.
7. Pinna, M., X. Guo, and A.V. Zvelindovsky, *Block copolymer nanoshells.* Polymer, 2008. **49**(12): p. 2797.
8. Spuch-Calvar, M., J. Pérez-Juste, and L.M. Liz-Marzán, *Hematite spindles with optical functionalities: Growth of gold nanoshells and assembly of gold nanorods.* Journal of Colloid and Interface Science, 2007. **310**(1): p. 297.
9. Huang, X., et al., *Cancer cell imaging and photothermal therapy in the near-infrared region by using gold nanorods.* Journal of the American Chemical Society, 2006. **128**: p. 2115.
10. Fahmy, T.M., J.P. Schneck, and W.M. Saltzman, *A nanoscopic multivalent antigen-presenting carrier for sensitive detection and drug delivery to T Cells.* Nanomedicine: Nanotechnology, Biology and Medicine, 2007. **3**(1): p. 75.

11. Wu, C., et al., *Metal-chelate-dendrimer-antibody constructs for use in radioimmunotherapy and imaging.* Bioorganic & Medicinal Chemistry Letters, 1994. **4**(3): p. 449.
12. Kennel, S.J., et al., *The fate of MAb-targeted Cd125mTe/ZnS nanoparticles in vivo.* Nuclear Medicine and Biology, 2008. **35**(4): p. 501.
13. Medintz, I.L., et al., *Self-assembled nanoscale biosensors based on quantum dot FRET donors.* Nature Materials, 2003. **2**: p. 630.
14. Xing, Y., et al., *Molecular profiling of single cancer cells and clinical tissue specimens with semiconductor quantum dots.* International Journal of Nanomedicine, 2006. **1**: p. 473.
15. Song, S., et al., *Peptide ligand-mediated liposome distribution and targeting to EGFR expressing tumor in vivo.* International Journal of Pharmaceutics, 2008. **363**(1-2): p. 155.
16. Katanasaka, Y., et al., *Antiangiogenic cancer therapy using tumor vasculature-targeted liposomes encapsulating 3-(3,5-dimethyl-1H-pyrrol-2-ylmethylene)-1,3-dihydro-indol-2-one, SU5416.* Cancer Letters, 2008. **270**(2): p. 260.
17. Tsuruta, W., et al., *Application of liposomes incorporating doxorubicin with sialyl Lewis X to prevent stenosis after rat carotid artery injury.* Biomaterials, 2009. **30**(1): p. 118.
18. Bista, R.K. and R.F. Bruch, *Near-infrared spectroscopy of newly developed PEGylated lipids.* Spectrochimica Acta Part A: Molecular and Biomolecular Spectroscopy, 2008. **71**(2): p. 410.
19. Vanniasinghe, A.S., V. Bender, and N. Manolios, *The potential of liposomal drug delivery for the treatment of inflammatory arthritis.* Seminars in Arthritis and Rheumatism. In Press, Corrected Proof, 2008. (doi:10.1016/j.semarthrit.2008.08.004).
20. Simon, F., et al., *Fullerene release from the inside of carbon nanotubes: A possible route toward drug delivery*. Chemical Physics Letters, 2007. **445**(4-6): p. 288.
21. Gallo, M., A. Favila, and D. Glossman-Mitnik, *DFT studies of functionalized carbon nanotubes and fullerenes as nanovectors for drug delivery of antitubercular compounds.* Chemical Physics Letters, 2007. **447**(1-3): p. 105.
22. Foley, S., et al., *Cellular localisation of a water-soluble fullerene derivative.* Biochemical and Biophysical Research Communications, 2002. **294**(1): p. 116.
23. Tanaka, K., et al., *Assembly system of direct modified superparamagnetic iron oxide nanoparticles for target-specific MRI contrast agents.* Bioorganic & Medicinal Chemistry Letters, 2008. **18**(20): p. 5463.
24. Maenosono, S., T. Suzuki, and S. Saita, *Superparamagnetic FePt nanoparticles as excellent MRI contrast agents.* Journal of Magnetism and Magnetic Materials, 2008. **320**(9): p. L79.

25. Patel, D., et al., *Poly(d,l-lactide-co-glycolide) coated superparamagnetic iron oxide nanoparticles: Synthesis, characterization and in vivo study as MRI contrast agent.* Colloids and Surfaces A: Physicochemical and Engineering Aspects, 2008. **313-314**: p. 91.
26. Galperin, A., et al., *Radiopaque iodinated polymeric nanoparticles for X-ray imaging applications.* Biomaterials, 2007. **28**(30): p. 4461.
27. Prinzen, L., et al., *Optical and magnetic resonance imaging of cell death and platelet activation using annexin A5-functionalized quantum dots.* Nano Letters, 2007. **7**(1): p. 93.
28. Wiener, E.C., et al., *Imaging folate binding protein expression with MRI.* Academic Radiology, 2002. **9**(2): p. 316-319.
29. Domnanich, P., et al., *Protein microarray for the analysis of human melanoma biomarkers.* Sensors and Actuators B: Chemical. In Press, Corrected Proof, 2008. (doi:10.1016/j.snb.2008.06.043).
30. Choi, J.-W., Y.-K. Kim, and B.-K. Oh, *The development of protein chip using protein G for the simultaneous detection of various pathogens.* Ultramicroscopy, 2008. **108**(10): p. 1396.
31. Scarlett, C.J., et al., *Proteomic classification of pancreatic adenocarcinoma tissue using protein chip technology.* Gastroenterology, 2006. **130**(6): p. 1670.
32. Roh, H.W., et al., *Development of a guideline for protein chip evaluation as medical devices.* Current Applied Physics, 2006. **6**(1): p. e261.
33. Marconi, S., et al., *A protein chip membrane-capture assay for botulinum neurotoxin activity.* Toxicology and Applied Pharmacology, 2008. **233**(3): p. 439.
34. Fissell, W.H., et al., *High-performance silicon nanopore hemofiltration membranes.* Journal of Membrane Science, 2009. **326**(1): p. 58.
35. Zhang, M., et al., *Strong, transparent, multifunctional, carbon nanotube sheets* Science, 2005. **309**: p. 1215.
36. Atkinson, K.R., et al., *Multifunctional carbon nanotube yarns and transparent sheets: Fabrication, properties, and applications.* Physica B: Condensed Matter, 2007. **394**(2): p. 339.
37. Flynn, E.R., et al., *Use of a SQUID array to detect T-cells with magnetic nanoparticles in determining transplant rejection.* Journal of Magnetism and Magnetic Materials, 2007. **311**(1): p. 429.
38. Martin, R. and J.K. Abba, *Peptides as targets of T cell-mediated immune responses*, in *Handbook of Biologically Active Peptides*. 2006, Academic Press: Burlington. p. 585.

39. Ghasemi-Mobarakeh, L., et al., *Electrospun poly(ε-caprolactone)/gelatin nanofibrous scaffolds for nerve tissue engineering.* Biomaterials, 2008. **29**(34): p. 4532.
40. Zhang, N., et al., *Fabrication of nanocrystalline hydroxyapatite doped degradable composite hollow fiber for guided and biomimetic bone tissue engineering.* Materials Science and Engineering: C, 2007. **27**(3): p. 599.
41. Janjanin, S., et al., *Mold-shaped, nanofiber scaffold-based cartilage engineering using human mesenchymal stem cells and bioreactor.* Journal of Surgical Research, 2008. **149**(1): p. 47.
42. Duan, X., et al., *Biofunctionalization of collagen for improved biological response: Scaffolds for corneal tissue engineering.* Biomaterials, 2007. **28**(1): p. 78.
43. Volcke, C., et al., *Influence of DNA condensation state on transfection efficiency in DNA/polymer complexes: An AFM and DLS comparative study.* Journal of Biotechnology, 2006. **125**(1): p. 11.
44. Yamagata, M., et al., *Structural advantage of dendritic poly(l-lysine) for gene delivery into cells.* Bioorganic & Medicinal Chemistry, 2007. **15**(1): p. 526.
45. Gómez-Valadés, A.G., et al., *Copolymers of poly-L-lysine with serine and tryptophan form stable DNA vectors: implications for receptor-mediated gene transfer.* Journal of Controlled Release, 2005. **102**(1): p. 277.
46. Suzuki, R., et al., *Effective gene delivery with novel liposomal bubbles and ultrasonic destruction technology.* International Journal of Pharmaceutics, 2008. **354**(1-2): p. 49.
47. De Rosa, G., et al., *Novel cationic liposome formulation for the delivery of an oligonucleotide decoy to NF-κB into activated macrophages.* European Journal of Pharmaceutics and Biopharmaceutics, 2008. **70**(1): p. 7.
48. Auguste, D.T., et al., *Triggered release of siRNA from poly(ethylene glycol)-protected, pH-dependent liposomes.* Journal of Controlled Release, 2008. **130**(3): p. 266.
49. Yuba, E., et al., *Gene delivery to dendritic cells mediated by complexes of lipoplexes and pH-sensitive fusogenic polymer-modified liposomes.* Journal of Controlled Release, 2008. **130**(1): p. 77.
50. Pan, X., et al., *Cationic lipid-coated magnetic nanoparticles associated with transferrin for gene delivery.* International Journal of Pharmaceutics, 2008. **358**(1-2): p. 263.
51. Han, S.-E., et al., *Novel cationic cholesterol derivative-based liposomes for serum-enhanced delivery of siRNA.* International Journal of Pharmaceutics, 2008. **353**(1-2): p. 260.
52. Smith, A.M., et al., *Bioconjugated quantum dots for in vivo molecular and cellular imaging.* Advanced Drug Delivery Reviews, 2008. **60**(11): p. 1226.

53. Courty, S., et al., *Tracking individual proteins in living cells using single quantum dot imaging*. Methods in Enzymology, ed. J.I. (Ed.). Vol. 414. 2006, Amsterdam: Elsevier, Inc., 211.
54. Howarth, M., et al., *Targeting quantum dots to surface proteins in living cells with biotin ligase.* Proceedings of the National Academy of Sciences of the United States of America, 2005. **102**: p. 7583.
55. Lagerholm, B., et al., *Multicolor coding of cells with cationic peptide coated quantum dots.* Nano Letters, 2004. **4**: p. 2019.
56. Kolhe, P., et al., *Preparation, cellular transport, and activity of polyamidoamine-based dendritic nanodevices with a high drug payload.* Biomaterials, 2006. **27**(4): p. 660.
57. Thaxton, C.S., D.G. Georganopoulou, and C.A. Mirkin, *Gold nanoparticle probes for the detection of nucleic acid targets.* Clinica Chimica Acta, 2006. **363**(1-2): p. 120.
58. Hien Pham, T.T., C. Cao, and S.J. Sim, *Application of citrate-stabilized gold-coated ferric oxide composite nanoparticles for biological separations.* Journal of Magnetism and Magnetic Materials, 2008. **320**(15): p. 2049.
59. Gong, J.-L., et al., *Ag/SiO_2 core-shell nanoparticle-based surface-enhanced Raman probes for immunoassay of cancer marker using silica-coated magnetic nanoparticles as separation tools.* Biosensors and Bioelectronics, 2007. **22**(7): p. 1501.
60. Yun, Y., et al., *A nanotube array immunosensor for direct electrochemical detection of antigen-antibody binding.* Sensors and Actuators B: Chemical, 2007. **123**(1): p. 177.
61. Yoon, H.C., D. Lee, and H.-S. Kim, *Reversible affinity interactions of antibody molecules at functionalized dendrimer monolayer: affinity-sensing surface with reusability.* Analytica Chimica Acta, 2002. **456**(2): p. 209.
62. Lee, J.H., et al., *Electrochemical immunosensor signaling by employing enzyme-tagged antibody for the determination of antigen or antibody under single competition reaction format.* Colloids and Surfaces A: Physicochemical and Engineering Aspects, 2008. **313-314**: p. 509.
63. Snejdarkova, M., et al., *Acetylcholinesterase sensors based on gold electrodes modified with dendrimer and polyaniline: A comparative research.* Analytica Chimica Acta, 2004. **514**(1): p. 79.
64. Yao, K., et al., *ENFET glucose biosensor produced with dendrimer encapsulated Pt nanoparticles.* Materials Science and Engineering: C, 2008. **28**(8): p. 1236.
65. Liu, Z.-M., et al., *A hydrogen peroxide biosensor based on nano-Au/PAMAM dendrimer/cystamine modified gold electrode.* Sensors and Actuators B: Chemical, 2005. **106**(1): p. 394.

66. Guo, F., et al., *Electrostatic layer-by-layer self-assembly of PAMAM-CdS nanocomposites on MF microspheres.* Materials Chemistry and Physics, 2007. **105**(2-3): p. 315.
67. Hsiao, C.-Y., et al., *Novel poly-silicon nanowire field effect transistor for biosensing application.* Biosensors and Bioelectronics. 2009. **24**(5): p. 1223.
68. He, B., T.J. Morrow, and C.D. Keating, *Nanowire sensors for multiplexed detection of biomolecules.* Current Opinion in Chemical Biology, 2008. **12**(5): p. 522.
69. Bailey, S.N., et al., *Microarrays of lentiviruses for gene function screens in immortalized and primary cells.* Nature Methods, 2006. **3**: p. 117.
70. Kang, L., et al., *Microfluidics for drug discovery and development: From target selection to product lifecycle management.* Drug Discovery Today, 2008. **13**(1-2): p. 1.
71. Underhill, G.H. and S.N. Bhatia, *High-throughput analysis of signals regulating stem cell fate and function.* Current Opinion in Chemical Biology, 2007. **11**(4): p. 357.
72. Roney, C., et al., *Targeted nanoparticles for drug delivery through the blood-brain barrier for Alzheimer's disease.* Journal of Controlled Release, 2005. **108**(2-3): p. 193.
73. Wolinsky, J.B. and M.W. Grinstaff, *Therapeutic and diagnostic applications of dendrimers for cancer treatment.* Advanced Drug Delivery Reviews, 2008. **60**(9): p. 1037.
74. Vail, D.M., et al., *Pegylated liposomal doxorubicin: Proof of principle using preclinical animal models and pharmacokinetic studies.* Seminars in Oncology, 2004. **31**(Supplement 13): p. 16.
75. Chow, T.-H., et al., *Diagnostic and therapeutic evaluation of ^{111}In-vinorelbine-liposomes in a human colorectal carcinoma HT-29/luc-bearing animal model.* Nuclear Medicine and Biology, 2008. **35**(5): p. 623.
76. Liu, J., et al., *Preparation of PEG-conjugated fullerene containing Gd^{3+} ions for photodynamic therapy.* Journal of Controlled Release, 2007. **117**(1): p. 104.
77. Holister, P., ed. *Nanotech: The tiny revolution*. 2002, CPM Cientifica: Madrid, Spain
78. Tomalia, D.A., *The dendritic state.* Materials Today, 2005. **8**(3): p. 34.
79. Tomalia, D.A., *Birth of a new macromolecular architecture: dendrimers as quantized building blocks for nanoscale synthetic polymer chemistry.* Progress in Polymer Science, 2005. **30**(3-4): p. 294.
80. D'Emanuele, A., et al., *The use of a dendrimer-propranolol prodrug to bypass efflux transporters and enhance oral bioavailability.* Journal of Controlled Release, 2004. **95**: p. 5447.
81. Jevprasesphant, R., et al., *Engineering of dendrimer surfaces to enhance transepithelial transport and reduce cytotoxicity.* Pharmaceutical Research, 2003. **20**(10): p. 1543.

82. Sashiwa, H., Y. Shigemasa, and R. Roy, *Chemical modification of chitosan 11: chitosan-dendrimer hybrid as a tree like molecule.* Carbohydrate Polymers, 2002. **49**(2): p. 195.
83. Domanski, D.M., B. Klajnert, and M. Bryszewska, *Incorporation of fluorescent probes into PAMAM dendrimers.* Bioelectrochemistry, 2004. **63**(1-2): p. 193.
84. Tomalia, D.A. and J.M.J. Fréchet, *Discovery of dendrimers and dendritic polymers: A brief historical perspective.* Journal of Polymer Science, Part A: Polymer Chemistry, 2002. **40**: p. 2719.
85. Tomalia, D.A. and J.M. Frechet, *Introduction to "Dendrimers and dendritic polymers".* Progress in Polymer Science, 2005. **30**(3-4): p. 217.
86. Svenson, S. and D.A. Tomalia, *Dendrimers in biomedical applications--reflections on the field.* Advanced Drug Delivery Reviews, 2005. **57**(15): p. 2106.
87. Esfand, R. and D.A. Tomalia, *Poly(amidoamine) (PAMAM) dendrimers: from biomimicry to drug delivery and biomedical applications.* Drug Discovery Today, 2001. **6**(8): p. 427.
88. Sadler, K. and J.P. Tam, *Peptide dendrimers: applications and synthesis.* Reviews in Molecular Biotechnology, 2002. **90**(3-4): p. 195.
89. Turnbull, W.B. and J.F. Stoddart, *Design and synthesis of glycodendrimers* Reviews in Molecular Biotechnology, 2002. **90**: p. 231.
90. Cloninger, M.J., *Biological applications of dendrimers.* Current Opinion in Chemical Biology, 2002. **6**: p. 742.
91. Niederhafner, P., S. Jaroslav, and J. Jezek, *Peptide dendrimers.* Journal of Peptide Science, 2005. **11**: p. 757.
92. Devarakonda, B., R.A. Hill, and M.M. de Villiers, *The effect of PAMAM dendrimer generation size and surface functional group on the aqueous solubility of nifedipine.* International Journal of Pharmaceutics, 2004. **284**(1-2): p. 133.
93. Fréchet, J.M.J., Y. Jiang, and C.J. Hawker. in *A. E. Proceedings of IUPAC International Symposium, Macromolecules*. 1989. Seoul, Korea.
94. Leu, C.-M., et al., *Dendritic poly(ether-imide)s: synthesis, characterization, and modification.* Polymer, 2001. **42**: p. 2339.
95. Leon, J.W. and J.M.J. Fréchet, *Analysis of aromatic polyether dendrimers and dendrimer-linear block copolymers by matrix-assisted laser desorption ionization mass spectrometry*. Polymer Bulletin, 1995. **35**: p. 449.
96. Lee, C.C., et al., *Designing dendrimers for biological applications.* Nature Biotechnology, 2005. **23**: p. 1517.

97. *Dendritic NanoTechnologies announces new low-cost dendrimers.* Focus on Surfactants, 2005. **2005**(8): p. 4.
98. *DNT Inc announces commercial roll out of Priostar dendrimers.* Focus on Surfactants, 2006. **2006**(9): p. 3.
99. Sakharov, D.V., et al., *Binding and retention of polycationic peptides and dendrimers in the vascular wall.* FEBS Letters, 2003. **573**: p. 6.
100. Chauhan, A.S., et al., *Dendrimer-mediated transdermal delivery: enhanced bioavailability of indomethacin.* Journal of Controlled Release, 2003. **90**(3): p. 335.
101. Tam, J.P., *Synthetic peptide vaccine design: synthesis and properties of a high-density multiple antigenic peptide system.* Proceedings of the National Academy of Sciences of the United States of America, 1988. **85**: p. 5409.
102. Choi, Y., et al., *Synthesis and functional evaluation of DNA-assembled polyamidoamine dendrimer clusters for cancer cell-specific targeting.* Chemistry & Biology, 2005. **12**(1): p. 35.
103. Barrett, T., et al., *Macromolecular MRI contrast agents for imaging tumor angiogenesis.* European Journal of Radiology, 2006. **60**(3): p. 353.
104. Ong, K.K., et al., *Dendrimer enhanced immunosensors for biological detection.* Analytica Chimica Acta, 2001. **444**: p. 143.
105. Tam, J.P. and J.K. Abba, *Peptide dendrimers as immunogens*, in *Handbook of Biologically Active Peptides*. 2006, Academic Press: Burlington. p. 541.
106. Han, S., et al., *Synthesis of new spherical and hemispherical oligosaccharides with polylysine core scaffold.* Carbohydrate Polymers, 2007. **68**(1): p. 26.
107. Tulu, M., et al., *Synthesis, characterization and antimicrobial activity of water soluble dendritic macromolecules.* European Journal of Medicinal Chemistry. In Press, Corrected Proof, 2008. (doi:10.1016/j.ejmech.2008.06.016).
108. Chen, C.Z. and S.L. Cooper, *Recent advances in antimicrobial dendrimers.* Advanced Materials, 2000. **12**: p. 843.
109. Gong, E., et al., *Evaluation of dendrimer SPL7013, a lead microbicide candidate against herpes simplex viruses.* Antiviral Research, 2005. **68**(3): p. 139.
110. Jiang, Y.-H., et al., *SPL7013 gel as a topical microbicide for prevention of vaginal transmission of $SHIV_{89.6}P$ in Macaques.* AIDS Research and Human Retroviruses, 2005. **21**: p. 207.
111. Helms, B. and E.W. Meijer, *Dendrimers at work.* Science, 2006. **313**: p. 929.

112. Dutta, T., M. Garg, and N.K. Jain, *Targeting of efavirenz loaded tuftsin conjugated poly(propyleneimine) dendrimers to HIV infected macrophages in vitro.* European Journal of Pharmaceutical Sciences, 2008. **34**(2-3): p. 181.
113. Dutta, T. and N.K. Jain, *Targeting potential and anti-HIV activity of lamivudine loaded mannosylated poly (propyleneimine) dendrimer.* Biochimica et Biophysica Acta (BBA) - General Subjects, 2007. **1770**(4): p. 681.
114. Klajnert, B., et al., *Influence of heparin and dendrimers on the aggregation of two amyloid peptides related to Alzheimer's and prion diseases.* Biochemical and Biophysical Research Communications, 2006. **339**(2): p. 577.
115. Klajnert, B., et al., *Influence of phosphorus dendrimers on the aggregation of the prion peptide PrP 185-208.* Biochemical and Biophysical Research Communications, 2007. **364**(1): p. 20.
116. Heegaard, P.M.H., et al., *Amyloid aggregates of the prion peptide PrP106-126 are destabilised by oxidation and by the action of dendrimers.* FEBS Letters, 2004. **577**(1-2): p. 127.
117. Kasai, S., et al., *Design and synthesis of antiangiogenic/heparin-binding arginine dendrimer mimicking the surface of endostatin.* Bioorganic & Medicinal Chemistry Letters 2002. **12**: p. 951.
118. Shimamura, M., et al., *Angiogenesis inhibition of arginine-rich dendrimers, TX-1943 and TX-1944, which mimic the surface structure of endostatin.* Vascular Pharmacology, 2006. **45**(3): p. e119.
119. Astruc, D., et al., *Metallodendrimers and dendronized gold colloids as nanocatalysts, nanosensors and nanomaterials for molecular electronics.* Comptes Rendus Chimie, 2003. **6**(8-10): p. 1117.
120. Auten, B.J., H. Lang, and B.D. Chandler, *Dendrimer templates for heterogeneous catalysts: Bimetallic Pt-Au nanoparticles on oxide supports.* Applied Catalysis B: Environmental, 2008. **81**(3-4): p. 225.
121. Balzani, V. and F. Vögtle, *Dendrimers as luminescent hosts for metal cations and organic molecules.* Comptes Rendus Chimie, 2003. **6**(8-10): p. 867.
122. Beakley, L.W., et al., *Nanocomposite catalysts: Dendrimer encapsulated nanoparticles immobilized in sol-gel silica.* Applied Catalysis A: General, 2005. **292**: p. 124.
123. Mazzaglia, A., et al., *Synthesis and characterization of poly(amidoamine)-platinum(II) complexes. detailed speciation by matrix-assisted laser desorption ionization mass spectrometry.* Journal of Organometallic Chemistry, 2005. **690**(8): p. 1978.

124. Mazzitelli, C.L. and J.S. Brodbelt, *Investigation of silver binding to polyamidoamine (PAMAM) dendrimers by ESI tandem mass spectrometry.* Journal of the American Society for Mass Spectrometry, 2006. **17**(5): p. 676.
125. Endo, T., T. Yoshimura, and K. Esumi, *Synthesis and catalytic activity of gold-silver binary nanoparticles stabilized by PAMAM dendrimer.* Journal of Colloid and Interface Science, 2005. **286**(2): p. 602.
126. Chessa, G., et al., *Synthesis of poly(pyridylthioether) dendrimers incorporating a Fe2(CO)6 cluster core.* Tetrahedron, 2005. **61**(7): p. 1755.
127. Martinovic, J., et al., *Metallo-functionalized first-generation salicylaldimine poly(propylenimine) tetraamine dendrimers: Electrochemical study and atomic force microscopy imaging.* Electrochimica Acta, 2008. **53**(14): p. 4907.
128. Benito, J.M., et al., *Carbosilane dendrimers containing peripheral cyclopentadienyl niobium- and tantalum-imido complexes.* Journal of Organometallic Chemistry, 2006. **691**(17): p. 3602.
129. Benito, J.M., et al., *Carbosilane dendrimers containing complexes N,N'-pyridylimine of molybdenum and platinum at their periphery.* Journal of Organometallic Chemistry, 2008. **693**(2): p. 278.
130. Al-Hamra, M. and T.H. Ghaddar, *Facile synthesis of poly-(l-lysine) dendrimers with a pentaaminecobalt(III) complex at the core.* Tetrahedron Letters, 2005. **46**(34): p. 5711.
131. Bellis, E. and G. Kokotos, *Proline-modified poly(propyleneimine) dendrimers as catalysts for asymmetric aldol reactions.* Journal of Molecular Catalysis A: Chemical, 2005. **241**(1-2): p. 166.
132. Alivertis, D., et al., *Searching for new host compounds: synthesis and characterization of novel crown ether-functionalized dendrimers.* Tetrahedron Letters, 2007. **48**(23): p. 4091.
133. Caminade, A.-M., et al., *Fluorinated dendrimers.* Current Opinion in Colloid & Interface Science, 2003. **8**(3): p. 282.
134. Caminade, A.-M., et al., *Phosphorus dendrimers: from synthesis to applications.* Comptes Rendus Chimie, 2003. **6**(8-10): p. 791.
135. Caminade, A.-M. and J.-P. Majoral, *Phosphorus dendrimers possessing metallic groups in their internal structure (core or branches): Syntheses and properties.* Coordination Chemistry Reviews, 2005. **249**(17-18): p. 1917.
136. Swallen, S.F., et al., *Exciton localization hierarchy and directed energy transfer in conjugated linear aromatic chains and dendrimeric supermolecules*. Journal of Luminescence, 1998. **76**: p. 193.

137. Devadoss, C., P. Bharathi, and J.S. Moore, Journal of the American Chemical Society, 1996. **118**: p. 9635.
138. Bentz, J.L. and J.J. Kozak, *Influence of geometry on light harvesting in dendrimeric systems. II. nth-nearest neighbor effects and the onset of percolation.* Journal of Luminescence, 2006. **121**(1): p. 62.
139. Balzani, V., et al., *Light-harvesting dendrimers.* Current Opinion in Chemical Biology, 2003. **7**(6): p. 657.
140. Akai, I., et al., *Rapid energy transfer in light-harvesting small dendrimers.* Journal of Luminescence, 2005. **112**(1-4): p. 449.
141. Akai, I., et al., *Energy transfer dynamics in wire-type dendrimers having oligophenylene peripheries.* Journal of Luminescence, 2008. **128**(5-6): p. 948.
142. Andrews, D.L. and S. Li, *Energy flow in dendrimers: An adjacency matrix representation.* Chemical Physics Letters, 2006. **433**(1-3): p. 239.
143. Araki, Y., et al., *Photoinduced intermolecular electron transfer and energy transfer of C60 dendrimers.* Comptes Rendus Chimie, 2006. **9**(7-8): p. 1014.
144. Anthopoulos, T.D., et al., *Influence of molecular structure on the properties of dendrimer light-emitting diodes.* Organic Electronics, 2003. **4**(2-3): p. 71.
145. Cho, J.-S., et al., *Phenylazomethine dendrimer complexes as novel hole-transporting materials of organic light-emitting diodes.* Synthetic Metals, 2005. **150**(1): p. 79.
146. Ceroni, P., et al., *Luminescent dendrimers as ligands for metal ions.* Journal of Organometallic Chemistry, 2004. **689**(24): p. 4375.
147. Bakshi, M.S. and A. Kaura, *Poly(amidoamine) dendrimer interactions with sodium dodecyl sulfate studied by viscosity measurements.* Colloids and Surfaces A: Physicochemical and Engineering Aspects, 2004. **244**(1-3): p. 45.
148. Alvarez-Venicio, V., et al., *Synthesis and incorporation in Langmuir films of oligophenylenevinylene dendrimers bearing a polar head group and different dendritic poly(benzyl ether) branches.* Polymer, 2008. **49**(18): p. 3911.
149. Bao, C., et al., *Preparation of Au nanoparticles in the presence of low generational poly(amidoamine) dendrimer with surface hydroxyl groups.* Materials Chemistry and Physics, 2003. **81**(1): p. 160.

150. Cho, M.Y., et al., *Fabrication and electrical characteristics of organic thin film transistor using [pi]-conjugated dendrimer.* Colloids and Surfaces A: Physicochemical and Engineering Aspects, 2008. **313-314**: p. 431.
151. Arrington, D., et al., *Copper electrodeposition onto the dendrimer-modified native oxide of silicon substrates.* Electrochimica Acta, 2008. **53**(5): p. 2644.
152. Alonso, B., et al., *Amperometric enzyme electrodes for aerobic and anaerobic glucose monitoring prepared by glucose oxidase immobilized in mixed ferrocene-cobaltocenium dendrimers.* Biosensors and Bioelectronics, 2004. **19**(12): p. 1617.
153. Armada, M.P.G., et al., *Electrocatalytical properties of polymethylferrocenyl dendrimers and their applications in biosensing.* Bioelectrochemistry, 2006. **69**(1): p. 65.
154. Yao, K., et al., *ENFET glucose biosensor produced with dendrimer encapsulated Pt nanoparticles.* Materials Science and Engineering: C, 2008. **28**(8): p. 1236.
155. Buschbeck, R. and H. Lang, *Triethylene glycol ether end-grafted carbosilane dendrimers: synthesis and complexation behaviour.* Inorganic Chemistry Communications, 2004. **7**(11): p. 1213.
156. Klajnert, B., M. Sadowska, and M. Bryszewska, *The effect of polyamidoamine dendrimers on human erythrocyte membrane acetylcholinesterase activity.* Bioelectrochemistry, 2004. **65**(1): p. 23.
157. Shcharbin, D., et al., *Effect of dendrimers on pure acetylcholinesterase activity and structure.* Bioelectrochemistry, 2006. **68**(1): p. 56.
158. Kubát, P., K. Lang, and Z. Zelinger, *Interaction of porphyrins with PAMAM dendrimers in aqueous solution.* Journal of Molecular Liquids, 2007. **131-132**: p. 200.
159. Shcharbin, D., et al., *Serum albumins have five sites for binding of cationic dendrimers.* Biochimica et Biophysica Acta (BBA) - Proteins & Proteomics, 2007. **1774**(7): p. 946.
160. Shcharbin, D., et al., *Impact of PAMAM G2 and G6 dendrimers on bovine serum albumin (fatty acids free and loaded with different fatty acids).* Colloids and Surfaces B: Biointerfaces, 2008. **63**(1): p. 27.
161. Bakshi, M.S., et al., *Sodium dodecyl sulfate-poly(amidoamine) interactions studied by AFM imaging, conductivity, and Krafft temperature measurements.* Journal of Colloid and Interface Science, 2004. **278**(2): p. 472.
162. Beezer, A.E., et al., *Dendrimers as potential drug carriers; encapsulation of acidic hydrophobes within water soluble PAMAM derivatives.* Tetrahedron, 2003. **59**(22): p. 3873.

163. Abdelhady, H.G., et al., *Atomic force microscopy studies of generation 4 poly(amidoamine) (PAMAM) dendrimers on functionalized surfaces.* Surface Science, 2004. **558**(1-3): p. 99.
164. Allabashi, R., et al., *Removal of some organic pollutants in water employing ceramic membranes impregnated with cross-linked silylated dendritic and cyclodextrin polymers.* Water Research, 2007. **41**(2): p. 476.
165. Cromer, J.R., et al., *Functionalized dendrimers as endotoxin sponges.* Bioorganic & Medicinal Chemistry Letters, 2005. **15**(5): p. 1295.
166. Labieniec, M., et al., *PAMAM G4 dendrimers lower high glucose but do not improve reduced survival in diabetic rats.* International Journal of Pharmaceutics. 2008. **364**(1): p. 142.
167. Krishna, T.R., et al., *Synthesis and biological evaluation of 3-amino-propan-1-ol based poly(ether imine) dendrimers.* Tetrahedron, 2005. **61**(17): p. 4281.
168. Jayamurugan, G. and N. Jayaraman, *Synthesis of large generation poly(propyl ether imine) (PETIM) dendrimers.* Tetrahedron, 2006. **62**(41): p. 9582.
169. Kofoed, J. and J.-L. Reymond, *Dendrimers as artificial enzymes.* Current Opinion in Chemical Biology, 2005. **9**(6): p. 656.
170. Jiang, D.-L. and T. Aida, *A dendritic iron porphyrin as a novel hemoprotein mimic: effects of the dendrimer cage on dioxygen-binding activity.* Chemical Communications, 1996. **13**: p. 1523-1524.
171. Jiang, D.-L. and T. Aida, *Bioinspired molecular design of functional dendrimers.* Progress in Polymer Science, 2005. **30**(3-4): p. 403.
172. Bezouska, K., *Design, functional evaluation and biomedical applications of carbohydrate dendrimers (glycodendrimers).* Reviews in Molecular Biotechnology 2002. **90**: p. 269.
173. Kobayashi, K., T. Akaike, and T. Usui, *Synthesis of poly (N-acetyl-□-lactosaminide-carrying acrylamide): chemical-enzymatic hybrid process.* Methods in Enzymology, 1994. **242**: p. 226-235.
174. de Paz, J.L., et al., *Potentiation of fibroblast growth factor activity by synthetic heparin oligosaccharide glycodendrimers.* Chemistry & Biology, 2007. **14**(8): p. 879.
175. Malik, N., et al., *Dendrimers: relationship between structure and biocompatibility in vitro, and preliminary studies on the biodistribution of ^{125}I-labelled polyamidoamine dendrimers in vivo.* Journal of Controlled Release, 2000. **65**: p. 133.
176. Domanski, D.M., B. Klajnert, and M. Bryszewska, *Influence of PAMAM dendrimers on human red blood cells.* Bioelectrochemistry, 2004. **63**(1-2): p. 189.
177. Jevprasesphant, R., et al., *The influence of surface modification on the cytotoxicity of PAMAM dendrimers.* International Journal of Pharmaceutics, 2003. **252**(1-2): p. 263.

178. King Heiden, T.C., et al., *Developmental toxicity of low generation PAMAM dendrimers in zebrafish.* Toxicology and Applied Pharmacology, 2007. **225**(1): p. 70.
179. Dutta, T., et al., *Poly(propyleneimine)dendrimer based nanocontainers for targeting of efavirenz to human monocytes/macrophages in vitro.* Journal Drug Targeting, 2007. **15**: p. 89.
180. Neerman, M.F., et al., *In vitro and in vivo evaluation of a melamine dendrimer as a vehicle for drug delivery*. International Journal of Pharmaceutics, 2004. **281**(1-2): p. 129.
181. Sashiwa, H., Y. Shigemasa, and R. Roy, *Chemical modification of chitosan. Part 9: Reaction of N-carboxyethylchitosan methyl ester with diamines of acetal ending PAMAM dendrimers.* Carbohydrate Polymers, 2002. **47**(2): p. 201.
182. Sashiwa, H., Y. Shigemasa, and R. Roy, *Chemical modification of chitosan 8: preparation of chitosan-dendrimer hybrids via short spacer.* Carbohydrate Polymers, 2002. **47**(2): p. 191.
183. Sashiwa, H. and S.-I. Aiba, *Chemically modified chitin and chitosan as biomaterials.* Progress in Polymer Science, 2004. **29**(9): p. 887.
184. Oliveira, J.M., et al., *Surface engineered carboxymethylchitosan/poly(amidoamine) dendrimer nanoparticles for intracellular targeting.* Advanced Functional Materials, 2008. **18**: p. 1840.
185. Dubber, M. and T.K. Lindhorst, *Treahalose-based octopus glycosides for the synthesis of carbohydrate-centered PAMAM dendrimers and thiourea-bridged glycoclusters.* Organic Letters, 2001. **3**: p. 4019.
186. Domanski, D.M., M. Bryszewska, and G. Salamonczyk, *Preliminary evaluation of the behavior of fifth-generation thiophosphate dendrimer in biological systems.* Biomacromolecules, 2004. **5**: p. 2007.
187. Dutta, T., et al., *Toxicological investigation of surface engineered fifth generation poly(propyleneimine) dendrimers in vivo.* Nanotoxicology, 2008. **2**: p. 62.
188. Makimura, Y., G. Zhonghong, and R. Roy, *Synthesis of novel sialic acid-containing polymers as inhibitors of hemagglutination.* International Congress Series, 2001. **1223**: p. 45.
189. Jevprasesphant, R., et al., *Engineering of dendrimer surfaces to enhance transepithelial transport and reduce cytotoxicity.* Pharmaceutical Research, 2003. **20**: p. 1543.
190. Kono, K., et al., *Preparation of poly(ethylene glycol)-modified poly(amidoamine) dendrimers with a shell of hydrophobic amino acid residues and their function as a nanocontainer.* Polymer, 2008. **49**(12): p. 2832.

191. Cheng, Y., M. Li, and T. Xu, *Potential of poly(amidoamine) dendrimers as drug carriers of camptothecin based on encapsulation studies.* European Journal of Medicinal Chemistry, 2008. **43**(8): p. 1791.
192. Cheng, Y., et al., *Polyamidoamine (PAMAM) dendrimers as biocompatible carriers of quinolone antimicrobials: An in vitro study.* European Journal of Medicinal Chemistry, 2007. **42**(7): p. 1032.
193. Yiyun, C. and X. Tongwen, *Dendrimers as potential drug carriers. Part I. Solubilization of non-steroidal anti-inflammatory drugs in the presence of polyamidoamine dendrimers.* European Journal of Medicinal Chemistry, 2005. **40**(11): p. 1188.
194. Yiyun, C., X. Tongwen, and F. Rongqiang, *Polyamidoamine dendrimers used as solubility enhancers of ketoprofen.* European Journal of Medicinal Chemistry, 2005. **40**(12): p. 1390.
195. Dhanikula, R.S. and P. Hildgen, *Influence of molecular architecture of polyether-co-polyester dendrimers on the encapsulation and release of methotrexate.* Biomaterials, 2007. **28**(20): p. 3140.
196. Canetta, E. and G. Maino, *Molecular dynamic analysis of the structure of dendrimers.* Nuclear Instruments and Methods in Physics Research Section B: Beam Interactions with Materials and Atoms, 2004. **213**: p. 71.
197. Cheng, Y. and T. Xu, *The effect of dendrimers on the pharmacodynamic and pharmacokinetic behaviors of non-covalently or covalently attached drugs.* European Journal of Medicinal Chemistry. 2008, **43**(11): p. 2291.
198. D'Emanuele, A., et al., *The use of a dendrimer-propranolol prodrug to bypass efflux transporters and enhance oral bioavailability.* Journal of Controlled Release, 2004. **95**(3): p. 447.
199. Devarakonda, B., et al., *Effect of pH on the solubility and release of furosemide from polyamidoamine (PAMAM) dendrimer complexes.* International Journal of Pharmaceutics, 2007. **345**(1-2): p. 142.
200. Aulenta, F., W. Hayes, and S. Rannard, *Dendrimers: a new class of nanoscopic containers and delivery devices.* European Polymer Journal, 2003. **39**(9): p. 1741.
201. Agashe, H.B., et al., *Investigations on biodistribution of technetium-99m-labeled carbohydrate-coated poly(propylene imine) dendrimers.* Nanomedicine: Nanotechnology, Biology and Medicine, 2007. **3**(2): p. 120.
202. Mano, J.F., *Stimuli-responsive polymeric systems for biomedical applications.* Advanced Engineering Materials, 2008. **10**(6): p. 515.

203. Lee, J.-K., et al., *Efficient synthesis of immolative carbamate dendrimer with olefinic periphery.* Tetrahedron Letters, 2007. **48**(28): p. 4919.
204. Li, S., et al., *Dendrimer disassembly by benzyl ether depolymerization.* Journal of the American Chemical Society, 2003. **125**: p. 10516.
205. Szalai, M.L., R.M. Kevwitch, and D.V. McGrath, *Geometric disassembly of dendrimers: dendritic amplification.* Journal of the American Chemical Society, 2003. **125**: p. 15688.
206. Szalai, M.L. and D.V. McGrath, *Phototriggering of geometric dendrimer disassembly: an improved synthesis of 2,4-bis(hydroxymethyl)phenol based dendrimers.* Tetrahedron, 2004. **60**(34): p. 7261.
207. Hui, H., F. Xiao-dong, and C. Zhong-lin, *Thermo- and pH-sensitive dendrimer derivatives with a shell of poly(N,N-dimethylaminoethyl methacrylate) and study of their controlled drug release behavior.* Polymer, 2005. **46**(22): p. 9514.
208. Pistolis, G., et al., *Poly(propyleneimine) dendrimers as pH-sensitive controlled-release systems.* Chemistry- A European Journal, 1999. **5**: p. 1440.
209. Zheng, Q. and C.-Y. Pan, *Preparation and characterization of dendrimer-star PNIPAAM using dithiobenzoate-terminated PPI dendrimer via RAFT polymerization.* European Polymer Journal, 2006. **42**(4): p. 807.
210. Lai, P.-S., et al., *Doxorubicin delivery by polyamidoamine dendrimer conjugation and photochemical internalization for cancer therapy.* Journal of Controlled Release, 2007. **122**(1): p. 39.
211. Papagiannaros, A., et al., *Doxorubicin-PAMAM dendrimer complex attached to liposomes: Cytotoxic studies against human cancer cell lines.* International Journal of Pharmaceutics, 2005. **302**(1-2): p. 29.
212. Wiwattanapatapee, R., L. Lomlim, and K. Saramunee, *Dendrimers conjugates for colonic delivery of 5-aminosalicylic acid.* Journal of Controlled Release, 2003. **88**(1): p. 1.
213. Ghorai, S., D. Bhattacharyya, and A. Bhattacharjya, *The first examples of anthracene capped chiral carbohydrate derived dendrimers: synthesis, fluorescence and chiroptical properties.* Tetrahedron Letters, 2004. **45**(32): p. 6191.
214. Yamada, A., et al., *Lactotriaose-containing carbosilane dendrimers: Syntheses and lectin-binding activities.* Bioorganic & Medicinal Chemistry, 2007. **15**(4): p. 1606.
215. Yamada, A., et al., *Syntheses of a series of lacto-N-neotetraose clusters using a carbosilane dendrimer scaffold.* Carbohydrate Research, 2006. **341**(4): p. 467.

216. Yamada, A., et al., *Syntheses and Vero toxin-binding activities of carbosilane dendrimers periphery-functionalized with galabiose.* Tetrahedron, 2006. **62**(21): p. 5074.
217. Bhadra, D., et al., *Glycodendrimeric nanoparticulate carriers of primaquine phosphate for liver targeting.* International Journal of Pharmaceutics, 2005. **295**(1-2): p. 221.
218. Agrawal, P., U. Gupta, and N.K. Jain, *Glycoconjugated peptide dendrimers-based nanoparticulate system for the delivery of chloroquine phosphate.* Biomaterials, 2007. **28**(22): p. 3349.
219. Matsuoka, K., et al., *Synthetic assembly of trisaccharide moieties of globotriaosyl ceramide using carbosilane dendrimers as cores. A new type of functional glyco-material.* Tetrahedron Letters, 1999. **40**: p. 7839.
220. Boysen, M.M.K. and T.K. Lindhorst, '*Sugaring' carbosilane dendrimers via hydrosilylation.* Tetrahedron, 2003. **59**(22): p. 3895.
221. Prieto, M.J., et al., *Brain and muscle of Wistar rats are the main targets of intravenous dendrimeric sulfadiazine.* International Journal of Pharmaceutics, 2008. **360**(1-2): p. 204.
222. Bhadra, D., et al., *A PEGylated dendritic nanoparticulate carrier of fluorouracil.* International Journal of Pharmaceutics, 2003. **257**(1-2): p. 111.
223. Gajbhiye, V., et al., *PEGylated PPI dendritic architectures for sustained delivery of H2 receptor antagonist.* European Journal of Medicinal Chemistry. In Press, Corrected Proof, 2008. (doi:10.1016/j.semarthrit.2008.08.004).
224. Haba, Y., et al., *Synthesis of biocompatible dendrimers with a peripheral network formed by linking of polymerizable groups.* Polymer, 2005. **46**(6): p. 1813.
225. Kono, K., et al., *Preparation and cytotoxic activity of poly(ethylene glycol)-modified poly(amidoamine) dendrimers bearing adriamycin.* Biomaterials, 2008. **29**(11): p. 1664.
226. Dodziuk, H., et al., *Synthesis and NMR study of a first generation dendrimer having four branches involving four glycine and one carbomoyl-(3,7-dimethoxy-2-naphthalene) groups and attempts to complex it with α-, β- or γ-cyclodextrins.* Journal of Molecular Structure, 2004. **693**(1-3): p. 145.
227. Muhanna, A.M.A., et al., *Synthesis of peptide dendrimers based on a [beta]-cyclodextrin core with guest binding ability.* Tetrahedron Letters, 2003. **44**(32): p. 6125.
228. Imae, T., et al., *Binding of poly(amido amine) dendrimer to sodium hyaluronate in aqueous NaCl solution.* Journal of Colloid and Interface Science, 2003. **263**(1): p. 306.
229. Kitchens, K.M., M.E.H. El-Sayed, and H. Ghandehari, *Transepithelial and endothelial transport of poly(amidoamine) dendrimers.* Advanced Drug Delivery Reviews, 2005. **57**(15): p. 2163.

230. Perumal, O.P., et al., *The effect of surface functionality on cellular trafficking of dendrimers.* Biomaterials, 2008. **29**(24-25): p. 3469.
231. Pisal, D.S., et al., *Permeability of surface-modified polyamidoamine (PAMAM) dendrimers across Caco-2 cell monolayers.* International Journal of Pharmaceutics, 2008. **350**(1-2): p. 113.
232. Seib, F.P., A.T. Jones, and R. Duncan, *Comparison of the endocytic properties of linear and branched PEIs, and cationic PAMAM dendrimers in B16f10 melanoma cells.* Journal of Controlled Release, 2007. **117**(3): p. 291.
233. Spangrude, G.J., *Stem cells and tissue regeneration: When is a stem cell really a stem cell?* Bone Marrow Transplantation, 2003. **32**: p. S7.
234. Langer, R. and J. Vacanti, *Tissue Engineering.* Science, 1993. **260**: p. 920.
235. Griffith, L.G. and G. Naughton, *Tissue engineering-current challenges and expanding opportunities.* Science, 2002. **295**: p. 1009.
236. Risbud, M.V. and M. Sittinger, *Tissue engineering: advances in in vitro cartilage generation.* Trends in Biotechnology, 2002. **20** (8): p. 351.
237. Zeng, X. and M.S. Rao, *Human embryonic stem cells: Long term stability, absence of senescence and a potential cell source for neural replacement.* Neuroscience, 2007. **145**(4): p. 1348.
238. McKay, R., *Stem cells - hype and hope.* Nature, 2000. **406**: p. 361.
239. McLaren, A., *Ethical and social considerations of stem cell research.* Nature, 2001. **414**: p. 129.
240. Dawson, L., et al., *Safety issues in cell-based intervention trials.* Fertility and Sterility, 2003. **80**: p. 1077.
241. Rando, T.A., *Stem cells, ageing and the quest for immortality.* Nature, 2006. **441**: p. 1080.
242. Vogel, G., *International standards proposed for stem cell work*, in *Science*. 2006. p. 26.
243. Verfaillie, C.M., *Adult stem cells: assessing the case for pluripotency.* Trends in Cell Biology, 2002. **12**: p. 502.
244. Pountos, I. and P.V. Giannoudis, *Biology of mesenchymal stem cells.* Injury, International Journal of the Care of the Injured, 2005. **365**: p. S8.
245. Wright, D.E., et al., *Physiological migration of hematopoietic stem and progenitor cells.* Science, 2001. **294**: p. 1933.
246. Trojani, C., et al., *Ectopic bone formation using an injectable biphasic calcium phosphate/Si-HPMC hydrogel composite loaded with undifferentiated bone marrow stromal cells.* Biomaterials 2006. **27**: p. 3256.

247. Dezawa, M., et al., *Specific induction of neuronal cells from bone marrow stromal cells and application for autologous transplantation.* The Journal of Clinical Investigation 2004. **113**: p. 1701.
248. Jiang, Y., et al., *Pluripotency of mesenchymal stem cells derived from adult marrow.* Nature, 2002. **418**: p. 41.
249. Miyahara, Y., et al., *Monolayered mesenchymal stem cells repair scarred myocardium after myocardial infarction.* Nature Medicine, 2006. **12**: p. 459.
250. Loebel, D.A.F., et al., *Lineage choice and differentiation in mouse embryos and embryonic stem cells.* Developmental Biology, 2003. **264**(1): p. 1.
251. Barry, F.P. and J.M. Murphy, *Mesenchymal stem cells: clinical applications and biological characterization.* The International Journal of Biochemistry & Cell Biology 2004. **36**: p. 568.
252. Anker, P.S., et al., *Mesenchymal stem cells in human second-trimester bone marrow, liver, lung, and spleen exhibit a similar immunophenotype but a heterogeneous multilineage differentiation potential.* Haematologica, 2003. **88**(8): p. 845.
253. Romanov, Y.A., V.A. Svintsitskaya, and V.N. Smirnov, *Searching for alternative sources of postnatal human mesenchymal stem cells: candidate MSC-like cells from umbilical cord.* Stem Cells, 2003. **21**(1): p. 105.
254. Fraser, J.K., et al., *Fat tissue: an underappreciated source of stem cells for biotechnology.* Trends in Biotechnology, 2006. **24**(4): p. 150.
255. Bongso, A. and M. Richards, *History and perspective of stem cell research.* Best Practice & Research Clinical Obstetrics and Gynaecology, 2004. **18**(6): p. 827.
256. De Coppi, P., et al., *Isolation of amniotic stem cell lines with potential for therapy.* Nature Biotechnology, 2007. **25**(1): p. 100.
257. Takahashi, K. and S. Yamanaka, *Induction of pluripotent stem cells from mouse embryonic and adult fibroblast cultures by defined factors.* Cell, 2006. **126**(4): p. 663.
258. Takahashi, K., et al., *Induction of pluripotent stem cells from fibroblast cultures.* Nature Protocols 2007. **2**(12): p. 3081.
259. Yamanaka, S., *Induction of pluripotent stem cells from mouse fibroblasts by four transcription factors.* Cell Proliferation, 2008. **41** (1): p. 51.
260. Park, I.-H., et al., *Reprogramming of human somatic cells to pluripotency with defined factors.* Nature, 2008. **451**(10): p. 141.

261. Le Nihouannen, D., et al., *Ectopic bone formation by microporous calcium phosphate ceramic particles in sheep muscles.* Bone 2005. **36**: p. 1086.
262. Rahaman, M.N. and J.J. Mao, *Stem cell-based composite tissue constructs for regenerative medicine.* Biotechnology and Bioengineering, 2005. **91**: p. 261.
263. Cancedda, R., et al., *Tissue engineering and cell therapy of cartilage and bone.* Matrix Biology 2003. **22**: p. 81.
264. Srouji, S. and E. Livne, *Bone marrow stromal cells and biological scaffold for bone repair in aging and disease.* Mechanisms of Ageing and Development, 2005. **126**: p. 281.
265. Hollister, S.J., *Porous scaffold design for tissue engineering.* Nature Materials, 2005. **4**: p. 518.
266. Van Thienen, T.G., et al., *On the synthesis and characterization of biodegradable dextran nanogels with tunable degradation properties.* Journal of Controlled Release, 2006. **116**(2): p. e12.
267. Haugh, M.G., et al., *The effect of pore size, crosslinking and collagen content on mechanical properties of collagen-GAG scaffolds.* Journal of Biomechanics, 2006. **39**(1): p. S216.
268. Dong, W., et al., *Biocompatible nanofiber scaffolds on metal for controlled release and cell colonization.* Nanomedicine: Nanotechnology, Biology and Medicine, 2006. **2**(4): p. 248.
269. Wang, H., et al., *Biocompatibility and osteogenesis of biomimetic nano-hydroxyapatite/polyamide composite scaffolds for bone tissue engineering.* Biomaterials, 2007. **28**(22): p. 3338.
270. Lutolf, M.P. and J.A. Hubbell, *Synthetic biomaterials as instructive extracellular microenvironments for morphogenesis in tissue engineering.* Nature Biotechnology, 2005. **23**: p. 47.
271. Liao, S., et al., *Processing nanoengineered scaffolds through electrospinning and mineralization suitable for biomimetic bone tissue engineering.* Journal of the Mechanical Behavior of Biomedical Materials, 2008. **1**(3): p. 252.
272. Mano, J.F., et al., *Bioinert, biodegradable and injectable polymeric matrix composites for hard tissue replacement: state of the art and recent developments.* Composites Science and Technology, 2004. **64**(6): p. 789.
273. Rezwan, K., et al., *Biodegradable and bioactive porous polymer/inorganic composite scaffolds for bone tissue engineering.* Biomaterials, 2006. **27**(18): p. 3413.
274. Marolt, D., et al., *Bone and cartilage tissue constructs grown using human bone marrow stromal cells, silk scaffolds and rotating bioreactors.* Biomaterials, 2006. **27**(36): p. 6138.

275. Gilbert, T.W., T.L. Sellaro, and S.F. Badylak, *Decellularization of tissues and organs.* Biomaterials, 2006. **27**(19): p. 3675.
276. Karageorgiou, V. and D. Kaplan, *Porosity of 3D biomaterial scaffolds and osteogenesis.* Biomaterials, 2005. **26**: p. 5474.
277. Chen, X., et al., *Effects of micropatterned surfaces coated with type I collagen on the proliferation and morphology of tenocytes.* Applied Surface Science, 2008. **255**(2): p. 368.
278. Stevens, M.M. and J.H. George, *Exploring and engineering the cell surface interface.* Science, 2005. **310**: p. 1135.
279. Vartanian, K.B., et al., *Endothelial cell cytoskeletal alignment independent of fluid shear stress on micropatterned surfaces.* Biochemical and Biophysical Research Communications, 2008. **371**(4): p. 787.
280. Andruzzi, L., et al., *Bio-selective surfaces by chemically amplified constructive microlithography.* Surface Science, 2007. **601**(21): p. 4984.
281. Dusseiller, M.R., et al., *An inverted microcontact printing method on topographically structured polystyrene chips for arrayed micro-3-D culturing of single cells.* Biomaterials, 2005. **26**(29): p. 5917.
282. Das, T., et al., *Microcontact printing of Concanavalin A and its effect on mammalian cell morphology.* Journal of Colloid and Interface Science, 2007. **314**(1): p. 71.
283. Heng, B.C., et al., *Strategies for directing the differentiation of stem cells into the cardiomyogenic lineage in vitro.* Cardiovascular Research, 2004. **62**: p. 34.
284. Zhang, J. and L. Li, *BMP signaling and stem cell regulation.* Developmental Biology, 2005. **284**: p. 1.
285. Kato, M., et al., *Ectopic bone formation in mice associated with a lactic acid/dioxanone/ethylene glycol copolymer–tricalcium phosphate composite with added recombinant human bone morphogenetic protein-2.* Biomaterials 2006. **27** p. 3927.
286. Hosseinkhani, H., et al., *Enhanced ectopic bone formation using a combination of plasmid DNA impregnation into 3-D scaffold and bioreactor perfusion culture.* Biomaterials 2006. **27**: p. 1387.
287. Marolt, D., et al., *Bone and cartilage tissue constructs grown using human bone marrow stromal cells, silk scaffolds and rotating bioreactors.* Biomaterials 2006. **27** p. 6138.
288. Marler, J.J., et al., *Transplantation of cells in matrices for tissue regeneration.* Advanced Drug Delivery Reviews 1998. **33**: p. 165.

289. Jeong, S.I., et al., *Mechano-active tissue engineering of vascular smooth muscle using pulsatile perfusion bioreactors and elastic PLCL scaffolds.* Biomaterials, 2005. **26**(12): p. 1405.
290. Wendt, D., M. Jakob, and I. Martin, *Bioreactor-based engineering of osteochondral grafts: from model systems to tissue manufacturing.* Journal of Bioscience and Bioengineering, 2005. **100**: p. 489.
291. Mano, J.F. and R.L. Reis, *Osteochondral defects: present situation and tissue engineering approaches.* Journal of Tissue Engineering and Regenerative Medicine, 2007. **1** (4): p. 261.
292. Sucosky, P., et al., *Fluid mechanics of a spinner-flask bioreactor.* Biotechnology and Bioengineering, 2003. **85**(1): p. 34.
293. Ruottinen, M., et al., *On-line monitoring of HeLa cell growth and cell cycle in spinner flask cultures.* Journal of Biotechnology, 2007. **131**(1): p. S70.
294. Jun, D., et al., *Impacts of aeration and active sludge addition on leachate recirculation bioreactor.* Journal of Hazardous Materials, 2007. **147**(1-2): p. 240.
295. Mahmoudifar, N. and P.M. Doran, *Tissue engineering of human cartilage and osteochondral composites using recirculation bioreactors.* Biomaterials, 2005. **26**(34): p. 7012.
296. Manley, P. and P.I. Lelkes, *A novel real-time system to monitor cell aggregation and trajectories in rotating wall vessel bioreactors.* Journal of Biotechnology, 2006. **125**(3): p. 416.
297. Singh, H., et al., *Flow modelling within a scaffold under the influence of uni-axial and bi-axial bioreactor rotation.* Journal of Biotechnology, 2005. **119** p. 181.
298. Ayyaswamy, P.S. and K. Mukundakrishnan, *Optimal conditions for simulating microgravity employing NASA designed rotating wall vessels.* Acta Astronautica, 2007. **60**(4-7): p. 397.
299. Heyes, C.D., et al., *Synthesis, patterning and applications of star-shaped poly(ethylene glycol) biofunctionalized surfaces.* Molecular Biosystems, 2007. **3**: p. 419.
300. Kawase, M., et al., *Effectiveness of polyamidoamine dendrimers modified with tripeptide growth factor, glycyl-L-histidyl-L-lysine, for enhancement of function of hepatoma cells.* Journal of Bioscience and Bioengineering, 1999. **88**: p. 433.
301. Tomalia, D.A., et al., *Structure control within poly(amidoamine) dendrimers: size, shape and regio-chemical mimicry of globular proteins.* Tetrahedron, 2003. **59**: p. 3799.
302. Tomalia, D.A., et al., *Partial shell-filled core-shell tecto(dendrimers): A strategy to surface differentiated nano-clefts and cusps.* Proceedings of the National Academy of Sciences of the United States of America, 2002. **99**(8): p. 5081.

303. Gabellieri, E., et al., *Dendrimer-protein interactions studied by tryptophan room temperature phosphorescence.* Biochimica et Biophysica Acta (BBA) - Proteins & Proteomics, 2006. **1764**(11): p. 1750.
304. Klajnert, B., et al., *Interactions between PAMAM dendrimers and bovine serum albumin.* Biochimica et Biophysica Acta (BBA) - Proteins & Proteomics, 2003. **1648**(1-2): p. 115.
305. Kim, M.-H., et al., *Response of human epithelial cells to culture surfaces with varied roughnesses prepared by immobilizing dendrimers with/without d-glucose display.* Journal of Bioscience and Bioengineering, 2007. **103**(2): p. 192.
306. Benhabbour, S.R., H. Sheardown, and A. Adronov, *Cell adhesion and proliferation on hydrophilic dendritically modified surfaces.* Biomaterials, 2008. **29**(31): p. 4177.
307. Abukawa, H., et al., *Reconstruction of mandibular defects with autologous tissue-engineered bone.* Journal of Oral and Maxillofacial Surgery, 2004. **62**(5): p. 601.
308. Herve Petite, et al., *Tissue-engineered bone regeneration.* Nature Biotechnology, 2000. **18**: p. 959.
309. Saint-Cyr, M., et al., *Immediate corticocancellous bone autografting in segmental bone defects of the hand.* The Journal of Hand Surgery: Journal of the British Society for Surgery of the Hand, 2006. **31**(2): p. 168.
310. Merkx, M.A.W., et al., *Incorporation of three types of bone block implants in the facial skeleton.* Biomaterials, 1999. **20**(7): p. 639.
311. Su-Gwan, K., K. Hak-Kyun, and L. Sung-Chul, *Combined implantation of particulate dentine, plaster of Paris, and a bone xenograft (Bio-Oss(R)) for bone regeneration in rats.* Journal of Cranio-Maxillofacial Surgery, 2001. **29**(5): p. 282.
312. Babensee, J.E., et al., *Host response to tissue engineered devices.* Advanced Drug Delivery Reviews, 1998. **33**(1-2): p. 111.
313. Kahan, B.D., *Immunosupressive therapy.* Current Opinion in Immunology, 1992. **4**: p. 553.
314. Langer, R. and J.P. Vacanti, *Tissue Engineering.* Science, 1993. **260**: p. 920.
315. Srouji, S. and E. Livne, *Bone marrow stem cells and biological scaffold for bone repair in aging and disease.* Mechanisms of Ageing and Development, 2005. **126**(2): p. 281.
316. Ohgushi, H., et al., *Tissue engineered ceramic artificial joint-ex vivo osteogenic differentiation of patient mesenchymal cells on total ankle joints for treatment of osteoarthritis.* Biomaterials, 2005. **26**(22): p. 4654.

317. Uemura, T., et al., *Transplantation of cultured bone cells using combinations of scaffolds and culture techniques.* Biomaterials, 2003. **24**(13): p. 2277.
318. Oliveira, J.M., et al., *Dexamethasone-loaded carboxymethylchitosan/Poly(amidoamine) dendrimer nanoparticles induces the osteogenic differentiation of rat bone marrow stromal cells seeded onto the surface of hydroxyapatite and starch-polycaprolactone scaffolds: In vitro study.* Biomaterials, 2009. **30**(5): p. 804.
319. Oliveira, J.M., et al., *Dexamethasone-loaded carboxymethylchitosan/poly(amidoamine) dendrimer nanoparticles enhances bone formation in vivo.* Tissue Engineering Part A, 2008. **14**(5): p. 721.
320. Lygre, H., *Prosthodontic biomaterials and adverse reactions: a critical review of the clinical and research literature.* Acta Odontologica Scandinavica, 2002. **60**: p. 1.
321. Viljanen, E.K., M. Skrifvars, and P.K. Vallittu, *Dendritic copolymers and particulate filler composites for dental applications: Degree of conversion and thermal properties.* Dental Materials, 2007. **23**(11): p. 1420.
322. Temenoff, J.S. and A.G. Mikos, *Review: tissue engineering for regeneration of articular cartilage.* Biomaterials, 2000. **21**: p. 431.
323. Aigner, T. and J. Stove, *Collagens-major component of the physiological cartilage matrix, major target of cartilage degeneration, major tool in the cartilage repair.* Advanced Drug Delivery Reviews, 2003. **55**: p. 1569.
324. Buckwalter, J.A., *Articular cartilage: injuries and potential for healing.* Journal of Orthopaedic & Sports Physical Therapy, 1998. **28**: p. 192.
325. Redman, S.N., S.F. Oldfield, and C.W. Archer, *Current strategies for articular cartilage repair.* European Cells and Materials, 2005. **9**: p. 23.
326. Glowacki, J., *In vitro engineering of cartilage.* Journal of Rehabilitation Research and Development, 2000. **37**: p. 171.
327. Miller, B.S., et al., *Patient satisfaction and outcome after microfracture of degenerative knee.* The Journal of Knee Surgery, 2004. **17**: p. 13.
328. Krishnan, S.P. and J.A. Skinner, *(i) Novel treatments for early osteoarthritis of the knee.* Current Orthopaedics, 2005. **19**: p. 407.
329. Akizuki, S., Y. Yasukawa, and T. Takizawa, *Does arthroscopic abrasion arthroplasty promote cartilage regeneration in osteoarthritic knees with eburnation? A prospective study of high tibial osteotomy with abrasion arthroplasty versus high tibial osteotomy alone.* Arthroscopy, 1997. **13**: p. 9.

330. Shapiro, F., S. Koide, and M.J. Glimcher, *Cell origin and differentiation in the repair of full-thickness defects of articular cartilage.* The Journal of Bone & Joint Surgery American Volume, 1993. **75**: p. 532.
331. Tibesku, C.O., et al., *Hyaline cartilage degenerates after autologous osteochondral transplantation.* Journal of Orthopaedic Research, 2004. **22**: p. 1210.
332. Sontjens, S.H.M., et al., *Biodendrimer-based hydrogel scaffolds for cartilge tissue repair.* Biomacromolecules, 2006. **7**: p. 310.
333. Khew, S.T., Q.J. Yang, and Y.W. Tong, *Enzymatically crosslinked collagen-mimetic dendrimers that promote integrin-targeted cell adhesion.* Biomaterials, 2008. **29**(20): p. 3034.
334. Duan, X. and H. Sheardown, *Dendrimer crosslinked collagen as a corneal tissue engineering scaffold: Mechanical properties and corneal epithelial cell interactions.* Biomaterials, 2006. **27**(26): p. 4608.
335. Grinstaff, M.W., *Designing hydrogel adhesives for corneal wound repair.* Biomaterials, 2007. **28**(35): p. 5205.
336. Hata, N., et al., *Dendrimer-immobilized culture surface as a tool to evaluate formation of cellular cytoskeleton of anchorage-dependent cells.* Journal of Bioscience and Bioengineering, 2004. **97**(4): p. 233.
337. Mellado, M. and Y.R. Carrasco, *Imaging techniques: New insights into chemokine/chemokine receptor biology at the immune system.* Pharmacology & Therapeutics, 2008. **119**: p. 24.
338. Hamann, I., F. Zipp, and C. Infante-Duarte, *Therapeutic targeting of chemokine signaling in multiple sclerosis.* Journal of the Neurological Sciences, 2008. **274**: p. 31.
339. Silva, T.A., et al., *Chemokines in oral inflammatory diseases: Apical periodontitis and periodontal disease.* Journal of Dental Research, 2007. **86**: p. 306.
340. Cascieri, M.A. and M.S. Springer, *The chemokine/chemokine-receptor family: potential and progress for therapeutic intervention.* Current Opinion in Chemical Biology, 2000. **4**: p. 420.
341. Neel, N.F., et al., *Chemokine receptor internalization and intracellular trafficking.* Cytokine & Growth Factor Reviews, 2005. **16**: p. 637.
342. Cartier, L., et al., *Chemokine receptors in the central nervous system: role in brain inflammation and neurodegenerative diseases.* Brain Research Reviews, 2005. **48**: p. 16.
343. Grainger, D.J. and J. Reckless, *Broad-spectrum chemokine inhibitors (BSCIs) and their anti-inflammatory effects in vivo.* Biochemical Pharmacology, 2003. **65**: p. 1027.

344. Honczarenko, M., et al., *Human bone marrow stromal cells express a distinct set of biologically functional chemokine receptors.* Stem Cells, 2006. **24**: p. 1030.
345. Fox, S., *Human Physiology*. 8th Edition, ed. M.-H. Companies. 2003.
346. Junqueira, L. and J. Carneiro, *Basic Histology*. 10th Edition, ed. G. Koogan. 2004, Rio de Janeiro.
347. Marieb, E., *Human Anatomy and Physiology*. 5th Edition, ed. B. Cummings. 1992, Redwood City, CA.
348. Marieb, E., *Human Anatomy and Physiology*, ed. Pearson. 2004, New York.
349. Purves, D., *Neuroscience*, ed. S.A. Publishing. 1997, New York.
350. Kabanov, A.V. and H.E. Gendelman, *Nanomedicine in the diagnosis and therapy of neurodegenerative disorders.* Progress in Polymer Science, 2007. **32**(8-9): p. 1054.
351. Partdrige, W., *The blood-brain barrier: bottlneck in brain drug development.* NeuroRx, 2005. **2**: p. 3.
352. Mayhan, W., *Regulation of blood-brain barrier permeability.* Microcirculation, 2001. **8**: p. 90.
353. Smith, M.W. and M. Gumbleton, *Endocytosis at the blood brain barrier: from basic understanding to drug delivery strategies.* Journal of Drug Targeting, 2006. **14**: p. 191.
354. da Cruz, M.T., et al., *Tf-lipoplex-mediated NGF gene transfer to the CNS: neuronal protection and recovery in an excitotoxic model of brain injury.* Gene Therapy 2005. **12**: p. 1242.
355. da Cruz, M.T., S. Simões, and M.C. de Lima, *Improving lipoplex-mediated gene transfer into C6 glioma cells and primary neurons.* Experimental Neurology, 2004. **187**(1): p. 65.
356. Rao, K.S., et al., *TAT-conjugated nanoparticles for the CNS delivery of anti-HIV drugs.* Biomaterials, 2008. **29**(33): p. 4429.
357. Pulkkinen, M., et al., *Three-step tumor targeting of paclitaxel using biotinylated PLA-PEG nanoparticles and avidin-biotin technology: Formulation development and in vitro anticancer activity.* European Journal of Pharmaceutics and Biopharmaceutics, 2008. **70**: p. 66.
358. Vinogradov, S.V., E.V. Batrakova, and A.V. Kabanov, *Nanogels for oligonucletide delivery to the brain.* Bioconjugate Chemistry, 2004. **15**: p. 50.
359. Dhanikula, R.S., et al., *Methotrexate loaded polyether-copolyester dendrimers for the treatment of gliomas: enhanced efficacy and intratumoral transport capability.* Molecular Pharmaceutics, 2008. **5**: p. 105.
360. Supattapone, S., et al., *Elimination of prions by branched polyamines and implications for therapeutics.* Proceedings of the National Academy of Sciences of the United States of America, 1999. **96**(25): p. 14529.

361. Supattapone, S., et al., *Branched polyamines cure prion-infected neuroblastoma cells.* Journal of Virology, 2001. **75**(7): p. 3453.
362. Klajnert, B., et al., *Influence of dendrimer's structure on its activity against amyloid fibril formation.* Biochemical and Biophysical Research Communications, 2006. **345**(1): p. 21.
363. Patel, D.A., J.E. Henry, and T.A. Good, *Attenuation of [beta]-amyloid-induced toxicity by sialic-acid-conjugated dendrimers: Role of sialic acid attachment.* Brain Research, 2007. **1161**: p. 95.
364. Kim, J.B., et al., *Enhanced transfection of primary cortical cultures using arginine-grafted PAMAM dendrimer, PAMAM-Arg.* Journal of Controlled Release, 2006. **114**: p. 110.
365. Choi, J.S., et al., *Enhanced transfection efficiency of PAMAM dendrimer by surface modification with L-arginine.* Journal of Controlled Release, 2004. **99**(3): p. 445.
366. Wu, G., et al., *Molecular targeting and treatment of an epidermal growth factor receptor-positive glioma using boronated cetuximab.* Clinical Cancer Research, 2007. **13**: p. 1260.
367. Morgan, M.T., et al., *Dendrimer-encapsulated camptothecins: increased solubility, cellular uptake, and cellular retention affords enhanced anticancer activity in vitro.* Cancer Research, 2006. **66**: p. 11913.
368. Salgado, A.J., et al., *In vitro characterization on the interactions between carboxymethylchitosan/poly(amidoamine) dendrimer nanoparticles and neurons/glial cells.* Tissue Engineering, 2008: p. submitted.
369. Kay, M.A., J.C. Glorioso, and L. Naldini, *Viral vectors for gene therapy: the art of turning infectious agents into vehicles of therapeutics.* Nature Medicine, 2001. **7**(1): p. 33.
370. Merdan, T., J. Kopecek, and T. Kissel, *Prospects for cationic polymers in gene and oligonucleotide therapy against cancer.* Advanced Drug Delivery Reviews, 2002. **54**(5): p. 715.
371. Haensler, J. and F.C. Szoka Jr., *Polyamidoamine cascade polymers mediate efficient transfection of cells in culture.* Bioconjugate Chemistry, 1993. **4**: p. 372.
372. Kim, H.J., et al., *Synthesis and characterization of poly(amino ester) for slow biodegradable gene delivery vector.* Bioorganic & Medicinal Chemistry, 2007. **15**: p. 1708.
373. Galletti, R., et al., *Inhibition of Epstein Barr Virus LMP1 gene expression in B lymphocytes by antisense oligonucleotides: Uptake and efficacy of lipid-based and receptor-mediated delivery systems.* Antiviral Research, 2007. **74**(2): p. 102.
374. Arima, H., et al., *Enhancement of gene transfer activity mediated by mannosylated dendrimer/[alpha]-cyclodextrin conjugate (generation 3, G3).* Journal of Controlled Release, 2006. **116**(1): p. 64.

375. Luo, D., et al., *Poly(ethylene glycol)-conjugated PAMAM dendrimer for biocompatible, high-efficiency DNA delivery.* Macromolecules, 2002. **35**: p. 3456.
376. Zhang, X.-Q., et al., *In vitro gene delivery using polyamidoamine dendrimers with a trimesyl core.* Biomacromolecules, 2005. **6**: p. 341.
377. Boussif, O., et al., *A versatile vector for gene and oligonucleotide transfer into cells in culture and in vivo: polyethylenimine.* Proceedings of the National Academy of Sciences of the United States of America, 1995. **92**: p. 7297.
378. Dung, T.H., et al., *Preparation and evaluation of cholesteryl PAMAM dendrimers as nano delivery agents for antisense oligonucleotides.* Colloids and Surfaces A: Physicochemical and Engineering Aspects, 2008. **313-314**: p. 273.
379. Russ, V., et al., *Oligoethylenimine-grafted polypropylenimine dendrimers as degradable and biocompatible synthetic vectors for gene delivery.* Journal of Controlled Release, 2008. **132**(2): p. 131.
380. Tziveleka, L.-A., et al., *Synthesis and characterization of guanidinylated poly(propylene imine) dendrimers as gene transfection agents.* Journal of Controlled Release, 2007. **117**(1): p. 137.
381. Tziveleka, L.-A., et al., *Synthesis and evaluation of functional hyperbranched polyether polyols as prospected gene carriers.* International Journal of Pharmaceutics, 2008. **356**(1-2): p. 314.
382. Choi, J.S., et al., *Dexamethsone conjugated poly(amidoamine) dendrimer as a gene carrier for efficient nuclear translocation.* International Journal of Pharmaceutics, 2006. **320**: p. 171.
383. Manunta, M., et al., *Gene delivery by dendrimers operates via different pathways in different cells, but is enhanced by the presence of caveolin.* Journal of Immunological Methods, 2006. **314**: p. 134.
384. Ruponen, M., et al., *Extracellular and intracellular barriers in non-viral gene delivery.* Journal of Controlled Release, 2003. **93**(2): p. 213.
385. Diaz-Mochon, J.J., et al., *Peptoid dendrimers-microwave-assisted solid-phase synthesis and transfection agent evaluation.* Tetrahedron Letters, 2008. **49**(5): p. 923.
386. Herrmann, A., et al., *Peptide-functionalized polyphenylene dendrimers.* Tetrahedron, 2003. **59**(22): p. 3925.
387. Mannisto, M., et al., *Structure-activity relationships of poly(L-lysines): effects of pegylation and molecular shape on physicochemical and biological properties in gene delivery.* Journal of Controlled Release, 2002. **83**: p. 169.

388. Higashi, N., et al., *Chain length effects of oligo(l-lysine)-shelled dendrimers on interaction with DNA.* International Journal of Biological Macromolecules, 2006. **38**(2): p. 120.
389. Okuda, T., et al., *Characters of dendritic poly(L-lysine) analogues with the terminal lysines replaced with arginines and histidines as gene carriers in vitro.* Biomaterials 2004. **25**: p. 537.
390. Hussain, M., et al., *A novel anionic dendrimer for improved cellular delivery of antisense oligonucleotides.* Journal of Controlled Release, 2004. **99**: p. 139.
391. Kuo, J.-H.S. and Y.-L. Lin, *Remnant cationic dendrimers block RNA migration in electrophoresis after monophasic lysis.* Journal of Biotechnology, 2007. **129**(3): p. 383.
392. Nishiyama, N., et al., *Light-induced gene transfer from packaged DNA enveloped in a dendrimeric photosensitizer.* Nature Materials, 2005. **4**: p. 934.
393. Shieh, M.-J., et al., *Non-toxic phototriggered gene transfection by PAMAM-porphyrin conjugates.* Journal of Controlled Release, 2008. **129**(3): p. 200.
394. Kuo, J.-h.S., M.-s. Jan, and Y.-L. Lin, *Interactions between U-937 human macrophages and poly(propyleneimine) dendrimers.* Journal of Controlled Release, 2007. **120**(1-2): p. 51.
395. Kobayashi, H., et al., *Renal tubular damage detected by dynamic micro-MRI with a dendrimer-based magnetic resonance contrast agent.* Kidney International, 2002. **61**: p. 1980.
396. Rietveld, I.B., E. Kim, and S.A. Vinogradov, *Dendrimers with tetrabenzoporphyrin cores: near infrared phosphors for in vivo oxygen imaging.* Tetrahedron, 2003. **59**(22): p. 3821.
397. Thomas, T.P., et al., *In vitro targeting of synthesized antibody-conjugated dendrimer nanoparticles.* Biomacromolecules, 2004. **5**: p. 2269.
398. Shukla, R., et al., *HER2 specific tumor targeting with dendrimer conjugated anti-HER2 mAb.* Bioconjugate Chemistry, 2006. **17**: p. 1109.
399. Kolhe, P., et al., *Drug complexation, in vitro release and cellular entry of dendrimers and hyperbranched polymers.* International Journal of Pharmaceutics, 2003. **259**(1-2): p. 143.
400. Agarwal, A., et al., *Ligand based dendritic systems for tumor targeting.* International Journal of Pharmaceutics, 2008. **350**(1-2): p. 3.
401. Pun, S.H., et al., *Targeted delivery of RNA cleaving DNA-enzyme (DNAzyme) to tumor tissue by transferrin-modified, cyclodextrin-based particles.* Cancer Biology & Therapy, 2004. **7:** p. 31.
402. Citro, G., et al., *Inhibition of leukemia cell proliferation by receptor-mediated uptake of cmyb antisense oligodeoxynucleotides.* Proceedings of the National Academy of Sciences of the United States of America, 1992. **89**: p. 7031.

403. Majoros, I.J., et al., *PAMAM dendrimer-based multifunctional conjugate for cancer therapy: synthesis, characterization, and functionality.* Biomacromolecules, 2006. **7**: p. 572.
404. Islam, M.T., I.J. Majoros, and J.J.R. Baker, *HPLC analysis of PAMAM dendrimer based multifunctional devices.* Journal of Chromatography B, 2005. **822**(1-2): p. 21.
405. Yang, W., et al., *Targeting cancer cells with biotin-dendrimer conjugates.* European Journal of Medicinal Chemistry. 2009. **44** (2): p. 862.
406. Artemov, D., et al., *Magnetic resonance molecular imaging of the HER-2/neu receptor.* Cancer Research, 2003. **63**: p. 2723.
407. Tomalia, D.A., *Dendrimers as multi-purpose nanodevices for oncology drug delivery and diagnostic imaging.* Nanomedicine: Nanotechnology, Biology and Medicine, 2006. **2**(4): p. 309.
408. Saad, M., et al., *Receptor targeted polymers, dendrimers, liposomes: Which nanocarrier is the most efficient for tumor-specific treatment and imaging?* Journal of Controlled Release, 2008. **130**(2): p. 107.

SECTION 2.

CHAPTER II.

Materials and methods

CHAPTER II.

Materials and methods

The main aim of this chapter is to describe in detail, the experimental work and protocols related to the obtained results that will be provided further, in Section 3. Along with Chapter I, it aims to be a guideline of the rationale for this research, namely on the aspects related with the selection of the materials, on the processing routes used, and characterization process adopted.

1. MATERIALS

1.1. CHITOSAN (CHT)

Chitin is a homopolymer of β(1→4)-linked *N*-acetyl-D-glucosamine residues (Figure 1A). Chitin is a natural polysaccharide and is the principal structural component of the exoskeleton of invertebrates such as crustaceans, insects and spiders and it can also be found in the cell walls of most fungi and many algae.

Chitosan (CHT) that is positively charged (interact easily with cell surface and negatively charged macromolecules), is an *N*-deacetylated derivative of chitin mainly composed of 2-amino-2-deoxy-D-glucopyranose units (Figure 1B) [1].

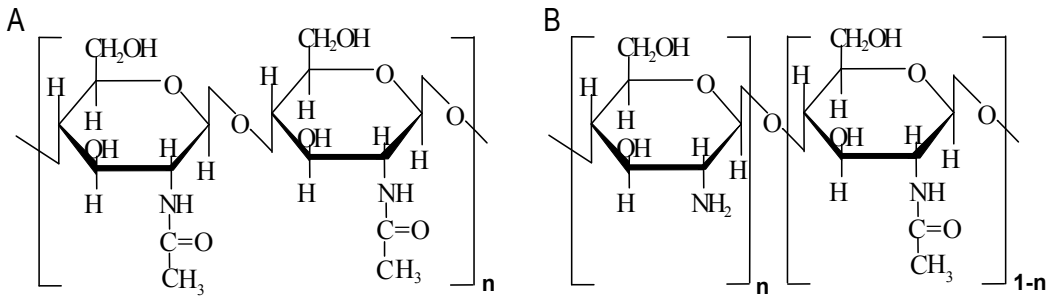

Figure 1. Schematic illustration of the structure of chitin (A), and chitosan (B).

It has also been reported that chitosan is biodegradable and non-toxic [2,3]. Important parameters affecting the characteristics of chitosan are its molecular weight (M_w) and its degree of deacetylation (DD), representing the proportion of deacetylated units [4]. It is a semi-crystalline polymer and the degree of crystallinity, depends on the degree of deacetylation, i.e. crystallinity is maximum for both chitin (0% deacetylated) and fully deacetylated (100%) chitosan. By its turn, minimum crystallinity is

achieved at intermediate degrees of deacetylation. Chitosan is insoluble in aqueous solutions above pH 7, but in dilute acids, the free amino groups are protonated and the molecule becomes fully soluble below ~pH 5. The pH-dependent solubility of chitosan provides a convenient mechanism for processing under mild conditions. For example, viscous solutions can be extruded and gelled in high pH solutions [5]. Freeze-drying techniques also allows obtaining highly porous structures by means of freezing a polymer solution (-20ºC and -196ºC) [6-9], following with the removal of solvent through lyophilization. Thus, chitosan scaffolds production is also conceivable. If we consider its biological properties such as biocompatibility and immunological, antibacterial and wound-healing activity [2, 10-12] and processability, chitosan is one of the most appealing biomaterials for prospective applications in tissue engineering. Moreover, given the importance of glucosaminoglycans (GAGs) in stimulating the chondrogenesis [13], the use of GAGs or GAG analogs as components of a cartilage tissue engineered scaffold is desired for improving chondrogenesis. One such candidate is chitosan, which shares structural characteristics with various GAGs and hyaluronic acid (HA) present in articular cartilage [1].

For the research work within this thesis, CHT was chosen for the being used in the production of bilayered scaffolds (cartilage layer) due to the highlighted advantages. Reagent grade CHT particles with a deacetylation degree of ~91% and size in the range of 125-250 μm were purchased from Vanson (USA). Since chitosan is a commercial product, it can contain impurities. Their elimination was performed using a re-precipitation method as described by Signini and coworkers [14].

1.2. CARBOXYMETHYLCHITOSAN (CMCHT)

Chitin and CHT are attractive macromolecules, but their use is limited due to its poor water-solubility. Chemical modifications in chitosan molecular structure are viable due to the existence of reactive functional groups (e.g. amine -NH_2 and hydroxyl -OH), allowing to tailor its degradation profile and widen its applications [15]. Thus, to develop biomaterials with improved physicochemical properties, attempts have been made to modify its structure by introducing acetyl [16], carboxymethyl [17], sulfuryl, or phosphoryl groups [18], among others.

Carboxymethylchitosan (CMCht) is a water-soluble biomacromolecule derived from deacetylation and insertion of carboxylic functions in chitosan (Figure 2) [19]. CMCht is soluble in a wide range of pH and its properties, namely low toxicity and antimicrobial activity [12], may wider its application, including medical and pharmaceutical areas - mainly for the controlled release of drugs.

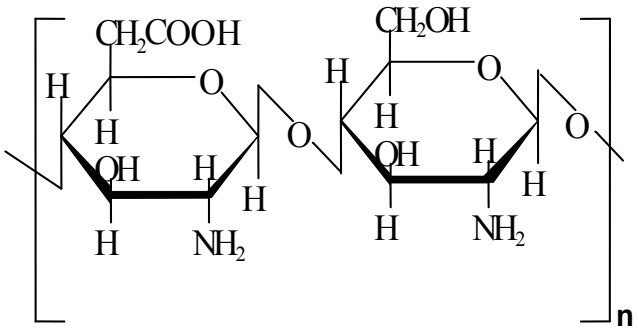

Figure 2. Schematic illustration of the structure of CMCht.

The choice of the appropriate reaction conditions and reagents allows the preparation of *N*-, *O*-, *N,O*- or *N,N*-dicarboxymethylchitosan [20]. Thus, the properties and applications of carboxymethylchitosan are strongly dependent on its structural characteristics, mainly the degree of substitution (DS) and the locus, amino or hydroxyl group.

For the purpose of this thesis, reagent grade chitosan particles with a DD of ~91%, monochloroacetic acid, 1% acetic acid solution, 40% sodium hydroxide solution, and acetone were used in the preparation of carboxymethylchitosan (CMCht). Sucessful preparation of CMCht was achieved using a reaction vessel apparatus as represented in Figure 3. The methodology used has been previously reported by Chen et al. [21]. Succintly, chitosan (5 g), 40% sodium hydroxide solution and solvent (100 mL) were added into a flask (500 mL) to swell and alkalize at room temperature for 1 hour. Then the monochloroacetic acid (18 g) was added into the reaction vessel dropwise for 30 minutes and reacted for 2 hours. During that time the temperature was maintained in a water bath at 60ºC. The reaction was stopped by adding 70% ethanol (200 mL). The solid was filtered and rinsed in 70-90% ethanol to de-salt and de-water, and vacuum dried at room temperature. Finally, the H-form of CMCht was obtained by suspending the Na salt CMCht in 80% ethanol aqueous solution (100 mL) and 37% hydrochloric acid (10 mL) for 30 minutes, under agitation. The solid was filtered and rinsed in 70-90% ethanol to neutral, freezed at -80ºC and freeze-dried (Telstar-Cryodos -80, Spain). CMCht with a DD of 80% and DS of 47% was chosen for the being used in the production of composite scaffolds and to surface modify the dendrimers, due to the previously highlighted advantages.

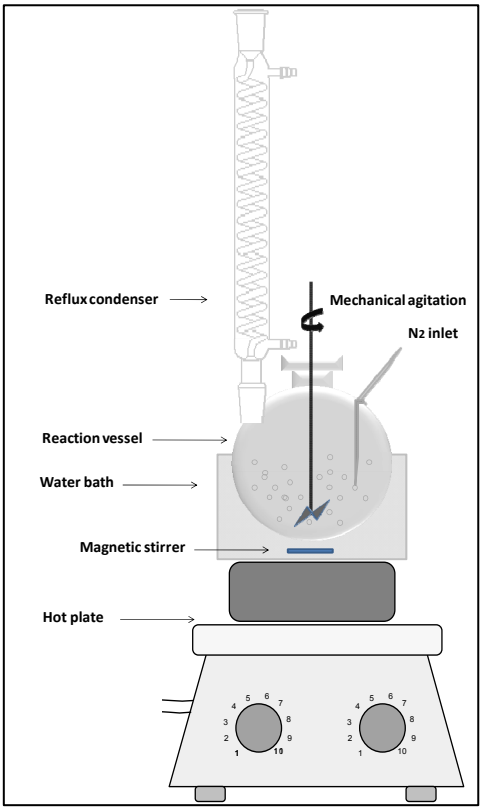

Figure 3. Schematic representation of the reaction vessel apparatus for the synthesis of CMCht.

For the composites scaffolds production, the incorporation of the bioactive ceramic filler has been carried out with two main goals. In one hand, a bioactive ceramic has always the potential capability of inducing a bioactive behaviour in a polymeric matrix [13-15]. On the other, being a ceramic filler, it can potentially improve the mechanical performance of the polymeric matrix where it is incorporated [13,16,17].

1.3. HYDROXYLAPATITE (HAP)

Hydroxylapatite (HAp) is represented by the chemical formula ($Ca_{10}(PO_4)_6(OH)_2$), and its structure resembles to the primary mineral component of bone. For some time now, bone substitute materials composed of HAp are available for use in surgery [22]. The reason for this is related with its biological characteristics namely its biocompatibility, non-immunogenic [23] and resorbability [24]. Moreover, it facilitates osteointegration of implants [25] and exhibits excellent osteoconductive ability [26,27], i.e. supports the ingrowth of bony tissue.

In this thesis, HAp powders were prepared by precipitation in an aqueous system (wet-chemistry) at room temperature. In the precipitation reaction, solutions of calcium hydroxide, $Ca(OH)_2$ and 85% ortho-phosphoric acid, H_3PO_4 were mixed for 2 hours. A controlled drop-wise automated apparatus was

developed using a peristaltic pump (Gilson Miniplus 3, France) for adding a diluted solution of ortho-phosphoric acid to the calcium hydroxide solution, in a reaction vessel. Synthesis conditions were adjusted to obtain a stoichiometric HAp, i.e. Ca/P ratio of 1.67. After complete addition of the acid solution, the final pH of medium was adjusted to 11 with concentrated ammonium hydroxide, NH_4OH. Vigorous stirring was continued during HAp precipitation. The supernatant was removed after 24 hours of maturation, and the precipitate filtered under vacuum. The resulting filtrate was dried at 60ºC for 24 hours, and milled in a mortar until obtaining a fine powder for further use.

1.4. STARCH-BASED BIOMATERIALS

Starch is a mixture of glucans composed of α-amylose and amylopectin (Figure 4) and is synthesized by plants. α-amylose is a linear polymer of several thousand glucose residues α(1→4)-linked. Amylopectin consists of α(1→4)-linked glucose residues but also possess α(1→6)-branch points.

A

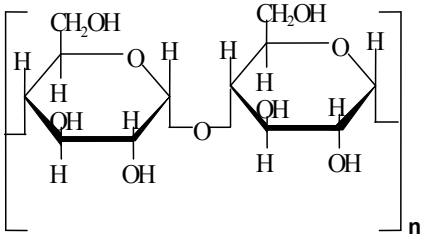

B

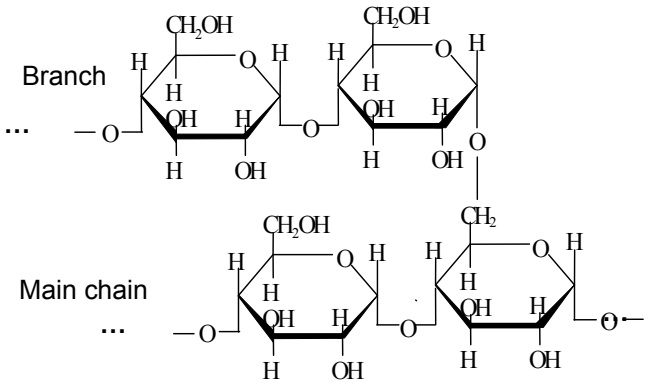

Figure 4. Starch is a mixture of glucans, composed of repeating units of α-amylose (A) and amylopectin with α(1→6) branch point (B).

Starch is a renewable and inherently biodegradable polymer [28]. Starch has been successfully incorporated in many polymeric systems in order to develop partially or totally biodegradable plastics [29].

Thus, the use of starch materials have attracted great attention in tissue engineering applications, as it can allow the designing of scaffolds with an adequate degradation rate, i.e. the degradation of the scaffold matching new tissue formation.

Our group [30-33] has been proposing the use of starch-based materials obtained from a blend of starch and polycaprolactone (SPCL) for bone tissue engineering applications. These starch-based materials have the advantages of being non-cytotoxicity, biodegradable, present good mechanical properties and can be processed by different methodologies.

1.5. REAGENTS

Chemicals used for the synthesis and purification of CHT, CMCht, CMCht/PAMAM dendrimer nanoparticles and HAp as well as their processing and characterization, were bought from the following companies: (Aldrich, USA), Fluka (Slovakia and Switzerland), Merck (Germany), Panreac (Spain), Pronalab (Portugal), Riedel-de Haën (Germany), and Sigma or Sigma-Aldrich (Germany).

2. SCAFFOLDS PRODUCTION

2.1. PROCESSING METHODOLOGIES FOR PRODUCTION OF SCAFFOLDS: OVERVIEW

Much attention has been given to choose the best processing techniques for the development of scaffolds of different shape, size and architecture for tissue engineering purposes. The processing technique must allow for the preparation of scaffolds with controlled porosity and adequate pore size, as well as tissue matching mechanical properties and an appropriate biological response. Among the processing methodologies myriad, a wide range have been exploited by our group. These are based on conventional melt-based processing routes, such as extrusion using blowing agents, and other based on multi-step processes such as compression moulding followed by particulate leaching [34]. Others include solvent casting and particle leaching, fibre bonding or more recently 3-D plotting [33,35]. Freeze-drying technique has also been widely used for the production of porous structures with different densities, shapes, porosities and pore sizes distributions by simply varying parameters such as polymer concentration [36-39], type of solvent [40], freezing temperature [6,9,40-42], type of moulds [8,43] and incorporating porogens [9,36,37]. In practice, the polymer solutions should be previously transferred into a mould and frozen before freeze-drying at temperatures which are typically comprised between -20ºC to -80ºC [6]. Thus, during freeze-drying the space occupied by the frozen solvent will became empty after sublimation and by this mean originating the pores [44]. It is important to guarantee that the final freezing

temperature is adequate to maintain all the molecules of solvent in the solid state [45]. Otherwise, the final structure will shrink during the drying process resulting on the formation of a dense external skin-like layer. By means of using the described methodologies, it is possible to tailor the properties of the different scaffolds, namely their degradation, architecture and mechanical properties, for several applications in tissue engineering.

In this thesis, the scaffolds were produced for applications in bone, cartilage and osteochondral tissue engineering by four distinct processing routes: (i) co-precipitation route and wax sphere leaching, (ii) sponge burn-out and sintering, (iii) two-step route, i.e. sponge burn-out and sintering, followed by impregnation of the polymer solution and freeze-drying, and (iv) by melt spinning followed by fibre bonding.

2.2. CARBOXYMETHYLCHITOSAN/HYDROXYLAPATITE (CMCHT/HAP) COMPOSITE SCAFFOLDS

The CMCht/HAp composite materials were prepared by a co-precipitation method using a acidic '*autocatalytic*' electroless bath [46]. This methodology is based on the possibility of chemisorption of Palladium (Pd^{2+}) on the surface of bioinert polymers, which acts as the catalyst to induce the precipitation of calcium-phosphate on its surface. A schematic representation of the principle of the electroless baths is shown in Chapter III. Thus, CMCht is able to chelate metal ions such as Pd^{2+}. The resulting excess of positive charge from the CMht/Pd^{2+} complex may build up an adjacent layer of negative charges (phosphate groups), which can originate a residual charge responsible for attracting other calcium ions. Consequently, composite scaffolds may be produced since calcium phosphate precipitation can occur in the presence of the CMht/Pd^{2+} complex.

For preparation of CMCht/HAp composite scaffolds, CMCht was synthesized as described above without further purification steps. Calcium chloride, $CaCl_2$, ortho-phosphoric acid, H_3PO_4 and palladium chloride, $PdCl_2$ were used to prepare the acidic '*autocatalytic*' electroless bath, and ammonium hydroxide 33%, NH_4OH solution to adjust the pH of the co-precipitation media. The acidic electroless bath was prepared by dissolving calcium chloride with a final concentration of 5.6 $g.L^{-1}$, ortho-phosphoric acid 3.4 $g.L^{-1}$, and palladium chloride 0.9 $g.L^{-1}$ in 500 mL distilled water, under agitation. A 10 wt% CMCht aqueous solution was added to the bath using a peristaltic pump (Gilson Miniplus 3, France) at a speed rate 2 $mL.minute^{-1}$. The composite precipitate was obtained by means of adjusting the pH of the bath to 6 with ammonium hydroxide. The precipitate was filtered under vacuum and the excess of water removed by drying at 37ºC for 24 hours. Porous structures were prepared by means of mixing the composite filtrate and 20 wt% wax spheres (Desert Whale Jojoba Company, Inc., USA), with

a diameter ranging from 50-450 μm, and transferring into a cylindrical mould with 4-7 mm diameter and 8-22 mm height. After drying at 60ºC, the wax spheres were eliminated off by soaking into tetrahydrofuran, in an ultrasound bath, for several hours. Once, the composite scaffolds were allowed to dry until constant weight and the scaffolds freeze at -80ºC overnight, followed by freeze-drying for the period of 2 days to completely remove the organic solvent.

2.3. HYDROXYLAPATITE (HAP) SCAFFOLDS

The HAp scaffolds were produced using a combined strategy consisting of a sponge burn-out followed by sintering. The procedure for obtaining the HAp scaffolds is summarized in Figure 5. The HAp powders were obtained by wet chemistry as previously described elsewhere. The obtained HAp pellets were milled until obtain a fine powder.

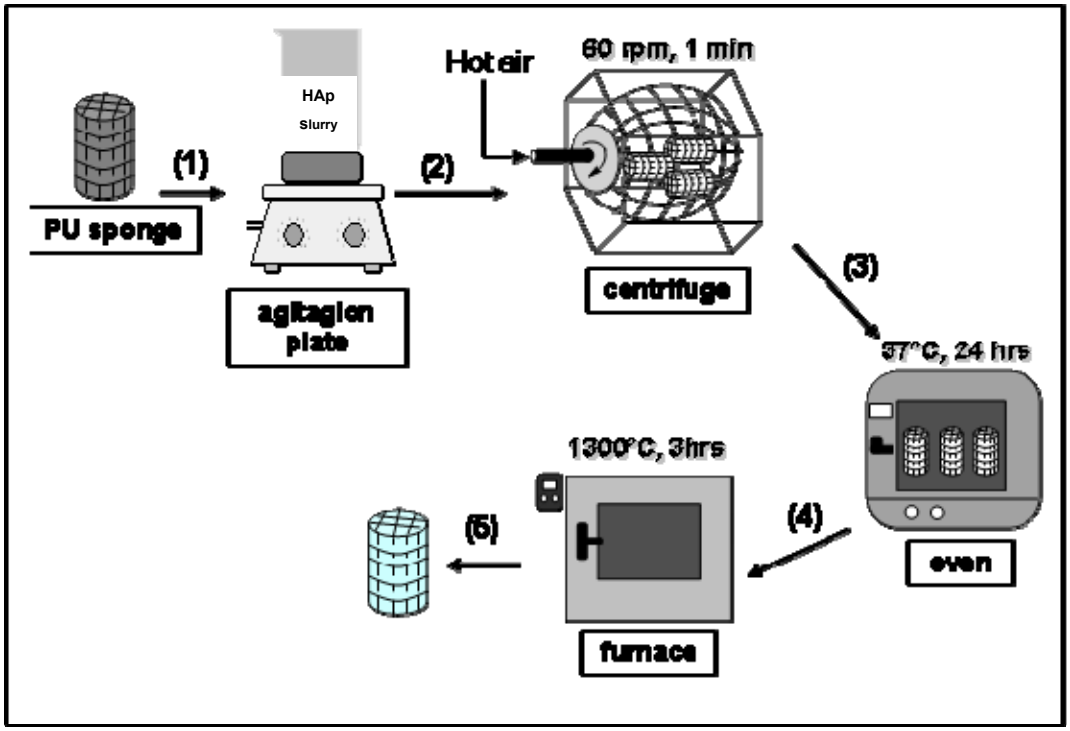

Figure 5. Schematic representation of the production route of the HAp scaffolds.

The HAp slurry was prepared by dispersing HAp powders in methanol for 48 hours. Then, polyurethane (PU, Eurospuma SA, Portugal) cylindrical sponges (10 x 8 mm) featuring fully interconnected pores were dipped into the slurry until total impregnation (step 1). To prevent the formation of an external skin-like layer, the impregnated PU sponges were transferred to a centrifuge and the excess of slurry was removed by centrifuging at 60 rpm for 1 minute (step 2), followed by drying at 37ºC, for 24 hours (step

3) to avoid the formation of cracks. Finally, the impregnated sponges were placed inside the furnace (Fornocerâmica, S.A., Portugal) and the PU matrices burned at 900ºC for 24 hours, followed by sintering the HAp scaffolds at 1300ºC for 3 hours (step 4). The HAp scaffolds were allowed to naturally cool inside the furnace (step 5). With this technique, the external shape and internal morphology of the PU sponge allow to produce HAp scaffolds with controlled internal architecture and external shape.

2.4. HYDROXYLAPATITE/CHITOSAN BILAYERED (HAP/CHT) SCAFFOLDS

In this thesis, an innovative technique was proposed for obtaining bilayered structures with improved architecture, stability and biological properties for osteochondral tissue engineering applications. Hydroxylapatite/chitosan (HAp/CHT) bilayered scaffolds were produced by adopting a two step procedure. Firstly, HAp porous layer (bone-like layer) with 10 mm height and 8 mm diameter were obtained by the sponge burn-out method as described elsewhere. Secondly, a 3 wt% chitosan solution was prepared by dissolving chitosan (CHT) of medium molecular weight and a degree of deacetylation of ~85% in 0.2 M acetic acid solution. The bilayered HAp/CHT scaffolds were fabricated by placing the HAp scaffolds into cylindrical silicon moulds (20 mm x 8 mm) and transferring the 3 wt% CHT solution. To guarantee that the chitosan solution penetrated into the HAp scaffolds it was left resting for 1 minute at room temperature. Moulds were freeze at -80°C and lyophilized (Telstar-Cryodos -80, Spain) up to 4 days to complete remove the frozen solvent, and allow obtaining the 'cartilage-like layer' on the top of the 'bone-like layer'. Then, HAp/CHT bilayered scaffolds were neutralized using a 0.1 M sodium hydroxide solution as previously described [38], freeze at -80°C and then lyophilized.

2.5. STARCH-POLYCAPROLACTONE (SPCL) SCAFFOLDS

In previous studies [35,47], our group demonstrated that SPCL fibre meshes are excellent scaffolds for rat bone marrow stromal cells, allowing for their proliferation and differentiation into osteoblasts. Thus, in the present thesis the starch-based materials were selected to evaluate the combinatorial strategy in tissue engineering principles employing carboxymethylchitosan/poly(amidoamine) dendrimer nanoparticles (see section 3) towards the intracellular release and regimented supply of dexamethasone (Dex) aimed at control stem cells osteogenic differentiation and *de novo bone* formation in the absence of typical osteogenic inducers, both *in vitro* and *in vivo* (Chapter VIII and IX).

Starch-polycaprolactone (SPCL) scaffolds were produced by adopting a two step procedure as previously reported [30]. The material used was a blend of starch with approximately 70% by weight of poly-ε-caprolactone (Novamont, Italy). Briefly, fibres of SPCL were produced by melt spinning using a

modular co-rotating twin screw extruder in two consecutive steps to a final draw ratio of approximately 1:100. Then, melt spun fibres were chopped. Fibre bundles were randomly displaced into the custom-designed mould cavities and subjected to thermal treatment at 60°C for 30 min before compression and fibre bonding. SPCL scaffolds (5 mm diameter and 4 mm height) were obtained through cutting of fibre bonded meshes with a circular die. Standardized fabrication conditions enabled the production of scaffolds with 67.4 ± 1.3% porosity (as determined by micro-computed tomography). More details on SPCL scaffolds can be found elsewhere [32,33].

2.6. STERILIZATION OF THE SCAFFOLDS

Prior to the cell culture studies CMCht, PAMAM-CT G 1.5, and CMCht/PAMAM dendrimer nanoparticles as well as all scaffolds were sterilized in an ethylene oxide gas atmosphere.

3. SYNTHESIS OF DENDRONIZED POLYMERS

Many scientific efforts are directed at improving the characteristics of biomacromolecules for applications as host-guest chemistry, nanocarriers, and catalysts, among others. As discussed in Chapter I, dendrimers are among such type of macromolecules since it offers a lot of possibilities in the molecular design. Such chemical versatility also allows producing multifunctional nanobiomaterials. Thus, in this thesis we focused on the development of novel nanoparticle systems with enhanced capabilities and performance should be developed specific to drug delivery. Research priorities for delivery and *in vivo* imaging should address simultaneously: (i) design of nanostructures with stealth properties that prevent them from being opsonised or cleared before reaching the target cells, (ii) ability to penetrate into cells and crossover biological barriers like the blood-brain barrier, uptake and recycling of nanostructures, (iii) trans-endocytosis of nanostructures, (iv) safety evaluation (*in vitro*/*in vivo* cytotoxicity, haemocompatibility and immunogenicity), *in vivo* carrier biodistribution, and (v) compatibility with external activation by magnetic field, ultrasound, X-ray, or optics to trigger the therapeutic activity.
For example, Sashiwa et al. [48] has demonstrated to be possible the development of tree-like hyperbranched chitosan-dendrimer hybrids. These macromolecules were described as based on chitosan (a trunk) linked to the dendrimer (sub-branch), which can possibly linking a variety of peptides or sugar molecules (the leaf's or flower's). In our approach, we modify amine-terminated poly(amidoamine) (PAMAM) dendrimers with water-soluble carboxymethylchitosan (CMCht) as an attempt to functionalize the dendrimers and neutralize the amine groups, which have been found to be

responsible for the toxicity of the dendrimers [49,50]. These macromolecules instead of trees can be called as dendrons or dendronized polymers due to their similar architecture (see Figure 5, Chapter I).

3.1. CARBOXYMETHYLCHITOSAN/POLY(AMIDOAMINE) DENDRIMER (CMCHT/PAMAM) NANOPARTICLES

For the synthesis of the CMCht/PAMAM dendrimer macromolecules, carboxymethylchitosan with a DD of 80% and DS of 47% was used. Starburst® poly(amidoamine)-carboxylic terminated dendrimers, PAMAM-CT (generation 1.5, 20% (w/v) methanolic solution) with an ethylenediamine core were purchased from Aldrich. Carboxymethylchitosan/poly(amidoamine) dendrimer (CMCht/PAMAM) nanoparticles were prepared in a stepwise manner as described in Figure 6: (i) increasing the generation of the PAMAM-CT (G 1.5), (ii) obtaining a PAMAM-methyl ester terminated dendrimer, (iii) reaction of PAMAM and CMCht, i.e. the reaction goes through a condensation reaction between the methyl ester and amine groups [51], and (iv) modifying the methyl ester groups that do not react to carboxylic ones in the CMCht/PAMAM dendrimer followed by precipitation. The increase of the dendrimers' generation was carried by transferring an appropriate volume of PAMAM-CT (G 1.5) in methanol (MeOH) to a 2 mL volumetric flask. The solvent was evaporated off under nitrogen gas, and the traces dried under vacuum in order to completely remove the methanol. The starting compound was re-dissolved in ultra-pure water to give a final concentration of 10 $mg.mL^{-1}$ and the pH was adjusted to 6.5 with dilute hydrochloric acid solution (HCl) solution. Then, 1-ethyl-3(3-dimethylaminopropyl) carbodiimide hydrochloride (EDC) was added to the solution at a molar ratio sufficient to modify the carboxylate residue of the dendrimers and kept under agitation for 30 minutes at room temperature. Ethylenediamine (EDA) was added to the solution at a molar ratio equal to that of EDC and let react for at least 4 hours. After this period the exceeding EDC was removed by dialysis (benzoylated cellulose tubing for separating compounds with a molecular weight of ≤ 1,200 from compounds with a molecular weight > 2,000). The compound was used without purification in the next step. After preparing the PAMAM-amine terminated compound, PAMAM-AT, an exhaustive alkylation of primary amines (Michael addition) was carried [52]. An appropriate volume of PAMAM-AT (~8.4 mmol) was transferred to a 50 mL flask and 30 mL of MeOH and 1.14 mL of methyl methacrylate (MA, ~12.6 mmol) were added. The solution was kept under agitation in a water bath for 24 hours at 50°C, to obtain the compound (PAMAM-methyl ester).

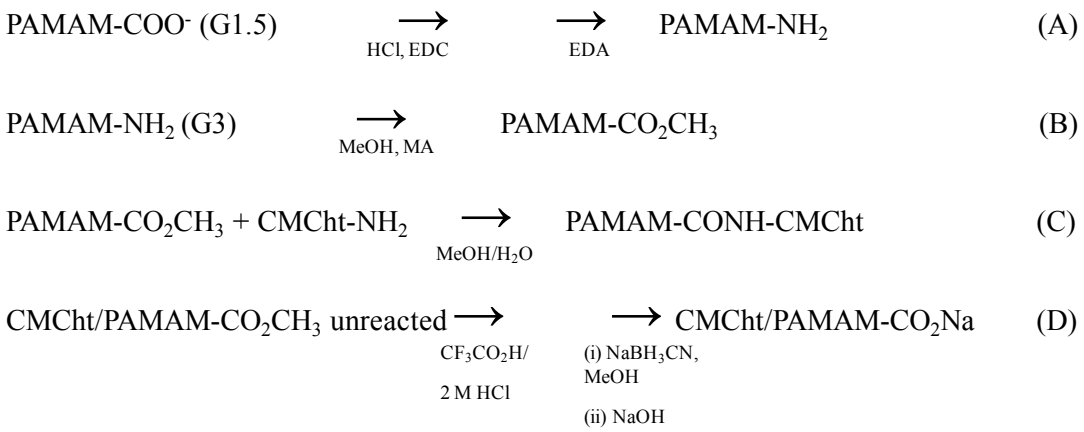

Figure 6. Reaction scheme showing the reaction steps for the synthesis of the CMCht/PAMAM dendrimer nanoparticles. (A) functionalization (increase generation), (B) Michael addition, (C) reaction of PAMAM-methyl ester dendrimers with the CMCht and (D) modification of the CMCht/PAMAM dendrimer methyl ester groups that do not react to carboxylic groups.

The carboxymethylchitosan (100 mg) dissolved in ultrapure water (10 mL) was mixed with the latter obtained PAMAM-methyl ester dendrimer (50 mg), which was previously dissolved in a 20/80 water/methanol (v/v) solution. The final solution was diluted by adding 30 mL of methanol and kept under agitation for 72 hours. After this period, CMCht/PAMAM dendrimer with carboxylic-terminated groups were obtained as described elsewhere [51]. CMCht/PAMAM dendrimer nanoparticles were then precipitated after addition of an appropriate volume of a saturated sodium carbonate, Na_2CO_3 solution and acetone.

3.2. Incorporation of dexamethasone (Dex) into the carboxymethylchitosan/poly(amidoamine) dendrimer nanoparticles

CMCht/PAMAM dendrimer nanoparticles were mixed with a Dex solution with a final concentration of 5 x 10^{-4} M under agitation (w/w). The mixture was then added to the precipitation media consisting of a saturated sodium carbonate, Na_2CO_3 and acetone solution, under vigorous agitation. Precipitates were collected by filtration and dispersed in ultrapure water for dialysis during the period of 48 hours. Both CMCht/PAMAM and Dex-loaded CMCht/PAMAM dendrimer nanoparticles were obtained by freezing the solution at -80°C and freeze-drying (Telstar-Cryodos -80, Spain) up to 4 days to complete remove the solvent. It is noteworthy that the CMCht/PAMAM dendrimer nanoparticles and Dex-loaded CMCht/PAMAM dendrimer nanoparticles are water-soluble at physiological pH.

3.3. LABELING OF CARBOXYMETHYLCHITOSAN/POLY(AMIDOAMINE) DENDRIMER NANOPARTICLES WITH FLUORESCEIN ISOTHIOCYANATE

In order to label the CMCht/PAMAM dendrimer with a fluorescent probe a 10 mg.mL^{-1} FITC solution was prepared in anhydrous dimethyl sulfoxide (DMSO), in dark conditions. Conjugates of CMCht/PAMAM-FITC were prepared by covalently bonding the amine group of CMCht and the isothyocianate group of FITC (thiourea bond), as illustrated in Figure 7.

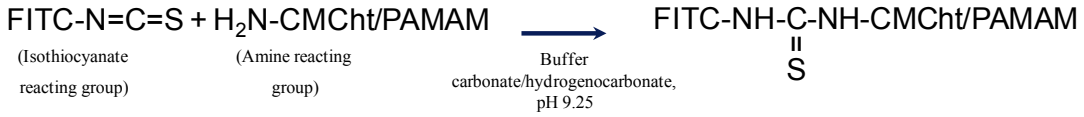

Figure 7. Reaction scheme showing the conditions for the linking of FITC with the CMCht/PAMAM dendrimer nanoparticles.

Firstly, a 10 mg.mL^{-1} CMCht/PAMAM dendrimer nanoparticles solution was prepared in a carbonate-bicarbonate coupling buffer of pH 9.2. Then, 50 μL of the FITC/DMSO solution was added per each mL of CMCht/PAMAM dendrimer nanoparticles buffered solution under agitation, and kept in dark at 4°C for 8 hours. The FITC-labeled CMCht/PAMAM dendrimer nanoparticles solution was dialyzed against ultra-pure water in order to remove unlinked FITC for 24 hours and filtered (pore size < 220 nm) in sterile and dark conditions. The final product was obtained as an orange powder after freeze-drying.

4. PHYSICOCHEMICAL CHARACTERIZATION TECHNIQUES

4.1. MORPHOLOGICAL/MORPHOMETRIC CHARACTERIZATION

4.1.1. Scanning electron microscopy (SEM)

In Chapter III, the microstructure of the CMCht/HAp composite scaffolds before and after immersion into the SBF solution, was investigated using scanning electron microscope, SEM (Leica Cambridge S-360, UK). Prior to the elemental and microstructure analysis, specimens were coated with carbon (Fisons Instruments, Polaron SC 508, UK) and gold (Fisons Instruments, Polaron SC 502, UK), respectively. The current was set at 18 mA with a coating time of 120 seconds. The phosphorus, calcium, sodium, carbon and oxygen elemental analysis was achieved by means of using an X-ray detector (Pentafet model 5526, UK) attached to the S-360 microscope, and a voltage of 10 keV was used.
The same equipment and procedure were used for analysis of HAp and HAp/CHT bilayered scaffolds.

For the *in vitro* studies using 3-D systems (Chapters IV and VIII), the surface morphology and pore size of the HAp scaffolds and SPCL scaffolds were also examined under a scanning electron microscope, SEM (SM-300, Topcon Corporation, Tokyo, Japan). Prior to microstructure analysis, specimens were sputter coated with platinum using an Ion coater (IB-3, Eiko Engineering Ltd., Ibaraki, Japan) with a current set at 6 mA, for a coating time of 2-3 minutes.

4.1.2. Transmission electron microscopy (TEM)

The morphology and size of the CMCht/PAMAM dendrimer nanoparticles was further analysed by transmission electron microscopy, TEM (Philips CM-12, FEI Company, The Netherlands, equipped with a MEGA VIEW-II DOCU camera and Image Software Analyzer SIS NT DOCU). The nanoparticles were stained with 2% of phosphotungstic acid and placed on copper grids for further observation.

4.1.3. Atomic force microscopy (AFM) studies

The morphology of the Dex-loaded CMCht/PAMAM and CMCht/PAMAM dendrimer nanoparticles was also investigated using atomic force microscopy (AFM). The dendrimer nanoparticles were dispersed in ultrapure water to obtain a solution with final concentration of 1 $mg.mL^{-1}$, and then 20 μL was placed over a 9.9 mm mica disc (Agar Scientific, England) and blown dried with nitrogen gas for subsequent characterization. The samples were analysed using the Tapping Mode™ with a MultiMode AFM connected to a NanoScope III controller, both from Veeco, USA, with non-contact silicon nanoprobes (ca 300 kHz) from Nanosensors, Switzerland. All images were plane-fitted using the third degree-flatten procedure included in the NanoScope software version 4.43r8. The particle size distribution was determined with the same software.

4.1.4. Micro-computed tomography (μ-CT) analysis

The structure and architecture of scaffolds are important factors affecting the performance of the tissue engineered cell-scaffold constructs. Micro-Computed Tomography (μ-CT) is an expedite and nondestructive technique for examining the morphological and architectural characteristics of the scaffolds, namely pore size, porosity and interconnectivity [53].

Micro-Computed Tomography (μ-CT) of the CMCht/HAp composite scaffolds was carried out using a Scanco 20 equipment (Scanco Medicals, Switzerland). Mimics® from Materialise (Belgium) was used as image processing software. The X-ray scans were performed in high resolution mode (9 μm) and 240 slices of the materials were obtained. The 2-D morphometric analysis of the scaffolds was performed

using a threshold 51 to identify the polymeric phase in order to determine the porosity, and a threshold 133 to identify the hydroxylapatite content along the scaffold (from 0-2000 μm).

The 3-D structural and architectural information of the HAp scaffolds was assessed quantitatively and qualitatively using μ-CT analysis. A series of c.a. 900 2-D slices with a scanning resolution of 11 μm were obtained by irradiating the specimen with penetrative X-rays of 50 keV. Mimics® was also used as image processing software. The porosity along the HAp scaffolds was also evaluated by 2-D morphometric analysis using a threshold 300. In addition, the qualitative information of the HAp/CHT bilayered scaffolds architecture was also investigated. From the CT data set, 300 slices of a region of interest corresponding to the interface between HAp and CHT was used to investigate the continuity of the HAp/CHT bilayered scaffolds. A customized threshold technique was used to enhance the CHT contrast and remove noise.

4.2. FOURIER-TRANSFORM INFRA-RED (FTIR) SPECTROSCOPY

The presence and also the environment of functional groups in organic molecules can be identified in a non destructive manner by infrared spectroscopy. Fourier-transform infra-red (FTIR) analysis was performed using a Perkin-Elmer spectroscope (Perkin-Elmer 1600 series equipment). Transparent Potassium bromide (KBr) pellets were prepared by mixing in the ratio of 1:10 of sample/KBr (wt/wt), and milling in an agate mortar, followed by uniaxially pressing the powders. All transmission spectra were recorded in the region of 4400-450 cm^{-1}, using a minimum of 32 scans, and a 2 cm^{-1} resolution.

For evaluation of Dex incorporation into the CMCht/PAMAM dendrimer nanoparticles FTIR analyses were also performed by means KBr pellets containing the samples. Moreover, the FITC labeling efficiency was also investigated.

4.3. X-RAY DIFFRACTION (XRD) ANALYSIS

X-ray diffraction (XRD) analysis was performed on powder samples of CMCht and CMCht/HAp composite scaffolds, using an X-ray diffractometer with Cu-Kα radiation at 50 mA and 40 kV (Philips PW 1710, The Netherlands). Using flat plate geometry, data were collected from 2 to 62º 2θ values, with a step size of 0.02º, and a counting time of 2 seconds.$step^{-1}$.

Crystallinity and phase content of HAp powder, sintered HAp and HAp scaffolds were also investigated. XRD patterns were examined in the region of 2º to 65º with a step size 0.02º for 2θ and scan speed of 0.6º.$minute^{-1}$.

4.4. NUCLEAR MAGNETIC RESONANCE (NMR) SPECTROSCOPY

Nuclear magnetic resonance (NMR) is a phenomenon which occurs when the nuclei of certain atoms are immersed in a static magnetic field and exposed to a second oscillating magnetic field. Some nuclei experience this phenomenon, and others do not, dependent upon whether they possess a property called spin. ^{1}H NMR (least expensive analysis) is the application of nuclear magnetic resonance in NMR spectroscopy with respect to hydrogen nuclei within the molecules of a substance. This is a non-destructive technique that allows determining the structure of organic compounds. Simple NMR spectra are recorded in solution, and solvent protons must not be allowed to interfere. In this thesis, ^{1}H NMR analysis of the CMCht/PAMAM dendrimer nanoparticles and Dex-loaded CMCht/PAMAM dendrimer nanoparticles was carried to investigate the structure of the nanoparticles and incorporation of Dex. For this purpose, nanoparticles were dissolved in deuterated water (D_2O). The NMR spectra were obtained with a Mercury -400BB operating at a frequency of 399.9 MHz at 50°C. The one-dimensional ^{1}H spectra were acquired using a 45° pulse, a spectral width of 6.3 kHz and an acquisition time of 2.001 seconds.

4.5. ZETA POTENTIAL AND PARTICLE SIZE ANALYSES

Zeta potential and particle size of the CMCht/PAMAM dendrimer nanoparticles and Dex-loaded CMCht/PAMAM dendrimer nanoparticles were measured in a particle size analyzer (Zetasizer Nano ZS, Malvern Instruments, UK).

Zeta potential was calculated by determining the electrophoretic mobility and then applying the Henry equation. The electrophoretic mobility is obtained by performing an electrophoresis experiment on the sample and measuring the velocity of the particles using Laser Doppler Velocimetry (LDV).

The Henry equation (1) is:

$$UE = \frac{2\varepsilon z\, f(Ka)}{3\eta} \qquad (1)$$

z: Zeta potential;

UE: Electrophoretic mobility;

ε: Dielectric constant;

η: Viscosity;

f(Ka): Henry's function; the value used was 1.5, and is referred to as the Smoluchowski approximation.

Electrophoretic determinations of Zeta potential were investigated using the universal 'dip' cell, at pH 3 and pH 7.4, in a citrate buffer and phosphate buffered saline (PBS) solutions, respectively.

Dynamic light scattering (DLS) that utilizes time variation of scattered light from suspended particles under Brownian motion to obtain their hydrodynamic size distribution is the most popular technology in sizing nanoparticles. DLS is a reliable technique that has been used to measure macromolecules and small particles in dilute suspension. Thus, for the present study, particle size analyses were performed using the DLS technique. The analyses were carried out in aqueous media with low concentration of nanoparticles and using disposable sizing cuvettes.

4.6. Ultraviolet-visible (UV-VIS) spectrophotometry

The FITC bonding to CMCht/PAMAM dendrimer nanoparticles and FITC:CMCht/PAMAM dendrimer nanoparticles ratio was also investigated by UV-VIS spectrophotometry (NanoDrop™ ND-1000; NanoDrop Technologies, USA). The labelling efficiency and stability was investigated by UV-VIS spectrophotometry.

4.7. Thermogravimetric analysis

Thermal stability and composition of the PU sponges, PU sponge impregnated with HAp before burning, and HAp scaffolds sintered at 1300°C was assessed by thermogravimetric (TGA) analysis. A TA-Q500 analyser (TA Instruments, USA) was used. The data was obtained using a ramp rate of 5°C.minute^{-1}.

4.8. Mechanical characterization

Compression tests in dry state were performed using a Universal Testing Machine (Instron 4505) possessing a load cell of 50 kN. A minimum number of 10 CMCht/HAp scaffolds were tested after storage at ~20°C and 55% relative humidity, to obtain an averaged result. Tests were conducted up to failure or until 60% reduction in specimen height as previously reported by Boesel et al. [54]. Complementarily, compression tests 'Push-out' in wet state were carried out by means of using a Miniature Materials Tester (Minimat Vsn 3.1, Rheometric Scientific Ltd, UK). This equipment is capable of sensing full scale load ranges from 20 N up to 1000 N at 37°C. Before conducting the tests, CMCht/HAp composite scaffolds were introduced inside the perforated stainless steel shells (6 mm of diameter and 11 mm height), and soaked into a phosphate buffered saline (PBS) solution for 24 hours at 37°C inside an oven. Afterwards, the shells containing the composite scaffolds were immersed into PBS solution at 37°C and a minimum number of 5 samples were tested. A baseline was also performed for each sample using the same experimental conditions but running the experiments with the empty stainless steel shells.

Mechanical properties of the HAp scaffolds were also investigated using the Universal Testing Machine (Instron 4505), at room temperature. The gauge length and diameter of all specimens was 16 mm and 8 mm, respectively. Tests were conducted with a constant strain rate of 2 mm.minute^{-1}, and up to failure or until 60% reduction in specimen height. The modulus (*E*) was determined by linear regression from the slopes in the initial elastic portion of the stress-strain diagram. A minimum number of 10 specimens were tested, and then *E* was averaged from the ten measurements.

4.9. SWELLING AND WEIGHT-LOSS STUDIES

Water-uptake or swelling and weight loss of the developed CMCht/HAp composite scaffolds, HAp and HAp/CHT bilayered scaffolds were performed, by soaking into a PBS solution for times up to 30 days, in triplicate. The solution was prepared by dissolving 1 tablet of PBS in 200 mL of distilled water to obtain a final concentration of 0.0027 M potassium chloride and 0.137 M sodium chloride, pH 7.4 at 25°C. The water-uptake was determined by the changes on the initial mass of the scaffolds (m_i) after incubation in the PBS solution at 37 $\pm$ 1°C. The scaffolds were removed after 1, 3, 7, 15, 21 and 30 days of immersion; then the excess of solution removed out with a filter paper, and the mass (m_w) determined using an analytical balance. Finally the scaffolds were dried at 60°C until constant weight and the mass was determined (m_d) in order to obtain the weight loss. The percentage of water-uptake of scaffolds (WUs) after each time of immersion (t) was calculated by means of using equation (2),

$$WUs,t = [(m_{w,t}-m_i)/ m_i] \times 100 \qquad (2)$$

The percentage of weight loss of the scaffolds (WLs) after each time of immersion (t) was calculated using equation (3),

$$WLs,t = [(m_{d,t}-m_i)/ m_i] \times 100 \qquad (3)$$

4.10. *IN VITRO* BIOACTIVITY ASSESSMENT

Bioactivity tests were performed by soaking the CMCht/HAp composite scaffolds and HAp scaffolds in a simulated body fluid (SBF) solution at 37 ± 1°C for periods of time ranging from 1 to 30 days. Note that this solution contains the inorganic ion concentrations resembling to those found in human blood plasma and pH of 7.4 [55]. After each soaking time the scaffolds were removed from the SBF solution and immediately rinsed with distilled water, dried at room temperature for 24 hours and in the oven at 60ºC until constant weight. The concentration of the Ca and P ions, after each soaking time, was measured by inductively-coupled plasma optical emission (ICP-OES, JY 70 plus, JobinYvon, France) spectrometry. Triplicate samples were analyzed for each soaking time and an averaged result calculated.

4.11. INVESTIGATION OF DEXAMETHASONE (DEX) RELEASE FROM CMCHT/PAMAM DENDRIMER NANOPARTICLES

The amounts of Dex from nanoparticles were measured using the high performance liquid chromatography (HPLC, ASI-Knauer, Germany) equipment with an UV detector set at 246 nm. The mobile phase consisted of acetonitrile:acetate buffer (2 mM, pH 4.8-adjusted with glacial acetic acid) (50:50 v/v) at flow-rate of 1 mL.minute^{-1}. In brief, Dex release was studied after dissolution of 10 mg of Dex-loaded CMCht/PAMAM dendrimer nanoparticles in 10 mL of phosphate buffer saline (pH 7.4, Sigma, USA) solution (PBS) in the absence or presence of 15% fetal bovine serum (FBS). Sodium azide 0.01% (w/v) was added to the buffer. The *in vitro* release studies were performed at 37°C and 60 rpm for times ranging from 1 hour until 7 days. At set time intervals, 1 mL of sample was taken for analysis and the same volume replaced by the respective buffer solution. Prior analysis, samples were centrifuged at 2,000 rpm for 10 minutes. A solution with sample/acetonitrile/acetate buffer (50:25:25, v/v) was prepared for further analysis. A Eurospher 100 C-18 analytical column (ASI-Knauer, Germany) was used. The retention time of Dex was 4 minutes. A calibration curve was obtained following the method described by Sun et al. [56]. Results were expressed as an average ± standard deviation, n=6.

5. *IN VITRO* BIOLOGICAL TESTING

5.1. CELL SOURCES

5.1.1. Bone marrow stromal cells isolation and culture

5.1.1.1. Rat bone marrow stromal cells (RBMSCs)

Rat bone marrow stromal cells (RBMSCs) isolated from Fisher 344 rat (F344/N) were used to evaluate the osteogenic potential of the Dex-loaded CMCht/PAMAM dendrimer nanoparticles, *in vitro* and *in vivo* (Chapters VI, VIII, IX, and X). Seven-week-old Fischer 344/N male rats were purchased from Japan SLC Inc. (Shizuoka, Japan) and sacrificed in accordance with the Ethics Committee at the Tissue Engineering Research Center (Amagasaki, Japan). The epiphyseal regions of the femora were removed and marrow plugs in the femoral shafts were flushed out using Eagle's minimum essential medium (MEM, Nacalai Tesque, Japan) supplemented with 15% FBS (JRH Biosciences, USA) and 1% antibiotic-antimycotic, A/B (Nacalai Tesque, Japan) solution [57]. The RBMSCs isolation was performed under aseptic conditions. RBMSCs were transferred to a T75 cm^2 culture flask and expanded in the presence of complete MEM medium at 37ºC in a 5% CO_2 incubator. Then, the culture medium was changed every 2 or 3 days. After reaching confluency, the cells (passage 1, P1) were released from substratum with 1 mL of 0.05% tripsin-0.53 mM EDTA (Invitrogen, USA) and centrifuged at 900 rpm for 5 minutes. A cell suspension was prepared and cell concentration determined using an automatic cell counter (Cell Counter Sysmex F-520, Japan).

5.1.1.2. Goat bone marrow stromal cells (GBMSCs)

Goat bone marrow stromal cells (GBMSCs) were isolated from the iliac crest of adult goats and cultured with basic culture medium - DMEM (Dulbecco's Modified Eagle's Medium, Sigma-Aldrich, USA) supplemented with 10% FBS and 1% A/B solution, under standard culture conditions. Cells were cultured until confluence and sub-cultured at P1 and P2 before seeding.

5.1.2. Primary cultures of hippocampal neurons

Hippocampal neuron cultures were prepared from P4 Wistar rats [58]. Upon dissection, hippocampus tissue samples were submitted to a trypsin based enzymatic digestion (0.05% Trypsin – Gibco; 3 $mg.mL^{-1}$ BSA; 0.0025% DNase in EBSS) for 10 minutes, followed by mechanical dissociation and centrifugation. Isolated cells were then plated on poly-D-lysine coated coverslips at a density of 4 x 10^4 $cells.cm^{-2}$. Cultures were maintained (37°C, 5% CO_2/95% air, 90% relative humidity) in Neurobasal A medium plus B27 Supplement, 1 mM GlutamaxI, 10 $ng.mL^{-1}$ basic fibroblast growth factor (b-FGF) and 0.1 $mg.mL^{-1}$ kanamycin (all from Gibco, USA) for 7 days. From day seven onwards two sets of experiments were performed: (i) in order to determine the internalization times of FITC-labeled CMCht/PAMAM dendrimer nanoparticles by hippocampal neurons, cultures were incubated with 200 $\mu g.mL^{-1}$ nanoparticles for periods of 1, 2, 6, 12, 15, 18, 24 and 48 hours; and (ii) to understand whether

the maintenance of the FITC-labeled CMCht/PAMAM concentration in the culture medium was essential to maintain the levels of internalization, cultures were incubated for periods up to 7 days in which FITC-labeled CMCht/PAMAM dendrimer nanoparticles were added to the culture medium every 48 hours in one group, while in the other nanoparticles were only added on the beginning of the experiment (day 0).

5.1.3. Primary cultures of cortical glial cells

Cortical glial cells were isolated from P4 newborns (Wistar Rats) as previously described [59]. Upon dissection, cortices were submitted to an enzymatic cocktail (30 $mg.mL^{-1}$ DNase, 0.25% Trypsin, both from Sigma) in Ca and Mg free HBSS followed by mechanical dissociation. Glial cells were then obtained by centrifuging the resulting cells suspension at 800 rpm for 2 minutes, and plated out on coverslips previously coated with poly-D-lysine at a density of 4×10^4 $cells.cm^{-2}$. Glial cells were then maintained for one week in DMEM supplemented with 1% A/B and 10% FBS. At this time point similar experiments to those performed with hippocampal cultures were carried out. In order to determine if astrocyte and oligodendrocyte cells proliferation was affecting the levels of internalization after 7 days of incubation with or without renovation, cultures were allow to grow and establish, being later on treated at day 7 (within a 14 day culturing period time frame) with 5-fluoro-2'-deoxiuridina (FUdR), a known inhibitor of glial cell proliferation.

5.2. CELL SEEDING TECHNIQUES

5.2.1. Seeding of GBMSCs onto the HAp porous layer of bilayered scaffolds and 3-D culturing

After expansion, GBMSCs were enzymatically lifted with 3 mL of trypsin after reaching 80% of confluence at P1 or P2. A cell suspension was prepared and seeded onto the HAp porous layer in a scaffold drop-wise manner, at a cellular density of 2.1×10^5 $cells.mL^{-1}$. GBMSCs-scaffolds constructs were cultured in 48-well plates for 3 days with basic medium in static conditions. For inducing osteogenic differentiation, cell-seeded scaffolds were cultured with an osteogenic media consisting of alpha-MEM (Minimal Essential Medium Eagle alpha modification) supplemented with osteogenic supplements namely, 10^{-8} M Dex, 50 $\mu g.mL^{-1}$ ascorbic acid and 10 mM β-glycerophosphate. The constructs were cultured for 3 days in static cultures with basal medium plus 14 days in osteogenic medium (17 days) and under dynamic conditions by using a lab rotator (Model DSR 2800 V, Digisystem

Laboratory Instruments Inc., Taiwan). Samples were collected on day 0 (12 hours after seeding), day 3 and day 17 for further studies.

5.2.2. Seeding of GBMSCs onto the CHT porous layer of bilayered scaffolds and 3-D culturing

To induce chondrogenic differentiation, CHT scaffolds were seeded with 2.5 x 10^5 GBMSCs and cultured for 7, 21 and 28 days with chondrogenic medium consisting of DMEM supplemented with 10 ng.mL^{-1} recombinant human transforming growth factor beta 1 (TGF-β1) (Sigma, USA), ITS+1 (100 x liquid media supplement), 0.1 M sodium pyruvate, 35 mM proline, 17 mM ascorbic acid and 1 mM Dex. The cell-scaffold constructs were also cultured under dynamic conditions by using a lab rotator system. Samples were retrieved after 7, 21 and 28 days of chondrogenic culture. Before chondrogenic medium was added, samples were cultured for 3 days in basal medium in static conditions. In both cases, culture media were changed every 2-3 days.

5.2.3. Seeding of RBMSCs onto the HAp and SPCL scaffolds for the in vitro and in vivo studies

The RBMSCs (passage 1, P1) were released from substratum with 1 mL of 0.05% tripsin-0.53 mM EDTA (Invitrogen, USA) and centrifuged at 900 rpm for 5 minutes, after reach confluence. The supernatant was aspirated and cells re-suspended with 10 mL of complete culture medium. Cell concentration was determined using an automatic cell counter (Cell Counter Sysmex F-520, Japan). Prior seeding, the viability of the RBMSCs was also analyzed with a NucleoCounter (ChemoMetec A/S, Denmark) [60]. In addition, the HAp scaffolds were de-aired in MEM medium under vacuum [61]. Then, one scaffold was placed in a well of 96-well tissue culture polystyrene (TCPS) plate and RBMSCs seeded in a drop-wise manner. RBMSCs expanded in complete MEM medium, MEM medium supplemented with 0.01 mg.mL^{-1} Dex-loaded CMCht/PAMAM dendrimer nanoparticles and MEM medium supplemented with 10^{-8} M Dex were seeded onto each HAp and SPCL scaffolds. The effect of cell density was evaluated by seeding different cell numbers (1 x 10^6 and 2 x 10^5) onto the HAp scaffolds. Finally, RBMSCs-HAp and RBMSCs-SPCL scaffolds constructs were cultured in complete MEM medium under standard culture conditions to allow cell adhesion, for the period of 12 hours. The same protocol was carried out for the in vitro studies, though different numbers of RBMSCs per scaffold were tested.

5.3. DNA QUANTIFICATION

Assessment of GBMSCs proliferation was carried out by DNA quantification. For this purpose, a fluorimetric dsDNA quantification kit (PicoGreen, Molecular Probes) was used. The samples were collected on day 0, day 3 and day 17, washed twice with a sterile PBS solution and transferred into 1.5 mL microtubes containing 1 mL of ultra-pure water. GBMSCs-HAp and -CHT were incubated for 1 hour at 37ºC in a water-bath and then stored in a -80ºC freezer until testing. Prior to DNA quantification constructs were thawed and sonicated for 15 minutes. Samples and standards (ranging between 0 and 2 $\mu g.mL^{-1}$) were prepared per each well of an opaque 96-well plate were added 28.7 µL of sample or standard plus 71.3 µL of PicoGreen solution and 100 µL of Tris-EDTA buffer. Triplicates were made for each sample or standard. The plate was incubated for 10 minutes in the dark and fluorescence was measured on a microplate ELISA reader (BioTek, USA) using an emission of 490 nm and an absorbance wavelength of 520 nm. A standard curve was created and sample DNA values were read off from the standard graph.

By its turn, DNA quantification in 2-D and 3-D cultures using RBMSCs (Chapters IV, VI and VIII) were performed using the nuclear dye Hoechst 33258 (Nacalai Tesque, Japan) according to the method previously described [62]. Prior to the assay, the RBMSCs-scaffold constructs were washed with a Ca and Mg-free PBS solution. Then, constructs were transferred to a 2 mL eppendorf, pulverized with zirconia's balls (milling time of ~2 minutes at 25 $shakes.second^{-1}$) using a ball mixer mill (Retsch GmbH, Germany), and sonicated in 0.2% Triton-X (Nacalai Tesque, Japan) solution for 5 minutes. Finally, the samples were sonicated and the DNA quantification carried out. The standard DNA solutions were prepared using salmon sperm DNA (Invitrogen, USA).

5.4. CYTOTOXICITY SCREENING

5.4.1. MTS assay

MTS (3-(4,5-dimethylthiazol-2-yl)-5-(3-carboxymethoxyphenyl)-2-(4-sulfophenyl)-2H-tetrazolium) viability test was performed to determine the cytotoxicity of HAp porous scaffolds and HAp/CHT bilayered scaffolds leachables that might result from the processing methodology used to obtain the HAp scaffolds and/or leachables of the polymeric component of the bilayered materials. Mouse fibroblastic-like cells (L929 cells; European collection of cell cultures-ECACC, UK), were cultured in basic medium: DMEM without phenol red supplemented with 10% FBS and 1% A/B solution containing 10,000 $units.mL^{-1}$ penicillin G sodium, 10,000 $\mu g.mL^{-1}$ streptomycin sulphate and 25 $\mu g.mL^{-1}$

amphotericin B as Fungizone® in 0.85% saline solution. L929 cells were incubated at 37ºC in an atmosphere containing 5% of CO_2, and after achieving confluence a cell suspension was prepared with a concentration of 8 x 10^4 cells.mL^{-1} and seeded onto 96-well TCPS plates. L929 cells were incubated for 3 days with different concentrations of HAp and HAp/CHT bilayered scaffolds extracts (25, 50, 75 and 100%). Eight replicates were considered per sample. Extracts of all samples were prepared as previously described by Gomes et al. [31]. L929 cells relative viability (%) was determined for each extract concentration and compared to TCPS. Latex extracts were used as a positive control of cellular death. All cytotoxicity tests were performed in triplicate.

For both neurons and glial cells, cell viability and metabolic activity was also assessed by the MTS test (Chapter VII), after seven days of incubation (with or without renovation) with FITC-labeled CMCht/PAMAM dendrimer nanoparticles. This assay, or others similar to it (MTT, WST-1), have been widely used to measure cellular viability and proliferation. Hippocampal neurons and glial cells cultures (n=3) were placed in culture medium containing MTS in a 5:1 ratio and incubated in a humidified atmosphere at 37ºC and 5% CO_2. After three hours of incubation 100 μL of solution from each well were transferred to a 96-well TCPS plate and the optical density was determined at 490 nm.

5.4.2. Total protein quantification

In order to complement the data obtained with the MTS test (Chapter VII), protein assay was carried out to relate the amount of adherent cells present in the cultures using the BCA Protein Assay kit (Pierce Chemical, USA). The bicinchoninic acid (BCA) assay is a rapid and convenient method for the determination of the relative number of adherent cells in tissue culture [63]. This system uses BCA as the detection reagent for Cu^{+1}, which is formed when Cu^{+2} is reduced by protein in an alkaline environment. The purple coloured reaction product is formed by the chelation of two molecules of BCA with one cuprous ion (Cu^{+1}). The BCA method provides a more rapid and sensitive procedure with greater stability of color than is obtained using the Lowry method. Cells were lysed in ultra-pure H_2O after which the total protein was quantified according to the manufacturer's protocol. At the end of the assay, 100 μL of each sample were transferred to a 96-well plate where a standard curve was prepared and the absorbance read at 562 nm in a multi-well plate reader (Tecan, USA).

5.4.3. Luminescent cell viability assay and osmolality

A luminescent cell viability assay based on the adenosine triphosphate (ATP) quantification was performed by exposing RBMSCs to CMCht/PAMAM dendrimer nanoparticles (Chapter VI). RBMSCs

were isolated from femora of 7 week-old male Fischer 344/N rats (SLC Inc. Japan), and expanded in T75 cm^2 culture flasks in the presence of MEM with 15% FBS (JRH Biosciences, USA) and 1% A/B (Nacalai Tesque, Japan) solution. The animals were sacrificed by administrating an excess of anesthesia, in accordance to the Ethics Committee at the Tissue Engineering Research Center (Amagasaki, Japan). After reaching confluency, the cells (passage 1, P1) were released from substratum and centrifuged at 900 rpm for 5 minutes. The supernatant was aspirated and cells re-suspended with 10 mL of complete culture medium. Cell concentration was determined using an automatic cell counter (Cell Counter Sysmex F-520, Japan). RBMSCs were seeded (sub-cultured) to each well of a 96-well TCPS plate at a cell density of 5 x 10^3 cells.mL^{-1}. A solution of CMCht/PAMAM dendrimer nanoparticles at a concentration of 10 mg.mL^{-1} was prepared in a complete culture medium. Serial dilutions (1, 0.1, 0.01 mg.mL^{-1}) were further prepared using the complete culture medium. Possible changes in the osmolality of the culture media were investigated using an automatic cryoscopic osmometer (OSMOMAT O 30-D, Gonotec, Germany). After a period of 24 hours, the culture medium was changed by the respective serial dilutions and the cells cultured under standard culture conditions for 1 and 3 days. A latex rubber extract was used as the positive control for cellular death. Finally, the ATP content was measured by means of performing a CellTiter-Glo® luminescent cell viability assay, following the protocol provided by the supplier (Promega Corporation, USA). Luminescence was measured using opaque-walled multi-well plate in a microplate reader (Wallac ARVOsx 1420, Perkin-Elmer Life and Analytical Sciences, USA).

Cytotoxicity screening of the HAp and SPCL scaffolds using RBMSCs was also investigated, *in vitro* (Chapter VIII) by luminescent cell viability assay [64]. Prior to RBMSCs seeding, the HAp and SPCL scaffolds were pretreated (de-airation) to prevent air bubble formation in the pores. Scaffolds were placed in 10 mL polystyrene tubes with ventilation caps. MEM medium was added and scaffolds were de-aired under vacuum using a 20 mL syringe with an attached 21G needle. Then, each scaffold was transferred into the respective well of a non-adherent 96-well TCPS plate. RBMSCs (P1) were seeded onto the surface of the HAp and SPCL scaffolds at a cell density of 5 x 10^2 cells.$scaffold^{-1}$, 1 x 10^3 cells.$scaffold^{-1}$, 5 x 10^3 cells.$scaffold^{-1}$ and 1 x 10^4 cells.$scaffold^{-1}$, and cultured in MEM medium under static conditions for 24 hours, 3 and 7 days. After each time period, the ATP content which signals the presence of metabolically active cells was measured by means of performing a CellTiter-Glo® luminescent cell viability assay (Promega Corporation, USA). Luminescence was measured in a microplate reader (Wallac ARVOsx 1420, Perkin-Elmer Life and Analytical Sciences, USA), following

the protocol provided by the supplier. All experiments were carried out 3 times using 3 replicates per experimental condition.

5.5. LIVE/DEAD VIABILITY ASSAY AND ADHESION STUDIES

For study cell adhesion and proliferation onto the surface of the HAp scaffolds (Chapter IV), RBMSCs were firstly, isolated and expanded as previously described. After that, RBMSCs were seeded onto the HAp scaffolds at a cellular density of 5 x 10^2 cells.scaffold^{-1}, 1 x 10^3 cells.scaffold^{-1}, 5 x10^3 cells.scaffold^{-1} and 1 x 10^4 cells.scaffold^{-1} and cultured in MEM medium for 24 hours, 3 and 7 days under static conditions. After each time period, the ATP content which signals the presence of metabolically active cells was measured by means of performing a CellTiter-Glo® luminescent cell viability assay (Promega Corporation, USA). The luminescence was measured using opaque-walled multi-well plate in a microplate reader (Wallac ARVOsx 1420, Perkin-Elmer Life and Analytical Sciences, USA). This assay is based on a luminescence signal that is proportional to the amount of ATP, which by its turn is directly proportional to the number of viable cells. Moreover, cell adhesion and proliferation was investigated by means of using a LIVE/DEAD viability assay kit (Molecular Probes). RBMSCs were incubated with two probes, calcein-AM (green colour) and ethidium homodimer-1 (EtdD-1, bright red colour), for intracellular esterase activity and plasma membrane integrity, respectively [65]. Then, specimens were observed under a 3-D fluorescence microscope (Olympus SZX12 stereomicroscope, OLYMPUS Co. Ltd., Japan) and SEM. All experiments were carried out three times using a minimum of 3 samples per experimental condition. By its turn, GBMSCs adhesion and morphology onto the surface of the HAp/CHT bilayered scaffolds was investigated by SEM analysis (Chapter V). For this purpose, after each culturing period, samples were removed from culture, washed in PBS, fixed in 2.5% glutaraldehyde, rinsed two times with PBS and dehydrated in series of ethanol concentrations. The samples were then dried at room temperature and sputter coated with gold before observation under the SEM.

5.6. ASSESSMENT OF FITC-LABELED CMCHT/PAMAM DENDRIMER NANOPARTICLES INTERNALIZATION

5.6.1. Fluorescence microscopy and fluorescence-activated cell sorting (FACS) analyses

In this thesis, the internalization of the FITC-labeled CMCht/PAMAM dendrimer nanoparticles was investigated using different cells types (Chapters VI, VII and X), both by fluorescence microscopy and fluorescence-activated cell sorting (FACS) analyses.

Human osteoblast-like cells (SaOs-2 cells, ECACC, UK) were used in preliminary tests to evaluate the internalization of the nanoparticles. SaOs-2 cells were maintained in T75 cm^2 culture flasks, cultured with basic culture medium - DMEM supplemented with 10% FBS and 1% A/B, and passaged after reaching confluence. A cell suspension was prepared and seeded on TCPS coverslips (Sarstedt Inc., USA) in 24-well plates (1 x 10^4 cells.$well^{-1}$) and cultured in standard culture conditions for 24 hours. The internalization of CMCht/PAMAM dendrimer nanoparticles by SaOs-2 cells was assessed after 3, 12, 24 hours, and 14 days. After each time point cells on the TCPS coverslips were fixed with 4% formalin and the nuclei stained with 4,6-diamidino-2-phenylindole, dilactate, DAPI blue (100 ng.mL^{-1}; Molecular Probes), for assessing possible cell morphological changes. Fluorescence was protected by using an antifade agent (ProLong® Antifade Kit, Invitrogen, USA), following the supplier procedure and cells were observed under the fluorescence microscope (AxioImager Z1, Zeiss Inc., Germany).

RBMSCs were isolated from rats and expanded until reaching 80% of confluency. The RBMSCs (P1) were trypsinized and transferred to a 6-well (1 x 10^5 cells.$well^{-1}$) and a TCPS coverslips in 24-well TCPS plates (2 x 10^4 cells.$well^{-1}$) for analysis under FACS and fluorescence microscopy, respectively. For fluorescence microscopy, RBMSCs were cultured in a MEM complete culture medium containing the 0.1 mg.mL^{-1} FITC-labeled CMCht/PAMAM dendrimer nanoparticles for a period of 12 hours until 14 days. For FACS analysis RBMSCs were cultured in the presence of 0.01 mg.mL^{-1} FITC-labeled CMCht/PAMAM dendrimer nanoparticles. All experiments were carried out in triplicate. The samples for fluorescence microscopy were prepared as follows: each well was washed with 1 mL of PBS, and cells fixed with 4% formalin (Nacalai Tesque, Japan) for 10 minutes at 4ºC followed by washing each well twice with PBS. After that cells were incubated with 0.5 mL of PBS containing Texas Red®-X phalloidin (Molecular Probes, Invitrogen, USA) and Hoechst 33258 (Invitrogen, USA) for staining the actin filaments of the cytoskeleton and nuclei of cells, respectively. The protocols provided by the supplier were followed with few modifications. The permeabilization of cells with Triton® X-100 was not carried out to avoid any undesired effect over the integrity of cells nuclei. TCPS coverslips were washed once with PBS and fluorescence protected using the ProLong® antifade kit. The specimens were observed under a fluorescence microscope (Olympus IX70, Olympus Co. Ltd., Japan). FACS analysis was carried out as follows: each well of the 6-well plate was washed with 2 mL of PBS. Then, PBS was aspirated and cells released from substratum as described above. Afterwards, it was added to each well 3.5 mL of MEM complete medium and samples transferred to a 15 mL Falcon tube. After centrifugation at 900 rpm for 5 min, cells were re-suspended in 0.5 mL of complete culture medium and passed through cell strainers [66]. Afterwards, 1 μL propidium iodide (Nacalai Tesque, Japan) was added to each sample for

determining the number of live cells. After this step, cells were loaded in a FACSCalibur flow cytometer (BD Biosciences Imunocytometry Systems, USA) and analyzed with a minimum of 10,000 events counting. Calibrite beads three-color kit (BD CaliBRITE™ beads, USA) was used to adjust the equipment instrument settings before samples are run on the flow cytometer. Finally, the FACS data was treated using the FLOWJO software.

5.6.2. Immunocytochemistry

For internalization studies using neurons and glial cells, immunocytochemistry studies were also carried out. The cells were fixed in 4% paraformaldehyde for 30 minutes, permeabilized by incubation with 100% methanol for 2 minutes, and washed three times in PBS. Cells were then blocked with 10% FBS/PBS (60 minutes), followed by a 1 hour incubation with the following primary antibodies: mouse anti-rat microtubule associated protein 2 (MAP-2) (Sigma, USA, 1:500) to detect mature hippocampal neurons, rabbit anti-rat glial fibrillary acid protein (GFAP) (Dako, Denmark, 1:500) for astrocytes, mouse anti-CD11b (BD Biosciences Pharmigen, USA, 1:100) for microglial cells and mouse anti-O4 (R&D systems, USA, 1:50) for oligodendrocytes. Cells were then washed in PBS and incubated with the secondary antibody: Alexa Fluor 594 goat anti-mouse immunoglobulin G (IgG) and Alexa Fluor goat anti-rabbit 488 (Molecular Probes, USA) for 60 minutes. The primary antibody was omitted to produce negative controls. Samples were further observed under an Olympus BX-61 Fluorescence Microscope (Olympus, Germany). Levels of FITC-labeled CMCht/PAMAM dendrimer nanoparticles internalization by the different cell populations was quantified by determining the rate between the number of positive cells for FITC-labeled CMCht/PAMAM internalization and the total number of cells (n=3, 5 random fields per coverslip).

5.7. Investigation of the mechanism of internalization of FITC-labeled CMCht/PAMAM dendrimer nanoparticles

For the investigation of the mechanism by which dendrimer nanoparticles are internalized by cells restrictive molecules were used, namely colchicine and apyrase known for inhibiting endocytosis and the active nuclear translocation, respectively. A cell suspension of RBMSCs (P1) in MEM complete culture medium was transferred to a 6-well (1 x 10^5 cells.well^{-1}) and TCPS coverslips in 24-well TCPS plates (2 x 10^4 cells.well^{-1}) for analysis under FACS and fluorescence microscopy, respectively. Stock solutions of 10 U.mL^{-1} apyrase (Nacalai Tesque, Japan) and 10 µM colchicine (Nacalai Tesque, Japan) were prepared in a phosphate-buffered saline solution. Cells were incubated in standard culture

conditions and after 24 hours, the culture medium was replaced by a different complete culture medium containing the FITC-labeled CMCht/PAMAM dendrimer nanoparticles (0.01 mg.mL^{-1} and 0.1 mg.mL^{-1}), and in the presence of 1 μM colchicine and 0.1 U.mL^{-1} apyrase or both, for a period of 12 hours to 14 days. Controls for internalization were performed by culturing RBMSCs in complete culture medium and in the presence of both colchicine and apyrase. All experiments were carried out in triplicate. After each time period, specimens were prepared as described previously. The tendency of FITC-labeled CMCht/PAMAM dendrimer nanoparticles to be internalized by RBMSCs was investigated by means of FACS analysis.

5.8. *IN VITRO* OSTEOGENIC DIFFERENTIATION STUDIES

For the evaluation of osteogenic differentiation of the RBMSCs cultured in the presence of Dex-loaded CMCht/PAMAM dendrimer nanoparticles, *in vitro*: RBMSCs were isolated from F344/N rats and expanded as described before. RBMSCs (P1) were cultured in a TCPS 24-well plate at a cell density of 2 x 10^4 cells.well^{-1}, and cultured in a complete MEM medium for 24 hours. After that time, culture medium was replaced by the different culture media, and RBMSCs cultured for times up to 14 days. The effect of the concentration of CMCht/PAMAM dendrimer nanoparticles loaded with Dex on the RBMSCs osteogenic differentiation was investigated. Dex-loaded CMCht/PAMAM dendrimer nanoparticles were dissolved in MEM medium supplemented with 0.28 mM ascorbic acid (Wako Pure Chemicals, Japan) and 10 mM β-glycerophosphate at a final concentration of 0.01 and 1 mg.mL^{-1}. RBMSCS were also cultured in a complete MEM medium, complete MEM medium containing 1 mg.mL^{-1} of CMCht/PAMAM dendrimer nanoparticles, and complete MEM medium containing 10 mM β-glycerophosphate (negative controls). Complete MEM medium supplemented with 10^{-8} M Dex, 0.28 mM ascorbic acid and 10 mM β-glycerophosphate was used as the positive control for osteogenic differentiation. Culture media were changed every 2-3 days. All experiments were carried out 3 times using a minimum of 4 replicates per experimental condition.

Moreover, the osteogenic differentiation of RBMSCs seeded onto the surface of the HAp and SPCL scaffolds and cultured with Dex-loaded CMCht/PAMAM dendrimer nanoparticles was also investigated. RBMSCs were isolated and expanded as mentioned above. HAp and SPCL scaffolds were placed in each well of a 96-well TCPS plate. Then, 1 x 10^6 RBMSCs (P1) were added per each HAp and SPCL scaffold, and the constructs were cultured in complete MEM medium under standard culture conditions for the period of 12 hours to allow cell adhesion. After that time, cell-scaffold constructs were transferred to a non-treated and non-protein coated flat bottom 12-well TCPS plate (Nunc, Japan), the different

culture medium was added, and RBMSCs were cultured for times up to 14 days. RBMSCs were exposed to a MEM medium supplemented with 0.01 mg.mL^{-1} Dex-loaded CMCht/PAMAM dendrimer nanoparticles, 0.28 mM ascorbic acid (Wako Pure Chemicals, Japan) and 10 mM β-glycerophosphate. RBMSCS were also cultured in a complete MEM medium (negative control for osteogenic differentiation). A complete MEM medium supplemented with 10^{-8} M Dex, 0.28 mM ascorbic acid and 10 mM β-glycerophosphate was used as the positive control for osteogenic differentiation. All experiments were carried out 3 times using a minimum of 3 replicates per experimental condition.

5.8.1. Qualitative analysis of mineralization

For 2-D *in vitro* studies (Chapter VI), Alizarin red S staining was performed to investigate possible calcium deposition after 14 days of culturing. RBMSCs were washed twice with PBS and fixed with 95% ethanol for 15 minutes. The fixed cells were then washed once with PBS and stained with 5 mg.mL^{-1} Alizarin red S in PBS for 5 minutes at room temperature. Then, it followed a washing step with ultra-pure water and mounting with Crystal/Mount™ (BiomedaCorporation, USA) for observation under the phase contrast microscope (Olympus CK40, Olympus Co. Ltd., Japan).
For the 3-D *in vitro* studies (Chapter VIII), RBMSCs-HAp and -SPCL scaffolds constructs were washed twice with Ca and Mg-free PBS solution and cells fixed with 95% ethanol for 15 minutes [67]. The fixed cells were then washed once with PBS and stained with 5 mg.mL^{-1} Alizarin red S in Ca and Mg-free PBS solution for 5 minutes at room temperature. After a washing step with ultra-pure water, RBMSCs-scaffold construct specimens were examined under a 3-D fluorescence microscope.

5.8.2. Quantitative analysis of mineralization (calcein uptake)

The degree of mineralization was quantitatively and qualitatively investigated following the method described by Uchimura et al. [68]. Succinctly, the method consists on the culturing of the RBMSCs in the presence of 1 μg.mL^{-1} of calcein (Dojindo Laboratories, Japan), which is incorporated in the mineralized extracellular matrix and allow us to investigate the calcium deposition. After each time period, each well was washed twice with PBS after which 1 mL of PBS was added. The fluorescence of calcein incorporated into the mineralized matrices was both visualized and quantified in a image analyzer equipment (Typhoon 8600 Variable Mode Imager, Amersham Biosciences, USA) using a 526 nm short pass filter. Afterwards, the fluorescence of the incorporated calcein was also observed under a fluorescence microscope (Olympus IX70, OLYMPUS Co. Ltd., Japan).

5.8.3. Qualitative analysis of alkaline phosphatase (ALP)

For the 2-D *in vitro* studies (Chapter VI), ALP staining the RBMSCs were washed twice the wells with PBS, after each culture period. Cells were fixed with 4% paraformaldehyde (Nacalai Tesque, Japan) for 15 minutes at 4ºC and then washed twice with AMP buffer (56 mM of 2-amino-2methyl-1,3-propanediol in ultrapure water, pH 9.9). It followed the soaking step with staining solution 0.5 mg naphtol AS-MX phosphate and 0.5 mg fast red violet LB salt per mL, in AMP buffer. Cells were incubated for 10 minutes at room temperature, washed with PBS and mounted (BiomedaCorporation, USA) for observation under the phase contrast microscope.

For the 3-D *in vitro* studies (Chapter VIII), ALP staining the RBMSCs-HAp and -SPCL scaffold constructs were washed twice with PBS, after 14 days of culturing. Cells were fixed with 4% paraformaldehyde/Ca and Mg-free PBS solution for 15 minutes at 4ºC. The RBMSCs-scaffold construct specimens were washed twice with AMP buffer and then soaked with staining solution 0.5 mg naphtol AS-MX phosphate and 0.5 mg fast red violet LB salt per mL, in AMP buffer. RBMSCs-scaffold construct specimens were incubated for 10 minutes at room temperature, washed with Ca and Mg-free PBS solution and examined under a 3-D fluorescence microscope.

5.8.4. Quantitative analysis of alkaline phosphatase (ALP)

GBMSCs osteoblastic differentiation was investigated by determining the alkaline phosphatase (ALP) activity (Chapter V). GBMSCs-HAp scaffold constructs used for DNA quantification assay were used to determine ALP levels. As cells were lysed during the above mentioned procedure, both DNA and other proteins produced by the cells were in suspension in the supernatant solution. So, to each well of a 96-well plate were added 20 µL of sample plus 60 µL of substrate solution consisting of 0.2% (w/v) p-nytrophenyl phosphate in a substrate buffer: 1 M diethanolamine HCl (Merck, Germany), at pH 9.8. The plate was then incubated in the dark for 45 minutes at 37ºC. After the incubation period, 80 µL of a stop solution (2 M NaOH containing 0.2 mM EDTA) was added to each well. Standards were prepared with 10 $\mu mol.mL^{-1}$ p-nytrophenol, pNP and the stop solutions in order to achieve the final concentrations ranging between 0 and 0.3 $\mu mol.mL^{-1}$. Triplicates were made for each sample and standard. Absorbance was read at 405 nm and sample concentrations were read off from standard graph.

In a different study (Chapter VI), ALP was also measured to evaluate osteoblast differentiation of RBMSCs cultured in the presence of Dex-loaded CMCht/PAMAM dendrimer nanoparticles. The samples used for DNA quantification assay were used to determine ALP levels. Prior to analysis the samples were centrifuged at 10,000 rpm for 1 minute at 4°C. To each well of a 96-well plate was added

an aliquot of supernatant and p-nytrophenyl phosphate substrate (ZYMED® Laboratories, Invitrogen, USA). The plate was then incubated in the dark for 30 minutes at 37ºC. After the incubation period, the reaction was stopped with 1 M NaOH. Standards were prepared with pNP. Triplicates were made for each sample and standard. Absorbance was read at 405 nm (Wallac ARVOsx 1420, Perkin-Elmer Life and Analytical Sciences, USA), and sample concentrations were read off from the standard graph. Enzyme activity was expressed either as nmol of pNP released/well/30 minutes and normalized by DNA content.

For quantification of ALP activity in 3-D systems (Chapter VIII), i.e. RBMSCs-HAp and RBMSCs-SPCL scaffolds, the remaining sonicated suspensions obtained from the DNA quantification assay were used. Prior to analysis the samples were sonicated once and centrifuged at 12,000 rpm for 1 minute at 4°C. To each well of a 96-well plate was added an aliquot of supernatant and p-nytrophenyl phosphate substrate (ZYMED® Laboratories, Invitrogen, USA), was added following the method described elsewhere [60] with minor modifications. Enzyme activity was determined as described above, expressed as nmol of pNP released/scaffold/30 minutes and normalized by DNA content.

5.8.5. Immunocytochemistry

Immunocytochemistry technique was used for evaluating the GBMSCs osteogenic differentiation after culturing onto the surface of the HAp scaffolds (Chapter V). GBMSCs-HAp scaffold constructs in an Accustain formalin solution, 10% neutral buffered for 1 hour at 4ºC, washing with PBS and including the constructs into methacrylate blocks. These blocks were cut into 10 μm thick slides and kept overnight at 80ºC before being used for subsequent immunocytochemistry analysis. The procedures immunocytochemistry were carried out following the instructions included in commercial kit: the RTU Vector Stain kit – Universal Elite ABC kit PK7200 (Vector Laboratories Inc., USA). This kit was used with a Peroxidase Substract Kit – DAB SK4100 (Vector Laboratories Inc., Burlingame, USA). For this study, samples were incubated with collagen type I (1/100, Chemicon, USA) for 1.6 hours and the biotinylated secondary antibody was incubated for 1 hour prior to wash and incubate the constructs with DAB for about 6 minutes. Also an osteopontin antibody (1/100, rabbit polyclonal to osteopontin, Abcam, UK) was tested using slides from the same constructs. Although in this particular case, a fluorescent secondary antibody was used instead of a biotinylated one and kept overnight at 80ºC. The methacrylate sections were incubated with osteopontin antibody, washed and then Alexa Fluor 488 secondary antibody (Molecular Probes, Invitrogen, UK) was added to GBMSCs-HAp scaffold constructs.

The incubation periods used were the same for both collagen type I and osteopontin antibodies. The observation of the constructs was performed using an Axio Imager Z1 microscope (Zeiss, Germany).

5.8.6. Osteocalcin content determined by enzyme-linked immunosorbent assay (ELISA)

Osteocalcin content was also determined to evaluate osteoblast differentiation of RBMSCs cultured in the presence of Dex-loaded CMCht/PAMAM dendrimer nanoparticles (2-D system, Chapter VI). The samples used for ALP activity were treated with a 20% formic acid solution immediately after concluding the assay and stored at 4°C for 2-3 days. Then, samples were centrifuged at 3,000 rpm for 10 minutes at 4°C and the supernatant passed through a Sephadex™ G-25 column (GE healthcare, Sweden) for desalting. The filtered samples were concentrated in a SPD SpeedVac® equipment attached to a UV Vacuum System (Thermo Electron Corporation, USA), prior to osteocalcin quantification. Finally, the osteocalcin content was determined by performing an Enzyme-linked immunosorbent assay, and using a Rat Osteocalcin EIA kit (N° BT-460, Biomedical Technologies Inc., USA). The experimental procedure was carried out following the instructions provided by the supplier. A 100 $ng.mL^{-1}$ standard solution of human osteocalcin was used to construct the standard curve. Data was read off from the standard graph and expressed as ng of deposited osteocalcin per μg of DNA.
For quantification of osteocalcin content in the 3-D systems (Chapter VIII), i.e. RBMSCs/HAp and RBMSCs/SPCL scaffolds, the remnants of each sample used for the ALP/DNA assays were treated with a 20% formic acid solution and stored at 4°C for 2-3 days. After that time, samples were centrifuged at 15,000 rpm for 10 minutes at 4°C. The supernatant was passed through a Sephadex™ G-25 column (GE healthcare, Sweden) for de-salting, and concentrated in order to carry out the ELISA assay. A Rat Osteocalcin EIA kit (N° BT-460, Biomedical Technologies Inc., MA, USA) was also used following the instructions provided by the supplier. Once, data was read off from the standard curve obtained with human osteocalcin and expressed as ng of deposited osteocalcin per μg of DNA.

5.9. *IN VITRO* CHONDROGENIC DIFFERENTIATION STUDIES

5.9.1. Quantification of glucosaminoglycans (GAGs)

GBMSCs chondrogenic differentiation onto the surface of CHT scaffold constructs was also investigated (Chapter V). Glucosaminoglycans (GAGs) quantification assay [69] was used to determine extracellular chondrogenic matrix formation after day 7, day 21 and day 28 of chondrogenic medium culture. GBMSCs-CHT scaffold constructs used for this assay were the same used for ALP and DNA assays.

GAGs standards were obtained by preparing a chondroitin sulphate solution ranging from 0 and 30 µg.mL^{-1}. In each well of a 96-well plate, 20 µL of sample or standard were added in triplicates and then 250 µL per well of dimethylmethylene blue (DMB) was added and mixed. The optical density was measured immediately at 525 nm on a microplate ELISA reader. A standard curve was created and GAGs sample values were read off from the standard graph.

6. *IN VIVO* STUDIES

6.1. IMPLANTS

For the *in vivo* studies, RBMSCs were expanded in different culture media namely, MEM, MEM supplemented with Dex and MEM supplemented with the Dex-loaded CMCht/PAMAM dendrimer nanoparticles. Then, the respective RBMSCs at different cell numbers (1 x 10^6 and 2 x 10^5) were seeded onto the surface of the HAp and SPCL scaffolds, cultured overnight for cell adhesion and then constructs were implanted subcutaneously and retrieved after 2 and 4 week of implantation (Figure 8). HAp and SPCL scaffolds without RBMSCs were also implanted (controls).

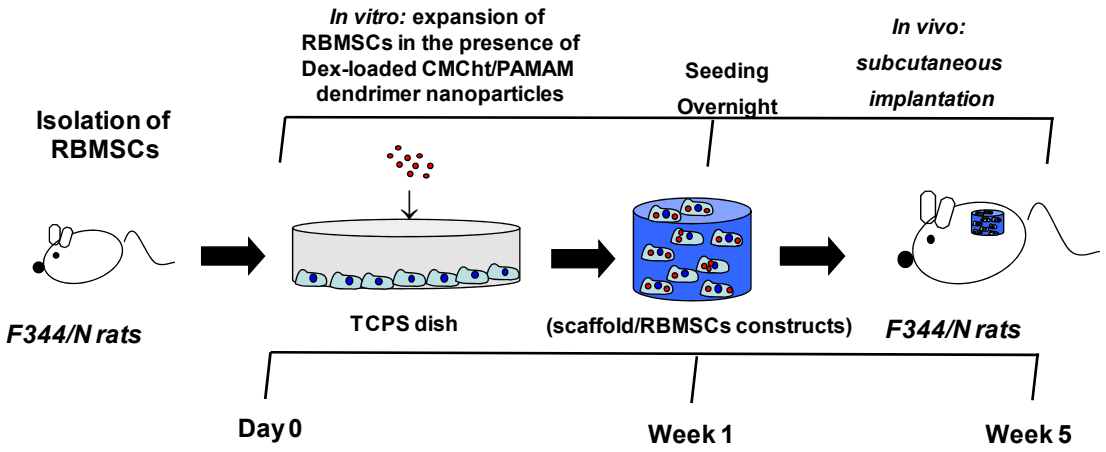

Figure 8. Schematic representation of the experimental strategy carried out to investigate the *in vivo* performance of the RBMSCs-scaffold constructs seeded with RBMSCs cultured in the presence of the Dex-loaded CMCht/PAMAM dendrimer nanoparticles.

6.2. SURGICAL PROCEDURE

Seven-week-old male Fischer 344 rat (Syngeneic F344/N rat), same as donor sub-strain and age, were anesthetized by intraperitoneal injection of pentobarbital (Nembutal, Dainippon Pharmaceutical Co. Ltd.,

Japan) at a final concentration of 3.5 mg per 100 g of body weight. The hair of the rat was cut at the implantation area, followed by washing with tap water and scrubbed with tincture of iodine and 70% ethanol. In each rat, three or four skin incisions (each 1 cm length) on the dorsal midline below the ear were made. Each RBMSCs-HAp and -SPCL constructs was implanted subcutaneously (1.5 to 2 cm away from the midline at both right and left sides) into the respective pocket and skin sutured. As a negative control, we used HAp and SPCL implants without RBMSCs. No prophylactic medication was administered post-surgery. After 2 and 4 weeks implantation, the animals were sacrificed with an overdose of anesthetic and RBMSCs-HAp and -SPCL constructs and controls were retrieved from the back of the F344/N rats. All experiments were carried out 3 times.

6.3. EXPLANTS CHARACTERIZATION

6.3.1. Micro-computed tomography (μ-CT) and morphometric analyses

New bone formation in the retrieved implants or explants was investigated by micro-computed tomography analysis (μ-CT: MCT-CB 100MF(Z); Hitachi Medical Corp., Tokyo, Japan). After 2 and 4 weeks of implantation, construct were retrieved, rinsed with PBS, and fixed with 10% formalin at room temperature, overnight. For the HAp-based constructs (Chapter IX), the explants were placed on the flat surface for analysis under the μ-CT. X-ray scans were acquired with a resolution mode of 10 μm (x/y/z) at 50 kV and 150 μA. The analytical conditions were: precision mode, 7 times magnification with an image intensifier field of 4.57 cm [70]. CT reconstruction has carried out using the 3D Bone Morphometry (TRI/3D-Bon, RATOC System Engineering Co. Ltd., Tokyo, Japan) software for evaluate the 2-D distribution of newly formed bone within the pores of the implanted constructs. Morphometric analysis was carried out using the public domain image-processing program IMAGE J (National Institutes of Health, Bethesda, MD) to obtain quantitative evaluation of histological section of bone. The light microscopy photographs of the 2-D histological decalcified sections of the HAp-based explants (Chapter IX) were converted to gray-value images and several filter steps were performed [71]. Shrinkage percentage observed in decalcified sections [70] was not considered in the calculations. New bone formation (NB) was expressed as a percentage of bone volume density (BV/TSV, Bone volume/Tissue plus Scaffold volume) ± standard deviation. A minimum of 12 sections per implant were analyzed.

For the SPCL-based constructs (Chapter X), new bone formation in the explants was evaluated with a high-resolution μ-CT Skyscan 1072 scanner (Skyscan, Kontich, Belgium) and using a resolution of pixel size of 6.59 μm and integration time of 1.7 ms. The X-ray source was set at 40 keV of energy and 250 μA of current. Approximately 400 projections were acquired over a rotation range of 180° with a rotation

step of 0.45°. Data sets were reconstructed using standardized cone-beam reconstruction software (NRecon v1.4.3, SkyScan). The output format for each sample was 500 serial 1024x1024 bitmap images. Representative data sets of 250 slices were segmented into binary images with a dynamic threshold of 220-255 (grey values) to access the new bone formation in the explants. The same representative volume of interest (VOI) was analysed for all the samples. These data sets were used for morphometric analysis (CT Analyser, v1.5.1.5, SkyScan) and to build the 3-D models (ANT 3D creator, v2.4, SkyScan). The morphometric analysis included scaffold characterization such as porosity and interconnectivity, histograms and new bone formation quantification. The distribution of this new bone formation in the scaffolds was assessed by 3-D virtual models that were created, visualized and registered using both image processing software's (CT Analyser and ANT 3D creator).

6.3.2. Histological evaluation

After μ-CT analyses, the explants were decalcified with K-CX solution (Falma Co., Tokyo, Japan) for histological analysis. Firstly, the explants were dehydrated in an ascending series grade ethanol/water solution (from 90-100%) using an automatic machine for 19 hours followed by washing three times with xylene. Secondly, specimens were immersed in paraffin at 62ºC and allowed to solidify at -5ºC. Slides were prepared by cutting the specimens into sections 5 μm thick using a microtome, and mounted in a micro-slide glass (Matsunami glass Ind. Ltd., Japan). Then, paraffin was melt by placing the slides in the oven at 71ºC for 20 minutes and allowed to let cool down at room temperature. The remnant paraffin was then eliminated off in hexane for 5 minutes (S.T. Chemical, Japan), followed by dipping into a ethylene/propylene mixture (Clear Plus, Falma Co., Tokyo, Japan) for 3 minutes. Finally, slides were immersed three times in 100% ethanol for 2 minutes each time of immersion.

6.3.2.1. Haematoxylin & Eosin (H&E) staining

For the Haematoxylin & Eosin (H&E) staining, slides were sequentially transferred to a 90% ethanol and then to a 70% and washed with tap water. It followed the staining step, which consisted in the immersion of the slides into the GM's Haematoxylin dye (Muto Pure Chemicals Co. Ltd, Tokyo, Japan, Nº 3008-1) for 10 minutes. It followed the washing step with tap water for 5 to 10 minutes. Then, slides were rinsed with de-ionized water and immersed in a 70% ethanol solution. Finally, slides were immersed in Eosin dye (Muto Pure Chemicals Co. Ltd, Tokyo, Japan, Nº 3204-2) solution for 2 minutes and dehydrated in a series of ethanol grades (70, 90, and 100%). At last, the specimens were immersed

three times in an ethylene/propylene mixture and then mounted avoiding the formation of bubbles for observation.

6.3.2.2. Toluidine blue staining

For Toluidine blue staining, paraffin was melt and slides rinsed with ultrapure water. The ground sections were stained with 0.05% Toluidine blue (Muto Pure Chemicals Co. Ltd., Tokyo, Japan) for 30 minutes. Finally, the slides were dehydrated in a series of ethanol grades (70, 90, and 100%) and mounted for further observation. All slides were examined under a light microscope (Olympus DP70, Olympus Co. Ltd, Japan). 2-D histological sections were obtained for bone specimens used in the micro-tomography analysis.

6.3.3. Quantification of ALP

Alkaline phosphatase activity was measured to evaluate osteoblast differentiation, *in vivo* (Chapters IX and X). Prior to the assay, the explants were washed with Ca and Mg-free PBS solution. Then, implants were transferred to a 2 mL eppendorf and pulverized with zirconia's balls as previously reported [61]. Prior to analysis the samples were sonicated and centrifuged at 12,000 rpm for 1 minute at 4°C. To each well of a 96-well plate was added an aliquot of supernatant and p-nytrophenyl phosphate substrate (ZYMED® Laboratories, Invitrogen, USA) [60]. The plate was then incubated in the dark for 30 minutes at 37ºC and after that time the reaction was stopped with 1 M NaOH (Panreac). Standards were prepared with pNP. Triplicates were made for each sample and standard. Absorbance was read at 405 nm (Wallac ARVOsx 1420, Perkin-Elmer Life and Analytical Sciences, USA), and sample concentrations were read off from the standard graph. Enzyme activity was expressed either as nmol of pNP released/explant/30 minutes.

6.3.4. Quantification of osteocalcin

The remnant of each sample used for the ALP assay of the explants, was treated with a 20% formic acid solution and stored at 4°C for 2-3 days (Chapters IX and X). Afterwards samples were centrifuged at 15,000 rpm for 10 minutes at 4°C. Then, the supernatant was passed through a Sephadex™ G-25 column (GE healthcare, Sweden), subsequently concentrated for performing the Enzyme-linked immunosorbent assay (ELISA). A Rat Osteocalcin EIA kit (N° BT-460, Biomedical Technologies Inc., MA, USA) was used following the instructions provided by the supplier. Data was read off from the

standard curve obtained with human osteocalcin and expressed as ng of deposited osteocalcin per explant.

6.3.5. Calcium assay

As an index of mineral bone formation, deposited calcium in the SPCL-based explants (Chapter X) was quantified as described by Kim et al. [72,73], with minor modifications. Briefly, SPCL-based explants were rinsed with Ca and Mg-free PBS solution and 0.2 mL of 1N HCl per explants was added. The tissues were chopped before being placed on an orbital shaker to extract calcium for 12 hours. Then, mixtures were centrifuged at 15,000 rpm for 10 minutes and supernatants were assayed using a commercial calcium assay kit (Calcium C-test™, Wako Pure Chemical Industries, Japan) and following the instructions provided by the supplier.

7. STATISTICAL ANALYSIS

Statistical evaluation was performed using one way ANOVA (internalization times experiments) and two-tailed paired *t*-student tests (MTS, total protein, comparison between renovation and non-renovation of CMCht/PAMAM dendrimer nanoparticles in the culture media), to assess the statistical differences between different groups. Statistical significance was defined as $p<0.05$ for a 95% confidence interval.
Results of *in vitro* cytotoxicity screening of the CMCht/PAMAM dendrimer nanoparticles were also analyzed for statistical significance using Student's t-test with the JMP 5.0.1 software (SAS Institute, Cary, N.C.).

REFERENCES

1. Suh, J.-K.F. and H.W.T. Matthew, *Application of chitosan-based polysaccharide biomaterials in cartilage tissue engineering: a review*. Biomaterials, 2000. **21**: p. 2589.
2. Kumar, M.N.V.R., *A review of chitin and chitosan applications*. Reactive & Functional Polymers, 2000. **46**: p. 1.
3. Khor, E. and L.Y. Lim, I*mplantable applications of chitin and chitosan*. Biomaterials, 2003. **24**: p. 2339.
4. Berger, J., et al., *Structure and interactions in covalently and ionically crosslinked chitosan hydrogels for biomedical applications*. European Journal of Pharmaceutis and Biopharmaceutics, 2004. **57**: p. 19.

5. Hsieh, C.Y., et al., *Analysis of freeze-gelation and cross-linking processes for preparing porous chitosan scaffolds*. Carbohydrate Polymers, 2007. **67**: p. 124.
6. Kang, H.W., Y. Tabata, and Y. Ikada, *Fabrication of porous gelatin scaffolds for tissue engineering*. Biomaterials, 1999. **20**(14): p. 1339.
7. Park, S.N., et al., *Characterization of porous collagen/hyaluronic acid scaffold modified by 1-ethyl-3-(3-dimethylaminopropyl)carbodiimide cross-linking*. Biomaterials, 2002. **23**(4): p. 1205.
8. Ren, L., et al., *Novel approach to fabricate porous gelatin-siloxane hybrids for bone tissue engineering*. Biomaterials, 2002. **23**(24): p. 4765.
9. Hou, Q., D.W. Grijpma, and J. Feijen, *Preparation of interconnected highly porous polymeric structures by replication and freeze-drying process*. Journal of Biomedical Materials Research Part B: Applied Biomaterials, 2003. **67B**: p. 732.
10. Muzzarelli, R.A.A., *Human enzymatic activities related to the therapeutic administration of chitin derivatives*. Cellular and Molecular Life Sciences, 1997. **53**: p. 131.
11. Kumar, R., et al., *Chitosan chemistry and pharmaceutical perspectives*. Chemical Reviews 2004. **104**: p. 6017.
12. Liu, X.F., et al., *Antibacterial action of chitosan and carboxymethyled chitosan*. Journal of Applied Polymer Science, 2001. **79**: p. 1324.
13. Kosher, R.A., J.W. Lash, and R.R. Minor, *Environmental enhancement of in vitro chondrogenesis. Stimulation of somite chondrogenesis by exogenous chondromucoprotein*. Developmental Biology, 1973. **35**(2): p. 210.
14. Signini, R. and S.P.C. Fillho, *On the preparation and characterization of chitosan hydrochloride*. Polymer Bulletin, 1999. **42**: p. 159.
15. Alves, N.M. and J.F. Mano, *Chitosan derivatives obtained by chemical modifications for biomedical and environmental applications*. International Journal of Biological Macromolecules 2008. **43**: p. 401.
16. Sashiwa, H., et al., *Chemical modification of chitosan. 14: Synthesis of water-soluble chitosan derivatives by simple acetylation*. Biomacromolecules, 2002. **3**: p. 1126.
17. Muzzarelli, R., *Carboxymethylated chitins and chitosans*. Carbohydrate Polymers, 1988. **8**: p. 1.
18. Sashiwa, H. and S.-i. Aiba, *Chemically modified chitin and chitosan as biomaterials*. Progress in Polymer Science, 2004. **29**(9): p. 887.
19. Muzzarelli, R.A.A., P. Ilari, and M. Petrarulo, *Solubility and structure of N-carboxymethylchitosan*. International Journal of Biological Macromolecules, 1994. **16**(4): p. 177.

20. An, N.T., et al., *Water-soluble N-carboxymethylchitosan derivatives: Preparation, characteristics and its application*. Carbohydrate Polymers, 2009. **75**(3): p. 489.
21. Chen, X.-G. and H.-J. Park, *Chemical characteristics of O-carboxymethylchitosans related to the preparation conditions*. Carbohydrate Polymers, 2003. **53**: p. 355.
22. Hollier, L.H. and S. Stal, *The use of hydroxyapatite cements in craniofacial surgery*. Clinics in Plastic Surgery, 2004. **31**(3): p. 423.
23. Hornez, J.C., et al., *Biological and physico-chemical assessment of hydroxyapatite (HA) with different porosity*. Biomolecular Engineering, 2007. **24**(5): p. 505.
24. Braye, F., et al. *Resorption kinetics of osseous substitute: natural coral and synthetic hydroxyapatite*. Biomaterials, 1996. **17**(13): p. 1345.
25. Kusakabe, H., et al., *Osseointegration of a hydroxyapatite-coated multilayered mesh stem*. Biomaterials, 2004. **25**(15): p. 2957.
26. Chang, B.S., et al., *Osteoconduction at porous hydroxyapatite with various pore configurations*. Biomaterials, 2000. **21**(12): p. 1291.
27. Boyde, A., et al. *Osteoconduction in large macroporous hydroxyapatite ceramic implants: evidence for a complementary integration and disintegration mechanism*. Bone, 1999. **24**(6): p. 579.
28. Kaneko, T., T. Ohno, and N. Ohisa, *Purification and characterization of a thermostable raw starch digesting amylase from a streptomyces sp. isolated in a milling factory*. Bioscience, Biotechnology, and Biochemistry, 2005. **69**(6): p. 1073.
29. Gattin, R., et al., *Biodegradation study of a starch and poly(lactic acid) co-extruded material in liquid, composting and inert mineral media*. International Biodeterioration & Biodegradation, 2002. **50**(1): p. 25.
30. Gomes, M.E., et al., *Alternative tissue engineering scaffolds based on starch: processing methodologies, morphology, degradation and mechanical properties*. Materials Science and Engineering: C, 2002. **20**(1-2): p. 19.
31. Gomes, M.E., et al., *Cytocompatibility and response of osteoblastic-like cells to starch-based polymers: effect of several additives and processing conditions*. Biomaterials, 2001. **22**(13): p. 1911.
32. Gomes, M.E., et al., *Starch-poly(caprolactone) and starch-poly(lactic acid) fibre-mesh scaffolds for bone tissue engineering applications: structure, mechanical properties and degradation behaviour*. Journal of Tissue Engineering and Regenerative Medicine, 2008. **2**(5): p. 243.

33. Oliveira, A.L., et al., *Micro-computed tomography (μ-CT) as a potential tool to assess the effect of dynamic coating routes on the formation of biomimetic apatite layers on 3D-plotted biodegradable polymeric scaffolds*. Journal of Materials Science: Materials in Medicine, 2007. **18**: p. 211.
34. Correlo, V.M., et al., *Tissue engineering using natural polymers*, In Biomedical Polymers. Cambridge, 2007: p. 197.
35. Tuzlakoglu, K., et al., *Nano- and micro-fiber combined scaffolds: a new architecture for bone tissue engineering*. Journal of Materials Science: Materials in Medicine, 2005. **16**(12): p. 1099.
36. Chen, G., T. Ushida, and T. Tateishi, *Development of biodegradable porous scaffolds for tissue engineering*. Materials Science and Engineering C, 2001. **17**: p. 63.
37. Weng, J., and M. Wang, *Producing chitin scaffolds with controlled pore size and interconnectivity for tissue engineering*. Journal of Materials Science Letters, 2001. **20**: p. 1401.
38. Silva, S.S., et al., *Preparation and characterization of novel chitosan/soy protein porous for tissue engineering applications*. Advanced Materials Forum, 2006. **514-516**: p. 1000.
39. Blacher, S., et al., Image analysis impedance spectroscopy and mercury porosimetry characterization of freeze-drying porous materials. Colloids and Surfaces A: Physicochemical and Engineering Aspects, 2001. **187-188**: p. 375.
40. Madihally, S.V. and H.W.T. Matthew, *Porous chitosan scaffolds for tissue engineering*. Biomaterials, 1999. **20**: p. 1133.
41. O' Brien, F.J., et al., *The effect of pore size on cell adhesion in collagen-GAG scaffolds*. Biomaterials, 2005. **26**(4): p. 433.
42. Mao, J.S., et al., S*tructure and properties of bilayer chitosan-gelatin scaffolds*. Biomaterials, 2003. **24**(6): p. 1067.
43. Oliveira, J.M., et al., *Innovative technique for the preparation of porous bilayer hydroxyapatite/chitosan scaffolds for osteochondral applications*. Kyoto (JPN): Key Engineering Materials, Trans Tech Pub, Zurich, Switzerland, 2006. **309-311**: p. 927.
44. Ho, M.H., et al., *Preparation of porous scaffolds by using freeze-extraction and freeze-gelation methods*. Biomaterials, 2004. **25**: p. 129.
45. Mladenov, D.A., T.D. Tsvetkov, and N.L. Vulchanov, *Freeze drying of biomaterials for the medical practice*. Cryobiology, 1993. **30**(3): p. 335.
46. Costa, S.A., et al., *Carboxymethylchitosan/calcium phosphate hybrid materials prepared by an innovative "auto-catalytic" co-precipitation method*. Key Engineering Materials, 2005. **284-286**: p. 701.

47. Gomes, M.E., et al., *Effect of flow perfusion on the osteogenic differentiation of bone marrow stromal cells cultured on starch-based three-dimensional scaffolds*. Journal of Biomedical Materials Research: Part A, 2003. **67**(1): p. 87.
48. Sashiwa, H., Y. Shigemasa, and R. Roy, *Chemical modification of chitosan 11: chitosan-dendrimer hybrid as a tree like molecule*. Carbohydrate Polymers, 2002. **49**(2): p. 195.
49. Domanski, D.M., B. Klajnert, and M. Bryszewska, *Influence of PAMAM dendrimers on human red blood cells*. Bioelectrochemistry, 2004. **63**(1-2): p. 189.
50. Jevprasesphant, R., et al., *Engineering of dendrimer surfaces to enhance transepithelial transport and reduce cytotoxicity*. Pharmaceutical Research, 2003. **20**(10): p. 1543.
51. Sashiwa, H., Y. Shigemasa, and R. Roy, *Chemical modification of chitosan. Part 9: Reaction of N-carboxyethylchitosan methyl ester with diamines of acetal ending PAMAM dendrimers*. Carbohydrate Polymers, 2002. **47**(2): p. 201.
52. Tomalia, D.A., A.M. Naylor, and W.A. Godard III, *Starburst dendrimers: Molecular-level control of size, shape, surface chemistry, topology, and flexibility from atoms to macroscopic matter.* Angewandte Chemie International Edition in English, 1990. **29**(2): p. 138.
53. Ho, S.T. and D.W. Hutmacher, *A comparison of micro CT with other techniques used in the characterization of scaffolds*. Biomaterials, 2006. **27**(8): p. 1362.
54. Boesel, L.F., J.F. Mano, and R.L. Reis, *Optimization of the formulation and mechanical properties of starch based partially degradable bone cements*. Journal of Materials Science: Materials in Medicine, 2004. **15**: p. 73.
55. Kokubo, T., et al., *Solutions able to reproduce in vivo surface-structure changes in bioactive glass-ceramic A-W*. Journal of Biomedical Materials Research, 1990. **24**: p. 721.
56. Sun, J.J., et al., *In vitro permeability of round window membrane to transforming dexamethasone with delivery vehicles — a dosage estimation*. Chinese Medical Journal, 2007. **120**: p. 2284.
57. Kihara, T., et al., *Three-dimensional visualization analysis of in vitro cultured bone fabricated by rat marrow mesenchymal stem cells*. Biochemical and Biophysical Research Communications, 2004. **316**: p. 943.
58. Lu, J., et al., *SMAD pathway mediation of BDNF and TGF beta 2 regulation of proliferation and differentiation of hippocampal granule neurons*. Development, 2005. **132**(14): p. 3231.
50. Salgado, A.J., et al. *Effects of starch/polycaprolactone based blends to be used for spinal cord injury regeneration in neurons/glial cells viability and proliferation*. Journal of Bioactive and Compatible Polymers, 2008. submitted.

60. Kotobuki, N., et al., *Viability and osteogenic potential of cryopreserved human bone marrow-derived mesenchymal cells*. Tissue Engineering, 2005. **11**: p. 663.
61. Oliveira, J.M., et al. *The osteogenic differentiation of rat bone marrow stromal cells cultured with dexamethasone-loaded carboxymethylchitosan/poly(amidoamine) dendrimer nanoparticles*. Biomaterials, 2009. **30**(5): p. 804.
62. Tanaka, T., et al., *Nano-scaled hydroxyapatite/silk fibroin sheets support osteogenic differentiation of rat bone marrow mesenchymal cells.* Materials Science and Engineering C, 2007. **27**: p. 817.
63. Tuszynski, G.P. and A. Murphy, *Spectrophotometric quantitation of anchorage-dependent cell numbers using the bicinchoninic acid protein assay reagent*. Analytical Biochemistry, 1990. **184**(1): p.189.
64. Oliveira, J.M., et al. *Surface engineered carboxymethylchitosan/poly(amidoamine) dendrimer nanoparticles for intracellular targeting*. Advanced Functional Materials, 2008. **18**: p. 1840.
65. Hirose, M., et al., *Osteogenic potential of cryopreserved human bone marrow-derived mesenchymal cells after thawing in culture*. Materials Science and Engineering C, 2004. **24**: p. 335.
66. Kotobuki, N., et al., *Cultured autologous human cells for hard tissue regeneration: preparation and characterization of mesenchymal stem cells from bone marrow*. Artificial Organs, 2004. **28**: p. 33.
67. Kotobuki, N., et al. *Observation and quantitative analysis of rat bone marrow stromal cells cultured in vitro on newly formed transparent b-tricalcium phosphate*. Journal of Materials Science: Materials in Medicine, 2006. **17**: p. 33.
68. Uchimura, E., et al., *In-situ visualization and quantification of mineralization of cultured osteogenetic cells*. Calcified Tissue International, 2003. **73**: p. 575.
69. Hollander, A.P. and P.V. Hatton, *Biopolymer methods in tissue engineering* (Methods in Molecular Biology Ser). Totowa, NJ: Human Press, 2003.
70. Tadokoro, M., Y. Hattori, and H. Ohgushi, *Rapid preparation of fresh frozen tissue-engineered bone sections for histological, histomorphometrical and histochemical analyses*. Bio-Medical Materials and Engineering, 2006. **16**: p. 405.
71. Muller, R., et al., *Morphometric analysis of human bone biopsies: A quantitative structural comparison of histological sections and micro-computed tomography*. Bone, 1998. **23**(1): p. 59.

72. Kim, H., H.W. Kim, and H. Suh, *Sustained release of ascorbate-2-phosphate and dexamethasone from porous PLGA scaffolds for bone tissue engineering using mesenchymal stem cells*. Biomaterials, 2003. **24**(25): p. 4671.
73. Kim, C.S., et al., *Ectopic bone formation associated with recombinant human bone morphogenetic proteins-2 using absorbable collagen sponge and beta tricalcium phosphate as carriers*. Biomaterials, 2005. **26**(15): p. 2501.

SECTION 3.

CHAPTER III.

Novel hydroxylapatite/carboxymethylchitosan composite scaffolds prepared combining an innovative '*autocatalytic*' electroless co-precipitation route

CHAPTER III.

Novel hydroxylapatite/carboxymethylchitosan composite scaffolds prepared combining an innovative '*autocatalytic*' electroless co-precipitation route

Abstract

A developmental composite scaffold for bone tissue engineering applications composed of hydroxylapatite (HAp) and carboxymethylchitosan (CMCht) was obtained using a co-precipitation method, which is based on the "*autocatalytic*" electroless deposition route. The obtained results revealed that the pores of the scaffold were regular, interconnected and possess a size comprised in the range of 20 to 500 μm. Furthermore, the Fourier-transform infra-red spectrum of the composite scaffolds exhibited all the characteristic peaks of apatite, and the appearing of typical bands from CMCht, thus showing that co-precipitation of both organic and inorganic phases was effective. The X-ray diffraction pattern of composite scaffolds demonstrated that calcium-phosphates consisted of crystalline HAp. From micro-computed tomography analysis, it was possible to determine that composite scaffolds possess a 58.9 ± 6% of porosity. Moreover, the 2-D morphometric analysis demonstrated that in average the scaffolds consisted of 24% HAp and 76% CMCht. The mechanical properties were assessed using compressive tests, both in dry and wet states. Additionally, *in vitro* tests were carried out to evaluate the water-uptake capability, weight loss and bioactive behaviour of the composite scaffolds. The novel hydroxylapatite/carboxymethylchitosan composite scaffolds show to be promising whenever degradability and bioactivity are simultaneously desired, such as in the case of bone tissue engineering scaffolding applications.

This chapter is based on the following publication: **Oliveira JM**, Costa SA, Leonor IB, Malafaya PB, Mano JF and Reis RL, 2009, Novel hydroxyapatite/carboxymethylchitosan composite scaffolds prepared combining an innovative '*autocatalytic*' electroless co-precipitation route, Journal Biomedical Materials Research: Part A, **88A(2)**: 470-480.

---

1. INTRODUCTION

The innovative Tissue Engineering (TE) concepts promises the creation of viable substitutes for the repair, replacement or regeneration of organs and tissues, and by this mean allowing a wide range of novel therapeutical possibilities [1]. This area of expertise deals with three main strategies: (i) combining of living cells with specially designed biomaterials [2,3], (ii) use of cells isolated or cells substitutes [4-6], and (iii) targeted-delivery of bioactive molecules, such as growth and differentiation factors by means of using drug-delivery carriers [7-9].

Scaffold technologies play a central role on the field of TE, since the main aim of the scaffold is to act as a support and guidance template for the development of a new tissue, both *in vitro* and *in vivo* [10]. Therefore, the size of the channels or pores as well as the 3-D architecture has a great effect on the cell seeding, infiltration and consequently on the tissue regeneration [11-13]. For instances, when engineering bone tissue, the scaffolds should meet other important criteria. It must be biocompatible [14], biodegradable in an appropriate time window, its degradation products should be non-toxic and easily eliminated by the metabolic pathways, support cell adhesion and growth, and possess adequate mechanical stability [1,10,15-18]. Moreover, the material should induce bone formation (osteoinductive) in addition to allow new bone ingrowths (osteoconductive) [19], while facilitating the angiogenesis [1,10] to supply with nutrients the newly formed tissue.

In recent years, great efforts have been made towards the development of new synthetic skeletal substitute products [20-22]. Among these, bioceramics and polymeric scaffolds have attracted much attention, such as hydroxylapatite (HAp, $Ca_{10}(PO_4)_6(OH)_2$) [23,24] and chitosan [25,26], respectively. Although, since there is not yet a single material that fulfils all the necessary requirements for bone tissue engineering scaffolds [27] composites have been developed [27-34]. Mechanical properties is one of the great advantages of composites, i.e. usually show a good balance between strength and toughness [17], but their improved osteoconductivity and biodegradability are also interesting [33]. From this point of view, composites materials are a better choice for such type of applications [35,18]. Bearing these premises in mind, Reis et al. [36] have been focusing its efforts at create innovative TE composite scaffolds based on natural-derived polymers and ceramics.

Carboxymethylchitosan (CMCht) is a biocompatible and biodegradable chitin or chitosan-derivative polymer [37] There are several types of carboxymethylated chitosans, which can be prepared through different methods [38,39] Of particular interest is the fact that contrarily to chitin and chitosan, CMCht is a water-soluble polymer [38,40]. Its versatility allowed many applications, namely as metal ion chelating agents [40,41], drug delivery [42,43], and medicine [44].

Muzzarelli et al. [38] reported that chitosan do not bind significantly calcium ions. On the contrary CMCht adsorb calcium ions to an extent that is dependent on proportion of protonation or if the molecule is in salt form of sodium. In this report an important particularity of CMCht was demonstrated. By attracting the calcium ions it is expected that one can have an effect on the precipitation of biominerals [45], or on the growth of the crystals either *in vitro* and *in vivo* [46,47].

Herein it is reported a co-precipitation route for the preparation of hydroxylapatite/carboxymethylchitosan (HAp/CMCht) composite materials. This method is based on a previously reported "*autocatalytic*" electroless bath [48,49] that has been used in our group to modify the surface of bioinert and biodegradable polymers (Figure 1) [49] This methodology is based on the possibility of chemisorption of Palladium (Pd^{2+}) on the surface of bioinert polymers (1), which acts as the catalyst to induce the precipitation of calcium-phosphate on its surface (2) [50-53]. Since it is known that CMCht is able to chelate metal ions [40], we expect CMCht to bind Pd^{2+}. As illustrated in Figure 1 the resulting excess of positive charge from the CMCht/Pd^{2+} complex may build up an adjacent layer of negative charges (phosphate groups), which can originate a residual charge responsible for attracting other calcium ions. Consequently, calcium phosphate precipitation may occur on the presence of CMCht due to a local supersaturation followed by calcium phosphate nucleation [32]. In this context, we hypothesized that by means of using an acidic "*autocatalytic*" electroless bath it may became possible to occur the co-precipitation of calcium-phosphates and CMCht.

As previously highlighted the porosity of scaffolds greatly dictates the performance of a 3-D template in the TE approaches.Therefore, the development of novel processing routes towards the fabrication of adequate porous structures is of great interest. The novelty of this work consists on the possibility of tailoring the porosity and 3-D architecture of the composite materials by means of using a wax spheres leaching methodology. The physicochemical characterization of composite scaffolds was performed by X-ray diffraction analysis, Fourier-transform infra-red spectroscopy, micro-computed tomography, and scanning electron microscopy attached with an X-ray detector. Complementarily, mechanical properties of composite scaffolds were determined under compression testing, in dry and wet states.

In vitro tests were carried out to assess the swelling and weight loss behaviour. The bioactive character of the composite scaffolds was also investigated by means of soaking the composite scaffolds in a simulated body fluid (SBF) solution. The elemental composition in the SBF solution was monitored by inductively-coupled plasma optical emission spectrometry.

2. MATERIALS AND METHODS

2.1. MATERIALS

Reagent grade chitosan particles with a deacetylation degree of ~91% and size in the range of 125-250 μm (Vanson, USA), monochloroacetic acid (Sigma, USA), acetic acid (Fluka, Switzerland), sodium hydroxide 40% (Merck, Germany) solution, and acetone (Pronalab, Portugal) were used in the preparation of carboxymethylchitosan (CMCht).

Calcium chloride, $CaCl_2$ (Merck, Germany), ortho-phosphoric acid, H_3PO_4 (Panreac, Spain) and palladium chloride, $PdCl_2$ (Aldrich, USA) were used to prepare the acidic "*autocatalytic*" electroless bath, and ammonium hydroxide 33%, NH_4OH (Riedel-de Haën, Germany) solution to adjust the pH of the co-precipitation media.

Hydration and weight loss tests were performed using phosphate-buffered saline (PBS) tablets supplied by Sigma (Sigma-Aldrich, Germany).

The Simulated Body Fluid (SBF) solution was prepared as previously reported by Kokubo et al. [54]. Potassium bromide, KBr (Riedel-de Haën, Germany) suitable for spectroscopy was used to prepare de FTIR pellets.

2.2. PREPARATION OF THE COMPOSITE SCAFFOLDS

CMCht was prepared by a modification of the reaction process that has been previously reported by Chen et al. [55] The composite materials were prepared by a co-precipitation method using a acidic "*autocatalytic*" electroless bath [48]. The acidic electroless bath was prepared by dissolving calcium chloride with a final concentration of 5.6 $g.L^{-1}$, ortho-phosphoric acid 3.4 $g.L^{-1}$, and palladium chloride 0.9 $g.L^{-1}$ in 500 ml distilled water, under agitation. A 10 wt% CMCht aqueous solution was added to the bath using a peristaltic pump (Gilson Miniplus 3, France) at a speed rate 2 $mL.minute^{-1}$. The composite precipitate was obtained by means of adjusting the pH of the bath to 6 with ammonium hydroxide. The precipitate was filtered under vacuum and the excess of water removed by drying at 37ºC for 24 hours. Porous structures were prepared by means of mixing the composite filtrate and 20 wt% wax spheres (Desert Whale Jojoba Company, Inc., USA), with a diameter ranging from 50-450 μm, and transferring into a cylindrical mould with 4-7 mm diameter and 8-22 mm height. After drying at 60ºC, the wax spheres were eliminated off by soaking into tetrahydrofuran (Riedel-de Haën, Germany), in an ultrasound bath, for several hours. Once composite scaffolds were allowed to dry until constant weight

and the scaffolds freeze at -80ºC overnight, followed by freeze-drying for the period of 2 days to completely remove the organic solvent.

2.3. SWELLING AND WEIGHT LOSS STUDIES

Water-uptake or swelling and weight loss of the developed composite scaffolds were performed, by soaking into a PBS solution for times up to 30 days, in triplicate. The solution was prepared by dissolving 1 tablet of PBS in 200 mL of distilled water to obtain a final concentration of 0.0027 M potassium chloride and 0.137 M sodium chloride, pH 7.4 at 25ºC. The water-uptake was determined by the changes on the initial mass of the scaffolds (m_i) after incubation in the PBS solution at 37 $\pm$ 1ºC. The scaffolds were removed after 1, 3, 7, 15, 21 and 30 days of immersion, the excess of solution removed out with a filter paper, and the mass (m_w) determined using an analytical balance. Then, scaffolds were dried at 60ºC until constant weight, the mass determined (m_d) in order to obtain the weight loss. The percentage of water-uptake of scaffolds (WUs) after each time of immersion (t) was calculated by means of using equation (1),

$$WUs,t = [(m_{w,t}-m_i)/ m_i] \times 100 \quad (1)$$

The percentage of weight loss of the scaffolds (WLs) after each time of immersion (t) was calculated using equation (2),

$$WLs,t = [(m_{d,t}-m_i)/ m_i] \times 100 \quad (2)$$

2.4. BIOACTIVITY TEST

Bioactivity tests were performed by soaking the scaffolds in a simulated body fluid (SBF) solution at 37 $\pm$ 1ºC. This solution contains the inorganic ion concentrations resembling to those found in human blood plasma and pH of 7.4 [54] for periods of time ranging from 1 to 30 days. After each soaking time the scaffolds were removed from the SBF solution and immediately rinsed with distilled water, dried at room temperature for 24 hours and in the oven at 60ºC until constant weight. The concentration of the Ca and P ions, after each soaking time, was measured by inductively-coupled plasma optical emission (ICP-OES, JY 70 plus, JobinYvon, France) spectrometry. Triplicate samples were analysed for each soaking time and an averaged result calculated.

2.5. MECHANICAL PROPERTIES

Compression tests in dry state were performed using a Universal Testing Machine (Instron 4505) possessing a load cell of 50 kN. A minimum number of 10 composite scaffolds were tested after storage at ~20ºC and 55% relative humidity, to obtain an averaged result. Tests were conducted up to failure or until 60% reduction in specimen height as previously reported by Boesel et al. [56]. Complementarily, compression tests "Push-out" in wet state were carried out by means of using a Miniature Materials Tester (Minimat Vsn 3.1, Rheometric Scientific Ltd, UK). This equipment is capable of sensing full scale load ranges from 20 N up to 1000 N at 37ºC. Before conducting the tests, composite scaffolds were introduced inside the perforated stainless steel shells (6 mm of diameter and 11 mm height), and soaked into a PBS solution for 24 hours at 37ºC inside an oven. Afterwards, the shells containing the composite scaffolds were immersed into a PBS solution at 37ºC and a minimum number of 5 samples were tested. A baseline was also performed for each sample using the same experimental conditions but running the experiments with the empty stainless steel shells.

2.6. SCANNING ELECTRON MICROSCOPY

The microstructure of the composite scaffolds before and after immersion into the SBF solution was performed using scanning electron microscope, SEM (Leica Cambridge S-360, UK). Previously to the elemental and microstructure analysis, specimens were coated with carbon (Fisons Instruments, Polaron SC 508, UK) and gold (Fisons Instruments, Polaron SC 502, UK), respectively. The current was set at 18 mA with a coating time of 120 seconds. The phosphorus, calcium, sodium, carbon and oxygen elemental analysis was achieved by means of using an X-ray detector, EDS (Pentafet model 5526, UK) attached to the S-360 microscope, and a voltage of 10 keV was used.

2.7. FOURIER-TRANSFORM INFRA-RED SPECTROSCOPY

Fourier-transform infra-red (FTIR) analysis was performed using a Perkin-Elmer spectroscope (Perkin-Elmer 1600 series equipment). Transparent KBr pellets were prepared by mixing in the ratio of 1:10 of sample/KBr (wt/wt), and milling in an agate mortar, followed by uniaxially pressing the powders. All transmission spectra were recorded in the region of 4400-450 cm^{-1}, using a minimum of 32 scans, and a 2 cm^{-1} resolution.

2.8. X-RAY DIFFRACTION

X-ray diffraction (XRD) analysis were performed on powder samples of CMCht and composite scaffolds, using an X-ray diffractometer with Cu-Kα radiation at 50 mA and 40 kV (Philips PW 1710, The Netherlands). Using flat plate geometry, data were collected from 2 to 62º 2θ values, with a step size of 0.02º, and a counting time of 2 seconds.step^{-1}.

2.9. MICRO-COMPUTED TOMOGRAPHY

Micro-computed tomography (μ-CT) of the composite scaffolds was carried out using a Scanco 20 equipment (Scanco Medicals, Switzerland). Mimics® from Materialise (Belgium) was used as image processing software. The X-ray scans were performed in high resolution mode (9 μm) and 240 slices of the materials were obtained. The 2-D histomorphometric analysis of the scaffolds was performed using a threshold 51 to identify the polymeric phase in order to determine the porosity, and a threshold 133 to identify the hydroxylapatite content along the scaffold (from 0-2000 μm).

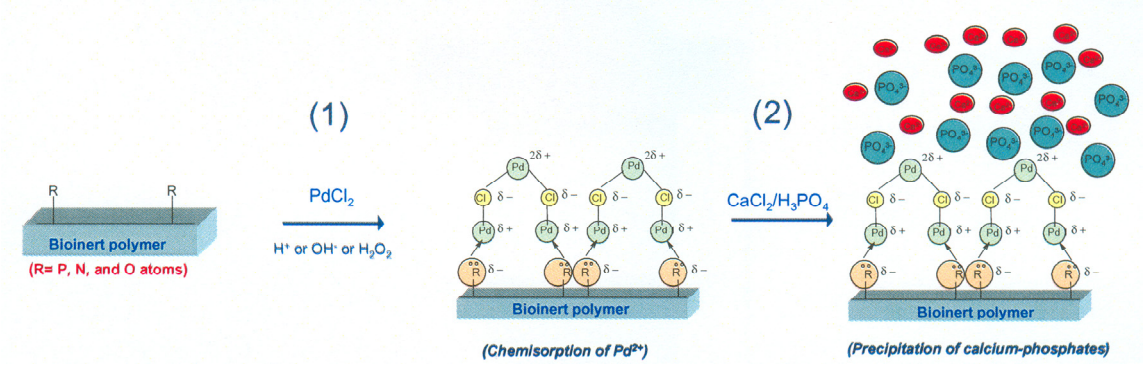

Figure 1. Schematic representation of the "*autocatalytic*" electroless route to modify the surface of bioinert and biodegradable polymers with calcium-phosphates.

3. RESULTS

Figure 2 shows the SEM morphology and EDS analysis of the composite scaffolds. These results revealed that the pores of the scaffolds were regular with size comprised in the range of 20 to 500 μm (Figure 2A). Additionally, it is possible to observe a typical interconnected macropores of size higher than 200 μm (Figure 2B). At high magnification, it is possible to observe that CMCht (white arrow) co-precipitated with ceramic particles (black arrow) (Figure 2C), and that these particles were

homogeneously distributed throughout the polymer network. Once, the EDS analysis corroborated previous studies showing that particles are calcium and phosphate in nature (Figure 2D).

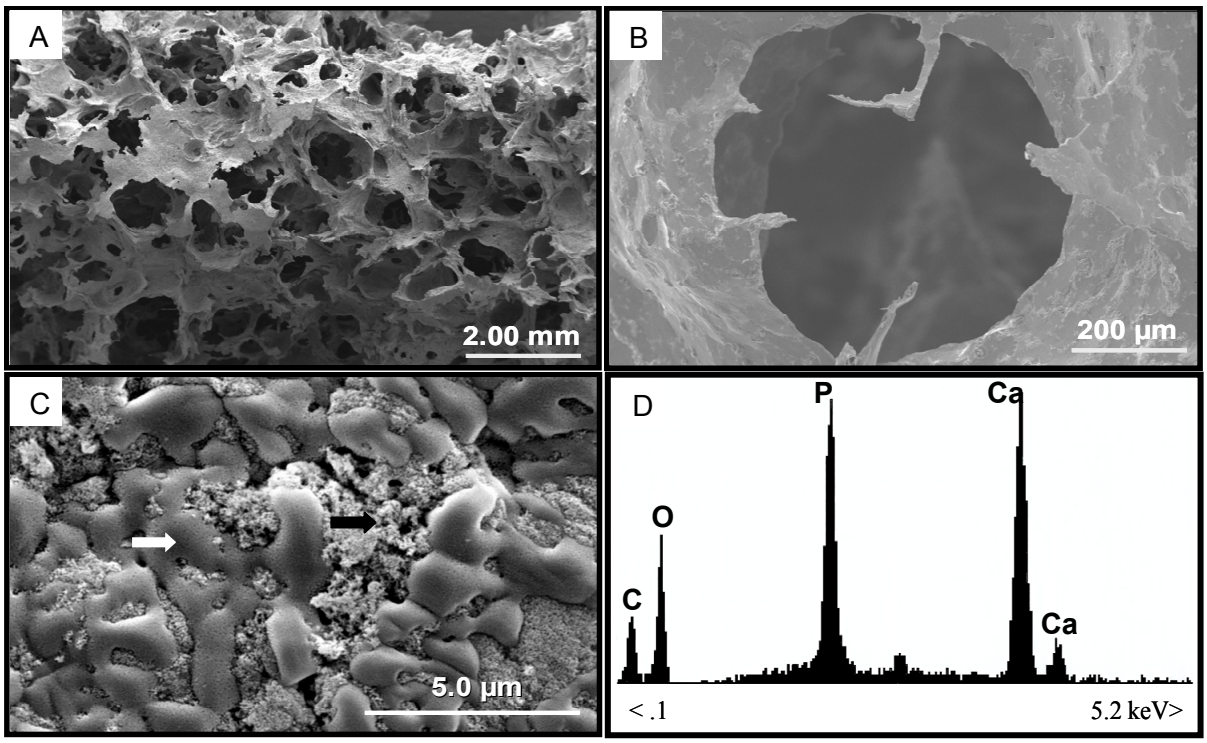

Figure 2. SEM micrographs of the hydroxylapatite/carboxymethylchitosan composite scaffolds: lateral view (A), typical pore (B), interface between the HAp and CMCht (C), and respective EDS (D).

The FTIR spectra of chitosan and CMCht demonstrated that the late was successfully synthesized, as detected by the presence of characteristic absorption bands of the carboxyl group (□) at 1593 cm^{-1} and 1417 cm^{-1} (υas COO^- and υs COO^-) (Figures 3A-B). On the other hand, the FTIR spectrum of the composite scaffolds revealed the presence of two types of phosphate absorption bands, PO_4^{3-} (ν3) at 1190-1020 cm^{-1} (+), and the PO_4^{3-} (ν4) bands at 601 cm^{-1} and 565 cm^{-1} (x) (Figure 3C). Additionally, it was detected the presence of the peaks corresponding to the carbonate groups, namely at 875 cm^{-1} attributed to carbonate ν2 (∗) and at 1650-1300 cm^{-1} assigned to carbonate ν3 (•), which can be indicative of the carbonate ion substitution. The appearing of a band (□) at 1417 cm^{-1} assigned to the COO^- group, and at 1731 cm^{-1} (♦) to COOH group, indicated that CMCht is present in the composite scaffold.

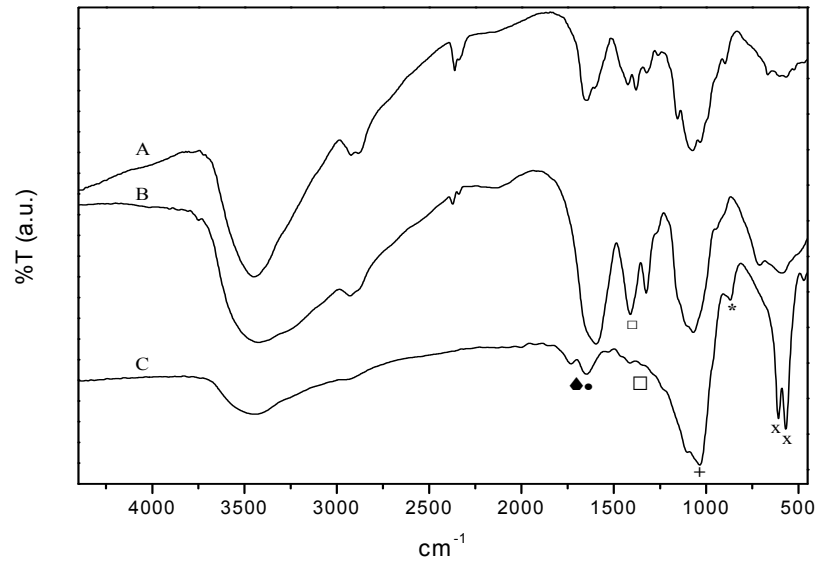

Figure 3. FTIR spectra of: chitosan (A), CMCht (B), and hydroxylapatite/carboxymethylchitosan composite scaffolds (C).

The XRD patterns of the novel composite scaffolds and pure CMCht synthesized in our laboratory are shown in Figure 4A and 4B, respectively. The diffractogram of composite scaffolds demonstrated that the calcium-phosphates consisted of crystalline HAp (Figure 4A). Figure 4B shows that CMCht is essentially amorphous.

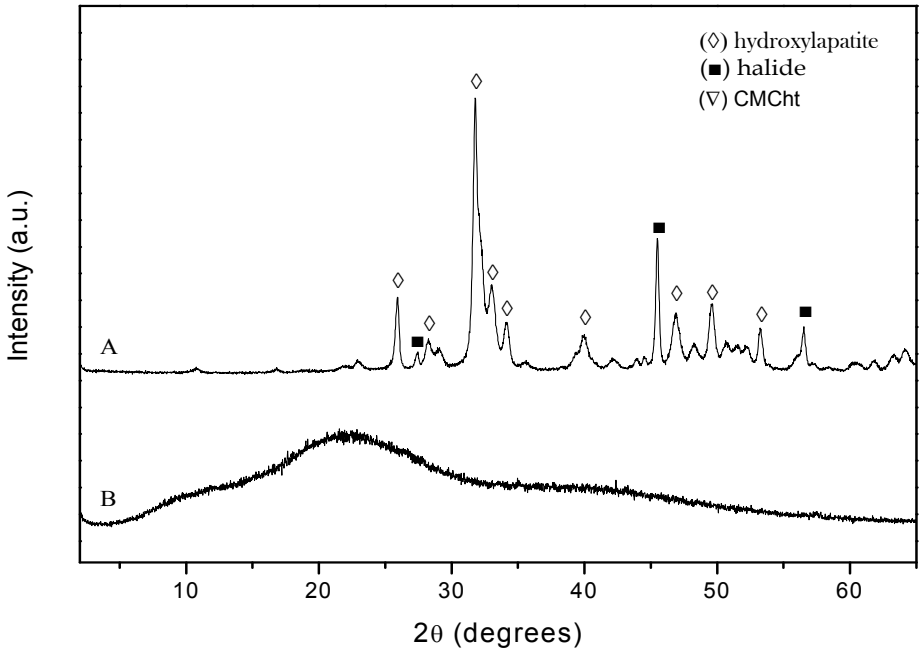

Figure 4. XRD patterns of powders of: hydroxylapatite/carboxymethylchitosan composite scaffolds (A) and CMCht (B).

From μ-CT, it can be seen that the porosity of the scaffolds extends from the top to the bottom (black arrows), showing the high interconnectivity of the scaffolds (Figures 5A-B). On the other hand, the 2-D morphometric analysis demonstrated that in average the scaffolds consisted of 24% HAp and 76% CMCht (Figure 5C). Moreover, it was also possible to determine that the composite scaffolds possess 58.9 ± 6% of porosity.

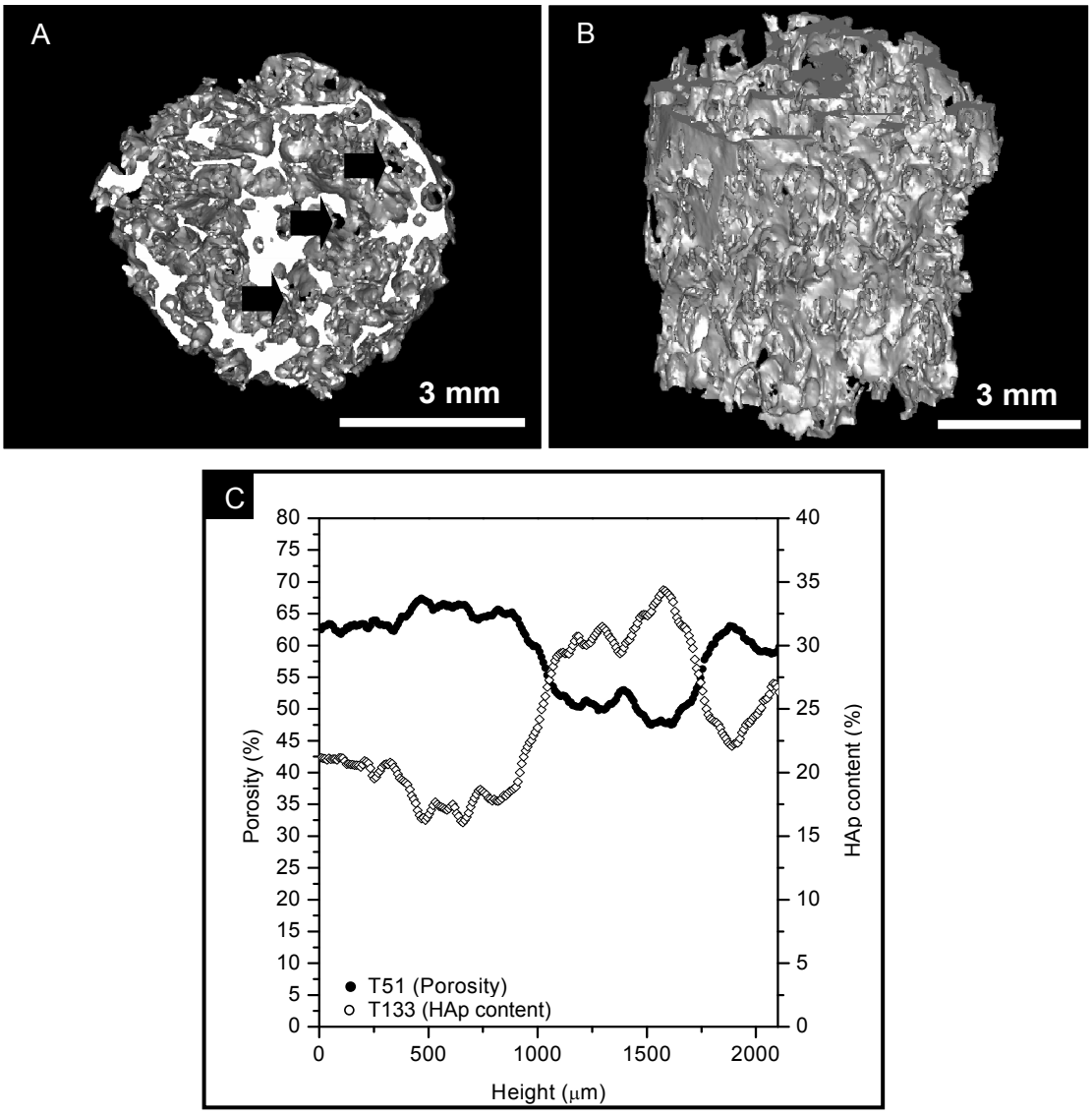

Figure 5. μ-CT of hydroxylapatite/carboxymethylchitosan composite scaffolds: top view (A), lateral view (B), and the respective 2-D histomorphometric analysis (C).

Figure 6 shows the profile of the water-uptake capability and weight loss of the composite scaffolds after soaking in a PBS solution for the period of 1 up to 30 days. The results have shown a dramatic increase of water absorption in the first hours after immersion in PBS (480%) solution. This trend can be seen

until day 7 and after this period a slight stabilisation around the day 15 occur (Figure 6A). After this period of time, it is possible to observe a slight decrease of the water-uptake.

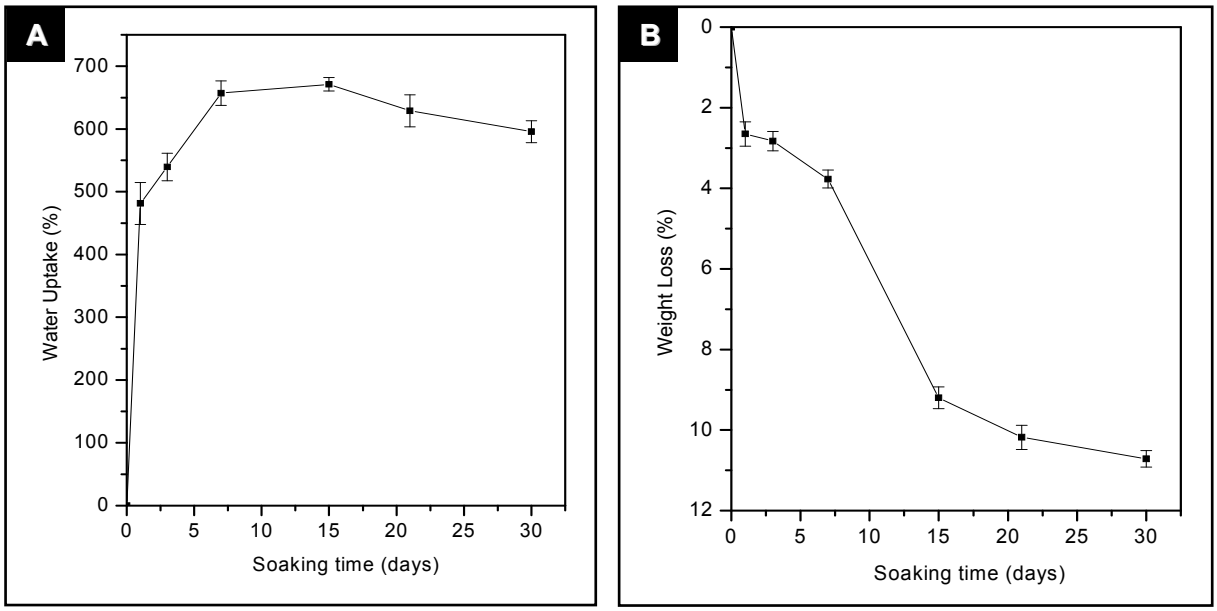

Figure 6. Hydroxylapatite/carboxymethylchitosan composite scaffolds after soaking in PBS solution for times ranging from 1 up to 30 days: water-uptake (A) and weight loss (B).

In respect to the weight loss, a decrease of 3.5% in mass can be seen around day 7. From day 7 until day 15, it is possible to observe a dramatic increase in weight loss (~ 9% in mass). This trend was observed until day 30 (Figure 6B).The mechanical properties of the composite scaffolds was assessed using compression tests in dry state. A modulus (*E*) of 57.3 ± 7 MPa and maximum percentage strength of 51.0 ± 6 MPa was obtained. Additionally, it was also carried out studies in wet state by measuring the "push-out" force (Figure 7) after soaking the composite scaffolds into a PBS solution for the period of 24 hours. A modulus (E) of 0.5 ± 0.3 MPa was calculated by linear regression.

The SEM studies revealed that deposition of aggregates occur after soaking 1d into a SBF solution (Figure 8A). From Figure 8B, it is possible to observe that the surface of the composite scaffolds was completely covered with a thick film with a typical apatite-like morphology, after 7 days.

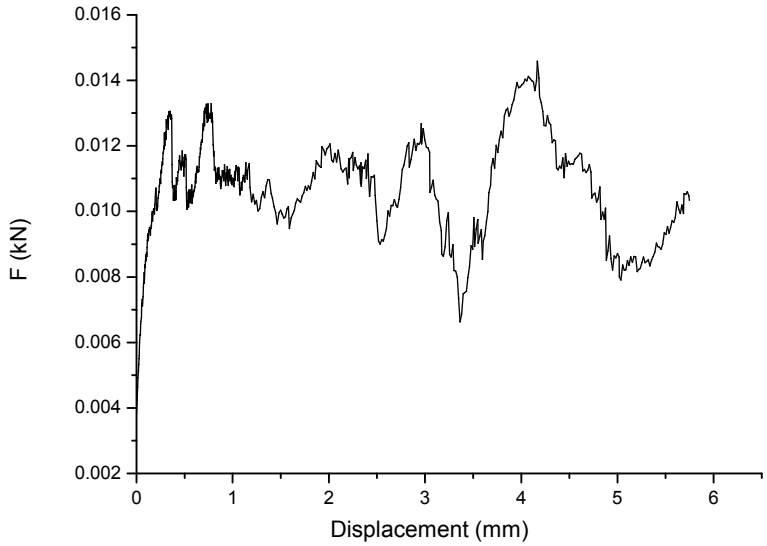

Figure 7. Push-out curve for the hydroxylapatite/carboxymethylchitosan composite scaffolds after soaking in a PBS solution for 24 hours.

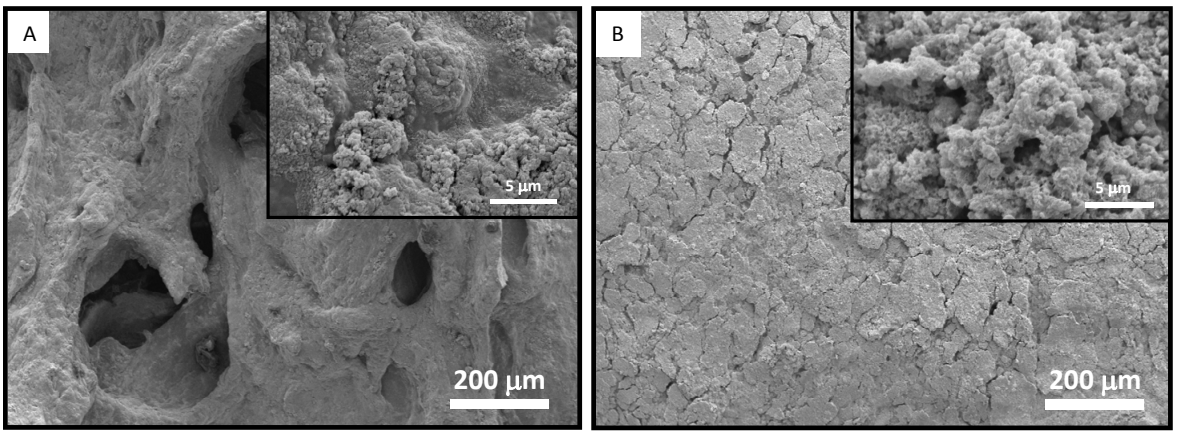

Figure 8. SEM micrographs hydroxylapatite/carboxymethylchitosan composite scaffolds surface after soaking in SBF: 1 day (A) and 7 days (B).

Figure 9 shows the variation on calcium and phosphorus ion concentrations in the SBF solution after soaking the composite scaffolds for the periods of 1 up to 30 days. It is possible to observe that both calcium and phosphorus concentration decreased from day 1 until day 15. In the period of time comprised between day 15 and day 21, it can be observed an increase of Ca concentration in solution.

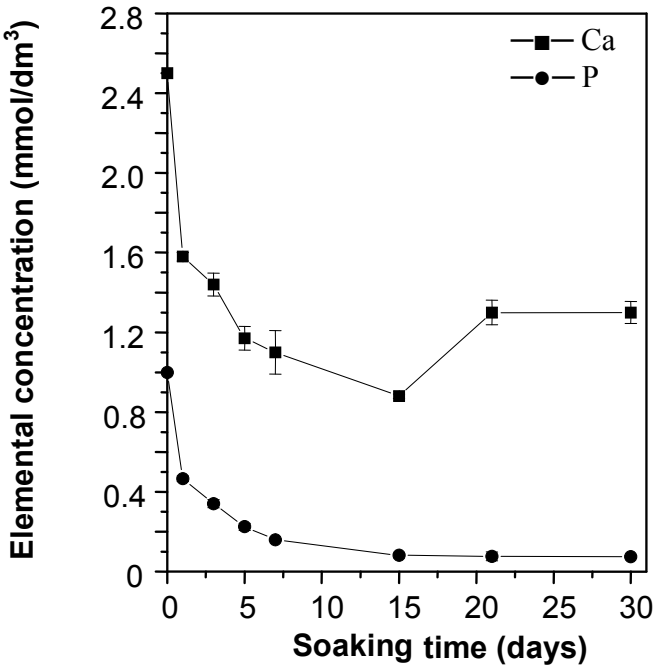

Figure 9. Profile of Ca and P ions in the SBF solution after soaking the hydroxylapatite/carboxymethylchitosan composite scaffolds from 1 up to 30 days.

4. DISCUSSION

Previously, we demonstrate that carboxymethylchitosan (CMCht) can react with $CaCl_2$ in two different "*autocatalytic*" electroless media containing Pd^{2+}, namely the acid and oxidant baths, resulting in the formation of opaque dispersions [48]. By performing a potentiometric titration, it was possible to verify that CMCht precipitation occurred preferentially in the range of pH's comprised between ~2-6 (data not shown). In the same report, we conclude that CMCht can co-precipitate with calcium-phosphates in a higher extent when using an acidic bath. This observation may be due to a more effective complexation of CMCht with Pd^{2+} ions. By this mean, we were able to produce a composite material, which is expected to possess improved mechanical and bioactive behaviour.

In the present investigation, SEM studies have shown the existence of two phases on the composite scaffolds, i.e. an organic and the inorganic one (Figure 2C). The EDS analysis showed that the inorganic phase consisted of calcium and phosphorus (Figure 2D). Therefore, the precipitation of CMCht enclosed the calcium phosphate particles inside the polymer. Moreover, using a wax spheres leaching methodology it was possible to develop 3D-macroporous structures with tailored porosity and interconnectivity (Figures 2A-B). The average pore size was found to be

comprised between 20 to 500 μm. Regarding materials porosity, Kaplan et al. [13] has been showing that the range of pore size observed in the composite scaffolds will be beneficial for the cells or tissue ingrowths, and formation of capillaries.

It has been reported [57] that the chelation of Ca^{2+} by the water soluble CMCht involves both carboxymethyl group and the 3-OH of a neighboring residue. From these findings, it is expected that the efficiency of CMCht on the Pd^{2+}/Ca^{2+} chelation would be dependent not only on the state of protonation of its carboxymethyl groups but also on the degree of substitution, i.e. percentage of carboxymethyl groups. Therefore, the degree of substitution of CMCht will dictate the number of chelation sites. These findings are extremely important because by either changing the pH of the precipitation bath and the initial degree of substituion of CMCht or even the molecular weight [58] we may be able to tailor the chemical composition of the composite scaffolds, i.e. the efficiency of calcium-phosphate co-precipitation, and ultimately its physicochemical properties.

Another advantage of using CMCht on the development of composite scaffolds for bone tissue applications, arises from the fact that CMCht allows to incorporate a larger variety of molecules (e.g. bovine serum albumin or bone morphogenetic proteins, BMPs) from precipitating media. But more importantly, this can be done in a wider range of pH's, which it is not possible when using chitosan, for example [59]. Therefore, we firmly believe that the herein proposed method is a feasible route to incorporate different pH-sensitive proteins in the bulk of the composite scaffolds without any detriment for its activity.

Structural changes of chitosan and its derivatives were assessed by FTIR spectroscopy (Figure 3). The overlaid IR spectra show that CMCht has been successfully synthesized from chitosan. In the region of 3600-3000 cm^{-1} the chitosan, CMCht and composite scaffolds exhibit a highly convoluted IR band due to the various OH stretching contributions. The presence of characteristic absorption bands assigned to the asymmetric (as) and symmetric(s) stretching modes COO^- group at 1593 cm^{-1} and 1417 cm^{-1} revealed that carboxymethylation was effective (Figures 3A-B). Previous studies have shown that CMCht possess a substitution degree (DS) of 47% (data not shown). By its turn, the FTIR spectrum of the composite scaffolds exhibited all the characteristic peaks of apatite, i.e. the presence of phosphate absorption bands, PO_4^{3-} ($\nu 3$) at 1190-1020 cm^{-1}, and the PO_4^{3-} ($\nu 4$) bands at 601 cm^{-1} and 565 cm^{-1} (Figure 3C). In the composite material, the appearing of a small band at 1417 cm^{-1} attributed to the carboxylic band, indicate that CMCht is also present. Besides, the band observed at 1731 cm^{-1} is also attributed to the –COOH group from CMCht. Additionally, it was also detected the peaks corresponding to the carbonate groups, namely at 875 cm^{-1} attributed

to carbonate $\nu 2$ and at 1650-1300 cm^{-1} assigned to carbonate $\nu 3$, which can be indicative of the carbonate ion substitution. The presence of the carbonate $\nu 2$ and $\nu 3$ vibrational modes, in the apatites may contribute to decrease the hydroxyl band, as seen in the FTIR spectra. It is known that the $\nu 2$ sites occur competitively between the OH^- and carbonate groups at the interface of growing crystal, whereas the $\nu 3$ sites depends on the competition between phosphate and carbonate ions.

The X-ray diffraction (XRD) analysis was conducted to investigate the phase content and cristallinity of the developed composite scaffolds. The XRD pattern of the composite scaffolds, clearly demonstrated that the calcium phosphates peaks perfectly matched with the standard file for HAp (JCPDS 9-432; Figure 4A). The wide peak appearing approximately at 22º was assigned to CMCht (Figure 4B). Therefore, the carbonate ions detected by FTIR are assigned to surface ones, rather than to carbonate ions in the lattice of phosphate ions. It is also possible to detect the presence of halide in the composite scaffolds, which can be due to the possibility of chemisorption of Pd^{2+} on the surface CMCht, as initially hypothesized. Therefore this data is an indication that CMCht is able to bind Pd^{2+}, which by its turn may promote the calcium phosphate precipitation. Besides being possible to control the CMCht precipitation, these results seems to corroborate previously reported ones, that showed that certain acidic "*autocatalytic*" electroless bath allows to control the Ca and P composition of composite, and the cristallinity of the inorganic phase [53].

By means of performing the μ-CT analysis of the novel composite scaffolds we were able to evaluate the porosity, both qualitative and quantitatively (Figure 5). Composite scaffolds showed to possess a high pore interconnectivity. Applying a threshold 133 (T133), it was possible to determine that in average the scaffolds consisted of 24% HAp and 76% CMCht. By its turn, when using the threshold 51 (T51), it was possible to calculate the porosity across the composite scaffolds. This study has shown that composite scaffolds have a porosity of 58.9 ± 6%, in average. Moreover, it is also possible to observe that porosity decreases where the HAp content increases. The reason for this observation and for the high interval of porosity may be due to the sedimentation of the HAp particles and wax spheres during the drying process. This can be prevented by agitating the moulds during the preparation of the composite scaffolds. From these results, it can be seen that the developed composite scaffolds have an appropriate porosity to find applications as bone substitutes. The method herein proposed presents and important advantage. Porosity and interconnectivity may be easily tailored by means of varying the content and granulometry of wax spheres.

Biodegradability or bioadsorbability [60] of the 3-D substrate is also an essential characteristic in TE applications. Since CMCht is a water soluble polymer we carried out *in vitro* tests, to determine the water-uptake capability (swelling) and weight loss of the developed composite scaffolds. The swelling profile showed a dramatic absorption of water (480%), from first hours until day 7. This swelling behaviour is often characteristic of a hydrogel. Nevertheless, it has been reported that CMCht swelling is dependent on the pH of the media [43]. Because CMCht contains both carboxyl and amino groups, it is possible to control the swelling of the composite scaffolds to load them with different proteins at different extents, for example. In fact, it has been reported that CMCht swell at low pH (<2.0) and at pH in the range of 4.0-13.0 due to the protonated amino groups and unprotonated carboxyl groups, respectively [43]. Therefore, the swelling behaviour of CMCht is affected by both degree of deacetylation and degree of substitution. Additionally, the charge of the composite scaffolds can be altered due to the possibility of CMCht to bind Ca^{2+} or Pd^{2+}, thus their swelling behavior is expected to be different from the typical CMCht gels.

In respect to the weight loss it was possible to observe that composite scaffolds were stable until day 7. After 30 days, a dramatic weight loss occur (~11% in mass). These results are in agreement with previous reported ones [43] and can be explained due to the water soluble behaviour of CMCht. Moreover, the slight decrease on the swelling of the composite scaffolds after day 15 until day 30 may be a consequence of this dissolution behaviour. Chen et al. [43] reported that carboxymethylchitin lose above 80% in weight after 20 days of immersion into a phosphate buffer at pH 7.4. Therefore, the lower weight loss of the novel composite scaffolds suggests that this trend may be a consequence of Ca^{2+} or Pd^{2+} ions chelation, thus resulting in the development of scaffolds more resistant to dissolution. In this context, future work will be carried out to evaluate the effect of Ca^{2+} or Pd^{2+} binding on the CMCht swelling and dissolution behaviour. A well known strategy to control the swelling of the polymers consists in performing the cross-linking [61]. In this context, after co-precipitation of CMCht and hydroxylapatite one may use cross-linking agents, such as silane-coupling agents. This strategy may allow controlling the swelling and pH-sensitivity of the composite scaffolds, and to improve the stability of the organic-inorganic network.

The mechanical properties of the composite scaffolds was assessed using compression tests in dry state. A modulus of 57.3 ± 7 MPa and maximum percentage strength of 51.0 ± 6 MPa at ~59% of macroporosity was obtained. Due to the high water-uptake capability of the composite scaffolds, its mechanical properties decrease dramatically after soaking into a PBS solution for 24 hours. Whilst mechanical strength of the composite scaffolds decreased after soaking into PBS solution, the

ductibility increased. These tests were carried out in confined cavities to mimic as much as possible the *in vivo* circumstances, i.e. at the implantation site the scaffold will be constrained by the bone compression. Interestingly, after undergoing the mechanical solicitation, the composite scaffolds showed a sponge-like behaviour, i.e. were capable of recover the initial shape without fracturing, thus keeping the scaffolds integrity. Based on these findings, the moldability of the composite scaffolds can be a major advantage if we take in consideration that the current orthopaedic implant materials such as sintered HAp are used in a hard form, thus requiring the surgeon to fit the surgical site around the implant or the need of a material of a desired shape [30].

Other important parameters have to be taken in consideration when developing a TE scaffold. Besides other things the scaffold must be capable of drug loading and its release in a controlled manner. In this context, Chen et al. [43] have described a reliable methodology to load CMCht based polyampholyte hydrogels with drugs by taking advantage of the high swelling behaviour. Due to composite scaffolds both mechanical stability in wet state and ability to form hydrogels, the authors believe that the herein described composite scaffolds have great advantage over other materials, namely because possess a lower dissolution behaviour when compared with CMCht alone.

In this study, bioactivty tests were also carried out. These have shown that deposition of apatite occur after soaking 1 day in a SBF solution. A thick film covering the surface of the composite scaffolds was observed after 7 days. This bioactive behaviour may be explained by the presence of HAp in the composite scaffold, which is known to accelerate the formation of bone-like apatite on the surface of implants [62]. The variation on calcium and phosphorus ion in SBF solution was monitored by ICP. From Figure 9 it can be seen that both calcium and phosphorus concentration decreased from day 1 until day 15. This trend may be a consequence of the consumption of both calcium and phosphorus during the precipitation of the apatite layer on the surface of the composite scaffolds (Figure 8). The increase of the Ca concentration (from day 15 until day 21) may be a result of CMCht dissolution. Moreover, since phosphate concentration remained constant, the release of calcium into the SBF solution can only be explained due to the release of calcium chelated to CMCht, and not due to a redissolution phenomena. Thus, this result is in agreement with the weight loss profile. Despite, further complimentary studies are required to elucidate the fast decrease of calcium and phosphorus in the SBF solution.

5. CONCLUSIONS

This work demonstrated that it is possible to prepare hydroxylapatite/carboxymethylchitosan composite scaffolds by means of combining a novel acidic "*autocatalytic*" co-precipitation route and a novel wax spheres leaching methodology. The physicochemical properties of the composite scaffolds may be tailored, especially the 3-D architecture, content in organic-inorganic phases, and dissolution behaviour. Therefore, these composite scaffolds are very promising whenever degradability and bioactivity are simultaneously desired, such as in the case of bone tissue engineering scaffolding applications. Moreover, the novel composite scaffolds can possibly the incorporation of pH-sensitive proteins up to physiological pH, which is known to be one major drawback of chitosan materials for such type of applications. Future work will be performed to study of cell adhesion, proliferation and screen the citotoxicity on the surface of the novel hydroxylapatite/carboxymethylchitosan composite scaffolds.

REFERENCES

1. Vacanti, J.P. and R. Langer, *Tissue engineering: the design and fabrication of living replacement devices for surgical reconstruction and transplantation*. Lancet, 1999. **354**: p. 32.
2. Langer, R. and J.P. Vacanti, *Tissue Engineering*. Science, 1993. **260**: p. 920.
3. Ohgushi, H., et al., *Tissue engineered ceramic artificial joint- ex vivo osteogenic differentiation of patient mesenchymal cells on total ankle joints for treatment of osteoarthritis*. Biomaterials, 2005. **26**: p. 4654.
4. Peterson, L., et al., *Autologous chondrocyte transplantation: biomechanics and long-term durability*. The American Journal of Sports Medicine, 2002. **30**: p. 2.
5. Cancedda, R., et al., *Tissue engineering and cell therapy of cartilage and bone*. Matrix Biology, 2003. **22**: p. 81.
6. Schliephake, H., et al., *Use of cultivated osteoprogenitor cells to increase bone formation in segmental mandibular defects: an experimental pilot study in sheep*. International Journal of Oral and Maxillofacial Surgery, 2001. **30**(6): p. 531.
7. Long, M.W., et al., *Regulation of human bone marrow-derived osteoprogenitor cells by osteogenic growth factors*. Journal of Clinical Investigation, 1995. **95**: p. 881.

8. Holland, T.A., et al., *Transforming growth factor-beta 1 release from oligo(poly(ethylene glycol) fumarate) hydrogels in conditions that model the cartilage wound healing environment*. Journal of Controlled Release, 2004. **94**: p. 101.
9. Ono, I., et al., *Combination of porous hydroxyapatite and cationic liposomes as a vector for BMP-2 gene therapy*. Biomaterials, 2004. **25**(19): p. 4709.
10. Honda, M., *Cartilage formation by cultured chondrocytes in a new scaffold made of poly(L-lactide-ε-caprolactone) sponge*. Journal of Maxillofacial Surgery, 2000. **58**: p. 767.
11. Yamamato, M., P*romotion of fibrovascular tissue ingrowth into porous sponges by basic fibroblast growth factor*. Journal of Materials Science: Materials in Medicine, 2000. **11**: p. 213.
12. Ma, P.X. and R. Langer, *Fabrication of biodegradable polymer foams for cell transplantation and tissue engineering*. In: Tissue Engineering Methods and Protocols, edited by M. Yarmush and J. Morgen. Totowa, NJ: Humana Press 1998: p. 47.
13. Karageorgiou, V. and D. Kaplan, *Porosity of 3D biomaterial scaffolds and osteogenesis*. Biomaterials, 2005. **26**: p. 5474.
14. Tomczok, J., et al., *Biomaterial-induced alterations of human neutrophils under fluid shear stress: scanning electron microscopical study in vitro*. Biomaterials, 1996. **17**: p. 1359.
15. Hutmacher, D.W., *Scaffold design and fabrication technologies for engineering tissues-state of the art and future perspectives*. Journal of Biomaterials Science, Polymer Edition, 2000. **12**: p. 107.
16. Ma, P.X., *Scaffolds for tissue engineering*. Materials Today, 2004. **7**: p. 30.
17. Liu, X. and P.X. Ma, *Polymeric scaffolds for bone tissue engineering*. Annals of Biomedical Engineering, 2004. **32**: p. 477.
18. Rizzi, S.C., et al., *Biodegradable polymer/hydroxyapatite composites: Surface analysis and initial attachment of human osteoblasts*. Journal of Biomedical Materials Research, 2001. **55**: p. 475.
19. Kawakami, T., et al., *Experimental study on osteoconductive properties of a chitosan-bonded hydroxyapatite self-hardening paste*. Biomaterials, 1992. **13**: p. 759.
20. Oliveira, J.M., et al., *Novel hydroxyapatite/chitosan bilayered scaffold for osteochondral tissue-engineering applications: Scaffold design and its performance when seeded with goat bone marrow stromal cells*. Biomaterials, 2006. **27**(36): p. 6123.
21. Solchaga, L.A., et al., *Repair of osteochondral defects with hyaluronan- and polyester-based scaffolds*. Osteoarthritis and Cartilage, 2005. **13**(4): p. 297.

22. Spoerke, E.D., et al., *A bioactive titanium foam scaffold for bone repair*. Acta Biomaterialia 2005. **1**(5): p. 523.
23. Turhani, D., et al., *In vitro growth and differentiation of osteoblast-like cells on hydroxyapatite ceramic granule calcified from red algae*. Journal of Oral and Maxillofacial Surgery, 2005. **63**: p. 793.
24. Kotobuki, N., et al., *Observation of osteogenic differentiation cascade of living mesenchymal stem cells on transparent hydroxyapatite ceramics*. Biomaterials, 2005. 26: p. 779.
25. Martino, A.D., M. Sittinger, and V.R. Makarand, *Chitosan: A versatile biopolymer for orthopaedic tissue-engineering*. Biomaterials, 2005. **26**: p. 5983.
26. Shi, C., et al., *Therapeutic potential of chitosan and its derivatives in regenerative medicine*. Journal of Surgical Research, 2006. **133**(2): p. 185.
27. Murugan, R. and S. Ramakrishna, *Bioresorbable composite bone paste using polysaccharide based nano hydroxyapatite*. Biomaterials, 2004. **25**: p. 3829.
28. Ma, P.X., et al., *Engineering new bone tissue in vitro on highly porous poly(α-hydroxyl acids)/hydroxyapatite composite scaffold*s. Journal of Biomedical Materials Research, 2001. **54**: p. 284.
29. Ge, Z., et al., *Hydroxyapatite-chitin materials as potential tissue engineered bone substitutes*. Biomaterials, 2004. **25**: p. 1049.
30. Xu, H.H.K. and C.G. Simon Jr., *Fast setting calcium phosphate-chitosan scaffold: mechanical properties and biocompatibility*. Biomaterials, 2005. **26**: p. 1337.
31. Zhang, Y. and M. Zhang, *Microstructural and mechanical characterization of chitosan scaffolds reinforced by calcium phosphates*. Journal of Non-Crystalline Solids, 2001. **282**: p. 159.
32. Wan, A.C.A., E. Khor, and G.W. Hastings, *Preparation of a chitin-apatite composite by in situ precipitation onto porous chitin scaffolds*. Journal of Biomedical Materials Research, 1998. **41**: p. 541.
33. Ang, T.H., et al., *Fabrication of 3D chitosan–hydroxyapatite scaffolds using a robotic dispensing system*. Materials Science and Engineering C, 2002. **20**: p. 35.
34. Kim, H.-W., J.C. Knowles, and H.-E. Kim, *Hydroxyapatite and gelatin composite foams processed via novel freeze-drying and crosslinking for use as temporary hard tissue scaffolds*. Journal of Biomedical Materials Research, 2005. **72A**: p. 136.
35. Hollinger, J.O., *Strategies for regenerating bone of the craniofacial complex*. Bone, 1993. **14**: p. 575.

36. Marques, A.P., R.L. Reis, and J.A. Hunt, *The biocompatibility of novel starch-based polymers and composites: in vitro studies*. Biomaterials, 2002. **23**: p. 1471.
37. Sun, T., et al., *Graft copolymerization of methacrylic acid onto carboxymethylchitosan*. European Polymer Journal, 2003. **39**: p. 189.
38. Muzzarelli, R., *Carboxymethylated chitins and chitosans*. Carbohydrate Polymers, 1988. **8**: p. 1.
39. Ge, H.-C. and D.-K. Luo, *Preparation of carboxymethylchitosan in aqueous solution under microwave irradiation*. Carbohydrate Research, 2005. **340**: p. 1351.
40. Dobetti, L. and F. Delben, *Binding of metal cations by N-carboxymethylchitosans in water*. Carbohydrate Polymers, 1992. **18**: p. 273.
41. Delben, F. and R.A.A. Muzzarelli, *Thermodynamic study of the interaction of N-carboxymethylchitosan with divalent metal ions*. Carbohydrate Polymers, 1989. **11**: p. 221.
42. Chen, S.-C., et al., *A novel pH-sensitive hydrogel composed of N,O carboxymethylchitosan and alginate cross-linked by genipin for protein drug delivery*. Journal of Controlled Release, 2004. **96**: p. 285.
43. Chen, L., Z. Tian, and Y. Du, *Synthesis and pH sensitivity of carboxymethyl chitosan-based polyampholyte hydrogels for protein carrier matrices*. Biomaterials, 2004. **25**: p. 3725.
44. Zhou, J., C. Elson, and T.D.G. Lee, *Reduction in postoperative adhesion formation and re-formation after an abdominal operation with the use of N,O - carboxymethylchitosan*. Surgery, 2004. **135**: p. 307.
45. Liang P, et al., *The effect of carboxymethylchitosan on the precipitation of calcium carbonate*. Journal of Crystal Growth, 2004. **261**: p. 571.
46. Muzzarelli, R.A.A., et al., *Osteogenesis promoted by calcium phosphate N,N-dicarboxymethylchitosan*. Carbohydrate Polymers, 1998. **36**: p. 267.
47. Viala, S., M. Freche, and J.L. Lacout, *Effect of chitosan on octacalcium phosphate crystal growth*. Carhohydrate Polymers, 1996. **29**: p. 197.
48. Costa, S.A., et al., *Carboxymethilchitosan/calcium phosphate hybrid materials prepared by an innovative "autocatalytic" co-precipitation method*. Key Engineering Materials, 2005. **284-286**: p. 701.
49. Leonor, I.B. and R.L. Reis, *An innovative "auto-catalytic" deposition route to produce calcium-phosphate coatings on polymeric biomaterials*. Journal of Materials Science: Materials in Medicine, 2003. **14**: p. 435.

50. Touchais-Papet, E., M. Charbonnier, and M. Romand, *Electroless metallization of carbon substrates*. Applied Surface Science, 1999. **138-139**: p. 557.
51. Charbonnier, M., et al., *Laser-assisted grafting onto polycarbonate: application to metallization by chemical means*. Applied Surface Science, 1997. **109-110**: p. 206.
52. Blaser, H.-U., et al., *Supported palladium catalysts for fine chemicals synthesis*. Journal of Molecular Catalysis A: Chemical, 2001. **173**(1-2): p. 3.
53. Oliveira, J.M., I.B. Leonor, and R.L. Reis, *Preparation of bioactive coatings on the surface of bioinert polymers through an innovative "auto-catalytic" electroless route*. Key Engineering Materials, 2005. **284-286**: p. 203.
54. Kokubo, T., et al., *Solutions able to reproduce in vivo surface-structure changes in bioactive glass-ceramic A-W*. Journal of Biomedical Materials Research, 1990. **24**: p. 721.
55. Chen, X.-G. and H.-J. Park, *Chemical characteristics of O-carboxymethylchitosans related to the preparation conditions*. Carbohydrate Polymers, 2003. **53**: p. 355.
56. Boesel, L.F., J.F. Mano, and R.L. Reis, *Optimization of the formulation and mechanical properties of starch based partially degradable bone cements*. Journal of Materials Science: Materials in Medicine, 2004. **15**: p. 73.
57. Uraki, Y., et al., *Site specific binding of calcium ions to anionic chitin derivatives*. Carbohydrate Polymers, 1993. **20**: p. 139.
58. Chen, X., et al., *The effect of carboxymethylchitosan on proliferation and collagen secretion of normal and keloid skin fibroblasts*. Biomaterials, 2002. **23**: p. 4609.
59. Chenite, A., et al., *Rheological characterisation of thermogelling chitosan/glycerol-phosphate solutions*. Carbohydrate Research, 2001. **46**: p. 39.
60. Hutmacher, D.W., *Scaffolds in tissue engineering bone and cartilage*. Biomaterials, 2000. **21**: p. 2529.
61. Berger, J., et al., *Structure and interactions in covalently and ionically crosslinked chitosan hydrogels for biomedical applications*. European Journal of Pharmaceutics and Biopharmaceutics, 2004. **57**: p. 19.
62. Sabokbar, A., et al., *Hydroxyapatite particles are capable of inducing osteoclast formation*. Journal of Materials Science: Materials in Medicine, 2001. **12**: p. 659.

CHAPTER IV.

Macroporous hydroxylapatite scaffolds for bone tissue engineering applications: physicochemical characterization and assessment of rat bone marrow stromal cell viability

CHAPTER IV.

Macroporous hydroxylapatite scaffolds for bone tissue engineering applications: physicochemical characterization and assessment of rat bone marrow stromal cell viability

Abstract

In this work, it is reported a new methodology for developing hydroxyapatite (HAp) scaffolds by using an organic sacrifice template. The novelty of work consists on the possibility of obtaining porous and highly interconnected scaffolds mimicking the sacrificial component. Our purpose consisted on evaluating the physicochemical properties of the HAp scaffolds by means of Fourier-transform infra-red spectroscopy, X-ray diffraction analysis, and scanning electron microscopy (SEM) attached with an X-ray detector. The HAp scaffolds obtained possess a porosity of ~70%, and macropores diameter in the range of 50-600 μm. On the other hand, results regarding the micro-computed tomography analysis have demonstrated both high pore uniformity and interconnectivity across the scaffolds. The compressive strength of the HAp scaffolds was found to be 30.2 ± 6.0 MPa. Bioactivity of the HAp scaffolds was assessed by immersion into a simulated body fluid solution, *in vitro*. SEM observations have showed a deposition of apatite on the surface of the HAp scaffolds, with a 'cauliflower-like' morphology after 1 day, and tend to be more pronounced with the immersion time. The changes in calcium and phosphorus concentration were monitored by inductively-coupled plasma optical emission spectrometry. Cytotoxicity of the HAp scaffolds was preliminarily investigated by carrying direct observation of mouse fibroblasts cells (L929 cell-line) death in the inverted microscope and then cell viability was determined by means of carrying out a MTS assay. Complementarily, a luminescent cell viability assay based on the quantification of adenosine triphosphate was performed using rat bone marrow stromal cells (RBMSCs). A LIVE/DEAD assay and SEM analysis allowed the visualization of the RBMSCs adhesion and proliferation on the surface of the HAp scaffolds. According to the results obtained from 3-D architecture, mechanical properties, biocompatibility and adhesion tests, it is suggested that HAp scaffolds has potential to find applications in bone tissue engineering scaffolding.

This chapter is based on the following publication: **Oliveira JM**, Silva SS, Malafaya PB, Rodrigues MT, Kotokuki N, Hirose M, Gomes ME, Mano JF, Ohgushi H and Reis RL, 2008, Macroporous hydroxyapatite scaffolds for bone tissue engineering applications: physicochemical characterization and

assessment of rat bone marrow stromal cell viability, Journal of Biomedical Materials Research: Part A – In Press, Corrected Proof, (doi:10.1002/jbm.a.32213).

---

1. INTRODUCTION

Bone lesions above a critical-sized segmental defect still remain a huge challenge to reconstructive surgery and regenerative medicine. This is mainly due to the fact that bone has a limited ability to heal [1,2]. In many clinical situations there is the need for a surgical intervention and the use of autografts [3,4], allografts or xenografts [4,5] transplantation. Still, the preferred clinical strategy is the autologous transplantation, since avoids the problem of immune rejection [6] and the consequent administration of drugs for immunosupression of the host [7]. Bone autografts consists on bone portions either cancellous or cortical [4], harvested from other skeletal locations, which are then transferred into the defect area that is aimed to repair [8]. Although, the limited bone graft volume available, consequent donor site morbidity [5,9] and *post*-operative pain [10] are seen as the major constraint in using autografts. Therefore, we can say that the currently available treatment possibilities are far from being a truly ideal solution. To circumvent these limitations great efforts are focused on developing implantable materials either synthetic and natural-based to be used as implants [11-13]. For instances, synthetic materials based on hydroxylapatite (HAp), $Ca_{10}(PO_4)_6(OH)_2$, have demonstrated a great potential for being used as bone substitutes [13-15] or fracture repair devices [16]. The great interest in using HAp or other ceramic materials arises from the possibility to improve the clinical outcome due to their osteoconductive behaviour [14,17]. However, these biomaterials alone are not always as effective as bone autografts, since they lack the osteogenic and osteoinductive properties [18,19].

More recently, it has been reported that by applying the tissue engineering (TE) principles [10], i.e. by seeding bone marrow stem cells into scaffolds, the so-called constructs [20] or prostheses [21] it was possible to recreate an regenerative environment at the defect area, which resulted in a more favourable healing. Despite the important advances, a wide range of problems related with the tissue engineering approaches remains unsolved. For example, many bone tissue engineering constructs developed showed that bone formation *in vitro*, only occurred at the surface [22]. Therefore, it seems that much has to be done and improvements of the cell culture techniques [23] and appropriate scaffolds architecture are needed for developing successful constructs that can be used in the clinical practice. Therefore, there is the need for continuously improving the development of processing routes towards the fabrication of biocompatible with adequate 3-D porous structures and mechanical properties.

In this work, we report a methodology for developing HAp scaffolds with a controllable architecture to find applications in tissue engineering of bone scaffolding. The physicochemical characterization of the macroporous HAp scaffolds was performed by using Fourier-transform infra-red (FTIR) spectroscopy, X-ray diffraction (XRD) analysis, and scanning electron microscopy attached with an X-ray detector

(SEM/EDS). The microstructure of the HAp scaffolds was examined using micro-computed tomography (μ-CT) analysis. The mechanical properties of the HAp scaffolds were assessed under compression testing.

The bioactive behaviour of the HAp scaffolds was assessed by immersion into a simulated body fluid (SBF) solution. The changes in calcium and phosphate concentration in the SBF solution were monitored by inductively-coupled plasma optical emission (ICP-OES) spectrometry.

Cytotoxicity of the HAp scaffolds leachables was evaluated by carrying out a cellular viability assay (MTS test) on mouse lung fibroblasts cells, which were previously in contact with the different HAp extract fluids. Rat bone marrow stromal cells adhesion and morphology were also analysed by SEM and under a 3-D fluorescence microscope, while the cell viability and proliferation were assessed by carrying out the Luminescent and LIVE/DEAD cell viability assays.

2. MATERIALS AND METHODS

2.1. PREPARATION OF HAP SCAFFOLDS

Calcium hydroxide (Riedel-de Haën, Germany) and ortho-phosphoric acid 85% (Panreac, Spain) solution were used to prepare separately, two precursors (Ca and P) solutions. HAp powders were obtained by adding in a controlled manner, appropriate amounts (Ca/P molar ratio of 1.67 was always used) of these solutions, using a peristaltic pump (Gilson Miniplus 3, France) at a speed rate 17 $mL.min^{-1}$. The precipitation of the HAp particles occurred by adjusting the pH of the media to 11 with a 33% ammonium hydroxide (Riedel-de Haën, Germany) solution. Then, precipitate was filtered under vacuum and the excess of water removed by drying the filtrate at 60ºC for 24 hrs. After milling the HAp pellets until obtain a fine powder, the HAp scaffolds were fabricated. The procedure for obtaining the HAp scaffolds is summarized in Figure 1. Firstly, the HAp slurry was prepared by dispersing HAp powders in methanol for 48 hrs (step 1). Then, polyurethane (PU, Eurospuma SA, Portugal) cylindrical sponges (10 x 8 mm) featuring fully interconnected pores were dipped into the slurry until total impregnation. To prevent the formation of an external skin-like layer, the impregnated PU sponges were transferred to a centrifuge and the excess of slurry was removed by centrifuging at 60 rpm for 1 min (step 2), followed by drying at 37ºC, for 24 hrs (step 3) to avoid the formation of cracks. Finally, the impregnated sponges were placed inside the furnace and the PU matrices burned at 900ºC for 24 hrs, followed by sintering the HAp scaffolds at 1300ºC for 3 hrs (step 4). The HAp scaffolds were allowed to

naturally cool inside the furnace (step 5) and finally sterilized by ethylene oxide gas. Figure 2 shows the typical HAp scaffolds obtained, where replica of the PU sponge pores can be observed.

2.2. CHARACTERIZATION OF THE HAP SCAFFOLDS

2.2.1. Fourier-transform infra-red spectroscopy

Potassium bromide (KBr, Riedel-de Haën, Germany) was used to prepare transparent discs (1:10 of sample/KBr (wt/wt)) for Fourier-transform infra-red (FTIR) analysis. A Perkin-Elmer 1600 series spectrophotometer (Perkin-Elmer, UK) was used to record the spectra that were collected with a minimum of 32 scans and resolution of 2 cm^{-1}. The chemical change of the HAp after sintering was examined over a region of 4400-450 cm^{-1}.

2.2.2. Thermogravimetric analyses

Thermal stability and composition of the PU sponges, PU sponge impregnated with HAp before burning, and HAp scaffolds sintered at 1300ºC was assessed by thermogravimetric (TGA) analysis. A TA-Q500 analyser (TA Instruments, USA) was used. The data was obtained using a ramp rate of 5ºC.min^{-1}.

2.2.3. X-ray diffraction measurements

Crystallinity and phase content of HAp powder, sintered HAp and HAp scaffolds were investigated with X-ray diffraction (XRD) analysis, using an X-ray diffractometer (Philips PW 1710, The Netherlands). XRD patterns were examined in the region of 2º to 65º with a step size 0.02º for 2θ and scan speed of 0.6º.min^{-1}.

2.2.4. Scanning electron microscopy

A scanning electron microscope attached with an energy dispersive electron probe X-ray analyzer (SEM-EDS, Leica Cambridge S-360, UK) was used to analyse both microstructure of HAp scaffolds before and after immersion into a simulated body fluid (SBF) solution, and PU sponges. All specimens were coated with gold using a Polaron SC 502 (Fisons Instruments, UK) coater, prior to observation.

2.2.5. Micro-computed tomography

The 3-D structural and architectural information of the HAp scaffolds was assessed quantitatively and qualitatively by means of micro-computed tomography (μ-CT) analysis and using a Scanco 20

equipment (Scanco Medicals, Switzerland). A series of c.a. 900 2-D slices with a scanning resolution of 11 μm were obtained by irradiating the specimen with penetrative X-rays of 50 keV. Mimics® from Materialise (Belgium) was used as image processing software. The porosity along the HAp scaffolds was also evaluated by 2-D morphometric analysis using a threshold 300 (Th 300).

2.2.6. Mechanical testing

Compression tests (dry state) were performed using a Universal Testing Machine (Instron 4505) containing a load cell of 50 kN. Experiments were conducted using a minimum number of 10 scaffolds.

2.2.7. Bioactivity test

HAp scaffolds were immersed in a simulated body fluid (SBF) solution at 37 ± 1ºC to assess the bioactivity, *in vitro* [24]. After each immersion time (1, 3, 7 and 15 days), the scaffolds were immediately rinsed with distilled water, dried at room temperature for 24 hrs and then dried in the oven at 60ºC until constant weight. The concentration of the Ca and P ions in the SBF solution was also measured by inductively-coupled plasma optical emission (ICP-OES, JY 70 plus, JobinYvon, France) spectrometry. Triplicate samples were analysed for each immersion time and averaged results calculated.

2.3. *IN VITRO* CELL CULTURE STUDIES

2.3.1. Cytotoxicity screening

The MTS viability test was performed to investigate the cytotoxicity of the HAp scaffolds leachables. A cell line of mouse lung fibroblasts (L929 cells) purchased from European Collection of Cell Cultures (ECACC, UK). This type of cells has been used in cytotoxicyty assays to preliminarily test biocompatibility of potential biomaterials [25]. L929 cells were cultured in an DMEM (Dulbecco's Modified Eagle's Medium, Sigma, Germany) medium supplemented with 10% foetal bovine serum (FBS, Gibco, UK), 1% antibiotic-antimycotic (Gibco, UK) solution containing 10,000 units.mL^{-1} penicillin G sodium, 10,000 μg.mL^{-1} streptomycin sulphate and 25 μg.mL^{-1} amphotericin B as Fungizone® in 0.85% saline. The L929 cells were incubated in an atmosphere containing 5% of CO_2 at 37ºC, and the medium changed every two days.

The extracts fluid were prepared as previously reported by Gomes et al. [25]. Succinctly, extracts fluids were obtained by introducing the HAp scaffolds in a 50 mL conical tube with flip-top cap (BD Falcon™, USA) and complete DMEM culture medium was added. For all tests a ratio of outer surface of HAp

scaffolds to DMEM medium equal to 30 $cm^2.mL^{-1}$ was used. Then, the tubes were transferred to a thermostatic bath at 37ºC and 60 rpm for the period of 3 d. Different concentrations of HAp scaffolds extracts (25%, 50%, 75% and 100%) were prepared. A latex rubber extract was used as positive control.

After reaching confluence, L929 cells were trypsinized (0.25% trypsin/EDTA solution, Sigma Chemical, USA) from a culture flask, and a diluted cell suspension was prepared in order to achieve a cellular concentration of 8 x 10^4 cells.mL^{-1}. Afterwards, 1.6 x 10^4 cells were seeded in each well of a 96-well plate (five replicates per sample). Cells were incubated for 48 hrs in a 5% CO_2 incubator at 37ºC, until achieving 80-90% of confluence. Afterwards, the culture medium in each well was replaced with the extraction fluids and incubated for 72 hrs. Then, an MTS assay was performed using 3-(4, 5-dimethylthiazol-2-yl)-5-(3-carboxymethoxyphenyl)-2-(4-sulfophenyl)-2H-tetrazolium) (MTS, Promega, USA), while cellular morphology was assessed by optical microscope (Zeiss-Axiovert 40, Germany). The cell viability (%) was calculated and compared to the tissue culture polystyrene (TCPS). All experiments were performed in triplicate.

2.3.2. Cell viability and adhesion studies

Rat bone marrow stromal cells (RBMSCs) were obtained from femora of 7 week-old male Fischer 344/N rats (SLC Inc. Japan). The animals were sacrificed following the protocol approved by the Ethics Committee at the Tissue Engineering Research Center (Amagasaki, Japan). Then, the femora's were collected under aseptic conditions and the soft tissue eliminated. The epiphyseal regions were removed and the marrow flushed out with freshly prepared complete Eagle's minimum essential medium (MEM, Nacalai Tesque, Japan) with 15% FBS (JRH Biosciences, USA) and 1% antibiotic-antimycotic (Nacalai Tesque, Japan) solution, into a 15 mL Falcon. The RBMSCs were expanded in T75 cm^2 (BD Biosciences Discovery Labware, Bedford, USA) culture flasks in the presence of complete culture medium and expanded under standard culturing conditions. The culture medium was changed each 2 or 3 d. After cells reach confluency, 1 mL of 0.05% tripsin-0.53 mM EDTA (Invitrogen, USA) solution was added to detach the cells from the substrate. Then, complete culture medium was added and RBMSCs (passage 1, P1) were centrifuged at 900 rpm for 5 min. The cells re-suspended with 10 mL of complete culture medium, and cells counted using an automated counter (Cell Counter Sysmex F-520, Japan). Viability of RBMSCs was also analyzed with a NucleoCounter (Chemometec, Denmark), prior seeding [26]. After that, RBMSCs were seeded onto the HAp scaffolds at a cellular density of 5 x 10^2 cells.$scaffold^{-1}$, 1 x 10^3 cells.$scaffold^{-1}$, 5 x 10^3 cells.$scaffold^{-1}$ and 1 x 10^4 cells.$scaffold^{-1}$ and cultured in

MEM medium for 24 hrs, 3 and 7 d under static conditions. After each time period, the ATP content which signals the presence of metabolically active cells was measured by means of performing a CellTiter-Glo® luminescent cell viability assay (Promega Corporation, USA). The luminescence was measured using opaque-walled multi-well plate in a microplate reader (Wallac ARVOsx 1420, Perkin-Elmer Life and Analytical Sciences, USA). This assay is based on a luminescence signal that is proportional to the amount of ATP, which by its turn is directly proportional to the number of viable cells. Moreover, cell adhesion and proliferation was investigated by means of using a LIVE/DEAD viability assay kit (Molecular Probes). RBMSCs were incubated with two probes, calcein-AM (green colour) and ethidium homodimer-1 (EtdD-1, bright red colour), for intracellular esterase activity and plasma membrane integrity, respectively [27]. Then, specimens were observed under a 3-D fluorescence microscope (Olympus SZX12 stereomicroscope, OLYMPUS Co. Ltd., Japan) and SEM. All experiments were carried out three times using a minimum of 3 samples per experimental condition.

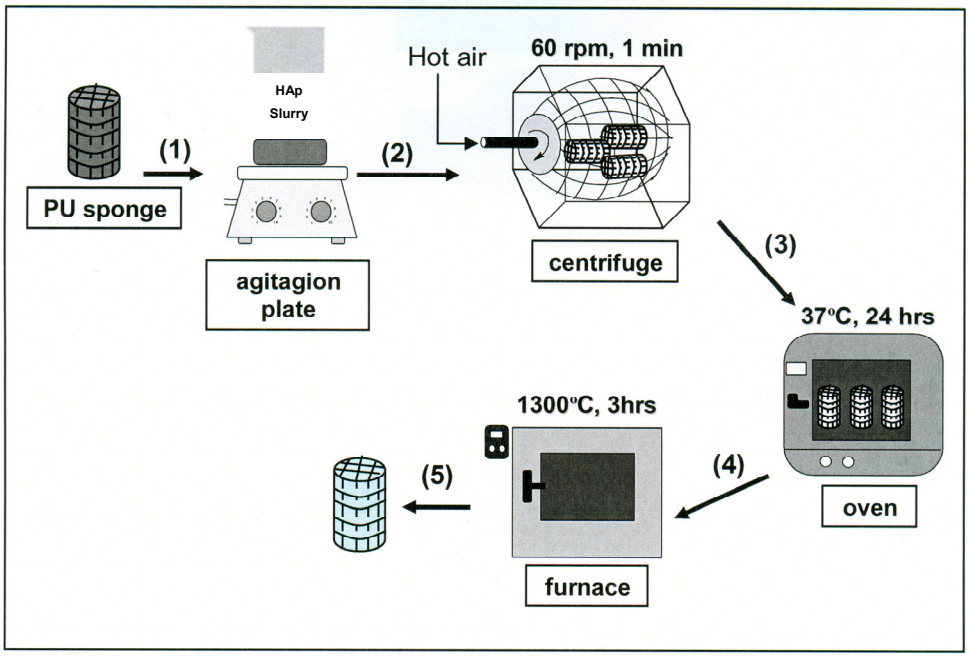

Figure 1. Schematic representation of the production route of the HAp scaffolds.

3. RESULTS AND DISCUSSION

There is a huge clinical demand for novel synthetic tissue engineered scaffolds. Porosity, pore size and interconnectivity of the biomaterial scaffolds are known to play a critical role in bone formation [28]. Therefore, among the key requirements that should be idealized, scaffolds architecture is one of the most important features. However, the balanced porosity/mechanical performance of the scaffolds is an

issue that must not be forgotten, and thus should also be explored. To address this issue the present work describes a methodology for the preparation of HAp scaffolds to find applications on bone tissue engineering. These scaffolds were successfully obtained by impregnating a PU sponge with Hap particles, followed by burning the sacrifice polymeric template and sintering the final HAp porous structure (Figure 1). It is noteworthy that centrifugation (step 2) is a crucial for optimizing the 3-D architecture of the scaffolds. It removes the excessive impregnation of HAp slurry and this method allows obtaining a uniform porosity across the scaffold and macro- and open pore structure.

The macroscopic appearance of the typical HAp scaffold is shown in Figure 2. It can be observed that the HAp scaffolds retained the typical shape of the original PU sponge and possess a trabeculae-like architecture.

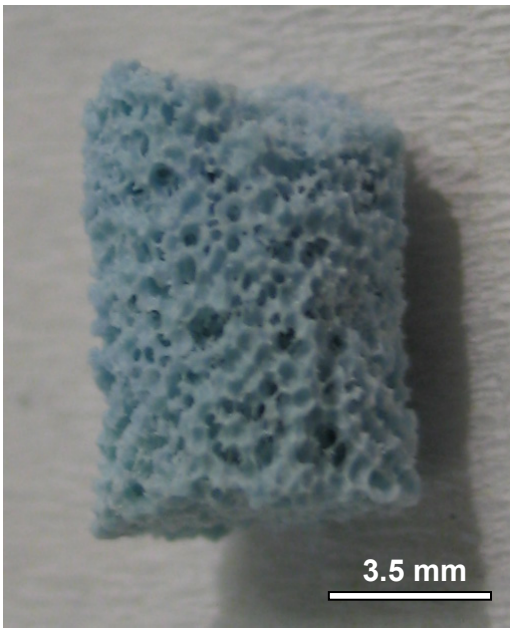

Figure 2. Macroscopic appearance of the HAp scaffolds after sintering at 1300ºC.

FTIR analysis was performed to assess the chemical changes on the HAp structures during processing. Figure 3 shows the FTIR spectra of HAp before and after sintering. The results confirmed previous ones [29] that demonstrated, in both cases the existence of characteristic bands of HAp, namely at 598 and 559 cm^{-1} (o), and at 1020 cm^{-1} (*) attributed to PO_4^{3-} ($\nu 4$) and PO_4^{3-} ($\nu 3$) groups, respectively (Figures 3a-c). Another typical HAp band that can be observed is assigned to the stretching mode of OH group at 3572 cm^{-1} (+). Moreover, it is also possible to observe the loosening of OH groups (θ) from adsorbed, and bending mode of H_2O after sintering HAp. Comparing the sintered HAp (Figure 3b) and HAp scaffolds (Figure 3c), it is possible to confirm that no differences were observed, and no characteristic

peaks of organic groups were found. This result clearly indicates that the heat treatment cycle applied is critical to avoid the undesired traces of PU sponge.

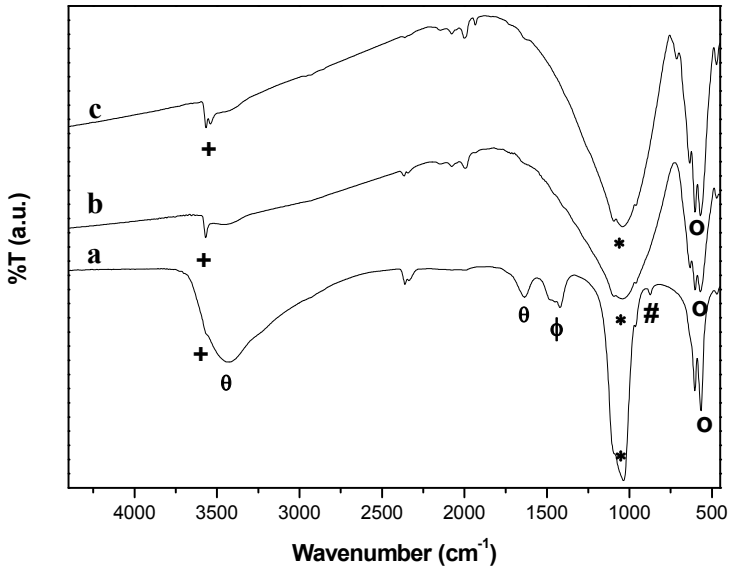

Figure 3. FTIR spectra of: (a) HAp synthesized by a precipitation method, (b) HAp sintered at 1300ºC, and (c) HAp scaffolds sintered at 1300ºC.

To further clarify this issue thermogravimetric analyses (TGA) were performed. Figure 4 shows the TGA of the PU sponges, PU sponges impregnated with HAp before burning and sintered HAp scaffolds. From results it can be seen that the ratio HAp:PU sponges was 80:20 wt% (Figure 4b).

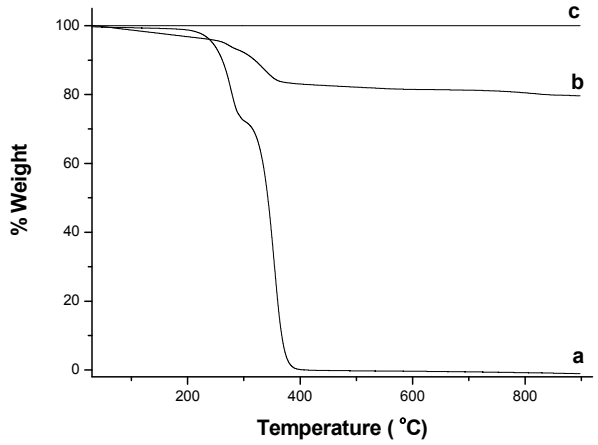

Figure 4. TGA analysis of: (a) PU sponges, (b) PU sponge impregnated with HAp before burning, and (c) HAp scaffolds sintered at 1300ºC.

Moreover, it can be seen that the melting point of PU sponges is about 300ºC, and PU sponge is completely burned around 400ºC. These findings have demonstrated that the thermal treatment of the HAp/PU sponges at 900ºC for the period of 24 hrs followed by sintering at 1300ºC proved to be adequate for the completely eliminating the PU sponges. This is particularly evident in Figure 4c, since no mass changes on the sintered HAp scaffolds were detected.

It has been reported that sintering temperatures and sintering time have great effect on sintered density of different apatites [30,31]. Therefore, by increasing the sintered density we expected to increase the final mechanical properties of the HAp scaffolds. However, it is also known that high temperatures may affect the crystallinity and phase content of HAp [32]. Figure 5 shows the XRD pattern of HAp before and after different heat treatments. Examining the XRD patterns (Figures 5a-c) and comparing with that of the standard file for HAp from JCPDS (9-432) it can be observed that the peaks are perfectly matching. The XRD pattern of synthesized HAp was found to be amorphous (Figure 5a). After sintering the crystallinity of HAp increased and no decomposition products such as α- or β-tricalcium phosphates (TCP) [32] were detected. The complementary FTIR data also revealed the presence of typical OH groups (Figures 3b-c) of the HAp [33] showing that the synthesized HAp is quite stable upon sintering of the materials at 1300ºC for 3 hrs.

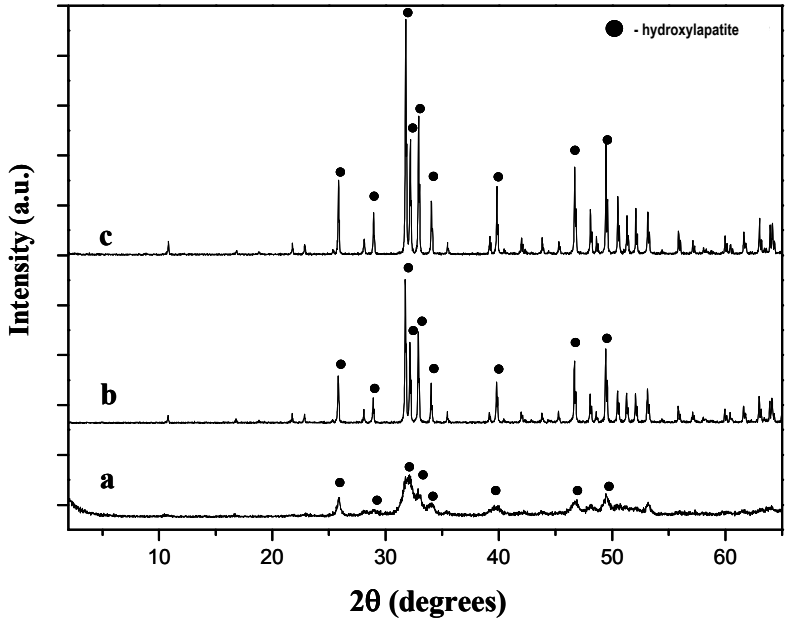

Figure 5. XRD patterns of: (a) HAp synthesized by a precipitation method, (b) HAp sintered at 1300ºC, and (c) HAp scaffolds sintered at 1300ºC.

As previously reported, the XRD data is also in good attainment with the FTIR spectra (Figure 3a). FTIR spectrum shows that carbonate ions are observed in the as synthetized HAp, the bands assigned to carbonate $\nu 2$ and $\nu 3$, at 875 cm^{-1} (#) and 1650-1300 cm^{-1}, respectively. The XRD study revealed that the carbonate ions observed by FTIR are assigned to surface ones, rather than being embedded within the lattice of phosphate ions [29]. To evaluate the microstructure of the HAp scaffolds, SEM analysis were performed as shown in Figure 6. The SEM images of the PU foams evidenced an "open-cell" and highly interconnected porous structure (Figures 6a-b), that facilitated the impregnation of hydroxylapatite particulates. From figure 6c it can be observed that the architecture of the obtained HAp scaffolds is analogous to the sacrifice template. In addition, the pore geometry is also quite similar (Figures 6b and d), showing a macroporous and highly interconnected structure with pore size comprised in the range of 50-600 μm. Such type of morphology and pore dimension has been shown to be adequate for bone tissue engineering purposes [28,34,35]. Note that the final pore architecture could be easily controlled by changing the structure of the PU foam. These results have demonstrated that the centrifugation step is required to prevent the formation of an external "skin-like" layer, i.e. non-porous HAp layer which can be a disadvantage for the cells adhesion and in-growths during seeding as well as proliferation and proper flow of culture medium [35,36].

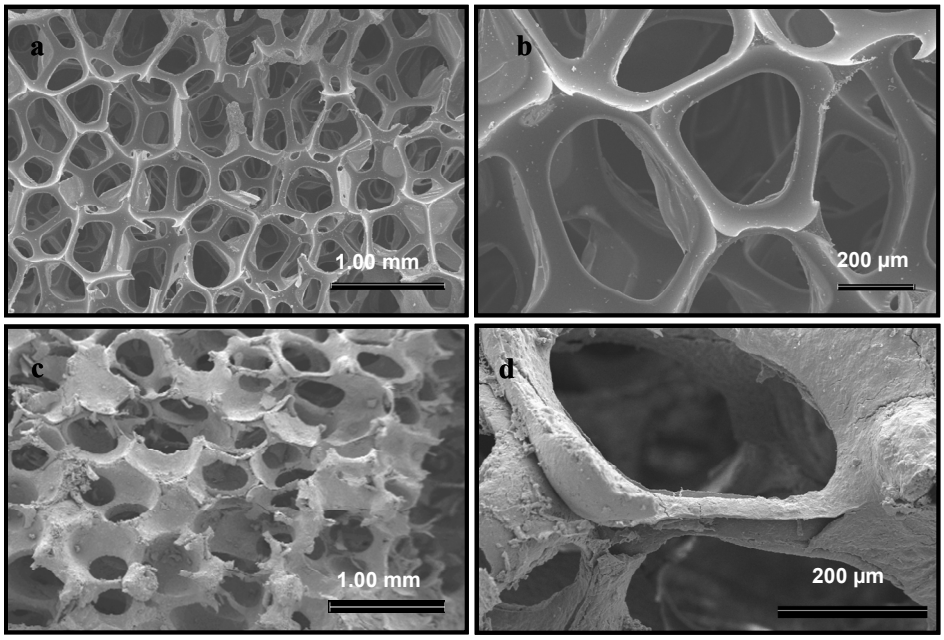

Figure 6. SEM micrographs of: (a) PU sponge, (b) typical PU "open-cell" pore, (c) HAp scaffold, and (d) typical macropore of the HAp scaffolds.

The structure and architecture of the HAp scaffolds was further examined in a non-destructive manner by means of μ-CT analysis (Figure 7). Figure 7a shows the 2-D morphometric analysis of the HAp scaffolds. It revealed that the mean porosity is about 67.8 ± 5.0%. Additionally, it can be seen that scaffolds present a uniform architecture and pore distribution. No gaps or empty spaces were observed, i.e. the impregnation technique allows obtaining 3-D structures mimicking the PU template. As previously mentioned, besides the need of scaffolds high porosity, the pores should be interconnected to allow the diffusion of culture medium, metabolic wastes and oxygen, and to facilitate the infiltration and proliferation of cells [37]. The transversal (Figure 7b) and longitudinal (Figure 7c) views of the HAp scaffolds, clearly showed that pore network is highly interconnected (black arrows). This result demonstrates that the centrifugation step not only prohibits the formation of an external 'skin-like' layer but also allows a uniform pore distribution and interconnectivity across the HAp scaffolds.

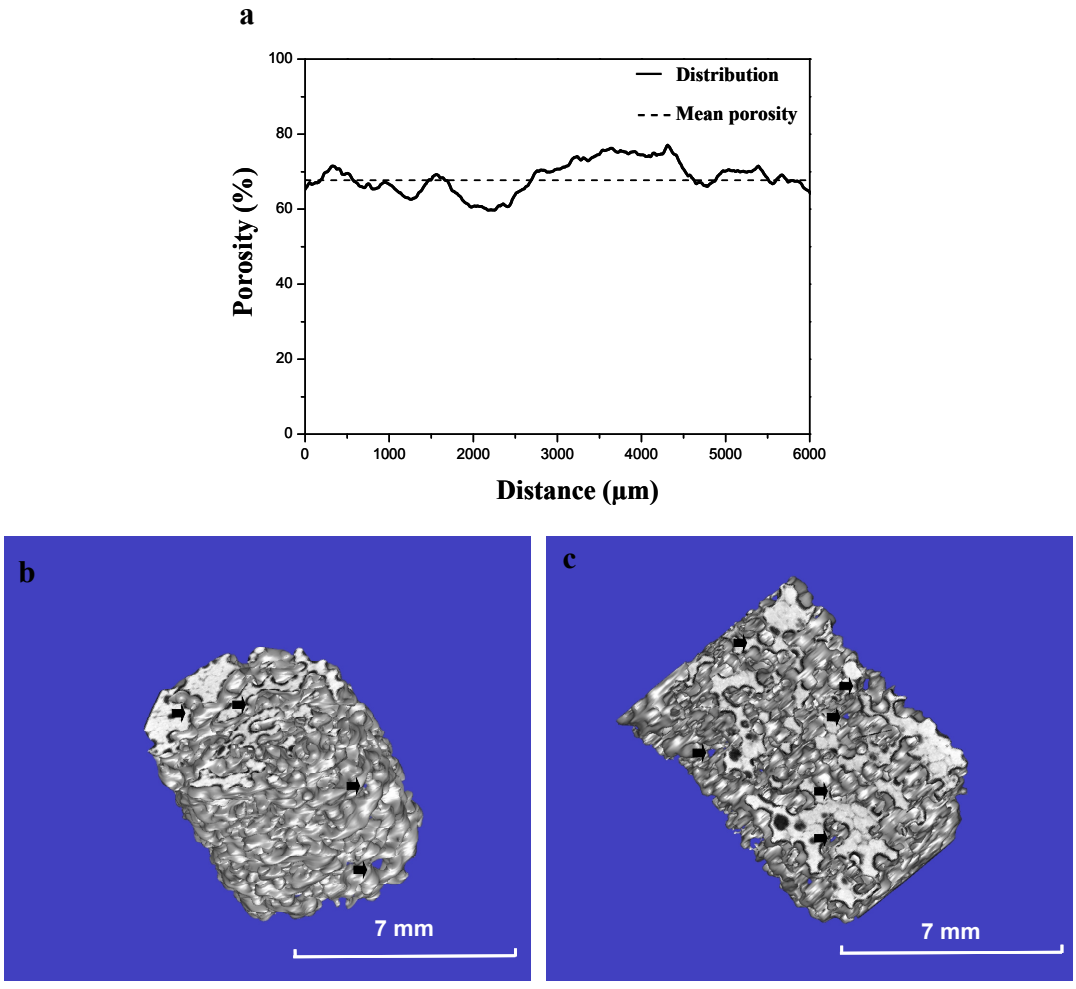

Figure 7. μ-CT analysis of HAp scaffolds: (a) 2-D morphometric analysis, (b) transversal view, and (c) longitudinal view.

It is well known that a compromise between porosity and mechanical properties exists, where higher porosity results in lower mechanical strength of the scaffold [38,39]. The compressive strength of the HAp scaffolds was found to be 30.2 ± 6.0 MPa. Previous reports have shown that for a HAp scaffolds possessing 77% of porosity compressive strength was about 17.4 MPa [40]. Therefore, as compared to others ceramic porous structures described in literature [23,40], our data presents a good compromise between porosity and mechanical performance, i.e. 67.8 ± 5.0% and 30.2 ± 6.0 MPa, respectively.

In the present work another issue that was address consisted on evaluating the bioactivity behaviour of HAp scaffolds, *in vitro*. Figure 8 shows the SEM images of the surface of HAp scaffolds before and after immersion in SBF for 1 to 15 d. It was possible to observe the deposition of precipitates after 1 d (Figure 8b), which tend to be more pronounced for longer soaking time (Figures 8c-d). The formation of these precipitates, which were covering the whole HAp surface, resembles the 'cauliflower-like' morphology of apatite formed *in vitro*, onto bioactive surfaces. Additionally, changes in calcium (Ca) and phosphorus (P) ions in SBF solution was also monitored by ICP. Figure 9 shows that Ca concentration increased in the SBF solution in the first 24 hrs. However, it is not detected an expected increase in P concentration during this period. This can be explained due to a fast consumption of P during apatite nucleation phase.

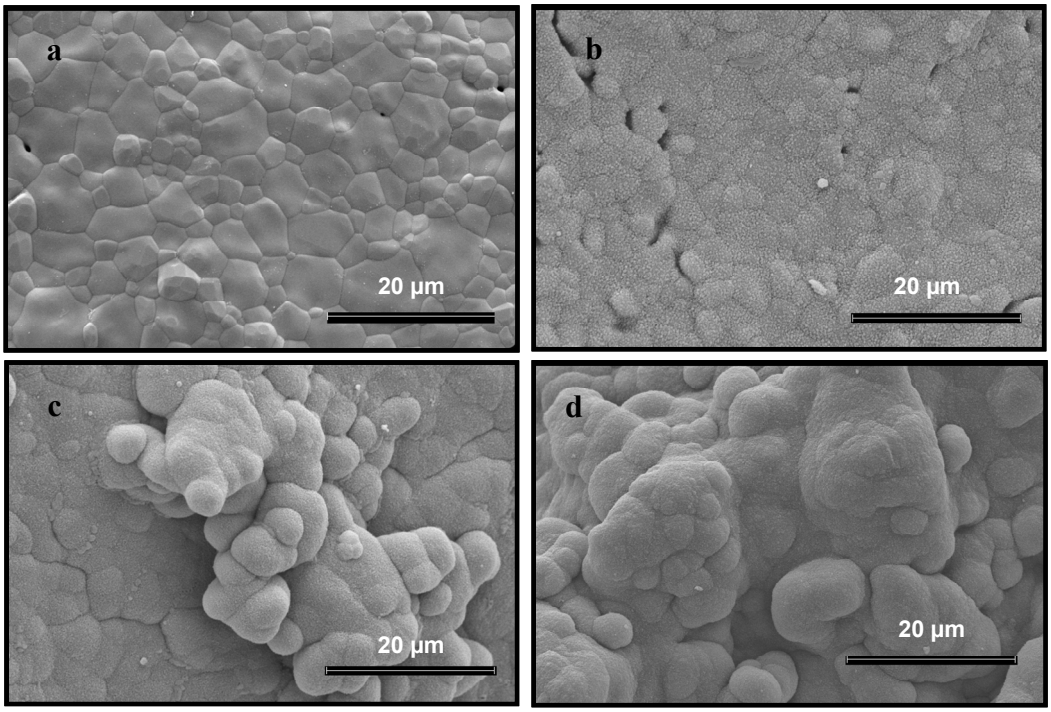

Figure 8. SEM micrographs of the surface of the macroporous HAp scaffolds after immersion in SBF for: (a) 0 d, (b) 1 d, (c) 7 d, and (d) 15 d.

From day 1 to day 15, we assist to both decrease in the concentration of Ca and P. This trend may be a consequence of the consumption of both calcium and phosphorus upon the deposition of the apatite layer at the surface of the HAp scaffolds, as detected by SEM (Figures 8b-d). These findings are in agreement with the data available in literature [41], which has been shown that HAp is bioactive in nature due to a phenomenon involving the dissolution of calcium and phosphate ions from the HAp.

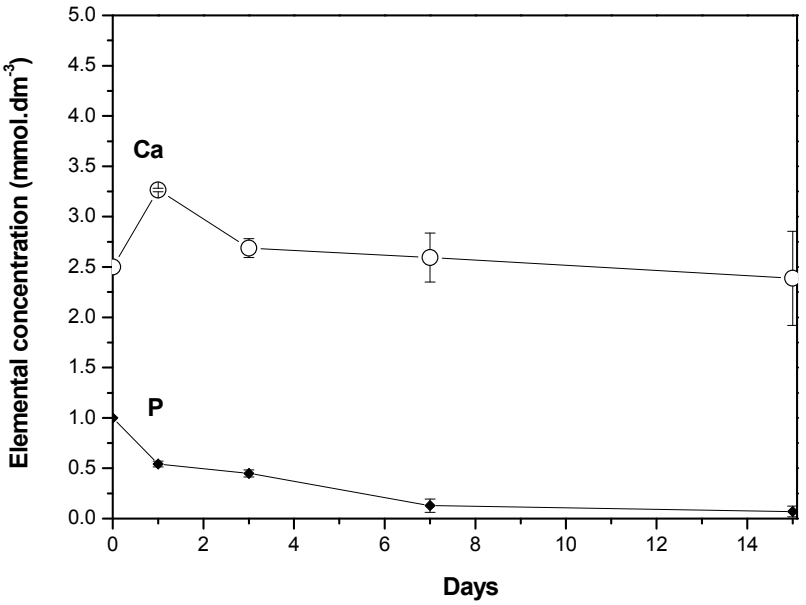

Figure 9. Profile of Ca and P ions in the SBF solution after soaking the macroporous HAp scaffolds from day 0 up to day 15.

As previously reported by Kirkpatrick et al. [42], there are several ways to assess the toxicity *in vitro.* In this study, L929 cells were used for preliminarily screen toxicity. Cytotoxicity of the HAp scaffolds was initially assessed through cell death observation in the inverted microscope (Figure 10). It can be observed that after 72 hrs in contact with a latex rubber extract (positive control), the L929 cells round up and detached from the culture substratum, which is indicative of the high cytotoxicity of the material (Figure 10b). On the contrary, when exposing to the different concentrations of HAp extract (Figures 10c-f), the L929 cells exhibited a normal morphology, proliferated well and established a monolayer when comparing to the negative control (Figure 10a). Therefore, these preliminary results show that no toxic traces of PU sponges remained on the HAp scaffolds, and that HAp scaffolds were biocompatible. Complementarily, cell viability was investigated by carrying out the MTS test (Figure 11). The results once corroborated the direct observation under the microscope which showed that L929 cells were viable after contacting with the different HAp extract fluids for the period of 72 hrs.

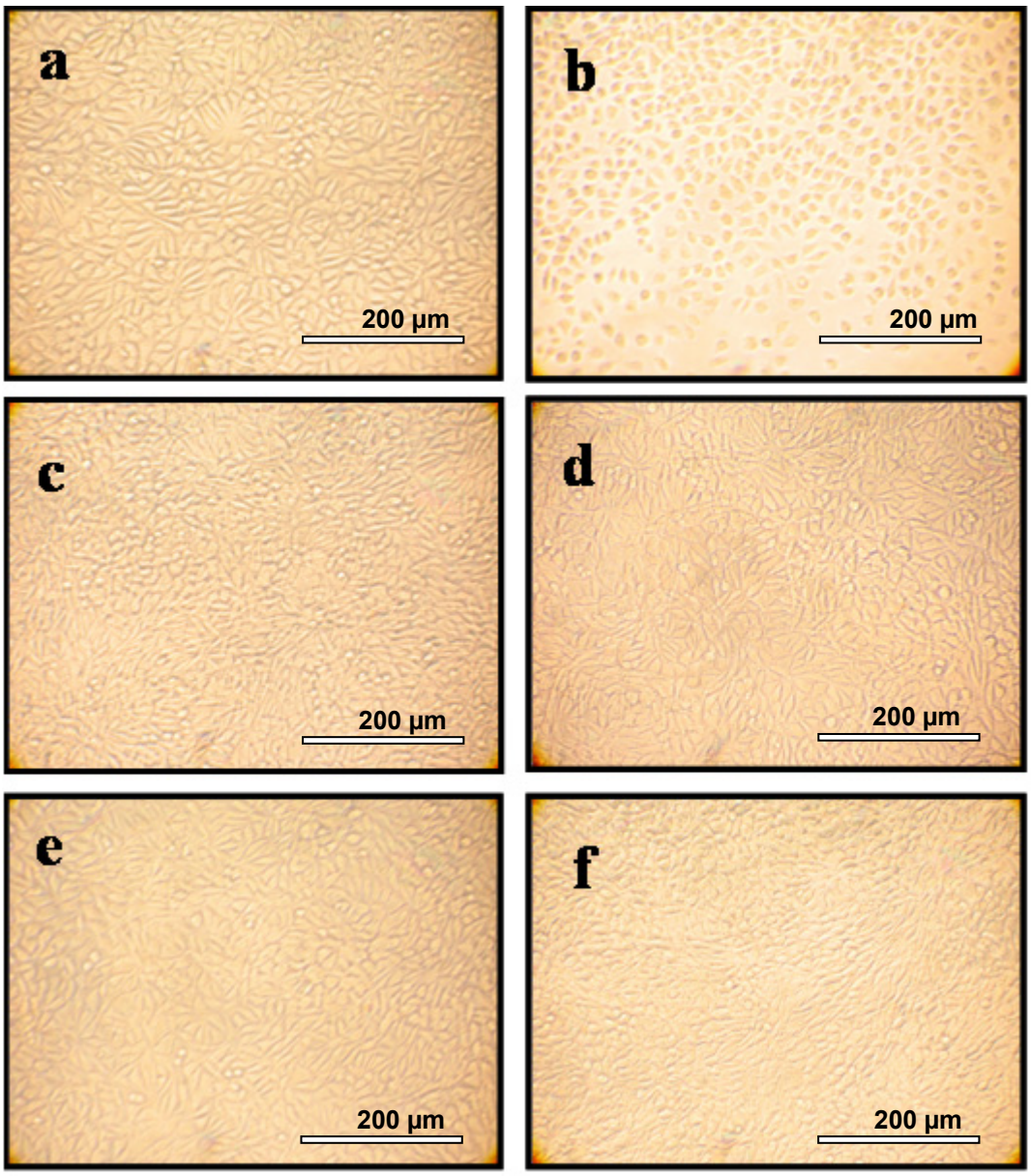

Figure 10. L929 cells after contacting 72 hrs with the extract fluids: (a) complete culture medium (negative control), (b) latex rubber leachables (positive control), (c) 25% HAp leachables, (d) 50% HAp leachables, (e) 75% HAp leachables, and (f) 100% HAp leachables.

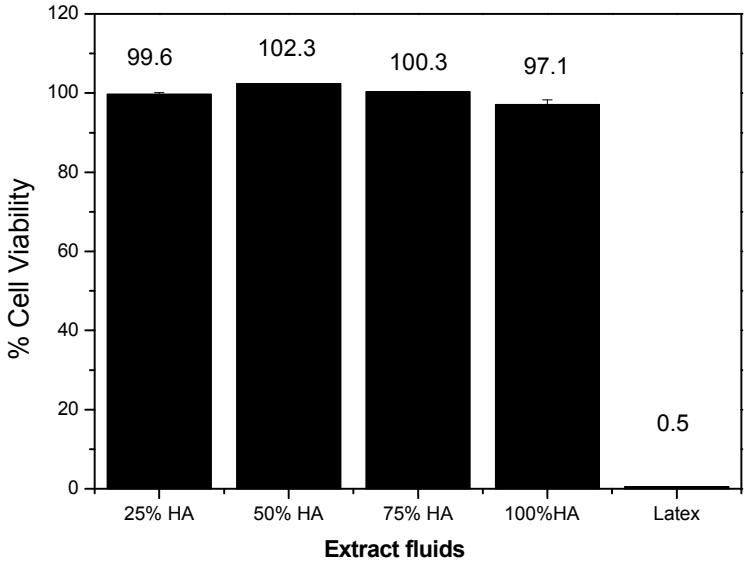

Figure 11. % of L929 cell viability versus extract fluids.

Cell viability and proliferation on the scaffolds is one of the prerequisite for the 3-D supports find applications in the TE [43]. In order to investigate other aspects of cytotoxicity, such as the cell/scaffold interactions, direct contact experiments were performed on the macroporous HAp scaffolds using rat bone marrow stromal cells (RBMSCs). On the other hand, for optimizing the cell seeding efficiency in respect to cell adhesion and proliferative capacity of RBMSCs onto the macroporous HAp scaffolds different cell numbers were tested. Figure 12 shows the luminescent cell viability assay of RBMSCs seeded onto the surface of the HAp scaffolds after culturing for 7 d.

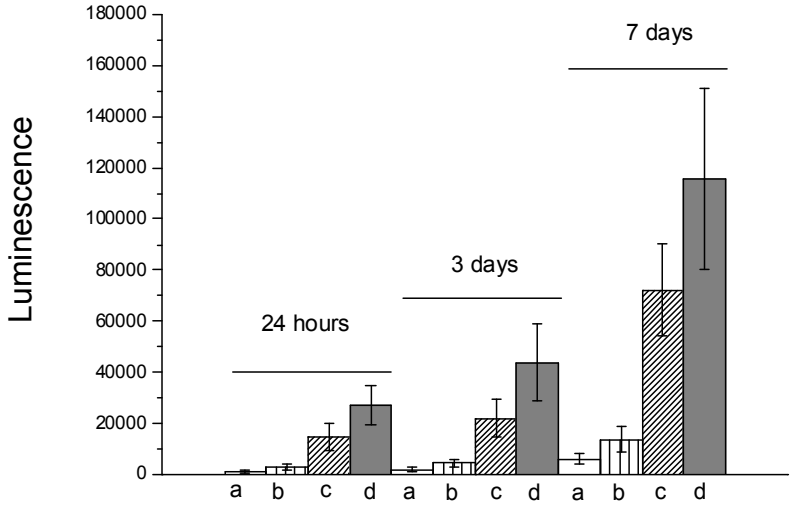

Figure 12. Cell viability assay of RBMSCs seeded at different cell densities onto the surface of the macroporous HAp scaffolds after 24 hrs, 3 d and 7 d: (a) 5 x 10^2 cells.scaffold^{-1}, (b) 1 x 10^3 cells.scaffold^{-1}, (c) 5 x 10^3 cells.scaffold^{-1}, and (d) 1 x 10^4 cells.scaffold^{-1}. Cell numbers correlates with luminescence.

This assay is based on a luminescence signal that is proportional to the amount of ATP, which signals the presence of metabolically active cells. From figure 12, it can be observed that RBMSCs seeded at higher cell numbers proliferated well and were viable after culturing onto the macroporous HAp scaffolds for 7 d. On the contrary, the low cell density has shown to influence negatively the proliferation of RBMSCs, as observed by the low cell numbers, after 7 d of culturing. Nevertheless, the number of viable cells increased with an increase of culture time for all cell densities tested. This data shows that cell seeding efficiency increased with the increase in cell concentration. This is an expected result since it has been shown that cells needs a proper microenvironment not only with respect to 3-D scaffold but also by means of interacting with other cells through cell-cell junctions and signaling [44,45]. Therefore, this data demonstrated that the cell seeding conditions, namely the cell numbers needs to be optimized. The high cell concentration used seems to be more adequate for the RBMSCs/HAp constructs fully achieve physiologic functions upon implantation. Figure 13 shows the fluorescence microscopy images of the HAp scaffolds seeded with RBMSCs after performing a two-colour fluorescence LIVE/DEAD cell viability assay. This type of assay allows distinguishing live from dead cells because calcein-AM is enzimatically converted into calcein, which is retained within live cells and produces an intense green fluorescence. On the other hand, dead cells are stained in a bright red fluorescence since EtdD-1 only enters cells with damaged membranes and binds to nucleic acids. From the fluorescence signals it can be observed that RBMSCs adhered, proliferated and remained viable after 7 d. Moreover, dead cells were present in low numbers as detected by the low bright red fluorescence. Moreover, it can be seen that RBMSCs were able to penetrate deeper into the core of the HAp scaffolds (Figure 13c). This is an important data since it has been shown [35,39] that cell infiltration and distribution within the whole scaffold will greatly affect the overall performance of the cells/scaffold construct.

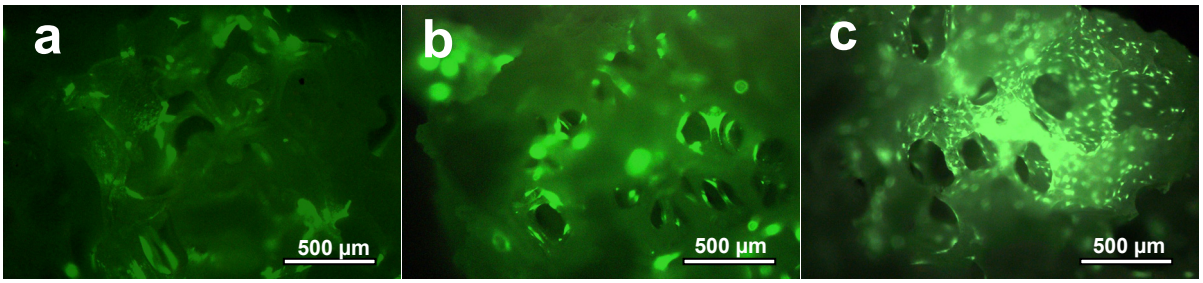

Figure 13. Fluorescence microscopy images of the macroporous HAp scaffolds seeded with RBMSCs at a cell density of 1 x 10^4 cells.scaffold^{-1} after culturing for: (a) 24 hrs, (b) 3 d, and (c) 7 d.

To further investigate the RBMSCs adhesion onto the surface of the macroporous HAp scaffolds SEM analysis were also carried out. Figure 14 shows the SEM images of the RBMSCs on the surface of the macroporous HAp scaffolds after 24 hrs and 7 d. It can be observed that RBMSCs aggregated and adhered onto the surface of the HAp scaffolds but presents a spherical morphology, after 24 hrs (Figure 14a). The morphology and small size are typical of the cells initial anchorage stage. After a longer period of culturing, RBMSCs spread actively and presented a flatten morphology showing a good anchoring to the substrate by multiple lamellipodia (Figure 14b).

Despite the biocompatibility and capacity of supporting normal cellular functions, the macroporous HAp scaffolds also have to support the differentiation of the stem cells both *in vitro* and *in vivo*. It can be seen from figure 14 that there are no indications of osteogenic differentiation, namely the extracellular mineralized matrix cannot be detected. This is an expected result since osteogenic factors medium were not added to culture medium. On the other hand hydroxylapatite is known to lack the osteoinductive capacity. This is an relevant feature that needs to be met in a variety of bone related clinical strategies and to which our research groups [46,47] have been giving great deal of attention. Moreover, the present data is promising since in future experiments, we propose to evaluate the HAp/RBMSCs constructs functionality, namely the ability of the HAp scaffolds to support the RBMSCs osteogenesis and bone formation, *in vitro and in vivo*, respectively.

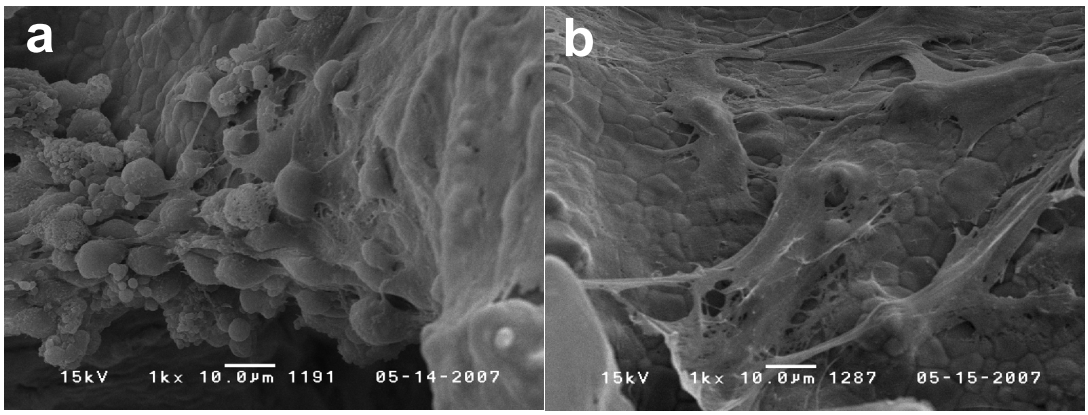

Figure 14. SEM images of the macroporous HAp scaffolds seeded with RBMSCs at a cell density of 1 x 10^4 cells.scaffold^{-1} after culturing for: (a) 24 hrs and (b) 7 d.

4. CONCLUSIONS

This work demonstrated that it is possible to prepare sintered hydroxylapatite (HAp) scaffolds with high interconnectivity by impregnating an 'open-cell' PU sponge into a HAp slurry, followed by burning the

"sacrifice template". The preparation route was optimized for producing macroporous HAp structures with controlled morphology, easily mediated by the architecture of the PU sponge. *In vitro* tests have demonstrated that such constructs are bioactive, as observed by the formation of an apatite layer after 1 day of immersion in SBF solution. The biocompatible behaviour of the macroporous HAp scaffold was demonstrated as evidenced by the non-cytotoxic effect over L929 cells. Moreover, the cell/material interaction tests have shown that the rat bone marrow stromal cells adhered, proliferated well and remained viable on the macroporous hydroxylapatite scaffolds. More importantly, the cells were able to populate the inner of the macroporous hydroxylapatite scaffolds. Therefore, the physicochemical and biological properties of the macroporous hydroxylapatite scaffolds have shown to suitable for find applications in bone tissue engineering scaffolding.

REFERENCES

1. Abukawa, H., et al., *Reconstruction of mandibular defects with autologous tissue-engineered bone*. Journal of Oral and Maxillofacial Surgery, 2004. **62**(5): p. 601.
2. Petite, H., et al., *Tissue-engineered bone regeneration*. Nature Biotechnology, 2000; **18**: p. 959.
3. Saint-Cyr, M., et al., *Immediate corticocancellous bone autografting in segmental bone defects of the hand*. The Journal of Hand Surgery, 2006. **31**(2): p. 168.
4. Merkx, M.A.W., et al., *Incorporation of three types of bone block implants in the facial skeleton.* Biomaterials, 1999. **20**(7): p. 639.
5. Su-Gwan, K., K. Hak-Kyun, and L. Sung-Chul, *Combined implantation of particulate dentine, plaster of Paris, and a bone xenograft (Bio-Oss(R)) for bone regeneration in rats*. Journal of Cranio-Maxillofacial Surgery, 2001. **29**(5): p. 282.
6. Babensee, J.E., et al., *Host response to tissue engineered devices*. Advanced Drug Delivery Reviews, 1998. **33**(1-2): p. 111.
7. Kahan, B.D., *Immunosupressive therapy*. Current Opinion in Immunology, 1992. **4**: p. 553.
8. Meinel, L., et al., *Silk implants for the healing of critical size bone defects*. Bone, 2005. **37**(5): p. 688.
9. Ahmad, C.S., W.B. Guiney, and C.J. Drinkwater, *Evaluation of donor site intrinsic healing response in autologous osteochondral grafting of the knee*. Arthroscopy, 2002. **18**: p. 95.
10. Langer, R. and J.P. Vacanti, *Tissue Engineering*. Science, 1993. **260**: p. 920.
11. Ozawa, S. and S. Kasugai, *Evaluation of implant materials (hydroxyapatite, glass-ceramics, titanium) in rat bone marrow stromal cell culture*. Biomaterials, 1996. **17**(1): p. 23.

12. Li, Z., et al., *Chitosan-alginate hybrid scaffolds for bone tissue engineering*. Biomaterials, 2005. **26**: p. 3919.
13. Chu, T.M.G., et al., *Mechanical and in vivo performance of hydroxyapatite implants with controlled architectures*. Biomaterials, 2002. **23**(5): p. 1283.
14. Sepulveda, P., et al., *In vivo evaluation of hydroxyapatite foams*. Journal of Biomedical Materials Research, 2002. **62**: p. 587.
15. Porter, A.E., et al., *Comparison of in vivo dissolution processes in hydroxyapatite and silicon-substituted hydroxyapatite bioceramics*. Biomaterials, 2003. **24**: p. 4609.
16. Hasegawa, S., et al., *A 5-7 year in vivo study of high-stength hydroxyapatite/poly(L-lactide) composite rods for the internal fixation of bone fractures*. Biomaterials, 2006. **27**: p. 1327.
17. Driessens, F.C.M., et al., *Chemical reactions of calcium phosphate implants after implantation in vivo*. Journal of Materials Science: Materials in Medicine, 1992. **3**: p. 413.
18. Schnettjer, R., et al., *Bone ingrowth in bFGF-coated hydroxyapatite ceramic implant*s. Biomaterials, 2003. **24**: p. 4603.
19. Dee, K.C., et al., *Conditions which promote mineralization at the bone-implant interface: a model in vitro study*. Biomaterials, 1996. **17**: p. 209.
20. Srouji, S. and E. Livne, *Bone marrow stem cells and biological scaffold for bone repair in aging and disease*. Mechanisms of Ageing and Development, 2005. **126**(2): p. 281.
21. Ohgushi, H., et al., *Tissue engineered ceramic artificial joint-ex vivo osteogenic differentiation of patient mesenchymal cells on total ankle joints for treatment of osteoarthritis*. Biomaterials, 2005. **26**(22): p. 4654.
22. Abukawa, H., et al., *Formation of a mandibular condyle in vitro by tissue engineering*. Journal of Oral and Maxillofacial Surgery, 2003. **61**(1): p. 94.
23. Uemura, T., et al., *Transplantation of cultured bone cells using combinations of scaffolds and culture techniques*. Biomaterials, 2003. **24**(13): p. 2277.
24. Kokubo, T., et al., *Solutions able to reproduce in vivo surface-structure changes in bioactive glass-ceramic A-W*. Journal of Biomedical Materials Research, 1990. **24**: p. 721.
25. Gomes, M.E., et al., *Cytocompatibility and response of osteoblastic-like cells to starch-based polymers: effect of several additives and processing conditions*. Biomaterials, 2001. **22**: p. 1911.
26. Muraki, K., et al., *Assessment of viability and osteogenic ability of human mesenchymal stem cells after being stored in suspension for clinical transplantation*. Tissue Engineering, 2006. **12**: p. 1711.

27. Hirose, M., et al., *Osteogenic potential of cryopreserved human bone marrow-derived mesenchymal cells after thawing in culture*. Materials Science and Engineering: C, 2004. **24**: p. 335.
28. Karageorgiou, V. and D. Kaplan, *Porosity of 3D biomaterial scaffolds and osteogenesis*. Biomaterials, 2005. **26**: p. 5474.
29. Oliveira, J.M., et al., *Innovative technique for the preparation of porous bilayer hydroxyapatite/chitosan scaffolds for osteochondral applications*. Kyoto (JPN): Key Engineering Materials, Trans Tech Pub, Zurich, Switzerland; 2006. **309-311**: p. 927.
30. Rao, W.R. and R.F. Boehm, *A study of sintered apatites*. Journal of Dental Research, 1974. **53**: p. 1351.
31. Kim, S.R., et al., *Synthesis of Si, Mg substituted hydroxyapatites and their sintering behaviours*. Biomaterials, 2003. **24**: p. 1389.
32. Tampieri, A., et al., *Sintering and characterization of HA and TCP bioceramics with control of their strength and phase purity*. Journal of Materials Science: Materials in Medicine, 1997. **8**: p. 29.
33. Weng, J., et al., *Intrinsic factors of apatite influencing its amorphization during plasma-spray coating*. Biomaterials, 1995. **16**(1): p. 39.
34. Hutmacher, D.W., M. Sittinger, and M.V. Risbud, *Scaffold-based tissue engineering: rationale for computer-aided design and solid free-form fabrication systems*. Trends in Biotechnology, 2004. 22: p. 354.
35. O' Brien, F.J., et al., *The effect of pore size on cell adhesion in collagen-GAG scaffolds*. Biomaterials, 2005. **26**: p. 433.
36. Ang, T.H., et al., *Fabrication of 3D chitosan–hydroxyapatite scaffolds using a robotic dispensing system*. Materials Science and Engineering: C , 2002. **20**: p. 35.
37. Ho, S.T. and D.W. Hutmacher, *A comparison of micro CT with other techniques used in the characterization of scaffolds*. Biomaterials, 2006. **27**: p. 1362.
38. Hollister, S.J., R.D. Maddox, and J.M. Taboas, *Optimal design and fabrication of scaffolds to mimic tissue properties and satisfy biological constraints*. Biomaterials, 2002. **23**(20): p. 4095.
39. Karageorgiou, V. and D. Kaplan, *Porosity of 3D biomaterial scaffolds and osteogenesis*. Biomaterials, 2005. **26**(27): p. 5474.
40. Dong, J., et al., *In vivo evaluation of a novel porous hydroxyapatite to sustain osteogenesis of transplanted bone marrow-derived osteoblastic cells*. Journal of Biomedical Materials Research, 2001. **57**: p. 208.

41. Weng, J., et al., *Formation and characteristics of the apatite layer on plasma-sprayed hydroxyapatite coatings in simulated body fluid*. Biomaterials, 1997. **18**(15): p. 1027.
42. Kirkpatrick, C.J. and C. Mittermayer, *Theoretical and practical aspects of testing potential biomaterials in vitro*. Journal of Materials Science: Materials in Medicine, 1990. **1**: p. 9.
43. Mauney, J.R., et al., *In vitro and in vivo evaluation of differentially demineralized cancellous bone scaffolds combined with human bone marrow stromal cells for tissue engineering*. Biomaterials, 2005. **26**(16): p. 3173.
44. Chen, G., et al., *Cell adhesion of bone marrow cells, chondrocytes, ligament cells and synovial cells on a PLGA-collagen hybrid mesh*. Materials Science and Engineering: C, 2004. **24**: p. 867.
45. Sun, S., I. Titushkin, and M. Cho, *Regulation of mesenhymal stem cell adhesion and orientation in 3D collagen scaffold by electrical stimulus*. Bioelectrochemistry, 2006. **69**: p. 133.
46. Oliveira, J.M., et al., *Novel hydroxyapatite/chitosan bilayered scaffolds for osteochondral tissue-engineering applications: Scaffold design and its performance when seeded with goat bone marrow stromal cells*. Biomaterials, 2006. **27**: p. 6123.
47. Kotobuki, N., et al., *Observation of osteogenic differentiation cascade of living mesenchymal stem cells on transparent hydroxyapatite ceramics*. Biomaterials, 2005. **26**(7): p. 779.

CHAPTER V.

Novel hydroxylapatite/chitosan bilayered scaffold for osteochondral tissue engineering applications: scaffold design and its performance when seeded with goat bone marrow stromal cells

CHAPTER V.

Novel hydroxylapatite/chitosan bilayered scaffold for osteochondral tissue engineering applications: scaffold design and its performance when seeded with goat bone marrow stromal cells

Abstract

Recent studies suggest that bone marrow stromal cells are a potential source of osteoblasts and chondrocytes and can be used to regenerate damaged tissues using a tissue engineering (TE) approach. However, these strategies require the use of an appropriate scaffold architecture that can support the formation de novo of either bone and cartilage tissue, or both, as in the case of osteochondral defects. The later has been attracting a great deal of attention since it is considered a difficult goal to achieve. This work consisted on developing novel hydroxylapatite/chitosan (HAp/CHT) bilayered scaffold by combining a sintering and a freeze-drying technique, and aims to show the potential of such type of scaffolds for being used in TE of osteochondral defects. The developed HAp/CHT bilayered scaffolds were characterized by Fourier-transform infra-red spectroscopy, X-ray diffraction analysis, micro-computed tomography, and scanning electron microscopy (SEM). Additionally, the mechanical properties of HAp/CHT bilayered scaffolds were assessed under compression. *In vitro* tests were also carried out, in order to study the water-uptake and weight loss profile of the HAp/CHT bilayered scaffolds. This was done by means of soaking the scaffolds into a phosphate buffered saline for 1 up to 30 days. The intrinsic cytotoxicity of the HAp scaffolds and HAp/CHT bilayered scaffolds extract fluids was investigated by carrying out a cellular viability assay (MTS test) using Mouse fibroblastic-like cells. Results have shown that materials do not exert any cytotoxic effect. Complementarily, *in vitro* (phase I) cell culture studies were carried out to evaluate the capacity of HAp and CHT layers to separately, support the growth and differentiation of goat marrow stromal cells (GBMSCs) into osteoblasts and chondrocytes, respectively. Cell adhesion and morphology were analysed by SEM while the cell viability and proliferation were assessed by MTS test and DNA quantification. The chondrogenic differentiation of GBMSCs was evaluated measuring the glucosaminoglycans synthesis. Data showed that GBMSCs were able to adhere, proliferate and osteogenic differentiation was evaluated by alkaline phosphatase activity and immunocytochemistry assays after 14 days in osteogenic medium and into chondrocytes after 21 days in culture with chondrogenic medium. The obtained results concerning the physicochemical and biological properties

of the developed HAp/CHT bilayered scaffolds show that these constructs exhibit great potential for their use in TE strategies leading to the formation of adequate tissue substitutes for the regeneration of osteochondral defects.

This chapter is based on the following publication: **Oliveira JM**, Rodrigues MT, Silva SS, Malafaya PB, Gomes ME, Viegas C A A, Azevedo JT, Dias IR, Mano JF and Reis RL, 2006, Novel hydroxyapatite/chitosan bilayered scaffold for osteochondral tissue engineering applications: scaffold design and its performance when seeded with goat bone marrow stromal cells, Biomaterials, **27**: 6123-6137 (Hot paper).

---

1. INTRODUCTION

In the skeleton, articular cartilages allows a stable movement with near frictionless and consequently act as a unique protective interface for the underlying bone. This is achieved in part, since articular cartilages resists to compressive forces due to the ability to distribute loads [1,2]. General features of cartilage tissue includes: (i) a small number of chondrocytes with low proliferation rate and having both catabolic and anabolic functions, (ii) a high content of water where metabolites and a large amount of electrolytes are dissolved, (iii) an abundant extracellular matrix (ECM) composed by different types of collagens (mainly type II) and proteoglycan aggrecan, which is the main responsible for the elasticity, and (iv) possess no nerve and vascular systems [1,3]. Actually, the different cell numbers, organization and distribution, as well as organic and water content across cartilage are responsible for the existence of three distinct layers with respect to depth, i.e. superficial, middle and deep [4]. In this respect, Kuettner et al. [4] have suggested that the variations among articular cartilages is mainly due to significant changes in biochemical composition and biomechanical properties of the three layers.

It is well known that cartilage has a limited regeneration capacity upon damage. In certain extent, this is explained by the fact of being an avascular tissue, regenerative cells cannot migrate to the defect void unless the lesion goes beyond the subchondral bone plate [5,6]. Therefore, a regenerative response will be only possible when it is provided an artificial access by the marrow [7]. This consideration is subjacent on several clinical strategies that are currently employed on the treatment of small cartilage lesions namely, the subchondral abrasion, Pridie perforations, micro-fracture, and transplantation of osteochondral plugs [6,8-10]. Although, in most cases after clinical intervention the repaired tissue tends to degenerate and occur the formation of the undesired fibrocartilage [5,11,12]. More recently, it was reported an alternative approach, which consists on injecting autologous chondrocytes at the defect void [13-15]. Even though, this strategy does not avoid the excision of healthy cartilage from the joint for further expansion of the freshly isolated chondrocytes *in vitro*. Despite the encouraging results, there are a few critical requirements for the success of this approach. For example, the need to obtain high cell numbers, while maintaining chondrocyte functions. In this respect, it is well known [16,17] that conditions favouring maintenance of phenotype are usually different from those that favour a high cell density, and consequently there are limitations in the number of cells obtained *in vitro* for subsequent clinical application. Therefore, the low rate of success especially in large lesions and in older people, and the procedural constraints are the major drawback of these techniques [18].

In order to eliminate donor site morbidity, which is one the major limitation of autografts, several tissue engineered (TE) cartilaginous cell-scaffolds constructs have been proposed [19,20]. But, since we have

been able to gain new insights related with the role of subchondral bone, it seems obvious the enormous implications in the field of tissue engineering namely, in respect to the development of more adequate scaffolds architectures for cartilage healing. In this respect, several authors have been proposing the use of bilayered osteochondral constructs for the improved regeneration of cartilage defects [21-23]. Basically, this conceptual approach consists on developing a single 3-D porous structure that combines a mechanical support resembling the subchondral bone (bone-like layer), while also providing a chondrogenic support in the top for the repairing of cartilage (cartilage-like layer) [24,25]. Materials like hydroxylapatite (HAp) [26-28] and chitosan (CHT) [29-31] have been widely employed to develop suitable 3-D supports for applications in tissue engineering of bone and cartilage, respectively. Therefore, on the basis of the osteochondral approaches, the development of bilayered osteochondral scaffolds combining both HAp and CHT layers thus seems a good approach. Although, a strong mechanical interface between mineral substrate and polymer matrix is required for preventing a premature failure of the scaffold. Schek et al. [25] has been described the use of poly lactic acid (PLA) rods for connecting a HAp and PLA phases of a biphasic composite scaffold. Nevertheless, the effect of the polymeric rods on bone and cartilage regeneration is not studied. Therefore, there is the need of more simple and reliable strategies to manufacture bilayered scaffolds for osteochondral applications.

Besides the choice of adequate materials and the optimization of the mechanical properties and architecture for the scaffolds, TE strategies requires the use of cell sources, that should be viable in terms of clinical practice and that can be effective in new tissue formation. Research focused on tissue regeneration by means of using mesenchymal stem cells (MSCs) is increasingly attracting a great deal of attention, since MSCs have the ability to differentiate into various mesenchymal lineages [32-34] under specific culture conditions [35]. In fact, MSCs are one of the most promising candidates for transplantation after seeding into tissue-engineered implants [36-39].

In this study it is described the developmental route, physicochemical characterization and biological evaluation of novel 3-D macroporous hydroxylapatite/chitosan (HAp/CHT) bilayered scaffolds. HAp scaffolds (bone-like layer) were firstly produced by means of sintering. Then, the CHT porous layer (cartilage-like layer) was obtained by means of freeze-drying a chitosan solution poured onto the top of the HAp scaffolds. The physicochemical characterization of both organic and inorganic layers was performed by Fourier-transform infra-red (FTIR) spectroscopy, X-ray diffraction (XRD) analysis, micro-computed tomography (μ-CT), and scanning electron microscopy attached with an X-ray detector (SEM/EDS). The mechanical properties of the HAp, CHT porous layers and HAp/CHT bilayered scaffolds were assessed by compression tests. *In vitro* tests were also carried out to investigate the

water-uptake and weight loss behaviour of the HAp/CHT bilayered scaffolds by soaking into a phosphate buffered saline (PBS) for 1 up to 30 days.

The intrinsic cytotoxicity of the HAp porous layer and HAp/CHT bilayered scaffolds leachables was examined by carrying out a cellular viability assay (MTS test) using Mouse fibroblastic-like cells, which were previously in contact with the different concentrations of the scaffolds extract fluids. Moreover, a preliminary *in vitro* cultivation, proliferation and differentiation study was performed upon seeding of goat bone marrow stromal cells (GBMSCs) onto HAp and CHT layers (Phase I). GBMSCs have showed to present high proliferation and viability rates in fresh or cryopreserved cultures. These cells are quite stable in 2-D cultures and differentiate into osteogenic and chondrogenic phenotypic cells in the presence of supplemented osteogenic and chondrogenic media, respectively. Beside that, it is possible to use an autologous approach with the goat animal model and, in future experiments, evaluate *in vivo*, the osteochondral constructs functionality of HAp and CHT using marrow cells harvested from same animal implanted with the *in vitro* TE construct. Relative GBMSCs viability and proliferation was assessed by MTS test and by DNA quantification, while cellular adhesion and morphology was investigated by SEM. Osteogenic differentiation was assessed by alkaline phosphatase activity (ALP) and immunocytochemistry techniques for type I collagen and osteopontin. Glucosaminoglycans quantification assay was performed to evaluate chondrogenic differentiation.

Future studies will be designed to investigate the capacity of the HAp/CHT bilayered scaffolds to favour simultaneous osteoblasts and chondrocytes proliferation and differentiation upon seeding GBMSCs, leading to the formation of adequate tissue substitutes for the regeneration of osteochondral defects. With this approach it is aimed to develop an autologous model for further implantantion *in vivo*.

2. MATERIALS AND METHODS

2.1. SYNTHESIS OF HAP

Analytical reagent grade calcium hydroxide, $Ca(OH)_2$ (Riedel-de Haën, Germany) and ortho-phosphoric acid, H_3PO_4 (Panreac, Spain) were used on the synthesis of the HAp powders. An controlled drop-wise automated apparatus was developed by means of using a peristaltic pump (Gilson Miniplus 3, France) for adding a diluted solution of ortho-phosphoric acid to the calcium hydroxide solution, in a reaction vessel. Synthesis conditions were adjusted to obtain a stoichiometric HAp, i.e. Ca/P ratio of 1.67. After complete addition of the acid solution, the final pH of medium was adjusted to 11 with concentrated ammonium hydroxide (Riedel-de Haën, Germany). Vigorous stirring was continued during HAp precipitation. The supernatant was removed after 24 hours of maturation, and the precipitate filtered

under vacuum. The resulting filtrate was dried at 60ºC for 24 hours and milled in a mortar until obtaining a fine powder.

2.2. PREPARATION OF HAP SCAFFOLDS AND HAP/CHT BILAYERED SCAFFOLDS

Hydroxyapatite/chitosan (HAp/CHT) bilayered scaffolds were produced by adopting a two step procedure. Firstly, hydroxylapatite (HAp) porous layer (bone-like layer) with 10 mm height and 8 mm diameter were obtained by means of impregnating a polyurethane (PU) sponge with HAp powders, as previously reported by Oliveira et al. [40]. The elimination of the organic matrix consisted on burning the impregnated sponges in the furnace (Fornocerâmica-ATR 901, Portugal) at 900ºC for 24 hours, followed by sintering at 1300ºC for 3 hours, at ramp rate of 2.5ºC.min^{-1}. Secondly, a 3 wt% chitosan solution was prepared by dissolving chitosan (CHT) of medium molecular weight (Aldrich, Germany) and a degree of deacetylation of ~85% in 0.2 M acetic acid solution. The bilayered HAp/CHT scaffolds were fabricated by placing the HAp scaffolds into cylindrical silicon moulds (20 mm x 8 mm) and transferring the 3 wt% CHT solution. To guarantee that chitosan interpenetrated into the HAp scaffolds it was left resting for 1 minute at room temperature. Moulds were freeze at -80ºC and lyophilized (Telstar-Cryodos -80, Spain) up to 4 days to complete remove the frozen solvent, and allow obtaining the 'cartilage-like layer' on the top of the 'bone-like layer'. Then, HAp/CHT bilayered scaffolds were neutralized using a 0.1 M sodium hydroxide solution as previously described elsewhere [41], freeze at -80ºC and once lyophilized. Finally, the resulting HAp/CHT bilayered scaffolds were sterilized using ethylene oxide before carrying out the cell culture studies.

2.3. PHYSICOCHEMICAL CHARACTERIZATION

2.3.1. FTIR spectroscopy

Infra-red spectra of specimen powders were recorded on a Perkin-Elmer spectrometer (Perkin-Elmer 1600 series equipment, USA). Prior analysis transparent KBr (Riedel-de Haën, Germany) pellets were prepared by mixing in the ratio of 1:10 of sample/KBr (wt/wt), followed by uniaxially pressing the powders under vacuum. All spectra were obtained between 4400-450 cm^{-1} at a 2 cm^{-1} resolution.

2.3.2. XRD analysis

X-ray diffractometer (Philips PW 1710, The Netherlands) employing Cu-Kα radiation was used to investigate the cristallinity and phase content of the HAp scaffolds on powder. Data was collected from 2 to 65º 2θ values, with a step size of 0.02º, and a counting time of 2 seconds.step^{-1}.

2.3.3. Surface topography characterization

The surface morphology and pore size of the HAp scaffolds and HAp/CHT bilayered scaffolds were examined under the scanning electron microscope attached with an X-ray detector, SEM/EDS (Leica Cambridge S-360, UK). Prior to the microstructure analysis, specimens were coated with gold using a Fisons Instruments Coater (Polaron SC 502, UK) with a current set at 18 mA, for a coating time of 120 seconds.

2.3.4. Micro-computed tomography

The qualitative information of the HAp/CHT bilayered scaffolds architecture was obtained by microtomography imaging using the Scanco 20 equipment (Scanco Medicals, Switzerland) with penetrative X-rays of 50 keV. The X-ray scans were acquired in high resolution mode (11 μm). Mimics® software (Materialise, Belgium) was used to visualize the 2-D X-ray sections images of the HAp/CHT bilayered scaffolds. From the CT data set, 300 slices of a region of interest corresponding to the interface between HAp and CHT was used to investigate the continuity of the HAp/CHT bilayered scaffolds. A customized threshold technique was used to enhance the CHT contrast and remove noise.

2.3.5. Mechanical testing

Compression tests (dry state) were performed using a Universal Testing Machine (Instron 4505) possessing a load cell of 50 kN, at room temperature. The gauge length and diameter of all specimens was 16 mm and 8 mm, respectively. Tests were conducted with a constant strain rate of 2 mm.minute^{-1}, and up to failure or until 60% reduction in specimen height. The modulus (*E*) was determined by linear regression from the slopes in the initial elastic portion of the stress-strain diagram. A minimum number of 10 specimens were tested, and then *E* was averaged from the 10 measurements.

2.3.6. Water uptake and weight loss studies

Water-uptake and weight loss of the HAp scaffolds and HAp/CHT bilayered scaffolds were evaluated after immersion into a phosphate-buffered saline, PBS (Sigma-Aldrich, Germany) solution at pH 7.4, for time periods up to 30 days. All experiments were conducted at 37 $\pm$ 1ºC, and in triplicate. Percentage of water-uptake (WUs) after each time of immersion (t) was calculated using equation (1), where W_d and W_w correspond to the weight of the HAp/CHT bilayered scaffolds before and after immersion into PBS solution, respectively:

$$WUs,t = [(W_{w,t}-W_d)/ W_d] \times 100 \quad (1)$$

The percentage of weight loss (WLs) after each time of immersion (t) was calculated using equation (2), where W_i and W_f corresponds to the weight they before and after immersion into PBS solution, respectively:

$$WLs,t = [(W_{f,t}-W_i)/ W_i] \times 100 \quad (2)$$

2.4. *IN VITRO* CELL CULTURE STUDIES

2.4.1. Cytotoxicity screening

MTS (3-(4,5-dimethylthiazol-2-yl)-5-(3-carboxymethoxyphenyl)-2-(4-sulfophenyl)-2H-tetrazolium) test was performed to determine the cytotoxicity of HAp porous scaffolds and HAp/CHT bilayered scaffolds leachables that might result from the processing methodology used to obtain the HAp scaffolds and/or leachables of the polymeric component of the bilayered materials. Mouse fibroblastic-like cells (L929 cells; ECACC, UK), were cultured in basic medium: D-MEM (Dulbecco's Modified Eagle's Medium, Sigma-Aldrich, USA) without phenol red supplemented with 10% foetal bovine serum, FBS (Gibco, UK) and antibiotic-antimycotic (1% A/B, Gibco, UK) solution containing 10,000 units.mL^{-1} penicillin G sodium, 10,000 μg.mL^{-1} streptomycin sulphate and 25 μg.mL^{-1} amphotericin B as Fungizone® in 0.85% saline. L929 cells were incubated at 37ºC in an atmosphere containing 5% of CO_2, and after achieving confluence a cell suspension was prepared with a concentration of 8 x 10^4 cells.mL^{-1} and seeded onto 96-well plates. L929 cells were incubated for 3 days with different concentrations of HAp and HAp/CHT bilayered scaffolds extracts (25%, 50%, 75% and 100%). Eight replicates were considered per sample. Extracts of all samples were prepared as previously described by Gomes et al. [42].

L929 cells relative viability (%) was determined for each extract concentration and compared to tissue culture polystyrene (TCPS). Latex extracts were used as a positive control of cellular death. All cytotoxicity tests were performed in triplicate.

2.4.2. Isolation and culture of GBMSCs

Bone marrow stromal cells were isolated from the iliac crest of adult goats and cultured with basic culture medium - DMEM supplemented with 10% FBS and 1% A/B. Cells were cultured until confluence and sub-cultured at P1 and P2 before seeding. The relative viability of GBMSCs on the HAp scaffolds was also determined by carrying out an MTS assay, after each time point. For this purpose, cells-HAp

scaffold constructs were transferred into a 48-well plate and washed twice with sterile PBS. Culture medium without FBS and without phenol red was mixed with MTS in a 5:1 ratio, added to the wells, until totally cover the constructs, and incubated for 3 hours at 37ºC in a 5% CO_2 incubator. After the incubation period, 100 μL of MTS and medium mixture were transferred into each well of a 96-well plate and absorbance was read at 490 nm.

2.4.3. Seeding of GBMSCs onto the HAp porous layer and 3-D culturing (Phase IA)

GBMSCs cells were enzymatically lifted with 3 mL of trypsin after reaching 80% of confluence at P1 or P2. A cell suspension was prepared and seeded onto the HAp porous layer in a scaffold drop-wise manner, at a cellular density of 2.1 x 10^5 cells.mL^{-1}. Cells/scaffolds constructs were cultured in 48-well plates for 3 days with basic medium in static conditions. For inducing osteogenic differentiation, cell-seeded scaffolds were cultured with an osteogenic media consisting of alpha-MEM (Minimal Essential Medium Eagle alpha modification, Sigma-Aldrich, USA) supplemented with osteogenic supplements namely, 10^{-8} M dexamethasone (Sigma-Aldrich, USA), 50 μg.mL^{-1} ascorbic acid (Sigma, USA) and 10 mM β-glycerophosphate (Sigma, USA). The constructs were cultured for 3 days in static cultures with basal medium plus 14 days in osteogenic medium (17 days) and under dynamic conditions by using a lab rotator (Model DSR 2800 V, Digisystem Laboratory Instruments Inc., Taiwan). Samples were collected on day 0 (12 hours after seeding), day 3 and day 17 for further studies.

2.4.4. Seeding of GBMSCs onto the CHT porous layer and 3-D culturing (Phase IB)

To induce chondrogenic differentiation, CHT scaffolds were seeded with 2.5 x 10^5 cells and cultured for 7, 21 and 28 days with chondrogenic medium consisting of DMEM (Dulbecco's Modified Eagle Medium, Sigma-Aldrich, USA) supplemented with 10 ηg.mL^{-1} TGF-β (Sigma-Aldrich, USA), ITS+1 (100 x liquid media supplement, Sigma, USA), 0.1 M sodium pyruvate (Sigma-Aldrich, USA), 35 mM proline (Sigma-Aldrich, USA), 17 mM ascorbic acid (Sigma-Aldrich, USA) and 1 mM dexamethasone (Sigma-Aldrich, USA). The cell-scaffold constructs were also cultured under dynamic conditions by using a lab rotator system. Samples were retrieved after 7, 21 and 28 days of chondrogenic culture. Before chondrogenic medium was added, samples were cultured for 3 days in basal medium in static conditions. In both cases, culture media were changed every 2-3 days.

2.4.5. Evaluation of GBMSCs adhesion and morphology

Culturing GBMSCs adhesion and morphology was investigated by SEM analysis. For this purpose, after each culturing period, samples were removed from culture, washed in PBS, fixed in 2.5% glutaraldehyde, rinsed two times with PBS and dehydrated in series of ethanol concentrations. The samples were then dried at room temperature and sputter coated with gold before observation under the SEM.

2.4.6. Assessment of GBMSCs proliferation and differentiation

GBMSCs-HAp and -CHT construct celullarity was determined using a fluorimetric dsDNA quantification kit (PicoGreen, Molecular Probes). For this purpose, samples collected on day 0, day 3 and day 17, were washed twice with a sterile phosphate buffered saline (PBS, Sigma, USA) solution and transferred into 1.5 mL microtubes containing 1 mL of ultra-pure water. GBMSCs-HAp and -CHT were incubated for 1 hour at 37ºC in a water-bath and then stored in a -80ºC freezer until testing. Prior to DNA quantification constructs were thawed and sonicated for 15 minutes. Samples and standards (ranging between 0 and 2 $\mu g.mL^{-1}$) were prepared per each well of an opaque 96-well plate were added 28.7 µL of sample or standard plus 71.3 µL of PicoGreen solution and 100 µL of Tris-EDTA buffer. Triplicates were made for each sample or standard. The plate was incubated for 10 minutes in the dark and fluorescence was measured on a microplate ELISA reader (BioTek, USA) using an emission of 490 nm and an absorbance wavelength of 520 nm. A standard curve was created and sample DNA values were read off from the standard graph.

Alkaline phosphatase (ALP) activity was measured to evaluate osteoblastic differentiation. Cell-HAp scaffold constructs used for DNA quantification assay were used to determine ALP levels. As cells were lysed during the above mentioned procedure, both DNA and other cell produced proteins were in suspension in the supernatant solution. So, to each well of a 96-well plate were added 20 µL of sample plus 60 µL of substrate solution: 0.2% (wt/v) p-nytrophenyl phosphate (Sigma) in a substrate buffer: 1 M diethanolamine HCl (Merck, Germany), at pH 9.8. The plate was then incubated in the dark for 45 minutes at 37ºC. After the incubation period, 80 µL of a stop solution: 2 M NaOH (Panreac) containing 0.2 mM EDTA (Sigma, USA), was added to each well. Standards were prepared with 10 $\mu mol.mL^{-1}$ p-nytrophenol, pNP (Sigma, USA) and the stop solutions in order to achieve the final concentrations ranging between 0 and 0.3 $\mu mol.mL^{-1}$. Triplicates were made for each sample and standard. Absorbance was read at 405 nm and sample concentrations were read off from standard graph.

Immunocytochemistry technique was performed by fixing cell-HAp scaffold constructs in an Accustain formalin solution, 10 % neutral buffered (Sigma-Aldrich, USA) for 1 hour at 4ºC, washing with PBS and

including the constructs into methacrylate blocks. These blocks were cut into 10 μm thick slides and kept overnight at 80ºC before being used for subsequent immunocytochemistry analysis. The procedures immunocytochemistry were carried out following the instructions included in commercial kit: the RTU Vector Stain kit – Universal Elite ABC kit PK7200 (Vector Laboratories Inc., Burlingame, USA). This kit was used with a Peroxidase Substract Kit – DAB SK4100 (Vector Laboratories Inc., Burlingame, USA). For this study, samples were incubated with collagen type I (1/100, Chemicon, USA) for 1.6 hours and the biotinylated secondary antibody was incubated for 1 hour prior to wash and incubate the constructs with DAB for about 6 minutes. Also an osteopontin antibody (1/100, Rabitt polyclonal to osteopontin, Abcam, UK) was tested using slides from the same constructs. Although in this particular case, a fluorescent secondary antibody was used instead of a biotinylated one and kept overnight at 80ºC. The metacrylate sections were incubated with osteopontin antibody, washed and then Alexa Fluor 488 secondary antibody (Molecular Probes, Invitrogen, UK) was added to cell-HAp scaffold constructs. The incubation periods used were the same for both type I collagen and osteopontin antibodies. The observation of the constructs was performed using an Axio Imager Z1 microscope (Zeiss, Germany).

Glucosaminoglycans (GAGs) quantification assay [43] was used to determine extracellular chondrogenic matrix formation after day 7, day 21 and day 28 of chondrogenic medium culture. Cell-CHT scaffold constructs used for this assay were the same used for ALP and DNA assays. GAGs standards were obtained by preparing a chondroitin sulphate solution ranging from 0 and 30 $\mu g.mL^{-1}$. In each well of a 96-well plate, 20 μL of sample or standard were added in triplicates and then 250 μL per well of dimethylmethylene blue (DMB, Sigma Aldrich, USA) was added and mixed. The optical density was measured immediately at 525 nm on a microplate ELISA reader. A standard curve was created and GAGs sample values were read off from the standard graph.

3. RESULTS AND DISCUSSION

3.1. CHARACTERIZATION

The exploitation of a variety of biomaterials and cultured cells in tissue engineering (TE) approaches offers a wide range of possibilities for the successful repair of different skeleton damages. The ideal strategy for the treatment of osteochondral defects requires a scaffold architecture possessing a 'cartilage-like' layer and a 'bone-like' layer (lower) [44]. With this approach, the porous bilayered structure is expected to act as a support for cells functions and ultimately, leading to the *de novo* formation of an articular cartilage-like tissue in the cartilage void, while providing a good fixation on the underlying bone.

Previously, it was shown [45] that it is possible to develop a 3-D macroporous HAp structures by impregnation of PU sponges with HAp particles, followed by burning the organic template and sintering the ceramic at 1300ºC. Moreover, it is well known that a wide number of highly porous scaffold systems may be prepared by means of freezing a polymer solution and subsequently freeze-drying. In this study, we developed a novel bilayered scaffold by means of pouring a 3 wt% chitosan solution upon the sintered HAp scaffolds followed by a freeze-drying procedure. Figure 1 shows the macroscopic appearance of the HAp/CHT bilayered scaffolds. The macro image shows two distinct layers, which corresponds to HAp (bottom layer) and CHT (upper layer). The improved stability at the inorganic-organic interface and overall integrity of the HAp/CHT bilayered scaffolds was achieved by partially impregnating the porous ceramic layer with the polymeric one.

Figure 1. Macroscopic appearance of the HAp/CHT bilayered scaffolds.

Figure 2 shows the FTIR spectra of the HAp and CHT layers of the HAp/CHT bilayered scaffolds. The FTIR analysis revealed the presence of the typical bands of CHT on the upper layer namely, the absorption bands of the amide I and amide II groups at 1650 cm^{-1} and 1586 cm^{-1} (θ), respectively [46,47]. On the other hand, the IR spectrum also exhibited the peaks at 900 and 1155 cm^{-1} (●) associated to saccharine structure, and aliphatic C-H stretching bands in the region of 2996-2882 cm^{-1} (x). The more intense and broad absorption band in the CHT is attributed to the N-H stretching and O-H stretching vibration (■) located in the spectral region of 3200-3500 cm^{-1}.

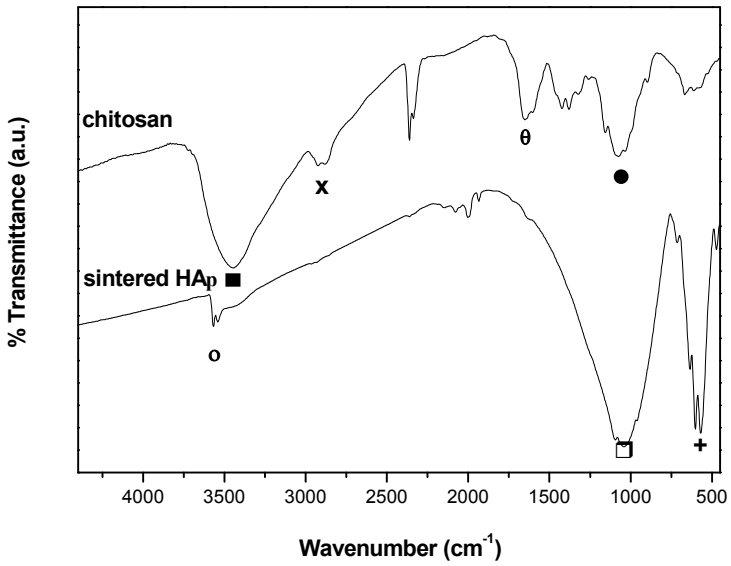

Figure 2. FTIR spectra of HAp and CHT layers of the HAp/CHT bilayered scaffolds.

Regarding the FTIR spectrum of lower layer of the HAp/CHT bilayered scaffolds, it were detected intense absorption bands at 598 and 559 cm^{-1} (+), and 1020 cm^{-1} (□), which are assigned to phosphate groups with the frequency of vibration $\nu 4$ and $\nu 3$, respectively. The small and sharp band observed at 3572 cm^{-1} (0) corresponds to the stretching mode of hydroxyl group, which is characteristic of calcium phosphates such as hydroxylapatite [48]. The FTIR data showed no typical peaks of the PU sponge in the HAp layer after performing the heat treatments. This result is an important one, because it shows that no traces of PU sponge were present in the HAp layer, thus avoiding the presence of organic matter that somehow could be responsible for eliciting some cytotoxic effect. Therefore, this result has shown that by means of using the burning and sintering cycle herein described, it is possible to completely eliminate the 'sacrifice matrix' consisting of PU sponge.

It has been reported that at temperatures higher than 1200ºC, HAp became unstable and frequently loses the -OH groups, and transforms in decomposition products such β-tricalcium phosphates (TCP) [48,49]. When the temperature exceeds 1250ºC, it may also occur a allotropic transformation and β-TCP may origin α-TCP [48,49]. Although, in a previous work we have shown that the synthesized HAp is highly stable upon sintering at 1300ºC for 3 hours, i.e. no -OH group loss was detected and no phase transformation observed [45]. Thus, understanding the sintering behaviour of hydroxylapatite allow us to control the chemical composition and design a porous ceramic structure with controlled grain size, microstructure and mechanical properties, since sintering temperature also has a dramatic effect on

densification. Actually, it has been shown that a decrease in porosity, i.e. increase in particle agglomeration is accompanied by an increase in the mechanical strength, due to the homogeneity and more closed packed HAp grains [50].

In this study, the XRD was also used to investigate the crystallinity and phase content of inorganic layer of the HAp/CHT bilayered scaffolds. Figure 3 shows the XRD pattern of the ceramic porous layer (on powder) after burning the organic template at 900ºC followed by sintering at 1300ºC for 3 hours. The XRD data is in good attainment with the FTIR, showing that the ceramic layer consists of highly crystalline form of hydroxyapaptite [51,52]. As expected, the pouring and freeze-drying of a chitosan solution upon the ceramic porous layer did not affect both crystallinity and phase content of the HAp.

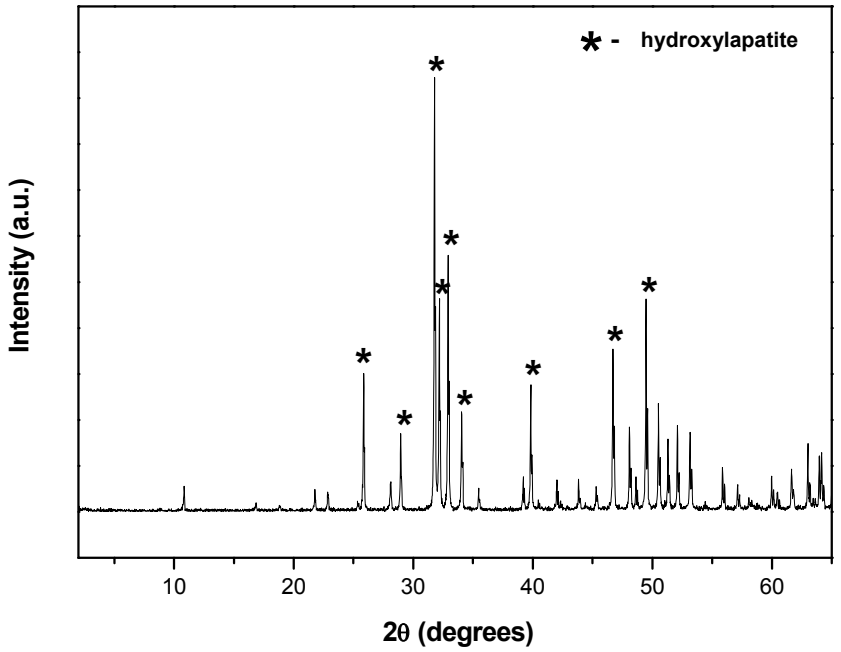

Figure 3. XRD pattern of the HAp scaffolds of the HAp/CHT bilayered scaffolds.

From the SEM images shown in Figure 4, it can be seen that HAp/CHT bilayered scaffolds microarchitecture consists of a highly porous and open pore structure. Figure 4A shows the interface of HAp/CHT bilayered scaffold at the surface, where it is possible to observe the two distinct porous layers. Figure 4B shows a typical HAp pore at the HAp/CHT interface, showing the good interpenetration of CHT into the HAp scaffolds. This observation suggests that a good bonding will exist between the two layers, which is known to be a requisite necessary to assure a good integrity and functionality of the osteochondral construct (scaffold+cells). Moreover, the SEM examination of the HAp scaffolds revealed that pores are highly interconnected and possess a size diameter in the range of 50-500 μm (Figure 4C).

Several authors [53,54] have shown that freezing conditions, concentration of polymer and freeze-drying parameters has great influence on the final microstructure and degree of interconnectivity of the scaffolds. Figure 4D shows the SEM micrograph of a CHT pore at the typical transversal cross-section of CHT layer. This study revealed that CHT pores quite resembles a typical spongy 3-D structure, with open pores, anisotropic porosity and pore size ranging from 20-600 μm. It is also possible to observe the formation of microfibres during the freeze-drying process. This can be an advantage since these fibres can act as an additional anchor-framework for improved cells adhesion. Therefore, the results depicted in figure 4 have shown that by combining a sintering and freeze-drying technique it is possible to develop HAp/CHT bilayered scaffolds with an adequate pore size and pore distribution for ingrowths of cells and diffusion of nutrients, while facilitating vascularization, and thus to be used in tissue engineering purposes [55,56]. Although, it is noteworthy that SEM analysis is only a reliable technique to obtain information about the 2-D systems, i.e. investigate the macro and micro-structure of the scaffold in a non-destructive way at the surface, and shows limited performance for assessing the pore interconnectivity of the materials.

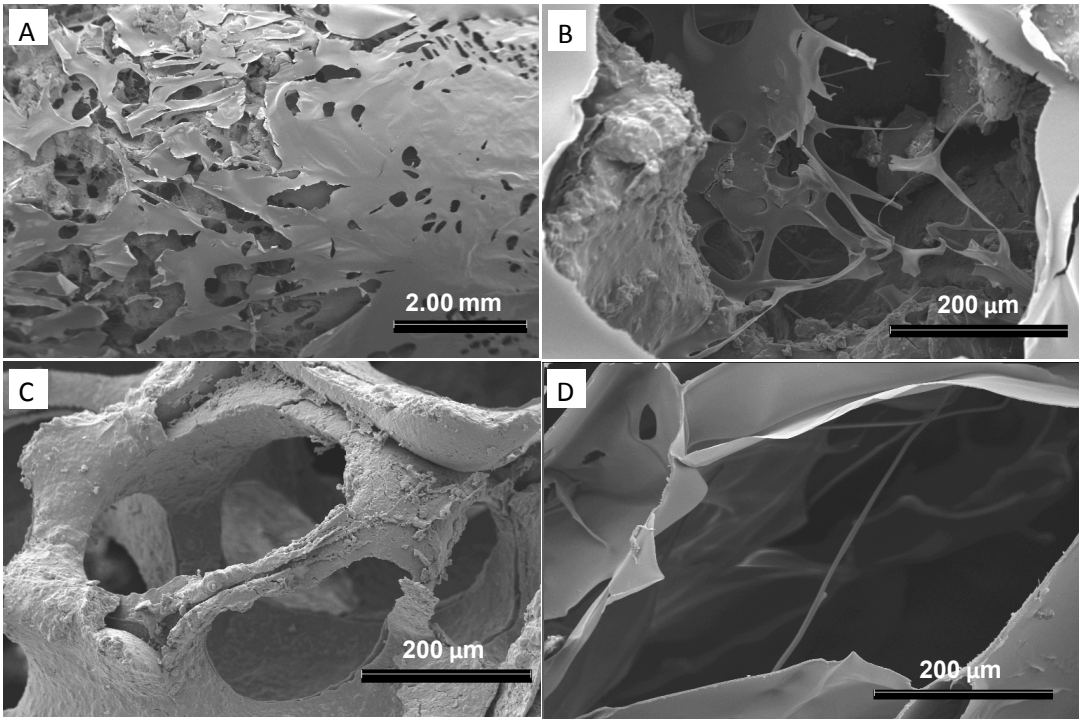

Figure 4. SEM micrographs of the HAp/CHT bilayered scaffolds: interface (A), typical pore at interface (B), pore of HAp scaffolds (C) and pore of CHT layer (D).

Moreover, the scaffold should be sectioned by destructive techniques towards obtaining the detailed information of their inner part using the SEM, thus the original morphology of the scaffold will be destroyed. Therefore, in this study the 3-D architecture of the materials was investigated in a non-destructive way, by means of using a micro-CT analysis.

Figure 5 shows the micro-computed tomography (μ-CT) analysis of the HAp/CHT bilayered scaffolds. A customized threshold technique was carried out and has shown to be effective on assessing the pore size and interconnectivity of CHT (Figure 5A). From the μ-CT 2-D scans it was possible to assess that pore size is higher than those obtained by the SEM (surface study). Actually, the inner pores of CHT was assessed to be up to 2 mm in length, which may be explained by the fact that μ-CT allows to study the inner 3-D architecture of the materials. Figure 5B shows the 2-D transversal view of the HAp scaffolds, which corroborated the SEM findings. These results clearly showed that the HAp pore network is highly interconnected. From figure 5C it became possible to observe that CHT perfectly interpenetrated into the HAp, thus showing the good continuity of the HAp/CHT bilayered scaffold. This result is encouraging since a strong mechanical interface between the HAp and CHT is required for the good performance of the construct.

Previous reported results have shown that the mean porosity of the HAp scaffolds (bottom layer) of the HAp/CHT bilayered scaffolds consisted of 67.8 ± 5.1% [45]. In this study, the percentage of porosity of the HAp and CHT layers were also determined (Figure 5D). The results have shown that HAp possess a porosity of 59.3 ± 1.7%, which is in good agreement with the previous reported data, and that CHT layer consisted of 74.6 ± 1.2%. Therefore, the HAp/CHT bilayered scaffolds have shown to possess adequate porosity [56] towards being used in tissue engineering scaffolding. Despite, the percentage of porosity at the interface was not possible to determine due to the limitation of the technique, i.e. since the coefficient of attenuation of HAp is much higher that that of CHT, the threshold applied for determining the porosity of HAp layer (T300) is different from that for assessing the porosity of CHT layer (T55). In fact, the observation of the dramatic lowering of porosity of CHT layer at the interface consists of an artefact and is a consequence of the interference of HAp layer. This data also shows that the overall integrity of the HAp/CHT bilayered scaffolds was achieved by partially impregnating the porous ceramic layer with the polymeric one, and is restricted to an area of 750 μm in length. Moreover, the results have shown that a physical interaction is the responsible for the stability of the bilayered scaffolds at the interface between hydroxylapatite and chitosan. Therefore, another biopolymer that can be processed by freeze-drying may serve the same role as the chitosan, i.e. top layer of the bilayered scaffold.

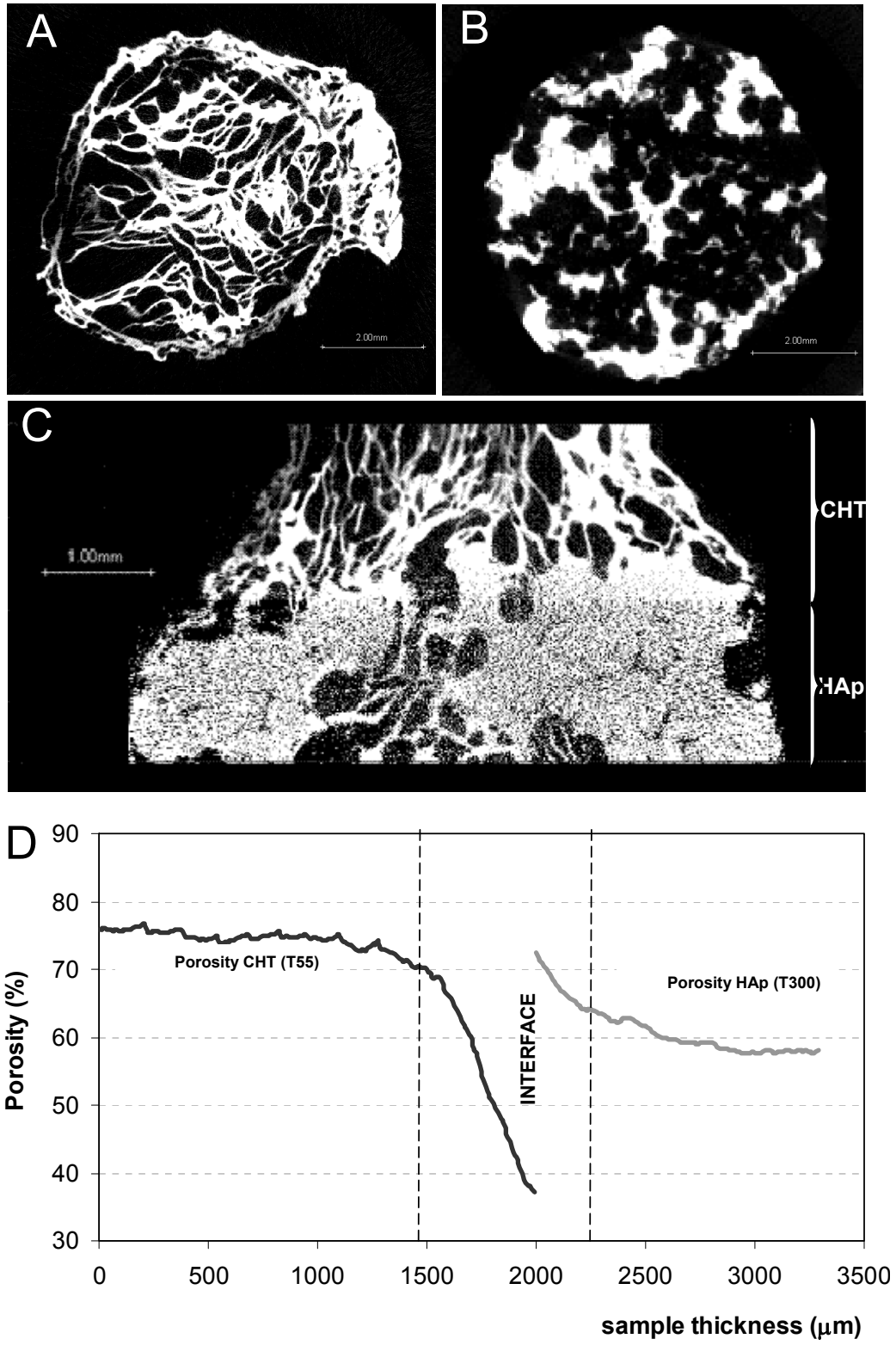

Figure 5. μ-CT images of the HAp/CHT bilayered scaffolds: transversal view of the CHT scaffold (A), transversal view of the HAp scaffold (B), and longitudinal view of the interface between HAp (bottom layer) and CHT (top layer) (C), and respective percentage of porosity.

To examine the mechanical properties of the HAp/CHT bilayered scaffolds, compression tests of the two layers were conducted separately, in dry conditions. The modulus (*E*) for the HAp and CHT in compression was found to be 153 ± 12 MPa and 2.9 ± 0.4 MPa, respectively. This results show that HAp scaffold possess quite good mechanical properties for being used in bone tissue engineering. On the other hand, the value for CHT scaffolds are in good attainment with those for normal human articular cartilage, which as been shown to have a compressive modulus ranging from 1.9 to 14.4 MPa [57,58]. Thus, the HAp/CHT bilayered scaffolds demonstrated quite promising mechanical properties for being used in TE of osteochondral defects. Actually, it has been shown that the biomechanical properties of articular cartilage greatly depends on composition, density of its ECM and interstitial fluid flow (water and solutes) [59]. Therefore, in wet conditions is expected a reduction of the mechanical properties. However, it must be noted that after implantation of the construct we expect to occur a matrix deposition and accumulation mediated by the cells, i.e. chondrocytes in the case of cartilage, and by this mean improve the mechanical function of the engineered cartilage [60].

The capability of a scaffold to uptake and preserve the water within the structure is an important feature for developing suitable tissue engineering constructs for regeneration of both cartilage and osteochondral defects, since cartilage possesses a high content of water where oxygen and nutrients are dissolved. The water-uptake and weight loss of the HAp/CHT bilayered scaffolds was investigated after soaking in PBS solution at physiological pH, for 1 up to 30 days (Figure 6). From figure 6A it can be seen that the water uptake profile of the HAp/CHT scaffolds reach a maximum of swelling of approximately 65% (w/w), after 5 days. From day 5 until day 30 the water uptake capability of the HAp/CHT remained constant (Figure 6A). After immersion of HAp/CHT bilayered scaffolds in PBS, no significant changes on the weight loss were observed. In fact, the weight loss profile showed that from day 3 until day 30, the HAp/CHT scaffolds showed a reduction in weight of approximately 0.8% (Figure 6B). It has been demonstrated that HAp dissolves slowly, both *in vitro* and *in vivo* [61,62]. Therefore, this gradual weight loss should be mainly due to the slow loss of the highly hydrophilic CHT scaffold by a solution-mediated dissolution, i.e. leaching of the water solubles rather than HAp scaffold. A decrease in CHT molecular weight lowers the water-uptake and favours dissolution [63]. Thus, the overall performance of the HAp/CHT scaffolds may be easily tailored by using different formulations namely, varying the CHT molecular weight and cross-linking [41]. Nevertheless, these results are quite interesting since the HAp/CHT bilayered scaffolds have shown to have enough stability, and preserve their size and physical integrity. This evidences their good performance for applications in TE of osteochondral defects and subsequent implantation.

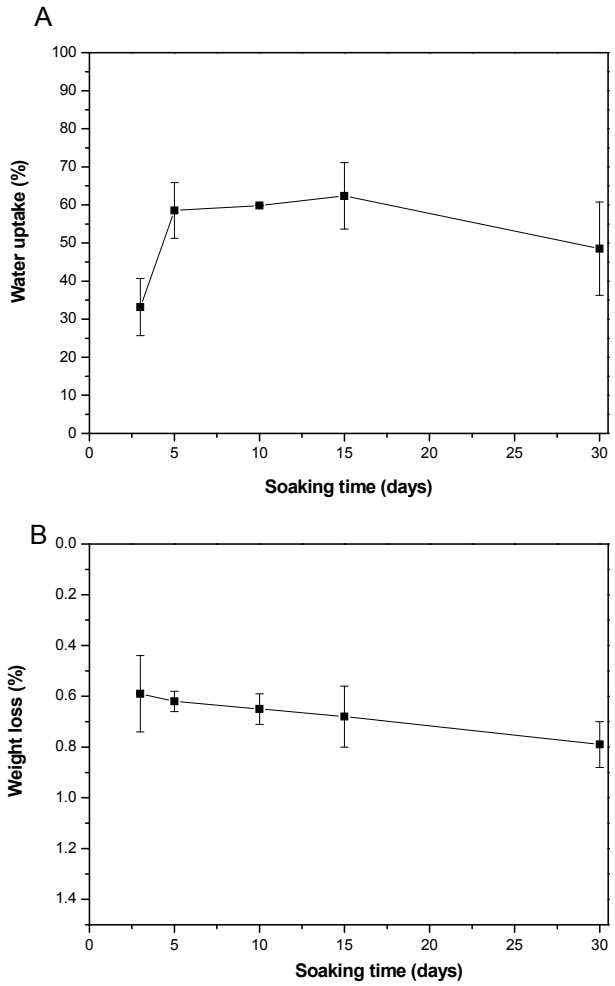

Figure 6. HAp/CHT scaffolds after soaking in PBS solution for times ranging from 1 up to 30 days: water-uptake (A) and weight loss (B).

3.2. CYTOTOXICITY SCREENING FOR THE HAP SCAFFOLDS AND HAP/CHT BILAYERED SCAFFOLDS

The intrinsic cytotoxicity of the HAp scaffolds and HAp/CHT bilayered scaffolds was assessed by culturing L929 cells with extract fluids for 72 hours. As observed in an inverted microscope cells exhibited a normal morphology proliferated well and established a monolayer (data not shown). Figure 7 shows the cell viability assessed by carrying out the MTS test. From results it is possible to assess that cells are viable in the presence of the HAp and HAp/CHT scaffold leachables. In fact, the viability levels are statistically similar among different HAp and HAp/CHT concentrations, reaching the maximum viability of ~100%. This shows that both HAp scaffolds and HAp/CHT scaffolds do not exert any cytotoxic effect on L929 cells. On the contrary, Latex rubber results (positive control) performed in the same conditions; do not overtake 1.0% of viable cells.

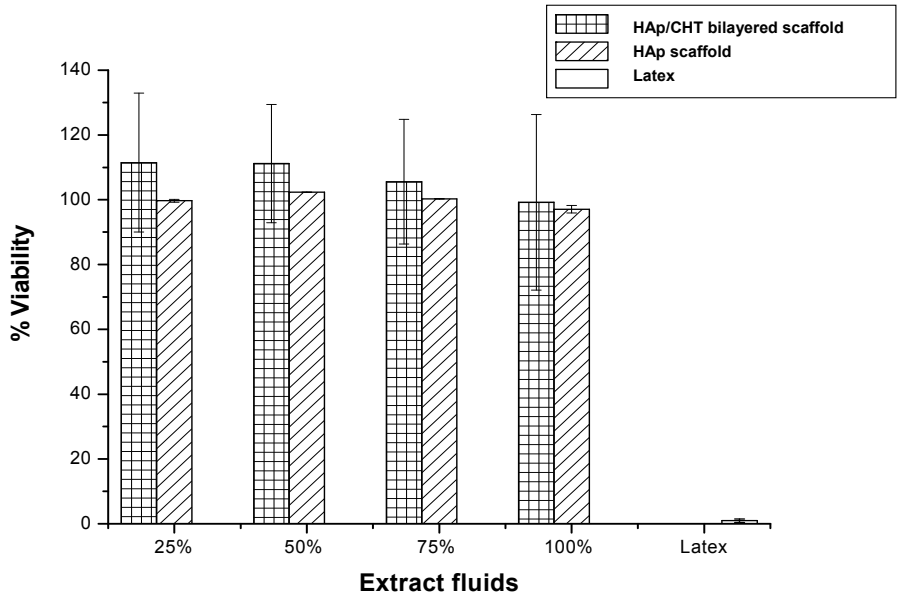

Figure 7. Cytotoxicity screening for the HAp scaffolds and HAp/CHT bilayered scaffolds. L929 cells were incubated with different concentrations of leachables obtained from HAp scaffolds, HAp/CHT bilayered scaffolds, and latex (positive control).

3.3. *IN VITRO* ASSESSMENT OF GBMSCS ADHESION, PROLIFERATION AND DIFFERENTIATION

The current investigations using biodegradable implants seeded mesenchymal stem cells have shown to be effective on the repair of osteochondral defects, *in vivo* [19]. In this work, we first analysed the ability of the HAp porous layer to successfully support the GBMSCs adhesion and functions, *in vitro* (Phase IA). As mentioned above, when treating a osteochondral defects this 'bone-like' layer is aimed at provide the repair of the subchondral bone [64], while providing a good fixation on the underlying bone, during cartilage regeneration. Figure 8 shows the SEM micrographs obtained from samples resulting from culturing GBMSCs onto the HAp porous layer in osteogenic medium, for 14 days. It is possible to observe the high cellular density on the surface of the HAp porous layer, which indicates that cells adhered and grew favourably (Figure 8A). Additionally, it is also possible to observe that cells did not obstruct the pores of the scaffold at the surface (Figure 8B), and perfectly adhere, spread actively and presented a flatten morphology onto the surface of the biomaterial (Figure 8C). In fact, the transversal section analysis indicate that cells were able to penetrate deeper into the scaffold core (Figure 8D). This is an important observation since a good cell distribution within the whole scaffold greatly affects the

overall performance of the construct (e.g. not limiting the diffusion of nutrients and oxygen) and shows that scaffold architecture allowed cells ingrowths and a sufficient diffusion of nutrients.

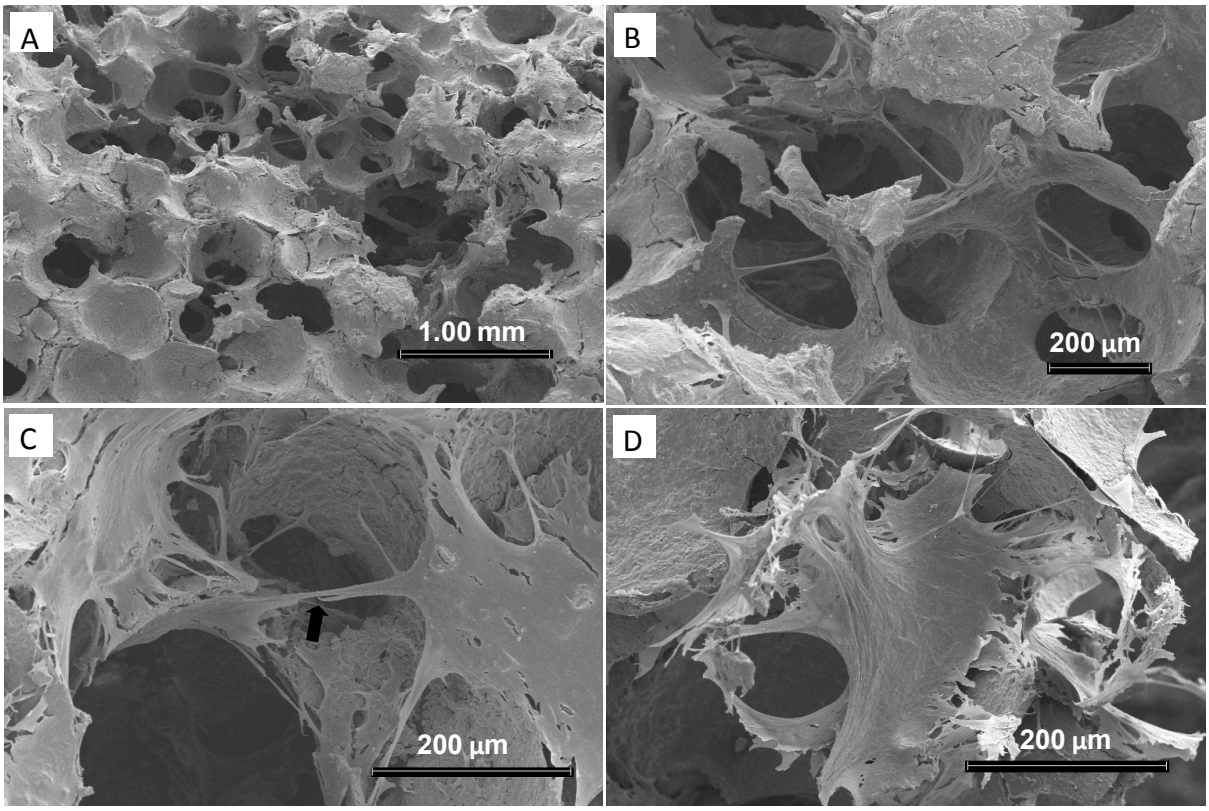

Figure 8. SEM micrographs of the HAp scaffold seeded with GBMSCs and cultured for 14 days in osteogenic media: surface of the cell-HAp constructs (A, B), GBMSCs infiltration into a HAp macropore (C), and GBMSCs on the core of the HAp scaffolds (D).

Additionally, it is also observed the formation of cells micovilli, which is suggestive of cell activation [65]. In our opinion, this result is quite promising since it demonstrates that the HAp porous layer possess an adequate pore size and pore distribution to effectively allow the cells to adhere and maintain their functions. Analysis of DNA values showed a significant enhancement comparatively to initial time points (Figure 9).

The cell number increased, and hence a high cellular proliferation occurred in the presence of osteogenic media. The DNA biochemical analysis was corroborated by MTS assay (Figure 10) showing that cells not only proliferated well in HAp porous layer but also were viable. These results illustrate that HAp porous layer is a suitable 3-D support for cellular proliferation.

The functional activity of the GBMSCs on the HAp porous layer was determined by quantifying the ALP activity (Figure 11). From day 0 to day 3, cells were not cultured with osteogenic medium so, ALP levels refer only to basal levels of alkaline phosphatase activity in GBMSCs. Although, the higher ALP results

shows that there is an enhancement of the osteoblastic phenotype expression levels, which evidences the presence of osteoblast cells, after 14 days (day 17) of culturing in the osteogenic medium (Figure 11).

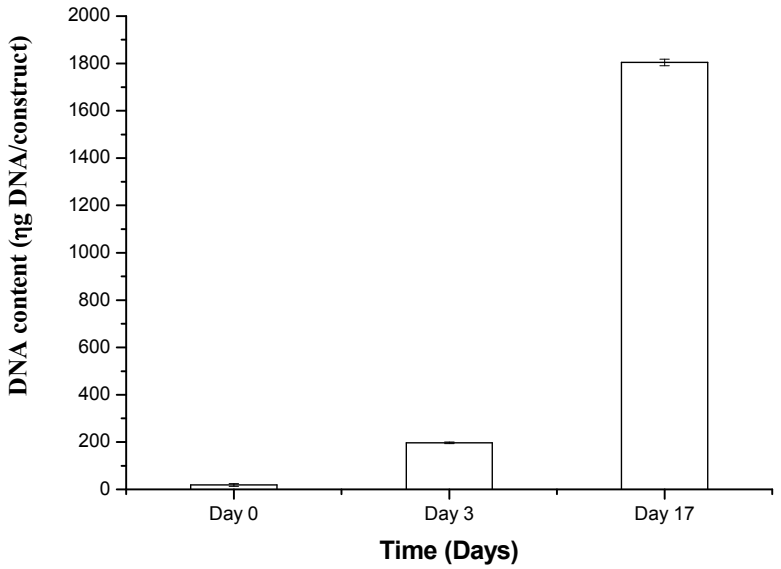

Figure 9. DNA content of GBMSCs cultured on the HAp scaffolds versus culture time.

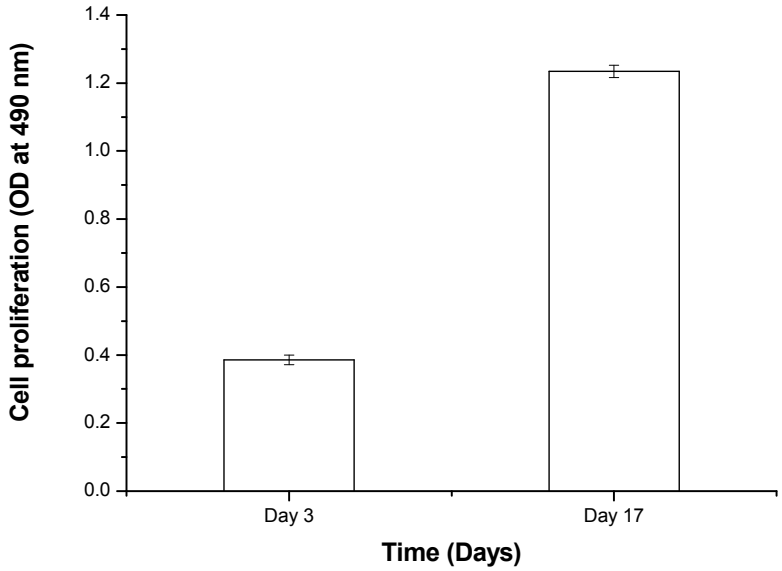

Figure 10. Proliferation levels of GBMSCs on the HAp scaffolds after 3 and 14 days of osteogenic culture, as assessed by an MTS method.

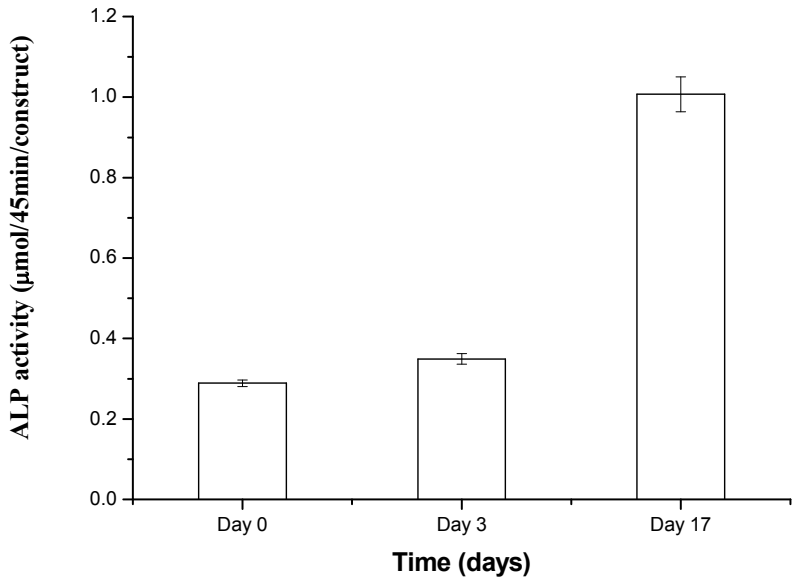

Figure 11. ALP activity assay of GBMSCs cultured on the HAp scaffolds.

Figure 12 shows the immunocytochemistry preliminary results for cell-HAp scaffold constructs after 14 days of culturing. The labelling was quite intense for osteopontin, which demonstrates that osteoblast differentiation was achieved in these constructs (Figure 12A). Immunolabeling for collagen type I was also detected, thus showing the production of collagenous matrix (Figure 12C). Therefore, this data confirm that GBMSCs were able to differentiate in the HAp layer after culturing in the osteogenic media for 14 days.

GBMSCs seeded onto chitosan layer present a good viability and proliferation (data not showed). SEM micrographs show the attachment of cells possessing size and shape consistent with those of chondrocytes throughout the scaffolds, i.e. round chondrocyte-like cells (Figure 13). It is also possible to observe a good distribution of cells and maintenance of the rounded cell morphology after day 28 (Figure 13A). At higher magnification it can also be seen the moderate cell adhesion to the substrate (Figure 13B), which is generally indicative of a cell performing its differentiation function [66]. Despite, cell numbers and penetration within scaffolds appeared to improve in areas presenting larger and interconnected pores.

Glycosaminoglycans (GAGs) are an important component of proteoglycan and are typically present in the cartilaginous extracellular matrix [67]. GAGs content was determined to assess the formation of newly formed extracellular matrix and thus if occur the differentiation of GBMSCs into chondrocytes in these cell-scaffold constructs, at day 7, 21 and 28 (Figure 14). The biochemical analysis demonstrated that the content of GAGs increased from day 7 to day 21, indicating that occur by synthesis due to the

differentiation of the GBMSCs into the chondrogenic lineage. GAGs levels seems to be low; however it was not found in the literature any reference values to compare with. Nevertheless, chitosan scaffolds obtained by a freeze-drying technique suggested being a suitable 3-D support for chondrogenic differentiation of GBMSCs, and their maintenance over a period of 28 days.

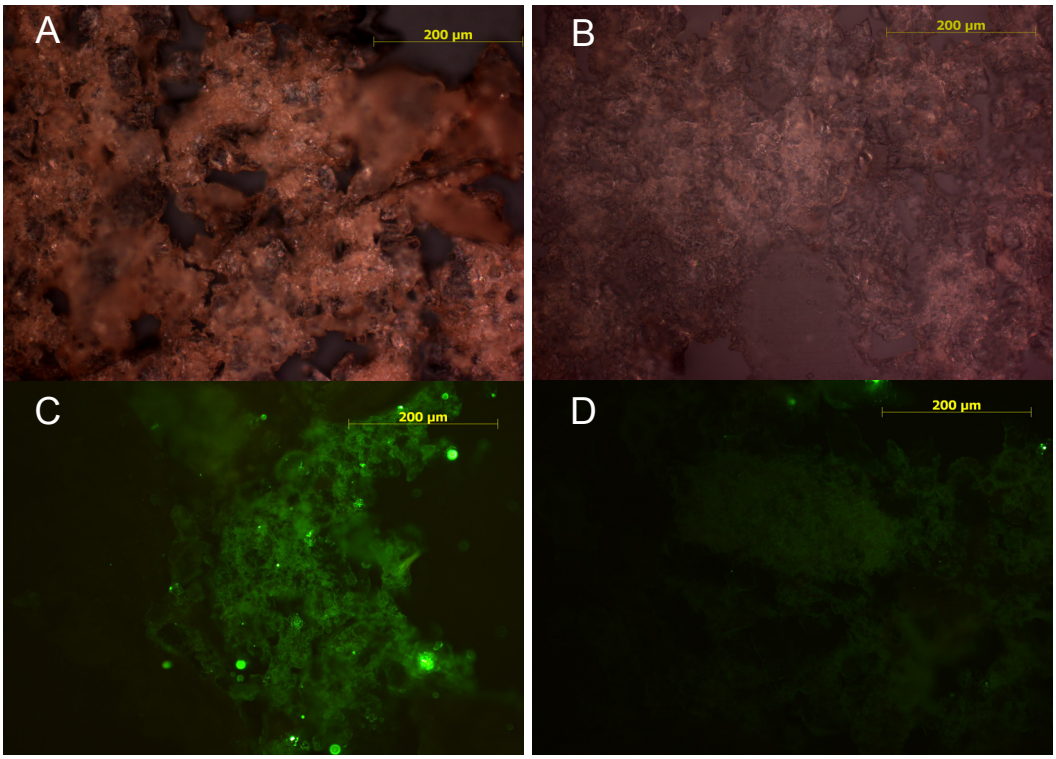

Figure 12. Immunolabeling for osteopontin marker (A) and respective negative control (without antibody) (B) on the cell-HAp scaffold constructs after 14 days of culturing. Immunolabeling for collagen type I marker (C) and respective negative control (without antibody) (D) on the cell-HAp scaffold constructs after 14 days of culturing.

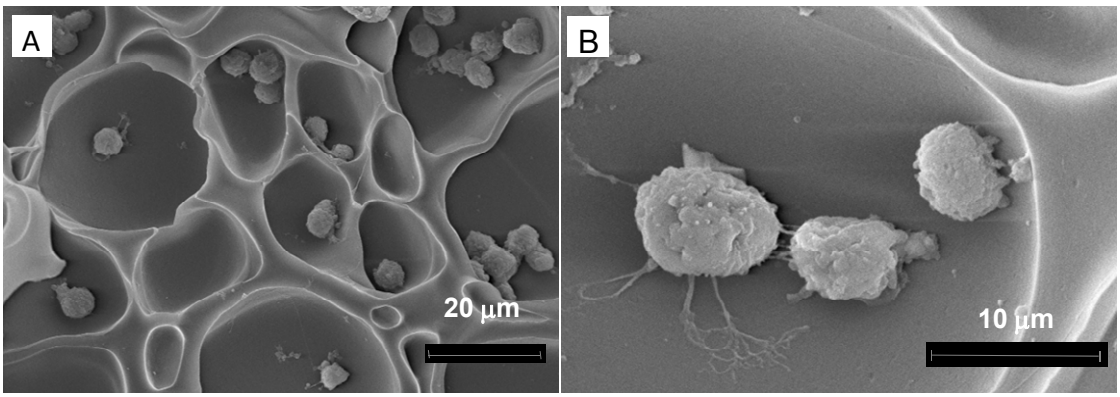

Figure 13. SEM micrographs of the CHT layer seeded with GBMSCs after 28 days of culturing (A, B).

Future studies will be designed to investigate the capacity of the HAp/CHT bilayered scaffolds to favour simultaneous but independent osteoblasts and chondrocytes proliferation and differentiation upon seeding GBMSCs, leading to the formation of adequate tissue substitutes for the regeneration of osteochondral defects (Phase II). This will be achieved using a culturing system such as the ones proposed by Wendt et al. [68], which are specifically designed for this purpose and allow to culture simultaneously the HAp and CHT layers in separate culture medium that will direct cell differentiation into the required phenotypes.

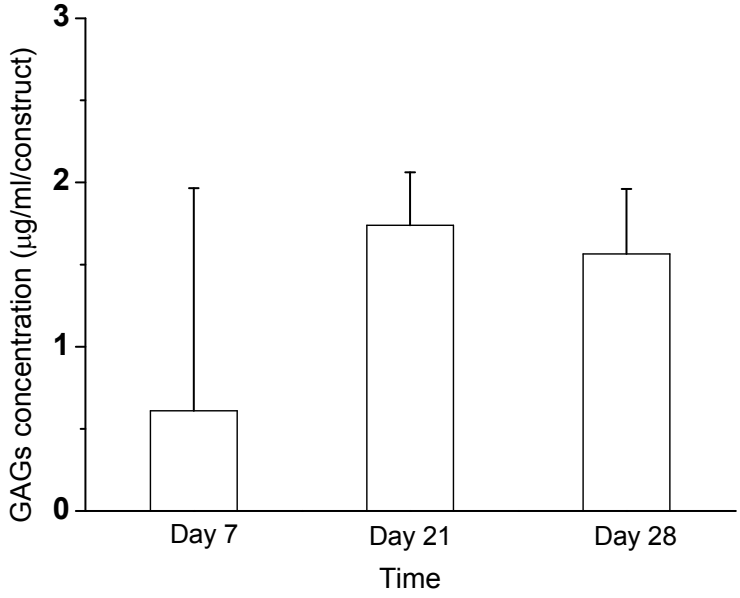

Figure 14. GAGs quantification assay of GBMSCs cultured on the CHT layer.

4. CONCLUSIONS

This work demonstrates the feasibility to prepare hydroxylapatite/chitosan bilayered scaffolds by means of an innovative method that combines a sintering and a freeze-drying technique. The novel 3-D macroporous hydroxylapatite/chitosan bilayered scaffolds exhibit physicochemical properties that appear to make them a suitable candidate to be used as a supportive structure for cells functions. Moreover, the *in vitro* cell culture studies demonstrated that both HAp and CHT layers provide an adequate 3-D support for the attachment, proliferation and differentiation of GBMSCs into osteoblasts and chondrocytes, respectively. The HAp/CHT bilayered scaffolds are advantageous by several reasons namely, they can be designed with several sizes and controlled architecture to fit patient specific injuries and cell functions, respectively. The HAp/CHT bilayered scaffolds showed promising biological behaviour and may therefore find applications in tissue engineering of bone and osteochondral defects.

REFERENCES

1. Temenoff, J.S. and A.G. Mikos, *Review: tissue engineering for regeneration of articular cartilage*. Biomaterials, 2000. 21: p. 431.
2. Cohen, N.P., R.J. Foster, and V.C. Mow, *Composition and dynamics of articular cartilage: structure, function and maintaining healthy state*. Journal of Orthopaedic & Sports Physical Therapy , 1998. **28**: p. 203.
3. Aigner, T. and J. Stove, *Collagens- major component of the physiological cartilage matrix, major target of cartilage degeneration, major tool in the cartilage repair*. Advanced Drug Delivery Reviews, 2003. **55**: p. 1569.
4. Kuettner, K.E. and A.A. Cole, *Review: Cartilage degeneration in different human joints*. Osteoarthritis and Cartilage, 2005. **13**: p. 93.
5. Buckwalter, J.A., *Articular cartilage: injuries and potential for healing*. Journal of Orthopaedic & Sports Physical Therapy , 1998. **28**: p. 192.
6. Redman, S.N., S.F. Oldfield, and C.W. Archer, *Current strategies for articular cartilage repair*. European Cells and Materials, 2005. **9**: p. 23.
7. Glowacki, J., *In vitro engineering of cartilage*. Journal of Rehabilitation Research and Development, 2000. **37**: p. 171.
8. Miller, B.S., et al., *Patient satisfaction and outcome after microfracture of degenerative knee*. J Knee Surgery, 2004. **17**: p. 13.
9. Krishnan, S.P. and J.A. Skinner, *(i) Novel treatments for early osteoarthritis of the knee*. Current Orthopaedics, 2005. **19**: p. 407.
10. Akizuki, S., Y. Yasukawa, and T. Takizawa, *Does arthroscopic abrasion arthroplasty promote cartilage regeneration in osteoarthritic knees with eburnation? A prospective study of high tibial osteotomy with abrasion arthroplasty versus high tibial osteotomy alone*. Arthroscopy, 1997. **13**: p. 9.
11. Shapiro, F., S. Koide, and M.J. Glimcher, *Cell origin and differentiation in the repair of full-thickness defects of articular cartilage*. Journal of Bone Joint Surgery (American Volume), 1993. **75**: p. 532.
12. Tibesku, C.O., et al., *Hyaline cartilage degenerates after autologous osteochondral transplantation*. Journal of Orthopaedic Research, 2004. **22**: p. 1210.

13. Gillogly, S.D., M. Voight, and T. Blackburn, *Treatment of articular cartilage defects of the knee with autologous chondrocyte implantation*. Journal of Orthopaedic & Sports Physical Therapy, 1998. **28**: p. 241.
14. Minas, T., *Autologous chondrocyte implantation in arthritic knee*. Orthopedics, 2003. **26**: p. 945.
15. Brittberg, M., *Autologous chondrocyte transplantation*. Clinical Orthopaedics, 1999. **367**: p. S147.
16. Glowacki, T.J., E. Trepman, and J. Folkman, *Cell shape and phenotypic expression in chondrocytes*. Proceedings of the Society for Experimental Biology and Medicine, 1983. **172**: p. 93.
17. Yoo, J., et al., *The chondrogenic potential of human bone-marrow-derived mesenchymal progenitor cells*. Journal of Bone Joint Surgery (American Volume), 1998. **80**: p. 1745.
18. O'Driscoll, S.W., *The healing and regeneration of articular cartilage*. Journal of Bone and Joint Surgery, 1998. **80-A**: p. 1795.
19. Uematsu, K., et al., *Cartilage regeneration using mesenchymal stem cells and a three-dimensional poly-lactic-glycolic acid (PLGA) scaffold*. Biomaterials, 2005. **26**: p. 4273.
20. Solchaga, L., et al., *Repair of osteochondral defects with hyaluronan- and polyester-based scaffolds*. Osteoarthritis and Cartilage, 2005. **13** p. 297.
21. Lima, E.G., et al., *Functional tissue engineering of chondral and osteochondral constructs*. Biorheology, 2004. **41**: p. 577.
22. Schaefer, D., et al., *In vitro generation of osteochondral composites*. Biomaterials, 2000. **21**: p. 2599.
23. Schaefer, D., et al., Tissue-engineered composites for the repair of large osteochondral defects. Arthritis & Rheumatism, 2002. **46**: p. 2524.
24. Gao, J., et al., *Repair of osteochondral defect with tissue-engineered two-phase composite material of injectable calcium phosphate and hyaluronan sponge.* Tissue Engineering, 2002. **8**: p. 827.
25. Schek, R.M., et al., *Engineered osteochondral grafts using biphasic composite solid free-form fabricated scaffolds*. Tissue Engineering, 2004. **10**: p. 1376.
26. Kotobuki, N., et al., *Observation of osteogenic differentiation cascade of living mesenchymal stem cells on transparent hydroxyapatite ceramics*. Biomaterials, 2005. **26**: p. 779.
27. Kasten, P., et al. *Ectopic bone formation associated with mesenchymal stem cells in a resorbable calcium deficient hydroxyapatite carrier*. Biomaterials, 2005. **26**: p. 5879.

28. Livingston, A.T., et al., *A comparative study of biphasic calcium phosphate ceramics for human mesenchymal stem-cell-induced bone formatio*n. Biomaterials, 2005. **26**: p. 3631.
29. Lu, J.X., et al., *Effects of chitosan on rat knee cartilages*. Biomaterials, 1999. **20**: p. 1937.
30. Di Martino, A., M. Sittinger, and M.V. Risbud, *Chitosan: A versatile biopolymer for orthopaedic tissue-engineering*. Biomaterials, 2005. **26**: p. 5983.
31. Yamane, S., et al. *Feasibility of chitosan-based hyaluronic acid hybrid biomaterial for a novel scaffold in cartilage tissue engineering*. Biomaterials, 2005. **26**: p. 611.
32. Jiang, Y., et al. *Pluripotency of mesenchymal stem cells derived from adult marrow*. Nature, 2002. **418**: p. 41.
33. Reyes, M., et al., *Purification and ex vivo expansion of postnatal human marrow mesodermal progenitor cells*. Blood, 2001. **98**: p. 2615.
34. Il Im, G., Y.-W. Shin, and K.-B. Lee, *Do adipose tissue-derived mesenchymal stem cells have the same osteogenic and chondrogenic potential as bone marrow-derived cells?* Osteoarthritis and Cartilage, 2005. **13**: p. 845.
35. Kitamura, S., et al., *Osteogenic differentiation of human bone marrow-derived mesenchymal cells cultured on alumina ceramics*. Artificial Organs, 2004. **28**: p. 72.
36. Caplan, A.I., et al., *Principles of cartilage repair and regeneration*. Clinical Orthopaedics and Related Research, 1997. **342**: p. 254.
37. Uemura, T., et al., *Transplantation of cultured bone cells using combinations of scaffolds and culture techniques*. Biomaterials, 2003. **24**: p. 2277.
38. Ohgushi, H., et al., *Tissue engineered ceramic artificial joint- ex vivo osteogenic differentiation of patient mesenchymal cells on total ankle joints for treatment of oseoarthritis*. Biomaterials, 2005. **26**: p. 4654.
39. Rahaman, M.N. and J.J. Mao, *Stem cell-based composite tissue constructs for regenerative medicine*. Biotechnology and Bioengineering, 2005. **91**: p. 261.
40. Oliveira, J.M., et al., *Innovative technique for the preparation of porous bilayer hydroxyapatite/chitosan scaffolds for osteochondral applications*. Kyoto (JPN): Key Engineering Materials, Trans Tech Pub, Zurich, Switzerland; 2006. **309-311**: p. 927.
41. Silva, S.S., et al., *Preparation and characterization of novel chitosan/soy protein porous for tissue engineering applications*. Advanced Materials Forum, 2006. **514-516**: p. 1000.
42. Gomes, M.E., et al., *Cytocompatibility and response of osteoblastic-like cells to starch-based polymers: effect of several additives and processing conditions*. Biomaterials, 2001. **22**: p. 1911.

43. Hollander, A.P. and P.V. Hatton, *Biopolymer methods in tissue engineering* (Methods in Molecular Biology Ser). Totowa, NJ: Human Press Inc.; 2004.
44. Kupper, J.H., L. van Gool, and A. Burkle, *Molecular genetic systems to study the role of poly(ADP-ribosyl)ation in the cellular response to DNA damage*. Biochimie, 1995. **77**(6): p. 450.
45. Oliveira, J.M., et al., *Macroporous hydroxyapatite scaffolds for bone tissue engineering applications: physicochemical characterization and assessment of rat bone marrow stromal cells viability*. Journal of Biomedical Materials Research: Part A – In Press (doi:10.1002/jbm.a.32213).
46. Yamaguchi, I., et al., *The chitosan prepared from crab tendon I: the characterization and mechanical properties*. Biomaterials, 2003. **24**: p. 2031.
47. Kolhe, P. and R.M. Kannan, *Improvement in ductibility of chitosan through blending and copolymerization with PEG: FTIR investigation of molecular interactions*. Biomacromolecules, 2003. **4**: p. 173.
48. Raynaud, S., et al., *Calcium phosphate with variable Ca/P atomic ratio I. Synthesis, characterization and thermal stability of powders*. Biomaterials, 2002. **23**: p. 1065.
49. Tampieri, A., et al., *Sintering and characterization of HA and TCP bioceramics with control of their strength and phase purity*. Journal of Materials Science: Materials in Medicine, 1997. **8**: p. 29.
50. Mostafa, N.Y., *Characterization, thermal stability and sintering of hydroxyapatite powders prepared by different routes*. Materials Chemistry and Physics, 2005. **94**: p. 333.
51. Kotobuki, N., et al., *Observation of osteogenic differentiation cascade of living mesenchymal stem cells on transparent hydroxyapatite ceramics*. Biomaterials, 2005. **26**: p. 779.
52. Cyster, L.A., et al., *The influence of dispersant concentration on the pore morphology of hydroxyapatite ceramics for bone tissue engineering*. Biomaterials, 2005. **26**: p. 697.
53. Ho, M.-H., et al., *Preparation of porous scaffolds by using freeze-extraction and freeze-gelation method*s. Biomaterials, 2004. **25**: p. 129.
54. Madihally, S.V. and H.W.T. Matthew, *Porous chitosan scaffolds for tissue engineering*. Biomaterials, 1999. **20**: p. 1133
55. Karageorgiou, V. and D. Kaplan, *Porosity of 3D biomaterial scaffolds and osteogenesis*. Biomaterials, 2005. **26**: p. 5474.
56. Hutmacher, D.W., *Scaffolds in tissue engineering bone and cartilage*. Biomaterials, 2000. **21**: p. 2529.
57. Zheng-Qiu, G., X. Jiu-Mei, and Z. Xiang-Hong, *The development of artificial articular cartilage - PVA-hydrogel*. Bio-Medical Materials and Engineering, 1998. **8**: p. 75.

58. Magnussen, R.A., F. Guilak, and T.P. Vail, *Cartilage degeneration in post-collapse cases of osteonecrosis of the human femoral head: Altered mechanical properties in tension, compression, and shear*. Journal of Orthopaedic Research, 2005. **23**: p. 576.
59. Evans, R.C. and T.M. Quinn, *Solute diffusivity correlates with mechanical properties and matrix density of compressed articular cartilage*. Archives of Biochemistry and Biophysics, 2005. **442**: p. 1.
60. Miyata, S., et al., *Static and dynamic mechanical properties of extracellular matrix synthesized by cultured chondrocytes*. Materials Science and Engineering: C, 2004. 24: p. 425.
61. Driessens, F.C.M., et al., *Chemical reactions of calcium phosphate implants after implantation in vivo*. Journal of Materials Science: Materials in Medicine, 1992. **3**: p. 413.
62. Klein, C.P.A.T., et al., *Studies of the solubility of different calcium phosphate ceramic particles in vitro*. Biomaterials, 1990. **11**: p. 509.
63. Berger, J., et al. *Structure and interactions in covalently and ionically crosslinked chitosan hydrogels for biomedical applications*. European Journal of Pharmaceutics and Biopharmaceutics, 2004. 57: p. 19.
64. Tamai, N., et al., *A new biotechnology for articular cartilage repair: subchondral implantation of a composite of interconnected porous hydroxyapatite, synthetic polymer (PLA-PEG), and bone morphogenetic protein-2 (rhBMP-2)*. Osteoarthritis and Cartilage, 2005. **13**: p. 405.
65. Xynos, I.D., et al., *Bioglass 45S5 stimulates osteoblast turnover and enhances bone formation in vitro: Implications and applications for bone tissue engineering*. Calcified Tissue International, 2000. **67**: p. 321.
66. Yaylaoglu, M.B., et al., *A novel osteochondral implant*. Biomaterials, 1999. **20**: p. 1513.
67. Barnewitz, D., et al., *Treatment of articular cartilage defects in horses with polymer-based cartilage tissue engineering grafts*. Biomaterials, 2006. **27**: p. 2882.
68. Wendt, D., M. Jakob, and I. Martin, *Bioreactor-based engineering of osteochondral grafts: from model systems to tissue manufacturing*. Journal of Bioscience and Bioengineering, 2005. **100**: p. 489.

CHAPTER VI.

Surface engineered carboxymethylchitosan/poly(amidoamine) dendrimer nanoparticles for intracellular targeting

CHAPTER VI.

Surface engineered carboxymethylchitosan/poly(amidoamine) dendrimer nanoparticles for intracellular targeting

Abstract

Novel highly branched biodegradable macromolecular systems were developed by grafting carboxymethylchitosan, CMCht onto low generation poly(amidoamine), PAMAM dendrimers. Such structures were organized into sphere-like nanoparticles that are proposed to be used as carriers to deliver bioactive molecules aimed at controlling the behaviour of stem cells, namely their proliferation and differentiation. The nanoparticles did not exhibit significant cytotoxicity in the range of concentrations below 1 $mg.mL^{-1}$ and fluorescent probe labeled nanoparticles were found to be internalized with highly efficiency by both human osteoblast-like cells and rat bone marrow stromal cells, under fluorescence-activated cell sorting and fluorescence microscopy analyses. Dexamethasone (Dex) was incorporated CMCht/PAMAM dendrimer nanoparticles and release rates were determined by high performance liquid chromatography. Moreover, the biochemical data demonstrated that the Dex-loaded CMCht/PAMAM dendrimer nanoparticles promote the osteogenic differentiation of rat bone marrow stromal cells, *in vitro*. The nanoparticles exhibited interesting physicochemical and biological properties and have great potential to be used in fundamental cell biology studies as well as in a variety of biomedical applications, including tissue engineering and regenerative medicine.

This chapter is based on the following publication: **Oliveira JM**, Kotokuki N, Marques AP, Pirraco RP, Benesch J, Hirose M, Costa SA, Mano JF, Ohgushi H and Reis RL, 2008, Surface engineered carboxymethyl-chitosan/poly(amidoamine) dendrimer nanoparticles for intracellular targeting, Advanced Functional Materials, **18**: 1840-1853.

---

1. INTRODUCTION

Dendrimers are a relatively new class of synthetic [1,2], highly branched, nanospherical and low dispersive macromolecules [3,4]. They can be designed to provide a quite versatile choice of external functional groups in order to reduce cytotoxicity and enhance transepithelial transport [5,6], for interaction with coupling molecules such as natural-based polymers [7] and fluorescent probes [8] and an inner hydrophobic core where other molecules can be trapped [6]. Among myriad possibilities, dendrimers can find applications as a delivery carrier of drugs [6,9] and DNA (transfection) [10], imaging agents [11,12], and tissue engineering scaffolding [13]. Although there are different routes to synthesise dendrimers [4], their maximum size is typically in the order of ~10-20 nm [12,14]. Moreover, it has also been found [15] that high generation dendrimers (G7) with amine capping-groups causes haemolysis and changes in red cell morphology, and in general are overall cytotoxic. Therefore, the strategy proposed herein envisions the surface engineering of a dendrimer core grafted to natural-based and biocompatible polymers (linear polymer chains) in order to obtain copolymers of new architectures with tuned nanoparticle size and more versatile macromolecules. These should make it possible to avoid the cytotoxic effects of high-generation dendrimers. This new class of materials is expected to exhibit entirely new properties since the structures might have sizes larger than 10 nm and different surface properties (dendronized polymer) [1]. It is expected that the dendronized polymers developed in the present work will have potential applications as novel drug or gene delivery carriers for targeting certain tissues or cell cultures. Such nano-devices could display a higher loading capacity, and allow the bulk incorporation of bioactive molecules of higher molecular weights and of different chemistry, while maintaining high internalization and transfection efficiency as compared to conventional dendrimers.

In this study, novel water-soluble nanoparticles consisting of a poly(amidoamine) (PAMAM) dendrimer core with grafted carboxymethylchitosan (CMCht) chains (dendronized polymer) were successfully synthesized. They were then characterized and screened for cytotoxicity using a fibroblast-cell line (L929) and rat bone marrow stromal Cells (RBMSCs) by means of performing a tetrazolium reduction (MTT) assay and luminescent cell viability assay based on the adenosine triphosphate (ATP) quantification, respectively. The internalization of fluorescein isothiocyanate (FITC)-labeled CMCht/PAMAM dendrimer nanoparticles was also investigated using both osteoblastic-cell line (SaOs-2) and RBMSCs as target cells. These types of cells are widely used in tissue engineering approaches [16,17] and are simple *in vitro* systems for assessing the internalization efficiency of fluorescent-labeled molecules. It is our particular interest to engineer these nanoparticles to find

applications in the intracellular controlled delivery of biological agents, including differentiation factors or genetic material, to modulate stem cell behaviour while avoiding undesired secondary effects. In this context, it was also investigated the capacity of dexamethasone-loaded CMCht/PAMAM nanoparticles to promote the osteogenic differentiation of rat bone marrow stromal cells. Alizarin red and ALP stainings were carried out to assess qualitatively the mineralization capacity and ALP activity, which are known to denote the osteogenic differentiation. The quantitative content of ALP and osteocalcin, the early and late markers of osteogenic differentiation respectively, were also determined.

2. EXPERIMENTAL

2.1. SYNTHESIS OF THE CMCHT/PAMAM NANOPARTICLES

Carboxymethylchitosan with a degree of deacetylation of 80% and degree of substitution of 47% was synthesized by a chemical modification route of chitin (Sigma, Germany) as described by Chen et al. [18]. Starburst® poly(amidoamine)-carboxylic terminated dendrimers, PAMAM-CT (generation 1.5, 20% (w/v) methanolic solution) with an ethylenediamine core were purchased from Aldrich. Carboxymethylchitosan/poly(amidoamine) dendrimer, CMCht/PAMAM dendrimer nanoparticles were prepared in a stepwise manner as follows: (i) increasing the generation of the PAMAM-CT (G 1.5), (ii) obtaining a PAMAM-methyl ester terminated dendrimer, (iii) reaction of PAMAM and CMCht, i.e. the reaction goes through a condensation reaction between the methyl ester and amine groups [19], and (iv) modifying the methyl ester groups that do not react to carboxylic ones in the CMCht/PAMAM dendrimer, followed by precipitation. Firstly, the increase of the dendrimers' generation was carried out as follows: an appropriate volume of PAMAM-CT (G 1.5) in methanol was transferred to a 2 mL volumetric flask and the solvent evaporated off under nitrogen gas, and the traces dried under vacuum in order to completely remove the methanol. The starting compound was re-dissolved in ultra-pure water to give a final concentration of 10 $mg.mL^{-1}$ and the pH was adjusted to 6.5 with dilute hydrochloric acid solution, HCl (Riedel de-Haen, Germany) solution. Then, 1-ethyl-3(3-dimethylaminopropyl) carbodiimide hydrochloride, EDC (Fluka, Slovakia) was added to the solution at a molar ratio sufficient to modify the carboxylate residue of the dendrimers and kept under agitation for 30 min at room temperature. Ethylenediamine, EDA (Sigma, Germany) was added to the solution at a molar ratio equal to that of EDC and let react for at least 4 hrs. After this period the exceeding EDC was removed by dialysis (cellulose tubing, benzoylated for separating compounds with a molecular weight of ≤ 1,200 from compounds with a molecular weight > 2,000, Sigma, Germany). The compound was used without

purification in the next step. After preparing the PAMAM-amine terminated compound, PAMAM-AT, an exhaustive alkylation of primary amines (Michael addition) was carried [20]. An appropriate volume of PAMAM-AT (~8.4 mmol) was transferred to a 50 mL flask and 30 mL of methanol (Sigma, Germany), and 1.14 mL of methyl methacrylate (~12.6 mmol) (Fluka, Germany) were added. The solution was kept under agitation in a water bath for 24 hrs at 50ºC, to obtain the compound (PAMAM-methyl ester). The carboxymethylchitosan (100 mg) dissolved in ultrapure water (10 mL) was mixed with the latter obtained PAMAM-methyl ester dendrimer (50 mg), which was previously dissolved in a 20/80 water/methanol (v/v) solution. The final solution was diluted by adding 30 mL of methanol and kept under agitation for 72 hrs. After this period, CMCht/PAMAM dendrimer with carboxylic-terminated groups were obtained as described elsewhere [19]. CMCht/PAMAM dendrimer nanoparticles were then precipitated after addition of an appropriate volume of a saturated sodium carbonate, Na_2CO_3 (Aldrich, Germany) solution and acetone (Pronalab, Portugal). On the other hand CMCht/PAMAM dendrimer nanoparticles were mixed with a dexamethasone solution with a final concentration of 5 x 10^{-4} M under agitation (w/w). The mixture was then added to the precipitation media consisting of a saturated sodium carbonate, Na_2CO_3 (Aldrich, Germany) and acetone solution, under vigorous agitation. Precipitates were collected by filtration and dispersed in ultrapure water for dialysis during the period of 48 hrs. Both CMCht/PAMAM and dexamethasone-loaded CMCht/PAMAM dendrimer nanoparticles were obtained by freezing the solution at -80ºC and freeze-drying (Telstar-Cryodos -80, Spain) up to 4 d to complete remove the solvent. It is noteworthy that the CMCht/PAMAM dendrimer nanoparticles are water-soluble at physiological pH.

2.2. Labeling of CMCht/PAMAM dendrimer nanoparticles with FITC

A 10 mg.mL^{-1} fluorescein isothiocyanate, FITC (Sigma, Germany) solution was prepared in dimethyl sulfoxide, DMSO anhydrous (Riedel de-Haen) (dark conditions). Conjugates of CMCht/PAMAM-FITC were prepared by covalently bonding the amine group of carboxymethylchitosan and the isothyocianate group of FITC (thiourea bond). Firstly, a 10 mg.mL^{-1} CMCht/PAMAM dendrimer nanoparticles solution was prepared in a carbonate-bicarbonate coupling buffer of pH 9.2. Then, 50 μL of the FITC/DMSO solution was added per each mL of CMCht/PAMAM dendrimer nanoparticles buffered solution under agitation, and kept in dark at 4ºC for 8 hrs. The FITC-labeled CMCht/PAMAM dendrimer nanoparticles solution was dialyzed against ultra-pure water in order to remove unlinked FITC for 24 hrs and filtered (pore size < 220 nm) in sterile and dark conditions. The final product was obtained as an orange powder after freeze-drying. The labelling efficiency was investigated by Fourier-transform infra-red, FTIR

spectroscopy (Perkin-Elmer 1600 series equipment, USA) and UV-VIS spectrophotometry (NanoDrop™ ND-1000; NanoDrop Technologies, USA).

2.3. CHARACTERIZATION OF THE CMCHT/PAMAM DENDRIMER NANOPARTICLES

Fourier transform infra-red (FTIR) analyses were performed by means of preparing transparent potassium bromide pellets containing the samples and using a Perkin-Elmer spectroscope (Perkin-Elmer 1600 series equipment, UK).

The morphology of the nanoparticles was investigated using atomic force microscopy (AFM). The lyophilized CMCht/PAMAM dendrimer nanoparticles were dispersed in ultrapure water to obtain a solution with final concentration of 1 $mg.mL^{-1}$, and then 20 μL was placed over a 9.9 mm mica disc (Agar Scientific, England) and blown dried with nitrogen gas for subsequent characterization. The samples were analysed using the Tapping Mode™ with a MultiMode AFM connected to a NanoScope III controller, both from Veeco, USA, with non-contact silicon nanoprobes (ca 300 kHz) from Nanosensors, Switzerland. All images were plane-fitted using the third degree-flatten procedure included in the NanoScope software version 4.43r8. The particle size distribution was determined with the same software. The morphology and size of the particles was further analysed by transmission electron microscopy, TEM (Philips CM-12, FEI Company, The Netherlands, equipped with a MEGA VIEW-II DOCU camera and Image Software Analyzer SIS NT DOCU). The nanoparticles were stained with 2% of phosphotungstic acid and placed on copper grids for further observation. The size of the CMCht/PAMAM dendrimer nanoparticles was also measured in a particle size analyzer (Zetasizer Nano ZS, Malvern Instruments, UK).

2.4. *IN VITRO* CYTOTOXICITY SCREENING OF THE CMCHT/PAMAM DENDRIMER NANOPARTICLES

A luminescent cell viability assay based on the adenosine triphosphate (ATP) quantification was performed by exposing Rat Bone Marrow Stromal Cells (RBMSCs) to CMCht/PAMAM dendrimer nanoparticles. Prior to the cell culture studies CMCht, PAMAM-CT G 1.5, and CMCht/PAMAM nanoparticles were sterilized under an ethylene oxide gas atmosphere. RBMSCs were isolated from femora of 7 week-old male Fischer 344/N rats (SLC Inc. Japan), and expanded in T75 cm^2 culture flasks in the presence of Eagle's minimum essential medium (MEM, Nacalai Tesque, Japan) with 15% fetal bovine serum, FBS (JRH Biosciences, USA) and 1 % antibiotic-antimycotic (Nacalai Tesque, Japan) solution. The animals were sacrificed by administrating an excess of anesthesia, in accordance to the Ethics Committee at the Tissue Engineering Research Center (Amagasaki, Japan). After reaching

confluency, the cells (passage 1, P1) were released from substratum and centrifuged at 900 rpm for 5 min. The supernatant was aspirated and cells re-suspended with 10 mL of complete culture medium. Cell concentration was determined using an automatic cell counter (Cell Counter Sysmex F-520, Japan). Viability of the RBMSCs was also analyzed with a NucleoCounter (Chemometec, Denmark), using prior seeding as described elsewhere [21]. RBMSCs were seeded (sub-cultured) to each well of a 96-well TCPS plate at a cell density of 5 x 10^3 cells.mL^{-1}. A solution of CMCht/PAMAM dendrimer nanoparticles at a concentration of 10 mg.mL^{-1} was prepared in a complete culture medium. Serial dilutions (1, 0.1, 0.01 mg.mL^{-1}) were further prepared using the complete culture medium. Possible changes in the osmolality of the culture media were investigated using an automatic cryoscopic osmometer (OSMOMAT O 30-D, Gonotec, Germany). After a period of 24 hrs, the culture medium was changed by the respective serial dilutions and the cells cultured under standard culture conditions for 1 and 3 d. A latex rubber extract was used as the positive control for cellular death. Finally, the ATP content was measured by means of performing a CellTiter-Glo® luminescent cell viability assay, following the protocol provided by the supplier (Promega Corporation, USA). Luminescence was measured using opaque-walled multi-well plate in a microplate reader (Wallac ARVOsx 1420, Perkin-Elmer Life and Analytical Sciences, USA). Results were analyzed for statistical significance using Student's *t*-test with the JMP 5.0.1 software (SAS Institute, Cary, N.C.).

2.5. Investigation of the internalization efficiency using SaOS-2 cells and RBMSCs under fluorescence microscopy and FACS analysis

Human osteoblast-like cells (SaOs-2 cells, ECACC, UK) were maintained in T75 cm^2 culture flasks, cultured with basic culture medium - DMEM supplemented with 10% FBS and 1% A/B, and passaged after reaching confluence. A cell suspension was prepared and seeded on TCPS coverslips (Sarstedt Inc., USA) in 24-well plates (1 x 10^4 cells.well^{-1}) and cultured in standard culture conditions for 24 hrs. The internalization of CMCht/PAMAM dendrimer nanoparticles by SaOs-2 cells was assessed after 3, 12, 24 hrs, and 14 d. After each time point cells on the TCPS coverslips were fixed with 4% formalin (Sigma, Germany) and the nuclei stained with 4,6-diamidino-2-phenylindole, dilactate, DAPI blue (100 ng.mL^{-1}; Molecular Probes), for assessing possible cell morphological changes. Fluorescence was protected by using an antifade agent (ProLong® Antifade Kit, Invitrogen, USA), following the supplier procedure and cells were observed under the fluorescence microscope (AxioImager Z1, Zeiss Inc., Germany).

RBMSCs were isolated from rats and expanded until reaching 80% of confluency. The RBMSCs (P1) were trypsinized and transferred to a 6-well (1 x 10^5 cells.well^{-1}) and a TCPS coverslips in 24-well TCPS plates (2 x 10^4 cells.well^{-1}) for analysis under FACS and fluorescence microscopy, respectively. For fluorescence microscopy, RBMSCs were cultured in a MEM complete culture medium containing the 0.1 mg.mL^{-1} FITC-labeled CMCht/PAMAM dendrimer nanoparticles for a period of 12 hrs until 14 d. For FACS analysis RBMSCs were cultured in the presence of 0.01 mg.mL^{-1} FITC-labeled CMCht/PAMAM dendrimer nanoparticles. All experiments were carried out in triplicate. The samples for fluorescence microscopy were prepared as follows: each well was washed with 1 mL of PBS, and cells fixed with 4% formalin (Nacalai Tesque, Japan) for 10 min at 4ºC followed by washing each well twice with PBS. After that cells were incubated with 0.5 mL of PBS containing Texas Red®-X phalloidin (Molecular Probes, Invitrogen, USA) and Hoechst 33258 (Invitrogen, USA) for staining the actin filaments of the cytoskeleton and nuclei of cells, respectively. The protocols provided by the supplier were followed with few modifications. The permeabilization of cells with Triton® X-100 was not carried out to avoid any undesired effect over the integrity of cells nuclei. TCPS coverslips were washed once with PBS and fluorescence protected using the ProLong® antifade kit. The specimens were observed under a fluorescence microscope (Olympus IX70, Olympus Co. Ltd., Japan). FACS analysis was carried out as follows: each well of the 6-well plate was washed with 2 mL of PBS. Then, PBS was aspirated and cells released from substratum as described above. Afterwards, it was added to each well 3.5 mL of MEM complete medium and samples transferred to a 15 mL Falcon. After centrifugation at 900 rpm for 5 min, cells were re-suspended in 0.5 mL of complete culture medium and passed through cell strainers [22]. Afterwards, 1 μL propidium iodide (Nacalai Tesque, Japan) was added to each sample for determining the number of live cells. After this step, cells were loaded in a FACSCalibur flow cytometer (BD Biosciences Imunocytometry Systems, USA) and analyzed with a minimum of 10,000 events counting. Calibrite beads three-color kit (BD CaliBRITE™ beads, USA) was used to adjust the equipment instrument settings before samples are run on the flow cytometer. Finally, the fluorescence-activated cell sorting (FACS) data was treated using the FLOWJO software.

2.6. Investigation of the effect of colchicine and apyrase on the internalization efficiency of FITC-labeled CMCht/PAMAM dendrimer nanoparticles by RBMSCs

A cell suspension of RBMSCs (P1) in MEM complete culture medium was transferred to a 6-well (1 x 10^5 cells.well^{-1}) and TCPS coverslips in 24-well TCPS plates (2 x 10^4 cells.well^{-1}) for analysis under FACS and fluorescence microscopy, respectively. Stock solutions of 10 U.mL^{-1} apyrase (Nacalai

Tesque, Japan) and 10 μM colchicine (Nacalai Tesque, Japan) were prepared in a phosphate-buffered saline solution. Cells were incubated in standard culture conditions and after 24 hrs, the culture medium was replaced by a different complete culture medium containing the FITC-labeled CMCht/PAMAM dendrimer nanoparticles (0.01 $mg.mL^{-1}$ and 0.1 $mg.mL^{-1}$), and in the presence of 1 μM colchicine and 0.1 $U.mL^{-1}$ apyrase or both, for a period of 12 hrs to 14 d. Controls for internalization were performed by culturing RBMSCs in complete culture medium and in the presence of both colchicine and apyrase. All experiments were carried out in triplicate. After each time period, specimens were prepared as described previously. The tendency of FITC-labeled CMCht/PAMAM dendrimer nanoparticles to be internalized by RBMSCs was investigated by means of FACS analysis.

2.7. Investigation of the dexamethasone release from CMCht/PAMAM dendrimer nanoparticles

The amounts of Dex from nanoparticles were measured using an HPLC (ASI-Knauer, Germany) with an UV detector set at 246 nm. The mobile phase consisted of acetonitrile:acetate buffer (2 mM, pH 4.8-adjusted with glacial acetic acid) (50:50 v/v) at flow-rate of 1 $mL.min^{-1}$. In brief, Dex release was studied after dissolution of 10 mg of Dex-loaded CMCht/PAMAM dendrimer nanoparticles in 10 mL of phosphate buffer saline, PBS (pH 7.4, Sigma, USA) solution in the absence or presence of 15% FBS. Sodium azide 0.01% (wt/v, Merck, Germany) was added to the buffer. The *in vitro* release studies were performed at 37°C and 60 rpm for times ranging from 1 h until 7 d. At set time intervals, 1 mL of sample was taken for analysis and the same volume replaced by the respective buffer solution. Prior analysis, samples were centrifuged at 2,000 rpm for 10 min. Samples were analyzed by means of preparing a solution with 1:1 (sample:acetonitrile:acetate buffer, 50:25:25 v/v). A Eurospher 100 C-18 analytical column (ASI-Knauer, Germany) was used. The retention time of Dex was 4 min. A calibration curve was obtained following the method described by Sun et al. [23]. Results were expressed as an average ± standard deviation, n=6.

2.8. Evaluation of osteogenic differentiation of the RBMSCs cultured in the presence of CMCht/PAMAM dendrimer nanoparticles loaded with dexamethasone, *in vitro*

RBMSCs were isolated from F344/N rats and expanded as described above. RBMSCs (P1) were cultured in a TCPS 24-well plate at a cell density of 2×10^4 $cells.well^{-1}$, and cultured in a complete MEM medium for 24 hrs. After that time, culture medium was replaced by the different culture media, and RBMSCs cultured for times up to 14 d. The effect of the concentration of CMCht/PAMAM dendrimer nanoparticles loaded with dexamethasone on the RBMSCs osteogenic differentiation was investigated.

Dexamethasone-loaded CMCht/PAMAM dendrimer nanoparticles were dissolved in MEM medium supplemented with 0.28 mM ascorbic acid (Wako Pure Chemicals, Japan) and 10 mM β-glycerophosphate (Sigma, USA) at a final concentration of 0.01 and 1 $mg.mL^{-1}$. RBMSCS were also cultured in a complete MEM medium, complete MEM medium containing 1 $mg.mL^{-1}$ of CMCht/PAMAM dendrimer nanoparticles, and complete MEM medium containing 10 mM β-glycerophosphate (negative controls). Complete MEM medium supplemented with 10^{-8} M dexamethasone, 0.28 mM ascorbic acid and 10 mM β-glycerophosphate was used as the positive control for osteogenic differentiation. Culture media were changed every 2-3 d. All experiments were carried out 3 times using a minimum of 4 replicates per experimental condition.

Alizarin red S staining was performed to investigate possible calcium deposition after 14 d of culturing. RBMSCs were washed twice with PBS and fixed with 95% ethanol for 15 min. The fixed cells were then washed once with PBS and stained with 5 $mg.mL^{-1}$ Alizarin red S in PBS for 5 min at room temperature. Then, it followed a washing step with ultra-pure water and mounting with Crystal/Mount™ (BiomedaCorporation, USA) for observation under the phase contrast microscope (Olympus CK40, Olympus Co. Ltd., Japan).

For the ALP staining the cells were washed twice the wells with PBS, after each culture period. Cells were fixed with 4% paraformaldehyde (Nacalai Tesque, Japan) for 15 min at 4ºC and then washed twice with AMP buffer (56 mM of 2-amino-2methyl-1,3-propanediol in ultrapure water, pH 9.9). It followed the soaking step with staining solution 0.5 mg naphtol AS-MX phosphate and 0.5 mg fast red violet LB salt per mL, in AMP buffer. Cells were incubated for 10 minutes at room temperature, washed with PBS and mounted (BiomedaCorporation, USA) for observation under the phase contrast microscope.

DNA quantification was performed using Hoechst 33258 (Nacalai Tesque, Japan), as previously described elsewhere [24].

Alkaline phosphatase was measured to evaluate osteoblast differentiation. The samples used for DNA quantification assay were used to determine ALP levels. Prior to analysis the samples were centrifuged at 10,000 rpm for 1 min at 4°C. To each well of a 96-well plate was added an aliquot of supernatant and p-nytrophenyl phosphate substrate (ZYMED® Laboratories, Invitrogen, USA). The plate was then incubated in the dark for 30 min at 37ºC. After the incubation period, the reaction was stopped with 1 M NaOH (Panreac). Standards were prepared with p-nytrophenol, pNP. Triplicates were made for each sample and standard. Absorbance was read at 405 nm (Wallac ARVOsx 1420, Perkin-Elmer Life and Analytical Sciences, USA), and sample concentrations were read off from the standard graph. Enzyme activity was expressed either as nmol of pNP released/well/30 min and normalized by DNA content.

The samples used for ALP activity were treated with a 20% formic acid solution immediately after concluding the assay and stored at 4°C for 2-3 d. Then, samples were centrifuged at 3,000 rpm for 10 min at 4°C and the supernatant passed through a Sephadex™ G-25 column (GE healthcare, Sweden) for desalting. The filtered samples were concentrated in a SPD SpeedVac® equipment attached to a UV Vacuum System (Thermo Electron Corporation, USA), prior to osteocalcin quantification. Finally, the osteocalcin content was determined by performing an Enzyme-linked immunosorbent assay, and using a Rat Osteocalcin EIA kit (N° BT-460, Biomedical Technologies Inc., USA). The experimental procedure was carried out following the instructions provided by the supplier. A 100 ng.mL^{-1} standard solution of human osteocalcin was used to construct the standard curve. Data was read off from the standard graph and expressed as ng of deposited osteocalcin per μg of DNA.

3. RESULTS AND DISCUSSION

3.1. CHARACTERIZATION OF THE CMCHT/PAMAM DENDRIMER NANOPARTICLES

Figure 1 shows FTIR spectra of the PAMAM-CT dendrimers, CMCht and CMCht/PAMAM dendrimer nanoparticles. The results suggest that CMCht was successfully synthesized, as evidenced by the presence of characteristic absorption bands of the carboxyl group (▲) at 1593 cm^{-1} and (◊) 1420 cm^{-1} (υas COO^- and υs COO^-). The characterization of molecular levels conjugate obtained by coupling reaction of CMCht with PAMAM dendrimer was investigated by FTIR analysis. We were able to detect characteristic absorption bands of groups attributed to both CMCht and PAMAM dendrimer structure in the CMCht/PAMAM dendrimer nanoparticles. There is an increase in intensity of the bands at 1570 and 1200 cm^{-1} (□) attributed to the Amide II and C-N stretching vibrations, which is evidence that substituted amines are present and there is possible chemical bonding between the CMCht and PAMAM. The effective degree of conjugation, measured by ^{1}H and ^{13}C NMR will be reported in a future work.

Some studies have been shown that PAMAM are hydrolytically degradable due to their amide skeletons, and hydrolysis occurs slowly at physiological temperatures [25]. On the other hand, chitosan and its derivatives have been shown to possess bonds that are enzyme substrates [26]. Thus, the surface engineering of dendrimers as proposed herein may enable obtain macromolecules with a different hydrolytic degradability, releasing also nontoxic products. As a consequence, the nanoparticles may show entirely new drug delivery profiles and elimination rates. In preliminary degradation studies, a decrease was observed in the intensity of the band at 1655-1630 cm^{-1} (*), which corresponds to amide I (n C=O) of the PAMAM dendrimer (see supporting information). Decreases were also detected in the

band at 1200 cm^{-1} (□) that corresponds to the C-N stretching vibration of the CMCht/PAMAM dendrimer nanoparticles, and also those at 1155 and 900 cm^{-1} (ϕ) attributed to the saccharine structure of CMCht. On the other hand, increased intensities of peaks attributed to the CH stretching bands (x) and N-H stretching vibrations (+) are observed. These preliminary data support the idea that the CMCht/PAMAM dendrimer nanoparticles are hydrolytically degradable at physiological temperature and pH, due to dissociation of their amide and glycosidic linkages. It has been shown that the architecture of nanoparticles strongly dictates the mechanisms and kinetics by which they are internalized by cells [27-28].

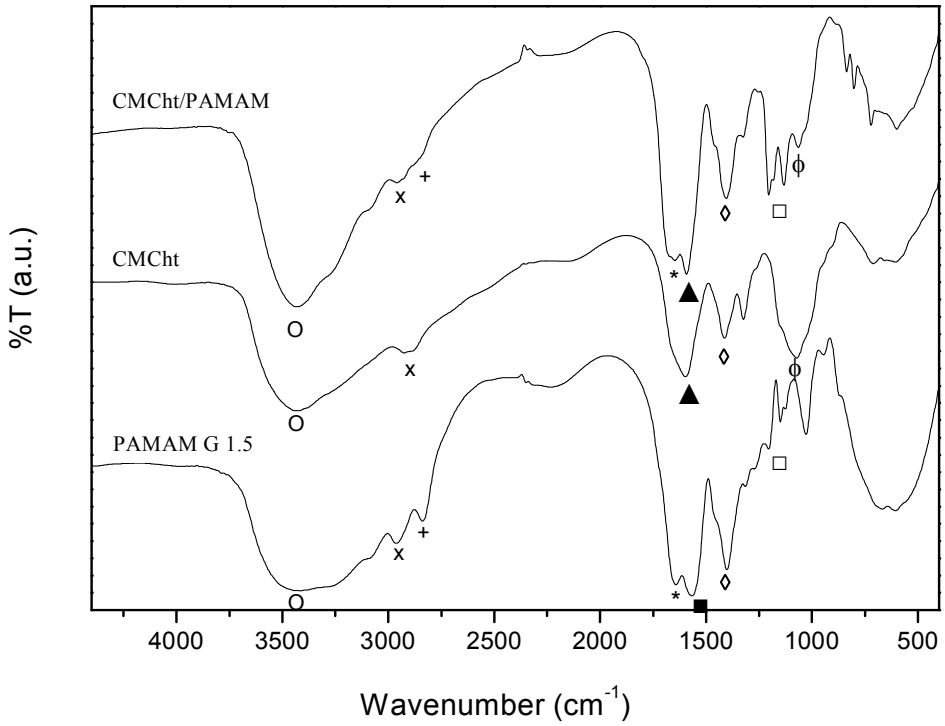

Figure 1. FTIR spectra of: Poly(amidoamine) dendrimer of generation 1.5 (PAMAM G1.5), carboxymethylchitosan (CMCht), and CMCht/PAMAM dendrimer nanoparticles. (O) 3450 cm^{-1} corresponds to –OH group; (x) 2996-2882 cm^{-1} is attributed to CH stretching bands; (+) 2860-2800 cm^{-1} corresponds to N-H stretching vibration; (*) 1655-1630 cm^{-1} corresponds to Amide I (n C=O); (▲) 1570 cm^{-1} corresponds to Amide II (n C-N + d NH); (■) 1556 cm^{-1} is attributed to C-N stretching vibration (C-N bond inside the core); (◊) 1420 cm^{-1} corresponds to symmetric (s) stretching mode of COO^-, (□) 1200 cm^{-1} corresponds to C-N stretching vibration, and (ϕ) 1155 and 900 cm^{-1} corresponds to saccharine structure.

Gao et al. [27] have recently demonstrated that the optimal cellular uptake of particles by endocytosis occurs with particles having diameters of ~50 nm. On the other hand, the mechanism of internalization of particles with larger diameters occurs preferentially by phagocytosis [27]. An AFM image of the CMCht/PAMAM nanoparticles is shown in Figure 2A. AFM characterization clearly demonstrated that the synthesized macromolecules consistently exhibit nanosphere-like shapes. It was also found that the CMCht/PAMAM dendrimer nanoparticles could be uniformly dispersed on a substrate by spreading a solution of dendronized polymers on a freshly cleaved mica surface and drying under a nitrogen gas stream. The results of a morphometric analysis by AFM indicated that the nanoparticles have an average diameter of 26 nm (dry state) and average total area of ~2123 nm^2. These data were corroborated by TEM observations. In Figures 2B-C it is possible to visualize the CMCht/PAMAM dendrimer nanoparticles in a greater detail. Additionally, it is also observed that the nanoparticles can form aggregates (Figure 2D).

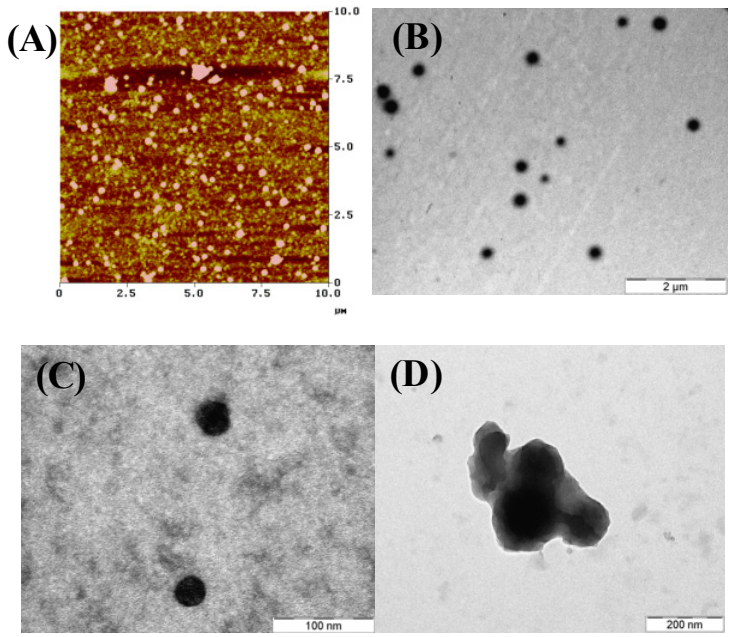

Figure 2. Representative A) Atomic force microscopy (AFM) and B-D) Transmission electron microscopy (TEM) images showing the morphology of the CMCht/PAMAM dendrimer nanoparticles. A) The AFM images show a uniform nanoparticle distribution, where it is also possible to observe some aggregated nanoparticles. B) Low-magnification TEM image of the CMCht/PAMAM dendrimer nanoparticles. C) High-magnification TEM image of the CMCht/PAMAM dendrimer nanoparticles (~40 nm). D) TEM image of aggregated CMCht/PAMAM dendrimer nanoparticles (~250 nm).

Carboxymethylchitosan with a degree of deacetylation (DA) of 80% and degree of substitution of 47% was used in the synthesis of the CMCht/PAMAM nanoparticles. Chitosan with high degree of acetylation is insoluble in water because the acetylated units can be involved in intramolecular hydrogen linkages, which in part explain the insolubility of chitosan in water [22]. Nevertheless, the modifications of amino groups with carboxylic-ones allowed us to obtain CMCht, a water soluble chitosan derivate. Using potentiometric titration it was possible to verify that the precipitation of CMCht occurred preferentially in a pH range from ~2-6 (data not shown). Thus, CMCht possesses protonated amino groups at pH 2, and negative COO^- ions at physiological pH. In other words, at physiological pH the CMCht behaves as a weak polyanionic polyelectrolyte, i.e. the amino groups are not protonated and most of carboxyl groups are not dissociated. Interactions between non-covalent free carboxyl groups of CMCht and/or PAMAM-CT dendrimer and amino groups of other CMCht particles are possible to occur, which may explain the formation of nanoparticle aggregates. It is noteworthy that Zhu et al. [30] proposed the use of CMCht aggregates for the effective loading and controlled release of drugs. On the other hand, during the synthesis of CMCht/PAMAM dendrimers nanoparticles there are several binding points available, onto which possible cross-linking reactions may occur. This may also explain the formation of nanoparticle aggregations. Nanoparticles aggregation might be prevented or minimized by optimizing the concentrations of both CMCht and PAMAM.

Figure 3 shows the data obtained from the particle size distribution analysis of the different nanoparticles in solution. Figure 3A shows the low dispersivity of the PAMAM-CT (G 1.5) dendrimers used in the synthesis of CMCht/PAMAM dendrimer nanoparticles. These nanoparticles have a diameter of 2 $\pm$ 1 nm, which is in agreement with previously reported data [31]. After the synthesis of the CMCht/PAMAM dendrimer nanoparticles, three kinds of particulate structures could be detected with sizes of approximately 6 $\pm$ 2 nm, 45 $\pm$ 15 nm and 250 $\pm$ 100 nm (Figure 3B). The first peak has an intensity of 5.5% and should correspond to the modified dendrimer. The second (36.2%) corresponds to the isolated CMCht/PAMAM dendrimer nanoparticles, and the third (58.2%) to the aggregated nanoparticles. Mammalian cells are sensitive to the osmolality of the ambient medium, and variations on this property may affect cell morphology and cell growth. It is known that most cell culture mediums are produced to have a osmolality in the range of 270-330 $mOsm.kg^{-1}$, since these values are acceptable for most cells [32]. In this study, MEM medium supplemented with FBS and A/B (standard) with an osmolality of 310 ± 2 $mOsm.kg^{-1}$ was used. The effect of the CMCht/PAMAM dendrimer nanoparticles on the osmolality of culture media was also investigated, since the addition of medium concentrates

may increase the osmolality of the media. The osmolality of the culture medium containing nanoparticles at a concentration ranging from 0.01 to 1 mg.mL^{-1} was assessed to be 315 ± 2 mOsm.kg^{-1}. It was observed that varying the concentration of the CMCht/PAMAM dendrimer nanoparticles did not significantly change the osmolality of media, which indicates that the cells are not cultured under osmotic stress.

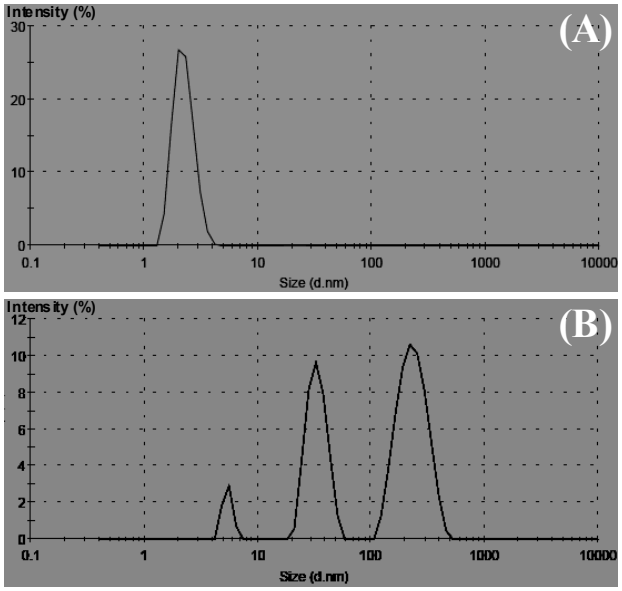

Figure 3. Particle size distribution of: A) PAMAM G 1.5, and B) CMCht/PAMAM dendrimer nanoparticles.

3.2. CYTOTOXICITY SCREENING

The cell viability in this work was preliminarily screened by performing a MTT test, which is a quite reliable method for assessing cytotoxicity [33,34]. A L929 fibroblast cell line was exposed to different concentrations of CMCht/PAMAM dendrimer nanoparticles over a period of 24 hrs (see supporting information). Two polymers, water-soluble carboxymethylchitosan (linear polymer) and PAMAM-CT G1.5 (spherical polymer), were selected for a comparative study considering the fact that biocompatibility is thought to be influenced by various characteristics including the polymer molecular weight, concentration, structure (linear, branched, cross-linked), surface charge density and flexibility [33,35-37]. Results indicate that dendronized polymers at concentrations of 0.01 mg.mL^{-1}, and 0.1 mg.mL^{-1} do not induce any toxicity for the investigated culturing times. However, for a concentration of 1 mg.mL^{-1}, after 24 hrs the viability of the L929 cells decreased in the presence of CMCht/PAMAM dendrimer nanoparticles, which suggests moderate cytotoxic effects. These results agree with previous

studies where the concentration was reported to affect the biocompatibility of polymers to a certain extent [33,37]. Moreover, our findings are also consistent with previous ones indicating that high molecular weight structures may exhibit more serious cytotoxic effects [33]. However, such trends are meaningful only when the same type of polymer is compared.

Figure 4 shows the luminescent cell viability assay that was carried out after culturing the RBMSCs in the presence of different concentrations of CMCht/PAMAM dendrimer nanoparticles for 24 and 72 hrs. This assay is a homogeneous method based on the quantification of ATP and thus a more feasible test for assessing the cytotoxicity of materials, since it signals the presence of metabolically active cells. The luminescence signal is proportional to the amount of ATP, which in turn is directly proportional to the number of cells in the culture medium. Statistically, it is possible to observe that increasing concentrations of CMCht/PAMAM dendrimer nanoparticles did not affect the viability (ATP content) of RBMSCs, after 24 hrs ($p > 0.05$).

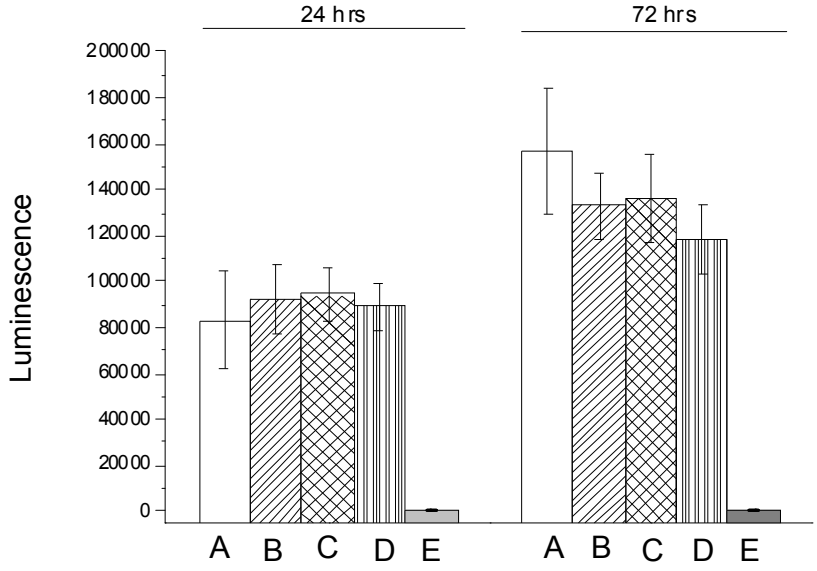

Figure 4. Viable RBMSCs after incubation in a culture medium with different concentrations of CMCht/PAMAM dendrimer nanoparticles for the period of 24 and 72 hrs. Cell number correlates with luminescence. A) MEM medium (negative control); B) CMCht/PAMAM dendrimer nanoparticles 0.01 $mg.mL^{-1}$; C) CMCht/PAMAM dendrimer nanoparticles 0.1 $mg.mL^{-1}$; D) CMCht/PAMAM dendrimer nanoparticles 1 $mg.mL^{-1}$, and E) MEM media containing an latex extract (positive control) ($p< 0.0001$). Results expressed as an average ± standard deviation, n=12. (Data were examined at a level of significance of $p < 0.05$).

When culturing the RBMSCs in a MEM medium and in the presence of CMCht/PAMAM dendrimer nanoparticles, a statistical increase in viability was observed from 24 to 72 hrs ($p < 0.0001$). A statistical difference on the viability of RBMSCs was not seen when culturing RBMSCs in the presence of MEM and CMCht/PAMAM dendrimer nanoparticles in the range of concentrations between 0.01 and 0.1 $mg.mL^{-1}$, after 72 hrs ($p > 0.05$). However, the viability of RBMSCs decreased in 8.5% when culturing in the presence of 1 $mg.mL^{-1}$ CMCht/PAMAM dendrimer nanoparticles ($p < 0.05$) as compared to control. The latex extracts (positive control) have shown a high cytotoxic effect over RBMSCs as seen by the low luminescence values after 24 and 72 hrs. These results demonstrate that RBMSCs remain viable in the presence of CMCht/PAMAM dendrimer nanoparticles at concentrations < 1 $mg.mL^{-1}$. Similar data was observed on the viability of L929 cells, which provides further evidence of the low cytotoxic effects of the CMCht/PAMAM dendrimer nanoparticles in the range of concentrations < 1 $mg.mL^{-1}$.

3.3. Internalization efficiency of the CMCht/PAMAM dendrimer nanoparticles

Several studies [5,9,38,39] have been performed to clarify the entry and retention mechanisms of nanoparticles on mammalian cells as well as to investigate cells death [40]. For instance, it has been reported [5] that the cationic surface charge of particles is responsible for their interactions with the anionic glycoproteins and phospholipids of the cell membrane surface, possibilitating the internalization. In the present case, it is expected that these types of interactions are responsible for the entry of CMCht/PAMAM dendrimer nanoparticles into the cell cytosol, either by passive transport caused through perturbations of the membrane or by endocytosis [5]. After being trapped within the endosome, the nanoparticles must be released into the cytosol before being subjected to acidic and/or enzymatic degradation. Nevertheless, due to the presence of protonated residues in the chain of the CMCht, which has a buffer capacity, it is expected that these nanoparticles can retard the degradation caused by acidification or enzymatic degradation within the endosomes. Theoretically, when loaded with drugs or DNA this type of nanocarriers may increase the availability of drugs inside the cells or the transfection efficiency. In this study, the internalization and intracellular end-condition of CMCht/PAMAM dendrimer nanoparticles were investigated by grafting a fluorescent label probe (FITC). This study was firstly performed using a SaOs-2 cell line and later on RBMSCs. Figure 5 shows the fluorescence microscopy images of SaOs-2 cells cultured in the presence of FITC-labeled CMCht/PAMAM dendrimer nanoparticles. The nanoparticles tested in this experiment consisted of the fraction of the total with size < 220 nm, which was easily obtained by a filtration technique. It is apparent that CMCht/PAMAM dendrimer nanoparticles (green) were present at the SaOs-2 cells membrane walls only in low numbers

after 3 hrs (white arrows), but in increasing amounts after a period of 12 hrs (Figures 5A-B). However, after 24 hrs it is clearly seen that CMCht/PAMAM dendrimer nanoparticles were internalized and widely distributed in the cytoplasm of SaOs-2 cells (Figure 5C). Moreover, there is also evidence of the presence of nanoparticles in the cell nuclei, as observed by the colocalization of the nuclei marker (blue) and FITC fluorescence (green). Cells continued to internalize the CMCht/PAMAM dendrimer nanoparticles (higher fluorescent signals) when cultured for longer periods of time, retaining their proliferation rate and remaining viable (Figure 5D).

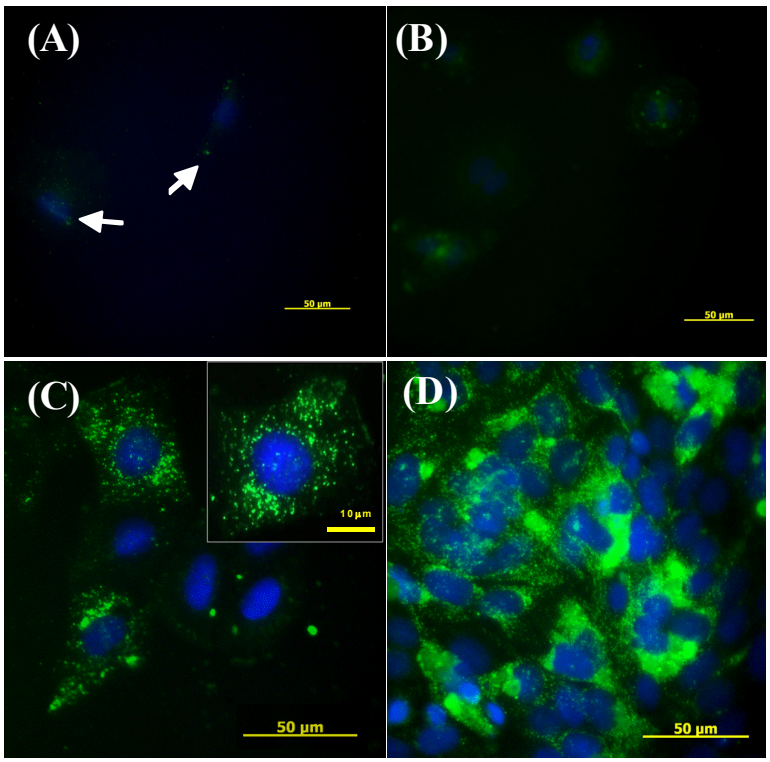

Figure 5. Fluorescence microscopy images of SaOs-2 cells after culturing in the presence of FITC-labeled CMCht/PAMAM dendrimer nanoparticles 1 mg.mL^{-1} (green) for: A) 3 hrs, B) 12 hrs, C) 24 hrs, and D) 14 d. Nuclear DNA was labeled with DAPI (blue).

A typical feature of apoptosis is the presence of chromatin condensation and nuclear fragmentation [35]. Apoptosis can be detected by nuclear morphology after staining with DAPI blue or Hoechst 33258, for example. In Figures 5C-D, it is seen that SaOs-2 exhibited a normal size and round nuclei with homogeneous chromatin. Microscopic observations during the course of cell culturing in the presence of FITC-labeled CMCht/PAMAM dendrimer nanoparticles showed no morphological changes or cellular senescence, which is a good indication of cell survival. On the other hand, significant cell death was

detected after 24 hrs for a culture of SaOs-2 cells in media containing FITC (control). These results also highlight the fact that the FITC-labeled CMCht/PAMAM dendrimer nanoparticles are quite stable, since their fluorescence was maintained over a period of 14 d. The fact that internalization of the nanoparticles was not well observed after 3 hrs can be attributed to the rather high detection limit of the fluorescence microscope. FACS analysis was performed towards circumventing this limitation. In this analysis, primary cultures and FITC-labeled CMCht/PAMAM dendrimer nanoparticles at a concentration of 0.01 mg.mL^{-1} were used. This concentration is impossible to detect by fluorescence microscopy and therefore makes a good test case for FACS.

Figure 6 shows the results of FACS analysis after culturing the RBMSCs in the presence of the FITC-labeled CMCht/PAMAM dendrimer nanoparticles for times up to 14 d. Flow-cytometry studies revealed increasing levels of fluorescence associated with cells after incubation of RBMSCs with CMCht/PAMAM dendrimer nanoparticles for the period of 12 hrs to 7 d. The present data show that nanoparticles were internalized with high efficiency by RBMSCs. The fraction of RBMSCs that internalized the nanoparticles reached 50.3% after 12 hrs and a maximum of 95.7% after 7 d of culturing (Table 1). Then, at day 14 a decrease of the internalization is detected which may be related to the fact that RBMSCs reach confluence around day 7. Moreover, the RBMSCs were stained with propidium iodide to quantify the fraction of live cells.

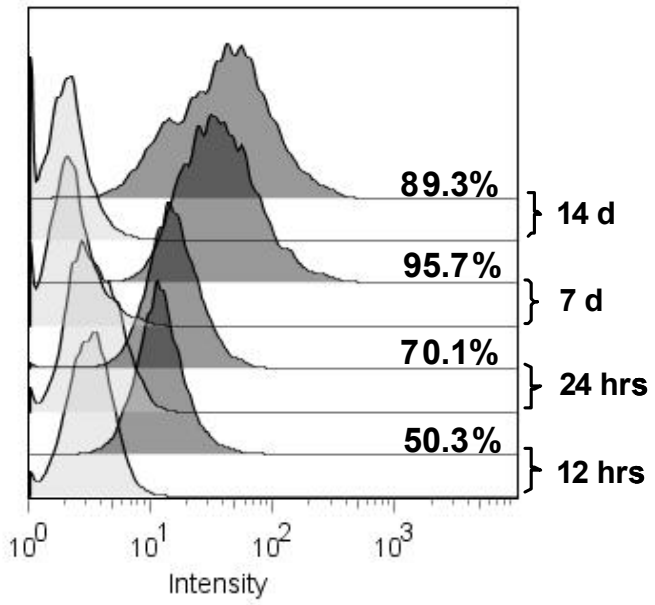

Figure 6. FACS data of live RBMSCs (% gated) after culturing in: MEM medium (light-grey peaks, control) and MEM medium with FITC-labeled dendrimer CMCht/PAMAM nanoparticles 0.01 mg.mL^{-1} (dark-grey peaks) for the period of 12 hrs, 24 hrs, 7 d and 14 d.

From Table 1, it is concluded that the fraction of live cells cultured in the presence of FITC-labeled CMCht/PAMAM dendrimer nanoparticles did not significantly differ from that of the control. This result also demonstrates the biocompatible nature of the FITC-labeled CMCht/PAMAM dendrimer nanoparticles.

Table 1. FACS data of the percentage of internalization of FITC-labeled CMCht/PAMAM dendrimer nanoparticles by the fraction of live RBMSCs, after the period of 12 hrs until 14 d. The percentage of live cells (stained with propidium iodide, PI method) was obtained from the analysis of a total number of 10,000 cells per sample.

Culture Conditions (medium)	% internalization (% gated)				% of live RBMSCs (PI stained)			
	12 hrs	24 hrs	7 d	14 d	12 hrs	24 hrs	7 d	14 d
FITC-labeled CMCht/PAMAM nanoparticles	50.3	70.1	95.7	89.3	96.0	93.7	75.4	62.6
MEM medium (control)	0.4	0.6	0.3	0.5	87.6	92.9	81.8	53.9

Fluorescence microscopy of RBMSCs cultured in the presence of FITC-labeled CMCht/PAMAM dendrimer nanoparticles corroborated the above-mentioned results of internalization studies carried out using a cell line, i.e. confirmed that the nanoparticles were internalized and widely distributed in the cytoplasm of RBMSCs (Figure 7). RBMSCs continued to internalize the nanoparticles (higher fluorescent signals) when cultured for longer periods of time. Additionally, RBMSCs were also stained with Texas-red phalloidin for observation of the cell cytoskeletons. This makes it possible to assess whether the presence of the FITC-labeled CMCht/PAMAM dendrimer nanoparticles affects the cytoskeleton. It is known that cell mutations involve rearrangements and morphological modifications [41]. From careful examinations it was concluded that no morphological changes could be detected compared to the control (data not shown). Interestingly, it appears that the FITC-labeled CMCht/PAMAM dendrimer nanoparticles are confined inside vesicular bodies resembling endosomes. This observation would support the idea that their transport may occur through an endocytotic transcellular pathway. As was also observed for SaOS-2 cells, there is evidence of the presence of nanoparticles in the RBMSCs nucleus.

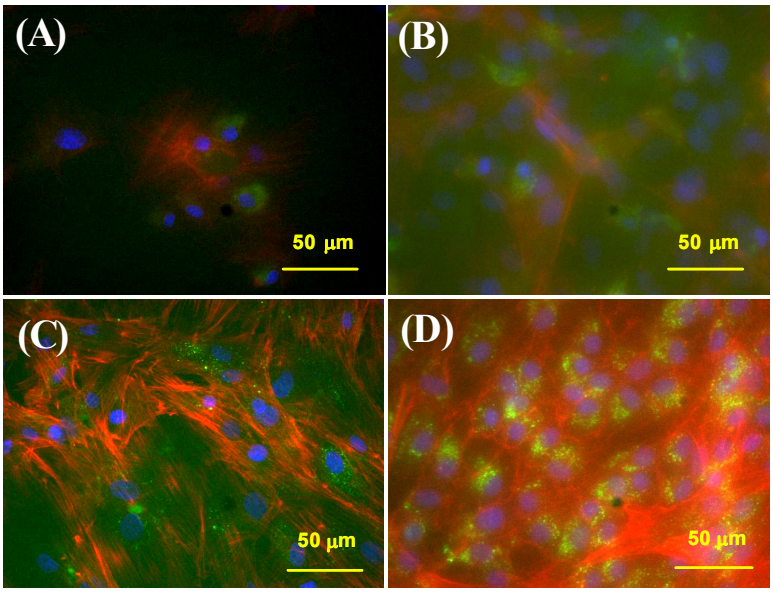

Figure 7. Fluorescence microscopy images of the RBMSCs cultured in the presence of FITC-labeled CMCht/PAMAM dendrimer nanoparticles 0.1 mg.mL^{-1} (green) for: A) 12 hrs, B) 24 hrs, C) 7 d and D) 14 d. Nuclear DNA and cytoskeleton were labeled with Hoechst 33258 (blue) and Texas-Red phalloidin (red), respectively.

3.4. Mechanism of CMCht/PAMAM dendrimer nanoparticles internalization

In order to gain further insights on the internalization mechanism, complementary experiments were carried out. The *in vitro* experimental design consisted of culturing the RBMSCs in the presence of FITC-labeled CMCht/PAMAM nanoparticles and restrictive endocytotic drugs such as colchicine [5]. It is known that colchicine binds tightly to microtubules causing microtubule depolymerisation, and by this mechanism affects endocytosis.

On the other hand, it has been reported [42,43] that the translocation of macromolecules larger than 10 nm from the cytoplasm to the nucleus is via active transport through the nuclear pore complex (NPC), whereas small molecules and proteins smaller than 20-40 kDa cross the 10 nm diameter channels of the NPC by passive diffusion. Thus, we also expose the RBMSCs to apyrase, a nuclear translocator inhibitor that causes ATP depletion, to study whether this treatment affects translocation of the FITC-labeled CMCht/PAMAM nanoparticles from the cytoplasm to the nucleus.

Figure 8 shows the percentage of RBMSCs-associated fluorescence due to nanoparticle internalization after culturing the cells in the presence and/or absence of the restrictive drugs, for periods of 12 hrs, 24 hrs, 7 d and 14 d. The results show that when culturing the RBMSCs in the presence of colchicine

(green peak), apyrase (dark-blue peak) or exposed to both (red peak), a decrease in nanoparticle internalization is always observed. In fact, when colchicine is not present in the culture medium the nanoparticle internalization efficiency doubles for the culturing periods comprising the first 24 hrs. However, the difference is not so pronounced after 7 and 14 d. Therefore, the present studies support the idea that not only nanoparticle internalization is highly dependent on the endocytosis mechanism, but also suggest that nanoparticles enter cells by a mechanism that might not be exclusively endocytotic. As previously discussed, the size of nanoparticles strongly dictates the mechanism by which they are internalized [27,44]. The nanoparticles described herein have sizes ranging from approximately 6 to 220 nm, and thus may be internalized by different mechanisms, i.e. cellular uptake of particles either by passive transport caused through perturbations of the membrane, endocytosis, and phagocytosis [5,27].

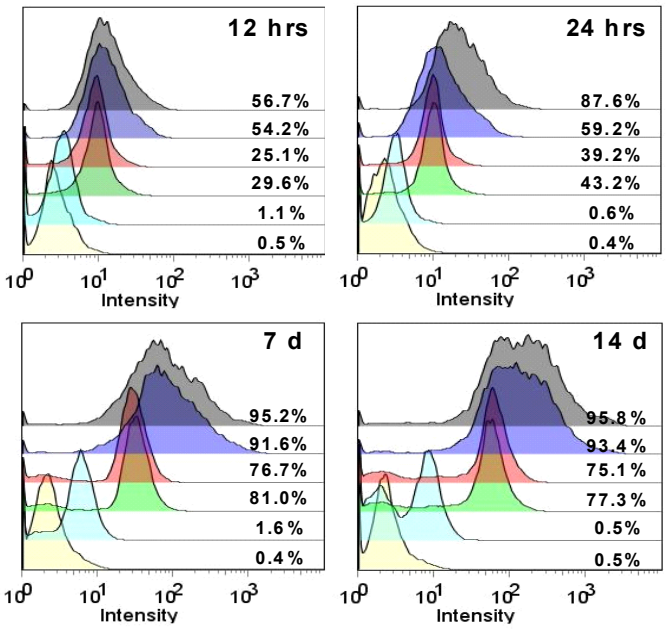

Figure 8. FACS data of RBMSCs-associated fluorescence (% gated) after culturing in different culture media for 12 hrs, 24 hrs, 7 d and 14 d. MEM medium (yellow); MEM medium with 0.1 U.mL^{-1} apyrase and 1 μM colchicine (light-blue); MEM medium containing FITC-labeled CMCht/PAMAM dendrimer nanoparticles 0.01 mg.mL^{-1}, and 1 μM colchicine (green); MEM medium containing FITC-labeled CMCht/PAMAM dendrimer nanoparticles 0.01 mg.mL^{-1}, 1 μM colchicine and 0.1 U.mL^{-1} apyrase (red); MEM medium containing FITC-labeled CMCht/PAMAM dendrimer nanoparticles 0.01 mg.mL^{-1}, and 0.1 U.mL^{-1} apyrase (dark-blue); MEM medium containing FITC-labeled CMCht/PAMAM dendrimer nanoparticles 0.01 mg.mL^{-1} (black).

On the other hand, FACS analysis showed that apyrase exposure did not affect nanoparticle internalization to a great extent after 7 and 14 d. However, after 24 hrs the observed internalization values with apyrase exposure (dark-blue peak) are significantly lower when compared to those of nanoparticle internalization without apyrase exposure (black peaks).

RBMSCs exposed to the restrictive drugs were also observed by fluorescence microscopy (Figure 9). As shown in Figure 9C, it was observed that the FITC-labeled CMCht/PAMAM dendrimer nanoparticles were internalized and widely distributed in the cytoplasm of RBMSCs, and the cells exhibited a normal morphology after 14 d. On the other hand, the depletion of ATP in the cells exposed to apyrase resulted in a decrease in nanoparticle internalization, which is more evident under fluorescence microscopy observation than by FACS analysis (Figure 9D). A preferential localization around the perinuclear area was observed when the cells were treated with apyrase. It should be noted that the cells were not exposed to permeabilizing agents to avoid any undesired effects on the integrity of the cell nuclei. This result suggests that the presence of apyrase also prevents the nanocarriers from entering the cell nuclei, at least to a certain extent, since small molecules cross the 10 nm diameter channels of the NPC by passive diffusion. However, further complimentary studies are needed to clearly elucidate the possible localization of nanoparticles in the nucleus and whether nuclear import is an energy-dependent active process, since no ATP and/or GTP regenerating systems or temperature-dependent assays were carried out [42,43]. On the other hand, when colchicine was present in the culture medium a dramatic decrease in nanoparticle internalization was observed (Figures 9E-F). In other words, the presence of colchicine restricted nanoparticle internalization. Additionally, the exposure of RBMSCs to colchicine seems to prevent the formation of vesicular structures, as evidenced by the observation of uniform fluorescence of the FITC-labeled CMCht/PAMAM dendrimer nanoparticles around the perinuclear area. This assay further suggests that nanoparticles enter in the cells by a mechanism that is not exclusively endocytotic. The colchicine treatment negatively affected cell growth, i.e. only a small number of stained nuclei were observed. Cytoskeleton morphology (Figures 9B, E and F) is also altered as evidenced by the increase in length of actin filaments when comparing to that of control (Figure 9A). This is not surprisingly, since it is well known that colchicine disrupts the cytoskeleton [45]. Tsai et al. [46] reported that colchicine at concentrations less than 1 μM caused disruption of microtubular structures of neutrophiles, but had little effect on either F-actin or on cellular mechanical properties. On the other hand, higher concentrations of colchicine disrupted microtubular structure, but also caused increased actin polymerization and cell rigidity. Thus, the present data demonstrate that the CMCht/PAMAM dendrimer nanoparticles have great potential for various applications as intracellular nanocarriers since

they show properties useful for launching cell-impermeable drugs/DNA within target cells, for example. Moreover, in addition to their applications in intracellular drug delivery systems (DDS), they can also be used for live-cell imaging during *in vitro* culturing. It is further emphasized that the low toxicity of CMCht/PAMAM nanoparticles is in contrast to those of most transfection agents and fluorescent labels, which exhibit significant cytotoxicity and have a period of use limited to only a few hours [38,47].

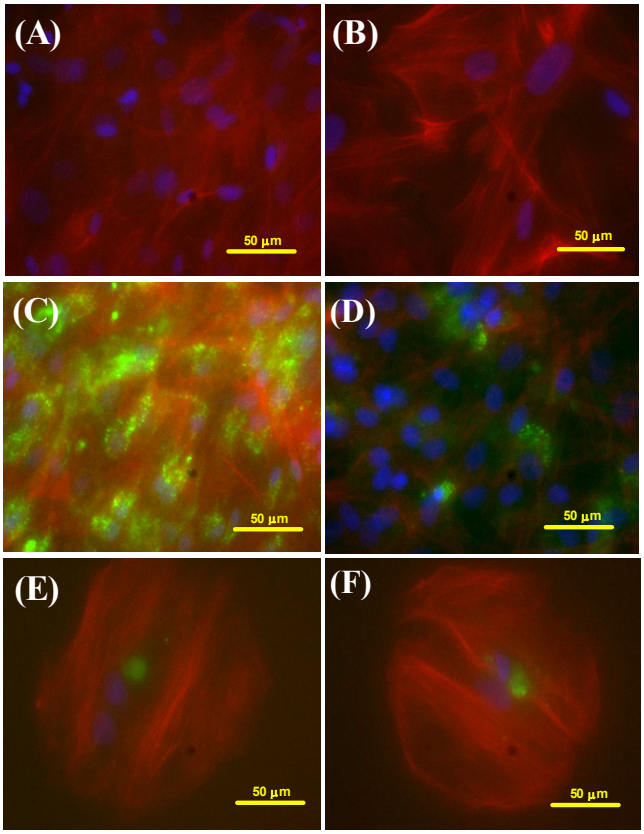

Figure 9. Fluorescence microscopy images of the RBMSCs cultured in different culture medium, after 14 d: A) MEM medium; B) MEM medium with 0.1 U.mL^{-1} apyrase and 1 µM colchicine; C) MEM medium with FITC-labeled CMCht/PAMAM dendrimer nanoparticles 0.1 mg.mL^{-1}; D) MEM medium with 0.1 U.mL^{-1} apyrase and FITC-labeled CMCht/PAMAM dendrimer nanoparticles 0.1 mg.mL^{-1}, E) MEM medium with 1 µM colchicine and FITC-labeled CMCht/PAMAM dendrimer nanoparticles 0.1 mg.mL^{-1} and F) MEM medium with 1 µM colchicine, 0.1 U.mL^{-1} apyrase and FITC-labeled CMCht/PAMAM nanoparticles 0.1 mg.mL^{-1}. FITC-labeled CMCht/PAMAM dendrimer nanoparticles (green). Nuclear DNA and cytoskeleton were labeled with Hoechst 33258 (blue) and Texas-Red phalloidin (red), respectively.

By means of optimizing parameters such as the size and surface chemistry of the nanoparticles, we expect to develop more stable and versatile intracellular nanocarriers aimed at maximizing the drug

availability to damaged tissues and decreasing the overall drug dosage and the need for frequent re-dosage, while simultaneously preventing drug exposure to healthy tissues.

3.5. *IN VITRO* RELEASE OF DEXAMETHASONE FROM THE CMCHT/PAMAM DENDRIMER NANOPARTICLES

Glucocorticoids such as dexamethasone (Dex) have been shown [48-50] to promote the osteogenic differentiation of stem cells. On the other hand glucocorticoids bind to the cytoplasmatic glucocorticoid receptor [51,52]. Therefore, Dex is the ideal drug to further investigate the loading and performance of the CMCht/PAMAM dendrimer nanoparticles as an intracellular drug delivery system. Figure 10 depicts the Dex release profile from CMCht/PAMAM dendrimer nanoparticles at physiological pH. We have studied the effect of serum proteins on the retention of Dex by adding 15% fetal bovine serum, FBS to PBS solution.

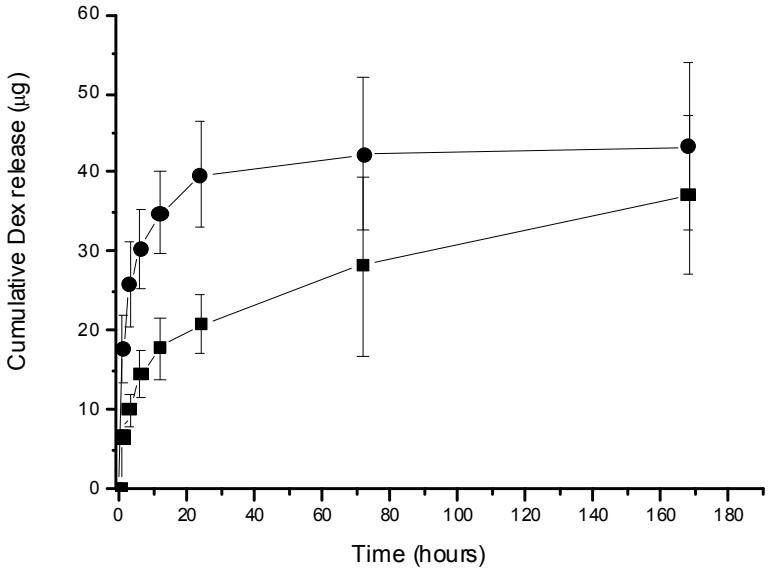

Figure 10. Dexamethasone release from CMCht/PAMAM dendrimer nanoparticles 1 mg.mL^{-1} at pH 7.4 PBS buffer in the presence (-●-) or absence (-■-) of 15% FBS under agitation at 37°C, 60 rpm and determined by high performance liquid chromatography for the period of 1 h until 7 d. The results are expressed as an average ± standard deviation, n=6.

A initial burst release of Dex is observed and the concentration reaches a maximum of 4 µg.mL^{-1} in PBS with 15% FBS, after 24 hrs. The release kinetics of Dex followed a steady release after the initial burst, which lasted for 7d. This data shows that Dex is released as free drug. The release of Dex from nanoparticles seems to be very slow for about 6 days after the initial release period, in the presence of

serum proteins. By comparing the release rate of Dex in absence of serum proteins, it can be seen that Dex is released more slowly, after the initial burst period and a higher amount of Dex is still being released at this second stage. This data shows that the presence of serum proteins increases the initial amount of Dex released from the nanoparticles. This data is in agreement with previous study [53], and may be related to nanoparticles degradation by serum proteins. Despite, further degradation studies need to be carried out to elucidate this issue. The time scale for the Dex release from the nanoparticles is of the same order of their internalization by cells. This could provide an indication of retention of dexamethasone within nanoparticles in culture media and its release rate after has been internalized by cells, *in vitro*. This and other issues such as what will be the Dex release profile inside the endosomes (pH 5) and *in vivo* situation remains to be examined in future studies.

3.6. *IN VITRO* OSTEOGENIC DIFFERENTIATION OF RBMSCS EXPOSED TO THE CMCHT/PAMAM DENDRIMER NANOPARTICLES

Osteodifferentiation study is an interesting *in vitro* model to validate the incorporation and release of dexamethasone from the nanocarriers, since osteogenic differentiation varies with the dose and duration of exposure to the glucocorticoids [48]. On the other hand, *in vitro* osteogenic differentiation of stem cells mimics many characteristics of the normal osteogenesis occurring *in vivo*. Under appropriate culture conditions stem cells are induced to express osteogenic markers such as bone-specific alkaline phosphatase (ALP), osteopontin and osteocalcin [49,54]. The deposition of an extracellular matrix namely type I collagen may occur, and as a consequence mineralization can be observed [50,55,56]. Calcium presence is a late marker of osteoblast differentiation. In this work, the mineralization was qualitatively investigated using the Alizarin red staining (Figure 11). These results have shown that RBMSCs cultures exposed to Dex-loaded CMCht/PAMAM dendrimer nanoparticles showed high mineralization, as seen by the calcium staining (Figures 11C-D). The extent of calcium deposition in cultures exposed to Dex-loaded CMCht/PAMAM dendrimer nanoparticles at a final concentration of 0.01 $mg.mL^{-1}$ was of same magnitude as in cultures treated with of standard culture media with Dex (osteogenic media), while RBMSCs cultured in the presence of CMCht/PAMAM dendrimer nanoparticles showed no mineralized nodules (Figure 11B). This is an important data since it shows that incorporation dexamethasone and nanoparticles concentration influence the intensity and extent of mineralization. Moreover, it can be seen an overall increase of calcium deposition in cultures exposed to Dex as compared to those lacking the glucocorticoid (Figures 11A, B and F). The *in vitro* release studies showed that Dex concentration reaches a maximum of 4 $\mu g.mL^{-1}$ in PBS with 15% FBS, after 24 hrs.

Therefore, in a culture media with 0.01 mg.mL^{-1} of Dex-loaded CMCht/PAMAM dendrimer nanoparticles, the concentration of Dex is expected to be in the magnitude of 40 ng.mL^{-1} (10 nM). Therefore, the Dex released from CMCht/PAMAM dendrimer nanoparticles resembles to that from osteogenic media. These range of concentrations of Dex has been shown to be effective for the osteogenic differentiation of MSCs [48,57].

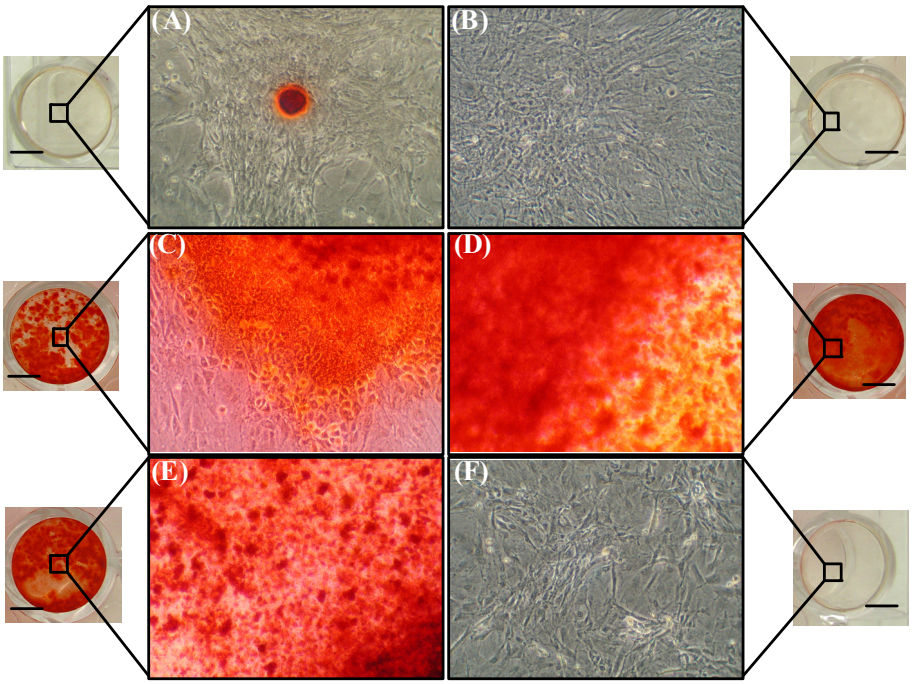

Figure 11. Calcium staining (Alizarin red) of RBMSCs after culturing in different culture medium for the period of 14 d: (A) MEM medium (negative control); (B) CMCht/PAMAM dendrimer nanoparticles 1 mg.mL^{-1}; (C) Dex-loaded CMCht/PAMAM dendrimer nanoparticles 1 mg.mL^{-1}; (D) Dex-loaded CMCht/PAMAM dendrimer nanoparticles 0.01 mg.mL^{-1}; (E) Osteogenic medium and (F) MEM medium with β-glycerophosphate. (Original magnification: x100). Bar: 5 mm.

It is known that ALP, a cell surface glycoprotein is an early marker of osteogenic differentiation [54,58]. To confirm the osteogenic differentiation of RBMSCs exposed to Dex-loaded CMCht/PAMAM dendrimer nanoparticles, we carried out an ALP staining (Figure 12). As seen in calcium staining, presence of the clusters of cuboid-shaped stained with ALP is higher in cultures exposed to Dex-loaded CMCht/PAMAM dendrimer nanoparticles (Figures 12C-D). It is possible to observe a strong ALP staining in cultures with Dex-loaded CMCht/PAMAM nanoparticles at a concentration of 0.01 mg.mL^{-1}. These results are further

corroborated by the above mineralization data which suggests that osteogenic differentiation of RBMSCs occurs in the presence of Dex-loaded CMCht/PAMAM dendrimer nanoparticles.

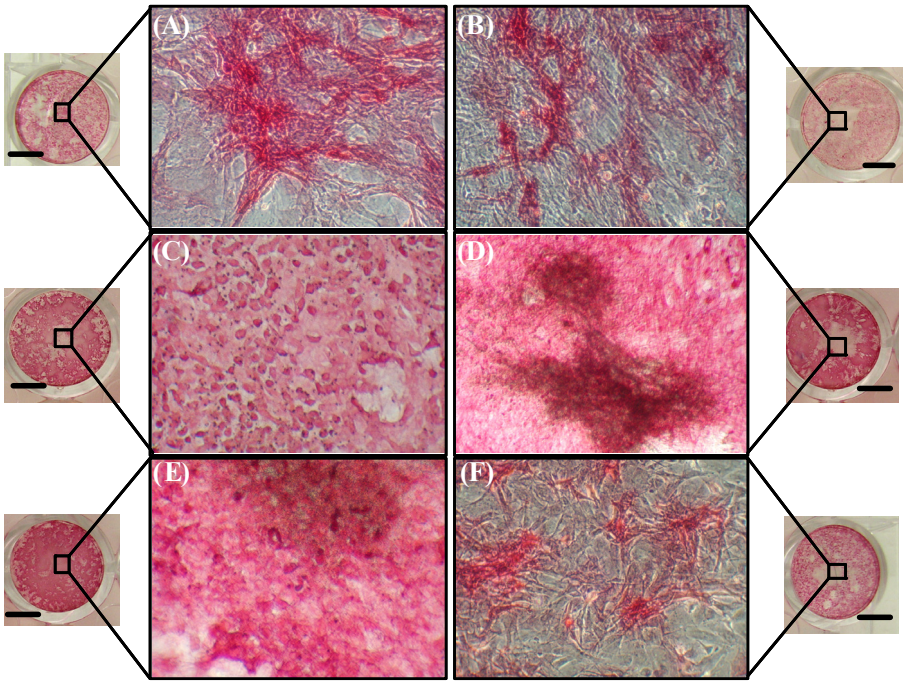

Figure 12. Alkaline phosphatase staining of the RBMSCs cultured in different culture medium for the period of 14 d: (A) MEM medium (negative control); (B) CMCht/PAMAM dendrimer nanoparticles 1 mg.mL^{-1}; (C) Dex-loaded CMCht/PAMAM dendrimer nanoparticles 1 mg.mL^{-1}; (D) Dex-loaded CMCht/PAMAM dendrimer nanoparticles 0.01 mg.mL^{-1}; (E) Osteogenic medium and (F) MEM medium with β-glycerophosphate. (Original magnification: x100). Bar: 5 mm.

Figure 13 shows the quantitative analysis of ALP activity, both normalized for DNA content (left) and non-normalized (right). Cultures grown in the presence of standard medium, CMCht/PAMAM dendrimer nanoparticles, and β-glycerophosphate presented similar ALP activity. It can be seen that ALP activity is increased in cultures with Dex-loaded CMCht/PAMAM dendrimer nanoparticles. No statistical differences were observed for cultures grown in the presence osteogenic medium and standard culture media with different concentrations of Dex-loaded CMCht/PAMAM dendrimer nanoparticles. As expected we observed the up-regulation of ALP in the RBMSCs exposed to Dex. Dex consistently increased ALP activity, but it should be noted that Dex does not globally stimulates all genes considered

to be part of osteoblast differentiation. On the other hand, the Dex actions are somehow species specific, or depend on the culture conditions [56].

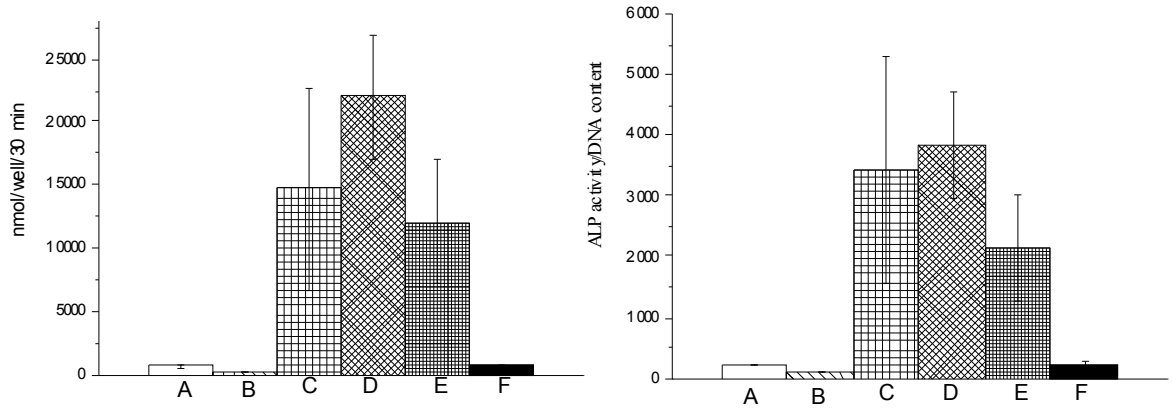

Figure 13. ALP activity (left) and ALP activity per DNA content (right) of RBMSCs cultured in the presence of different culture medium after 14 d: (A) MEM medium (negative control); (B) CMCht/PAMAM dendrimer nanoparticles 1 mg.mL^{-1}; (C) Dex-loaded CMCht/PAMAM dendrimer nanoparticles 1 mg.mL^{-1}; (D) Dex-loaded CMCht/PAMAM dendrimer nanoparticles 0.01 mg.mL^{-1}; (E) Osteogenic medium and (F) MEM medium with β-glycerophosphate. Results expressed as an average ± standard deviation, n=12.

The late osteogenic marker and bone-specific osteocalcin was also measured by performing an Enzyme-linked immunosorbent assay, ELISA (Figure 14). It is possible to observe that osteocalcin deposition occur in cultures exposed to the Dex-loaded CMCht/PAMAM dendrimer nanoparticles.

In addition, higher osteocalcin content in cultures treated with osteogenic media can be seen. Despite, the magnitude of osteocalcin deposition do not present significant differences when comparing to that of cultures with 0.01 mg.mL^{-1} Dex-loaded CMCht/PAMAM dendrimer nanoparticles. These observations can be explained by the fact that differentiation proceed to mineralization and the responsiveness of osteocalcin synthesis to long-term exposure to Dex, as this late marker appears to reach a maximum just before or during mineralized tissue formation [59]. Therefore, the present biochemical findings demonstrate that RBMSCs differentiate into osteoblasts and organize into a mineralized matrix when culturing in the presence of Dex-loaded CMCht/PAMAM dendrimer nanoparticles.

While it is yet to be determined the intracellular Dex release profile, the *in vitro* release and differentiation studies have proved particularly useful to demonstrate that dexamethasone was incorporated into the CMCht/PAMAM dendrimer nanoparticles and it was released at a concentration that caused no negative effects on the RBMSCs osteogenic differentiation.

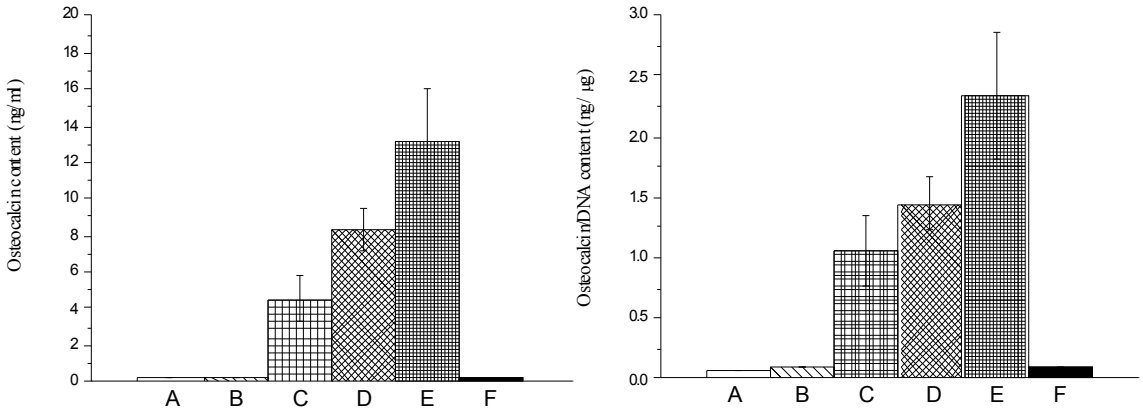

Figure 14. Osteocalcin quantification (left) and osteocalcin per DNA content (right) of RBMSCs cultured in the presence of different culture medium after 14 d: (A) MEM medium (negative control); (B) CMCht/PAMAM dendrimer nanoparticles 1 mg.mL^{-1}; (C) Dex-loaded CMCht/PAMAM dendrimer nanoparticles 1 mg.mL^{-1}; (D) Dex-loaded CMCht/PAMAM dendrimer nanoparticles 0.01 mg.mL^{-1}; (E) Osteogenic medium and (F) MEM medium with β-glycerophosphate. Results expressed as an average ± standard deviation, n=12.

4. CONCLUSIONS

The results in this paper demonstrated that the combination of synthetic and natural-based polymers enable to prepare CMCht/PAMAM dendrimer nanoparticles of suitable diameters to cover a wide range of intracellular delivery applications. *In vitro* tests showed that the carboxymethylchitosan/poly(amidoamine) dendrimer nanoparticles do not exert any significant cytotoxic effect over both L929 fibroblast and RBMSCs for concentrations below 1 mg.mL^{-1}. Furthermore, the successful internalization of the nanoparticles by two different types of cells, i.e. cell lines and primary cultures, was also demonstrated. The biochemical data presented herein also proved that the dexamethasone-loaded carboxymethylchitosan/poly(amidoamine) dendrimer nanoparticles induced the

osteogenic differentiation of rat bone marrow stem cells, *in vitro*. Therefore, the novel carboxymethylchitosan/poly(amidoamine) dendrimer nanoparticles may be used as targeted-drug delivery carriers covering a wide range of applications involving the efficient intracellular delivery of biological agents to modulate the behaviour of cells. These might include the use of differentiation factors to act from the inside the cell or genetic material. The incorporation of fluorescent labels for live-cell imaging and monitoring of the final intracellular fate of such structures is also possible.

REFERENCES

1. Tomalia, D.A. and J.M.J. Fréchet, *Introduction to "Dendrimers and Dendritic Polymers"*. Progress in Polymer Science, 2005. **30**: p. 217.
2. Svenson, S. and D.A. Tomalia, *Dendrimers in biomedical applications—reflections on the field.* Advanced Drug Delivery Reviews, 2005. **57**: p. 2106.
3. Tomalia, D.A., *Birth of a new macromolecular architecture: dendrimers as quantized building blocks for nanoscale synthetic polymer chemistry*. Progress in Polymer Science, 2005. **30**: p. 294.
4. Esfand, R. and D.A. Tomalia, *Poly(amidoamine) (PAMAM) dendrimers: from biomimicry to drug delivery and biomedical applications*. Drug Discovery Today, 2001. **6**: p. 427.
5. Jevprasesphant, R., et al., *Engineering of dendrimer surfaces to enhance transepithelial transport and reduce cytotoxicity*. Pharmaceutical Research, 2003. **20**: p. 1543.
6. D'Emanuele, A., et al., *The use of a dendrimer-propranolol prodrug to bypass efflux transporters and enhance oral bioavailability*. Journal of Controlled Release, 2004. **95**: p. 5447.
7. Sashiwa, H., Y. Shigemasa, and R. Roy, *Chemical modification of chitosan 11: chitosan-dendrimer hybrid as a tree like molecule*. Carbohydrate Polymers, 2002. **49**: p. 195.
8. Domanski, D.M., B. Klajnert, and M. Bryszewska, *Incorporation of fluorescent probes into PAMAM dendrimers*. Bioelectrochemistry, 2004. **63**: p. 193.
9. Sakharov, D.V., et al., *Binding and retention of polycationic peptides and dendrimers in the vascular wal*l. FEBS Letters, 2003. **573**: p. 6.
10. Luo, D., et al., *Poly(ethylene glycol)-Conjugated PAMAM dendrimer for biocompatible, high-efficiency DNA delivery*. Macromolecules, 2002. **35**: p. 3456.
11. Hata, N., et al., *Dendrimer-immobilized culture surface as a tool to evaluate formation of cellular cytoskeleton of anchorage-dependent cells*. Journal of Bioscience and Bioengineering, 2004. **97**: p. 233.

12. Lee, C.C., et al., *Designing dendrimers for biological applications*. Nature Biotechnololy, 2005. **23**: p. 1517.
13. Sontjens, S.H.M., et al., *Biodendrimer-based hydrogel scaffolds for cartilge tissue repair*. Biomacromolecules, 2006. **7**: p. 310.
14. Tomalia, D.A., *The dendritic state*. Materials Today, 2005. **8**: p. 34.
15. Malik, N., et al., *Dendrimers: relationship between structure and biocompatibility in vitro, and preliminary studies on the biodistribution of ^{125}I-labelled polyamidoamine dendrimers in vivo*. Journal of Controlled Release, 2000. 65: p. 133.
16. Marques, A.P. and R.L. Reis, *Hydroxyapatite reinforcement of different starch-based polymers affects osteoblast-like cells adhesion/spreading and proliferation*. Materials Science and Engineering: C, 2005. **25**: p. 215.
17. Wiesmann, H.P., et al., *Bone tissue engineering by primary osteoblast-like cells in a monolayer system and 3-dimensional collagen gel*. Journal of Oral and Maxillofacial Surgery, 2003. **61**: p. 1455.
18. Chen, X.-G. and H.-J. Park, *Chemical characteristics of O-carboxymethyl chitosans related to the preparation conditions*. Carbohydrate Polymers, 2003. **53**: p. 355.
19. Sashiwa, H., Y. Shigemasa, and R. Roy, *Chemical modification of chitosan. Part 9: Reaction of N-carboxyethylchitosan methyl ester with diamines of acetal ending PAMAM dendrimers*. Carbohydrate Polymers, 2002. **47**: p. 201.
20. Tomalia, D.A., A.M. Naylor, and W.A. Godard, *Starburst dendrimers: Molecular-level control of size, shape, surface chemistry, topology, and flexibility from atoms to macroscopic matter*. Angewandte Chemie International Edition in English, 1990. **29**: p. 138.
21. Kotobuki, N., et al., *Viability and osteogenic potential of cryopreserved human bone marrow-derived mesenchymal cells*. Tissue Engineering, 2005. **11**: p. 663.
22. Kotobuki, N., et al., *Cultured autologous human cells for hard tissue regeneration: Preparation and characterization of mesenchymal stem cells from bone marrow*. Artificial Organs, 2004. **28**: p. 33.
23. Sun, J.-J., et al., *In vitro permeability of round window membrane to transforming dexamethasone with delivery vehicles- a dosage estimation*. Clinical Medicine - Journal, 2007. **120**: p. 2284.
24. Kitamura, S., et al., *Osteogenic differentiation of human bone marrow-derived mesenchymal cells cultured on alumina ceramics*. Artificial Organs, 2004. **28**: p. 72.

25. Tang, M. X., C.T. Redemann, and F.C. Szoka, *In vitro gene delivery by degraded polyamidoamine dendrimers*. Bioconjugate Chemistry, 1996. **4**: p. 372.
26. Li, J., Y. Du, and H. Liang, *Influence of molecular parameters on the degradation of chitosan by a commercial enzyme*. Polymer Degradation and Stability, 2007. **92**: p. 515.
27. Gao, H., W. Shi, and L.B. Freund, *Mechanics of receptor-mediated endocytosis*. Proceedings of the National Academy of Sciences of the United States of America, 2005. **102**: p. 9469.
28. Sato, H., et al., *Importance of receptor-mediated endocytosis in peptide delivery and targeting: kinetic aspects*. Advanced Drug Delivery Reviews, 1996. **19**: p. 445.
29. Zhu, A.P., et al., *The aggregation behavior of O-carboxymethylchitosan in dilute aqueous solution*. Colloids and Surfaces B: Biointerfaces, 2005. **43**: p. 143.
30. Zhu, A.P., L. Jianhong, and Y. Wenhui, *Effective loading and controlled release of camptothecin by O-carboxymethylchitosan aggregates*. Carbohydrate Polymers, 2006. **63**: p. 89.
31. Brothers II, H.M., L.T. Piehler, and D.A. Tomalia, *Slab-gel and capillary electrophoretic characterization of polyamidoamine dendrimers*. Journal of Chromatography A, 1998. **814**: p. 233.
32. Ryu, J.S. and G.M. Lee, *Effect of hypoosmotic stress on hybridoma cell growth and antibody production*. Biotechnology and Bioengineering, 1997. **55**: p. 565.
33. Huang, M., E. Khor, and L.-Y. Lim, *Uptake and cytotoxicity of chitosan molecules and nanoparticles: Effects of molecular weight and degree of deacetylation*. Pharmaceutical Researc*h*, 2004. **21**: p. 344.
34. Marques, A.P., R.L. Reis, and J.A. Hunt, *The biocompatibility of novel starch-based polymers and composites: in vitro studies*. Biomaterials, 2002. **23**: p. 1471.
35. Fischer, D., et al., *In vitro cytotoxicity testing of polycations: influence of polymer structure on cell viability and hemolysis*. Biomaterials, 2003. **24**: p. 1121.
36. Choksakulnimitr, S., et al., *In vitro cytotoxicity of macromolecules in different cell culture systems*. Journal of Controlled Release, 1995. **34**: p. 233.
37. Domanski, D.M., B. Klajnert, and M. Bryszewska, *Influence of PAMAM dendrimers on human red blood cells.* Bioelectrochemistry, 2004. **63**: p. 189.
38. Luo, D. and W.M. Saltzman, *Enhancement of transfection by physical concentration of DNA at the cell surface*. Nature Biotechnology, 2000. **18**: p. 893.
39. Jevprasesphant, R., et al., *Transport of dendrimer nanocarriers through epithelial cells via the transcellular route*. Journal of Controlled Release, 2004. **97**: p. 259.

40. Prinzen, L., et al., O*ptical and magnetic resonance imaging of cell death and platelet activation using annexin A5-functionalized quantum dots*. NanoLetters. 2007. **7**: p. 93.
41. Huo, X., et al., *Filamentous-actins in human hepatocarcinoma cells with CLSM*. World Journal of Gastroenterology, 2004. **10**: p. 1666.
42. Thompson, K.J., et al., *Regulation, mechanisms and proposed function of ferritin translocation to cell nuclei.* Journal of Cell Science, 2002. **115**: p. 2165.
43. Yokoya, F., et al., *Beta-Catretin can be transported into the nucleus in a Ran-unassisted manner*. Molecular Biology of the Cell, 1999. **10**: p. 1119.
44. Yan, A., et al., *Biocompatible, hydrophylic, supramolecular carbon nanoparticles for cell delivery*. Advanced Materials, 2006. **18**: p. 2373.
45. Kallard, E., K.J. Johnson, and K. Boekelheide, *Colchicine disrupts the cytoskeleton of rat testis seminiferous epithelium in a stage-dependent manner*. Biology of Reproduction, 1993. **48**: p. 143.
46. Tsai, M.A., R.E. Waugh, and P.C. Keng, *Passive mechanical behavior of human neutrophils: effects of colchicine and paclitaxel*. Biophysical Journal, 1998. **74**: p. 3282.
47. Trevors, J.T., *Fluorescent probes for bacterial cytoplasmic membrane research*. Journal of Biochemical and Biophysical Methods, 2003. **57**: p. 87.
48. Beresford, J., et al., *The effects of dexamethasone and 1,25-Dihydroxyvitamin D_3 on osteogenic differentiation of human marrow stromal cells in vitro.* Archives of Oral Biology, 1994. **39**: p. 941.
49. Blum, J., et al., *Early osteoblastic differentiation induced by dexamethasone enhances adenoviral gene delivery to marrow stromal cells*. *Journal of Orthopaedic Research*, 2004. **22**: p. 411.
50. Eijken, M., et al., *The essential role of glucocorticoids for proper osteoblast differentiation and matrix mineralization*. Molecular and Cellular Endocrinology, 2006. **248**: p. 87.
51. Hayashi, R., et al., *Effects of glucocorticoids on gene transcription*. European Journal of Pharmacology, 2004. **500**: p. 51.
52. Vorgias, C., et al., *Colchicine, colcemide and cytochalasin B do not affect translocation of the glucocorticoid hormoe-receptor in rat thymocytes or Ehrlich ascites cells*. Bioscience Reports, 1988. **8**: p. 193.
53. Kallinteri, P., et al., *Dexamathasone incorporating liposomes: an in vitro study of their applicability as a slow releasing delivery system of dexamethasone from covered metallic stents*. Biomaterials, 2002. **23**: p. 4819.

54. Beck, G., B. Zerler, and E. Moran, *Phosphate is a specific signal for induction of osteopontin gene expression*. Proceedings of the National Academy of Sciences of the United States of America, 2000. **97**: p. 8352.
55. Uchimura, E., et al., *In-situ visualization and quantification of mineralization of cultured osteogenetic cells*. Calcified Tissue International, 2003. **73**: p. 575.
56. Jorgensen, N., et al., *Dexamethasone, BMP-12, and 1,25-dihydroxyvitamin D enhance a more differentiated osteoblast phenotype: validation of an in vitro model for human bone marrow-derived primary osteoblasts*. Steroids, 2004. **69**: p. 219.
57. Jaiswal, N., et al., *Osteogenic differentiation of purified, culture-expanded human mesenchymal stem cells in vitro*. Journal of Cellular Biochemistry, 1997. **64**: p. 295.
58. Harris, H., *The human alkaline phosphatases: what we know and what we don't know*. Clinica Chimica Acta, 1989. **186**: p. 133.
59. Ogston, N., et al., *Dexamathasone and retinoic acid differentially regulate growth and differentiation in immortalised human clonal bone marrow stromal cell line with osteoblastic characteristics*. Steroids, 2002. **67**: p. 895.

CHAPTER VII.

Carboxymethylchitosan/poly(amidoamine) dendrimer nanoparticles in central nervous system regenerative medicine: Effects on neurons/glial cell viability/proliferation and internalization efficiency

CHAPTER VII.

Carboxymethylchitosan/poly(amidoamine) dendrimer nanoparticles in central nervous system regenerative medicine: Effects on neurons/glial cell viability/proliferation and internalization efficiency

Abstract

Central nervous system associated disorders are the leading cause of disability worldwide. In recent years targeted drug delivery nanoparticle based systems for intracellular application have been put forward has a possible therapeutic route to follow. In this sense the objective of the present report was to characterize and evaluate the possible applicability of the recently developed carboxymethylchitosan/poly(amidoamine) (CMCht/PAMAM) dendrimer nanoparticles for central nervous system (CNS) regenerative medicine. Atomic force and transmission electron microscopy observations have revealed that the nanoparticles possessed a nanosphere-like shape, with a mean size ranging from 22.0 to 30.7 nm. Moreover it was also possible to confirm by UV-Vis spectrophotometry that these nanoparticles could be bound to the fluorescent-probe fluorescein isothiocyanate (FITC) for tracing purposes. Experiments with post-natal hippocampal neurons and cortical glial cells revealed that both cell populations were able to internalize the FITC-labeled CMCht/PAMAM dendrimer nanoparticles with high efficiency. The internalization rates changed according to the cell populations, reaching a peak after 48 hours of incubation. Overall astrocytes and microglial cells disclosed higher internalization rates (around 100% of the total cell sub-population) followed by neurons and oligodendrocytes (up to 80-90% of the observed cells). Further experiments for periods up to 7 days revealed that the periodical addition of FITC-labeled CMCht/PAMAM dendrimer nanoparticles was needed to maintain the levels of internalization. This fact was attributed to the proliferation of neuroprogenitors, astrocytes and oligodendrocytes in hippocampal neurons and cortical glial cells cultures, respectively. Finally, it was also observed that cell viability and proliferation were not significantly affected by the presence of the above referred nanoparticles. Further studies will be focused on loading relevant drugs for future CNS applications.

This chapter is based on the following publication: **Oliveira JM**, Salgado AJ, Pirraco RP , Pereira VH, Fraga JS, Marques AP, Neves NM, Mano JF, Reis RL and Sousa N,

Carboxymethylchitosan/poly(amidoamine) dendrimer nanoparticles in central nervous system regenerative medicine: Effects on neurons/glial cell viability/proliferation and internalization efficiency, (2009), submitted.

---

1. INTRODUCTION

Central nervous system associated disorders are a leading cause of disability worldwide. Although in recent years several new drugs have been put forward to tackle problems such as Parkinson's and Alzheimer's Disease, Multiple Sclerosis, and Spinal Cord Injury, one still faces the low efficacy that the latter are delivered into the brain. The greatest treatment obstacle is not the drug potency itself, but rather the physical barriers, such as the blood brain barrier (BBB), that render the typical circulatory routes of delivery ineffective [1-3]. In fact the same mechanisms that protect the brain from foreign substances, also restrict the entry of many potentially therapeutic agents [1-4], such as larger molecular weight molecules, like peptides, proteins and oligonucleotides [1,3]. Therefore there is an urgent need for the development of new routes that can efficiently overcome this problem.

One of such routes could be trough the use of nanomedicine based approaches, namely those dealing with the development of targeted drug delivery nanoparticle-based systems. The latter do not only possess the advantage of their size, but simultaneously could be surface engineered in order to present the adequate properties (e.g. surface chemistry) that would allow them to cross the BBB [1,4]. In general terms, drugs could be dissolved, entrapped, encapsulated or attached to a nanoparticle matrix, serving in this sense as a "*Trojan horse*" for a variety of chemical and biological entities [5-7]. Moreover as they are normally able to be internalized by CNS derived cells, they could be quite useful in the modulation of the activity of neuronal/glial cells intracellular receptors.

Baring this in mind several nanoparticle based systems have been developed throughout the years. For instance, different authors have shown that poly(butyl)cyanoacrylate based nanoparticles could be used as efficient dug delivery agents within the brain [8-11]. Other studies [12-15] have also revealed that liposomes, which commonly disclosed a non-toxic and biodegradable behaviour, could be quite effective for the transport of drugs into the brain. Still within this topic, dendrimers have also been put forward as yet another route for the above referred applications [16-19]. Dendrimers are synthetic highly branched, spherical, monodisperse macromolecules of nanometer dimension [16]. They are easily internalized by cells, property that might be of use if the goal is to deal with, for instance, intracellular receptors of CNS derived cells. Their multiple surface functional groups can be easily modified to potentially attack a large number of ligands for a selected targeted drug delivery application, while its inner hydrophobic core is amenable for drug entrapment [16,20,21]. However, the non-covalent encapsulation of drugs into dendrimers presents a general drawback as it is difficult to control the release of the molecules from the dendrimer core [21]. Furthermore, in order to increase the rate of drug incorporation, it is common to use

higher generation of dendrimers (G7) with amine capping-groups which has been shown to cause haemolysis and changes in red cell morphology, leading to a general overall cytotoxic behaviour [22].

In order to obviate these problems Oliveira et al. [23] have recently proposed a new strategy consisting on poly(amidoamine) (PAMAM) dendrimer core with grafted carboxymethylchitosan (CMCht) chains. By doing so, this novel class of CMCht/PAMAM dendrimer nanoparticles could display a higher loading capacity due to peripheral congestion, which can improve container properties, and also can allow the bulk incorporation of bioactive molecules of higher molecular weights and of different chemistry. Simultaneously they could maintain the high internalization efficiency with improved biological properties, when compared to conventional dendrimers [23].

Following on this initial report the objectives of the present work consists in determining the possible application of these systems for CNS related applications by studying their role on the viability and proliferation of hippocampal neurons and cortical glial cells, as well as to investigate the internalization rate of the CMCht/PAMAM dendrimer nanoparticles by the latter. Results revealed that CMCht/PAMAM dendrimer nanoparticles were not deleterious to both hippocampal neurons and cortical glial cells and did not impaired cell proliferation in these two systems. Furthermore it was also possible to observe that neurons, astrocytes, oligodendrocytes and microglial cells were able to internalize the CMCht/PAMAM nanoparticles at different rates. The latter varied along the different cell populations, but overall started after 1 hour of incubation reaching a peak, that ranged between 80-100%, after 48 hours of exposure. Moreover it was also observed, namely for oligodendrocytes and neurons, that the periodical addition of CMCht/PAMAM dendrimer nanoparticles was needed to maintain the internalization rate for periods of up to 7 days in culture.

2. MATERIALS AND METHODS

2.1. CMCHT/PAMAM DENDRIMER NANOPARTICLES SYNTHESIS

The synthesis of the CMCht/PAMAM dendrimer nanoparticles was carried out as described elsewhere [23]. Succinctly, CMCht/PAMAM dendrimer nanoparticles were prepared using a step-by-step method: (i) increasing the generation of the PAMAM-carboxylic terminated dendrimer, PAMAM-CT (G 1.5), (ii) obtaining a PAMAM-methyl ester terminated dendrimer, (iii) reaction of PAMAM with carboxymethylchitosan possessing a degree of deacetylation of 80% and degree of substitution of 47%. Then, the CMCht/PAMAM dendrimer nanoparticles were precipitated after addition of an appropriate volume of a saturated sodium carbonate, Na_2CO_3 (Aldrich, Germany) solution and acetone (Pronalab,

Portugal), under vigorous agitation. Precipitates were collected by filtration, dispersed in ultra-pure water for extensive dialysis and freeze-dried (Telstar-Cryodos -80, Spain) at -80ºC. In order to trade down the CMCht/PAMAM dendrimer nanoparticles within the intracellular compartment the latter were labeled with fluorescein isothiocyanate, FITC (Sigma, Germany). For this purpose conjugates of FITC-labeled CMCht/PAMAM dendrimer nanoparticles were prepared by covalently bonding the amine group of carboxymethylchitosan and the isothyocianate group of FITC (thiourea bond). The labeling efficiency was investigated by UV-Vis spectrophotometry (NanoDrop™ ND-1000; NanoDrop Technologies, USA) by reading the absorvance at 280 nm and 495 nm, and the determination of FITC:CMCht/PAMAM dendrimer nanoparticles molar ratio calculated using a standard curve.

2.2. CMCHT/PAMAM DENDRIMER NANOPARTICLES PHYSICAL CHARACTERIZATION

The morphology of the nanoparticles was investigated using atomic force microscopy (AFM). The freeze-dried CMCht/PAMAM dendrimer nanoparticles were dispersed in ultrapure water to obtain a solution with final concentration of 1 $mg.mL^{-1}$, and then 20 μL was placed over a 9.9 mm mica disc (Agar Scientific, England) and blown dried with nitrogen gas for subsequent characterization. The samples were analyzed using the Tapping Mode™ with a MultiMode AFM connected to a NanoScope III controller, both from Veeco, USA, with non-contact silicon nanoprobes (ca 300 kHz) from Nanosensors, Switzerland. All images were plane-fitted using the third degree-flatten procedure included in the NanoScope software version 4.43r8. The morphometric analysis was performed using the same software. Complementarily, the morphology of the particles was also analysed under a transmission electron microscope, TEM (Philips CM-12, FEI Company, The Netherlands, equipped with a MEGA VIEW-II DOCU camera and Image Software Analyzer SIS NT DOCU).

2.3. CELL CULTURE

2.3.1. Primary cultures of hippocampal neurons

Hippocampal neuron cultures were prepared from P4 Wistar rats [24]. Upon dissection, hippocampus tissue samples were submitted to trypsin based enzymatic digestion (0.05% Trypsin – Gibco; 3 $mg.mL^{-1}$ BSA – Sigma; 0.0025% DNase – Sigma, in EBSS - Gibco) for 10 minutes, followed by mechanical dissociation and centrifugation. Isolated cells were then plated on poly-D-lysine coated coverslips at a density of 4×10^4 $cells.cm^{-2}$. Cultures were maintained (37°C, 5% CO_2/95% air, 90% relative humidity) in Neurobasal A medium/B27 supplemented with 1 mM Glutamax I, 10 $ng.mL^{-1}$ basic fibroblast growth

factor (b-FGF) and 0.1 mg.mL^{-1} kanamycin (all from Gibco, USA) for 7 days. From day seven onwards two sets of experiments were performed: 1) In order to determine the internalization time of FITC-labeled CMCht/PAMAM dendrimer nanoparticles by hippocampal neurons, cultures were incubated with 200 μg.mL^{-1} nanoparticles for periods of 1, 2, 6, 12, 15, 18, 24 and 48 hours; 2) To understand whether the maintenance of the CMCht/PAMAM concentration in the culture medium was essential to maintain the levels of internalization, cultures were incubated for periods up to 7 days in which CMCht/PAMAM dendrimer nanoparticles were added to the culture medium every 48 hours in one group, while in the other nanoparticles were only added on the first day of the experiment.

2.3.2. Primary cultures of cortical glial cells

Cortical glial cells were isolated from P4 newborns (Wistar Rats) as previously described [25]. Upon dissection, cortices were submitted to an enzymatic cocktail (30 mg.mL^{-1} DNase, 0.25% Trypsin, both from Sigma) in Ca^{2+}/Mg^{2+} free HBSS (Gibco) followed by mechanical dissociation. Glial cells were then obtained by centrifuging the cells suspension at 800 rpm for 2 minutes, and plated out on coverslips previously coated with Poly-D-Lysine at a density of 4 x 10^4 cells.cm^{-2}. Glial cells were then maintained for one week in DMEM (Sigma) supplemented with 1% antibiotics/antimycotics solution and 10% FBS. At this time point similar experiments to those performed with hippocampal cultures were carried out. In order to determine if astrocytes and oligodendrocyte cells proliferation was affecting internalization rate after 7 days of incubation with or without renovation, cultures were treated at day 7 with '5-fluoro-2'-deoxiuridina (FDU, Sigma), a known inhibitor of glial cell proliferation.

2.3.3. Primary cultures of hippocampal neurons

Cortical glial cells were isolated from P4 newborns (Wistar Rats) as previously described [25]. Upon dissection, cortices were submitted to an enzymatic cocktail (30 mg.mL^{-1} DNase, 0.25% Trypsin, both from Sigma) in Ca^{2+}/Mg^{2+} free HBSS (Gibco) followed by mechanical dissociation. Glial cells were then obtained by centrifuging the cells suspension at 800 rpm for 2 minutes, and plated out on coverslips previously coated with Poly-D-Lysine at a density of 4 x 10^4 cells.cm^{-2}. Glial cells were then maintained for one week in DMEM (Sigma) supplemented with 1% antibiotics/antimycotics solution and 10% FBS. At this time point similar experiments to those performed with hippocampal cultures were carried out. In order to determine if astrocytes and oligodendrocyte cells proliferation was affecting internalization rate after 7 days of incubation with or without renovation, cultures were treated at day 7 with '5-fluoro-2'-deoxiuridina (FDU, Sigma), a known inhibitor of glial cell proliferation.

2.4. MTS ASSAY

For both neurons and glial cells, cell viability was assessed by the MTS test, after 7 days of incubation (with or without renovation) with FITC-labeled CMCht/PAMAM dendrimer nanoparticles. The MTS (3-(4,5-dimethylthiazol-2-yl)-5-(3-carboxymethoxyphenyl)-2(4-sulfophenyl)-2H tetrazolium) (Promega, USA) test is an assay in which the substrate – MTS – is bioreduced into a brown formazan product by NADPH or NADP produced by mitochondrial enzymes, which are active in living cells [26,27]. This assay, or others similar to it (MTT, WST-1), have been widely used to measure cellular viability and proliferation. Hippocampal neurons and glial cells cultures (n=3) were placed in culture medium containing MTS in a 5:1 ratio and incubated in a humidified atmosphere at 37ºC and 5% CO_2. After three hours of incubation 100 μL of solution from each well were transferred to 96-well plates and the optical density was determined at 490 nm.

2.5. TOTAL PROTEIN QUANTIFICATION

In order to complement the data obtained with the MTS test, total protein was quantified by using the BCA Protein Assay kit (Pierce Chemical, USA). This system uses bicinchoninic acid (BCA) as the detection reagent for Cu^{+1}, which is formed when Cu^{+2} is reduced by protein in an alkaline environment. The purple coloured reaction product is formed by the chelation of two molecules of BCA with one cuprous ion (Cu^{+1}). Cells were lysed in ultra-pure H_2O after which the total protein was quantified according to the manufacturer's protocol. At the end of the assay, 100 μL of each sample were transferred to 96-well plates where a standard curve was prepared and the absorbance read at 562 nm in a multi-well plate reader (Tecan, USA).

2.6. IMMUNOCYTOCHEMISTRY

Following each culture period, the cells were fixed in 4% paraformaldehyde for 30 minutes, permeabilized by incubation with 100% methanol for 2 minutes at room temperature, and washed three times in PBS. Cells were then blocked with 10% FBS/PBS (60 minutes) and followed by a 60 minutes incubation with the following primary antibodies: mouse anti-rat microtubule associated protein-2 (MAP-2) (Sigma, USA, 1:500) to detect mature hippocampal neurons, rabbit anti-rat glial fibrillary acid protein (GFAP) (Dako, Denmark, 1:500) for astrocytes, mouse anti-CD11b (BD Biosciences Pharmigen, USA, 1:100) for microglial cells and mouse anti-O4 (R&D systems, USA, 1:50) for oligodendrocytes. Cells were then washed in PBS and incubated with the secondary antibody: Alexa Fluor 594 goat anti-

mouse immunoglobulin G (IgG) and Alexa Fluor goat anti-rabbit 488 (Molecular Probes, USA) for 60 minutes. The primary antibody was omitted to produce negative controls. Samples were further observed under an Olympus BX-61 Fluorescence Microscope (Olympus, Germany). Levels of FITC-labeled CMCht/PAMAM dendrimer nanoparticles internalization by the different cell population was achieved by the following (n=3, 5 random fields/coverslip):

% of positive cells for internalization= number of cells positive for FITC-labeled CMCht/PAMAM dendrimer nanoparticles internalization/total number of cells

2.7. STATISTICAL ANALYSIS

Statistical evaluation was performed using one way ANOVA (internalization times experiments) and two-tailed paired *t*-student tests (MTS, total protein, comparison between renovation and no-renovation of FITC-labeled CMCht/PAMAM dendrimer nanoparticles in the culture medium), to assess the statistical differences between different groups. Statistical significance was defined as $p<0.05$ for a 95% confidence interval.

3. RESULTS AND DISCUSSION

In the present study we aimed at determining the interactions between a new class of nanoparticle based systems, known as CMCht/PAMAM dendrimer nanoparticles, with hippocampal neurons and cortical glial cells in order to develop future strategies for CNS regenerative medicine. For this purpose the CMCht/PAMAM nanoparticles were firstly characterized under AFM and TEM after which hippocampal neurons and cortical glial cells were exposed to the latter for different culture periods.

Initially and in order to further characterize the CMCht/PAMAM dendrimer nanoparticles an AFM study was performed to both evaluate their size and morphology (Figure 1). From Figure 1A it is possible to observe the 3-D AFM image of the PAMAM-carboxylic terminated (G1.5) dendrimers. This data reveals the monodispersive character of these macromolecules. On the other hand, Figure 1B shows the 3-D image of the CMCht/PAMAM dendrimer nanoparticles, which clearly shows the consistency of these molecules, i.e. nanosphere-like shape. By performing a threshold technique it became possible to perform the morphometric analysis of the latter. This study revealed that the CMCht/PAMAM dendrimer nanoparticles have a mean size ranging from 22.0 to 30.7 nm for a confidence level of 95%, and a confidence level of ± 4.4 (Figure 1D). This data was further confirmed by TEM analysis (Figure 1E) that revealed the nanosphere-like morphology of the nanoparticles.

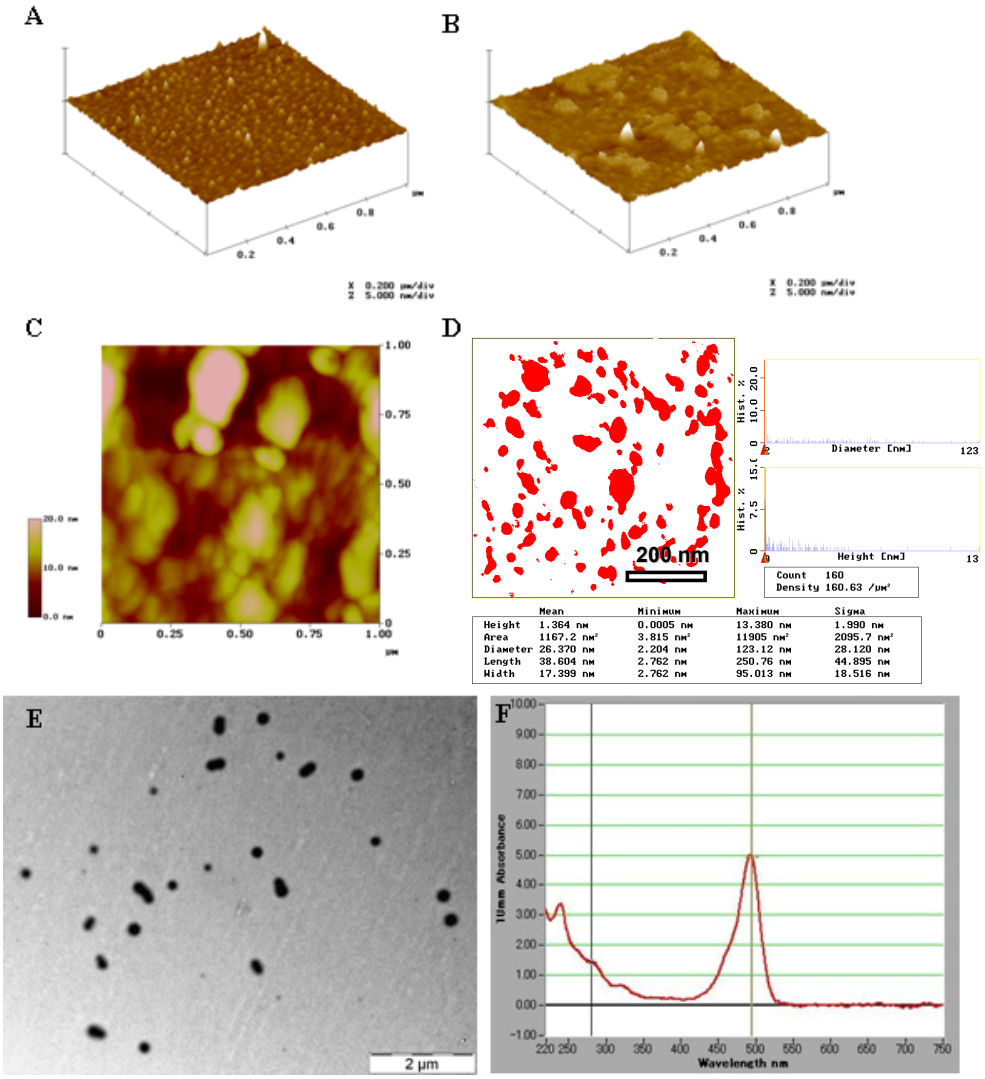

Figure 1. Characterization of the dendrimer nanoparticles. A) AFM 3-D images of the PAMAM-CT, G1.5; B) CMCht/PAMAM dendrimer nanoparticles spread on a mica surface after the solute (water) being wick off with filter paper; C) AFM 2-D image of the CMCht/PAMAM dendrimer nanoparticles and D) respective morphometric analysis; E) Transmission electron microscope micrograph of the CMCht/PAMAM dendrimer nanoparticles; F) UV-Vis spectrum of FITC-labeled CMCht/PAMAM dendrimer nanoparticles.

For the qualitative and quantitative evaluation of CMCht/PAMAM dendrimer nanoparticles internalization and intracellular trafficking within cells, the dendrimers were labeled with fluorescein isothiocyanate (FITC). The labeling efficiency and stability was investigated by UV-Vis spectrophotometry. Figure 1F shows the UV-Vis spectrum of the FITC-labeled CMCht/PAMAM dendrimer nanoparticles. The FITC:CMCht/PAMAM dendrimer nanoparticles ratio was 1:1.1.

Regarding the biological assays, the effects of the CMCht/PAMAM dendrimer nanoparticles on neurons and glial cells viability and proliferation, were the first parameters to be assessed. For this purpose both cell cultures systems were incubated for one week with the nanoparticles under study. In one of the groups CMCht/PAMAM dendrimer nanoparticle concentration was renewed every 48 hours, while in the other, nanoparticles were only added to the culture medium at day 0 of the experiment with no further additions. Figure 2 shows the results of the MTS and total protein assays. MTS test (Figure 2) was used in order to determine the cell viability/metabolic activity of hippocampal neurons and cortical glial cells.

Hippocampal Neurons cultured with CMCht/PAMAM dendrimer nanoparticles

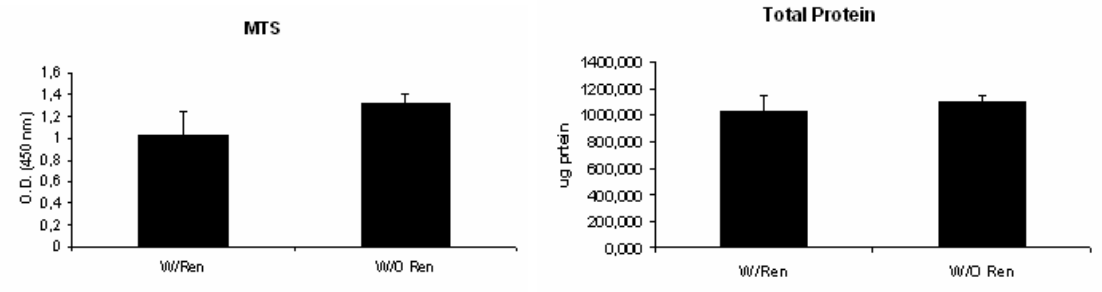

Glial cells cultured with CMCht/PAMAM dendrimer nanoparticles

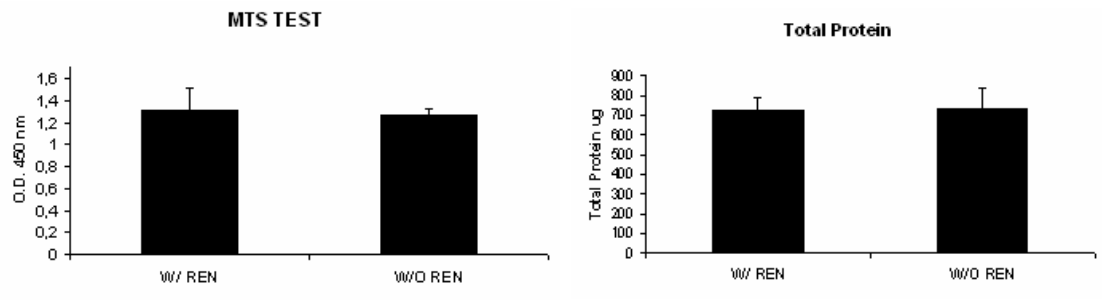

Figure 2. Cell viability and proliferation assays on cultures of hippocampal neurons and cortical glial cells after incubation for 7 days with the FITC-labeled CMCht/PAMAM dendrimer nanoparticles (200 $\mu g.mL^{-1}$) with or without periodical renovations every 48 hours. MTS results showed that the metabolic activity/cell viability of both cell populations was not dramatically altered between the two tested groups. Similar results were also obtained for the total protein quantification (n=3, mean $\pm$ SD, $p>0.05$).

Results revealed that both cell populations were producing large amounts of a brown formazan product which is an indication of normal cell viability and metabolism, as cells were able to incorporate and

metabolize MTS. However it should be referred that for the hippocampal neurons there was a slight difference, non significant ($p>0.05$), between the two groups. This effect could be attributed to the periodical renovation of the CMCht/PAMAM nanoparticles concentration, as the latter lead to a small acidification of the culture medium

The data obtained with the MTS test was subsequently confirmed by a total protein quantification assay (Figure 2), which can be considered as an indication of cell proliferation. Similar to the results achieved by the MTS test, some slight or no differences were found between the tested and control samples ($p>0.05$), and therefore it was demonstrated that cell proliferation of both cell populations in the two tested conditions was not affected by the presence the CMCht/PAMAM dendrimer nanoparticles.

After testing if the CMCht/PAMAM nanoparticles had any deleterious effect on cell viability and proliferation of both neuronal and glial cell populations, the objectives of the present report were focused on the determination of the internalization time and rate in two different sets of experiments. Figure 3 shows the results obtained in primary cultures of post-natal hippocampal neurons. As it can be observed hippocampal neurons were able to internalize the FITC-labeled CMCht/PAMAM dendronized nanoparticles (Figure 3A, after 24 hours of exposure to a concentration of 200 $\mu g.mL^{-1}$). Furthermore the same experiments also revealed that the internalization rate tended to increase with time, presenting three different plateaus: 1) between 1-3 hours the rates are around 5-10%; 2) between 6-18 hours around 40-50% and 3) after 18 hours the values were above 50%. Groups 1-3 hours presented statistically significant difference ($p<0.05$) when compared to groups 15 to 48 hours. Another feature noticed with these experiments was the high variability (high standard deviations) obtained among the different incubation time. This fact indicates that not all hippocampal neurons disclosed the same internalization response at earlier incubation time points. However, and as can be observed in Figure 3B, this tendency tended to fade way with time as after 24 and 48 hours the obtained results were much more homogenous, as it can be seen by the indicative values of the error bars. Although it was not an objective of the present study to understand the mechanisms by which CMCht/PAMAM dendrimer nanoparticles are internalized by hippocampal neurons, similar experiments performed with other cell populations [23] indicate that this phenomena is mediated by endocytosis followed by endosomal transport within the intracellular compartment. Finally, it was also observed that the periodical renovation of the FITC-labeled CMCht/PAMAM dendrimer nanoparticles in the culture medium is essential for the maintenance of the internalization rates by hippocampal neuron populations (Figures 3C-D, $p<0.05$). It is believed that this fact is related with the proliferation of other cell populations present in this culture system, namely neuroprogenitor cells.

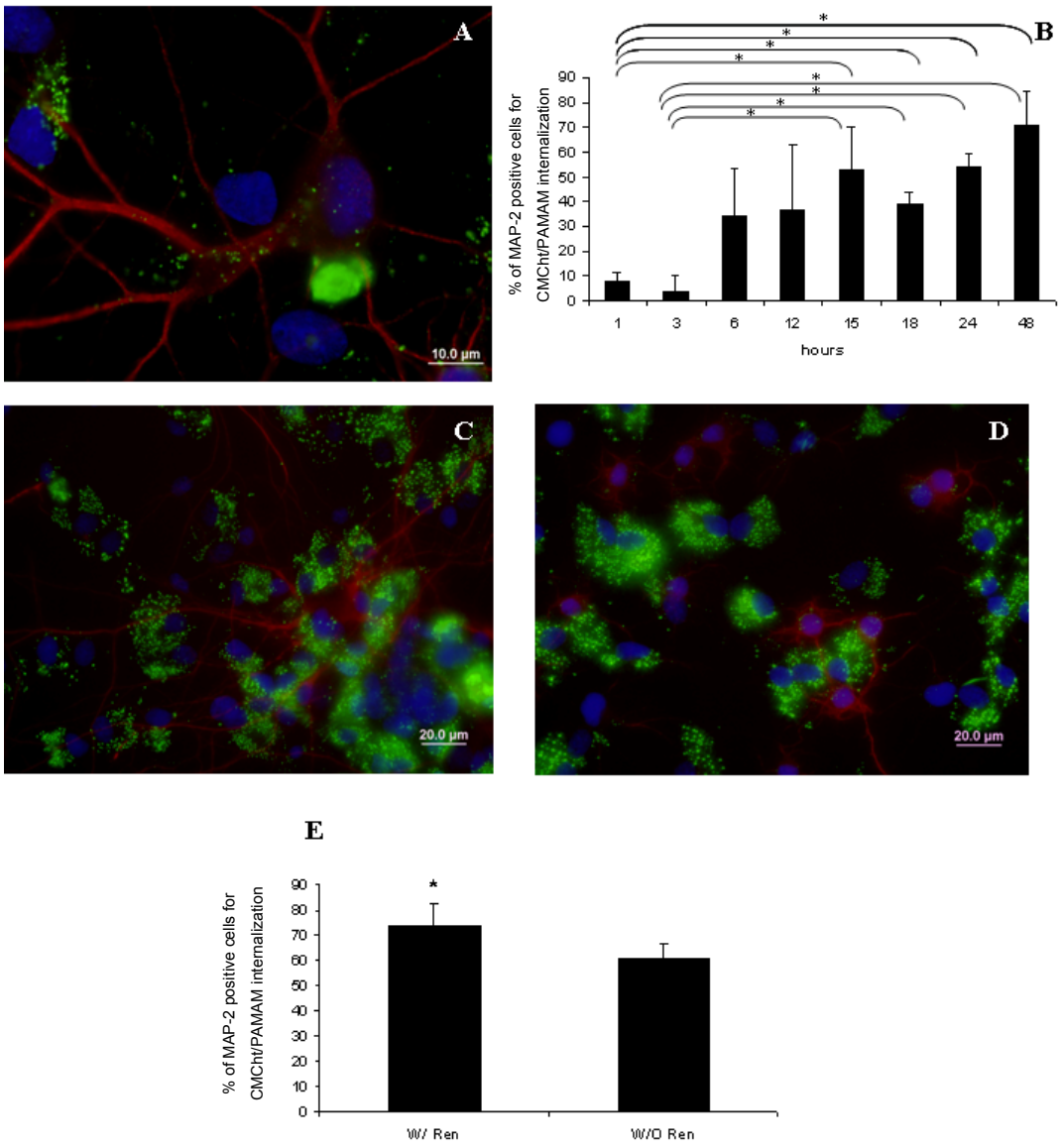

Figure 3. Post-natal hippocampal neurons were able to internalize the FITC-labeled CMCht/PAMAM dendrimer nanoparticles (A). Initially neuronal cells disclosed a high variability on the capacity of internalizing the nanoparticles. However results tended to be more homogeneous after 24 hours of incubations, reaching a maximum of internalization (around 80-90%) after 48 hours of incubation (B). Further experiments (C-E) also showed that the maintenance of the FITC-labeled CMCht/PAMAM dendrimer nanoparticle concentration in the culture medium was essential to maintain the levels of internalization. The differences observed in C-E were attributed to the proliferation of other cell populations within the hippocampal neuron cultures, namely neuroprogenitor cells (n=3; 5 fields/coverslip; mean $\pm$ SD; $p<0.05$).

Similar to what had been observed for hippocampal neurons, all three glial cell types were able to internalize the FITC-labeled CMCht/PAMAM dendrimer nanoparticles (Figures 4-6).

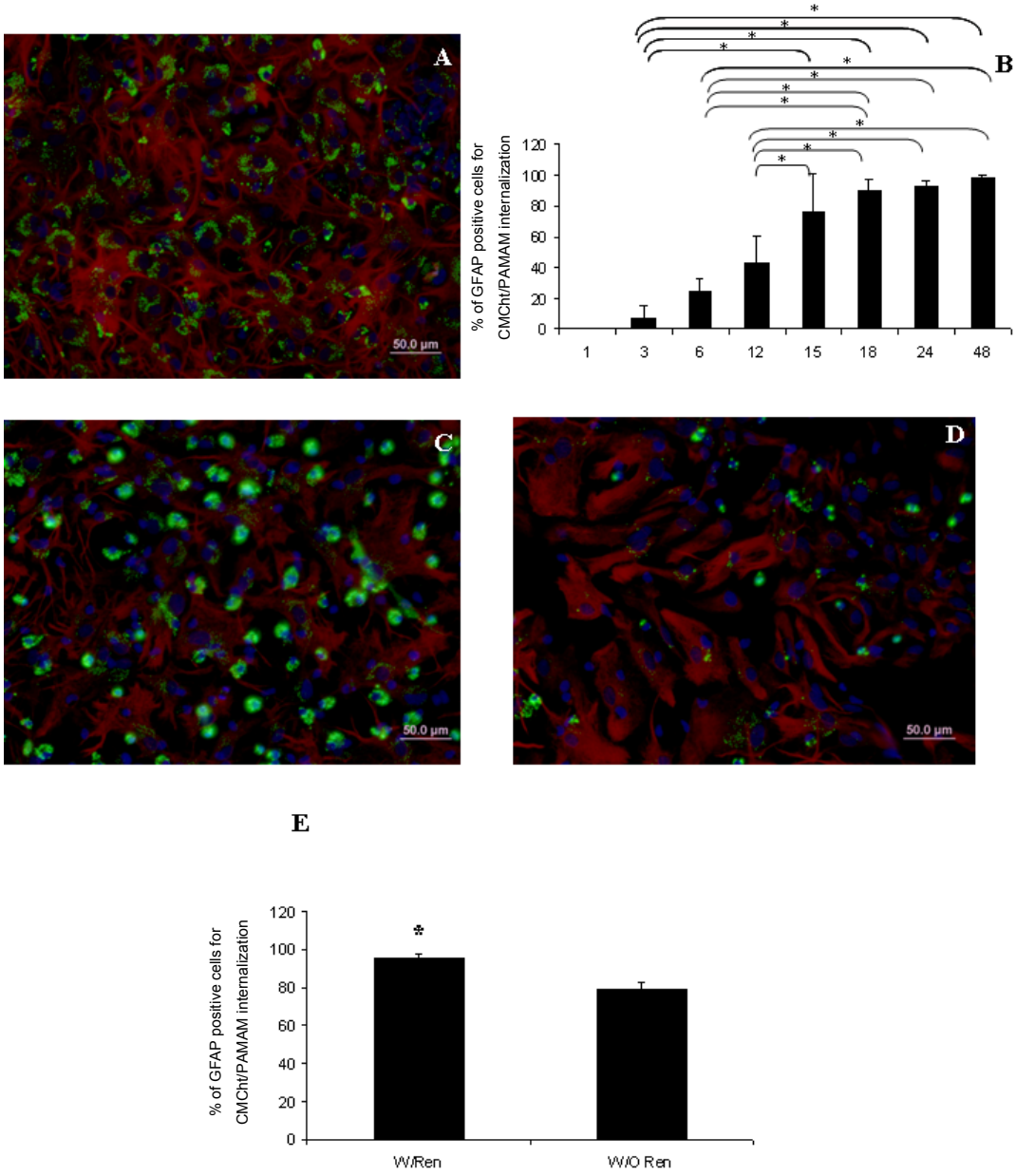

Figure 4. Internalization experiments within cortical glial cell cultures showed that astrocytes were also able to internalize the FITC-labeled CMCht/PAMAM dendrimer nanoparticles (A- after 48 hours of incubation). As it can be observed in (B) the internalization occurred in a gradual manner reaching a peak (around 100% of internalization) after 48 hours of incubation). When exposed for longer periods of time it was observed that the periodical addition of nanoparticles to the culture medium was needed to stabilize the levels of internalization (C-E); (n=3; 5 fields/coverslip; mean ± SD; $p<0.05$).

This fact is noteworthy to mention, as in the culture system used in the present work all glial cell types were present, and therefore is an indicative that the nanoparticles under study are not preferentially up taken and consequently phagocytised by microglial cells. Nevertheless, all glial cell populations disclosed different internalization patterns. For instance, astrocytes (Figure 4) revealed a steady constant increase on the number of positive cells for FITC-labeled CMCht/PAMAM dendrimer nanoparticles internalization reaching the highest value after 48 hours of incubation (around 100%). On the other hand oligodendrocytes (Figure 5) disclosed a similar pattern to what had been observed with hippocampal cultures, disclosing three different levels of internalization, with the highest value around 80-90%. Finally, and as expected due to its phagocytotic nature, microglia (Figure 6) had the fastest and highest rates of internalization, showing levels of around 100% after 12 hours of incubation. The differences obtained between astrocytes and oligodendrocytes to the same concentration of FITC-labeled CMCht/PAMAM dendrimer nanoparticles are probably related with their different endocytotic capabilities. Moreover it was also seen that the size of the nanoparticles that could be found within the intracellular compartment varied according to the cell type observed. For instance, microglial cells (Figure 6A) tended to internalize particles with an increased size when compared to neurons (Figure 3A) and oligodendrocytes (Figure 5A). This fact is mainly related with phagocytotic activity of microglial cells, that commonly phagocytise particles above 100 nm [1]. Moreover this data also indicate that neurons and oligodendrocytes preferentially internalize particles bellow this size.

As for the hippocampal neurons, all glia cell types, namely oligodendrocytes, had reduced internalization rates ($p<0.05$) whenever FITC-labeled CMCht/PAMAM dendrimer nanoparticles concentration was not renewed in the culture medium. For microglial cels this fact was attributed to the macrophage behaviour of the latter, which lead to the degradation of the particles within the intracellular compartment. However for astrocytes and oligodendrocytes the observed phenomena was attributed to cell proliferation, as these cells tend to possess higher proliferation rates when compared to microglial cells. This hypothesis was further assessed by stopping cell proliferation within the cortical glial cell primary cultures (Figure 7). In these conditions, and as it can be observed in Figure 7, no differences were found between the two tested groups ($p>0.05$).

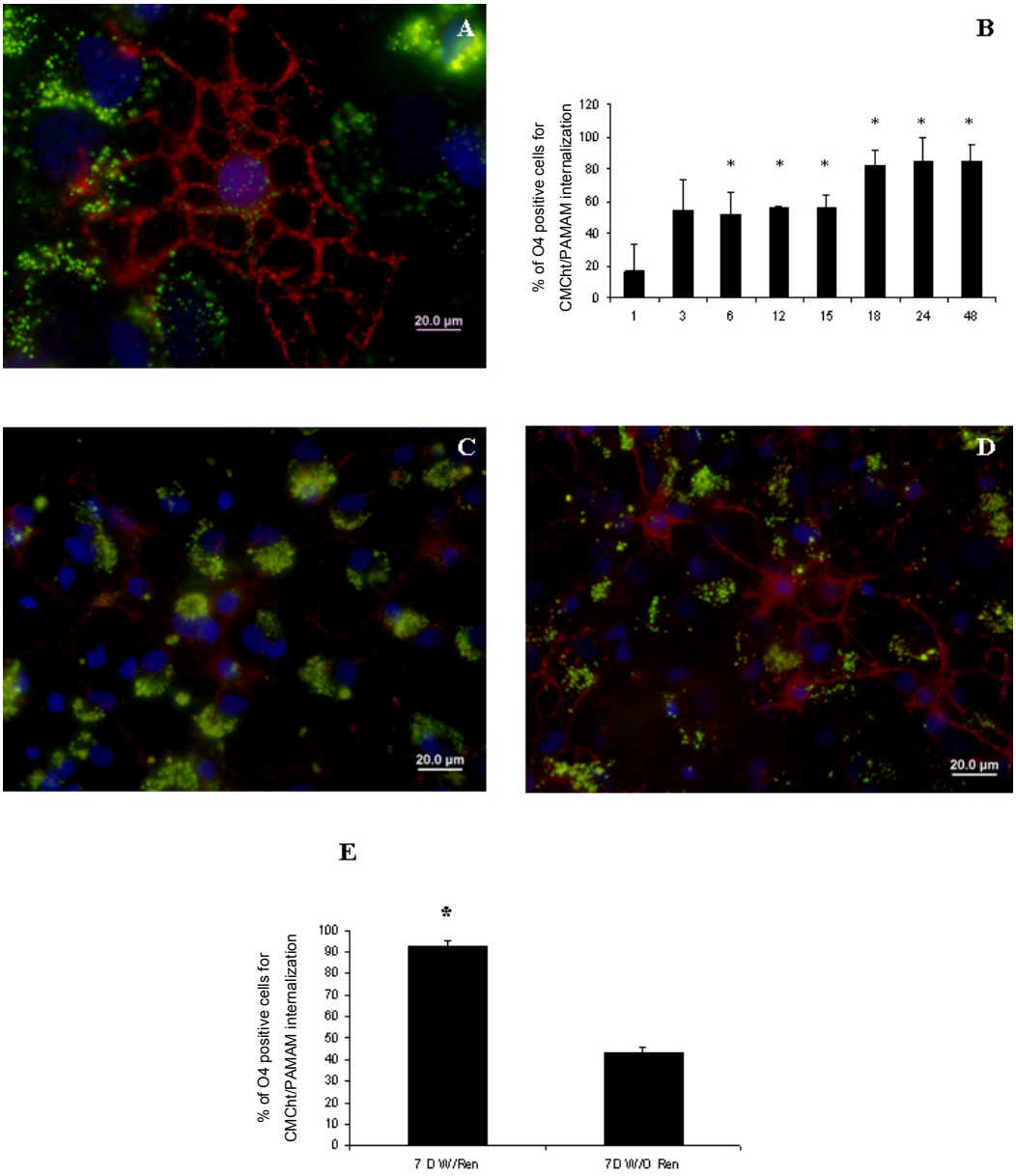

Figure 5. Oligodendrocytes also reveal to be capable of internalizing the FITC-labeled CMCht/PAMAM dendrimer nanoparticles. (A) representative image of the nanoparticles distributed along the intracellular compartment. As it can be observed they were scattered around the nucleus, as well as distributed along the cytoplasmatic processes of the cells. Within the oligodendrocyte population it was possible to observe three plateau of internalization, being the highest obtained after 48 hours of incubation (B-around 80-90%). Similarly to what happened with neurons and astrocytes, the maintenance of the internalization levels within the oligodendrocyte cell population was dependent on the maintenance of the concentration of the FITC-labeled CMCht/PAMAM dendrimer nanoparticles in the culture medium (C-E); (n=3; 5 fields/coverslip; mean $\pm$ SD; $p<0.05$).

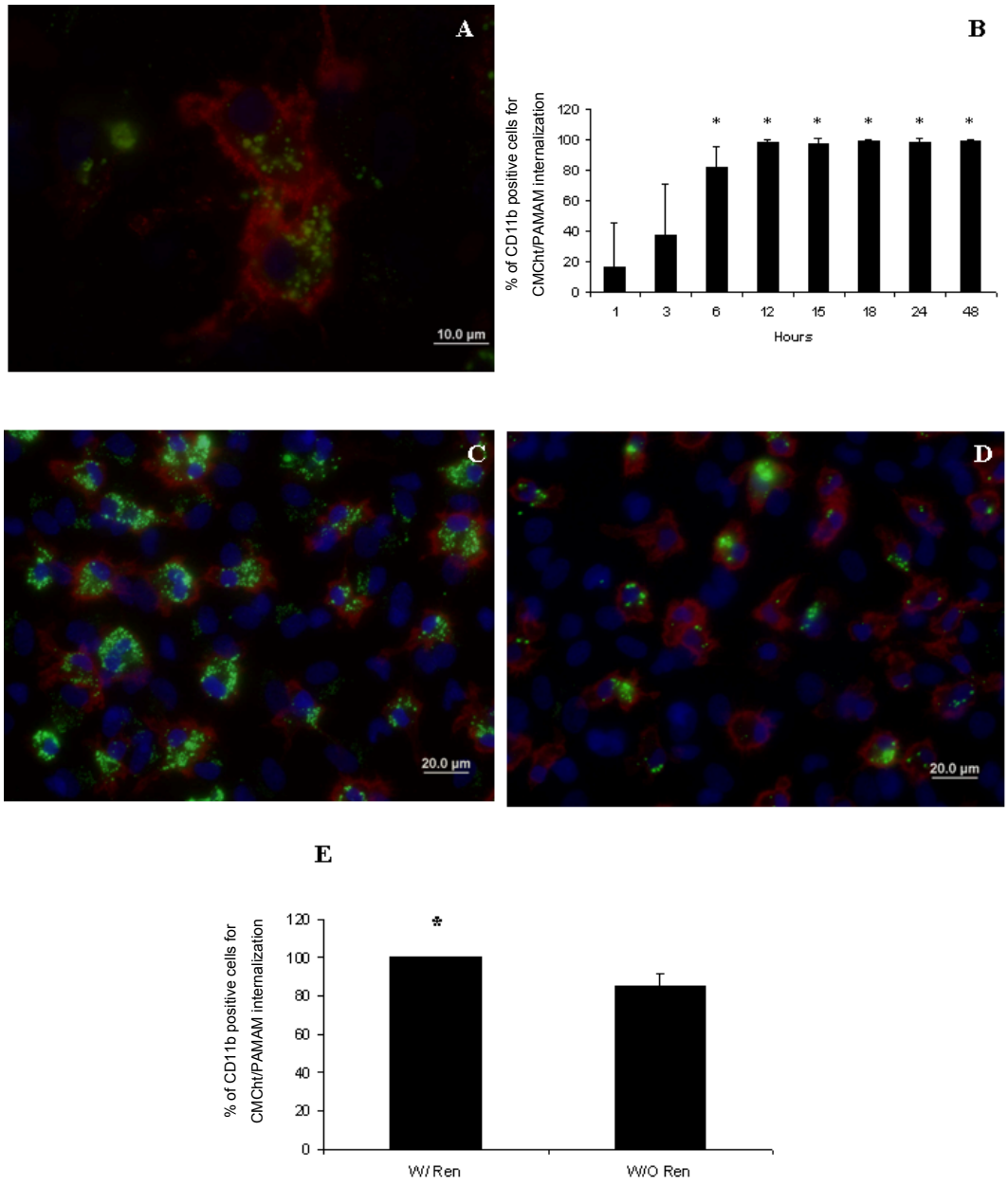

Figure 6. Microglial cells were able to internalize FITC-labeled CMCht/PAMAM dendrimer nanoparticles at a faster rate (A,B) when compared to other neuronal and glial cell populations. This fact cannot be dissociated from the phagocytotic capability of these cells. Furthermore, figure A also allowed observe that the size of the particles internalized by microglial cells was higher when compared to the one disclosed by other cell populations. Similar effects to those previously observed with other cell populations regarding the influence of the periodical addition of nanoparticles on the levels of internalization were also observed (C-E). This result is probably related with the macrophage-like behaviour of these cells.

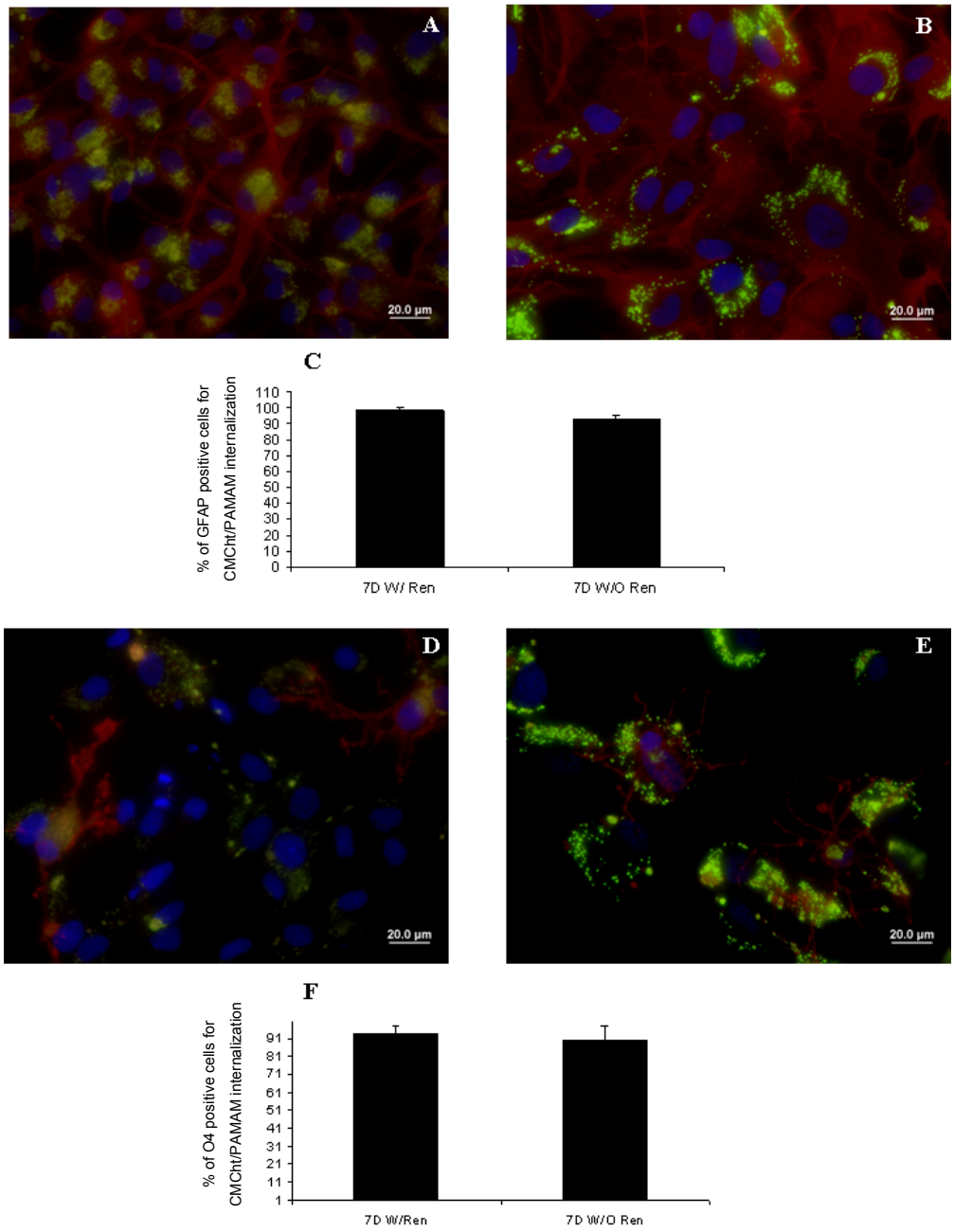

Figure 7. Cortical glial cells cultures were treated with FDU in order to determine if the decrease on the rates of FITC-labeled CMCht/PAMAM dendrimer nanoparticles internalization by astrocytes (A-C) and oligodendrocytes (D-F) was related to their cell proliferation. As it can be observed, whenever astrocyte and oligodendrocyte cells proliferation is impaired, the levels of internalization are not dependent on the periodical additions of FITC-labeled CMCht/PAMAM dendrimer nanoparticles to the culture medium. This fact is an indication that the results observed in Figures 4 and 5 are related with the cell proliferation of the above referred cell populations.

4. CONCLUSIONS

With the present work it was possible to demonstrate that carboxymethylchitosan/poly(amidoamine) dendrimer nanoparticles disclosed a nanosphere-like shape. Furthermore it was also revealed that the binding of these nanoparticles to fluorescent probes (e.g. FITC) for tracing purposes was also possible. At the biological level it was possible to determine that the cell viability and proliferation of post-natal neurons and glial cells was not affected upon exposure to the above referred nanoparticles. Moreover, it was possible to observe that neurons, astrocytes, oligodendrocytes and microglial cells were able to internalize, at different rate, the FITC-labeled CMCht/PAMAM dendrimer nanoparticles, probably through endocytotic processes. Finally, it was also observed that cell proliferation of astrocytes and oligodendrocytes lead to a decrease on the internalization rate within their total cell populations. Further studies will be focused on the loading of relevant drugs for CNS related applications into the CMCht/PAMAM dendrimer nanoparticles.

REFERENCES

1. Emerich, D.F. and C.G. Thanos, *Targeted nanoparticle-based drug delivery and diagnosis*. Journal of Drug Targeting, 2007. **15**: p. 163.
2. Partdrige, W.M., *The blood-brain barrier: Bottleneck in brain drug development*. The Journal of The American Society for Experimental NeuroTherapeutics, 2005. **2**: p. 3.
3. Tiwiri, S.B. and M.M. Amuji, *A review of nanocarrier-based CNS delivery systems*. Current Drug Delivery, 2006. **3**: p. 219.
4. Garcia-Garcia, E., et al., *A relevant in vitro rat model for the evaluation of blood-brain barrier translocation of nanoparticles*. Cellular and Molecular Life Sciences, 2005. **62**: p. 1400.
5. Shinoda, S., M. Ohashi, and H. Tsukube, *"Pocket Dendrimers" as nanoscale receptors for bimolecular guest accommodation*. Chemistry - A European Journal, 2007; **13**: p. 81.
6. Hussain, M., et al., *A novel anionic dendrimer for improved cellular delivery of antisense oligonucleotides*. Journal of Controlled Release, 2004. **99**: p. 139.
7. Chen, C.Z. and S.L. Cooper, *Recent advances in antimicrobial dendrimers*. Advanced Materials, 2000. **12**: p. 843.
8. Kreuter, J., et al., *Passage of peptides through the blood-brain barrier with collidal polymer particles (nanoparticles)*. Brain Research, 1995; **674**: p. 171.

9. Alyautdin, R.N., et al., *Delivery of loperamide across the blood-brain barrier with polysorbate 80-coated polybutylcyaniacrilate nanoparticles*. Pharmaceutical Research, 1997. **14**: p. 325.
10. Gulyaev, A.E., et al., *Significant transport of doxorubicin into the brain with polysorbate 80-coated nanoparticles*. Pharmaceutical Research, 1999. **16**: p. 1564.
11. Kreuter, J., et al., *Direct evidence that polysorbate-80-coated poly(butylcyanoacrylate) nanoparticles deliver drugs to the CNS via specific mechanisms requiring prior binding of drug to the nanoparticles*. Pharmaceutical Research, 2003. **20**: p. 409.
12. Shi, N., et al., *Brain-specific expression of an exogenous gene after in vivo administration*. Proceedings of the National Academy of Sciences of the United States of America, 2001. **98**: p. 12754.
13. Jiang, C., et al., *In vivo delivery of glial cell derived neurotrophic factor across the blood brain barrier by gene transfer into brain capillary endothelial cells*. Human Gene Therapy, 2003. **14**: p. 1181.
14. da Cruz, M.T., S. Simões, and M.C. de Lima, *Improving lipoplex-mediated gene transfer into C6 glioma cells and primary neurons*. Experimental Neurology, 2004. **187**: p. 65.
15. da Cruz, M.T., et al., *Tf-lipoplex-mediated NGF gene transfer to the CNS: neuronal protection and recovery in an excitotoxic model of brain injury*. Gene Therapy, 2005. **12**: p. 1242.
16. Costantino, L., et al., *Nanoparticulate drug carriers based on hybrid poly(D,L-lactide-co-glycolide)-dendron structures*. Biomaterials, 2006. **27**: p. 4635.
17. Kim, J.-B., et al., *Enhanced transfection of primary cortical cultures using arginine-grafted PAMAM dendrimer, PAMAM-Arg*. Journal of Controlled Release, 2006. **114**: p.110.
18. Bracci, L., et al., *Synthetic peptides in the form of dendrimers become resistant to protease activity*. Journal of Biological Chemistry, 2003. **278**: p. 46590.
19. Wu, G., et al., *Targeted delivery of methotrexate to epidermal growth factor receptor-positive brain tumors by means of cetuximab (IMC-C225) dendrimer bioconjugates*. Molecular Cancer Therapeutics, 2006. **5**: p. 52.
20. Lee, C.C., et al., *Designing dendrimers for biological applications*. Nature Biotechnology, 2005. **23**: p. 1517.
21. Gillies, E.R., and J.M. Fréchet, *Dendrimers and dendritic polymers in drug delivery*. Drug Discovery Today, 2005. **10**: p. 35.

22. Malik, N., et al., *Dendrimers: relationship between structure and biocompatibility in vitro, and preliminary studies on the biodistribution of ^{125}I-labelled polyamidoamine dendrimers in vivo*. Journal of Controlled Release, 2000. **65**: p. 133.
23. Oliveira, J.M., et al., *Surface engineered carboxymethylchitosan/poly(amidoamine) dendrimer nanoparticles for intracellular targeting*. Advanced Functional Materials, 2008. **18**: p. 1840.
24. Lu, J., et al., *SMAD pathway mediation of BDNF and TGF beta 2 regulation of proliferation and differentiation of hippocampal granule neurons*. Development, 2005. **132**: p. 3231.
25. Salgado, A.J., et al., *Effects of starch/polycaprolactone based blends to be used for spinal cord injury regeneration in neurons/glial cells viability and proliferation*. Journal of Biomedical Materials Research, 2007, *submitted*.
26. Cory, A.H., et al., *Use of an aqueous soluble tetrazolium/formazan assay for cell growth assays in culture*. Cancer Communications, 1991. **3**: 207.
27. Salih, V., et al., *Development of soluble glasses for biomedical use Part II: The biological response of human osteoblast cell lines to phosphate-based soluble glasses*. Journal of Materials Science: Materials in Medicine, 2000. **11**: p. 615.

CHAPTER VIII.

The osteogenic differentiation of rat bone marrow stromal cells cultured with dexamethasone-loaded carboxymethylchitosan/poly(amidoamine) dendrimer nanoparticles

CHAPTER VIII.

The osteogenic differentiation of rat bone marrow stromal cells cultured with dexamethasone-loaded carboxymethylchitosan/poly(amidoamine) dendrimer nanoparticles

Abstract

There is an increasing interest in developing novel macromolecular vehicles for the intracellular and controlled delivery of bioactive molecules, since they can allow modulation of the cellular functions in a more effective manner *ex vivo*, and maintain the cellular phenotype *in vivo* upon re-implantation. The present study was designed to investigate the effect of combining novel dexamethasone-loaded carboxymethylchitosan/poly(amidoamine) dendrimer (Dex-loaded CMCht/PAMAM) nanoparticles and, both HAp and SPCL scaffolds (3-D system) on the proliferation and osteogenic differentiation of rat bone marrow stromal cells (RBMSCs) *in vitro*. A luminescent cell viability assay using RBMSCs was performed for screening cytotoxicity of the developed HAp and SPCL scaffolds. Results corroborated previous ones which have demonstrated *in vitro*, the superior performance of the HAp and SPCL scaffolds on supporting cells adhesion and proliferation. Furthermore, this work showed that RBMSCs seeded onto the surface of both HAp and SPCL scaffolds differentiate into osteoblasts when cultured in the presence of 0.01 $mg.mL^{-1}$ Dex-loaded CMCht/PAMAM dendrimer nanoparticles. In addition, results demonstrated that Dex-loaded CMCht/PAMAM dendrimer nanoparticles combined with the HAp enhance osteogenesis by increasing ALP activity and mineralization of the extracellular matrix. The pre-incubation of stem cells with these kinds of nanoparticles allows the delivery of Dex inside the cells and directly influences their cellular fate, being a promising new tool to be used in cells and tissue engineering strategies.

This chapter is based on the following publication: **Oliveira JM**, Sousa RA, Kotobuki N, Tadokoro M, Hirose M, Mano JF, Reis RL and Ohgushi H, 2009, The osteogenic differentiation of rat bone marrow stromal cells cultured with dexamethasone-loaded carboxymethylchitosan/poly(amidoamine) dendrimer nanoparticles, Biomaterials, **30**: 804-813.

---

1. INTRODUCTION

Mesenchymal stem cells (MSCs) are a valuable therapeutic tool in tissue engineering (TE) [1], since they can proliferate and differentiate either *in vitro* or *in vivo* into a multitude of distinct cellular phenotypes [2-4]. It is well known that the process of stem cell maintenance and differentiation occurs *in vitro*, under optimal culture conditions [5,6]. For example, it has been shown that dexamethasone (Dex) delivered as a medium supplement promotes the osteogenic differentiation of marrow stromal cells [4,7]. Despite its use in clinical practice [8], Dex and other glucocorticoids have been restricted to few applications mainly due to adverse side-effects [9,10]. Therefore, the development of novel strategies that can stimulate stem cells to become osteoblasts *in vitro* and *in vivo*, and that provide a more effective treatment route with diminished complications is still regarded as a hot issue [11] that needs to be exploited further. In this context, the use of nanocarriers that possess high cellular uptake efficiency to deliver and target drugs can be seen as a possible and reliable solution [12]. Ultimately, these vehicles are expected to increase the solubility of drugs [13] and their bioavailability [14], and their delivery to the targets where they are required [15,16], thus suppressing harmful secondary effects on the patients during drug/cell based treatments.

A huge portfolio of controlled-release vehicles are being investigated for their ability to process into nanocarriers [17,18], while several new emerging nanomaterials are being studied for their biodegradability [19,20] and for their controlled-release and stimuli-responsive properties [21,22]. In this context, we focus our present work on the surface engineering of poly(amidoamine) (PAMAM) dendrimers with natural-based and biodegradable polymers such as the water-soluble carboxymethylchitosan (CMCht) [23]. Previously [24], we have clearly demonstrated that the CMCht/PAMAM dendrimer nanoparticles are efficiently internalized by different cell types. Since glucocorticoids bind to and activate a cytoplasmatic glucocorticoid receptor [25,26], our particular interest is in the loading of these novel macromolecular architectures with Dex in order to study their internalization and effects on the proliferation and osteogenic differentiation of stem cells, *in vitro* and *in vivo*.

In this work, we applied a TE strategy consisting of the combination of stem cells and either ceramic or polymeric scaffolds as a way to qualitatively and quantitatively evaluate their performance in supporting the osteogenic differentiation of rat bone marrow stromal cells (RBMSCs) exposed to the intracellular Dex-loaded CMCht/PAMAM dendrimer nanocarrier. The herein chosen scaffolds were the macroporous hydroxylapatite (HAp) [27] and starch-polycaprolactone (SPCL) [28,29] scaffolds which have been found to exhibit a unique architecture and adequate physicochemical and biological properties to be used in

bone related applications. However, the novelty of the present paper lies in deeper *in vitro* studies that illustrated the potential applications of combining nanoparticles and scaffolds for cells and tissue engineering. Therefore, we went a step further and reported on the osteogenic efficacy of this system, and how to make use of this potential in bone TE and regenerative medicine. *In vitro* studies were carried out in order to evaluate the viability of RBMSCs seeded onto the surface of the HAp and SPCL scaffolds. In addition, RBMSCs-scaffold constructs specimens were also examined using microscopic analyses to assess the cell adhesion and proliferation. Complementarily, scanning electron microscopy, LIVE/DEAD viability assay and DNA quantification were carried out after 14 d of culturing. Alizarin red and ALP stainings were also performed to qualitatively assess calcium deposition and ALP activity, which are parameters denoting osteogenic differentiation. Quantification of the alkaline phosphatase activity and osteocalcin content were carried out in order to evaluate the osteoblastic phenotype expression levels.

2. MATERIALS AND METHODS

2.1. PREPARATION OF THE HYDROXYLAPATITE (HAP) AND STARCH-POLYCAPROLACTONE (SPCL) SCAFFOLDS

Hydroxylapatite (HAp) scaffolds were prepared by impregnating a polyurethane sacrifice sponge (PU, 5 mm diameter and 4 mm height, Eurospuma S.A., Portugal) with HAp powders obtained as previously reported [27]. The elimination of the organic matrix consisted of burning the impregnated sponges in a furnace (Fornocerâmica-ATR 901, Portugal) at 900ºC for 24 hrs, then sintering at 1300ºC for 3 hrs.

Starch-polycaprolactone (SPCL) scaffolds were produced by adopting a two step procedure as previously reported elsewhere [28]. The material used was a blend of starch with approximately 70% by weight of poly-ε-caprolactone, SPCL. Briefly, fibres of SPCL were produced by melt spinning using a modular co-rotating twin screw extruder in two consecutive steps to a final draw ratio of approximately 1:100. Then, melt spun fibres were chopped. Fibre bundles were randomly displaced into the custom-designed mould cavities and subjected to thermal treatment at 60°C for 30 min before compression and fibre bonding. SPCL scaffolds (5 mm diameter and 4 mm height) were obtained through cutting of fibre bonded meshes with a circular die. Standardized fabrication conditions enabled the production of scaffolds with 67.4 ± 1.3% porosity (as determined by micro-computed tomography). More details on SPCL scaffolds can be found elsewhere [30,31].

Prior to the cell culture studies HAp and SPCL scaffolds were sterilized in an ethylene oxide gas atmosphere.

2.2. SYNTHESIS OF DEXAMETHASONE-LOADED CARBOXYMETHYLCHITOSAN/POLY(AMIDOAMINE) (DEX-LOADED CMCHT/PAMAM) DENDRIMER NANOPARTICLES

Carboxymethylchitosan (CMCht) was synthesized by a chemical modification of chitin (Sigma, Germany) as described by Chen et al. [32]. Starburst® poly(amidoamine)-carboxylic terminated dendrimers, PAMAM-CT (generation 1.5, 20% (w/v) methanolic solution) with an ethylenediamine core were purchased from Aldrich. CMCht/PAMAM dendrimer nanoparticles were prepared stepwise as previously reported [24]. Succinctly, Dex-loaded CMCht/PAMAM dendrimer nanoparticles were prepared by means of mixing CMCht/PAMAM dendrimer nanoparticles in an aqueous solution with a dexamethasone (Dex) solution with a final concentration of 5 x 10^{-4} M, under vigorous agitation. The mixture was then added to the precipitation media consisting of a saturated sodium carbonate (Aldrich, Germany) and acetone solution. Precipitates were collected and extensive dialysis (cellulose tubing, benzoylated for separating compounds with a cut-off of 1,200 from (Sigma, Germany) was carried out for 2 d. Dex-loaded CMCht/PAMAM dendrimer nanoparticles were obtained by freezing the solution at -80ºC and freeze-drying (Telstar-Cryodos -80, Spain).

2.3. CHARACTERIZATION OF THE HAP AND SPCL SCAFFOLDS, AND DEX-LOADED CMCHT/PAMAM DENDRIMER NANOPARTICLES

2.3.1. Surface topography characterization

The surface morphology and pore size of the HAp scaffolds and SPCL scaffolds were examined under a scanning electron microscope, SEM (SM-300, Topcon Corporation, Tokyo, Japan). Prior to microstructure analysis, specimens were sputter coated with platinum using an Ion coater (IB-3, Eiko Engineering Ltd., Ibaraki, Japan) with a current set at 6 mA, for a coating time of 2-3 min.

2.3.2. Micro-computed tomography

The qualitative and quantitative information about the microstructure of the HAp and SPCL scaffolds was obtained by micro-computed tomography, µ-CT 20 equipment (SCANCO Medicals, Switzerland). The X-ray scans were acquired in high resolution mode of 11 µm x/y/z [27]. Mimics® (Materialise, Belgium) was used as image processing software for CT reconstruction to create and visualize the 3-D representations.

2.3.3. Transmission electron microscopy

The morphology of the Dex-loaded CMCht/PAMAM dendrimer nanoparticles was investigated by transmission electron microscopy, TEM (Philips CM-12, FEI Company, The Netherlands, equipped with a MEGA VIEW-II DOCU camera and Image Software Analyzer SIS NT DOCU). The nanoparticles were stained with 2% of phosphotungstic acid and placed on copper grids for observation.

2.4. *IN VITRO* CELL CULTURE STUDIES

2.4.1. Isolation and culturing of rat bone marrow stromal cells (RBMSCs)

Seven-week-old Fischer 344/N male rats were purchased from Japan SLC Inc. (Shizuoka, Japan) and sacrificed in accordance with the Ethics Committee at the Tissue Engineering Research Center (Amagasaki, Japan). The epiphyseal regions of the femora were removed and marrow plugs in the femoral shafts were flushed out using Eagle's minimum essential medium (MEM, Nacalai Tesque, Japan) supplemented with 15% fetal bovine serum, FBS (JRH Biosciences, USA) and 1% antibiotic-antimycotic (Nacalai Tesque, Japan) solution. The RBMSCs isolation was performed under aseptic conditions. RBMSCs were transferred to a T75 cm^2 culture flask and expanded in the presence of complete MEM medium at 37ºC in a 5% CO_2 incubator. Then, the culture medium was changed every 2 or 3 d. After reaching confluency, the cells (passage 1, P1) were released from substratum with 1 mL of 0.05% tripsin-0.53 mM EDTA (Invitrogen, USA) and centrifuged at 900 rpm for 5 min. A cell suspension was prepared and cell concentration determined using an automatic cell counter (Cell Counter Sysmex F-520, Japan).

Viability of the RBMSCs was also analyzed with a NucleoCounter (ChemoMetec A/S, Denmark) as described elsewhere [33].

2.4.2. Cytotoxicity screening of the HAp and SPCL scaffolds

A luminescent cell viability assay [24] based on the adenosine triphosphate (ATP) quantification was performed in order to evaluate the viability of RBMSCs seeded onto the surface of the HAp and SPCL scaffolds. Prior to RBMSCs seeding, the HAp and SPCL scaffolds were pretreated (de-airation) to prevent air bubble formation in the pores. Scaffolds were placed in 10 mL polystyrene tubes with ventilation caps. MEM medium was added and scaffolds were de-aired under vacuum using a 20 mL syringe with an attached 21G needle. Then, each scaffold was transferred into the respective well of a non-adherent 96-well tissue culture polystyrene (TCPS) plate. RBMSCs (P1) were seeded onto the

surface of the HAp and SPCL scaffolds at a cell density of 5 x 10^2 cells/scaffold, 1 x 10^3 cells/scaffold, 5 x 10^3 cells/scaffold and 1 x 10^4 cells/scaffold, and cultured in MEM medium under static conditions for 24 hrs, 3 and 7 d. After each time period, the ATP content which signals the presence of metabolically active cells was measured by means of performing a CellTiter-Glo® luminescent cell viability assay (Promega Corporation, USA). Luminescence was measured in a microplate reader (Wallac ARVOsx 1420, Perkin-Elmer Life and Analytical Sciences, USA), following the protocol provided by the supplier. All experiments were carried out 3 times using 3 replicates per experimental condition.

2.4.3. Assessment of proliferation and osteogenic differentiation of RBMSCs seeded onto the surface of the HAp and SPCL scaffolds and cultured with Dex-loaded CMCht/PAMAM dendrimer nanoparticles

RBMSCs were isolated and expanded as mentioned above. HAp and SPCL scaffolds were placed in each well of a 96-well TCPS plate. Then, 1 x 10^6 RBMSCs (P1) were added per each HAp and SPCL scaffold, and the constructs were cultured in complete MEM medium under standard culture conditions for the period of 12 hrs to allow cell adhesion. After that time, cell-scaffold constructs were transferred to a non-treated and non-protein coated flat bottom 12-well TCPS plate (Nunc, Japan), the different culture medium was added, and RBMSCs were cultured for times up to 14 d. RBMSCs were exposed to a MEM medium supplemented with 0.01 mg.mL^{-1} Dex-loaded CMCht/PAMAM dendrimer nanoparticles, 0.28 mM ascorbic acid (Wako Pure Chemicals, Japan) and 10 mM β-glycerophosphate (Sigma, USA). RBMSCS were also cultured in a complete MEM medium (negative control for osteogenic differentiation). A complete MEM medium supplemented with 10^{-8} M Dex, 0.28 mM ascorbic acid and 10 mM β-glycerophosphate was used as the positive control for osteogenic differentiation. All experiments were carried out 3 times using a minimum of 3 replicates per experimental condition.

2.4.4. LIVE/DEAD viability assay

Cell adhesion and proliferation was also investigated with a LIVE/DEAD viability assay kit (Molecular Probes, USA) after 14 d of culturing. RBMSCs-scaffold constructs were incubated with two probes, calcein-AM (green colour) and ethidium homodimer-1 (bright red colour), for intracellular esterase activity and plasma membrane integrity, respectively [34]. Then, RBMSCs-scaffold construct specimens were washed with Ca and Mg-free PBS solution and observed under a 3-D fluorescence microscope (Olympus SZX12 stereomicroscope, OLYMPUS Co. Ltd., Japan). RBMSCs-scaffold constructs specimens were also prepared for SEM observation using standard fixative and dehydration methods.

2.4.5. DNA quantification

DNA quantification was performed using the nuclear dye Hoechst 33258 (Nacalai Tesque, Japan) according to the method previously described [34]. Prior to the assay, the RBMSCs-scaffold constructs were washed with a Ca and Mg-free PBS solution. Then, constructs were transferred to a 2 mL eppendorf, pulverized with zirconia's balls (milling time of ~2 min at 25 shakes.s^{-1}) using a ball mixer mill (Retsch GmbH, Germany), and sonicated in 0.2% Triton-X (Nacalai Tesque, Japan) solution for 5 min. Finally, the samples were sonicated and the DNA quantification carried out. The standard DNA solutions were prepared using salmon sperm DNA (Invitrogen, USA).

2.4.6. Qualitative analysis of mineralization

Alizarin red S staining was performed to investigate possible calcium deposition after 14 d of culturing. RBMSCs-scaffold construct specimens were washed twice with Ca and Mg-free PBS solution and cells fixed with 95% ethanol for 15 min [35]. The fixed cells were then washed once with PBS and stained with 5 $mg.mL^{-1}$ Alizarin red S in Ca and Mg-free PBS solution for 5 min at room temperature. After a washing step with ultra-pure water, RBMSCs-scaffold construct specimens were examined under a 3-D fluorescence microscope.

2.4.7. Qualitative and quantitative analysis of alkaline phosphatase (ALP)

ALP activity was investigated either, qualitatively and quantitatively in order to evaluate osteoblastic differentiation. For the ALP staining the RBMSCs-scaffold construct specimens were washed twice with PBS, after 14 d of culturing. Cells were fixed with 4% paraformaldehyde/Ca and Mg-free PBS solution for 15 min at 4°C. The RBMSCs-scaffold construct specimens were washed twice with AMP buffer (56 mM of 2-amino-2-methyl-1,3-propanediol in ultra-pure water, pH 9.9) and then soaked with staining solution 0.5 mg naphtol AS-MX phosphate and 0.5 mg fast red violet LB salt per mL, in AMP buffer. RBMSCs-scaffold construct specimens were incubated for 10 min at room temperature, washed with Ca and Mg-free PBS solution and examined under a 3-D fluorescence microscope.

The remaining sonicated suspensions obtained from the DNA quantification assay were used to determine ALP levels. Prior to analysis the samples were sonicated once and centrifuged at 12,000 rpm for 1 min at 4°C. To each well of a 96-well plate was added an aliquot of supernatant and p-nytrophenyl phosphate substrate (ZYMED® Laboratories, Invitrogen, USA), following the method described elsewhere [33] with minor modifications. Standards were prepared with p-nytrophenol, pNP. Triplicates

were made for each sample and standard. Absorbance was read at 405 nm (Wallac ARVOsx 1420, Perkin-Elmer Life and Analytical Sciences, USA), and sample concentrations were read off from the standard graph. Enzyme activity was expressed as nmol of pNP released/scaffold/30 min and normalized by DNA content.

2.4.8. Osteocalcin content determined by enzyme-linked immunosorbent assay (ELISA)

The remnants of each sample used for the ALP/DNA assays were treated with a 20% formic acid solution and stored at 4°C for 2-3 d. After that time, samples were centrifuged at 15,000 rpm for 10 min at 4°C. The supernatant was passed through a Sephadex™ G-25 column (GE healthcare, Sweden) for de-salting, and concentrated in order to carry out the ELISA assay. A Rat Osteocalcin EIA kit (N° BT-460, Biomedical Technologies Inc., MA, USA) was used following the instructions provided by the supplier. Data was read off from the standard curve obtained with human osteocalcin and expressed as ng of deposited osteocalcin per μg of DNA.

3. RESULTS AND DISCUSSION

3.1. MORPHOLOGY OF THE HAP AND SPCL SCAFFOLDS, AND DEX-LOADED CMCHT/PAMAM DENDRIMER NANOPARTICLES

It is well known that the ability of a scaffold to support cells proliferation and differentiation is one of the key issues for the success of a tissue engineered cells-scaffold construct. In the current work, an extensive *in vitro* study was carried out in order to investigate the effect of the intracellular delivery of dexamethasone by the carboxymethylchitosan/poly(amidoamine) dendrimer (Dex-loaded CMCht/PAMAM) nanoparticles supplemented from a culture medium on the proliferation and osteogenic differentiation of RBMSCs when cultured onto the surface of two types of scaffolds. From Figure 1, it is possible to observe the microstructure of the HAp (A-B) and SPCL (C-D) scaffolds examined under SEM. Figures 1A-B revealed that the architecture of the obtained HAp scaffolds possess a trabeculae-like structure and highly interconnected macropores. Figures 1C-D show the typical SPCL macroporosity, which can be obtained by randomly assembling the fibres. The polymeric scaffolds also exhibited a high level of interconnectivity.

Several groups [27,29,31] have shown that these scaffolds exhibit adequate porosity and mechanical properties to support cell adhesion and proliferation and tissue ingrowth upon implantation of the construct. Moreover, we have also demonstrated that these starch-based scaffolds are biodegradable,

and thus have the potential to be used in tissue engineering strategies to regenerate bone tissue defects.

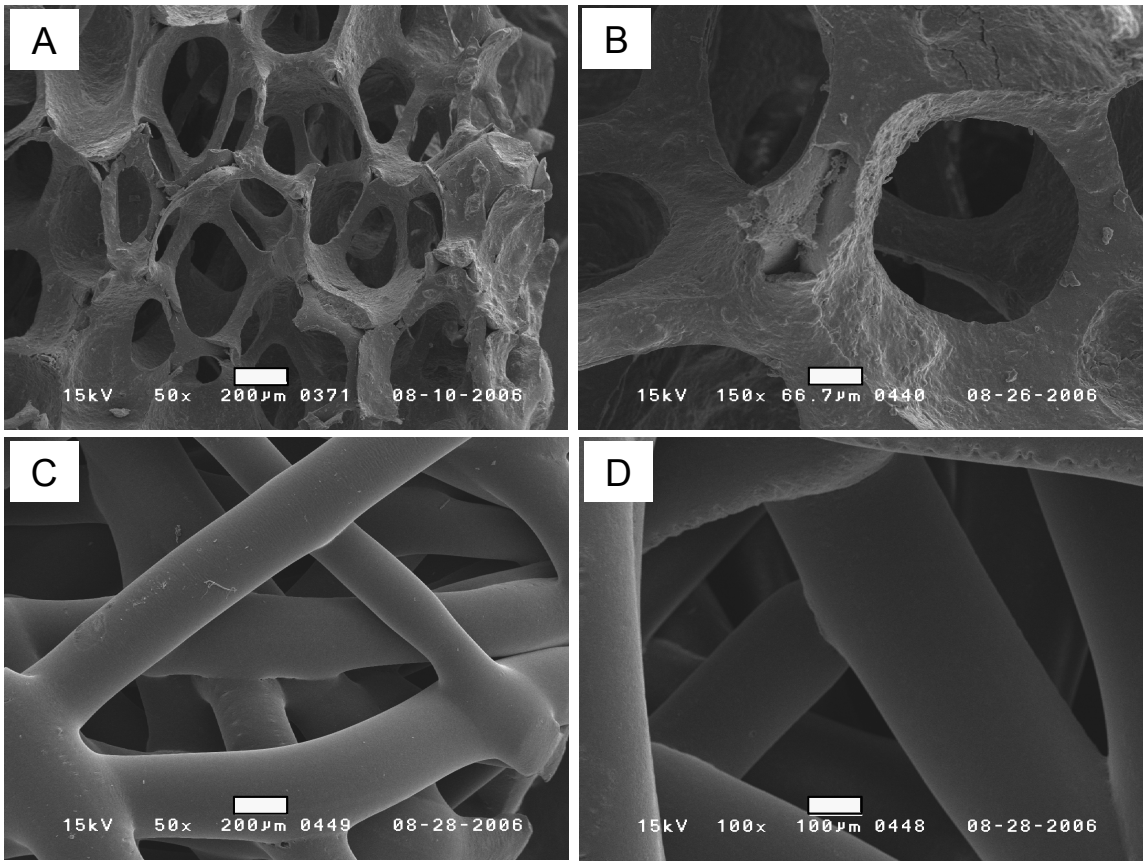

Figure 1. SEM micrographs of the HAp (A-B) and SPCL (C-D) scaffolds.

Figure 2 shows the 3-D micro-computed tomography images of the HAp and SPCL scaffolds. This study revealed that the HAp scaffolds possess a mean porosity of 67.8 ± 5.1% and pore size in the range of 50-600 μm. The SPCL scaffolds showed a mean porosity of 67.4 ± 1.3% and pore size in the range of 50-1000 μm. The selected scaffolds present a similar porosity and pore size as well as high levels of interconnectivity, which is ideal for carrying out a comparative study in terms of scaffold composition as these features play a critical role in bone formation *in vitro* and *in vivo* [36]. Issues that will not be addressed in the present work are of course related to the mechanical properties and degradation rate of the scaffolds, but more details on this can be found elsewhere [31].

Figure 3 shows the TEM image of the developed Dex-loaded CMCht/PAMAM dendrimer nanoparticles. It can be seen that the novel macromolecular nanocarriers possess a dendron-like morphology. These have been shown to be effective in the loading and controlled release of Dex [24]. In this study, we have also demonstrated that the Dex-loaded CMCht/PAMAM dendrimer nanoparticles did not exhibit

significant cytotoxicity in the range of concentrations below 1 mg.mL^{-1} and fluorescent probe labeled nanoparticles were found to be internalized with high efficiency by different cell types. In this first study, we also proved that the Dex-loaded CMCht/PAMAM dendrimer nanoparticles promote the osteogenic differentiation of rat bone marrow stromal cells in a 2-D system, *in vitro*.

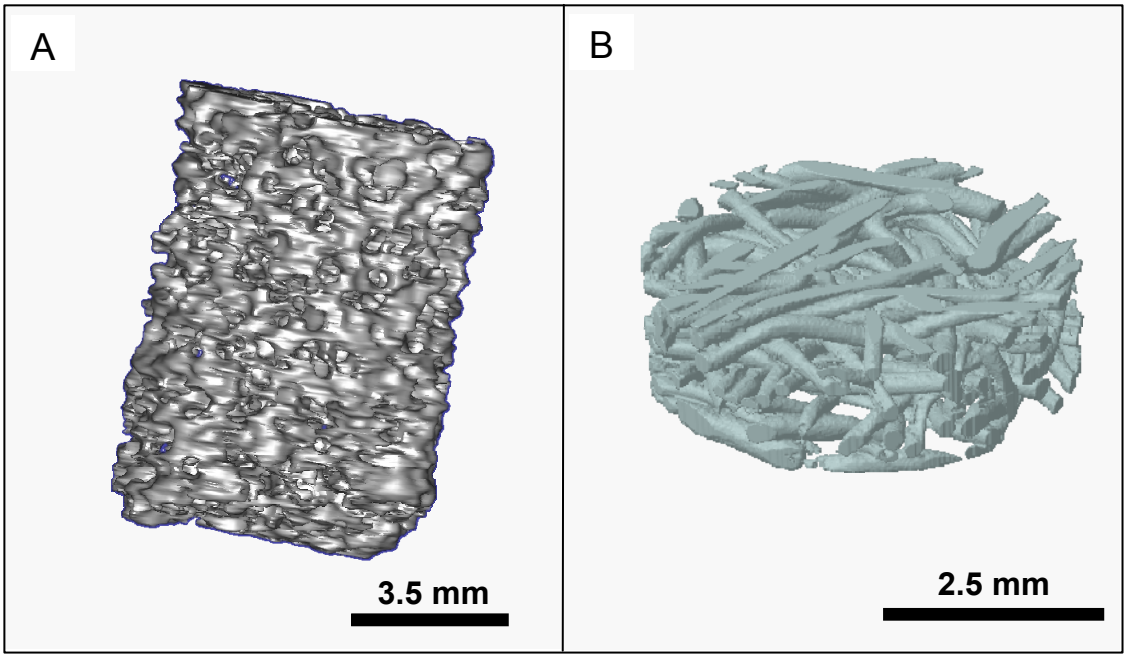

Figure 2. 3-D μ-CT images of the HAp (A) and SPCL (B) scaffolds.

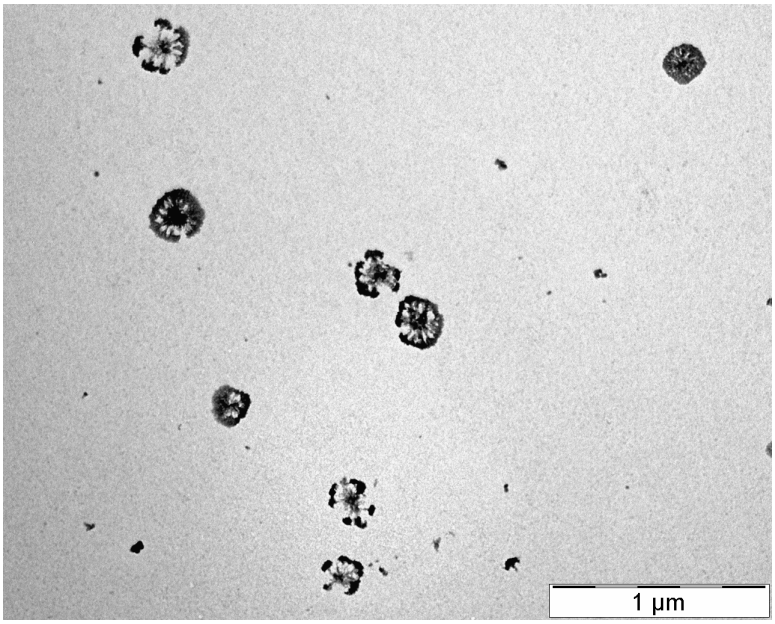

Figure 3. TEM image showing the morphology of the Dex-loaded CMCht/PAMAM dendrimer nanoparticles.

3.2. RAT BONE MARROW STROMAL CELLS VIABILITY, ADHESION AND PROLIFERATION

A luminescent cell viability assay based on adenosine triphosphate (ATP) quantification was performed to evaluate the viability of RBMSCs seeded at different cell densities onto the surface of the HAp and SPCL scaffolds, and results are disclosed in Figure 4.

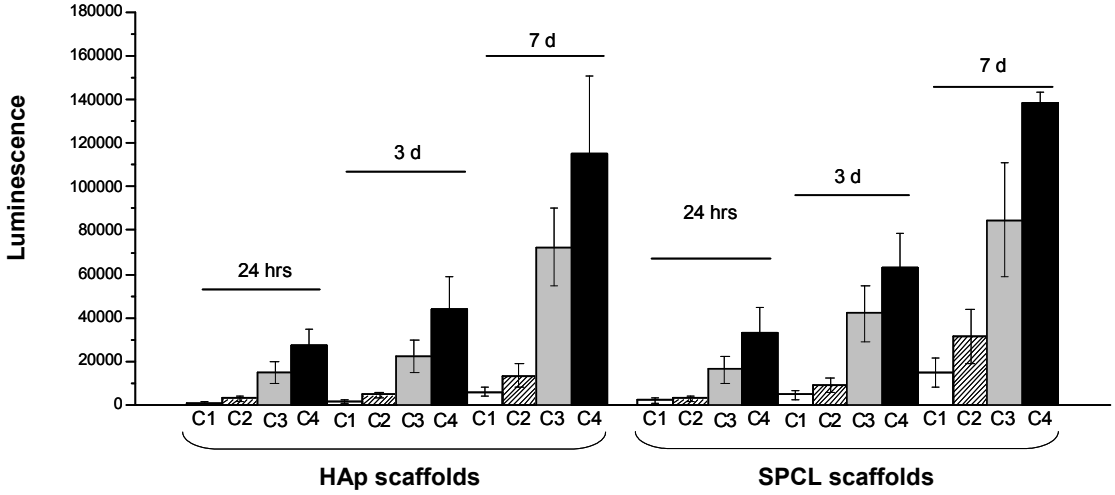

Figure 4. Cell viability assay of RBMSCs seeded at different cell densities onto the surface of the HAp and SPCL scaffolds after 24 hrs, 3 d and 7 d: (C1) 5 x 10^2 cells/scaffold (C2) 1 x 10^3 cells/scaffold, (C3) 5 x 10^3 cells/scaffold, and (C4) 1 x 10^4 cells/scaffold. Cell numbers correlate with luminescence. Results expressed as an average ± standard deviation, n=9.

This assay is a feasible test for assessing the cytotoxicity of materials, since it signals the presence of metabolically active cells. Results have shown that the HAp and SPCL materials are not cytotoxic over RBMSCs. As seen in the present work, no significant differences in the RBMSCs viability were observed when culturing on the surface of the HAp as compared to the SPCL scaffolds. By its turn, it is possible to observe that the initial RBMSCs seeding density affects the viability (ATP content) of RBMSCs.

Additional studies were carried out to evaluate the capacity of HAp and SPCL scaffolds to support the proliferation and differentiation of rat bone marrow stromal cells (RBMSCs) after exposure to Dex-loaded CMCht/PAMAM dendrimer nanoparticles. In the present paper, RBMSCs proliferation was investigated by DNA quantification (Figure 5). From that figure it is possible to observe that the cell seeding efficiency is similar for HAp and SPCL scaffolds as observed by the DNA content after 12 hrs of culturing. However, a slightly higher cellular density was detected for the HAp as compared to that for

SPCL, after 7 and 14 d. This result shows that the HAp scaffolds allows for a higher proliferation of the RBMSCs.

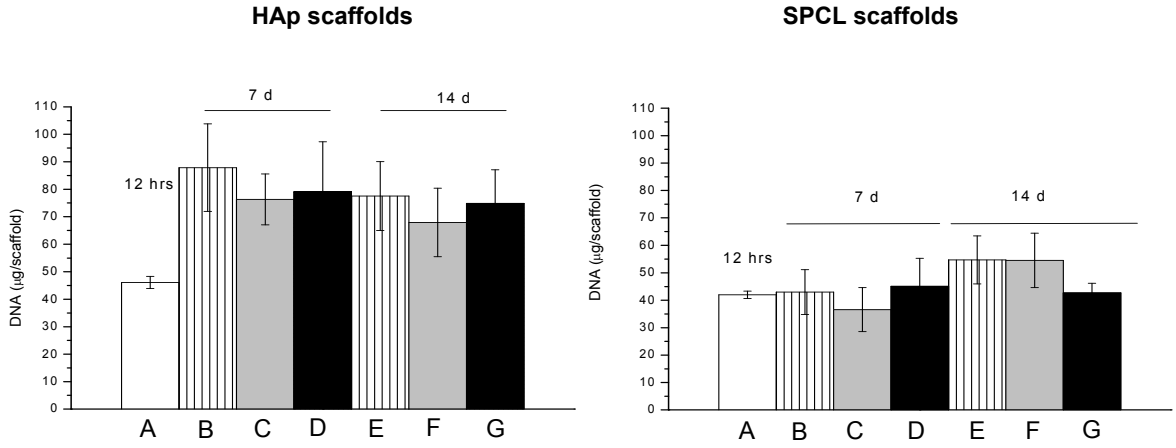

Figure 5. DNA content of RBMSCs seeded (1 x 10^6 cells/scaffold) onto the surface of the HAp (left) and SPCL (right) scaffolds and cultured for 12 hrs, 7 and 14 d, in different culture media: (A, B and E) Complete MEM medium; (C, F) MEM medium supplemented with 10^{-8} M Dex, 0.28 mM ascorbic acid and 10 mM β-glycerophosphate (osteogenic medium); (D, G) MEM medium with 0.01 mg.mL^{-1} Dex-loaded CMCht/PAMAM dendrimer nanoparticles, 0.28 mM ascorbic acid and 10 mM β-glycerophosphate. Results expressed as an average ± standard deviation, n=9.

To a certain extent, this observation may also be related with the fact that proliferation rates are reduced during differentiation [37], as seen by lower cell numbers in cultures when osteogenic factors were present. Then, RBMSCs-scaffold constructs were also examined under microscopic analyses in order to assess cell adhesion and proliferation, after 14 d of culturing (Figure 6). It is possible to observe a higher cellular density on the surface of the HAp as compared to the SPCL. This data thus reflects the findings of the DNA quantification. This data also indicates that cells adhere perfectly, spread actively, and present a flattened morphology (*). Moreover, the (calcein-AM, green colour) images of the RBMSCs-HAp and -SPCL construtcs revealed that cells were alive, after 14 d. Despite the high cellular density it is clear that cells did not obstruct the pores of either. This is an important condition, since the overall performance of the construct [38-40] may be affected by limiting the diffusion of nutrients, oxygen, and metabolites to or from its core.

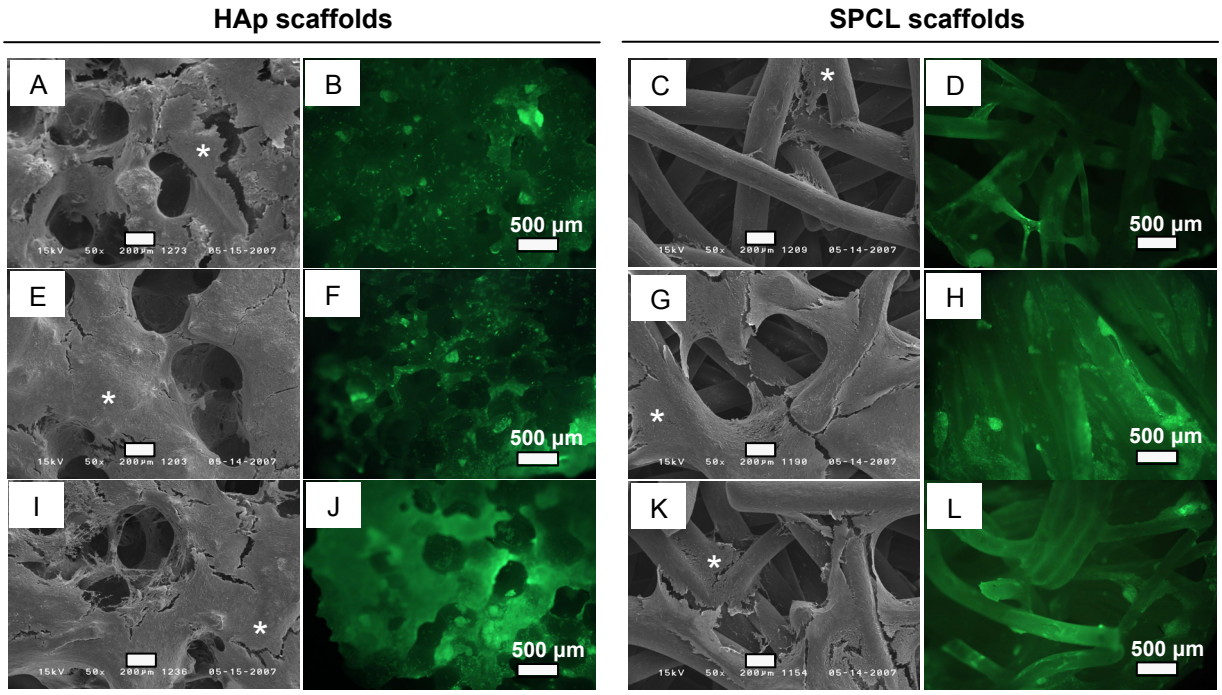

Figure 6. SEM and respective fluorescence microscopy (calcein-AM, green colour) images of the HAp (left) and SPCL (right) scaffolds seeded with RBMSCs (1 x 10^6 cells/scaffold) after culturing in different culture media for the period of 14 d: (A-D) Complete MEM medium, (E-H) MEM medium with 0.01 mg.mL^{-1} Dex-loaded CMCht/PAMAM dendrimer nanoparticles, 0.28 mM ascorbic acid and 10 mM β-glycerophosphate; (I-L) MEM medium supplemented with 10^{-8} M Dex, 0.28 mM ascorbic acid and 10 mM β-glycerophosphate (osteogenic medium). It is also possible to observe that cells perfectly adhere, spread actively and presented a flatten morphology (*).

3.3. Effect of the Dex-loaded CMCht/PAMAM dendrimer nanoparticles on the osteogenic differentiation of rat bone marrow stromal cells

In the present study we have also investigated the osteogenic differentiation of RBMSCs seeded onto the surface of the HAp and SPCL scaffolds that were cultured in: (i) absence of Dex and, (ii) with Dex delivered as a medium supplement and via cellular uptake using the CMCht/PAMAM dendrimer nanoparticles. Mendes et al. [29] showed that the SPCL supports the proliferation and osteogenic differentiation of RBMSCs, *in vitro*. Despite the *in vitro* and *in vivo* characterization on the performance of the SPCL scaffolds, the report lacks in quantitative data. To our knowledge, no qualitative and quantitative studies were performed to investigate the effect of combining Dex-loaded CMCht/PAMAM

dendrimer nanoparticles and both HAp and SPCL scaffolds (3-D system) on the osteogenic differentiation of the RBMSCs, *in vitro*.

Production of mineral deposits is an important indicator of osteogenesis and osteogenic differentiation [41,42]. In order to be able to assess mineralization, calcium staining (Alizarin red) and SEM analyses of RBMSCs-scaffold constructs cultured in different culture media were carried out (Figure 7).

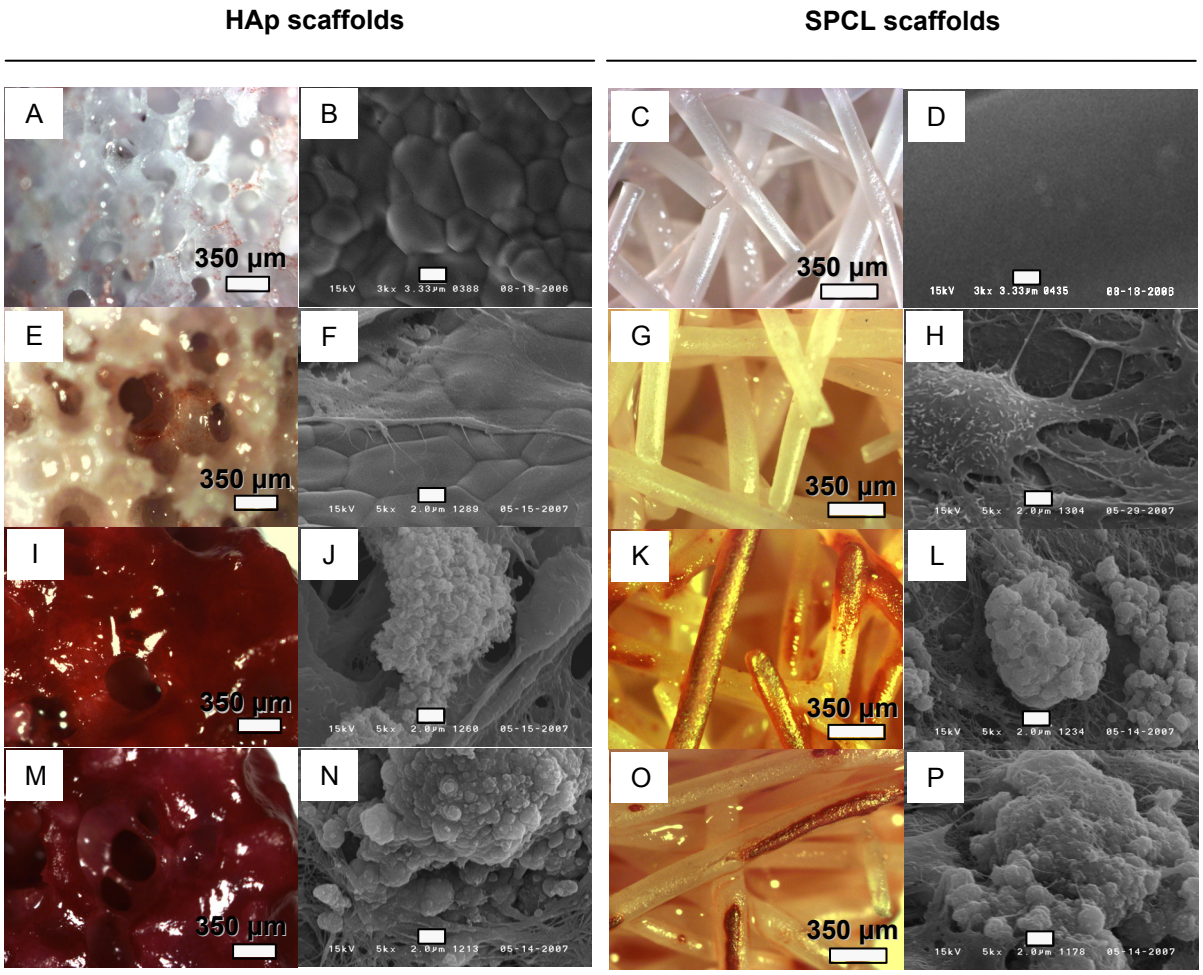

Figure 7. Optical microscopy and respective SEM images of the HAp (left) and SPCL (right) scaffolds seeded with RBMSCs (1 x 10^6 cells/scaffold), which were stained with Alizarin Red (mineralization) after culturing in different culture media for the period of 14 d: (A-D) Controls (scaffolds without RBMSCs); (E-H) Complete MEM medium, (I-L) MEM medium with 0.01 mg.mL^{-1} Dex-loaded CMCht/PAMAM dendrimer nanoparticles, 0.28 mM ascorbic acid and 10 mM β-glycerophosphate; (M-P) MEM medium supplemented with 10^{-8} M Dex, 0.28 mM ascorbic acid and 10 mM β-glycerophosphate (osteogenic medium).

At 14 d, it was possible to observe a higher calcium deposition in the RBMSCs-scaffold constructs exposed to Dex-loaded CMCht/PAMAM dendrimer nanoparticles as compared to that of RBMSCs-scaffold constructs cultured in the standard culture medium (Figures 7I, K, and E, G). The extent of mineralization in cultures exposed to Dex-loaded CMCht/PAMAM dendrimer nanoparticles at a final concentration of 0.01 $mg.mL^{-1}$ was of the same magnitude as for cultures exposed to a standard osteogenic media (Figures 7I, K and M, O). Moreover, from SEM images it is possible to observe the typical mineralized nodules (Figures 7J, L and N, P), which are not seen in RBMSCs-scaffold constructs cultured in complete MEM medium (Figures 7F, H).

Finally, the osteoblastic phenotype expression levels were evaluated both, qualitatively and quantitatively for alkaline phosphatase and osteocalcin, which are known to be the early and late markers of osteogenic differentiation [43], respectively. It is well known that Dex triggers the osteogenic differentiation of MSCs at an early stage and directs the cells toward terminal maturation at the late stages of differentiation and matrix mineralization [44]. Thus, we hypothesized that the continuous exposure of RBMSCs to Dex via the sustained release from the nanoparticles, either intracellularly or in culture media results in the differentiation of RBMSCs into mature osteoblasts. Figure 8 shows the ALP staining of RBMSCs-scaffold constructs after culturing in a different culture medium for a period of 14 d. As seen for mineralization, the ALP activity is higher for cultures in which RBMSCs were exposed to Dex-loaded CMCht/PAMAM dendrimer nanoparticles and osteogenic medium (Figures 8E, F and G, H). These findings demonstrate strong evidence that osteogenic differentiation only occured in cultures with Dex either, supplemented from culture media and delivered via the Dex-loaded CMCht/PAMAM dendrimer nanoparticles.

The ALP activity per DNA content of the HAp (top) and SPCL (bottom) scaffolds seeded with RBMSCs and cultured in different culture media for a period of 12 hrs, 7 and 14 d is presented in Figure 9. It is possible to observe that ALP activity is increased in cultures where RBMSCs-scaffold constructs were exposed to Dex, i.e. Dex-loaded CMCht/PAMAM dendrimer nanoparticles, and osteogenic medium. The present data is not surprising, since the *in vitro* release studies of Dex from the CMCht/PAMAM dendrimer nanoparticles [24] revealed that Dex concentration resembles to that of osteogenic media. In addition, a significant increase in the ALP activity of RBMSCs-HAp scaffold constructs that were cultured with Dex delivered via the CMCht/PAMAM dendrimer nanoparticles was observed as compared to the constructs supplemented with Dex in culture media, after 7 d. In contrast, the ALP activity is higher when RBMSCs are cultured with 10^{-8} M Dex supplied from culture medium (Figure 9 bottom, F), after 14 d.

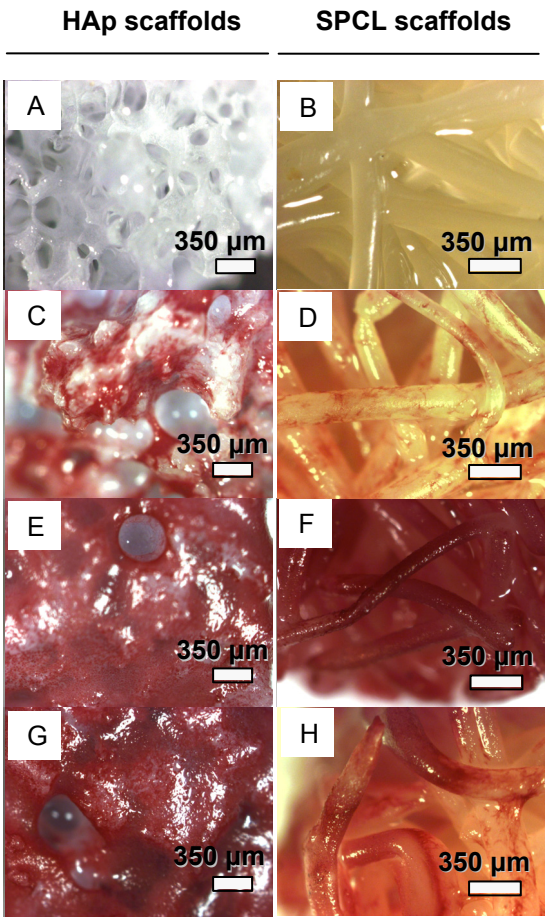

Figure 8. Optical microscopy images of the HAp (left) and SPCL (right) scaffolds seeded with RBMSCs (1 x 10^6 cells/scaffold) which were stained for ALP after culturing in different culture medium for the period of 14 d: (A, B) Controls (scaffolds without RBMSCs); (C, D) Complete MEM medium, (E, F) MEM medium with 0.01 mg.mL^{-1} Dex-loaded CMCht/PAMAM dendrimer nanoparticles, 0.28 mM ascorbic acid and 10 mM β-glycerophosphate; (G, H) MEM medium supplemented with 10^{-8} M Dex 0.28 mM ascorbic acid and 10 mM β-glycerophosphate (osteogenic medium).

No significant differences in the ALP activity were observed for RBMSCs-SPCL scaffold constructs, after 7 d although, sub-figure 9 (bottom, G) shows a higher ALP activity in the RBMSCs-SPCL constructs that were cultured with Dex-loaded CMCht/PAMAM dendrimer nanoparticles after 14 d. We have also observed that ALP activity is higher for the RBMSCs-HAp constructs as compared to that for the RBMSCs-SPCL constructs. Thus, results demonstrated that Dex-loaded CMCht/PAMAM dendrimer nanoparticles combined with HAp enhance osteogenesis by increasing ALP activity and mineralization of the extracellular matrix. Therefore, the present data show that the Dex-loaded CMCht/PAMAM

dendrimer nanoparticle may be useful in TE strategies since it promotes the early osteogenic differentiation of RBMSCs.

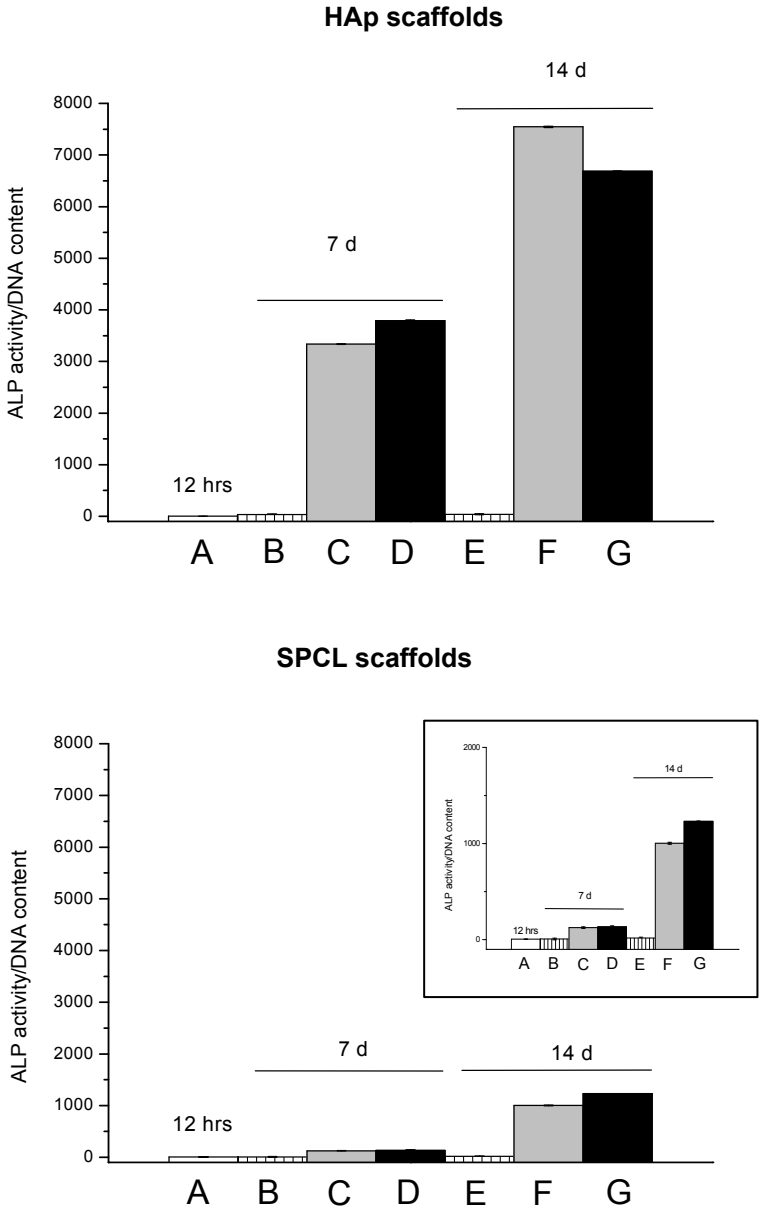

Figure 9. ALP activity per DNA content of the HAp (left) and SPCL (right) scaffolds seeded with RBMSCs (1 x 10^6 cells/scaffold) after culturing in different culture medium for the period of 12 hrs, 7 and 14 d: (A, B and E) Complete MEM medium; (C, F) MEM medium supplemented with 10^{-8} M Dex, 0.28 mM ascorbic acid and 10 mM β-glycerophosphate (osteogenic medium); (D, G) MEM medium with 0.01 mg.mL^{-1} Dex-loaded CMCht/PAMAM dendrimer nanoparticles, 0.28 mM ascorbic acid and 10 mM β-glycerophosphate. Results expressed as an average ± standard deviation, n=9.

In its turn, this data corroborates previous works [27,42,45] that demonstrated the important role of HAp in the adhesion, proliferation and osteogenic differentiation of the RBMSCs, *in vitro* and *in vivo*. This data is not surprising since HAp which has a crystal structure similar to that of bone mineral [46], and is considered the 'gold-standard' of the osteoconductive materials. The obtained results also demonstrated that SPCL scaffolds are effective in supporting the osteogenic differentiation of RBMSCs, since ALP activity is in the same order of magnitude to that of RBMSCs-HAp constructs. On the other hand, the SPCL scaffolds has been shown [31] to be degraded enzymatically, which allows an increase in the scaffold porosity over time and consequently may favour tissue ingrowth during implantation time.
Figure 10 shows the content of the late osteogenic marker and bone-specific osteocalcin normalized by DNA content of RBMSCs cultured onto the surface of the HAp (top) and SPCL (bottom) scaffolds and exposed to a different culture medium for the period of 12 hrs, 7 and 14 d.
This data corroborates the previous ALP assay demonstrating that RBMSCs differentiate into osteoblasts when culturing in the presence of Dex-loaded CMCht/PAMAM dendrimer nanoparticles and osteogenic medium. However, no significant differences in osteocalcin content were observed for the RBMSCs-HAp and RBMSCs-SPCL scaffold constructs supplemented with Dex delivered via the CMCht/PAMAM dendrimer nanoparticles and free in culture media, after 7 and 14 d of culturing. In the light of these results, we have shown that RBMSCs proliferated well, and both differentiate into osteoblasts and organize into a mineralized matrix by combining Dex-loaded CMCht/PAMAM dendrimer nanoparticles and scaffolds (3-D systems), *in vitro*.
This work has demonstrated the efficacy of the system Dex-loaded CMCht/PAMAM dendrimer nanoparticles and scaffolds in promoting the proliferation and osteodifferentiation of RBMSCs, and the success in the intracellular delivery of Dex, *in vitro*. Thus, it is conceivable that intracellular controlled drug delivery using biodegradable nanocarriers or cell-based carrying nanoparticles strategies may be an excellent candidate for *in vivo* TE applications, as these nanosystems may possibly to: (i) reduce the drug dosage needs and, (ii) improve efficacy, since the drug would only concentrate in the damaged/diseased cells and tissues.

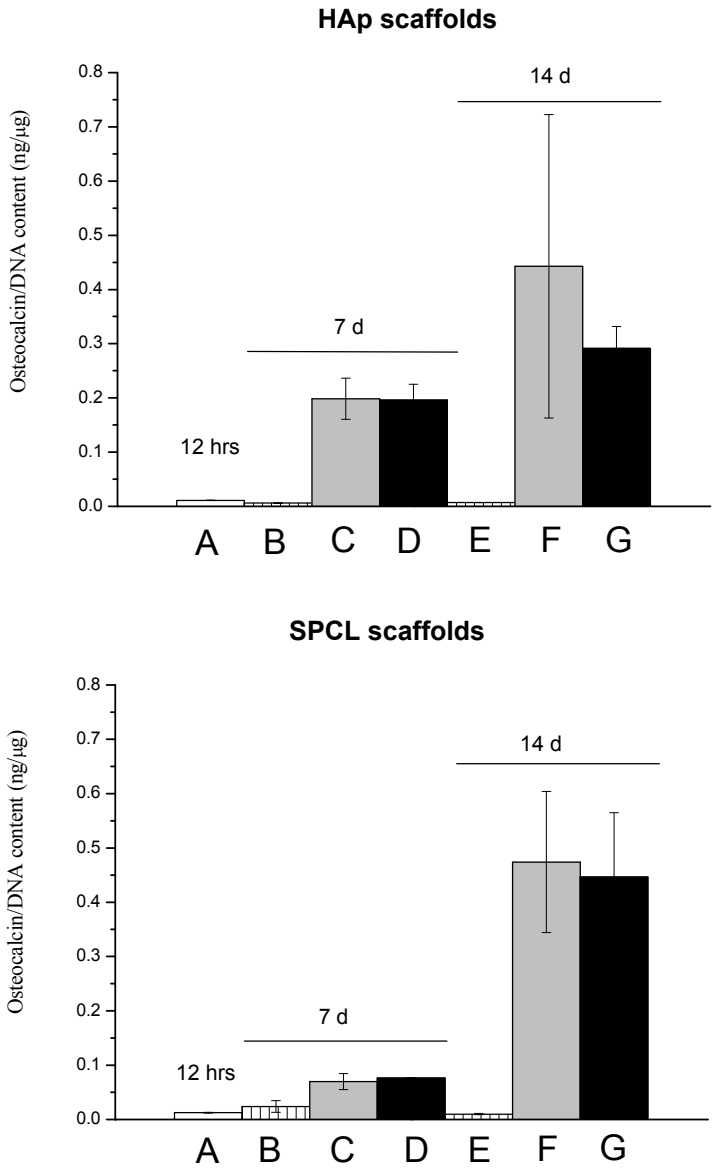

Figure 10. Osteocalcin per DNA content of the HAp (top) and SPCL (bottom) scaffolds seeded with RBMSCs (1 x 10^6 cells/scaffold) after culturing in different culture medium for the period of 12 hrs, 7 and 14 d: (A, B and E) Complete MEM medium; (C, F) MEM medium supplemented with 10^{-8} M Dex, 0.28 mM ascorbic acid and 10 mM β-glycerophosphate (osteogenic medium); (D, G) MEM medium with 0.01 mg.mL^{-1} Dex-loaded CMCht/PAMAM dendrimer nanoparticles, 0.28 mM ascorbic acid and 10 mM β-glycerophosphate. Results expressed as an average ± standard deviation, n=9.

4. CONCLUSIONS

In this work we demonstrate the biological performance of previously prepared macroporous HAp and SPCL scaffolds. These have shown to be adequate for culturing RBMSCs, namely for adhesion,

proliferation and osteogenic differentiation. Results showed that the RBMSCs proliferation and osteogenic differentiation are favored when cultured onto the surface of the HAp scaffolds, but the results obtained for SPCL are quite similar and much better than one could expect for a biodegradable polymer. On the other hand, the biochemical data presented herein demonstrated that the Dex-loaded CMCht/PAMAM dendrimer nanoparticles enhanced the early osteogenic differentiation of RBMSCs, *in vitro*. Therefore, the Dex-loaded CMCht/PAMAM dendrimer nanoparticles may be used as intracellular nanocarriers of biological agents being able to modulate the behaviour of stem cells.

REFERENCES

1. Langer, R. and J. Vacanti, *Tissue Engineering*. Science, 1993. **260**: p. 920.
2. Rice, C.M. and N.J. Scolding, *Autologous bone marrow stem cells - properties and advantages*. Journal of the Neurological Sciences, 2008. **265**(1-2): p. 59.
3. Ke, Z., et al. *Down-regulation of Wnt signaling could promote bone marrow-derived mesenchymal stem cells to differentiate into hepatocytes*. Biochem Biophys Res Commun, 2008. **367**(2): p. 342.
4. Ciapetti, G., et al., *Human bone marrow stromal cells: In vitro expansion and differentiation for bone engineering*. Biomaterials, 2006. **27**(36): p. 6150.
5. Lei, Z., et al., *Culture and neural differentiation of rat bone marrow mesenchymal stem cells in vitro*. Cell Biol Int, 2007. **31**(9): p. 916.
6. Donzelli, E., et al., *Mesenchymal stem cells cultured on a collagen scaffold: In vitro osteogenic differentiation*. Arch Oral Biol, 2007. **52**(1): p. 64.
7. Oshina, H., et al., *Effects of continuous dexamethasone treatment on differentiation capabilities of bone marrow-derived mesenchymal cells*. Bone, 2007. **41**(4): p. 575.
8. Graziani, F., et al., *Perioperative dexamethasone reduces post-surgical sequelae of wisdom tooth removal. A split-mouth randomized double-masked clinical trial*. International Journal of Oral and Maxillofacial Surgery, 2006. **35**(3): p. 241.
9. Stahn, C., et al., *Molecular mechanisms of glucocorticoid action and selective glucocorticoid receptor agonists*. Molecular and Cellular Endocrinology, 2007. **275**(1-2): p. 71.
10. Ebrecht, M., et al., *Tissue specificity of glucocorticoid sensitivity in healthy adults*. Journal of Clinical Endocrinology & Metabolism, 2007. **85**: p. 3733.
11. Hwang, N.S., S. Varghese, and J. Elisseeff, *Controlled differentiation of stem cells*. Advanced Drug Delivery Reviews, 2008. **60**(2): p. 199.

12. Breunig, M., S. Bauer, and A. Goepferich, *Polymers and nanoparticles: Intelligent tools for intracellular targeting?* European Journal of Pharmaceutics and Biopharmaceutics, 2008. **68**(1): p. 112.
13. Zimmer, A. and J. Kreuter, *Microspheres and nanoparticles used in ocular delivery systems*. Advanced Drug Delivery Reviews, 1995. **16**(1): p. 61.
14. He, W., S.W. Horn, and M.D. Hussain, *Improved bioavailability of orally administered mifepristone from PLGA nanoparticles*. International Journal of Pharmaceutics, 2007. **334**(1-2): p. 173.
15. Byrappa, K., S. Ohara, and T. Adschiri, *Nanoparticles synthesis using supercritical fluid technology - towards biomedical applications*. Advanced Drug Delivery Reviews, 2008. **60**(3): p. 299.
16. Li, F.-Q., et al., *Preparation and characterization of sodium ferulate entrapped bovine serum albumin nanoparticles for liver targeting*. International Journal of Pharmaceutics, 2008. **349**(1-2): p. 274.
17. Zhang, W., X. Qiao, and J. Chen, *Synthesis of silver nanoparticles-Effects of concerned parameters in water/oil microemulsion*. Materials Science and Engineering: B, 2007. **142**(1): p. 1.
18. Matsumura, Y., *Poly (amino acid) micelle nanocarriers in preclinical and clinical studies*. Advanced Drug Delivery Reviews, 2008. **60**(8): p. 899.
19. Luten, J., et al., *Biodegradable polymers as non-viral carriers for plasmid DNA delivery*. Journal of Controlled Release, 2008. **126**(2): p. 97.
20. Lee, P.-W., et al., *The use of biodegradable polymeric nanoparticles in combination with a low-pressure gene gun for transdermal DNA delivery*. Biomaterials, 2008. **29**(6): p. 742.
21. Stover, T.C., et al., T*hermoresponsive and biodegradable linear-dendritic nanoparticles for targeted and sustained release of a pro-apoptotic drug*. Biomaterials, 2008. **29**(3): p. 359.
22. Xiang, Y. and D. Chen, *Preparation of a novel pH-responsive silver nanoparticle/poly(HEMA-PEGMA-MAA) composite hydrogel*. European Polymer Journal, 2007. **43**(10): p. 4178.
23. Muzzarelli, R.A.A., P. Ilari, and M. Petrarulo, *Solubility and structure of N-carboxymethylchitosan*. International Journal of Biological Macromolecules, 1994. **16**(4): p. 177.
24. Oliveira, J.M., et al., *Surface engineered carboxymethylchitosan/poly(amidoamine) dendrimer nanoparticles for intracellular targeting*. Advanced Functional Materials, 2008. **18**: p. 1840.
25. Hayashi, R., et al., *Effects of glucocorticoids on gene transcription*. European Journal of Pharmacology, 2004. **500**: p. 51.

26. Zhang, X., et al., *Dexamethasone inhibition of trabecular meshwork cell phagocytosis and its modulation by glucocorticoid receptor b*. Experimental Eye Research, 2007. **84**: p. 275.
27. Oliveira, J.M., et al., *Novel hydroxyapatite/chitosan bilayered scaffold for osteochondral tissue-engineering applications: Scaffold design and its performance when seeded with goat bone marrow stromal cells*. Biomaterials, 2006. **27**(36): p. 6123.
28. Gomes, M.E, et al., *Alternative tissue engineering scaffolds based on starch: processing methodologies, morphology, degradation and mechanical properties*. Materials Science and Engineering: C, 2002. **20**(1-2): p. 19.
29. Mendes, S.C., et al., *Evaluation of two biodegradable polymeric systems as substrates for bone tissue engineering*. Tissue Engineering, 2003. **9**(1): p. 91.
30. Oliveira, A.L., et al., *Micro-computed tomography (μ-CT) as a potential tool to assess the effect of dynamic coating routes on the formation of biomimetic apatite layers on 3D-plotted biodegradable polymeric scaffolds*. Journal of Materials Science: Materials in Medicine, 2007. **18**: p. 211.
31. Gomes, M.E., et al., *Starch-poly(caprolactone) and starch-poly(lactic acid) fibre-mesh scaffolds for bone tissue engineering applications: structure, mechanical properties and degradation behaviour*. Journal of Tissue Engineering and Regenerative Medicine, 2008. **2**(5): p. 243.
32. Chen, X.-G., and H.-J. Park, *Chemical characteristics of O-carboxymethyl chitosans related to the preparation conditions*. Carbohydrate Polymers, 2003. **53**: p. 355.
33. Kotobuki, N., et al., *Viability and osteogenic potential of cryopreserved human bone marrow-derived mesenchymal cells*. Tisssue Engineering, 2005. **11**: p. 663.
34. Tanaka, T., et al., *Nano-scaled hydroxyapatite/silk fibroin sheets support osteogenic differentiation of rat bone marrow mesenchymal cells*. Materials Science and Engineering: C, 2007. **27**: p. 817.
35. Kotobuki, N., et al., *Observation and quantitative analysis of rat bone marrow stromal cells cultured in vitro on newly formed transparent b-tricalcium phosphate*. Journal of Materials Science: Materials in Medicine, 2006. **17**: p. 33.
36. Karageorgiou, V. and D. Kaplan, *Porosity of 3D biomaterial scaffolds and osteogenesis*. Biomaterials, 2005. **26**: p. 5474.
37. Leberbauer, C., et al., *Different steroids co-regulate long-term expansion versus terminal differentiation in primary human erythroid progenitors*. Blood, 2005. **105**(1): p. 85.
38. Li, J.P., et al., *Bone ingrowth in porous titanium implants produced by 3D fiber deposition*. Biomaterials, 2007. **28**(18): p. 2810.

39. Silva, M.M.C.G., et al., *The effect of anisotropic architecture on cell and tissue infiltration into tissue engineering scaffolds*. Biomaterials, 2006. **27**(35): p. 5909.
40. Miot, S., et al., *Effects of scaffold composition and architecture on human nasal chondrocyte redifferentiation and cartilaginous matrix deposition*. Biomaterials, 2005. **26**(15): p. 2479.
41. Pittenger, M.F., et al., *Multilineage potential of adult human mesenchymal stem cells*. Science, 1999. **284**: p. 143.
42. Kotobuki, N., et al., *Observation of osteogenic differentiation cascade of living mesenchymal stem cells on transparent hydroxyapatite ceramics*. Biomaterials, 2005. **26**: p. 779.
43. Beck, G.R., B. Zerler, and E. Moran, *Phosphate is a specific signal for induction of osteopontin gene expression*. Proceedings of the National Academy of Sciences of the United States of America, 2000. **97**: p. 8352.
44. Eijken, M., et al., *The essential role of glucocorticoids for proper human osteoblast differentiation and matrix mineralization*. Molecular and Cellular Endocrinology, 2006. **248**: p. 87.
45. Yoshikawa, T., et al., *Biochemical and histological sequences of membranous ossification in ectopic site*. Calcified Tissue International, 1992. **50**: p. 184.
46. Hing, K.A., et al., *Biomechanical assessment of bone ingrowth in porous hydroxyapatite*. Journal of Materials Science: Materials in Medicine, 1997. **8**: p. 731.

CHAPTER IX.

Ex vivo culturing of rat bone marrow stromal cells with dexamethasone-loaded carboxymethylchitosan/poly(amidoamine) dendrimer nanoparticles enhances ectopic bone formation on tissue engineered constructs

CHAPTER IX.

Ex vivo culturing of rat bone marrow stromal cells with dexamethasone-loaded carboxymethylchitosan/poly(amidoamine) dendrimer nanoparticles enhances ectopic bone formation on tissue engineered constructs

Abstract

Recently, our group has proposed a combinatorial strategy in tissue engineering principles employing carboxymethylchitosan/poly(amidoamine) dendrimer nanoparticles (CMCht/PAMAM) towards the intracellular release and regimented supply of dexamethasone (Dex) aimed at control stem cells osteogenic differentiation in the absence of typical osteogenic inducers, *in vivo.* In this work, we have investigated if the Dex-loaded CMCht/PAMAM dendrimer nanoparticles could play a crucial role in the regulation of osteogenesis, *in vivo*. Macroporous hydroxylapatite (HAp) scaffolds were seeded with rat bone marrow stromal cells (RBMSCs), whose cells were expanded in MEM medium supplemented with 0.01 mg.mL^{-1} Dex-loaded CMCht/PAMAM dendrimer nanoparticles and implanted subcutaneously on the back of rats for the period of 2 and 4 weeks. HAp porous ceramics without RBMSCs and RBMSCs/HAp scaffold constructs seeded with cells expanded in the presence and absence of 10^{-8} M Dex were used as controls. The effect of initial cell number seeded in the HAp scaffolds on the bone forming ability of the constructs was also investigated. Qualitative and quantitative new bone formation was evaluated using micro-computed tomography analysis of the implants, Haematoxylin & Eosin staining of the implant sections and histomorphometrical analysis. Toluidine blue staining was also carried out to investigate the synthesis of proteoglycan extracellular matrix. In addition, alkaline phosphatase and osteocalcin levels were quantified, since these markers denote osteogenic differentiation. At four-weeks post-implantation results have shown that the novel Dex-loaded carboxymethylchitosan/poly(amidoamine) dendrimer nanoparticles may be beneficial as intracellular nanocarrier, supplying Dex in a regimented manner leading to superior ectopic *de novo* bone formation. The superior role of the Dex-loaded CMCht/PAMAM dendrimer nanoparticles in enhancing new bone formation was particularly evident when seeding 2 x 10^5 RBMSCs per HAp scaffold.

This chapter is based on the following publication: **Oliveira JM**, Kotobuki N, Tadokoro M, Hirose M, Mano JF, Reis RL and Ohgushi H, *Ex vivo* culturing of rat bone marrow stromal cells with dexamethasone-

loaded carboxymethylchitosan/poly(amidoamine) dendrimer nanoparticles enhances ectopic bone formation on tissue engineered constructs (2009), submitted.

1. INTRODUCTION

A variety of hydroxylapatite (HAp) ceramics with controlled architectures [1-3] has been developed for find applications as bone substitutes in clinic. Despite, their interesting architecture namely pore size, shape and interconnectivity, mechanical properties and important biological role in the *in vivo* performance, these porous implants lack on their osteoinductive capacity [4-6]. In this regard, it has been shown that porous HAp ceramics alone, do not induce bone formation in soft tissues when implanted in rabbits [7], or upon subcutaneous implantation in mice [8,9], rats [10-12] and goats [13]. By its turn, bone marrow stromal cells (BMSCs) have shown to inherently possess a huge therapeutic potential [14-20]. Therefore, in bone tissue engineering strategies, combination of bone marrow stromal cells (BMSCs) with porous scaffolds [10,11,13,21] and use of bioreactors [22,23], have been widely explored as possible alternatives. On the other hand, it has been shown that glucocorticoids such as dexamethasone (Dex) has an essential role for osteoblast differentiation and matrix mineralization [24-26]. In fact, it has been reported that Dex regulation depends on the degree of cellular differentiation, the donor species, and dosage, dose duration and dosing regimen [27]. Several authors [9,10,28] reported that stem cells need to be under the influence of such type of osteogenic factors for superior *de novo bone* formation. Actually, cell-scaffold constructs showed bone formation within the pores of the scaffolds when constructs were *in vitro* cultured under osteogenic factors post-implantation [10,11]. However, the long culturing time is a major drawback of this strategy and may not be the most feasible for satisfactorily meet clinical demands. In addition, we foresee that cells may not maintain *in vivo* the cellular phenotype upon withdrawal of Dex, since Dex acts at both early and late stages to direct proliferative osteoprogenitor cells toward terminal maturation [29]. Therefore, a great deal of attention has been paid for finding alternative approaches to improve the limited cell-derived osteogenesis. In this context, we have been hypothesizing that the *ex vivo* culturing of stem cells with functional nanoparticles which can be efficiently taken up by cells may influence their cellular fate in the absence of typical osteogenic inducers, *in vivo*. It has been shown that glucocorticoids such as Dex bind to and triggers the cytoplasmatic glucocorticoid receptor [30,31]. Thus, we expect that the culturing of stem cells in the presence of nanoparticles that release Dex from inside, and in a regimented manner may be an effective strategy for *in vivo* control of stem cells osteogenic differentiation and maturation. In this regard, we have surface engineered low generation poly(amidoamine) dendrimers with carboxymethylchitosan, CMCht/PAMAM dendrimer nanoparticles and loaded them with Dex [32]. These are expected to possess high payload, and improved biocompatibility when compared to that of typical dendrimers. The use of Dex-loaded CMCht/PAMAM

dendrimer nanoparticles can also allow avoid the need and frequency of drug administration since Dex is available at the target site, and thus possibly minimize the undesired side-effects [31].

In previous *in vitro* studies [32,33], we have shown the high efficiency of Dex-loaded CMCht/PAMAM dendrimer nanoparticles on being internalized by different cell types. The Dex release profile from the CMCht/PAMAM nanoparticles was monitored, in the presence and absence of serum proteins at physiological pH. This study has shown that Dex is released as free drug in the range of concentrations similar to that of typical osteogenic cocktails. Complementarily, we demonstrated their role in promoting the osteogenic differentiation of rat bone marrow stromal cells (RBMSCs) in tissue culture polystyrene, TCPS dishes.

Our group [34] has recently developed HAp scaffolds with macroporous structure and reported that these scaffolds are biocompatible and efficiently support the adhesion, proliferation and osteogenic differentiation of RBMSCs in the presence of 0.01 mg.mL^{-1} Dex-loaded CMCht/PAMAM dendrimer nanoparticles, *in vitro* [35]. Thus, the HAp scaffolds have shown *in vitro* to possess suitable physicochemical and biological properties for being used in bone tissue engineering approaches. To further evaluate the *in vivo* performance of the cell-scaffold constructs, several groups [10,11,28,36] have been proposing the well established ectopic implantation model in rats. This is a cost effective model [37] and allows to avoid the presence of growth factors found at the orthotopic site whose influences may affect the performances of the constructs [38].

In the current experimental study, we investigate if the Dex-loaded CMCht/PAMAM dendrimer nanoparticles play a crucial role in the regulation of osteogenesis, *in vivo*. We therefore used RBMSCs/HAp constructs where cells were exposed to 0.01 mg.mL^{-1} Dex-loaded CMCht/PAMAM dendrimer nanoparticles during the expansion time (Figure 1, top) and assess their efficiency in promoting the osteogenic differentiation and *de novo* bone formation upon subcutaneous implantation on the back of rats for the period of 2 and 4 weeks. HAp porous ceramics and RBMSCs/HAp constructs seeded with different cells number and cultured either, presence and absence of Dex were used as controls for elucidating the role of the Dex-loaded CMCht/PAMAM dendrimer nanoparticles in promoting osteogenesis. Micro-computed tomography analysis was performed to investigate new bone formation in the RBMSCs/HAp constructs. Histological studies were also carried out using Haematoxylin & Eosin staining. Histomorphometrical analysis of the implants sections was performed to quantify new bone formation. Toluidine blue staining was also performed to investigate the synthesis of proteoglycan extracellular matrix. Complementarily, osteoblastic phenotype expression levels were determined by

quantification of the surface-membrane alkaline phosphatase (ALP) glycoprotein and osteocalcin, the early and late markers of osteogenic differentiation, respectively [39,40].

2. MATERIALS AND METHODS

2.1. PREPARATION OF THE HYDROXYLAPATITE (HAP) SCAFFOLDS AND SYNTHESIS OF DEXAMETHASONE-LOADED CARBOXYMETHYLCHITOSAN/POLY(AMIDOAMINE) DENDRIMER (DEX-LOADED CMCHT/PAMAM DENDRIMER NANOPARTICLES)

Sintered HAp scaffolds with 5 mm diameter and 4 mm height were obtained by means of impregnating a polyurethane (PU, Eurospuma S.A., Portugal) sponge with HAp powders, as previously reported [34,41,42]. Carboxymethylchitosan was synthesized by a chemical modification route of chitin (Sigma, Germany) as described by Chen et al. [43]. Starburst® poly(amidoamine)-carboxylic terminated dendrimers, PAMAM-CT (generation 1.5, 20% (w/v) methanolic solution) with an ethylenediamine core were purchased from Aldrich (Germany). Dexamethasone-loaded carboxymethylchitosan/poly(amidoamine) dendrimer nanoparticles (Dex-loaded CMCht/PAMAM) were prepared in a stepwise manner as described elsewhere [32].

Prior to the *in vitro* cell culture the HAp scaffolds and Dex-loaded CMCht/PAMAM dendrimer nanoparticles were sterilized under an ethylene oxide gas atmosphere.

2.2. *IN VITRO* CELL CULTURE

2.2.1. Isolation and expansion of rat bone marrow stromal cells (RBMSCs)

Seven-week-old Fischer 344/N male rats (Japan SLC Inc., Shizuoka, Japan) were sacrificed by administrating an excess of anesthesia, in accordance to the Ethics Committee at the Tissue Engineering Research Center (Amagasaki, Japan). The marrow plugs in the femoral shafts were flush out using Eagle's minimum essential medium (MEM, Nacalai Tesque, Japan) supplemented with 15% fetal bovine serum (FBS, JRH Biosciences, USA) and 1% antibiotic-antimycotic (A/B, Nacalai Tesque, Japan) solution, as previously reported [44]. RBMSCs were transferred to T75 cm^2 culture flask and expanded in the presence of different culture medium: complete MEM medium, MEM medium supplemented with 0.01 $mg.mL^{-1}$ Dex-loaded CMCht/PAMAM dendrimer nanoparticles and MEM medium supplemented with 10^{-8} M dexamethasone at 37ºC in a 5% CO_2 incubator. The culture medium was changed within 3 days to remove non-adherent cells. Then, culture medium was changed each 2 or 3 days.

2.2.2. Seeding of RBMSCs onto the surface of the HAp scaffolds

The RBMSCs (passage 1, P1) were released from substratum with 1 mL of 0.05% tripsin-0.53 mM EDTA (Invitrogen, USA) and centrifuged at 900 rpm for 5 minutes, after reach confluence. The supernatant was aspirated and cells re-suspended with 10 mL of complete culture medium. Cell concentration was determined using an automatic cell counter (Cell Counter Sysmex F-520, Japan). Prior seeding, the viability of the RBMSCs was also analyzed with a NucleoCounter (ChemoMetec A/S, Denmark) [45]. In addition, the HAp scaffolds were de-aired in MEM medium under vacuum [35]. Then, one scaffold was placed in a well of a 96-well TCPS plate and RBMSCs seeded in a drop-wise manner. RBMSCs expanded in complete MEM medium, MEM medium supplemented with 0.01 $mg.mL^{-1}$ Dex-loaded CMCht/PAMAM dendrimer nanoparticles and MEM medium supplemented with 10^{-8} M dexamethasone were seeded onto each HAp scaffold. The effect of cell density was evaluated by seeding different cell numbers (1×10^6 and 2×10^5) onto the HAp scaffolds. Finally, RBMSCs/HAp scaffolds constructs were cultured in complete MEM medium under standard culture conditions to allow cell adhesion, for the period of 12 hours.

2.3. *IN VIVO* STUDY

2.3.1. Subcutaneous implantation

Seven-week-old male Fisher 344 rat (Syngeneic F344/N rat), same as donor sub-strain and age, were anesthetized by intraperitoneal injection of pentobarbital (Nembutal, Dainippon Pharmaceutical Co. Ltd., Japan) at a final concentration of 3.5 mg per 100 g of body weight. The hair of the rat was cut at the implantation area, followed by washing with tap water and scrubbed with tincture of iodine and 70% ethanol. In each rat, three or four skin incisions (each 1 cm length) on the dorsal midline below the ear were made. Each RBMSCs/HAp construct was implanted subcutaneously (1.5 to 2 cm away from the midline at both right and left sides) into the respective pocket and skin sutured. As a negative control, we used HAp implants without RBMSCs. No prophylactic medication was administered post-surgery.
After 2 and 4 weeks implantation, the animals were sacrificed with an overdose of anesthetic and the implants retrieved. All experiments were carried out 3 times.

2.3.2. Micro-computed tomography analysis

New bone formation in the retrieved implants was investigated by micro-computed tomography analysis (μ-CT: MCT-CB 100MF(Z); Hitachi Medical Corp., Tokyo, Japan). After 2 and 4 weeks of implantation,

implants were retrieved, rinsed with PBS, and fixed with 10 % formalin at room temperature, overnight. Constructs were placed on the flat surface for analysis under the μ-CT. X-ray scans were acquired with a resolution mode of 10 μm (x/y/z) at 50 kV and 150 μA. The analytical conditions were: precision mode, 7 times magnification with an image intensifier field of 4.57 cm [46]. CT reconstruction has carried out using the 3-D Bone Morphometry (TRI/3D-Bon, RATOC System Engineering Co. Ltd., Tokyo, Japan) software for evaluate the 2-D distribution of newly formed bone within the pores of the explants.

2.3.3. Histological evaluation of the explants

After μ-CT, implants were decalcified with K-CX solution (Falma Co., Tokyo, Japan) for histological analysis. Firstly, the constructs were dehydrated in an ascending series grade ethanol/water solution (from 90-100%) using an automatic machine for 19 hours followed by washing three times with xylene. Then, specimens were immersed in paraffin at 62ºC and allowed to solidify at -5ºC. Slides were prepared by cutting the specimens into sections 5 μm thick using a microtome, and mounted in a micro-slide glass (Matsunami glass Ind. Ltd., Japan). Paraffin was melt by placing the slides in the oven at 71ºC for 20 minutes and allowed to let cool down at room temperature. The remnant paraffin was then eliminated off in hexane for 5 minutes (S.T. Chemical, Japan), followed by dipping into a ethylene/propylene mixture (Clear Plus, Falma Co., Tokyo, Japan) for 3 minutes. Then, slides were immersed three times in 100% ethanol for 2 minutes each time of immersion.

For the Haematoxylin & Eosin (H&E) staining, slides were sequentially transferred to a 90% ethanol and then to a 70% and washed with tap water. It followed the staining step, which consisted in the immersion of the slides into the GM's Haematoxylin dye (Muto Pure Chemicals Co. Ltd, Tokyo, Japan, GM Haematoxylin Staining for H&E staining Nº 3008-1) for 10 minutes. It followed the washing step with tap water for 5 to 10 minutes. Then, slides were rinsed with de-ionized water and immersed in a 70% ethanol solution. Finally, slides were immersed in Eosin dye (Muto Pure Chemicals Co. Ltd, Tokyo, Japan Nº 3204-2) solution for 2 minutes and dehydrated in a series of ethanol grades (70%, 90%, and 100%). At last were immersed three times in an ethylene/propylene mixture and then mounted avoiding the formation of bubbles for observation.

For Toluidine blue staining, paraffin was melt and slides rinsed with ultrapure water. The ground sections were stained with 0.05% toluidine blue (Muto Pure Chemicals Co. Ltd., Tokyo, Japan) for 30 minutes. Finally, the slides were dehydrated in a series of ethanol grades (70%, 90%, and 100%) and mounted for further observation. All slides were examined under a light microscope (Olympus

DP70, Olympus Co. Ltd, Japan). 2-D histological sections are given for the same bone specimens used in the micro-computed tomography analysis.

2.3.4. Histomorphometry

Histomorphometrical analysis was carried out using the public domain image-processing program IMAGE J (National Institutes of Health, Bethesda, MD) to obtain quantitative evaluation of histological section of bone. The light microscopy photographs of the 2-D histological decalcified sections of each sample were converted to gray-value images and several filter steps were performed [47]. Shrinkage percentage observed in decalcified sections [46] was not considered in the calculations. New bone formation (NB) was expressed as a percentage of bone volume density (BV/TSV, Bone volume/Tissue plus Scaffold volume) ± standard deviation. A minimum of 12 sections per implant were analyzed.

2.3.5. Quantification of alkaline phosphatase (ALP)

Alkaline phosphatase was measured to evaluate osteoblast differentiation. Prior to the assay, the explants were washed with Ca and Mg-free PBS solution. Then, implants were transferred to a 2 mL eppendorf and pulverized with zirconia's balls as previously reported [35]. Prior to analysis the samples were sonicated and centrifuged at 12,000 rpm for 1 minute at 4°C. To each well of a 96-well plate was added an aliquot of supernatant and p-nytrophenyl phosphate substrate (ZYMED® Laboratories, Invitrogen, USA) [46]. The plate was then incubated in the dark for 30 minutes at 37ºC and after that time the reaction was stopped with 1 M NaOH (Panreac, Japan). Standards were prepared with p-nytrophenol, pNP. Triplicates were made for each sample and standard. Absorbance was read at 405 nm (Wallac ARVOsx 1420, Perkin-Elmer Life and Analytical Sciences, USA), and sample concentrations were read off from the standard graph. Enzyme activity was expressed either as nmol of pNP released/explant/30 minutes.

2.3.6. Quantification of osteocalcin

The remnant of each sample used for the ALP assay was treated with a 20% formic acid solution and stored at 4°C for 2-3 days. Afterwards samples were centrifuged at 15,000 rpm for 10 minutes at 4°C. Then, the supernatant was passed through a Sephadex™ G-25 column (GE healthcare, Sweden), subsequently concentrated for performing the Enzyme-linked immunosorbent assay (ELISA). A Rat Osteocalcin EIA kit (N° BT-460, Biomedical Technologies Inc., MA, USA) was used following the

instructions provided by the supplier. Data was read off from the standard curve obtained with human osteocalcin and expressed as ng of deposited osteocalcin per explant.

3. RESULTS AND DISCUSSION

Recently, our group [32] has proposed the combinatorial strategy of tissue engineering principles with nanocarriers towards the intracellular release and regimented supply of Dex aimed at control the stem cells osteogenic differentiation in the absence of typical osteogenic cocktails, *in vivo*. In this context, we have shown that is possible to develop CMCht/PAMAM dendrimer nanoparticles and load these macromolecules with Dex. The *in vitro* release studies have shown that Dex is released as free drug in the range of concentrations similar to that of typical osteogenic cocktails when using concentrations of nanoparticles in the range of 0.01 $mg.mL^{-1}$. Moreover, we have shown that osteogenic differentiation occurs in RBMSCs seeded onto the HAp scaffolds in the presence of 0.01 $mg.mL^{-1}$ Dex-loaded CMCht/PAMAM dendrimer nanoparticles, *in vitro* [35].

In the current work, we have investigated if the Dex-loaded CMCht/PAMAM dendrimer nanoparticles can allow improving *in vivo* bone formation. We therefore exposed RBMSCs to 0.01 $mg.mL^{-1}$ Dex-loaded CMCht/PAMAM dendrimer nanoparticles during expansion time, seeded the RBMSCs onto the surface of the HAp scaffolds and implanted the constructs subcutaneously on the back of F344/N rats (Figure 1, top). The effect of cell number on the bone forming capacity was also investigated, since has been shown that influences ectopic bone formation [37]. Ohgushi et al. [45] observed that fresh RBMSCs cultured in the presence of Dex and seeded onto the HAp scaffolds can show a high level of *in vivo* bone-forming ability. Therefore, in this study we also used as control the RBMSCs/HAp constructs, where RBMSCs were pre-cultured in a MEM medium with Dex at a final concentration of 10^{-8} M. We preliminary assessed histologically, new bone formation on the RBMSCs/HAp constructs, after 2 weeks of subcutaneous implantation. At 2 weeks post-implantation no bone formation was detected in the RBMSCs/HAp constructs with RBMSCs expanded in complete MEM medium, MEM medium supplemented with 0.01 $mg.mL^{-1}$ Dex-loaded CMCht/PAMAM dendrimer nanoparticles and MEM medium supplemented with 10^{-8} M dexamethasone and HAp scaffolds without cells (data not shown). Therefore, to observe the effect of pre-culturing RBMSCs in the presence of Dex-loaded CMCht/PAMAM dendrimer nanoparticles in the *de novo* bone formation, we implanted subcutaneously the RBMSCs/HAp constructs for 4 weeks.

Figure 1 (bottom) shows the photograph of the RBMSCs/HAp construct in the back of the F344/N rats, where RBMSCs were pre-incubated with 0.01 $mg.mL^{-1}$ Dex-loaded CMCht/PAMAM dendrimer

nanoparticles, after 4 weeks of subcutaneous implantation. No signs of infection or acute inflammatory reaction were detected at the implantation sites, for all implants.

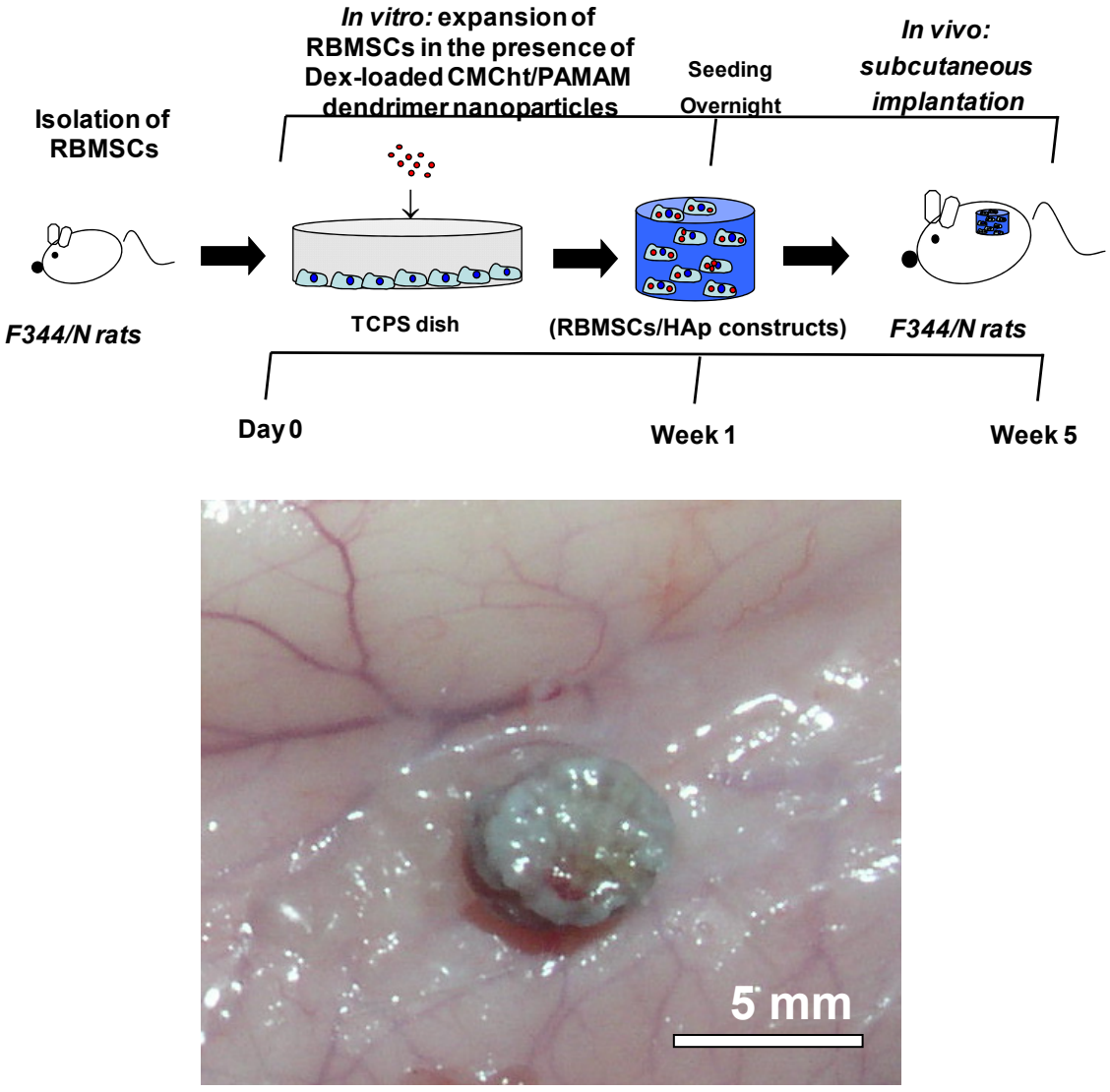

Figure 1. Schematic representation of the experimental strategy (top) and photo of the RBMSCs/HAp explants with RBMSCs expanded in MEM medium supplemented with 0.01 mg.mL^{-1} Dex-loaded CMCht/PAMAM dendrimer nanoparticles, after 4 weeks of subcutaneous implantation (bottom).

Figure 2 shows the 2-D μ-CT images and respective microradiographs of the RBMSCs/HAp constructs after 4 weeks of subcutaneous implantation. We can observe different attenuation areas, having high (white), medium (light gray), and low (dark gray) intensities. We defined the white, light gray, and dark gray areas as HAp scaffold, *de novo* bone (NB, gray arrows), and fibrovascular tissue with fat cells, respectively.

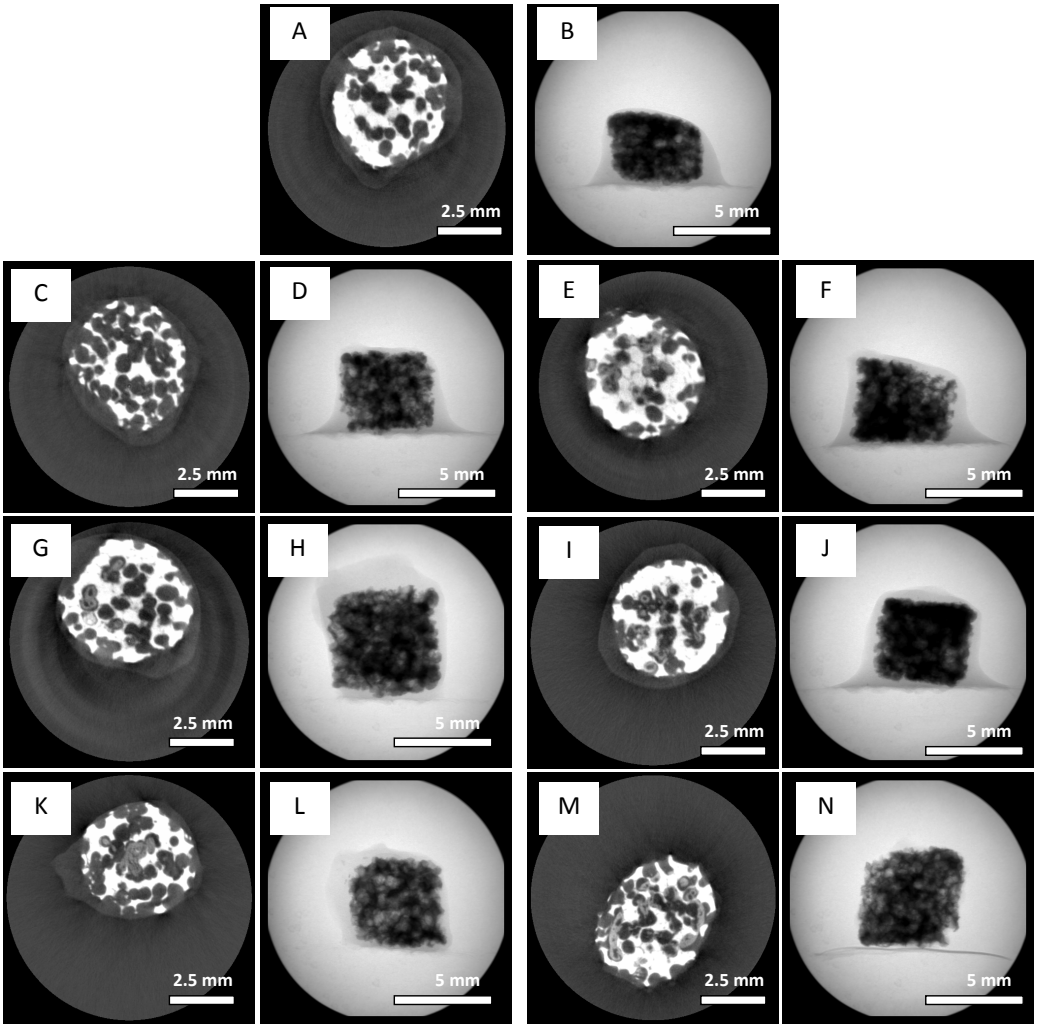

Figure 2. 2-D μ-CT images and respective X-ray photographs of the explants, after 4 weeks of subcutaneous implantation: HAp scaffolds (A-B), HAp seeded with 2 x 10^5 RBMSCs which were expanded in MEM medium (C-D), HAp seeded with 1 x 10^6 RBMSCs which were expanded in MEM medium (E-F), HAp seeded with 2 x 10^5 RBMSCs which were expanded in MEM medium supplemented with 10^{-8} M dexamethasone (G-H), HAp seeded with 1 x 10^6 RBMSCs which were expanded in MEM medium supplemented with 10^{-8} M dexamethasone (I-J), HAp seeded with 2 x 10^5 RBMSCs which were expanded in MEM medium supplemented with 0.01 mg.mL^{-1} Dex-loaded CMCht/PAMAM dendrimer nanoparticles (K-L), and HAp seeded with 1 x 10^6 RBMSCs which were expanded in MEM medium supplemented with 0.01 mg.mL^{-1} Dex-loaded CMCht/PAMAM dendrimer nanoparticles (M-N). We defined the white, light gray, and dark gray areas as HAp scaffold, new bone formation formed bone (gray arrows), and fibrovascular tissue with fat cells, respectively.

Massive areas of NB (gray areas) were detected in all RBMSCs/HAp scaffold constructs seeded with 1 x 10^6 RBMSCs (Figures 2E, I and M) as compared to those of HAp constructs without cells (Figure 2A)

and RBMSCs/HAp constructs seeded with 2 x 10^5 RBMSCs (Figure 2C) that were pre-cultured in MEM medium.

Figure 3 shows the light microscopy photographs of the different RBMSCs/HAp explants decalcified sections after 4 weeks of subcutaneous implantation, which were stained with Haematoxylin & Eosin. The histological findings showed extensive *de novo bone* formation inside the HAp pores with cuboid osteoblasts lining (black arrows) the forming bone matrix in all HAp scaffolds seeded with 1 x 10^6 RBMSCs (Figures 3E, F, I, J, M, N), indicating an active bone formation site. In fact, it is also possible to observe the lacunar spaces and reminiscent osteocyte-like cells entrapped in the bone matrix (see Figures 3H, J and L). Thus, osteocytic lacunae in the lamellar bone are uniform and regularly distributed with osteoblasts forming a continuous layer of bone in a unidirectional way typical of mature bone (NB). In addition, we also detect new bone formation in the HAp scaffolds seeded with 2 x 10^5 RBMSCs that were previously expanded in the presence of 10^{-8} M Dex (Figures 3G-H) and 0.01 $mg.mL^{-1}$ Dex-loaded CMCht/PAMAM dendrimer nanoparticles (Figures 3K-L). In the late, we can observe a higher new bone formation as compared to that of constructs seeded with RBMSCs that were expanded in the presence of 10^{-8} M (Figures 3G-H). This data thus confirm the μ-CT observations in Figure 2, which showed that the gray areas are in fact newly formed bone. From Figures 3A-B it can be seen that fibrovascular tissue (F) with fat cells was formed and there is no evidence of *de novo* bone formation within the scaffolds. No bone formation was also observed for the RBMSCs/HAp constructs seeded with 2 x 10^5 RBMSCs that were expanded in MEM medium (Figures 3C-D), thus once corroborating the μ-CT findings. Despite, this data shows the importance of the porous size and interpore connectivity on the cells in-growth since fibrovascular tissue can be seen in the core of the scaffolds. Moreover, we can also observe that bone formation in the implants seeded with 1 x 10^6 RBMSCs expanded in the presence of 10^{-8} M Dex for 7 days, is restricted to the walls of the HAp scaffolds (Figure 3I). In addition, it can also be seen extensive formation of adipocytes (A) in inner part of the pores of the implants. This result is not surprisingly since Porter et al. [29] have shown that the sustained exposure of bone marrow stromal cells (BMSCs) to Dex induce the maturation of an adipocyte subpopulation within BMSCs, *in vitro*. Actually, in their studies they proposed that these side effects can be reduced if Dex is supplied in a regimented manner. In fact this hypothesis is supported by our histological findings, since we can detect that the pores of the RBMSCs/HAp constructs, where cells were pre-cultured with Dex-loaded CMCht/PAMAM dendrimer nanoparticles are completely filled with calcified bone like-matrix (Figure 3M), and the presence of adipocytes is decreased. Thus this data supports the idea that the supply of Dex in a regimented

manner may be an effective strategy to, on one hand avoid the RBMSCs adipogenic differentiation in the inner part of the pores and, on the other, direct RBMSCs towards osteogenic differentiation.

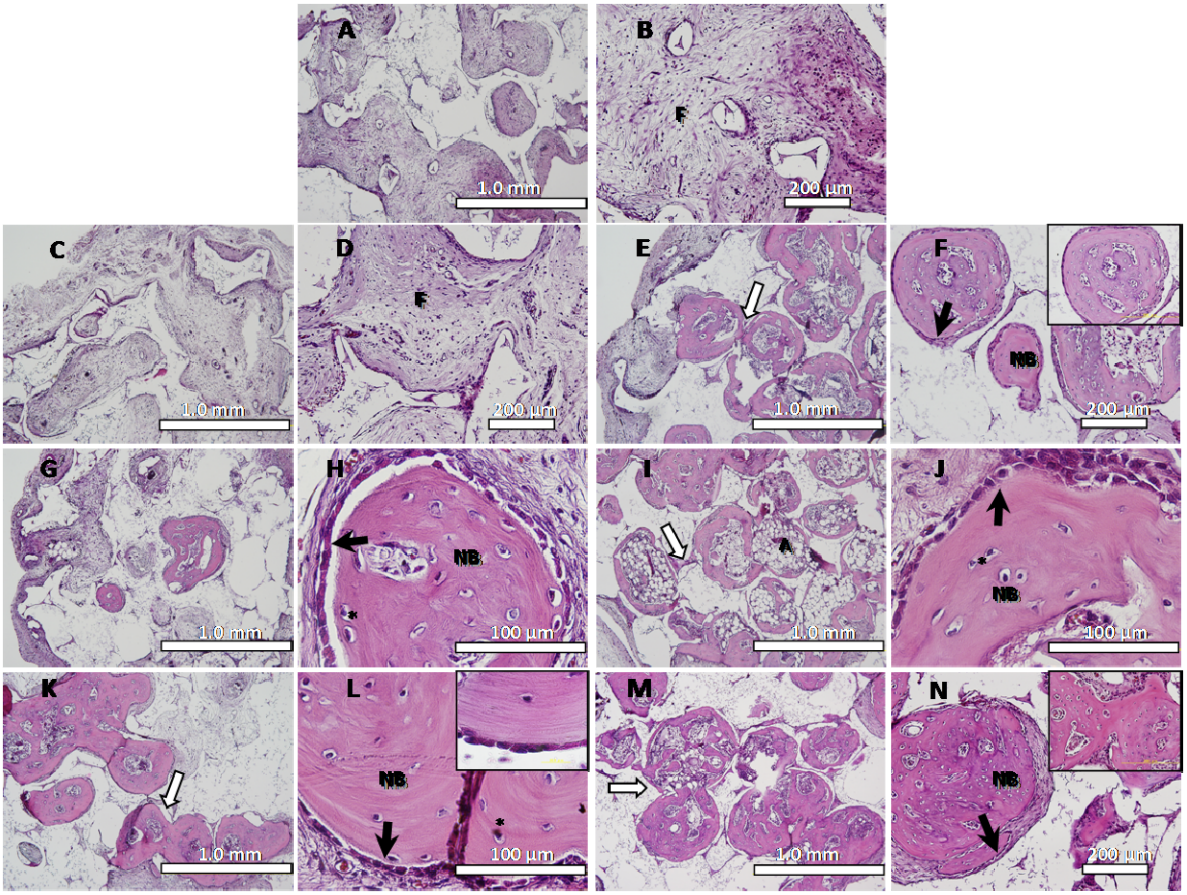

Figure 3. Light microscopy photographs of the explants sections stained with Haematoxylin & Eosin (decalcified sections), after 4 weeks of subcutaneous implantation: HAp scaffolds (A-B), HAp seeded with 2 x 10^5 RBMSCs which were expanded in MEM medium (C-D), HAp seeded with 1 x 10^6 RBMSCs which were expanded in MEM medium (E-F), HAp seeded with 2 x 10^5 RBMSCs which were expanded in MEM medium supplemented with 10^{-8} M dexamethasone (G-H), HAp seeded with 1 x 10^6 RBMSCs which were expanded in MEM medium supplemented with 10^{-8} M dexamethasone (I-J), HAp seeded with 2 x 10^5 RBMSCs which were expanded in MEM medium supplemented with 0.01 mg.mL^{-1} Dex-loaded CMCht/PAMAM dendrimer nanoparticles (K-L), and HAp seeded with 1 x 10^6 RBMSCs which were expanded in MEM medium supplemented with 0.01 mg.mL^{-1} Dex-loaded CMCht/PAMAM dendrimer nanoparticles (M-N). It is possible to observe representative areas of *de novo* bone formation (NB), fibrous tissue (F) and adipocytes (A). White arrows indicate the interconnected pores. Black arrows shows the cells lining which is suggestive of active osteoblasts. Osteocytes can also be visualized (*).

Several authors [8,10,48,49] have been considering that degradation rate, pore geometry and degree of interconnectivity are important features for successfully induce *de novo* bone formation, since they control the diffusion of oxygen, nutrients and metabolites to and from the cells. Therefore, the developed HAp scaffolds should own an adequate pore size and interconnectivity, since extensive new bone formation within the macropores was observed. From 2-D μ-CT images and histological findings we observe that new bone was connected at the interpores (Figures 2 and 3). It has been shown that the interpore connections below 3 μm do not allow cell migration and vascularization [50]. Actually, we may observe bone formation in the core (osteoconduction) of the HAp scaffolds which reveals that the scaffolds posses an adequate interpore size and connection.

Figure 4 shows a representative light microscopy photograph of a decalcified section (H&E staining) of HAp scaffolds seeded with 1 x 10^6 RBMSCs which were expanded in MEM medium supplemented with 0.01 mg.mL^{-1} Dex-loaded CMCht/PAMAM dendrimer nanoparticles, after 4 weeks of subcutaneous implantation, and the respective imaging processing that was carried out to perform the histomorphometrical analyses.

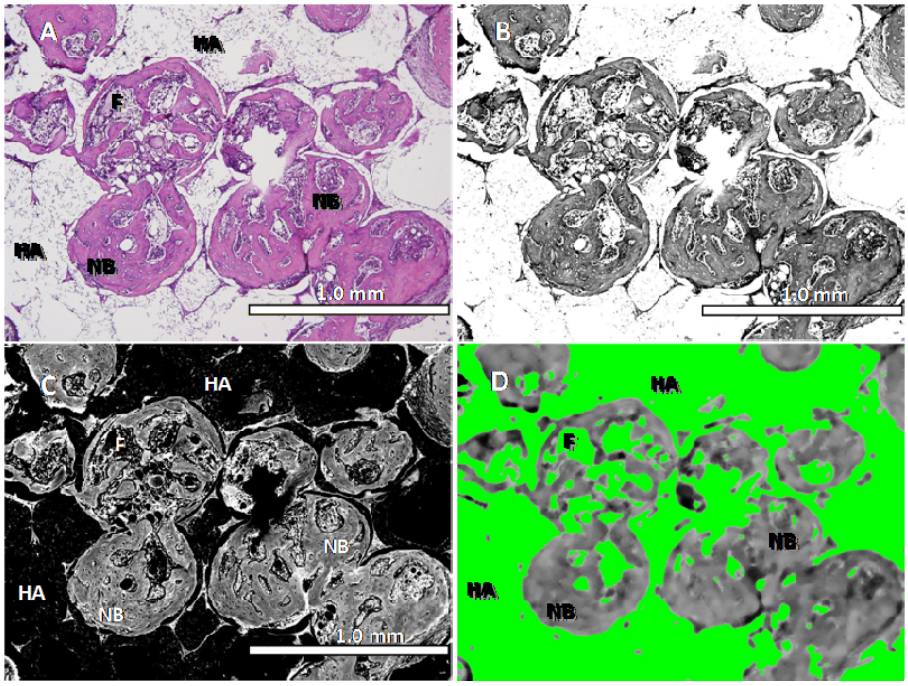

Figure 4. Light microscopy photographs of a explant section corresponding to the HAp seeded with 1 x 10^6 RBMSCs which were expanded in MEM medium supplemented with 0.01 mg.mL^{-1} Dex-loaded CMCht/PAMAM dendrimer nanoparticles, after 4 weeks of subcutaneous implantation: Decalcified section stained with H&E (A), and respective imaging processing (B-D). It is possible to observe representative areas of *de novo* bone formation (NB), HAp scaffolds (HAp) and fibrous tissue (F).

Table 1 shows the percentage of bone volume density in the different implants determined from the histomorphometrical analysis of the 2-D histological sections. Results have shown that no bone formation was observed in the HAp scaffolds without RBMSCs and HAp seeded with 2 x 10^5 RBMSCs expanded in MEM medium. Bone volume density in HAp seeded with 1 x 10^6 RBMSCs expanded in MEM medium was 27.1 ± 7.1%. By its turn, HAp seeded with 2 x 10^5 and 1 x 10^6 RBMSCs expanded in MEM medium supplemented with 10^{-8} M Dex was 6.9 ± 4.7% and 36.4 ± 9.2%, respectively. Finally, HAp seeded with 2 x 10^5 and 1 x 10^6 RBMSCs expanded in MEM medium supplemented with 0.01 mg.mL^{-1} Dex-loaded CMCht/PAMAM dendrimer nanoparticles was 30.5 ± 6.0% and 38.1 ± 5.7%, respectively. This data shows that porous HAp ceramics alone do not induce bone formation upon subcutaneous implantation in the back of the F344/N rats. However by seeding bone marrow stromal cells (BMSCs) onto the scaffolds bone formation could be detected, when cell number was 1 x 10^6 cells.

Table 1. Percentage of bone volume density (BV/TSV) calculated from the histomorphometrical analysis of the 2-D histological sections of the different explants, after 4 weeks of subcutaneous implantation. A minimum of 12 sections per explant were analyzed.

Explant	% Bone volume density (Mean ± Std. dev.)
HAp scaffolds without RBMSCs	0
HAp seeded with 2x10^5 RBMSCs expanded in MEM medium	0
HAp seeded with 2x10^5 RBMSCs expanded in MEM medium supplemented with 10^{-8} M Dex	6.9 ± 4.7
HAp seeded with 2x10^5 RBMSCs expanded in MEM medium supplemented with 0.01 mg.ml^{-1} Dex-loaded CMCht/PAMAM dendrimer nanoparticles	30.5 ± 6.0
HAp seeded with 1x10^6 RBMSCs expanded in MEM medium	27.1 ± 7.1
HAp seeded with 1x10^6 RBMSCs expanded in MEM medium supplemented with 10^{-8} M Dex	36.4 ± 9.2
HAp seeded with 1x10^6 RBMSCs expanded in MEM medium supplemented with 0.01 mg.ml^{-1} Dex-loaded CMCht/PAMAM dendrimer nanoparticles	38.1 ± 5.7

Moreover, this study corroborates previous findings [24-26] that showed the role of Dex for superior *de novo* bone formation. Despite, in this work we have shown that Dex-loaded CMCht/PAMAM dendrimer nanoparticles induced a higher new bone formation as compared to that of RBMSCs expanded in MEM medium supplemented with 10^{-8} M Dex, the typical concentration used in osteogenic media [44]. This is particularly evident when seeding low cell numbers onto the surface of the HAp scaffolds. Thus these findings demonstrate that Dex was available inside the RBMSCs and could be release from the CMCht/PAMAM dendrimer nanoparticles with an adequate profile. Our present data is relevant if we

consider that, to our knowledge, no reports have been shown pores of implanted ceramics completely filled with newly formed bone when seeded with low cell numbers, after 4 weeks of implantation. Nishikawa et al. [10] have demonstrated bone formation in the RBMSCs/HAp scaffolds after 2 weeks of ectopic implantation, but constructs were previously cultured *in vitro* in a osteogenic medium. On the other hand, Arinzeh et al. [8] observed low amounts of new bone formation in the HAp scaffolds seeded with 5 x 10^6 cells, and mainly restricted to peripheral pores, after 6 weeks.

It has been reported [29,51,52] that sustained exposure of bone marrow stromal cells to Dex down-regulate collagen type I production *in vitro* both in humans and animal models. To further investigate proteoglycan extracellular matrix synthesis (ECM) [37], we stained the implants sections with the methacromatic toluidine blue (Figure 5). Methacromasia was weakly observed in implants where new bone formation was formed (Figures 5E-F, G-H, I-J, and K-L). The other implants had no such findings (Figures 5A-B, and C-D). However, enhanced methacromasia was evidenced in the RBMSCs/HAp constructs where RBMSCs were expanded in the presence of Dex-loaded CMCht/PAMAM dendrimer nanoparticles (Figures 5M-N), which shows the ECM rich of proteoglycans. This data suggests that supply of Dex in a regimented manner can enhance proteoglycan extracellular matrix synthesis. No cartilaginous like-matrix [53] was observed.

Osteoblast differentiation is accompanied by the differential and temporal expression of several osteoblastic markers such as ALP, osteopontin, collagen type I, and osteocalcin [39]. To demonstrate the quantitatively the osteogenic capacity of the different implants, we measured the ALP activity and osteocalcin contents, after 4 weeks of implantation. Figure 6 shows the ALP activity of the HAp scaffolds without RBMSCs and the several RBMSCs/HAp constructs post-implantation. As seen for bone formation, the ALP activity is higher in the HAp implants seeded with 1 x 10^6 RBMSCs as compared to that seeded with 2 x 10^5 RBMSCs. This data thus suggests that osteogenic differentiation did occur in cultures with and without Dex which corroborates previous histological findings. It can be seen that ALP is higher when RBMSCs were expanded in a culture medium with 0.01 mg.mL^{-1} Dex-loaded CMCht/PAMAM dendrimer nanoparticles and 10^{-8} M Dex. In addition, no significant differences were observed between the implants seeded with 1 x 10^6 RBMSCs where RBMSCs were expanded in a culture medium with Dex-loaded CMCht/PAMAM dendrimer nanoparticles and 10^{-8} M Dex.

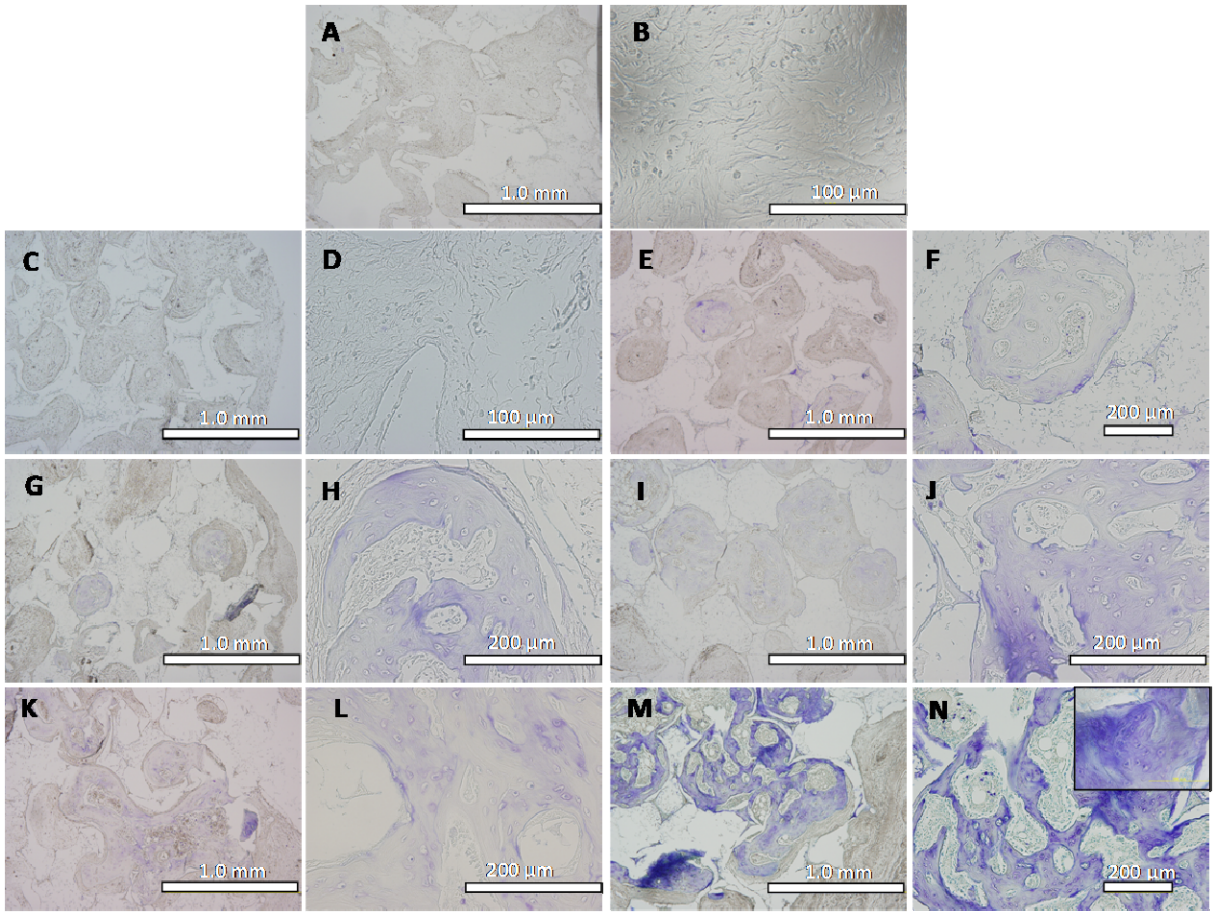

Figure 5. Light microscopy photographs of the different explants sections stained with Toluidine Blue staining (decalcified sections), after 4 weeks of subcutaneous implantation: HAp scaffolds (A-B), HAp seeded with 2 x 10^5 RBMSCs which were expanded in MEM medium (C-D), HAp seeded with 1 x 10^6 RBMSCs which were expanded in MEM medium (E-F), HAp seeded with 2 x 10^5 RBMSCs which were expanded in MEM medium supplemented with 10^{-8} M dexamethasone (G-H), HAp seeded with 1 x 10^6 RBMSCs which were expanded in MEM medium supplemented with 10^{-8} M dexamethasone (I-J), HAp seeded with 2 x 10^5 RBMSCs which were expanded in MEM medium supplemented with 0.01 mg.mL^{-1} Dex-loaded CMCht/PAMAM dendrimer nanoparticles (K-L), and HAp seeded with 1 x 10^6 RBMSCs which were expanded in MEM medium supplemented with 0.01 mg.mL^{-1} Dex-loaded CMCht/PAMAM dendrimer nanoparticles (M-N). It is possible to observe representative weak and strong methacromasia for proteoglycan extracellular matrix (ECM), in explants where new bone formation was detected.

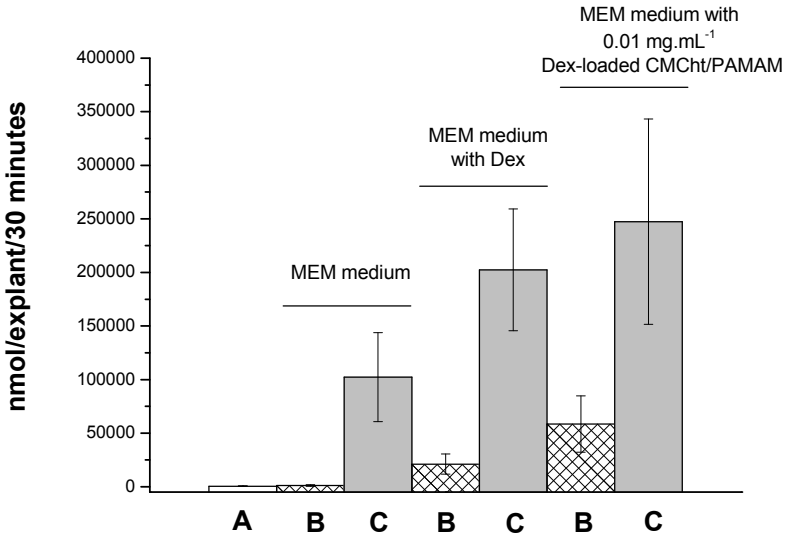

Figure 6. ALP activity of the different explants after 4 weeks of subcutaneous implantation: HAp scaffolds (A), HAp seeded with 2 x 10^5 RBMSCs (B), HAp seeded with 1 x 10^6 RBMSCs (C). Results expressed as an average ± standard deviation, n=9.

On the contrary, significant differences in ALP activity were observed in the implants seeded with 2 x 10^5 RBMSCs. It can be seen that ALP activity in the implants where RBMSCs were expanded in a culture medium with 0.01 mg.mL^{-1} Dex-loaded CMCht/PAMAM dendrimer nanoparticles presented higher ALP levels as compared to that of culture medium with 10^{-8} M Dex, which is consistent with the higher bone formation observed. In other words, our data are is in full agreement with previous findings [28,54], as we found that continuous treatment with Dex consistently increases the ALP activity, which is an indication of the osteogenic commitment of RBMSCs. Thus, Dex induced the early osteoblastic differentiation and potentate new bone formation. Moreover, HAp scaffolds without RBMSCs and RBMSC/HAp constructs seeded with 2 x 10^5 RBMSCs expanded in MEM medium presents low ALP activities, which demonstrates the important role of Dex and cell number on the formation of new bone.

Figure 7 shows the osteocalcin content of the RBMSCs/HAp constructs, after 4 weeks of subcutaneous implantation. Osteocalcin content is higher both when RBMSCs were expanded in a culture medium with 0.01 mg.mL^{-1} Dex-loaded CMCht/PAMAM dendrimer nanoparticles and 10^{-8} M Dex as compared to that of implants where RBMSCs were cultured in MEM medium. Increasing osteocalcin expression indicated advancing differentiation. By its turn, as observed for ALP, osteocalcin content in the HAp scaffolds without cells is low, which explains the absence of bone formation. In addition, it is possible to observe that the osteocalcin content did not vary significantly in the implants where RBMSCs were

expanded in the same conditions but seeded with different cell number (B-C). Moreover, no significant differences were found in explants with RBMSCs exposed to Dex. These results can be explained by the unresponsiveness of osteocalcin to long-term exposure to Dex in our experimental study as this late osteoblastic marker appears to reach a maximum just before or during mineralized tissue formation [55].

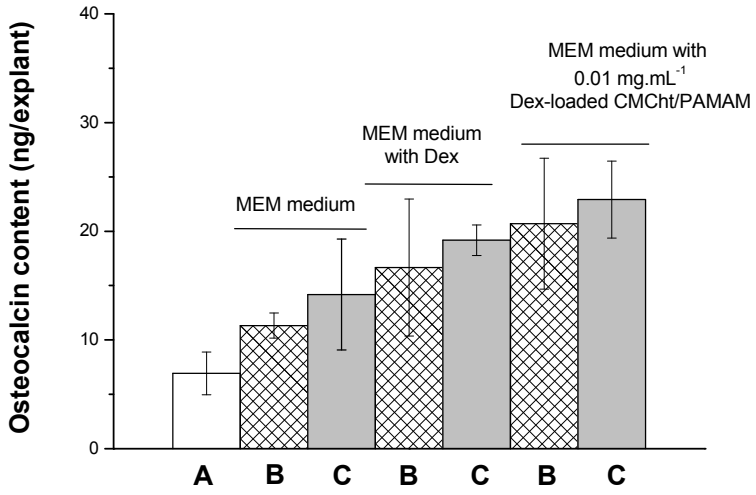

Figure 7. Osteocalcin content of the different explants after 4 weeks of subcutaneous implantation: HAp scaffolds (A), HAp seeded with 2 x 10^5 RBMSCs (B), HAp seeded with 1 x 10^6 RBMSCs (C). Results expressed as an average ± standard deviation, n=9.

It has been shown that the expression of osteocalcin increases [56] with mineral deposition, while ALP levels decreases [57]. In fact Porter et al. [29] reported that Dex induces the expression of bone sialoprotein, but not osteocalcin expression which may be stimulated through a different pathway. Despite, all these results confirmed the osteogenic capacity of the HAp scaffolds seeded with 1 x 10^6 RBMSCs and showed that exposure of Dex prior and during implantation resulted in a superior new bone formation. Moreover, this study demonstrate that CMCht/PAMAM dendrimer nanoparticles could supply Dex to RBMSCS in a regimented manner, thus acting at both early and late stages to direct proliferative osteoprogenitor cells toward terminal maturation. The superior role of the Dex-loaded CMCht/PAMAM dendrimer nanoparticles in increasing the ALP levels was particularly evident when seeding 2 x 10^5 RBMSCs per HAp scaffold.

4. CONCLUSIONS

In this work, we have demonstrated that cell number and *ex vivo* culturing strategies greatly influences the osteogenesis and *de novo bone* formation, *in vivo*. RBMSCs expanded with 0.01 mg.mL^{-1}

dexamethasone-loaded carboxymethylchitosan/poly(amido-amine) dendrimer nanoparticles and seeded at low cell number on the surface of the HAp scaffolds enhanced the ectopic bone formation, after 4 weeks of subcutaneous implantation in the back of F344/N rats. This study reveals that the novel dexamethasone-carboxymethylchitosan/poly(amidoamine) dendrimer nanoparticles may be beneficial as intracellular nanocarrier and supply of Dex in a regimented manner to modulate and direct stem cells differentiation towards osteogenic phenotype, enhance proteoglycan extracellular matrix synthesis and superior ectopic *de novo* bone formation. The architecture of HAp scaffolds proved to be a good support for osteogenic differentiation of bone marrow derived osteoblast and bone formation, *in vivo*. Thus, the tissue engineering strategy proposed in this work showed to be effective on promoting *de novo* bone formation *in vivo* and avoid the long time of *in vitro* culturing in the presence of osteogenic cocktails which is seen as major drawback for most clinical applications.

REFERENCES

1. Chu, T.M.G., et al., *Mechanical and in vivo performance of hydroxyapatite implants with controlled architectures.* Biomaterials, 2002. **23**(5): p. 1283.
2. Schnettler, R., et al., *Bone ingrowth in bFGF-coated hydroxyapatite ceramic implants.* Biomaterials, 2003. **24**(25): p. 4603.
3. Jones, A.C., et al., *Assessment of bone ingrowth into porous biomaterials using micro-CT.* Biomaterials, 2007. **28**(15): p. 2491.
4. Woodard, J.R., et al., *The mechanical properties and osteoconductivity of hydroxyapatite bone scaffolds with multi-scale porosity.* Biomaterials, 2007. **28**(1): p. 45.
5. Boyde, A., et al., *Osteoconduction in large macroporous hydroxyapatite ceramic implants: evidence for a complementary integration and disintegration mechanism.* Bone, 1999. **24**(6): p. 579.
6. Kozo, O., et al., *Quantitative study on osteoconduction of apatite-wollastonite containing glass ceramic granules, hydroxyapatite granules and alumina granules.* Biomaterials, 1990. **11**(4): p. 265.
7. Kurashina, K., et al., *Osteogenesis in muscle with composite graft of hydroxyapatite and autogenous calvarial periostium: a preliminary report.* Biomaterials, 1995. **16**: p. 119.
8. Arinzeh, T.L., et al., *A comparative study of biphasic calcium phosphate ceramics for human mesenchymal stem-cell-induced bone formation.* Biomaterials, 2005. **26**(17): p. 3631.

9. Kim, H., et al., *In vivo bone formation by human marrow stromal cells in biodegradable scaffolds that release dexamethasone and ascorbate-2-phosphate.* Biochemical and Biophysical Research Communications, 2005. **332**(4): p. 1053.
10. Nishikawa, M., et al., *Bone Tissue Engineering Using Novel Interconnected Porous Hydroxyapaptite ceramics Combined With Marrow mesenchymal cells: Quantitative and Three-Dimensional Image Analysis.* Cell Transplantation, 2004. **13**: p. 367.
11. Uemura, T., et al., *Transplantation of cultured bone cells using combinations of scaffolds and culture techniques.* Biomaterials, 2003. **24**(13): p. 2277.
12. Hosseinkhani, H., et al., *Enhanced ectopic bone formation using a combination of plasmid DNA impregnation into 3-D scaffold and bioreactor perfusion culture.* Biomaterials, 2006. **27**(8): p. 1387.
13. Kruyt, M.C., et al., *Analysis of ectopic and orthotopic bone formation in cell-based tissue-engineered constructs in goats.* Biomaterials, 2007. **28**(10): p. 1798.
14. Srouji, S. and E. Livne, *Bone marrow stem cells and biological scaffold for bone repair in aging and disease.* Mechanisms of Ageing and Development, 2005. **126**(2): p. 281.
15. Bianco, P. and P.G. Robey, *Stem cells in tissue engineering.* Nature, 2001. **414**: p. 118.
16. Karussis, D., et al., *Immunomodulation and neuroprotection with mesenchymal bone marrow stem cells (MSCs): A proposed treatment for multiple sclerosis and other neuroimmunological/neurodegenerative diseases.* Journal of the Neurological Sciences, 2008. **265**(1-2): p. 131.
17. Hou, M., et al., *Transplantation of mesenchymal stem cells from human bone marrow improves damaged heart function in rats.* International Journal of Cardiology, 2007. **115**(2): p. 220.
18. Liu, W., et al., *Bone Reconstruction with Bone Marrow Stromal Cells*, in *Methods in Enzymology*. 2006, Academic Press. p. 362.
19. Banfi, A., et al., *Proliferation kinetics and differentiation potential of ex vivo expanded human bone marrow stromal cells: Implications for their use in cell therapy.* Experimental Hematology, 2000. **28**(6): p. 707.
20. Krampera, M., et al., *Mesenchymal stem cells for bone, cartilage, tendon and skeletal muscle repair.* Bone, 2006. **39**(4): p. 678.
21. Mauney, J.R., et al., *In vitro and in vivo evaluation of differentially demineralized cancellous bone scaffolds combined with human bone marrow stromal cells for tissue engineering.* Biomaterials, 2005. **26**(16): p. 3173.

22. Pound, J.C., et al., *An ex vivo model for chondrogenesis and osteogenesis.* Biomaterials, 2007. **28**(18): p. 2839.
23. Martin, Y. and P. Vermette, *Bioreactors for tissue mass culture: Design, characterization, and recent advances.* Biomaterials, 2005. **26**(35): p. 7481.
24. N. Ogston, et al., *Dexamethasone and retinoic acid differentially regulate growth and differentiation in an immortalised human clonal bone marrow stromal cell line with osteoblastic characteristics.* Steroids, 2002. **67**: p. 895.
25. Eijken, M., et al., *The essential role of glucocorticoids for proper human osteoblast differentiation and matrix mineralization.* Molecular and Cellular Endocrinology, 2006. **248**: p. 87.
26. Blum, J.S., et al., *Early osteoblastic differentiation induced by dexamethasone enhances adenoviral gene delivery to marrow stromal cells.* Journal of Orthopaedic Research, 2004. **22**(2): p. 411.
27. Jorgensen, N.R., et al., *Dexamethasone, BMP-2, and 1,25-dihydroxyvitamin D enhance a more differentiated osteoblast phenotype: validation of an in vitro model for human bone marrow-derived primary osteoblasts.* Steroids, 2004. **69**(4): p. 219.
28. Holtorf, H.L., J.A. Jansen, and A.G. Mikos, *Ectopic bone formation in rat marrow stromal cell/titanium fiber mesh scaffold constructs: Effect of initial cell phenotype.* Biomaterials, 2005. **26**(31): p. 6208.
29. Porter, R.M., W.R. Huckle, and A.S. Goldstein, *Effect of dexamethasone withdrawal on osteoblastic differentiation of bone marrow stromal cells.* Journal of Cellular Biochemistry, 2003. **90**: p. 13.
30. Hayashi, R., et al., *Effects of glucocorticoids on gene transcription.* European Journal of Pharmacology, 2004. **500**: p. 51-62.
31. Schäcke, H., W.D. Döcke, and K. Asadullah, *Mechanisms involved in the side effects of glucocorticoids.* Pharmacology & Therapeutics, 2002. **96**: p. 23-43.
32. Oliveira, J.M., et al., *Surface engineered carboxymethylchitosan/poly(amidoamine) dendrimer nanoparticles for intracellular targeting.* Advanced Functional Materials, 2008. **18**(12): p. 1840.
33. Oliveira, J.M., et al. *Intracellular carboxymethylchitosan/poly(amidoamine) nanocarriers loaded with dexamethasone enhances osteogenic differentiation of RBMSCs in vitro*. Tissue Engineering, 2007. **13(7)**: p. 1719.
34. Oliveira, J.M., et al., *Macroporous hydroxyapatite scaffolds for bone tissue engineering applications: Physicochemical characterization and assessment of rat bone marrow stromal cells*

viability. Journal Biomedical Materials Research: Part A, In Press, Corrected Proof, 2008. (doi:10.1002/jbm.a.32213).

35. Oliveira, J.M., et al., *The osteogenic differentiation of rat bone marrow stromal cells cultured with dexamethasone-loaded carboxymethylchitosan/poly(amidoamine) dendrimer nanoparticles*. Biomaterials, 2008. **30(5)**: p.804.
36. Ito, A., et al., *Zinc-containing tricalcium phosphate and related materials for promoting bone formation.* Current Applied Physics, 2005. **5**: p. 402.
37. Kasten, P., et al., *Ectopic bone formation associated with mesenchymal stem cells in a resorbable calcium deficient hydroxyapatite carrier.* Biomaterials, 2005. **26**(29): p. 5879.
38. Haynesworth, S.E., et al., *Characterization of cells with osteogenic potential from human marrow.* Bone, 1992. **13**: p. 81.
39. Beck, G.R., B. Zerler, and E. Moran, *Phosphate is a specific signal for induction of osteopontin gene expression.* Proc. Nat. Acad. Sci., 2000. **97**: p. 8352.
40. Harris, H., *The human alkaline phosphatases: wahat we know and what we don't know.* Clinica Chimica Acta, 1989. **186**: p. 133.
41. Oliveira, J.M., et al., *Innovative technique for the preparation of porous bilayer hydroxyapatite/chitosan scaffolds for osteochondral applications*. In: Bioceramics 18, Kyoto (JPN): Key Engineering Materials, Trans Tech Pub, Zurich, Switzerland, 2006. **309-311**: p. 927.
42. Oliveira, J.M., et al., *Novel hydroxyapatite/chitosan bilayered scaffold for osteochondral tissue-engineering applications: Scaffold design and its performance when seeded with goat bone marrow stromal cells.* Biomaterials, 2006. **27**(36): p. 6123.
43. Chen, X.-G. and H.-J. Park, *Chemical characteristics of O-carboxymethyl chitosans related to the preparation conditions.* Carbohydrate Polymers, 2003. **53**: p. 355.
44. Kihara, T., et al., *Three-dimensional visualization analysis of in vitro cultured bone fabricated by rat marrow mesenchymal stem cells.* Biochemical and Biophysical Research Communications, 2004. **316**: p. 943.
45. Kotobuki, N., et al., *Viability and Osteogenic Potential of Cryopreserved Human Bone Marrow-derived Mesenchymal Cells.* Tisssue Engineering, 2005. **11**: p. 663.
46. Tadokoro, M., Y. Hattori, and H. Ohgushi, *Rapid preparation of fresh frozen tissue-engineered bone sections for histological, histomorphometrical and histochemical analyses.* Bio-Medical Materials and Engineering, 2006. **16**: p. 405.

47. Muller, R., et al., *Morphometric Analysis of Human Bone Biopsies: A Quantitative Structural Comparison of Histological Sections and Micro-Computed Tomography.* Bone, 1998. **23**(1): p. 59.
48. Zeltinger, J., et al., *Effect of pore size and void fraction on cellular adhesion, proliferation, and matrix deposition.* Tissue Engineering, 2001. **7**: p. 557.
49. Simon, J.L., et al., *Engineered cellular response to scaffold architecture in a rabbit trephine defect.* Journal of Biomedical Materials Research: Part A, 2003. **66A**: p. 275.
50. Tamai, N., et al., *Novel hydroxyapatite ceramics with an interconnective porous structure exhibit superior osteoconduction in vivo.* Journal of Biomedical Materials Research, 2002. **59**: p. 110.
51. Hicok, K.C., et al., *Development and characterisation of conditionally immortalised osteoblast precursor cell lines from human bone marrow stroma.* Journal of Bone and Mineral Research, 1998. **13**: p. 205.
52. Mahonen, A., et al., *Type 1 procollagen synthesis is regulated by steroids and related hormones in human osteosarcoma cells.* Journal of Cellular Biochemistry, 1998. **68**: p. 151.
53. Chen, G., et al., *Chondrogenic differentiation of human mesenchymal stem cells cultured in a cobweb-like biodegradable scaffold.* Biochemical and Biophysical Research Communications, 2004. **322**(1): p. 50.
54. Wong, M.M., et al., *Long-term effects of physiologic concentrations of dexamethasone on human bone-derived cells.* Journal of Bone and Mineral Research, 1990. **5**: p. 803.
55. Kondo, H., et al., *Temporal changes of mRNA expression of matrix proteins and parathyroid hormonerelated protein (PTH/PTH-rp) receptor in bone development.* Journal of Bone and Mineral Research, 1997. **12**: p. 2089.
56. Owen, T.A., et al., *Reciprocal relationships in expression of genes associated with osteoblast proliferation and differentiation during formation of bone extracellular matrix.* Journal of Cellular Physiology, 1990. **143**: p. 420.
57. Malaval, L., et al., *Cellular expression of bone related proteins during in vitro osteogenesis in rat bone marrow stromal cultures.* Journal of Cellular Physiology, 1994. **138**: p. 555.

CHAPTER X.

Dexamethasone-loaded carboxymethylchitosan/poly(amidoamine) dendrimer nanoparticles induces osteogenic differentiation of rat bone marrow stromal cells and ectopic bone formation

CHAPTER X.

Dexamethasone-loaded carboxymethylchitosan/poly(amidoamine) dendrimer nanoparticles induces osteogenic differentiation of rat bone marrow stromal cells and ectopic bone formation

Abstract

Among the myriad of possibilities in bone tissue engineering, the development novel strategies that can stimulate stem cell differentiation to become osteoblasts in the absence of typical osteogenic cocktails *in vivo*, it is still regarded as a very appealing challenge. Biodegradable and biocompatible sphere-like nanoparticles were previously developed by means of grafting carboxymethylchitosan onto poly(amidoamine) dendrimers (CMCht/PAMAM dendrimer nanoparticles). Such structures have been proposed to be used in tissue engineering and regenerative medicine as an intracellular drug delivery system of bioactive molecules to modulate stem cells fate *in vivo*, namely proliferation and differentiation. In this work deeper studies on the physicochemical properties and morphology of the nanoparticles were carried out, including proton nuclear magnetic resonance (^{1}H NMR), transmission electron microscopy (TEM), dynamic light scattering (DLS) and zeta potential analyses. Upon dexamethasone (Dex) loading into the CMCht/PAMAM dendrimer nanoparticles, we have assisted to a particle size increase, while no significant variation on the zeta potential was observed. Moreover, the effect of Dex loading on the viability of rat bone marrow stromal cells (RBMSCs) and internalization efficiency were also investigated by quantification of ATP and fluorescence studies, respectively. These studies reveal that Dex did not affect cells viability, but decrease nanoparticles internalization by RBMSCs, *in vitro*. Dex-loaded CMCht/PAMAM dendrimer nanoparticles osteogenic potential and bone forming ability were also evaluated, *in vitro* and *in vivo*. *In vitro* studies revealed that mineralization occur in 2-D RBMSCs cultures exposed to the Dex-loaded CMCht/PAMAM dendrimer nanoparticles to an extent similar to that for osteogenic medium. For *in vivo* studies, RBMSCs were incubated with Dex-loaded CMCht/PAMAM dendrimer nanoparticles during the expansion period and the cells were then seeded onto the surface of starch-polycaprolactone (SPCL) scaffolds before being implanted subcutaneously into the back of Fischer 344 rats for 4 weeks. Interestingly, the μ-CT and morphometric analyses, histology (H&E staining), biochemical parameters denoting osteogenesis and mineral bone formation content, demonstrate the superior performance of the developed nanoparticle system for the intracellular delivery of Dex as it stimulate RBMSCs to produce superior bone mineral in the absence of the typical osteogenic supplements, *in vivo*.

This chapter is based on the following publication: **Oliveira JM**, Malafaya PB, Silva SS, Kotobuki N, Hirose M, Sousa RA, Mano JF, Reis RL and Ohgushi H, Dexamethasone-loaded carboxymethylchitosan/poly(amidoamine) dendrimer nanoparticles induces osteogenic differentiation of rat bone marrow stromal cells and ectopic bone formation (2009), submitted.

1. INTRODUCTION

Cell and tissue engineering [1-7] has benefited from the development of novel strategies that can stimulate and control cells functions, *in vitro* and *in vivo.* This issue it is still regarded as a very appealing challenge [4,8,9] since there is the need to target-deliver biological agents, including differentiation factors or genetic material towards modulating from inside stem cells behavior. Nanocarrier systems have generated a significant amount of interest in the *ex vivo* cell maintenance and co-culturing [10,11], and control of the cellular fate *in vivo* mainly due to their internalization efficiency, drug loading capacity, and to favorably modulate the solubility and pharmacokinetics of drugs [12-14].

Likewise, a great deal of attention has been given [15,16] to understanding the fundamental problem of the entry and retention mechanisms of nanoparticles on mammalian cells since the nano-devices may be incorporated into membrane-bounded endosomes and fail to access the cytosolic cell targets. In this regard, dendrimers have attracted growing interest as nanocarriers as they can pass through cell membranes [17-19]. Despite the interesting architecture and multivalency, it has been found [20] that high generation dendrimers are often cytotoxic. The designing of dendrimers for biological and medical applications has been exploited by many researchers [21-23]; however, a fundamental paradigm still remains: how can we improve dendrimers biocompatibility without compromising their multivalency?

To the best of our knowledge, nanoparticle systems that are biocompatible, possess higher loading capacity, and allow the bulk incorporation of bioactive molecules of higher molecular weights and of different chemistry, while maintaining high internalization and transfection efficiency as compared to conventional dendrimers still have not been successfully developed. We focused our attention in this fundamental problem, and have been proposing a novel surface engineering strategy which consists of using a low generation dendrimer backbone grafted to the carboxymethylchitosan (CMCht), a natural amphoteric polyelectrolyte derived from chitosan, with the aim of obtaining copolymers of new architectures and physichochemical properties. We develop novel macromolecules [24] by grafting carboxymethylchitosan (CMCht) onto poly(amidoamine) dendrimers, the so-called CMCht/PAMAM dendrimer nanoparticles. This new class of nanobiomaterials has been proposed to act intracellularly in the control of the stem cells fate *in vivo*, in tissue engineering and regenerative medicine applications. However, this remains '*proof-of-concept'* with previous report [24] showing that the surface engineering of PAMAM dendrimer nanoparticles with the biodegradable CMCht possibly to manipulate the chemical composition and improve biocompatibility, thus avoiding the cytotoxic effects of high-generation dendrimers. Moreover, upon loading of dexamethasone (Dex), the dendron-like nanocarriers promote the osteogenic differentiation of rat bone marrow stromal cells (RBMSCs), *in vitro* [24,25].

Here we report deeper studies on the physicochemical characteristics of the novel nanoparticles, namely the influence of incorporating Dex, measured by proton nuclear magnetic resonance (^{1}H NMR) spectroscopy. The effect of Dex loading on the architecture, Zeta potential and size of the nanoparticles was investigated under transmission electron microscope (TEM) and a particle size analyzer. A luminescent cell viability assay based on the adenosine triphosphate (ATP) quantification was carried for screening nanoparticles cytotoxicity over RBMSCs. Fluorescence-activated cell sorting and fluorescence microscopic studies were carried out to investigate the internalization efficiency of the Dex-loaded CMCht/PAMAM dendron-like nanoparticles nanoparticles. Moreover, to further investigate on their osteogenic potential, *in vitro* and *in vivo* studies were performed. *In vitro* mineralization was evaluated by measuring the levels of calcein uptake. For *in vivo* studies, Dex-loaded CMCht/PAMAM dendron-like nanoparticles were exposed from culture media to RBMSCs during the expansion period. Then, RBMSCs were seeded onto the surface of starch-polycaprolactone (SPCL) scaffolds overnight followed by subcutaneous implantation in the back of Fischer 344 rats for 4 weeks. Bone formation was evaluated by micro-computed tomography and morphometric analyses, and histological studies (Haematoxylin & Eosin staining). Complementarily, biochemical analyses such as ALP activity, osteocalcin content and calcium assay were also carried out.

2. MATERIALS AND METHODS

2.1. SYNTHESIS OF THE CARBOXYMETHYLCHITOSAN/POLY(AMIDOAMINE) (CMCHT/PAMAM) DENDRIMER NANOPARTICLES AND LOADING WITH DEXAMETHASONE (DEX)

Carboxymethylchitosan/poly(amidoamine) dendrimer, CMCht/PAMAM dendrimer nanoparticles were prepared in a stepwise manner as described elsewhere [24]. A CMCht/PAMAM dendrimer nanoparticles solution was mixed with dexamethasone (Dex) at final concentration of $5x10^{-5}$ M, under agitation. Dex-loaded CMCht/PAMAM dendrimer nanoparticles were obtained by a precipitation route. Then, precipitate was collected by filtration, dialyzed and freeze-dried (Telstar-Cryodos -80, Spain). Fluorescent probe nanoparticles were also prepared using fluorescein isothiocyanate (FITC) [24].

2.2. CHARACTERIZATION OF THE DEVELOPED NANOPARTICLES

The incorporation of Dex into the CMCht/PAMAM dendrimer nanoparticles was investigated by ^{1}H nuclear magnetic resonance (NMR) spectroscopy. CMCht/PAMAM dendrimer nanoparticles and Dex-loaded CMCht/PAMAM dendrimer nanoparticles were dissolved in deuterated water, D_2O (Aldrich,

USA). The NMR spectra were obtained with a Mercury -400BB operating at a frequency of 399.9 MHz at 50°C. The one-dimensional ^{1}H spectra were acquired using a 45° pulse, a spectral width of 6.3 kHz and an acquisition time of 2.001 seconds.

Zeta potential and particle size of the CMCht/PAMAM dendrimer nanoparticles and Dex-loaded CMCht/PAMAM dendrimer nanoparticles were measured in a particle size analyzer (Zetasizer Nano ZS, Malvern Instruments, UK). For the present study, particle size analyses were performed by dynamic light scattering (DLS), in an aqueous solution with low concentration of nanoparticles and using disposable sizing cuvettes. Electrophoretic determinations of Zeta potential were investigated using the universal 'dip' cell, at pH 3 and pH 7.4, in a citrate buffer and phosphate buffered saline (PBS) solutions, respectively. Zeta potential was also investigated in water.

The changes on the morphology of the CMCht/PAMAM dendrimer nanoparticles after incorporation of Dex was investigated under transmission electron microscopy, TEM (Philips CM-12**,** FEI Company, The Netherlands) equipped with a MEGA VIEW-II DOCU camera and Image Software Analyzer SIS NT DOCU, as previously described elsewhere [24].

2.3. STARCH-POLYCAPROLACTONE (SPCL) SCAFFOLDS

A blend of starch and poly-ε-caprolactone from Novamont (Italy) 30/70 (w/w) was used to produce fibres of starch-polycaprolactone (SPCL) by melt spinning using a modular co-rotating twin screw extruder. SPCL scaffolds with 5 mm diameter and 4 mm height were obtained by fibre bonding as reported elsewhere [25,26]. More details on SPCL scaffolds can be found elsewhere [27]. Prior in vivo studies all the SPCL scaffolds were sterilized under an ethylene oxide gas atmosphere.

2.4. *IN VITRO* STUDIES

2.4.1. Luminescent viability assay

Rat bone marrow stromal cells (RBMSCs) were isolated from femora of 7 week-old male Fischer 344/N rats (SLC Inc. Japan), and expanded in T75 cm^2 culture flasks in the presence of Eagle's minimum essential medium (MEM, Nacalai Tesque, Japan) with 15% fetal bovine serum (FBS, JRH Biosciences, USA) and 1% antibiotic-antimycotic (A/B, Nacalai Tesque, Japan) solution, the so-called MEM complete medium. Firstly, the animals were sacrificed following the protocol approved by Ethics Committee at the Tissue Engineering Research Center (Amagasaki, Japan). The femora's were collected, marrow flushed out and marrow cells from each shaft were transferred into a T75 cm^2 culture flask (BD Biosciences

Discovery Labware, Bedford, USA) and expanded under standard culturing conditions. The culture medium was changed within a 3 days period to remove non-adherent cells, followed by changing the culture medium each 2 or 3 days, until reaching about 80% confluence. RBMSCs were trypsinized with 1 mL of 0.05% tripsin-0.53 mM EDTA (Invitrogen, USA) solution, and incubated for 3 minutes at 37ºC. Complete culture medium was added and RBMSCs (passage 1, P1) were centrifuged at 900 rpm for 5 minutes. Then, supernatant was aspirated and cells re-suspended with 10 mL of complete culture medium. Cell counting was performed using an automated counter (Cell Counter Sysmex F-520, Japan). Viability of RBMSCs was analyzed with a NucleoCounter (Chemometec, Denmark), prior seeding [28].

RBMSCs were seeded (sub-cultured) to each well of a 96-well tissue culture polystyrene (TCPS) plate at a cell density of 5 x 10^3 cells.mL^{-1}, as previously described elsewhere [24]. Serial dilutions (1, 0.1, and 0.01 mg.mL^{-1}) of CMCht/PAMAM dendrimer nanoparticles and Dex-loaded CMCht/PAMAM dendrimer nanoparticles were prepared using the MEM complete culture medium, and RBMSCs cultured with the respective media for 24 and 72 hours. A latex rubber extract was used as the positive control for cellular death. After each time period, the ATP content was measured by means of performing a CellTiter-Glo® luminescent cell viability assay (Promega Corporation, USA). Luminescence was measured in a microplate reader (Wallac ARVOsx 1420, Perkin-Elmer Life and Analytical Sciences, USA). All experiments were carried out in triplicate using 4 replicates per experimental condition.

2.4.2. Investigation of the internalization efficiency upon incorporation of dexamethasone into the CMCht/PAMAM dendrimer nanoparticles

RBMSCs were isolated and expanded as described above. Then, RBMSCs were sub-cultured in a 6-well (1 x 10^5 cells.well^{-1}) and a tissue culture polystyrene (TCPS) coverslips in 24-well TCPS plates (2 x 10^4 cells.well^{-1}) for analysis under FACS and fluorescence microscopy, respectively.

For fluorescence microscopy, RBMSCs were cultured in a MEM complete culture medium supplemented with the FITC-labeled CMCht/PAMAM dendrimer nanoparticles and MEM complete culture medium with the FITC-labeled CMCht/PAMAM dendrimer nanoparticles at a concentration of 0.1 mg.mL^{-1} for the period of 12 hours until 14 days. By its turn, for FACS analysis RBMSCs were cultured in the presence of 0.01 mg.mL^{-1} FITC-labeled CMCht/PAMAM dendrimer nanoparticles nanoparticles, for the period of 12 hours until 14 days. All experiments were carried out in triplicate. After each time period, the RBMSCs were fixed with 4% formalin (Nacalai Tesque, Japan) and incubated with Texas Red®-X phalloidin (Molecular Probes, Invitrogen, USA) and Hoechst 33258

(Invitrogen, USA) for staining the actin filaments of cytoskeleton and nuclei of cells, respectively. We followed the protocols provided by the supplier, with few modifications. The specimens were observed under a fluorescence microscope (Olympus IX70, OLYMPUS Co. Ltd., Japan).

Prior FACS analysis each well of the 6-well plate was washed with PBS and cells released from substratum as described above. After centrifugation at 900 rpm for 5 minutes, RBMSCs were re-suspended in 0.5 mL of complete culture medium and passed through cell strainers [29]. Propidium iodide (Nacalai Tesque, Japan) was added to each sample for determining the number of live cells. Then, RBMSCs were loaded in a FACSCalibur flow cytometer (BD Biosciences Imunocytometry Systems, USA) and analyzed with a minimum of 10,000 events counting [24].

2.4.3. Assessment of calcein uptake (mineralization), in vitro

RBMSCs were isolated from F344/N rats and expanded as described above. RBMSCs (P1) were cultured in a TCPS 24-well plate at a cell density of 2 x 10^4 cells.well^{-1} and cultured in a complete MEM medium for 24 hours. After that time, culture medium was replaced by the different culture media, and RBMSCs cultured for times up to 14 days. The effect of the concentration of Dex-loaded CMCht/PAMAM dendrimer nanoparticles on the RBMSCs osteogenic differentiation was investigated as previously reported elsewhere [24]. Dex-loaded CMCht/PAMAM dendrimer nanoparticles were dissolved in MEM complete medium supplemented with 0.28 mM ascorbic acid (Wako Pure Chemicals, Japan) and 10 mM β-glycerophosphate (Sigma, USA) at a final concentration of 0.01 and 1 mg.mL^{-1}. RBMSCs were also cultured in a MEM complete medium (negative control for osteogenic differentiation), MEM complete medium containing 1 mg.mL^{-1} of CMCht/PAMAM dendrimer nanoparticles, and MEM complete medium containing 10 mM β-glycerophosphate (negative controls). MEM complete medium supplemented with 10^{-8} M Dex, 0.28 mM ascorbic acid and 10 mM β-glycerophosphate was used as the positive control for osteogenic differentiation. Culture media were changed every 2-3 days.

The degree of mineralization was qualitatively and quantitatively investigated following the method described by Uchimura et al. [30]. Succinctly, the method consists on the culturing of the RBMSCs in the presence of 1 μg.mL^{-1} of calcein (Dojindo Laboratories, Japan), which is incorporated in the mineralized extracellular matrix and allow us to investigate the calcium deposition. After each time period (1, 7 and 14 days), each well was washed twice with PBS after which 1 mL of PBS was added. The fluorescence of calcein incorporated into the mineralized matrices was both visualized and quantified in a image analyzer equipment (Typhoon 8600 Variable Mode Imager, Amersham Biosciences, USA) using a 526 nm short pass filter. Afterwards, the fluorescence of the incorporated calcein was also observed under a

fluorescence microscope (Olympus IX70, OLYMPUS Co. Ltd., Japan). All experiments were carried out 3 times using a minimum of 4 replicates per experimental condition.

2.5. *IN VIVO* STUDIES

RBMSCs were expanded in different culture media namely, MEM, MEM supplemented with Dex and MEM supplemented with the Dex-loaded CMCht/PAMAM dendrimer nanoparticles. Then, the respective RBMSCs at different cell numbers (1 x 10^6 and 2 x 10^5) were seeded onto the surface of the SPCL scaffolds, cultured overnight in MEM complete medium for cell adhesion, and then constructs were implanted subcutaneously. Seven-week-old male Fisher 344 rat (Syngeneic F344/N rat), same as donor sub-strain and age, were anesthetized by intraperitoneal injection of pentobarbital (Nembutal, Dainippon Pharmaceutical Co. Ltd., Japan) at a final concentration of 3.5 mg per 100 g of body weight. The hair of the rat was cut at the implantation area, followed by washing with tap water and scrubbed with tincture of iodine and 70% ethanol. In each rat, three or four skin incisions (each 1 cm length) on the dorsal midline below the ear were made. Each RBMSCs-SPCL constructs was implanted subcutaneously (1.5 to 2 cm away from the midline at both right and left sides) into the respective pocket and skin sutured. As a negative control, we used SPCL implants without RBMSCs. No prophylactic medication was administered post-surgery. After 4 weeks implantation, the animals were sacrificed with an overdose of anesthetic and RBMSCs-SPCL constructs and controls were retrieved. All experiments were carried out 3 times.

2.5.1. Micro-computed tomography (μ-CT) and morphometric analyses

New bone formation in the explants was evaluated using micro-Computed Tomography (micro-CT). Micro-CT was carried out with a high-resolution μ-CT Skyscan 1072 scanner (Skyscan, Kontich, Belgium) using a resolution of pixel size of 6.59 μm and integration time of 1.7 ms. The X-ray source was set at 40 keV of energy and 250 μA of current. Approximately 400 projections were acquired over a rotation range of 180° with a rotation step of 0.45°. Data sets were reconstructed using standardized cone-beam reconstruction software (NRecon v1.4.3, SkyScan). The output format for each sample was 500 serial 1024x1024 bitmap images. Representative data set of 250 slices were segmented into binary images with a dynamic threshold of 220-255 (grey values) to assess new bone formation. The same representative volume of interest (VOI) was analysed for all the samples. These data sets were used for morphometric analysis (CT Analyser, v1.5.1.5, SkyScan) and to build the 3-D models (ANT 3-D creator, v2.4, SkyScan). The morphometric analysis included scaffold characterization such as porosity and

interconnectivity, histograms and new bone formation quantification. The distribution of this new bone formation in the scaffolds was assessed by 3-D virtual models that were created, visualized and registered using both image processing software's (CT Analyser and ANT 3-D creator).

2.5.2. Histological studies

After μ-CT analysis, the explants were decalcified with K-CX solution (Falma Co., Tokyo, Japan) for histological analysis. Firstly, the explants were dehydrated in an ascending series grade ethanol/water solution (from 90-100%) for 19 hours followed by washing three times with xylene. Then, explants were immersed in paraffin at 62ºC and allowed to solidify at -5ºC. Slides were prepared by cutting the explants into sections 5 μm thick using a microtome, and mounted in a micro-slide glass (Matsunami glass Ind. Ltd., Japan). Paraffin was melt by placing the slides in the oven at 71ºC for 20 minutes and allowed to let cool down at room temperature. The remnant paraffin was then subsequently removed from slides by immersion in hexane for 5 minutes (S.T. Chemical, Japan), and in a ethylene/propylene mixture (Clear Plus, Falma Co., Tokyo, Japan) for 3 minutes. Then, slides were immersed three times in 100% ethanol for 2 minutes each time of immersion.
For the Haematoxylin & Eosin (H&E) staining, slides were sequentially transferred to a 90% ethanol and then to a 70% and washed with tap water. It followed the staining steps and mounted for observation as described elsewhere [31].

2.5.3. Analyses of biochemical parameters

Alkaline phosphatase activity (ALP) and osteocalcin content were measured to evaluate osteoblast differentiation, *in vivo*. Prior to the assay, the explants were washed with Ca and Mg-free PBS solution. Then, explants were transferred to a 2 mL eppendorf and pulverized with zirconia balls as previously reported [25]. Prior to analysis the samples were sonicated and centrifuged at 12,000 rpm for 1 minute at 4°C. To each well of a 96-well plate was added an aliquot of supernatant and p-nytrophenyl phosphate substrate (ZYMED® Laboratories, Invitrogen, USA) [28]. The plate was then incubated in the dark for 30 minutes at 37ºC and after that time the reaction was stopped with 1 M NaOH (Panreac). Standards were prepared with p-nytrophenol, pNP. Triplicates were made for each sample and standard. Absorbance was read at 405 nm (Wallac ARVOsx 1420, Perkin-Elmer Life and Analytical Sciences, USA), and sample concentrations were read off from the standard graph. Enzyme activity was expressed either as nmol of pNP released/explant/30 minutes.

The remnant of each sample used for the ALP assay of the explants, was treated with a 20% formic acid solution and stored at 4°C for 2-3 days. Afterwards samples were centrifuged at 15,000 rpm for 10 minutes at 4°C. Then, the supernatant was passed through a Sephadex™ G-25 column (GE healthcare, Sweden), subsequently concentrated for performing the Enzyme-linked immunosorbent assay (ELISA). A Rat Osteocalcin EIA kit (N° BT-460, Biomedical Technologies Inc., MA, USA) was used following the instructions provided by the supplier. Data was read off from the standard curve obtained with human osteocalcin and expressed as ng of deposited osteocalcin per explant.

2.5.4. Calcium content

As an index of mineral bone formation, deposited calcium in the explants was quantified as described by Kim et al. [32,33], with minor modifications. Succinctly, explants were rinsed with Ca and Mg-free PBS solution and 0.2 mL of 1N HCl per explants was added. The tissues were chopped before being placed on an orbital shaker to extract calcium for 12 hours. Then, mixtures were centrifuged at 15,000 rpm for 10 minutes and supernatants were assayed using a commercial calcium assay kit (Calcium C-test™, Wako Pure Chemical Industries, Japan) and following the instructions provided by the supplier.

3. RESULTS AND DISCUSSION

The water soluble nanoparticles could easily be characterized by NMR. ^{1}H NMR spectra (in D_2O) of the nanoparticles is shown in Figure 1 (albeit broad peaks). The ^{1}H NMR spectrum of CMCht/PAMAM dendrimer nanoparticles (Figure 1A) is relatively complex but showed a singlet at 2.49 ppm, and multiplets δ from 3.1 to 3.73 ppm and 4.07 ppm, which were ascribed to the H2 protons, the ring methine protons (H3, H4, H5 and H6), and protons of $–CH_2COO-$ groups of the CMCht [34,35]. Also, the presence of the PAMAM dendrimer is revealed by distinct peaks from 1.98 to 3.46 ppm. These have been attributed to CH_2COO, CH_2CO and CH_2CN groups. In addition, new signals were not detected, but the peaks at 2.49 and 3.46 ppm appears overlapped as a result of the resonances of the CH_2COO and CH_2 protons of both CMCht and PAMAM. The presence of the peak at ca. 3 ppm and the absence of a peak at 4.3 ppm can indicate that the substitutions occurred mainly on the C2 amino group of CMCht. The spectrum of the Dex-loaded CMCht/PAMAM dendrimer nanoparticles (Figure 1B) shows the typical signals from CMCht, PAMAM dendrimers and Dex. From spectrum it is possible to observe small singlets at 1.14, 1.28 ppm and 1.86 ppm from CH_3 and CH_2 groups, and a doublet at 7.55 ppm and 7.96 ppm which are attributed to the chemical shifts of the protons attached to C1 atoms and to aromatic ring

(*) of Dex [36], respectively. The latter signal has a low intensity but clearly shows that Dex was effectively incorporated into the CMCht/PAMAM dendrimer nanoparticles.

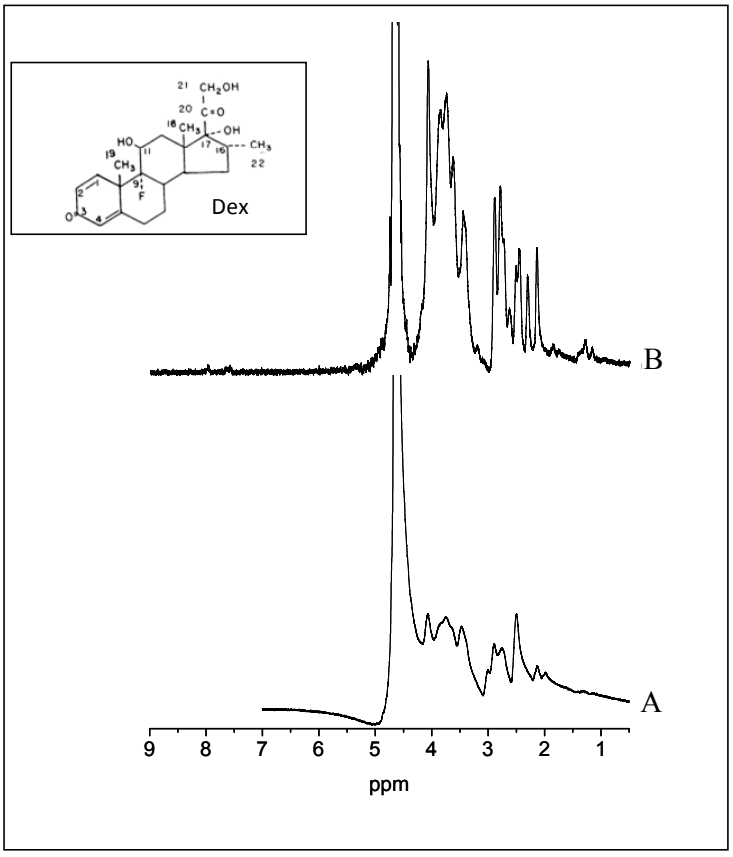

Figure 1. ^{1}H NMR spectra of the CMCht/PAMAM dendrimer nanoparticles (A), and Dex-loaded CMCht/PAMAM dendrimer nanoparticles (B), in D_2O. The signal around at ca. 4.61 ppm is ascribed to D_2O.

Figure 2 shows the TEM image of the CMCht/PAMAM nanoparticles before and after incorporation of Dex. This study clearly demonstrated the consistency in respect to shape of the synthesized macromolecules, which exhibit a nanosphere-like shape. Moreover, we can observe that incorporation of Dex affect the morphology of the nanoparticles. In fact, it is possible to observe the formation dendron-like nanoparticles instead of the nanosphere-like structure. From Figure 2B it is possible to observe aggregation of nanoparticles with ~4 nm. A possible explanation for this may be related with the self-aggregation behavior of CMCht.

On the other hand, since particle size is one of the most important parameters in drug carriers for intracellular delivery, we thus investigated here mainly the particle size and surface charge by dynamic

light scattering, DLS (Table 1). Moreover, to explore the influence of pH on the particle properties, Zeta potential was studied at physiological and lysosomal typical pH´s.

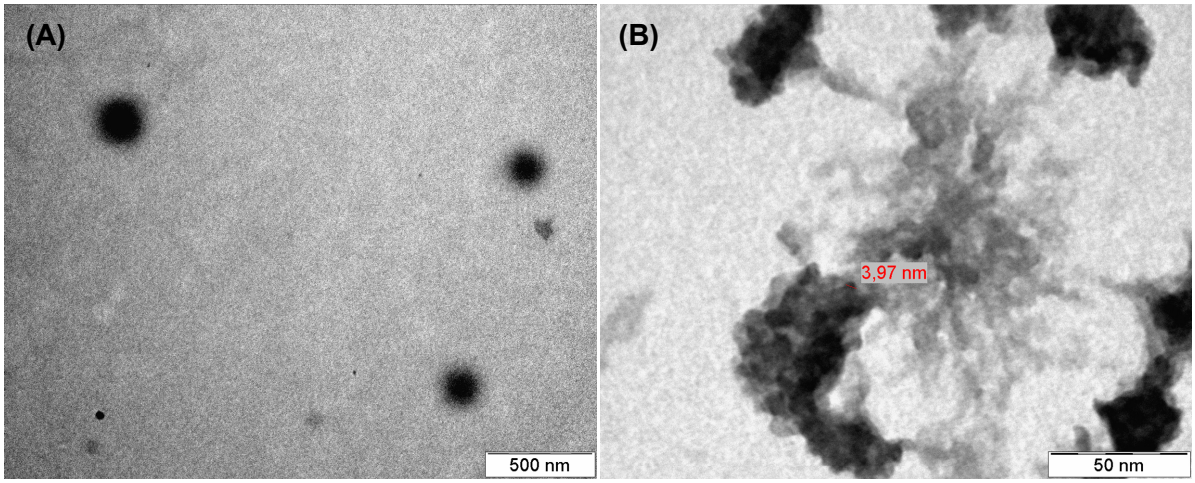

Figure 2. Representative TEM images of the CMCht/PAMAM dendrimer nanoparticles (A), and Dex-loaded CMCht/PAMAM dendrimer nanoparticle (B).

The results are resumed in Table 1 and show that upon Dex loading into the CMCht/PAMAM dendrimer nanoparticles the hydrodynamic diameter of the particles increase, while no significant variation on the zeta potential was observed.

Zeta potential is a property involving not only the particles but also their environment, e.g. pH, ionic strength, and even the type of ions in the suspension [37]. By its turn, it is expected that CMCht has a good pH and ion sensitivity in aqueous solution due to abundant –COOH and $–NH_2$ groups. This is relatively evident by the observed values of Zeta potential measured in a PBS solution (pH 7.4) and in water. On the other hand, since zeta potential of particles is decided by their surface properties [38], this data shows that the negatively charged carboxymethyl groups in the CMCht/PAMAM dendrimer nanoparticles were mainly distribute at the surface of the nanoparticles, which clearly reveals the successful surface engineering of the PAMAM dendrimers.

Upon incorporation of Dex the absolute value of Zeta potential decrease from 32.8 to 27.3 mV. The observed decrease can explain in part, the particle agglomeration observed under the TEM. Moreover, the increase the nanoparticle size in water can be related with particle agglomeration. Another possible explanation for the aggregation of Dex-loaded CMCht/PAMAM dendrimer nanoparticles can be related with the increase of hydrophobicity upon incorporation of Dex. The present data is in agreement with other report by Yinsong et al. [39] that demonstrated the important role of the surface negatively charged

carboxymethyl groups and hydrophobic interactions of cholesterol moieties on the stability of self-aggregation behavior of cholesterol-modified *O*-carboxymethylchitosan conjugates.

Table 1. Zeta potential as a function of pH, and particle size distribution of unloaded and Dex-loaded CMCht/PAMAM dendrimer nanoparticles. Data is shown as mean ± standard deviation (S.D.).

Sample	Zeta potential (mV) ± S.D.			Mean particle diameter (nm) ± S.D.	Intensity (%) ± S.D.
	pH 3	pH 7.4	Water		
CMCht/PAMAM nanoparticles	2.2 ± 1.2	-14.7 ± 3.0	-32.8 ± 1.8	52 ± 26 473 ± 222 1477 ± 551	12 ± 7 41 ± 3 47 ±4
Dex-loaded CMCht/PAMAM nanoparticles	1.5 ± 0.7	-17.4 ± 5.9	-27.3 ± 1.19	102 ±21 407 ± 80 2129 ± 543	26 ± 8 41 ± 5 33 ± 4

In an acidic medium, the amino and carboxylic groups of CMCht are protonated. Thus, as expected, the Zeta potential of the nanoparticles at pH 3 loosed the strong negative character. This would mean that within the lysosomes (pH<<5.5), nanoparticles will gradually lead to neutralization of surface charge, i.e. ‘‘proton sponge’’ effect. The neutralization of the surface charge will cause coagulation of the particles and prevent Dex release within lysosomes. In fact, the charge conversion has been reported to be beneficial for lysosomal escape [40], and subsequently release Dex in the cytoplasm, where it can bind and activate the glucocorticoid receptor [41].

Figure 3 shows the RBMSCs viability when cultured in the presence of different culture medium, for 24 and 72 hours. Results have shown that the nanoparticles are not cytotoxic over RBMSCs at concentrations bellow 1 $mg.mL^{-1}$. As seen in the present work, no significant differences in the RBMSCs viability were observed when culturing in the presence of the Dex-loaded CMCht/PAMAM dendrimer nanoparticles as compared to that for unloaded nanoparticles.

As previously stated, particle size can affect internalization. On the other hand, in a report by Zhang et al. [42] it was demonstrated that Dex treatment decrease the phagocytosis of *Straphylococcus aureus* bioparticles in normal primary trabecular meshwork cells.

To investigate if the incorporation of Dex into the nanoparticles affects the internalization by RBMSCs, a FITC-probe was linked to the nanoparticles. Fluorescence microscopy images of RBMSCs cultured in the presence of FITC-labeled CMCht/PAMAM dendrimer nanoparticles once corroborated previous internalization studies, i.e. also revealed that the FITC-labeled and Dex-loaded CMCht/PAMAM

dendrimer nanoparticles were taken up by RBMSCs, after 12 hours (Figure 4). RBMSCs continued to internalize the nanoparticles (higher fluorescent signals) when cultured for longer period of time. Additionally, RBMSCs were also stained with Texas-red phalloidin for observation of cells cytoskeleton. From the observations, no rearrangements and morphological changes were detected in the cytoskeleton, which is a good indication of its non cytotoxicity.

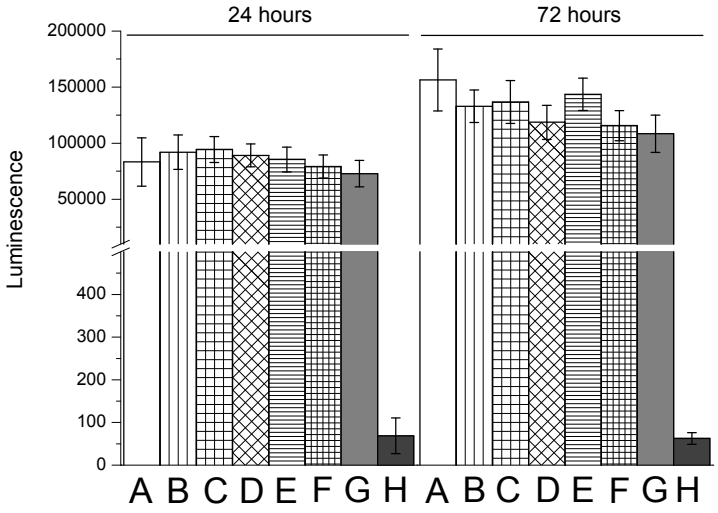

Figure 3. Cell viability assay of RBMSCs cultured in the presence of different culture medium, for 24 and 72 hours. Cell number correlates with luminescence. (A) MEM medium (negative control); (B) CMCht/PAMAM dendrimer nanoparticles 0.01 mg.mL^{-1}, (C) CMCht/PAMAM dendrimer nanoparticles 0.1 mg.mL^{-1}, (D) CMCht/PAMAM dendrimer nanoparticles 1 mg.mL^{-1}, and (E) Dex-loaded CMCht/PAMAM dendrimer nanoparticles 0.01 mg.mL^{-1}, (F) Dex-loaded CMCht/PAMAM dendrimer nanoparticles 0.1 mg.mL^{-1}, (G) Dex-loaded CMCht/PAMAM dendrimer nanoparticles 1 mg.mL^{-1}, (H) MEM media containing an latex extract (positive control).

FACS analysis was performed after culturing the RBMSCs in the presence of the FITC-labeled nanoparticles for times up to 14 days (Figure 5). The flow cytometry studies revealed increasing levels of fluorescence associated with cells after incubation RBMSCs with CMCht/PAMAM dendrimer nanoparticles for the period of 12 hours until 7 days. The fraction of RBMSCs that internalized the CMCht/PAMAM dendrimer nanoparticles reached a maximum of 95.7% after 7 days of culturing, while the peak for RBMSCs cultured with Dex-loaded CMCht/PAMAM dendrimer nanoparticles was seen at 14 days of culturing.

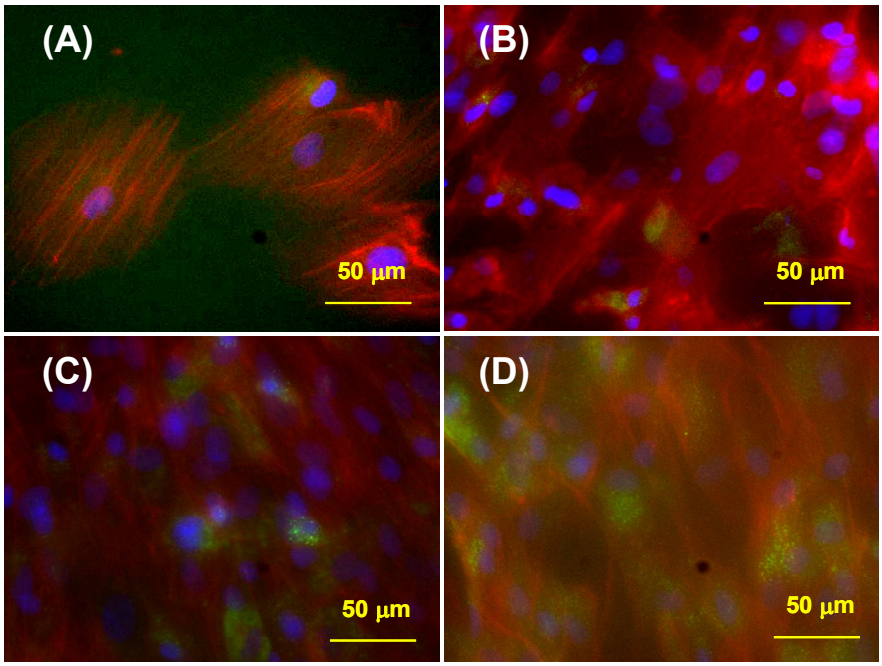

Figure 4. Fluorescence microscopy images of the RBMSCs cultured in the presence of FITC-labeled Dex-loaded CMCht/PAMAM dendrimer nanoparticles 0.1 mg.mL^{-1} (green) for: 12 hours (A), 24 hours (B), 7 days (C) and 14 days (D). Nuclear DNA and cytoskeleton were labeled with Hoechst 33258 (blue) and Texas-Red phalloidin (red), respectively.

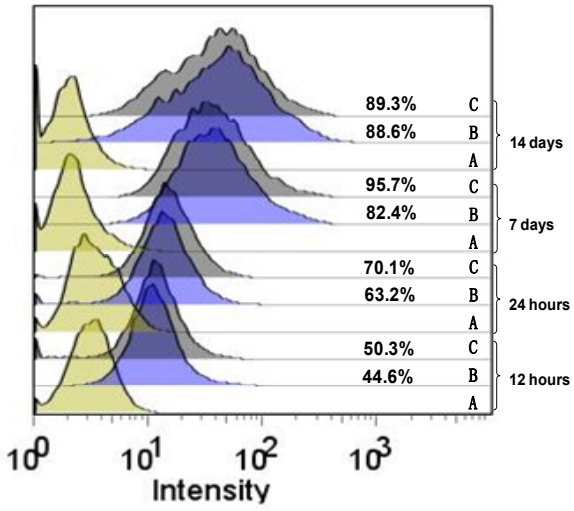

Figure 5. FACS data of live RBMSCs (% gated) after culturing in different culture media for the period of 12 hours until 14 days: MEM medium (A, control), MEM medium with FITC-labeled Dex-loaded dendrimer CMCht/PAMAM nanoparticles 0.01 mg.mL^{-1} (B), and MEM medium with FITC-labeled CMCht/PAMAM dendrimer nanoparticles 0.01 mg.mL^{-1} (C).

Thus, internalization efficiency is lower in cultures supplemented with Dex-loaded CMCht/PAMAM dendrimer nanoparticles as compared to that without Dex. This can be associated to a dual effect that includes on one hand the larger size of Dex-loaded nanoparticles and on the other the Dex-induced suppression of phagocytotic activity [42]. Moreover, the RBMSCs were stained with propidium iodide to assess the fraction of live cells. From Table 2, it is possible to observe that the fraction of live cells cultured in the presence of FITC-labeled Dex-loaded CMCht/PAMAM dendrimer nanoparticles did not significantly differ from that of controls, i.e. RBMSCs cultured with the FITC-labeled CMCht/PAMAM dendrimer nanoparticles and in MEM medium. This corroborates the luminescent viability assay, demonstrating that incorporation of Dex into the CMCht/PAMAM dendrimer nanoparticles did not elicit any cytotoxic effect over RBMSCs.

Table 2. Percentage of internalization of FITC-labeled CMCht/PAMAM dendrimer nanoparticles and Dex-loaded CMCht/PAMAM dendrimer nanoparticles and fraction of live RBMSCs obtained from FACS analyses, after the period of 12 hours until 14 days.

Culture Conditions (medium)	% internalization (% gated)				% of live RBMSCs (PI stained)			
	12 hours	24 hours	7 days	14 days	12 hours	24 hours	7 days	14 days
FITC-labeled CMCht/PAMAM nanoparticles	50.3	70.1	95.7	89.3	96.0	93.7	75.4	62.6
FITC-labeled Dex-loaded CMCht/PAMAM nanoparticles	44.6	63.2	82.4	88.6	92.5	92.5	76.2	62.6
MEM medium (control)	0.40	0.58	0.31	0.45	87.6	92.9	81.8	53.9

The later stage of the osteogenic differentiation of mesenchymal stem cells give rises to cells that are able to produce mineralized ECM. The osteogenic ability of Dex-loaded CMCht/PAMAM dendrimer nanoparticles was investigated by qualitatively and quantitatively determining the levels of calcein uptake. This method was developed by Uchimura et al. [30] that demonstrated the linear correlation between the calcium content and amount of fluorescence emitted by calcein. This method allows monitoring the calcein fluorescence arising from the mineralization process which denotes the osteogenic activity in a culture. Figure 6 shows the photograph of a 24-well TCPS plate obtained from the Typhoon image analyzer.

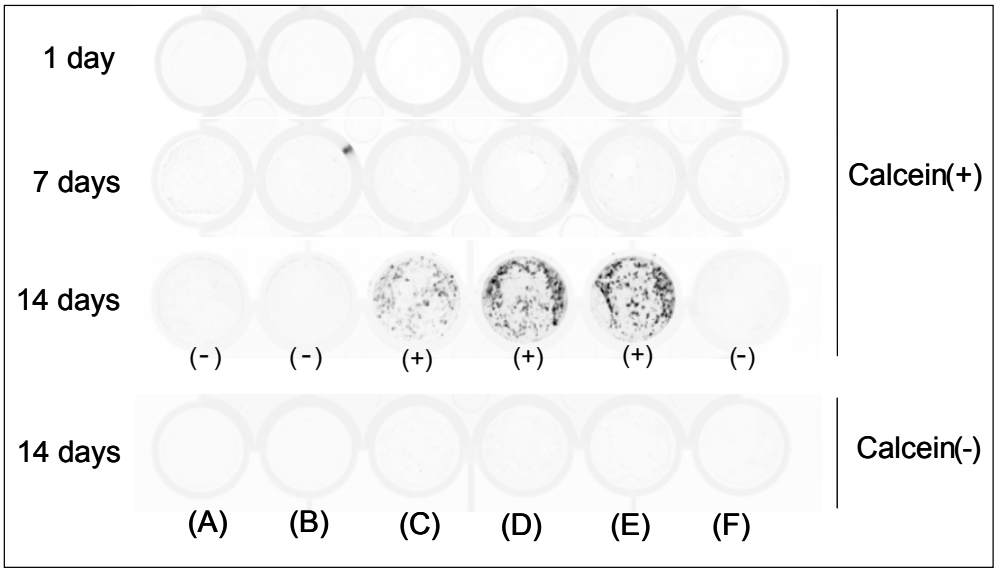

Figure 6. Images of RBMSCs cultured in a 24-well TCPS plate obtained from the Typhoon image analyzer, which detects fluorescence (calcein uptake). RBMSCs were cultured in different culture medium in the absence (bottom, control) and presence of calcein (top) for the period of 1, 7 and 14 days: (A) MEM medium (negative control); (B) CMCht/PAMAM dendrimer nanoparticles 1 mg.mL^{-1}, (C) Dex-loaded CMCht/PAMAM dendrimer nanoparticles 1 mg.mL^{-1}, (D) Dex-loaded CMCht/PAMAM dendrimer nanoparticles 0.01 mg.mL^{-1}, (E) Osteogenic medium, and (F) MEM medium with β-glycerophosphate. No mineralization (-) and mineralization occur (+).

It is possible to observe that mineralization only occur in cultures, whose RBMSCs were supplemented with Dex-loaded CMCht/PAMAM dendrimer nanoparticles and osteogenic medium. Figure 7 shows the fluorescence intensity values of RBMSCs cultured in the presence of calcein. These results revealed that no significant differences in mineralization were observed for cultures supplemented with 0.01 mg.mL^{-1} Dex-loaded CMCht/PAMAM dendrimer nanoparticles as compared to that for osteogenic medium. This is a good indication that the nanoparticles possess osteogenic ability. On the contrary, calcein uptake is decrease in cultures supplemented with Dex-loaded CMCht/PAMAM dendrimer nanoparticles at a concentration of 1 mg.mL^{-1}. This data is not surprisingly since it has been reported that dosage and regimented supply of Dex is required for proper osteoblast differentiation and mineralization [43,44]. These results are supported by phase contrast (left) and respective fluorescence microscopy images of RBMSCs after culturing in different culture medium and in the presence of calcein for 14 days (Figure 8). From the image, we can observe the typical mineral nodule formation in

RBMSCs cultures that were exposed to Dex, both from culture media or from the Dex-loaded CMCht/PAMAM dendrimer nanoparticles.

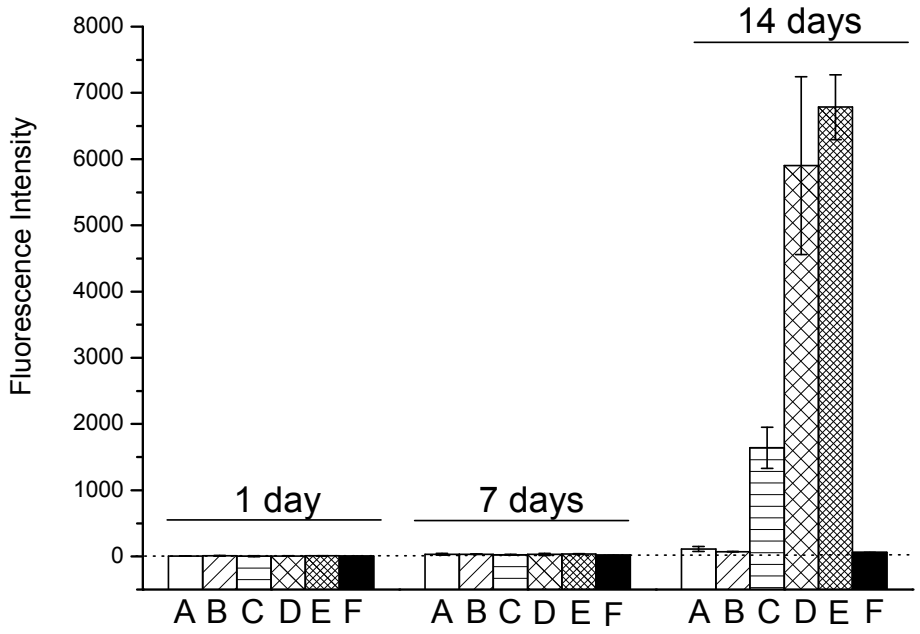

Figure 7. Fluorescence intensity values of RBMSCs cultured in the presence of calcein, for the period of 1 until 14 days. Values were related to fluorescence intensity of RBMSCs cultured in the absence of calcein, for each condition. (A) MEM medium (negative control); (B) CMCht/PAMAM dendrimer nanoparticles 1 mg.mL^{-1}; (C) Dex-loaded CMCht/PAMAM dendrimer nanoparticles 1 mg.mL^{-1}; (D) Dex-loaded CMCht/PAMAM dendrimer nanoparticles 0.01 mg.mL^{-1}; (E) Osteogenic medium and (F) MEM medium with β-glycerophosphate.

Histology, scanning electron and fluorescence microscopy imaging are the current methods used for evaluating new bone formation and osteointegration of tissue-engineered constructs [45]. These methods provide 2-D information of the samples, but the need for processing the sample prior analysis is a disadvantage as can modify its original structure. Moreover, the 3-D qualitative and quantitative analysis of the newly formed bone within the tissue-engineered constructs are difficult to obtain by these techniques. Micro-computed tomography (μ-CT), a non destructive and time-saving technique based on X-ray radiation may provide 3-D data such as the total volume, thickness distribution and remodeling of newly formed bone into implants in a small animal model [46,47].

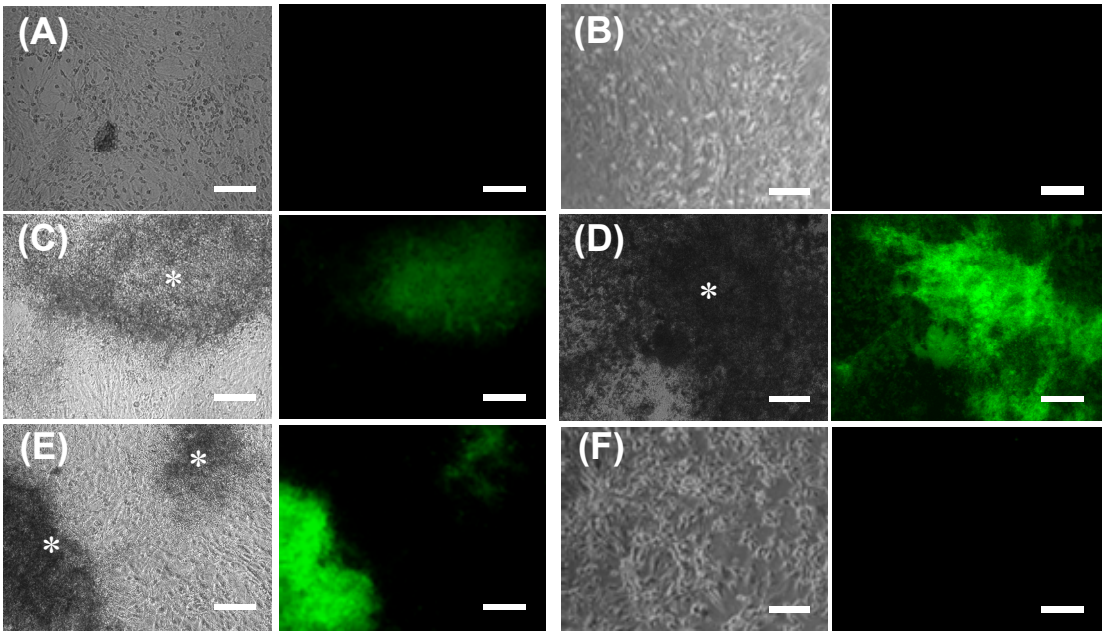

Figure 8. Phase contrast (left) and respective fluorescence microscopy (right) images of RBMSCs after culturing in different culture medium and in the presence of calcein for 14 days: (A) MEM medium (negative control); (B) CMCht/PAMAM dendrimer nanoparticles 1 mg.mL^{-1}; (C) Dex-loaded CMCht/PAMAM dendrimer nanoparticles 1 mg.mL^{-1}; (D) Dex-loaded CMCht/PAMAM dendrimer nanoparticles 0.01 mg.mL^{-1}; (E) Osteogenic medium, and (F) MEM medium with β-glycerophosphate. Indication of clustered cells and bone mineral nodules (∗) (Scale bar: 100 μm).

In the present work, *in vivo* studies were conducted to elucidate the ability of the Dex-loaded CMCht/PAMAM dendrimer nanoparticles towards the production of new bone. SPCL scaffolds with 67.4 ± 1.3% porosity (as determined by μ-CT) were used as the 3-D matrix, since it have been shown to be adequate for supporting RBMSCs osteogenic differentiation, *in vitro* [25]. Since these scaffolds exhibit lower attenuation coefficient than that for bone or calcium phosphates, i.e. the intensity of the x-ray beam is reduced less as it passes through the SPCL material [26], we can envision to obtain images and determine the total volume of newly formed bone into implants by using the micro-CT technique. We therefore cultured *in vitro*, RBMSCs in the presence of 0.01 mg.mL^{-1} Dex-loaded CMCht/PAMAM dendrimer nanoparticles until reaching confluence, seeded the RBMSCs onto the surface of the SPCL scaffolds overnight followed by subcutaneous implantation into the back of F344/N rats, for 4 weeks. The effect of cell number on the bone forming ability was also investigated, since previously we demonstrated that it influences new bone formation [31]. After 4 weeks of implantation, no signs of infection or acute inflammatory reaction were detected at the implantation sites for all implants.

Micro-CT analyses of the explants were performed to investigate new bone formation. Figure 9 shows the attenuation coefficient data for the SPCL scaffolds and explants obtained from μ-CT. It is possible to observe regions of higher attenuation between 0.7 and 0.8 cm^{-1} (black arrow) in the constructs seeded with 1 x 10^6 RBMSCs that were exposed to Dex and Dex-loaded CMCht/PAMAM dendrimer nanoparticles. On the contrary, explants with SPCL alone and SPCL scaffolds seeded with 2 x 10^5 and 1 x 10^6 RBMSCs (explants) whose cells were expanded in MEM medium, no areas of high attenuation were observed.

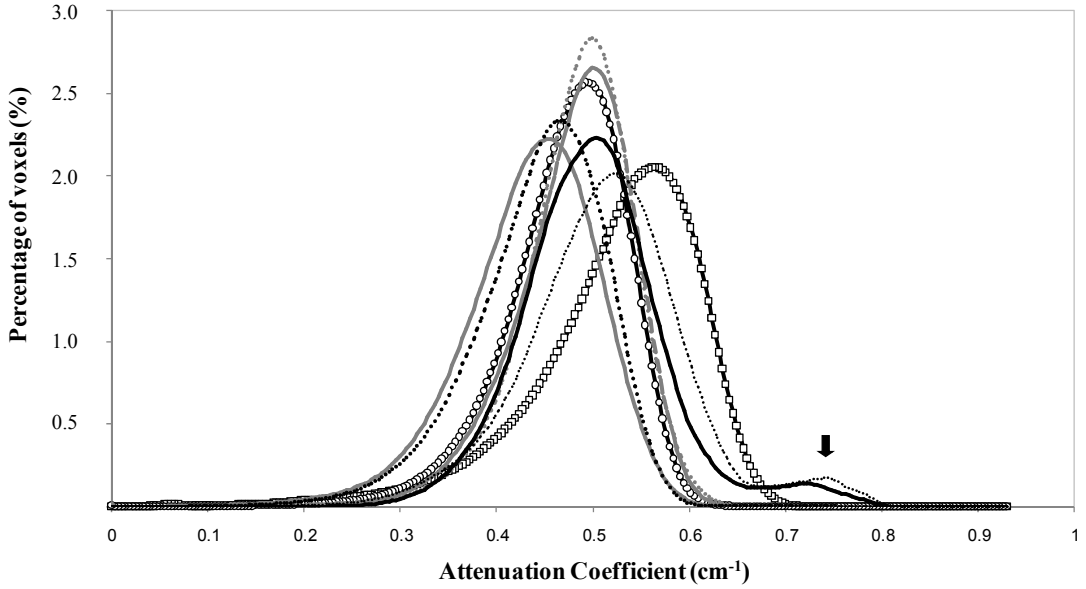

Figure 9. Attenuation coefficient data for the SPCL scaffolds and explants obtained from μ-CT analyses, prior and after 4 weeks of subcutaneous implantation, respectively. SPCL scaffold (-□-), SPCL scaffold explant (-○-), explant with 2 x 10^5 RBMSCs cultured in MEM (···), explant with 2 x 10^5 RBMSCs cultured in MEM with Dex (---), explant with 2 x 10^5 RBMSCs cultured in MEM with Dex-loaded CMCht/PAMAM dendrimer nanoparticles (——), explant with 1 x 10^6 RBMSCs cultured in MEM (•••), explant with 1 x 10^6 RBMSCs cultured in MEM with Dex (···), explant with 1 x 10^6 RBMSCs cultured in MEM with Dex-loaded CMCht/PAMAM dendrimer nanoparticles (**---**). Arrow shows the areas of higher attenuation.

The areas of higher attenuation detected can be an indication of *de novo* bone formation, since the SPCL scaffolds and SPCL explants have an attenuation coefficient between 0.3 and 0.6 cm^{-1}, which is lower than that for ceramics and mineralized matrix. To elucidate this issue, histological studies were carried out. Figure 10 shows the 3-D images of the SPCL scaffolds and explants obtained from μ-CT analyses and respective microscopic images of the explants histological sections stained with

Haematoxylin & Eosin. By analysing the images imposing a threshold criterion to evidence the high density regions, it is possible to observe that the region of higher attenuation observed in Figure 9 corresponds to the white areas in the 3-D μ-CT images.

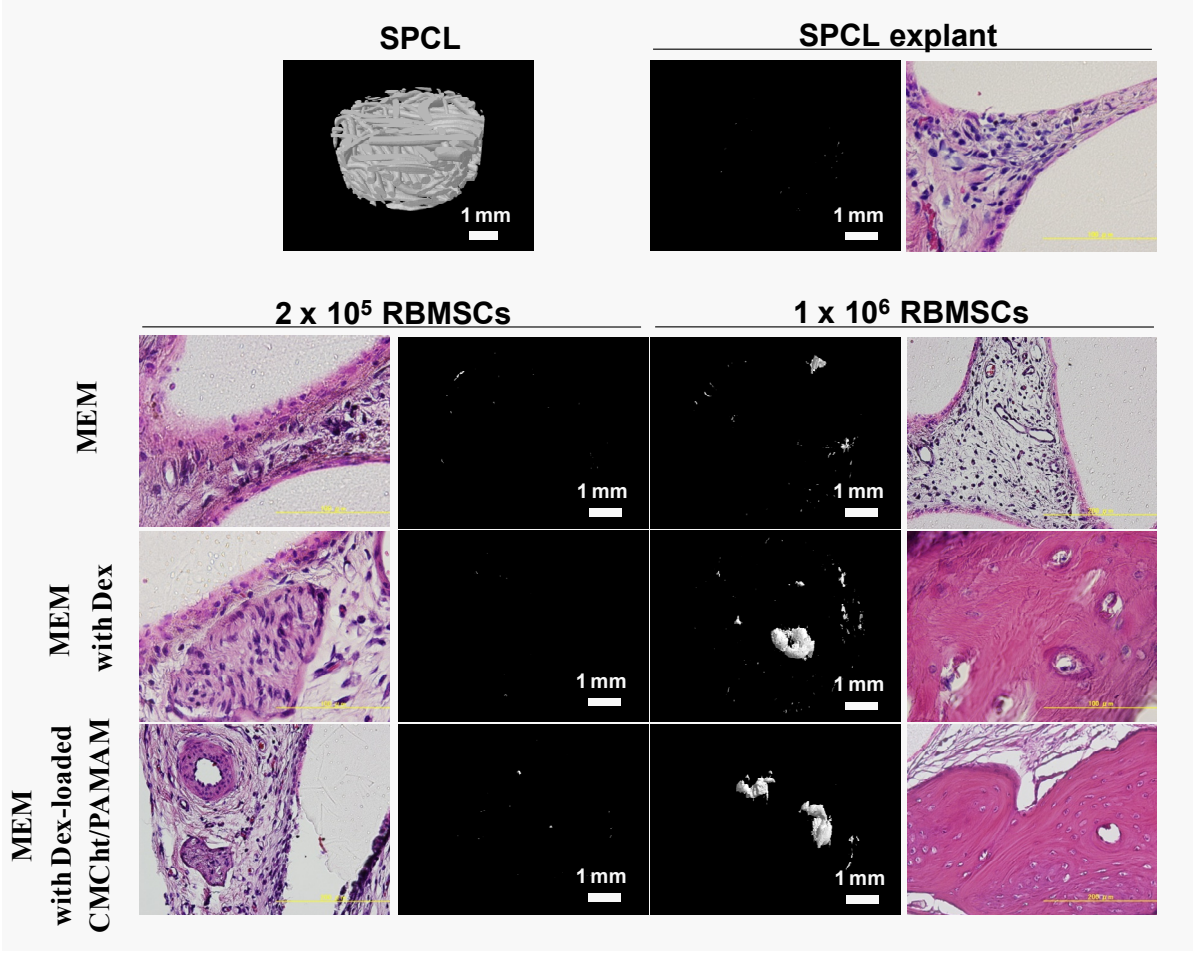

Figure 10. 3-D μ-CT images and respective Haematoxylin & Eosin stained sections of the explants after 4 weeks of subcutaneous implantation.

The white areas were observed in all explants seeded with 1 x 10^6 cells. On the contrary, in the SPCL explants and SPCL scaffolds seeded with 2 x 10^5 RBMSCs, no white areas were observed. In fact, compact masses were only observed in the explants whose RBMSCs were exposed to Dex and Dex-loaded CMCht/PAMAM dendrimer nanoparticles during expansion *in vitro*. From the histological photographs of the explants, it is evident that the massive areas of high attenuation (white areas) correspond to newly formed bone. By its turn, explants where RBMSCs were not exposed to Dex, fibrous tissue formation within the pores of SPCL scaffolds can be observed. Despite, this data shows the importance of the porous size and interconnectivity on the cells in-growth since fibrovascular tissue

could be seen in the core of the scaffolds (data not shown). Interestingly, the histological image of the explants whose RBMSCs were supplemented with Dex-loaded CMCht/PAMAM dendrimer nanoparticles shows a superior bone organization as compare to explants whose RBMSCs were supplemented with Dex from culture media. Cuboid osteoblasts lining the forming bone matrix in SPCL scaffolds seeded with 1 x 10^6 RBMSCs indicate an active bone formation site (black arrow). Moreover, it is also possible to observe the lacunar spaces and reminiscent osteocyte-like cells entrapped in the bone matrix (white arrows). Thus, osteocytic lacunae in the lamellar bone are uniform and regularly distributed with osteoblasts forming a continuous layer of bone in a unidirectional way typical of mature bone. Moreover, we observe that new bone formation occurs primarily at the core of the scaffold, which reveals that the scaffolds possess an adequate pore size and interconnectivity.

Figure 11 shows a representative microscopy photograph of a decalcified section (H&E staining) of SPCL explants seeded with 1 x 10^6 RBMSCs exposed to the Dex-loaded CMCht/PAMAM dendrimer nanoparticles, after 4 weeks of subcutaneous implantation.

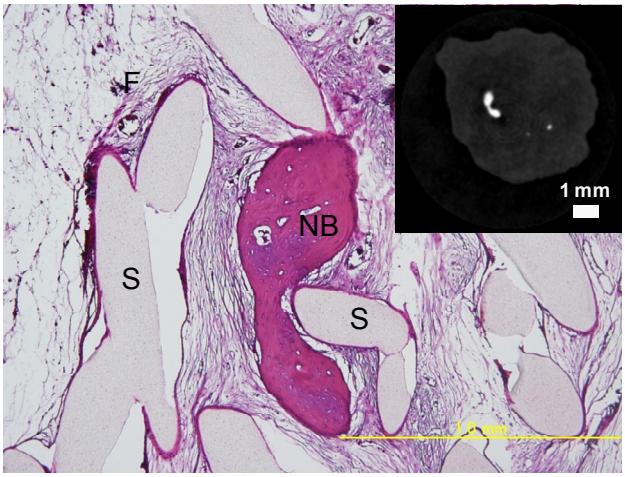

Figure 11. Haematoxylin & Eosin stained section of the explant whose SPCL scaffolds were seeded with 1 x 10^6 RBMSCs cultured in MEM medium supplemented with Dex-loaded CMCht/PAMAM dendrimer nanoparticles, after 4 weeks of subcutaneous implantation. It is possible to observe representative areas of *de novo* bone formation (NB), SPCL fibre (S) and fibrous tissue (F). Inserted image is the respective 2-D µ-CT slice of the explants and white area correspond the newly formed bone.

From the histological image of the explant section it is possible to observe that the area of *de novo* bone (NB) match to that of high attenuation (white area) in the 2-D µ-CT image. These data proof that the

SPCL scaffolds exhibit radiological features that possibly to investigate the new bone formation into the implants in a non destructive manner by using the μ-CT technique.

Complementarily, morphometric analyses corroborated the histological data which reveal that new bone formation only occurs in the explants seeded with 1 x 10^6 RBMSCs and that were exposed to Dex and Dex-loaded CMCht/PAMAM nanoparticles from culture media (Figure 12). Micro-CT analysis reveal that in the explants with 1 x 10^6 RBMSCs cultured in MEM media, bone formation occurs though in low amounts. Thus, this data shows that RBMSCs cultured with Dex-loaded CMCht/PAMAM nanoparticles prior implantation might be beneficial in TE strategies for enhancing new bone formation.

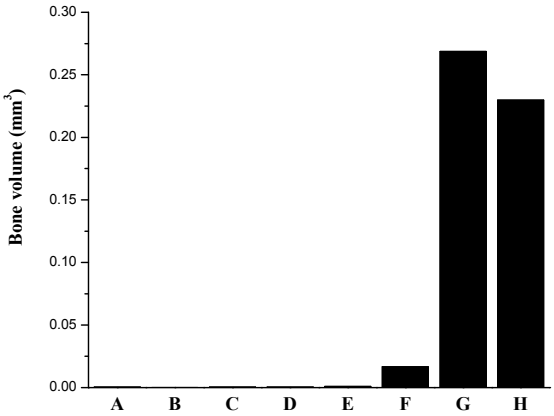

Figure 12. Morphometric analysis (% volume of bone) of the SPCL scaffolds and explants obtained from μ-CT, prior and after 4 weeks of subcutaneous implantation, respectively. SPCL scaffold (A), SPCL scaffold explant (B), explant with 2 x 10^5 RBMSCs cultured in MEM (C), explant with 2 x 10^5 RBMSCs cultured in MEM with Dex (D), explant with 2 x 10^5 RBMSCs cultured in MEM with Dex-loaded CMCht/PAMAM dendrimer nanoparticles (E), explant with 1 x 10^6 RBMSCs cultured in MEM (F), explant with 1 x 10^6 RBMSCs cultured in MEM with Dex (G), explant with 1 x 10^6 RBMSCs cultured in MEM with Dex-loaded CMCht/PAMAM dendrimer nanoparticles (H).

Alkaline phosphatase was measured to evaluate the osteoblast differentiation, *in vivo* (Figure 13, top). Results demonstrated that ALP activity is increased in cultures where RBMSCs were exposed to Dex, i.e. Dex-loaded CMCht/PAMAM dendrimer nanoparticles, and Dex supplemented from culture media. This data is not surprisingly, since the previous *in vitro* release studies [24] of Dex from the CMCht/PAMAM dendrimer nanoparticles showed that Dex concentration resembles to that from osteogenic media. Therefore, this data shows that SPCL scaffolds are effective on supporting the osteogenic differentiation of RBMSCs and new bone formation, *in vivo*. Figure 13 (bottom) shows the

content of the late osteogenic marker and bone-specific osteocalcin in the explants, after 4 weeks of implantation. No significant differences in osteocalcin levels were seen for SPCL explants without cells and seeded with 2 x 10^5 RBMSCs cultured in MEM and MEM supplemented with Dex.

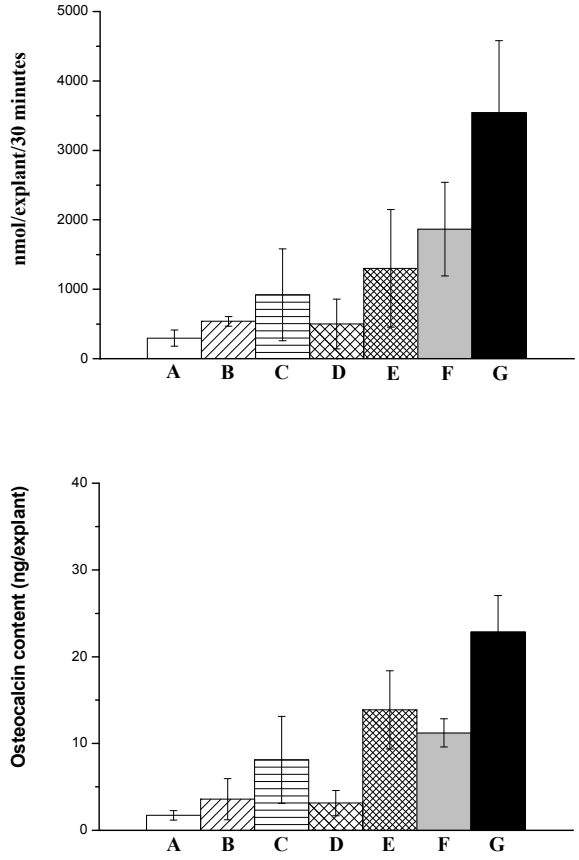

Figure 13. ALP activity (top) and Osteocalcin content (bottom) of the explants after 4 weeks of subcutaneous implantation: SPCL scaffold explant (A), explant with 2 x 10^5 RBMSCs cultured in MEM (B), explant with 1 x 10^6 RBMSCs cultured in MEM (C), explant with 2 x 10^5 RBMSCs cultured in MEM with Dex (D), explant with 1 x 10^6 RBMSCs cultured in MEM with Dex (E), explant with 2 x 10^5 RBMSCs cultured in MEM with Dex-loaded CMCht/PAMAM dendrimer nanoparticles (F), and explant with 1 x 10^6 RBMSCs cultured in MEM with Dex-loaded CMCht/PAMAM dendrimer nanoparticles (G).

Although, the osteocalcin levels for the explants seeded with 2 x 10^5 RBMSCs exposed to Dex-loaded CMCht/PAMAM dendrimer nanoparticles resembles to that of the explants seeded with 1 x 10^6 RBMSCs exposed or not, to Dex. Moreover, a significant enhancement of the osteocalcin content can be observed for the explants seeded with 1 x 10^6 RBMSCs supplement with the Dex-loaded CMCht/PAMAM nanoparticles from culture media.

Significant differences in the organization of the newly formed bone were observed under the histological studies. To elucidate these findings, calcium was extracted from the explants by acid treatment to investigate the quality and degree of mineralization of the newly bone formed. Figure 14 shows the calcium content in the several explants after 4 weeks of subcutaneous implantation. As expected no considerable calcium deposition was found in the SPCL scaffold explants and SPCL scaffolds seeded with the RBMSCs that were cultured in the absence of Dex.

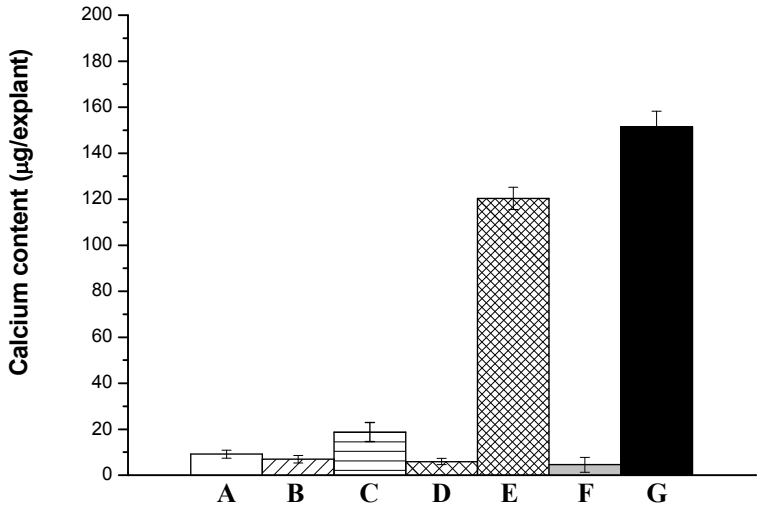

Figure 14. Calcium content in the SPCL scaffolds seeded with RBMSCs expanded in the presence of Dex-loaded CMCht/PAMAM dendrimer nanoparticles after 4 weeks of subcutaneous implantation: SPCL scaffold explant (A), explant with 2 x 10^5 RBMSCs cultured in MEM (B), explant with 1 x 10^6 RBMSCs cultured in MEM (C), explant with 2 x 10^5 RBMSCs cultured in MEM with Dex (D), explant with 1 x 10^6 RBMSCs cultured in MEM with Dex (E), explant with 2 x 10^5 RBMSCs cultured in MEM with Dex-loaded CMCht/PAMAM dendrimer nanoparticles (F), and explant with 1 x 10^6 RBMSCs cultured in MEM with Dex-loaded CMCht/PAMAM dendrimer nanoparticles (G).

These results corroborates the histological and μ-CT findings, demonstrating that bone formation only occurs in the explants seeded with 1 x 10^6 RBMSCs exposed to Dex and Dex-loaded CMCht/PAMAM dendrimer nanoparticles. Moreover, a significant increase in the calcium deposited is observed when expanding the RBMSCs with Dex-loaded CMCht/PAMAM dendrimer nanoparticles, which denotes the superior mineralization of the newly bone formed. We advance with a possible explanation for the superior bone organization and mineralization observed in the explants with 1 x 10^6 RBMSCs supplemented with Dex-loaded CMCht/PAMAM dendrimer nanoparticles, which can be due to the

supply of Dex for longer time and in a regimented manner, as Dex can be released from the nanoparticles inside cells during *in vivo* implantation time.

Succinctly, the biochemical data shows that porous SPCL scaffolds alone do not induce bone formation upon subcutaneous implantation in the back of the F344/N rats. However, by seeding RBMSCS supplemented with Dex onto the scaffolds bone formation could be detected, when cell number was 1×10^6. Moreover, the use of CMCht/PAMAM nanoparticles for the intracellular delivery of Dex stimulate stem cells differentiation towards production of bone mineral in the absence of the typical osteogenic supplements, *in vivo*.

As revealed by μ-CT analyses, histology and calcium assay, the Dex-loaded CMCht/PAMAM dendrimer nanoparticles internalization by RBMSCs *ex vivo* can afford a regimented supply of Dex *in vivo*, and stimulate RBMSCs to produce superior bone mineral. Remarkably, the SPCL scaffolds proved to be adequate for fundamental studies as they studies support bone formation *in vivo*, allowing also the analysis of new bone using a nondestructive technique such as micro-computed tomography.

4. CONCLUSIONS

Dex-loaded CMCht/PAMAM dendrimer nanoparticles were successfully developed. Results obtained from ^{1}H NMR, TEM, Zeta potential and particle size analysis revealed that Dex incorporation greatly influences the structure and the surface characteristics of the nanoparticles. These were found to possess pH and ionic-responsive nature. The *in vitro* tests showed that the Dex-loaded CMCht/PAMAM dendrimer nanoparticles at concentrations bellow 1 $mg.mL^{-1}$ do not exert any significant cytotoxic effect over RBMSCs. Furthermore, its ability for being taken up by RBMSCs was shown and incorporation of Dex into the nanoparticles showed to decrease their internalization efficiency. Complementarily, it was shown that these Dex-loaded CMCht/PAMAM dendrimer nanoparticles have the ability to promote *in vitro* mineralization, denoting its osteogenic ability. Moreover, the *in vivo* studies proved that the Dex-loaded CMCht/PAMAM dendrimer nanoparticles may find applications in bone tissue engineering and regenerative medicine strategies, namely as an intracellular drug delivery nanocarrier able to promote the osteogenic differentiation of RBMSCs and inducing superior *de novo* bone formation. To our knowledge the present work demonstrate for the first time, the use of non cytotoxic nanoparticles able to program the differentiation pathway from the interior of stem cells, being able, in particular to promote superior bone formation *in vivo* when using stromal cells. This work mark the transition from '*proof-of-concept'* to useful intracellular nanocarrier tool as these nanoparticles show promise in clinically relevant approaches for bone regeneration.

REFERENCES

1. Bianco, P. and P.G. Robey, *Stem cells in tissue engineering*. Nature, 2001. **414**: p. 118.
2. Griffith, L.G. and G. Naughton, *Tissue engineering-current challenges and expanding opportunities*. Science, 2002. **295**: p. 1009.
3. Lutolf, M.P. and J.A. Hubbell, *Synthetic biomaterials as instructive extracellular microenvironments for morphogenesis in tissue engineering*. Nature Biotechnology, 2005. **23**: p. 47.
4. Wang, Y., et al., *Co-delivery of drugs and DNA from cationic core-shell nanoparticles self-assembled from a biodegradable copolymer.* Nature Materials, 2006. 5: p. 791.
5. Dalby, M.J., et al., *The control of human mesenchymal cell differentiation using nanoscale symmetry and disorder*. Nature Materials, 2007. **6**: p. 997.
6. Sontjens, S.H.M., et al., *Biodendrimer-based hydrogel scaffolds for cartilge tissue repair*. Biomacromolecules, 2006. **7**: p. 310.
7. Du, Y., et al., Directed assembly of cell-laden microgels for fabrication of 3D tissue constructs. Proceedings of the National Academy of Sciences of the United States of America, 2008. **105**: p. 9522.
8. Kraljevic, S. and K. Pavelic, *Navigare necessere est*. EMBO reports, 2005. **6**: p. 695.
9. Nishiyama, N., et al., *Light-induced gene transfer from packaged DNA enveloped in a dendrimeric photosensitizer*. Nature Materials, 2005. **4**: p. 934.
10. Neu, M., et al., *Crosslinked nanocarriers based upon poly(ethylene imine) for systemic plasmid delivery: In vitro characterization and in vivo studies in mic*e. Journal of Controlled Release, 2007. **118**: p. 370.
11. Kocbek, P., et al., *Targeting cancer cells using PLGA nanoparticles surface modified with monoclonal antibody*. Journal of Controlled Release, 2007. **120**: p. 18.
12. Lee, C.C., et al., *A single dose of doxorubicin-functionalized bow-tie dendrimer cures mice bearing C-26 colon carcinomas*. Proceedings of the National Academy of Sciences of the United States of America, 2006. **103**: p. 16649.
13. Kano, M.R., et al., *Improvement of cancer-targeting therapy, using nanocarriers for intractable solid tumors by inhibition of TGF-Î²² signaling*. Proceedings of the National Academy of Sciences of the United States of America, 2007. **104**: p. 3460.
14. Beezer, A.E., et al., *Dendrimers as potential drug carriers; encapsulation of acidic hydrophobes within water soluble PAMAM derivatives*. Tetrahedron, 2003. **59**: p. 3873.

15. Medintz, I.L., et al., Q*uantum dot bioconjugates for imaging, labelling and sensing*. Nature Materials, 2005. **4**: p. 435.
16. Tsogas, I., et al., *Interactive transport of guanidinylated poly(propylene-imine)-based dendrimers through liposomal and cellular membranes*. ChemBioChem, 2007. **8**: p. 1865.
17. Tomalia, D.A. and J.M.J. Fréchet, *Introduction to "Dendrimers and dendritic polymers"*. Progress in Polymer Science, 2005. **30**: p. 217.
18. Kukowska-Latallo, J.F., et al., *Efficient transfer of genetic material into mammalian cells using Starburst polyamidoamine dendrimers*. Proceedings of the National Academy of Sciences of the United States of America, 1996. **93**: p. 4897.
19. Tomalia, D.A., et al., *Partial shell-filled core-shell tecto(dendrimers): A strategy to surface differentiated nano-clefts and cusps*. Proceedings of the National Academy of Sciences of the United States of America, 2002. **99**: p. 5081.
20. Malik, N., et al., *Dendrimers: relationship between structure and biocompatibility in vitro, and preliminary studies on the biodistribution of ^{125}I-labelled polyamidoamine dendrimers in vivo*. Journal of Controlled Release, 2000. **65**: p. 133.
21. Lee, C.C., et al., *Designing dendrimers for biological applications*. Nature Biotechnology, 2005. **23**: p. 1517.
22. Choi, Y., et al., *Synthesis and functional evaluation of DNA-assembled polyamidoamine dendrimer clusters for cancer cell-specific targeting*. Chemistry & Biology, 2005. **12**: p. 35.
23. Kobayashi, H., et al., *Renal tubular damage detected by dynamic micro-MRI with a dendrimer-based magnetic resonance contrast agent*. Kidney International, 2002. **61**: p. 1980.
24. Oliveira, J.M., et al., *Surface engineered carboxymethylchitosan/poly(amidoamine) dendrimer nanoparticles for intracellular targeting*. Advanced Functional Materials, 2008. **18**: p. 1840.
25. Oliveira, J.M., et al., *The osteogenic differentiation of rat bone marrow stromal cells cultured with dexamethasone-loaded carboxymethylchitosan/polyamidoamine dendrimer nanoparticles*. Biomaterials, 2009. **30**: p. 804.
26. Oliveira, A.L., et al., *Micro-computed tomography (μ-CT) as a potential tool to assess the effect of dynamic coating routes on the formation of biomimetic apatite layers on 3D-plotted biodegradable polymeric scaffolds*. Journal of Materials Science: Materials in Medicine, 2007. **18**: p. 211.
27. Gomes, M.E., et al., *Starch-poly(caprolactone) and starch-poly(lactic acid) fibre-mesh scaffolds for bone tissue engineering applications: structure, mechanical properties and degradation behaviour*. Journal of Tissue Engineering and Regenerative Medicine, 2008. **2**: p. 243.

28. Kotobuki, N., et al., *Viability and osteogenic potential of cryopreserved human bone marrow-derived mesenchymal cells*. Tisssue Engineering, 2005. **11**: p. 663.
29. Kotobuki, N., et al., *Cultured autologous human cells for hard tissue regeneration: Preparation and characterization of mesenchymal stem cells from bone marrow*. Artificial Organs, 2004. **28**: p. 33.
30. Uchimura, E., et al., *In-situ visualization and quantification of mineralization of cultured osteogenetic cells*. Calcified Tissue International, 2003. **73**: p. 575.
31. Oliveira, J.M., et al., *Ex vivo culturing of rat bone marrow stromal cells with dexamethasone-loaded carboxymethylchitosan/poly(amidoamine) dendrimer nanoparticles enhances ectopic bone formation on tissue engineered constructs*. 2009; submitted.
32. Kim, H., H.W. Kim, and H. Suh, *Sustained release of ascorbate-2-phosphate and dexamethasone from porous PLGA scaffolds for bone tissue engineering using mesenchymal stem cells*. Biomaterials, 2003. **24**: p. 4671.
33. Kim, C.-S., et al., *Ectopic bone formation associated with recombinant human bone morphogenetic proteins-2 using absorbable collagen sponge and beta tricalcium phosphate as carriers*. Biomaterials, 2005. **26**: p. 2501.
34. Du, J. and Y.-L. Hsieh, *Nanofibrous membranes from aqueous electrospinning of carboxymethyl chitosan*. Nanotechnology, 2008. (doi:10.1088/0957-4484/19/12/125707).
35. Sun, L., et al., *Preparation, characterization and antimicrobial activity of quaternized carboxymethyl chitosan and application as pulp-cap*. Polymer, 2006. **47**: p. 1796.
36. Midelfart, A., et al. *Dexamethasone and dexamethasone phosphate detected by ^{1}H and ^{19}F NMR spectroscopy in the aqueous humour*. Experimental Eye Research, 1998. **66**: p. 327.
37. Xu, R., *Progress in nanoparticles characterization: Sizing and zeta potential measurement*. Particuology, 2008. **6**: p. 112.
38. Jiang, B., et al., *Ibuprofen-loaded nanoparticles prepared by a co-precipitation method and their release properties*. International Journal of Pharmaceutics, 2005. **304**: p. 220.
39. Yinsong, W., et al., *Preparation and characterization of self-aggregated nanoparticles of cholesterol-modified O-carboxymethylchitosan conjugates*. Carbohydrate Polymers, 2007. **69**: p. 597.
40. Lee, Y., et al., *Charge-conversion ternary polyplex with endosome disruption moiety: A technique for efficient and safe gene delivery13*. Angewandte Chemie, 2008. **120**: p. 5241.

41. Hayashi, R., et al., *Effects of glucocorticoids on gene transcription*. European Journal of Pharmacology, 2004. 500: p. 51.
42. Zhang, X., et al., *Dexamethasone inhibition of trabecular meshwork cell phagocytosis and its modulation by glucocorticoid receptor b*. Experimental Eye Research, 2007. **84**: p. 275.
43. Beresford, J.N., et al., *Evidence for an inverse relationship between the differentiation of adipocytic and osteogenic cells in rat bone marrow stromal cell cultures*. Journal of Cell Science, 1992. **102**: p. 341.
44. Porter, R.M., W.R. Huckle, and A.S. Goldstein, *Effect of dexamethasone withdrawal on osteoblastic differentiation of bone marrow stromal cells*. Journal of Cellular Biochemistry, 2003. **90**: p. 13.
45. Cancedda, R., et al., *Bulk and interface investigations of scaffolds and tissue-engineered bones by X-ray microtomography and X-ray microdiffraction*. Biomaterials, 2007. **28**: p. 2505.
46. Muller, R., et al., *Morphometric analysis of human bone biopsies: A quantitative structural comparison of histological sections and micro-computed tomography*. Bone, 1998. **23**: p. 59.
47. Mastrogiacomo, M., et al., *Engineering of bone using bone marrow stromal cells and a silicon-stabilized tricalcium phosphate bioceramic: Evidence for a coupling between bone formation and scaffold resorption*. Biomaterials, 2007. **28**: p. 1376.

SECTION 4.

CHAPTER XI.

Summary and general conclusions

CHAPTER XI.

Summary and general conclusions

1. SUMMARY AND GENERAL CONCLUSIONS

Nanotechnology and medicine research are merging with other fields leading to completely new science and superior technological platforms such as those recently reported for regenerative medicine and neurosciences. The main aim of this thesis was to exploit a new concept based on combining nanotechnology and traditional tissue engineering strategies towards developing more efficient approaches for the treatment of damage/diseased cells and tissues. The use of surface engineered dendrimers to deliver bioactive agents from inside the cells is aimed at improve *in vivo*, the biological performance of stem cell alone or combined with scaffolds, the so-called cells-scaffold constructs.

Dendrimers and their derivatives have been exhibiting unique physicochemical properties which have great potential to be used as nanocarriers in a variety of applications, including tissue engineering and regenerative medicine, which have been discussed in the first chapter of this thesis. Though, high generation dendrimers with amine capping-groups causes haemolysis and changes in red cell morphology, since they bind to negatively charged membranes of cells in a non-specific manner and can cause toxicity *in vitro* and *in vivo*. To circumvent this drawback, we modified the surface of low generation poly(amidoamine) (PAMAM) dendrimers with carboxymethylchitosan (CMCht), to reduce the cytotoxic effects of cationic and high-generation dendrimers and reduce the haemolytic toxicity by reduction/shielding of the positive charge on the dendrimer surface, while enhancing the peripheral congestion to improve container properties. Carboxymethylchitosan was chosen due to its water solubility, low toxicity and antimicrobial activity making it attractive for applications in the controlled release of drugs. Thus, carboxymethylchitosan/poly(amidoamine) dendrimer (CMCht/PAMAM) nanoparticles were prepared in a stepwise manner as follows: (i) increasing the generation of the PAMAM-carboxylic terminated (G 1.5), (ii) obtaining a PAMAM-methyl ester terminated dendrimer, (iii) reaction of PAMAM and CMCht, i.e. the reaction goes through a condensation reaction between the methyl ester and amine groups, and (iv) modifying the methyl ester groups that do not react to carboxylic ones in the CMCht/PAMAM dendrimer, followed by precipitation. As a model drug, dexamethasone (Dex) was incorporated into CMCht/PAMAM dendrimer nanoparticles due to its important role in osteogenesis and clinical relevance.

To assess the potential of using the Dex-loaded CMCht/PAMAM dendrimer nanoparticles systems for application in tissue engineering, we used different biomaterials to develop a set of novel scaffolds (3-D systems) suitable for applications in bone, cartilage and osteochondral tissue engineering.

Chitosan was used a biomaterial for developing support for cartilage due to its easy processability and biological properties such as biocompatibility and immunological, antibacterial and wound-healing activity. Moreover, chitosan shares structural characteristics with various glucosaminoglycans (GAGs) and given its importance in stimulating the chondrogenesis, the use of GAG analogs as components of a cartilage tissue engineered scaffold is desired for improving chondrogenesis.

Hydroxylapatite was used a a biomaterial to develop scaffolds for bone applications since its structure resembles to the primary mineral component of bone. Other advantages include the good processability, non-cytotoxicity, non-immunogenicity, resorbability and osteoconductivity.

Starch-based biomaterials such as the starch-polycaprolactone (SPCL) were also used within the scope of this thesis mainly due to the advantages of being non-cytotoxicity, biodegradable, present good mechanical properties and can be processed by different methodologies. Processability is an important feature which can allow us to tailor the final properties of the scaffolds, and can be a major advantage in comparative studies. Moreover, it can be possible to investigate qualitatively and quantitatively the calcified tissue within the explants using a non-destructive and time-saving technique such as micro-computed tomography, as polymeric materials exhibit lower attenuation coefficient as compared to bone or ceramics.

The general conclusions of the research work produced in the present thesis, which extends from Chapter III to X, are summarized as follows.

1.1. NOVEL HYDROXYLAPATITE/CARBOXYMETHYLCHITOSAN COMPOSITE SCAFFOLDS PREPARED THROUGH AN INNOVATIVE "*AUTOCATALYTIC*" ELECTROLESS CO-PRECIPITATION ROUTE

Chapter III describes the "*autocatalytic*" electroless deposition route for production of a composite scaffolds composed of hydroxylapatite (HAp) and carboxymethylchitosan (CMCht) for bone tissue-engineering scaffolding applications. This work demonstrated that it is possible to prepare such composite scaffolds by means of combining a novel acidic "*autocatalytic*" co-precipitation route and a novel wax spheres leaching methodology. The physicochemical properties of the composite scaffolds may be tailored, especially the 3-D architecture, content in organic-inorganic phases, and dissolution behaviour. Therefore, these composite scaffolds are very promising whenever degradability and bioactivity are simultaneously desired, such as in the case of bone tissue-engineering scaffolding

applications. Moreover, these novel composite scaffolds can possibly support the incorporation of pH-sensitive proteins up to physiological pH, which is known to be one major drawback of chitosan materials for such type of applications. Despite, the promissing data, no cell culture studies were carried out in order to fully exploit its potential usefulness in tissue engineering applications.

1.2. MACROPOROUS HYDROXYLAPATITE SCAFFOLDS FOR BONE TISSUE ENGINEERING APPLICATIONS: PHYSICOCHEMICAL CHARACTERIZATION AND ASSESSMENT OF RAT BONE MARROW STROMAL CELL VIABILITY

Chapter IV reports a new methodology for developing HAp scaffolds by using an organic sacrifice template, and its potential to find applications in bone tissue engineering scaffolding investigated. The novelty of this work consists on the possibility of obtaining porous and highly interconnected scaffolds mimicking the sacrificial component. In fact, this work demonstrated that it is possible to prepare sintered hydroxylapatite scaffolds with high interconnectivity by impregnating the template of 'open-cell' polyurethane (PU) sponge into the HAp slurry, followed by sponge burn-out. The preparation route was optimized for producing macroporous HAp structures with controlled morphology, easily mediated by the architecture of the PU sponge. *In vitro* tests have demonstrated that such constructs are bioactive, as observed by the formation of an apatite layer after 1 day of immersion in SBF solution. The biocompatible behaviour of the macroporous HAp scaffold was demonstrated as evidenced by the non-cytotoxic effect over L929 cells. Moreover, the cell/material interaction tests have shown that the RBMSCs adhered, proliferated well and remained viable on the macroporous hydroxylapatite scaffolds. More importantly, the cells were able to populate the inner of the macroporous HAp scaffolds. Therefore, the physicochemical and biological properties of the macroporous HAp scaffolds have shown to be suitable for bone tissue-engineering applications.

1.3. NOVEL HYDROXYLAPATITE/CHITOSAN BILAYERED SCAFFOLD FOR OSTEOCHONDRAL TISSUE ENGINEERING APPLICATIONS

Chapter V demonstrates the feasibility to prepare hydroxylapatite/chitosan bilayered scaffolds by means of an innovative method that combines a sintering and a freeze-drying technique. The novel macroporous hydroxylapatite/chitosan bilayered scaffolds exhibit physicochemical properties that appear to make them a suitable candidate to be used as a supportive structure for cells functions. Moreover, the *in vitro* cell culture studies demonstrated that both HAp and CHT layers provide an adequate 3-D support for the attachment, proliferation and differentiation of goat bone marrow stromal cells (GBMSCs) into osteoblasts and chondrocytes, respectively. The HAp/CHT bilayered scaffolds are

advantageous by several reasons, namely they can be designed with several sizes and controlled architecture to fit patient specific injuries and cell functions, respectively. The HAp/CHT bilayered scaffolds showed promising biological behavior and may therefore find applications in tissue engineering of bone and osteochondral defects.

1.4. *IN VITRO* INVESTIGATION OF DEX-LOADED AND CMCHT/PAMAM DENDRIMER NANOPARTICLES: INTERNALIZATION EFFICIENCY AND MECHANISM, AND OSTEOGENIC POTENTIAL (2-D SYSTEM)

In this thesis we demonstrated that the combination of synthetic and natural-based polymers enable to prepare CMCht/PAMAM dendrimer nanoparticles of suitable diameters to cover a wide range of intracellular delivery applications (Chapter VI and VII). *In vitro* tests showed that the carboxymethylchitosan/poly(amidoamine) dendrimer nanoparticles do not exert any significant cytotoxic effect over both L929 fibroblast, post-natal neurons and glial cells and RBMSCs for concentrations below 1 $mg.mL^{-1}$. Furthermore, the successful internalization of the nanoparticles by two different types of cells, i.e. cell lines and primary cultures, was also demonstrated. We also proved that the mechanism by which these nanoparticles are taken up by cells is not exclusively endocytotic. The biochemical data presented herein also proved that the Dex-loaded CMCht/PAMAM dendrimer nanoparticles induced the osteogenic differentiation of RBMSCs *in vitro*, in TCPS 2-D substrates. Therefore, the novel CMCht/PAMAM dendrimer nanoparticles may be used as targeted-drug delivery carriers covering a wide range of applications involving the efficient intracellular delivery of biological agents to modulate the behaviour of cells. These might include the use of differentiation factors to act from the inside the cell or genetic material. The incorporation of fluorescent labels for live-cell imaging and monitoring of the final intracellular fate of such structures is also possible.

1.5. *IN VITRO* ASSESSMENT OF OSTEOGENIC DIFFERENTIATION WHEN COMBINING DEX-LOADED CMCHT/PAMAM DENDRIMER NANOPARTICLES, STEM CELLS AND, EITHER HAP AND SPCL SCAFFOLDS (3-D SYSTEM)

In this thesis, it was our aim to fully investigate the biological performance of the macroporous HAp and SPCL scaffolds when seeded with RBMSCs exposed to Dex-loaded CMCht/PAMAM dendrimer nanoparticles. These two types of scaffolds were chosen for their similar architecture, i.e. porosity, interconnectivity and pore size, while possessing different composition. Both were found to be adequate for culturing RBMSCs, namely for adhesion, proliferation and osteogenic differentiation, *in vitro* (Chapter VIII). Despite, RBMSCs proliferation and osteogenic differentiation are favoured when cultured onto the

surface of the HAp scaffolds, but the results obtained for SPCL are quite similar and much better than one could expect for a biodegradable polymer. On the other hand, the biochemical data demonstrated that the Dex-loaded CMCht/PAMAM dendrimer nanoparticles enhanced the early osteogenic differentiation of RBMSCs in a 3-D environment, *in vitro*.

1.6. *IN VIVO PROOF-OF-CONCEPT*

Chapter IX exploited the potential of the combinatorial strategy in tissue engineering principles employing CMCht/PAMAM dendrimer nanoparticles towards the intracellular release and regimented supply of dexamethasone (Dex) aimed at control stem cells osteogenic differentiation in the absence of typical osteogenic inducers, *in vivo*. In this work, we have demonstrated that cell number and *ex vivo* culturing strategies greatly influences the osteogenesis and *de novo bone* formation, *in vivo*. RBMSCs expanded with 0.01 $mg.mL^{-1}$ Dex-loaded CMCht/PAMAM dendrimer nanoparticles and seeded at low cell number on the surface of the HAp scaffolds enhanced the ectopic bone formation, after 4 weeks of subcutaneous implantation in the back of F344/N rats. This study revealed that the novel Dex-loaded CMCht/PAMAM dendrimer nanoparticles may be beneficial as intracellular nanocarrier and supply of Dex in a regimented manner to modulate and direct stem cells differentiation towards osteogenic phenotype, enhance proteoglycan extracellular matrix synthesis and superior ectopic *de novo* bone formation. The architecture of HAp scaffolds proved to be a good support for osteogenic differentiation of bone marrow derived osteoblast and new bone formation, *in vivo*. Thus, the tissue engineering strategy proposed in this thesis showed to be effective on promoting *de novo* bone formation *in vivo* and avoid the long time of *in vitro* culturing in the presence of osteogenic cocktails which is seen as major drawback for most clinical applications.

Complementarily, Chapter X report deeper studies on the chemistry of the Dex-loaded CMCht/PAMAM dendrimer nanoparticles and also the *in vivo* osteogenic ability. These nanoparticles were found to possess pH and ionic-responsive nature. Moreover, we have observed that Dex incorporation greatly influences the structure of the nanoparticles. The *in vitro* tests showed that the Dex-loaded CMCht/PAMAM dendrimer nanoparticles at concentrations bellow 1 $mg.mL^{-1}$ do not exert any significant cytotoxic effect over RBMSCs. Furthermore, its ability for being taken up by RBMSCs was shown and incorporation of Dex into the nanoparticles decreases their internalization efficiency. It was shown that these Dex-loaded CMCht/PAMAM dendrimer nanoparticles have the ability to promote *in vitro* mineralization, denoting its osteogenic ability. *In vivo*, the biochemical data revealed that porous SPCL scaffolds alone do not induce bone formation upon subcutaneous implantation in the back of the F344/N

rats. However, by seeding RBMSCs supplemented with Dex onto the scaffolds bone formation could be detected, when cell number was 1 x 10^6 cells. Moreover, these studies proved that the Dex-loaded CMCht/PAMAM dendrimer nanoparticles internalization by RBMSCs *ex vivo*, can afford a regimented supply of Dex *in vivo*, and stimulate RBMSCs to produce superior bone mineral. Remarkably, the SPCL scaffolds proved to be adequate for fundamental studies as it revealed by *in vivo* studies supported bone formation, while allow qualitative and quantitative analyses of the newly bone formed using a non-destructive technique such as the micro-computed tomography.

As a final remark, this thesis mark the transition from '*proof-of-concept'* to useful intracellular nanocarrier tool, as the Dex-loaded CMCht/PAMAM dendrimer nanoparticles show promise for applications in several cells and tissues therapies. The use of these nanocarriers towards the incorporation of multiple bioactive agents and formulations aimed at find applications in osteochondral tissue engineering or for targeting central nervous system can also be envisioned.